UNIVERSITAT DE BARCELONA

# The biogeochemical imprint of the Azores Archipelago lacustrine sedimentary infill

## A linkage between the climatic effects of the north Atlantic atmospheric circulation and the tectono-volcanic landscape of the triple junction during the late Holocene

Mario Benavente Marín

# The biogeochemical imprint of the Azores Archipelago lacustrine sedimentary infill

## A linkage between the climatic effects of the north Atlantic atmospheric circulation and the tectono-volcanic landscape of the triple junction during the late Holocene

UNIVERSITAT DE BARCELONA

Mario Benavente Marín

**PhD thesis**

**July 2024**

# The biogeochemical imprint of the Azores Archipelago lacustrine sedimentary infill

## A linkage between the climatic effects of the north Atlantic atmospheric circulation and the tectono-volcanic landscape of the triple junction during the late Holocene

Programa de doctorado: Ciencias de la Tierra

Línea de investigación: Estratigrafía y análisis de cuencas

Facultad de Ciencias de la Tierra

UNIVERSITAT DE BARCELONA

**Mario Benavente Marín**

Directores:

Santiago Giralt Romeu — GEO3BCN Geosciences Barcelona - CSIC

Armand Hernández Hernández — UNIVERSIDADE DA CORUÑA

Tutor:

Alberto Sáez Ruiz — UNIVERSITAT DE BARCELONA

# Index

## Agradecimientos

Santi y Armand, gracias por guiarme, aconsejarme y ayudarme en los momentos que mas lo necesitaba. Gracias también por no hacerlo en los momentos en los que no tocaba, fue entonces cuando el crecimiento fue máximo. Supisteis perfectamente como ponerme en el camino para encontrarme con mi potencial, que hoy, es el mayor regalo que me llevo de esta experiencia. La confianza que habéis depositado en mi durante estos años ha marcado la diferencia para dar a esta tesis la forma que hoy tiene. Armand, desde luego nuestro paso por el congreso de Argentina fue un momento único, me alegro mucho de haber compartido aquella experiencia contigo. Santi, nuestra campaña en Groenlandia aun la vivo como si hubiera sido un sueño, nunca me imagine que la vida me pondría en aquel lugar tan especial, gracias por hacerlo posible. En definitiva, gracias a los dos por cada una de las oportunidades que me habéis ofrecido durante todo este tiempo.

Marc, Mari y Encarni, si hay algo que me haya hecho sentir como en casa durante estos años ha sido compartir las alegrías y los momentos difíciles con vosotros. Marc, gracias por ayudarme a encontrar propósito en lo que hago, trabajar contigo siempre fue como un juego. Creo que desde ahí es como las cosas salen bien de verdad. Me has enseñado el valor de la sencillez, y tu contribución en esta tesis ha sido clave para que hoy queden aquí plasmadas las ideas que me rondaban. Mari, quizás si, es posible que debiera haber salido corriendo el día que llegue, pero, al igual que tu no lo hice, y hoy me alegro, por que me encuentro saliendo del bosque cargando con la piel de oso, para decirte que esta tesis también lleva un poco de ti. Sea como sea, solo por haber conocido a personas como tu ya ha merecido la pena llegar hasta aquí. Gracias por prepárame para los momentos duros de verdad. Encarni, no sé cómo lo haces, pero siempre has sabido como ponérmelo fácil. Una vez tras otra me has sorprendido con nuevas formas de hacer que mi paso por el Instituto en concreto, y por Barcelona en general, fuera lo mas agradable posible. La calidad que tienes como persona es algo que admiro mucho. Gracias por tanto a los tres.

Vitor, Pedro, Matín y Bea, la experiencia en Azores fue única gracias a vosotros. Parte de las líneas de esta tesis están inspiradas en las observaciones de las campañas de campo que vosotros hicisteis posibles. También en las charlas que mantuve con vosotros y con el resto de compañeros del CIBIO y del INOVA: Antonio, Rita, Ana... Me llevasteis a los lugares mas increíbles del archipiélago y gracias a vosotros por fin pude conocer mis tres lagos. Además, sin vosotros no habría sido nada fácil dar con los sitios mas auténticos de Ponta Delgada. Fueron unas semanas inolvidables.

Mariana, fue un placer haber dado los primeros pasos de este camino contigo. Además, te estoy muy agradecido por tu ayuda con la vulcanología. Alberto, mientras hablábamos sobre la tesis no me daba ni cuenta de que las horas pasaban, gracias por esos ratos y por ponerlo siempre tan fácil con los tramites del doctorado. Gracias al resto del equipo de trabajo, Sergi, Catarina, Nora, Ricardo, Joan Albert, Carolina, Roberto … ha sido un placer contar con vuestra colaboración durante estos años.

Celia, mi paso por Londres y las semanas en la RHUL es uno de los mejores recuerdos que me llevo de estos años, gracias por aquella oportunidad. También te agradezco la implicación que tuviste con mi trabajo meses después de la estancia y los buenos ratos compartidos en Argentina.

Compañeros del Almera, Irene, Jorge, Enric…, os eché de menos durante la segunda etapa del doctorado. Los buenos recuerdos que me quedan de la primera, son sobre todo gracias a los momentos compartidos con vosotros. Comapañer@s del Geo3BCN gracias por vuestra compañía durante todos estos años. Erandi y Daniela, siempre me hicisteis sentir en confianza para compartir con vosotras mis inquietudes, es algo que valoro mucho. Wentao… we are so hard working! XD, thanks a lot for being my partner, your happiness at work was contagious. Hanneke, Alejandra, Lara,

Olaya, gracias por contar siempre conmigo. Marc Español, mil gracias por mantener a raya los “incendios” informáticos que han comprometido la evolución de la tesis. El viejo Mac cuenta con una tesis más a sus espaldas gracias a ti. Xavi, contar con tu felicitación año tras año y con tu bienvenida cada mañana ha sido algo que recordare siempre de forma muy positiva.

Además, esta investigación ha sido financiada por los proyectos PaleoNAO, RapidNAO and PaleoModes (CGL 2010-15767, CGL 2013-40608-R and CGL 2016-75281-C2, respectivamente) del Ministerio de Economía y Competitividad del Gobierno de España y por la Fundação para a Ciência e Tecnologia (PTDC/CTA-AMB/28,511/2017). Quiero expresar mi gratitud a estas estas instituciones por el apoyo económico recibido.

Gracias a mi geogente de Granada, de una forma u otra os he tenido presentes durante estos años lejos del sur. Bob, esta aventura empezaba contigo en el Candela, intentando decidir si me convenía embarcarme en ella o no. Hoy te agradezco que me aportaras tu visión para lanzarme. Gersan, Alvaro, Esteban, JD y el resto de compañeros de carrera… eché de menos los grandes momentos compartidos con vosotros y nuestra particular forma de entender la Geología, observándola desde el ángulo que ofrece la Bética.

Antonio Jabaloy, me animaste a dar mis primeros pasos en la academia y creo que esta tesis nunca se habría escrito sin la fe que depositaste en mi entonces. Alguien me dijo una vez que este no era lugar para el altruismo, sea o no cierto, tu ejemplo sería la excepción que confirma la regla.

Gracias a mis compañer@s de piso, especialmente a Shanti, Oli, Lau y Lu, por la paciencia infinita y por acompañarme día tras día en la etapa mas dura de esta carrera de fondo. Siempre habéis estado ahí apoyando y celebrando cada pequeña victoria. Teneros cerca me ha dado fuerza para llegar hoy hasta aquí.

Hoy no estaría escribiendo estas líneas sin el apoyo de mi familia, que ante todo pronostico, a veces favorable, a veces no tanto, siempre se mantuvo convencida de que mi plan, era el plan. Juanka, gracias por marcar el camino mas firme que conozco, al que siempre volver cuando los demás se pierden. Sin esa guía ni esta tesis ni muchas otras cosas que he logrado en mi vida serian una realidad hoy. Padre, si hoy he llegado hasta aquí ha sido gracias a tu ejemplo, por enseñarme el valor del sacrificio y a mantenerme de una pieza ante las situaciones exigentes. Madre, tu cariño ha sido mi mayor fuente de energía para seguir adelante. Entre los tres me habéis aportado dirección, fuerza y confianza para llegar hoy hasta aquí. Os quiero.

Sobre todo, gracias a mi mismo… por poner el trabajo, la determinación, el foco y la perseverancia, por aplicar lo que esta vida me ha enseñado en el proceso y por atreverme a escuchar a mi intuición para ofrecer lo que soy. También me gustaría disculparme conmigo mismo… por todas las veces que me perdí el respeto en el proceso, poniendo en juego mi salud, normalizando situaciones que, como mínimo, rozaban la excentricidad, por los momentos de auto-exigencia desmedida y por las veces que me he forzado a encajar en espacios que me quedaban pequeños.

## Abstract

The spatiotemporal evolution of atmospheric dynamics in the North Atlantic has a considerable socioeconomic impact on the European continent. Furthermore, the evolution of the relationship between the North Atlantic Oscillation (NAO) and the East Atlantic pattern (EA) has a significant influence on the climate of this region, as the combination of these two modes of climate variability largely determines the position of the jet stream and the associated storm tracks. The location of the Azores Archipelago, in the central North Atlantic Ocean, coincides with the high-pressure zone that determines the sign of the NAO, making this archipelago a strategic point for the analysis of regional atmospheric dynamics. Therefore, possible climate reconstructions derived from the multidisciplinary study of sediments deposited on the lake bottoms of the Azores Archipelago allow for establishing the temporal evolution of North Atlantic atmospheric dynamics beyond instrumental records. However, the use of such sediments for climate and environmental reconstructions include complexities, as the origin and evolution of these oceanic islands are governed by one of the most complex geodynamics on the planet. The triple junction between the African, Eurasian, and North American plates shapes the archipelago and its lake basins through tectono-volcanism, which determines the sedimentary processes occurring in them. Additionally, in this complicated atmospheric and geological scenario, the colonization of the archipelago occurred much earlier than the official date, contributing to greater environmental complexity through increasing anthropogenic pressure on the ecosystems of the archipelago since its colonization.

The multi-proxy approach to study the lake basin sediments, supported by novel limnogeomorphic spatial analysis techniques, has allowed investigating the relationship between landscape evolution and the geological substrate on which it develops. This approach integrates the normalized slope geomorphic index (Ksn) and bathymetric data from lake-basin systems with multi-proxy data of lithological, biogeochemical, and biological nature obtained from sedimentary sequences of the lakes. Thus, erosive power in the basin is related to its sedimentary response, allowing the establishment of process-response models indicative of morphosedimentary dynamics. In this context, the significant role played by the sedimentary cascade in the biogeochemical cycle of lake-basin systems highlights. The stratigraphic distribution of sediments and depositional forms of relief, supported by radiometric chronologies, permit establishing the spatiotemporal evolution of depositional environments during the last 5200 years. This evolution has demonstrated the existence of annual sedimentation patterns that allow inferring depositional dynamics at a seasonal temporal scale.

The sediments used belong to Lake Funda, located within one of the phreatomagmatic craters of a group that responds to orthogonal tectonic controls on Flores Island. Sediments from Lake Caldeirão on Corvo Island, which lies in the flat and central domain of the bottom of a collapsed volcanic caldera through annular faulting, were also used, sharing a structural domain with Flores in the western group of islands of the archipelago. Finally, Lake Caveiro on Pico Island was selected, whose sedimentary infill fills the crater of a small scoria cone fragmented by a fault associated with the transtensive dynamics of the central group of the Azores archipelago. The lacustrine systems of these basins are affected by a relatively similar climate, however, they have demonstrated variable depositional evolution dominated, in part, by the geological configuration of their basins. The last 1000 years of Lake Funda system evolution are marked by the transition of deltaic depositional environments, reflecting basin erosion as the main mechanism of pelagic sediment accumulation, resulting in a subsequent varved laminated pattern composed of diatom remains and resuspended clayey and silty material. The last 3700 years of Lake Caldeirão system evolution were dominated by runoff fluctuations provoking cyclic changes in the extension of the lake, affecting soil formation and degradation in the basin. Finally, Lake Caveiro experienced rapid infilling during the last 5200 years, where its limited accommodation space dominated the depositional evolution of the system,

controlled by the dominant tectonic alignment favoring the preferential progradation of the morphosedimentary system. Hydroclimatic changes modulated this effect, determining erosion and sediment accumulation rates within the basin.

The analysis of the rate of change in sediment composition has revealed the increasing anthropogenic transformation of the landscape, resulting in reduced rates of evapotranspiration, biological weathering, and soil cohesion through deforestation. The sedimentary response to deforestation effects varied depending on basin configuration, emphasizing some effects over others. In Funda, the reduction of evapotranspiration led to system deepening, favoring the formation of a summer thermocline whose rupture during autumn controls varved sedimentation. Reductions in biological weathering and soil cohesion in Caldeirão affected ecological dynamics within the lake through changes in nutrient concentrations released from the basin into the lake. In Caveiro, the effects of deforestation were practically null due to the small size of its basin. However, neotectonic dynamics in the islands of the central group greatly influenced sedimentation by increasing system infiltration.

Pearson correlation coefficients established between instrumental climate records in the study area and data obtained from paleolimnological records have allowed reconstructing the climatic signals contained in biogeochemical records. Erosion and runoff are indicators of precipitation, while Lake Funda level and soil formation rates in Caldeirão respond to temperature variations. These signals have allowed determining the climate of the western sector of the archipelago during the last 3700 years.

Thus, a regional climate comparison has been established, allowing the spatiotemporal evolution of North Atlantic atmospheric dynamics to be reconstructed. This evolution was marked by 5 stages: Stage 1 (approximately 3700 to 2700 years cal. before present): Negative NAO in winter and negative EA in summer; Stage 2 (approximately 2700 to 1800 years cal. before present): Negative NAO in winter and positive EA in summer; Stage 3 (approximately 1800 to 650 years cal. before present): Positive NAO in winter and negative EA in summer; Stage 4 (approximately 650 to 250 years cal. before present): Negative NAO in winter and negative EA in summer; Stage 5 (approximately 250 years cal. before present to present): Positive NAO in winter and positive EA in summer. This last phase highlights the effect that global warming is having on the lacustrine sedimentation of the archipelago.

## Resumen

La evolución espacio-temporal de la dinámica atmosférica en el Atlántico Norte tiene un considerable impacto socio-económico en el continente europeo. A su vez, la evolución de la relación entre la Oscilación del Atlántico Norte (NAO, por sus siglas en inglés) y el patrón del Atlántico Este (EA, por sus siglas en inglés) tiene una importante influencia en el clima de esta región, ya que la combinación de estos dos modos de variabilidad climática determina, en gran medida, la posición de la corriente de chorro y los frentes de tormenta asociados a ella. La ubicación del Archipiélago de las Azores, en la zona central del océano Atlántico norte, coincide con la zona de altas presiones que determina el signo de la NAO y, de este modo, este archipiélago se convierte en un punto estratégico para el análisis de la dinámica atmosférica regional. Por lo tanto, las posibles reconstrucciones climáticas derivadas del estudio multidisciplinar de los sedimentos depositados en el fondo de los lagos del Archipiélago de la Azores permiten establecer la evolución temporal de la dinámica atmosférica del Atlántico Norte más allá del registro instrumental. Sin embargo, el uso de dichos sedimentos para reconstrucciones climáticas y ambientales no está exento de complicaciones, y es que el origen y evolución de estas islas oceánicas está regido por una de las geodinámicas más complejas sobre el planeta. El punto triple entre las placas africana, euroasiática y norteamericana da origen y forma al archipiélago y a sus cuencas lacustres a través del tectono-vulcanismo, determinando los procesos sedimentarios que tienen lugar en ellas. Además, en este complicado escenario atmosférico y geológico, hay que añadir que la colonización del archipiélago tuvo lugar mucho antes de la fecha oficial, lo que contribuyó a dar una mayor complejidad ambiental mediante la creciente presión antrópica a la que se han visto sometidos los ecosistemas del archipiélago desde su colonización.

El enfoque multi-indicador (multi-proxy, en inglés) de los sedimentos de las cuencas lacustres, apoyado por novedosas técnicas limnogeomorfólogicas de análisis espacial, ha permitido investigar la relación entre la evolución del paisaje y el sustrato geológico sobre el que este se desarrolla. Este enfoque integra el índice geomórfico de pendiente normalizada (Ksn) y datos batimétricos de los sistemas lago-cuenca con datos *multi-proxy* de carácter litológico, biogeoquímico y biológico obtenidos de las secuencias sedimentarias de los lagos. De esta forma, se relaciona el poder erosivo en la cuenca con su respuesta sedimentaria permitiendo establecer modelos proceso-respuesta indicativos de la dinámica morfosedimentaria. En esta dinámica destaca el relevante papel que juega la cascada sedimentaria en el ciclo biogeoquímico de los sistemas lago-cuenca. La distribución estratigráfica de los sedimentos y las formas deposicionales del relieve, apoyadas en las cronologías radiométricas, permiten establecer la evolución espacio-temporal de los ambientes deposicionales durante los últimos 5200 años. Esta evolución ha demostrado que existen patrones de sedimentación de carácter anual que permiten inferir la dinámica deposicional a escala temporal estacional.

Los sedimentos empleados pertenecen a la laguna de Funda, localizada dentro de uno de los cráteres freato-magmáticos de una agrupación que responde a controles tectónicos ortogonales en la Isla de Flores. También se han utilizado sedimentos del Lago Caldeirão, en la isla de Corvo, el cual se encuentra en el dominio llano y central del fondo de una caldera volcánica colapsada mediante fallamiento anular, compartiendo dominio estructural con Flores en el grupo occidental de islas del archipiélago. Por último, se seleccionó el lago Caveiro en la isla de Pico, cuyo relleno sedimentario colmata el cráter de un pequeño cono de escorias fragmentado por una falla asociada a la dinámica transtensiva del grupo central del archipiélago de las Azores. Los sistemas lacustres de estas cuencas están afectados por un clima relativamente similar, sin embargo han demostrado una evolución deposicional variable, dominada, en parte, por la configuración geológica de sus cuencas. Los últimos 1000 años de evolución del sistema de Funda están marcados por el tránsito de ambientes deposicionales deltaicos que son el reflejo de la erosión de la cuenca como principal

mecanismo de acumulación de sedimentos pelágicos, dando paso a un posterior patrón de laminación varvado compuesto por restos de diatomeas y material arcilloso y limoso resuspendido. Por su parte, los últimos 3700 años de evolución del sistema de Caldeirão estuvieron dominados por fluctuaciones de la escorrentía que impulsaron cambios cíclicos de la extensión del lago. Estas fluctuaciones afectaron a la formación y degradación del suelo en la cuenca. Por último, el Lago Caveiro experimentó una rápida colmatación durante los últimos 5200 años, donde su limitado espacio de acomodación dominó la evolución deposicional del sistema. El espacio de acomodación estuvo controlado por la alineación tectónica dominante que favoreció la progradación preferencial del sistema morfo-sedimentario. Los cambios hidroclimáticos modularon este efecto y, ambos factores, determinaron las tasas de erosión y acumulación de sedimentos dentro de la cuenca.

El análisis de la tasa de cambio de la composición de los sedimentos ha revelado la creciente transformación antrópica del paisaje, que provocó una reducción de las tasas de evapotranspiración, de meteorización biológica y de cohesión del suelo a través de la deforestación. La respuesta sedimentaria a los efectos de la deforestación fue variable en función de la configuración de las cuencas, que enfatiza unos efectos sobre otros. En Funda la reducción de evapotranspiración indujo a la profundización del sistema favoreciendo la formación de una termoclina de verano cuya ruptura durante el otoño controla la sedimentación varvada. La reducción de la meteorización biológica y de la cohesión del suelo en Caldeirão afectó a la dinámica ecológica dentro del lago a través de cambios en las concentraciones de nutrientes liberados desde la cuenca hacia el mismo. En Caveiro los efectos de la deforestación fueron prácticamente nulos debido al pequeño tamaño de su cuenca. Sin embargo, la dinámica neotectónica en las islas del grupo central influyó en gran medida a su sedimentación al aumentar la infiltración del sistema.

Los coeficientes de correlación de Pearson establecidos entre los registros climáticos instrumentales en el área de estudio y los datos obtenidos de registros paleolimnologicos han permitido reconstruir las señales climáticas que contienen los registros biogeoquímicos. La erosión y la escorrentía son indicadores de la precipitación mientras que el nivel del lago de Funda y las tasas de formación de suelo en Caldeirão responden a variaciones de temperatura. Estas señales han permitido determinar el clima del sector occidental del archipiélago durante los últimos 3700 años.

Así, se ha establecido una comparación climática regional que ha permitido reconstruir la evolución espacio-temporal de la dinámica atmosférica del Atlántico Norte. Esta evolución estuvo marcada por 5 fases: Etapa 1 (entre aprox. 3700 y 2700 años cal. antes del presente): NAO negativa en invierno y EA negativa en verano; Etapa 2 (entre aprox. 2700 y 1800 años cal. antes del presente): NAO negativa en invierno y EA positiva en verano; Etapa 3 (entre aprox. 1800 y 650 años cal. antes del presente): NAO positiva en invierno y EA negativa en verano; Etapa 4 (entre aprox. 650 y 250 años cal. antes del presente): NAO negativa en invierno y EA negativa en verano; Etapa 5 (entre aprox. 250 años cal. antes del presente y hasta la actualidad): NAO positiva en invierno y EA positiva en verano. En esta última etapa se destaca el efecto que el calentamiento global está teniendo sobre la sedimentación lacustre del archipiélago.

## Resum

L'evolució espaial i temporal de la dinàmica atmosfèrica a l'Atlàntic Nord té un considerable impacte socioeconòmic al continent europeu. A la vegada, l'evolució de la relació entre l'Oscil·lació de l'Atlàntic Nord (NAO, per les seves sigles en anglès) i el patró de l'Atlàntic Est (EA, per les seves sigles en anglès) té una important influència en el clima d'aquesta regió. La combinació d'aquests dos modes de variabilitat climàtica determina, en gran mesura, la posició de la corrent en jet i els fronts de tempesta associats a aquest. La ubicació de l'arxipèlag de les Açores, a la zona central de l'oceà Atlàntic Nord, coincideix amb la zona d'altes pressions del dipol que defineix la NAO i, d'aquesta manera, aquest arxipèlag es converteix en un dels punts estratègics per a l'anàlisi de la dinàmica atmosfèrica regional. Per tant, les possibles reconstruccions climàtiques derivades de l'estudi dels sediments dels llacs presents a l'arxipèlag permeten establir l'evolució temporal de la dinàmica atmosfèrica de l'Atlàntic Nord més enllà del registre instrumental. Tanmateix, l'ús d'aquests sediments per a les reconstruccions climàtiques i ambientals no està absent de complicacions, ja que l'origen i evolució d'aquestes illes oceàniques estan controlats per una de les geodinàmiques més complexes del planeta. El punt triple entre les plaques africana, euroasiàtica i nord-americana determina l'origen i forma de l'arxipèlag i de les seves conques lacustres a través de la tectònica i el vulcanisme determinant, a la vegada, els processos sedimentaris que hi tenen lloc en elles. A més, en aquest escenari atmosfèric i geològic tan complicat, cal afegir-hi que la colonització de l'arxipèlag va tenir lloc molt abans de la data oficial, contribuint amb una complexitat ambiental molt més acusada a causa de la creixent pressió antropogènica a la que s'han vist sotmesos els ecosistemes de l'arxipèlag des de la seva colonització.

L'estudi multi-indicador (multi-proxy, en anglès) dels sediments de les conques lacustres, recolzat per noves tècniques limnogeomorfòlogiques d'anàlisi espaial, ha permès investigar la relació entre l'evolució del paisatge i el substrat geològic. Aquesta aproximació utilitza l'índex geomorfològic de pendent normalitzada (Ksn) i les dades batimètriques i topogràfiques dels sistemes llac-conca amb dades litològiques, biogeoquímiques i biològiques obtingudes de l'estudi multi-indicador de les seqüències sedimentàries dels llacs. D'aquesta manera, es relaciona el poder erosiu a la conca amb la seva resposta sedimentària establint models procés-resposta indicatius de la dinàmica morfosedimentària. En aquesta dinàmica cal destacar el paper que juga la cascada sedimentària en el cicle biogeoquímic dels sistemes llac-conca. L'estratigrafia dels sediments junt amb les formes deposicionals del relleu, tot recolzat per les cronologies radiomètriques, permet establir l'evolució espaial i temporal dels ambients deposicionals pels darrers 5200 anys. Aquestes evolucions posen de manifest que existeixen patrons de sedimentació de caràcter anual que ajuden a inferir la dinàmica deposicional a escala estacional.

Els sediments emprats en aquesta Tesi Doctoral pertanyen al Llac de Funda, localitzat en un dels cràters freàtico-magmàtics d'una agrupació de volcans que responen a controls tectònics ortogonals de l'illa de Flores. També s'han utilitzat sediments del Llac Caldeirão, situat a l'illa de Corvo, i que es troba al domini pla i central del fons d'una caldera volcànica col·lapsada degut a un sistema de falles anulars. Aquesta illa comparteix domini estructural amb l'illa de Flores al grup occidental d'illes de l'arxipèlag. Finalment, també es va seleccionar el Llac Caveiro, localitzat a l'illa de Pico, i que llur rebliment sedimentari omple el cràter d'un petit con d'escòries fragmentat per una falla associada a la dinàmica transtensiva que afecta el grup central d'illes de l'arxipèlag de les Açores. Els sistemes lacustres de totes aquestes conques estan afectats per un clima relativament similar però les respectives evolucions deposicionals depenen, en part, de la configuració geològica de les seves conques.

Els últims 1000 anys de l'evolució del sistema llac-conca de Funda han estan marcats pel trànsit d'ambients deposicionals deltaics, que són el reflex de l'erosió de la conca com a principal mecanisme d'acumulació de sediments pelàgics, donant lloc a un posterior patró de sedimentació

dominat per la deposició de laminació varvada formada per restes de diatomees i material argilós i llimós en resuspensió. Els últims 3700 anys de l'evolució del sistema llac-conca de Caldeirão han estat dominats per fluctuacions de l'escolament superficial que han impulsat canvis cíclics a l'extensió de l'àrea del llac. Aquestes fluctuacions van afectar la formació i degradació del sòl a la conca. Finalment, el sistema llac-conca del Llac Caveiro va experimentar un ràpida rebliment durant els darrers 5200 anys. El seu limitat espai d'acomodació va controlar l'evolució deposicional del sistema. L'alienació tectònica regional dominant va afavorir la progradació preferencial del sistema morfo-sedimentari. Els canvis hidroclimàtics van modular aquest efecte i, ambdós factors, van determinar les taxes d'erosió i acumulació de sediments dins de la conca.

L'anàlisi de la taxa de canvi de la composició dels sediments ha posat de manifest la creixent transformació antropogènica del paisatge que ha provocat una reducció de les taxes d'evapotranspiració, de meteorització biològica i de cohesió del sòl a través de la desforestació. La resposta sedimentària als efectes de la desforestació va ser variable en funció de la configuració de les conques, la qual cosa emfatitza el predomini d'uns efectes sobre d'altres. La reducció de l'evapotranspiració al Llac de Funda va induir a la profundització del sistema afavorint la formació d'una termoclina d'estiu. La ruptura d'aquesta termoclina durant la tardor dona lloc a la sedimentació varvada. La reducció de la meteorització biològica i de la cohesió del sòl al Llac de Caldeirão va afectar la dinàmica ecològica dins el llac a través de canvis en les concentracions de nutrients alliberats des de la conca cap aquest. Al Llac de Caveiro, els efectes de la desforestació van ser pràcticament nuls com a conseqüència de la mida tan petita de la seva conca. No obstant, la dinàmica neotectònica que ha afectat a les illes del grup central va influir en gran mesura en la sedimentació dels llacs presents en aquestes illes a l'augmentar la infiltració del sistema.

Els coeficients de correlació de Pearson establerts entre els registres meteorològics instrumentals presents a l'àrea d'estudi i les dades obtingudes de registres paleolimnològics han permès reconstruir les senyals climàtiques contingudes en els registres biogeoquímics. L'erosió i l'escolament superficial són indicadors de la precipitació, mentre que el nivell del Llac de Funda i les taxes de formació de sòl a la conca del Llac de Caldeirão responen a variacions de temperatura. Aquestes senyals han permès determinar el clima del sector occidental de l'arxipèlag durant els darrers 3700 anys.

Així doncs, s'ha establert una comparació climàtica regional que ha permès reconstruir l'evolució espaial i temporal de la dinàmica atmosfèrica a l'Atlàntic Nord. Aquesta evolució va estar marcada per 5 fases: Fase 1 (entre aprox. 3700 i 2700 anys calendari abans del present): NAO negativa a l'hivern i EA negativa a l'estiu; Fase 2 (entre aprox. 2700 i 1800 anys calendari abans del present): NAO negativa a l'hivern i EA positiva a l'estiu; Fase 3 (entre aprox. 1800 i 650 anys calendari abans del present): NAO positiva a l'hivern i EA negativa a l'estiu; 4. Fase 4 (entre aprox. 650 i 250 anys calendari abans del present): NAO negativa a l'hivern i EA negativa a l'estiu; Fase 5 (entre aprox. 250 anys calendari abans del present i fins a l'actualitat): NAO positiva a l'hivern i EA positiva a l'estiu. Durant aquesta darrera etapa cal destacar-ne l'efecte que l'escalfament global està tenint sobre la sedimentació lacustre dels llacs presents a l'arxipèlag.

## Keywords

North Atlantic atmospheric circulation, Azores Archipelago, volcano-tectonic lake basins, Paleolimnology, landscape, sediment cascading, Biogeochemistry, Anthropocene, varves.

## List of acronyms

**abl** Above base level
**Acc.** Accommodation
**Al** Aluminium
**AMV** Atlantic Multidecadal Variability
**asl** Above sea level
**$_{B}$DEM** Bathymetry Digital Elevation Model
**BP** Before Present
**Br** Bromine
**BSFR** Basal Surface of Forced Regression
**BSi** Biogenic Silica
**C** Carbon
**Ca** Calcium
**ca.** Circa
**$_{cald}$** Caldeirão
**$_{cav}$** Caveiro
**CC** Correlative Conformity
**CCiTUB** Centres Científics i Tecnològics at Universitat
**CE** Common Era
**$_{C}$F** Chemofacies
**CG** Central Group
**Cl** Chlorine
**cm** Centimetres
**Cpx** Clinopiroxene
**Cr** Chrome
**CSIC** Consejo Superior de Investigaciones Científicas
**$_{C}$Z** Chemozone
**DEM** Digital Elevation Model
**DIC** Dissolved inorganic carbón
**DTM** Digital Terrain Model
**E** East
**EA** East Atlantic pattern
**EAi** Eastern Atlantic pattern index
**EG** Eastern Group
**EMA** Early Middle Ages
**ENSO** El Niño–Southern Oscillation
**EOF** Empirical orthogonal function
**EPSG** European Petroleum Survey Group
**Eq.** Equation
**ESE** East-southeast
**F** Facies
**Fe** Iron
**Fig.** Figure
**FPFZ** Faial-Pico Fracture Zone
**FSST** Falling Stage System Tract
**$_{fun}$** Funda
**GDGT** Glycerol dialkyl glycerol tetraether
**Geo3BCN** Geociencias Barcelona
**GIS** Geographic Information System
**H** Hydrogen
**HAK** Lake Haukadalsvatn
**HST** Highstand Systems Tract
**HVT** Lake Hvítárvatn
**IA** Iron Age
**IDM** Inverse Distance Weighting
**IE** Industrial Era
**IGeoE** Instituto Geográfico do Exército
**Inc/coh** Incoherent/ Coherent
**IOD** Indian Ocean Dipole
**IP** Iberian Peninsula
**IPCC** Intergovernmental Panel on Climate Change
**JJA** June to August
**K** Potassium
**Kcps** Kilo counts per second
**Km** Kilometres
**Ksn** Normalized Steepness Index
**L** Litre
**LBA** Late Bronce Age
**LIA** Little Ice Age
**LOI** Loss on ignition
**LST** Lowstand Systems Tract
**$_{L}$Z** Lithozone
**m** Meter
**MAR** Mid Atlantic Ridge
**MCA** Medieval Climate Anomaly
**MFS** Maximum Flooding Surface
**$_{ML}$Z** Microlithozone
**Mn** Manganese
**MRS** Maximum Regressive Surface
**N** Nitrogen
**N** North

**NAM** Northern Annular Mode
**NAO** North Atlantic Oscillation
**NAOi** North Atlantic Oscillation index
**NE** Northeast
**NNE** North-northeast
**NTU** Nephelometric turbidity unit
**O** Oxygen
**Ol** Olivine
**OM** Organic matter
**ONDJFM** October to March
**PCA** Principal Component Analysis
**PDB** Pee Dee Belemnite
**PDV** Pacific Decadal Variability
**Pl** Plagioclase
**Rb** Rubidium
**RDA** Redundancy Analysis
**$_R$DEM** Relief Digital Elevation Model
**REEA** Relatorio do Estado do Ambiente dos Açores
**$_R$F** Rhythmic Facies
**RP** Roman Period
**RS** Ravinement Surface
**RSME** Regressive Surface of Marine Erosion
**S** Sulphur
**S** South
**SAM** Southern Annular Modes
**SCAi** Scandinavian pattern index
**SCAND** Scandinavian pattern
**SDR** sediment delivery ratio
**SEM** Scanning Electron Microscope
**Si** Silicon
**SLP** Sea Level Pressure
**Sr** Strontium
**SSP** Shared Socioeconomic Pathways
**SST** Sea Surface Temperature
**SSW** South-southwest
**St** Stream
**SU** Subaerial Unconformity
**SW** Southwest
**Ti** Titanium
**TIN** Triangulated Irregular Network
**Tmax** Maximum temperature
**Tmin** Minimum temperature
**TN** Total Nitrogen
**TOC** Total Organic Carbon
**TR** Terceira Rift
**TST** Transgressive Systems Tract
**UK** United Kingdom
**UTM** Universal Transverse Mercator
**V** Vanadium
**V** Volume
**VDB** Varves Data Base
**Ves** Vesuvianite
**VQI** Varve quality index
**VSA** Variable Source Area
**W** West
**WG** Western Group
**WGS** World Geodetic System
**WNW** West-northwest
**XRD** X-Ray Diffraction
**XRF** X-Ray Fluorescence
**Zr** Zirconium
**δDwax** Delta deuterium wax

**θ** Concavity
**µS** Microsiemens
**χ** Chi index

# 1. Introduction

The environment is made up of a number of components in dynamic interaction. Abiotic (physical and chemical factors) and biotic (living organisms) components in a specific environment are interconnected. To understand these interactions, the environment is usually analyzed by isolating its components into small pieces that are “easy to handle” (White et al., 1998). This reductionism allows seeing which are the components constituting the environment and how they work in the medium, thereby constituting environmental systems (White et al., 1998; Deaton and Winebrake, 1999).

Environmental systems operate across different spatiotemporal scales, ranging from fundamental levels to specific phenomena (White et al., 1998). They exchange matter and energy with the surroundings, constituting open systems, governed by thermodynamics laws. They also experience changes of state through processes. If the processes guide the system to a new state without returning to the initial state, they are considered lineal, whereas if the process returns the system to the initial state, they constitute cycles (Fig. 1.1).

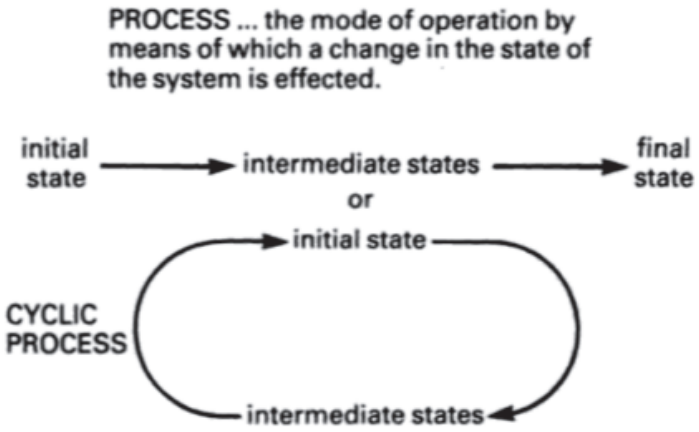


*Fig. 1.1: Cyclic and linear processes within environmental systems (from White et al., 1998).*

As open systems, environmental systems are controlled by the inputs, throughputs and outputs of energy and matter (White et al., 1998; Deaton and Winebrake, 1999). While no changes are observable at the macroscopic scale, ongoing processes at the microscopic scale move the environmental systems away from an ideal equilibrium state, which is essentially a statistical abstraction representing an average state. Therefore, environmental systems that maintain stability between their elements, attributes and relationships at the macroscopic scale are considered stationary or steady. The evolution of processes within environmental systems must imply steadiness to prevent the collapse, which is conditioned by feedback mechanisms among their constituents. Negative feedback mechanisms counteract initial actions, whereas positive feedback mechanisms amplify initial actions, leading to cumulative directional changes in the system, reinforcing a particular direction of change (Fig. 1.2).

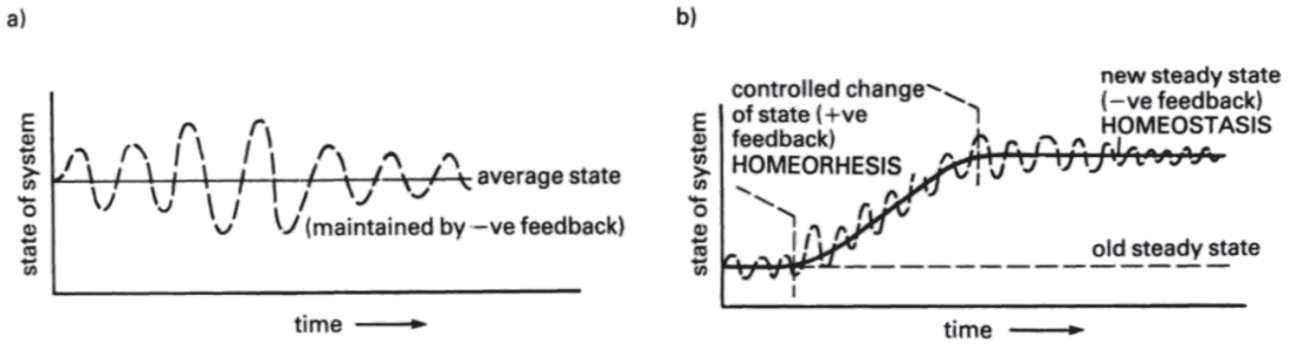


*Fig. 1.2: States of environmental systems (from White et al., 1998).*

The evolution of environmental systems is regulated by the establishment of various feedback positive and/or negative mechanisms resulting in feedback loops (Fig. 1.3). When these cycles are driven by negative feedback mechanisms, the stable state of the environmental system is maintained by self-regulation (homeostatic systems). On the contrary, when positive feedback mechanisms dominate, the system increases in the order and complexity over time (homeorhetic systems). Positive feedback mechanisms can induce a new stable state different from the original causing system instability if uncontrolled. They can also generate abrupt changes and signal amplification in some systems. However, generally, positive feedback is considered less favourable than negative feedback in terms of stability and system control (Deaton and Winebrake, 1999).

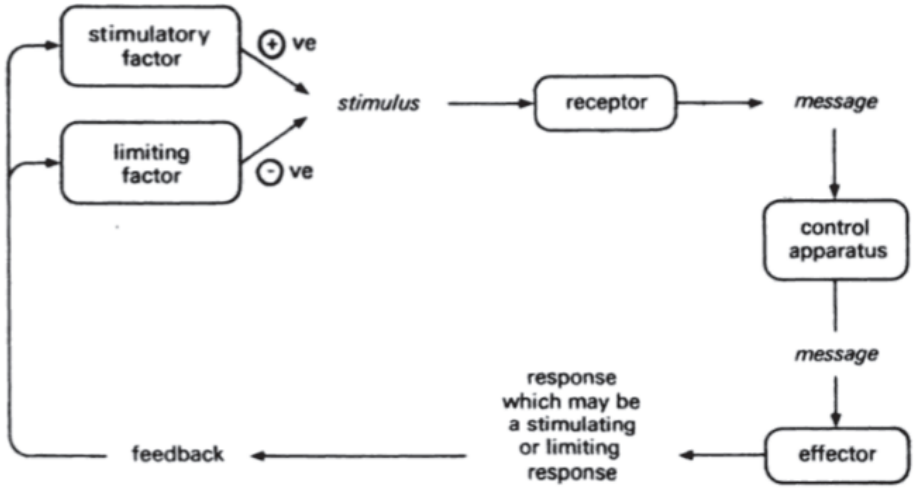


*Fig. 1.3: Feedback loops established within environmental systems (from White et al., 1998).*

Models are used as representations of reality to predict the behaviour of the environmental system (Deaton and Winebrake, 1999; White et al., 1998). Usually models are homomorphic, meaning they are imperfect representations of reality rather than reality itself. This is partly due to the scale of discrimination of compartments within. Egler (1964) called compartment models to homomorphic models whose function can be evaluated without specifying their contents. Models can be hardware, mathematical or conceptual (Fig. 1.4).

In particular, conceptual model construction involves delineating compartments, defining boundaries, elements, attributes, and structural relationships. These morphological models, which can vary in sophistication, commonly employ statistical or mathematical expressions to describe relationships between system variables. Functional linkages between compartments facilitate system operation, emphasizing flux pathways of matter and energy transfer, store residence times, and transfer regulation variables.

Some compartments serve as subsystems, interconnected to form cascades, representing the progression of matter and energy through the system. These cascading models are structural and they prioritize functional structure. To depict system dynamics, models must incorporate processes—mechanisms driving matter and energy transformation and state changes, even when maintaining a steady state.

Combining process modelling with system response yields higher-level process-response models, integrating morphological and cascade models. Pertinent variables regulate processes, inherently involving energy (and matter in open systems) transformation and transfer, elucidating system dynamics and functionality.

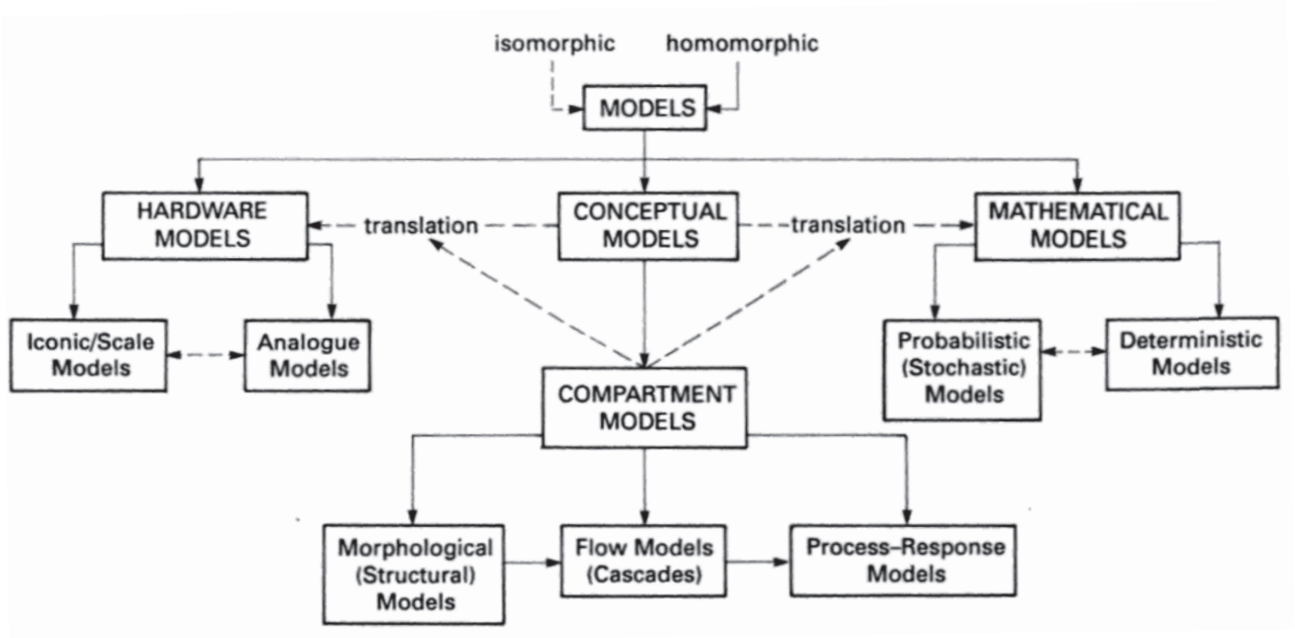


*Fig. 1.4: Kind of models (from white et al., 1998).*

Environmental systems comprise a wide range of ecosystems, such as forests, oceans, deserts, urban environments, lakes, the atmosphere and the complete planet. These systems perform through interconnected processes like energy flow, nutrient cycling, species interactions, and the water cycle. Understanding these mechanisms is essential for effective resource management and conservation. Additionally, it is crucial for urgently addressing current global challenges as climate change, biodiversity decline, and soil degradation.

## 1.1 The climate system

Climate is the long-term statistical representation of weather patterns, including variables like temperature, precipitation, and wind over a region for a certain time period (Le Treut et al., 2007). Unlike weather, which focuses on short-term atmospheric conditions (Gutro, 2005), climate analysis typically spans 30 years (Le Treut et al., 2007), although climatologists may extend their analysis to include broader time frames. Understanding climate dynamics involves the entire climate system, comprising the atmosphere, hydrosphere, cryosphere, pedosphere, and biosphere, along with their interactions and energy exchanges (Goosse et al., 2010; Siedler et al., 2013). This system evolves over time due to internal variability and external forcings like volcanic and solar activity and human actions (Le Treut et al., 2007; Siedler et al., 2013) (Fig. 1.5).

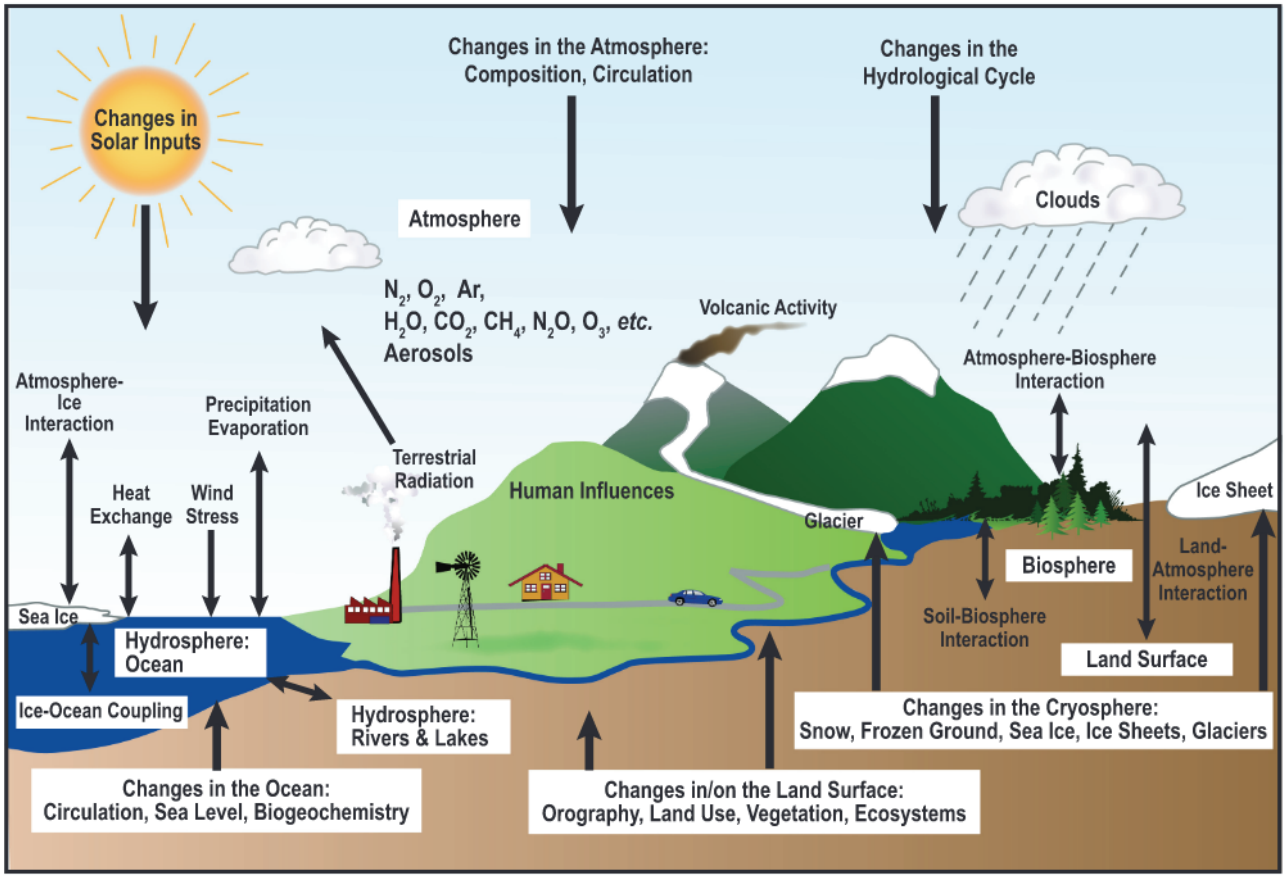


*Fig. 1.5: Schematic view of the components that compose the climatic system, their processes and interactions (from LeTreut, 2007).*

Hence, the significance of climate goes beyond its immediate effects on weather; it profoundly shapes human civilization and development (Huntington, 1922; Fagan, 2009). Despite technological advancements, human societies remain vulnerable to climate variability and change (Hartmann, 2015). Understanding past, present, and future climate trends is essential for both human progress and environmental conservation.

### 1.1.1. Modes of climate variability

A significant portion of climate variability adheres to recurrent patterns, often termed modes of climate variability (Stephenson et al., 2004). Climate modes are typically identified using statistical analyses of observational and model data, giving distinct spatial patterns and associated time series (Christensen et al., 2013). Empirical orthogonal function analysis is the most widely used method for calculating climate indices, enabling dimensionality reduction and pattern extraction, although it may suffer from issues such as bias in variance (Hannachi et al., 2007; Beguería et al., 2016). Alternatively, traditional station-based indices, derived from fixed meteorological stations, provide continuous time series extending back centuries, but they are limited in representing the centers of action of some modes (Comas-Bru and Hernández, 2018; Cropper et al., 2015; Hurrell, 1995; Jones et al., 1997; Vinther et al., 2003a; Visbeck, 2009). Consequently, modes of variability are often defined using gridded data to overcome these limitations (Folland et al., 2009; Moore et al., 2013; Roundy, 2014).

The importance of the study and reconstruct over time prominent modes like El Niño–Southern Oscillation (ENSO), North Atlantic Oscillation (NAO), Pacific Decadal Variability (PDV), Atlantic Multidecadal Variability (AMV), Northern and Southern Annular Modes (NAM and SAM), and the

Indian Ocean Dipole (IOD) is that they significantly impact large geographical areas (Fig. 1.6). These modes are often associated with severe climate events (Benito et al., 2015; Cook et al., 2015; Ionita et al., 2012), affecting socio-economic sectors like agriculture, water resources, and economies. They also have cascading effects on air quality, fire risk, energy availability, and human health (Bastos et al., 2016; Jerez et al., 2013; Zubiate et al., 2017). Besides, as environmental subsystems, disturbances of these modes may trigger a set of chain-reactions known as climate cascading, compromising the steady state of the climatic system, thereby catalyzing global changes (Lawrence et al., 2020). However, instrumental measurements of climatic variables, available for only a couple of centuries at best, limit their study and understanding (Casty et al., 2005; Jones, 2001; Luterbacher et al., 1999, 2001, 2002, 2016; Parker et al., 2007, 1992; Prohom et al., 2016).

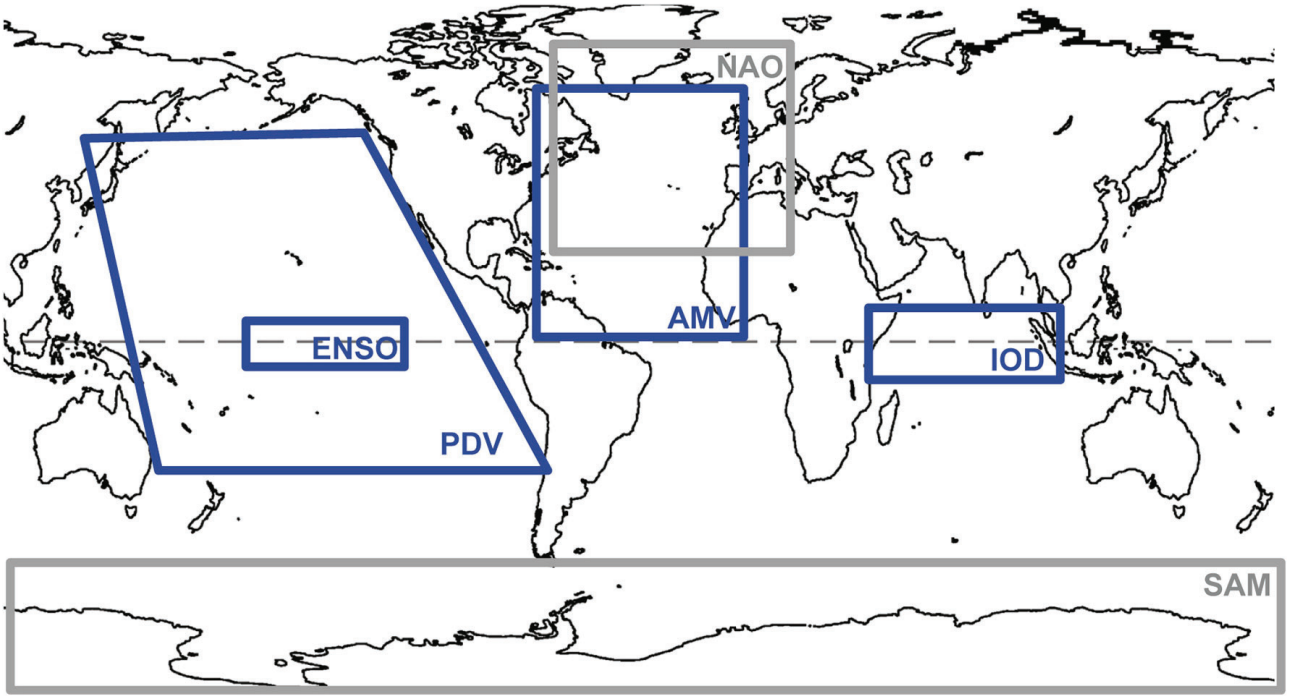


*Fig. 1.6: Some of the most prominent modes of climatic variability. Grey and blue colors correspond to atmospheric and oceanic modes, respectively (from Hernandez et al. 2020).*

To address limitations in directly measuring climate modes of variability, indirect climate indicators from natural archives (otherwise called proxy-based records) are crucial (Gornitz, 2009; Marcott et al., 2013; Neukom et al., 2019). These proxy-based records, responding to environmental factors like temperature and precipitation, indirectly link to modes of variability through their response to atmospheric and oceanic circulation (Bradley, 2015; Jones et al., 2009; Zorita and Gonzalez-Rouco, 2002). Studies reconstructing modes of climate variability across different timescales using different proxy-based records such as historical documents and natural archives reveal spatio-temporal patterns, impacts, interactions, and links to external forcings, particularly evident for the Holocene in general and the last millennium in particular (Ivanochko et al., 2008; Koutavas and Joanides, 2012; Dätwyler et al., 2018; Mann et al., 2009; Ortega et al., 2015; Wang et al., 2017). Limitations like chronological uncertainties associated with absolute radiometric dating of these proxy-based records and oversimplification between the relationship of these proxy-based records and a given mode of climate variability challenge these reconstructions (Evans et al., 2013; Raible et al., 2014).

### 1.1.2. Past climates

The Earth's climate exhibits variability across various timescales, from millions of years to multi years, influenced by both external forcings (e.g., tectonic plates, solar activity, Earth orbital

parameters, volcanism) and internal variability within the climate system (e.g., Earth system feedbacks; Fig. 1.2) (Jones and Mann, 2004; Mann, 2007). Enhancing our ability to predict future climate changes requires a thorough comprehension of the dynamics of the climate system (Bradley, 2015). This understanding relies on documenting and elucidating past variations, achieved through the study of natural archives such as ice cores, marine and lacustrine sediments, cave deposits, tree rings, and corals (Juggins and Birks, 2012; Bradley, 2015).

Natural archives contain proxy-based records that act as indirect indicators of past environmental conditions, accumulating and preserving information over time (Smol, 2008). For example, ice cores provide records of various climate parameters, including precipitation, temperature, atmospheric composition, and solar activity, analyzed through stable isotopes (Dansgaard et al., 1993; Grootes and Stuiver, 1997; Jouzel et al., 2007). Marine sediment records, composed of a mix of silts, clays, and remains from calcareous and siliceous organisms, offer insights into temperature, sea level variations, and past atmospheric compositions (Ravelo and Hillaire-Marcel, 2007). Lacustrine records, using proxies like varve thickness, inorganic and organic chemical biomarkers, physical proxies, and biological indicators, are also widely employed for paleoclimate reconstructions (Ojala and Alenius, 2005; Bakke et al., 2010; Birks, 2003). Speleothems offer high-resolution records of environmental changes through stable isotopes of oxygen and carbon (Martín-Chivelet et al., 2011; Medina-Elizalde et al., 2010), while tree-ring widths offer information on temperature, droughts, and climate modes (Cook et al., 2002, 2007).

Analyzing multiple proxy-based records from the same natural archive is advantageous because it offers a more comprehensive view of the spatial and temporal evolution of a given ecosystem, providing a broader perspective than single proxy data alone—a methodology known as multiproxy study (Cuenca-Cambronero et al., 2022). However, challenges persist in validating the often simplistic approach relating the proxy-based record with a given meteorological variable and addressing uncertainties mainly associated with the absolute age determination of the sediments (Piovano et al., 2014). Proxy data represent estimations rather than direct measurements, and using multiple proxy sources might introduce statistical distortions to the reconstructed variables.

The paleoclimate record illustrates with a high degree of accuracy Earth's dynamic climate history over the past ca. 540 million years, from the onset of the Cambrian to the warm mid-Cretaceous era (92 million years ago) to the recent cold ice ages, including the Last Glacial Maximum (21,000 years ago), reflecting remarkable climate variability (Lauretano et al., 2018; Hodell et al., 2008; Scotese et al., 2021) (Fig. 1.7). These changes featured brief hyperthermal and cold events at different time scales, influenced by fluctuations in atmospheric $CO_2$ concentrations (Walker et al., 1981). Therefore, studying past climates offers valuable insights into climate processes across different $CO_2$ concentrations, serving as benchmarks for future climate prediction under various emissions scenarios (Henehan et al., 2019). Ancient climates, although not perfect analogs for future states, can be employed as essential targets for evaluating the reliability of climate models and understanding critical climate feedbacks and sensitivities (Goddéris et al., 2014).

Climate forecast suggest profound alterations in regional and seasonal rainfall and temperature patterns, with significant implications for human society (McMichael et al., 2006; Wilby, 2007). These changes have the potential to trigger biogeochemical feedbacks, which may either exacerbate or mitigate initial radiative forcing effects (Arneth et al., 2010). While current global climate models exhibit discrepancies regarding the direction and magnitude of future regional rainfall changes (Knutti & Sedláček, 2013) all of them clearly suggest that by the end of this century temperature will significantly increase (IPCC, 2023). To improve predictions, it is crucial to distinguish internal climate system variability from externally forced changes, a task where paleoclimate data play a paramount role (Deser et al., 2012; PAGES Hydro2k Consortium, 2017).

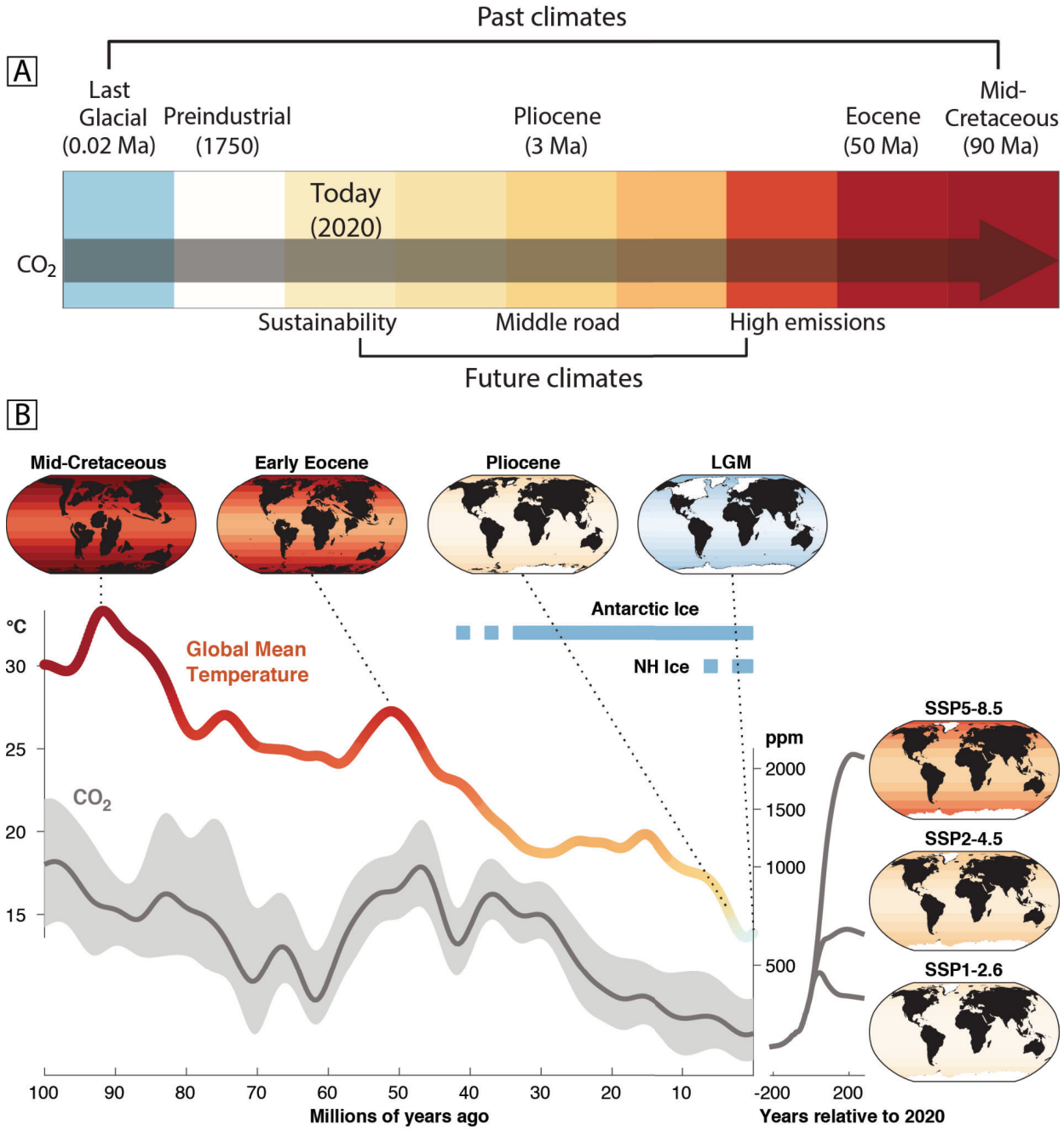


*Fig. 1.7: A) Understanding past climates is key for contextualizing future climate scenarios. Both past (top) and future (bottom) climates are depicted with colors reflecting their anticipated shifts in global mean annual surface temperature compared to preindustrial norms, spanning from cooler blues to warmer reds. The terms "Sustainability," "Middle road," and "High emissions" represent projected global temperature anomalies for the year 2300 under the Shared Socioeconomic Pathways (SSPs) SSP1-2.6, SSP2-4.5, and SSP5-8.5, respectively. Warmer climates in both historical and future contexts align with increased $CO_2$ levels, illustrated by directional arrows. Ma: millions of years ago. (modified from Tierney et al., 2020). B) Global mean surface temperature for the past 100 million years estimated from benthic $\delta^{18}O$ (Zachos et al. 2001; Friedrich et al. 2012). $CO_2$ was mainly estimated from the multiproxy dataset compiled by Foster et al. (2017). The $CO_2$ error envelopes represent 1σ uncertainties. Note the logarithmic scale for $CO_2$. Gaussian smoothing was applied to both the temperature and $CO_2$ curves to emphasize long-term trends. Temperature colors are scaled relative to preindustrial conditions. The maps show simplified representations of surface temperature. Projected $CO_2$ concentrations are from the extended SSP scenarios (Meinshausen et al. 2020). Blue bars indicate when there are well-developed ice sheets (solid lines) and intermittent ice sheets (dashed lines), according to previous syntheses (Zachos et al. 2001). NH: Northern Hemisphere. Figure from Tierney et al. (2020).*

Comparisons between proxy-based data and models aid in understanding hydroclimate variability, particularly concerning wet-dry patterns (Burls & Fedorov, 2017). While future models predict subtropical drying, paleoclimate intervals suggest alternative patterns, with wetter conditions in the subtropics and high latitudes (Burls & Fedorov, 2017). This divergence emphasizes the importance of paleoclimates in constraining future projections, especially for arid regions (DiNezio et al., 2018). In conclusion, these advancements are revolutionizing paleoclimate research, enabling the explicit use of paleoclimate data to assess and refine climate models (Tierney et al., 2019). They allow for the inference of key climatic processes and the evaluation of models across various time periods, addressing longstanding challenges in paleoclimate research.

### 1.1.3. Lakes as sentinels of climate change

Lakes serve as indicators of climate change by reflecting its influence across broader lake catchments (Williamson et al., 2009; Adrian et al., 2009). Sensitivity to climate makes lakes responsive in physical, chemical, and biological aspects (ACIA 2004; Rosenzweig et al. 2007), highlighting them as potential climate change indicators (Carpenter et al. 2007; Pham et al. 2008; Williamson et al. 2008). Climate change, recognized as a significant threat to global ecosystems, poses challenges for monitoring and understanding its effects due to ecosystem variability and landscape diversity (ACIA 2004; Rosenzweig et al. 2007). Early lake studies have revealed climate change effects on ecosystem structure, function and services (Schindler et al. 1996a; Magnuson et al. 2000; Verburg et al. 2003; O'Reilly et al. 2003). Observable signs of climate change in lakes include water level fluctuations and shifts in ice formation timing (Magnuson et al. 2000; Williamson et al. 2009).

Paleolimnological records offer insights into less visible climate-related changes (Smol 2009; Leavitt et al. 2009), aiding our understanding and prediction of climate effects. Lakes serve as sentinels by providing measurable indicators of climate change, either directly or indirectly through catchment influence, such as water temperature and plankton composition (Schindler et al. 1996a; Magnuson et al. 2000; Verburg et al. 2003). However, the use of lakes as sentinels presents challenges due to their complexity, internal feedbacks (Fig. 1.2), and varying catchment influences (Schindler et al. 1996a; Magnuson et al. 2000; Verburg et al. 2003). Limnological variables serve as climate change indicators, including physical, chemical, and biological properties, reflecting direct or indirect climate effects on lakes (ACIA 2004; Rosenzweig et al. 2007). The complexity and applicability of these variables change across different lake types and climate regions. Nevertheless, the wide range in lake morphology, catchment characteristics, and geographic locations suggests caution in making generalized statements about the ability of lakes to capture the effects of the current, rapidly changing climate (Adrian et al., 2009).

The processes transferring the climate signal from the atmosphere to lake sediments are complex, establishing intricate relationships within basin-lake systems (lake, drainage, soils, geology, vegetation, etc.). These constituents continuously interact and respond to regional environmental changes through different mechanisms (Cohen, 2003), complicating straightforward environmental reconstructions (Giralt et al., 2011). Some discrepancies in analyzed climate signals may be related to an incomplete understanding of these processes (Hernández et al., 2015). Previous studies have employed multi-proxy analyses of lake sediments to reconstruct paleoclimate, revealing the complex interaction among climatic and non-climatic factors shaping landscape dynamics. Non-climatic factors, including tectonic and human impacts, have been explored alongside long-term factors such as variable geomorphic configurations between lake basins (e.g., Wünnemann et al., 2015, 2006, Lu et al., 2018; Rubensdotter and Rosqvist, 2003; Sánchez-López et al., 2015). These analyses underscore the spatially and temporally variable responses of different magnitudes and frequencies. However, the implications of these findings have not consistently been incorporated, potentially contributing to the observed heterogeneity and partial incomparability of reported high-resolution

paleoclimate records (Dietze et al., 2010). Some discrepancies may be attributed to an incomplete understanding of the processes transferring the climate signal from the atmosphere to the natural archive (Hernández et al., 2015).

## 1.2. Lake basins

The presence of a lake on Earth requires two essential components: a topographically enclosed depression and water. Historically, discussions surrounding lakes have focused on their origin, emphasizing the formation of the depression. However, it is crucial to recognize that the depression itself has a distinct history, partly independent of the lake it eventually contains, and this history interacts with the water body development (Cohen, 2003). Freshwater ecosystems are categorized into three main types: Lentic, which encompasses standing water bodies like lakes and ponds; Lotic, referring to running water bodies such as springs, streams, and rivers; and Wetlands, which consist of marshes and swamps, characterized by fluctuating water levels both seasonally and annually. The dynamic interplay between a lake and its underlying substrate throughout the lake history advocates for the concept of lake basin evolution over the static notion of lake origin. Basin evolution encompasses various aspects, including the three-dimensional geometry of underlying lake deposits, sediment accumulation rates, and the likely history of the lake (e.g., Hernández et al. 2023). The importance of lake basin evolution lies in its ability to influence both the quality and characteristics of the responses provided. Different types of lakes are inclined to address specific paleolimnological questions, with some preserving records for millions of years, while others offer high-resolution records for shorter durations (Camuera et al., 2021; Leroy et al., 2023; Lan et al., 2020; Ruiz-Fernández et al., 2022). A comprehensive understanding of lake basin evolution is essential in designing paleolimnological studies, as the quality of paleolimnological records directly depends on the mechanisms of basin evolution (Cohen, 2003, Jones et al., 2022).

Efforts to classify lakes encounter challenges due to the intricate evolution of lake basins (Hutchinson, 1957; Cohen, 2003). The evolution of lake basins is deduced by analyzing geomorphic and sedimentological evidence. For lakes with fresh geomorphic features, the shape and lithology of lake outlets provide insights into their formation (Leverington & Teller, 2003). The formation of lakes is primarily attributed to glacial, tectonic, or fluvial processes (Hutchinson, 1957; Brosius et al., 2021). Features such as moraines or basalt flows can indicate an origin by blocking pre-existing drainage systems. Seismic reflection data offers additional clues by revealing the shape of bedrock surfaces beneath lake deposits (De Batist et al., 2002; Sabatier et al., 2022). Furthermore, seismic stratigraphy interprets glacial and post-glacial sedimentation, lake-level fluctuations, and neotectonic impacts in lake basins (Niessen et al., 1999; Colman et al., 2002; D'Agostino et al., 2002; Brooks et al., 2005; Anselmetti et al., 2006; Colman, 2006; Hofmann et al., 2006; Beres et al., 2008; Wagner et al., 2008). However, uncertainty arises when the constructional feature blocking the outlet is higher than the ultimate spillway, making the timing of dam construction and spillway incision uncertain. The most challenging origins to interpret occur when the geomorphology of the basin is no longer discernible. In pre-Pleistocene lake deposits, tectonic influences may be evident through the association of lake deposits with structural basins. However, secondary features like ice dams, which may not have left a permanent signal, could have controlled the spillway elevation of a paleolake (Cohen, 2003).

After their formation, the ontogeny of lakes involves a gradual shallowing and reduction in area due to sedimentation. However, erosive events, particularly in shallow lakes, may deepen basins, influenced by factors like deflation or wind-blown material accumulation from emergent vegetation. Sedimentation rates vary widely, ranging from 1 to 5 mm annually, with oligotrophic lakes sometimes experiencing rates below 1 mm per year (Kemp et al., 1976, 1978). Lakes with depths between 10 and 500 m are expected to have lifespans between $10^4$ and $10^5$ years, with deeper lakes having

longer lifespans (De Batist et al., 2002; Ulfers et al., 2022). Transient lakes formed by glaciers during the late Pleistocene fill rapidly within one to a few thousand years (e.g., Hernández et al. 2023). Changes in shoreline configuration are driven by factors such as delta formation, talus fan growth, and sand dune movement, which can be influenced by natural processes or human activities. Shoreline morphologies can be significantly altered by sand dunes, especially in arid or coastal zones. Volcanic activity, glacier retreat, and major floods also contribute to shoreline modifications, whereas lakes can undergo spatial displacement over long periods due to volcanic and tectonic events. This illustrates the dynamic nature of lakes and their susceptibility to environmental changes (O'Sullivan and Reynolds, 2005).

Current lake distribution reflects latitudinal belts influenced by Pleistocene glaciation and present-day climatic conditions (Talbot and Kelts, 1989; Foster, 2010; Brosius et al., 2021). Mid-latitudes, roughly between 40–60ºN and 40–50ºS, host a concentration of lakes due to abundant precipitation, low evapotranspiration rates, and remnants of glacial activity (Talbot and Kelts, 1989; Meek, 1999; Reheis and Redwine, 2008; Verpoorter et al., 2014). Equatorial regions, with positive precipitation balance and absence of Pleistocene glaciation, feature lakes formed mainly by tectonic and fluvial processes (Talbot and Kelts, 1989) (Fig. 1.8). In contrast, subtropical zones, characterized by minimal precipitation and high evapotranspiration rates, have fewer closed-basin lakes mainly of tectonic origin (Street-Perrott and Roberts, 1983; Gasse, 1990; Korup, 2002; Dunning et al., 2006). Despite their scarcity, these lakes are crucial for paleolimnological studies due to their sensitivity to climate changes (Street-Perrott and Roberts, 1983; Gasse, 1990) (Fig. 1.8). Regional factors such as orographic effects and atmospheric circulation patterns also influence lake formation likelihood (Chenggao and Renaut, 1994). Variations in seasonal insolation impact areas with favourable precipitation-to-evaporation balance for lake formation (Cohen, 2003). Evidence from the Sahara Desert suggests a history of abundant large lakes during the late Pleistocene and early Holocene, indicating dynamic shifts in lake distribution under changing climate conditions (Street-Perrott and Roberts, 1983; Gasse et al., 1990; Fontes and Gasse, 1991; Drake et al., 2022; Li et al., 2023).

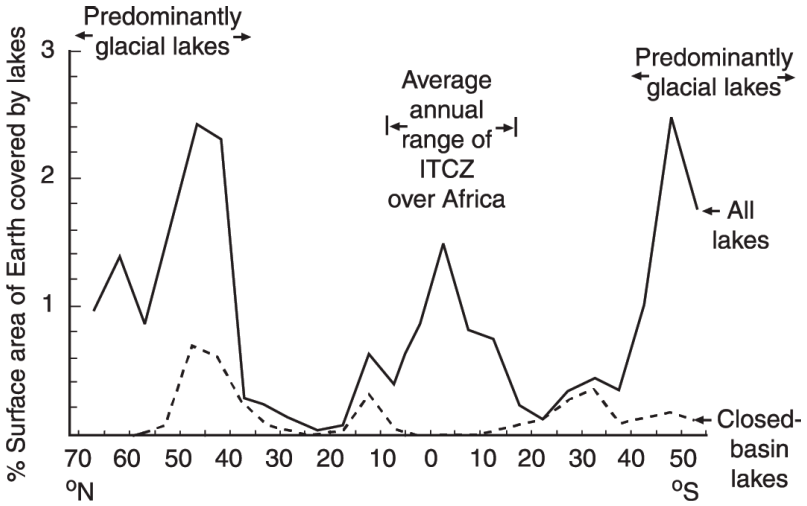


*Fig. 1.8: Modern lakes latitudinal distribution. ITCZ: intertropical convergence zone. Modified from Cohen (2003).*

Numerous palaeolimnological studies have revealed how sediment properties reflect catchment processes (Coulthard et al., 2005; Dietze et al., 2010; Zhang et al., 2012; Ghimire and Higaki, 2015). Recently, there has been a focus on expanding contemporary erosional studies through sediment column analysis. Figure 1.9 illustrates a lake-catchment system, highlighting subsystems controlling material influx and sediment deposition. The cascading nature of the system and varied sediment sources present challenges in isolating specific processes from sediment analysis alone (Coulthard et al., 2005; Dietze et al., 2010; Zhang et al., 2012; Ghimire and Higaki, 2015). Additionally,

interpreting deposited material quantities in terms of catchment-erosion relationships is complex due to varying transporting energies and temporal dynamics (Dingle et al., 2018; Bhattacharjee et al., 2022). Recent studies have provided reliable data on erosion, sediment yields, and sources, quantifying sediment flows over time (Wünnemann et al., 2015). Long-term erosion records are paramount for defining erosion rates, understanding responses to environmental changes, reconstructing sediment budgets, identifying erosion processes, and testing erosional models across different timescales (Fig. 1.10) (Dearing, 1991; Amasi et al., 2021).

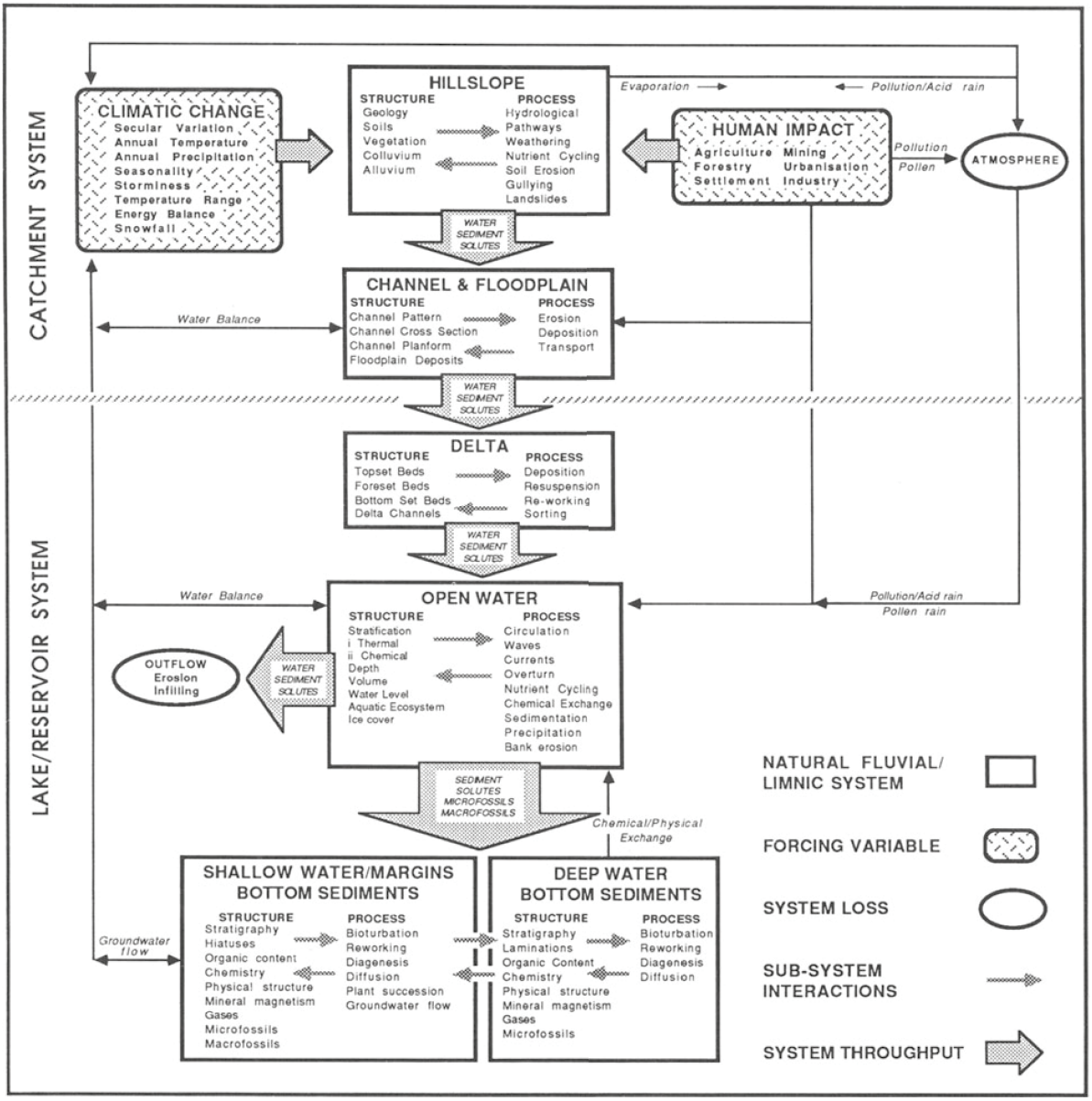


*Fig. 1.9: The lake-catchment system (modified from Dearing 1991), showing the range of environmental processes and factors which control the movements of materials between sub-systems.*

Hence, integrating spatial and temporal paleoenvironmental data, including sediment cascade dynamics, is crucial for understanding terrestrial and lacustrine archives. Lake basin morphology, shaped primarily by non-climatic factors like tectonics, reflects both terrestrial landscape dynamics and lacustrine processes over extended periods (Fig. 1.10) (Dietze et al., 2010). Basin morphology studies unravel internal lake system dynamics and aid in assessing climatic sensitivity when combined with seismic stratigraphy.

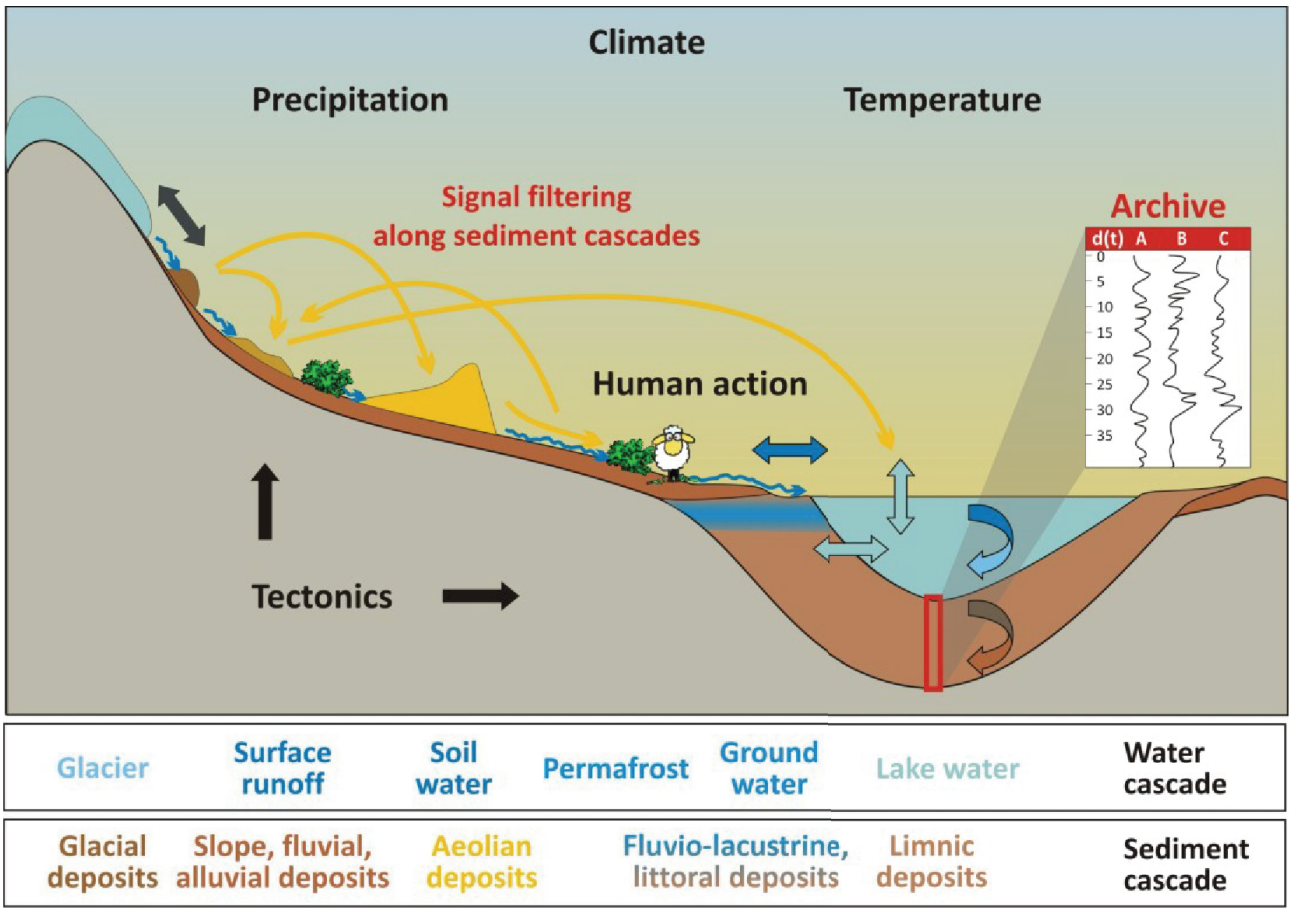


*Fig. 1.10: Sediment and water pathways along a sediment cascade in a lake-catchment system, reflecting key environmental drivers within a sediment archive (figure from Dietze, 2012).*

### 1.2.1. Catchments and sediment cascading

In a lake-catchment system, materials originating from both external forcings such as melting and rainfall and internal ones like tectonic activity in the catchment can either be transported to the lake or deposited within the catchment (Fig. 1.10). The ratio of lake size to catchment size influences the rate of sedimentation per unit area in a lake, assuming other conditions remain relatively stable (Singh et al., 2023). The grain size of transported materials correlates with flow velocity; coarse particles tend to be deposited near river mouths, while finer particles carried by lake currents settle farther onto the lake bottom (Ochiai and Kashiwaya, 2003). Consequently, a given grain size is also affected by depositional sites which, in turn, are influenced by changes in water level (Fig. 1.11). Significant changes in the exposed floor zone during low-water periods greatly affect erosion and sedimentation processes. The exposed zone is susceptible to erosion from external forcings such as rainfall and wind, particularly influenced by climatic conditions, with a negative correlation to temperature. Therefore, climatic conditions may intensify erosion processes in this context (Kashiwaya, 2017).

Understanding the evolution of drainage systems in catchments involves two main aspects: (1) the fractal nature of these systems, and (2) their coherence across different zones, known as "ergodic" reasoning. The fractal nature is evident in the self-similarity observed between small-scale and large-scale systems, emphasizing cyclical patterns crucial for structural development. "Ergodic" reasoning allows arranging a chronological sequence of drainage system development by comparing systems in various stages under similar environmental conditions and structures (Paine, 1985; Yatsu, 1986). Quantifying and relating the major processes responsible for sediment generation and transport is challenging due to their slow and highly variable nature in space and time. Short-term monitoring

data are difficult to extrapolate to compute average values for large areas (Dietrich and Dunne, 1978).

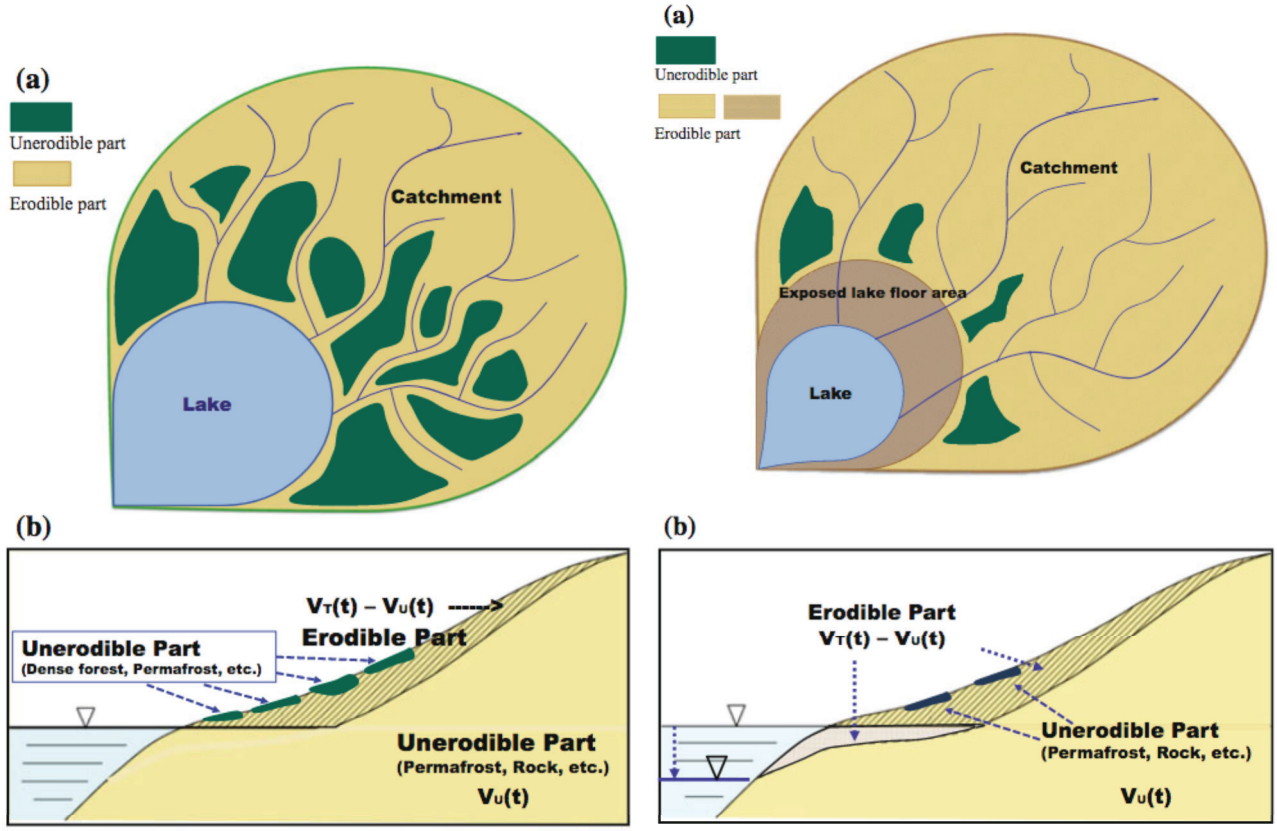


*Fig. 1.11: Left side: a) Plane figure and b) cross section of an ideal lake-catchment system depicting the lake (light blue), erodible part (hatched ocher), unerodible part (green and ocher), and river (dark blue). Right side: a) Plane figure and b) cross section of an ideal lake-catchment system with large change in water level. In this scenario, the erodible part is indicated by hatched ocher and hatched brown. Figure adapted from Kashiwaya et al. (2017).*

Finally, identifying sedimentation areas in small lakes is challenging, especially when sediment limits change due to water-level fluctuations (Dearing, 1991). Assessing catchment-derived sediment yield requires subtracting components like lake margin erosion, the atmosphere, and autochthonous production. Ergodic reconstructions of erosional processes may oversimplify transition phases and, consequently, studies have tried to link lake sediment data to contemporary erosion data using 'fingerprinting' techniques.

#### 1.2.1.1. Active landscapes

Active landscapes evolve through the interaction of rock uplift and erosion rates, influencing relief and hillslope steepness (Whipple, 2004; Finnegan et al., 2008). River incision into bedrock responds to uplift, whereas sediment dynamics are influenced by adjacent sediment sources (Korup, 2005). Sediment reservoir formation and failure significantly impact sediment transport rates and landscape dynamics (Davies and Korup, 2010).

In active mountain ranges, uplifted rocks undergo fracturing and disaggregation before erosion and transport (Davies and Korup, 2010). This process involves physical, chemical, and biological weathering, as well as mechanical fracturing from tectonic stresses (Molnar et al., 2007). Various factors contribute to rock fracturing, including earthquake shaking, temperature changes, freeze-thaw cycles, plant root growth, and chemical activity (Taylor & Eggleton, 2001). Stress corrosion also fragments rock masses through the gradual growth of microcracks at low stress levels (Molnar et al., 2007).

Sediment transport in mountainous regions involves gravity-driven movement facilitated by water, ice, and wind. Frictional resistance must be overcome for sediment to move, with slopes of approximately 35 degrees (McSaveney & Davies, 2007), although some large landslides can begin at lower angles and travel extraordinary distances. Water presence reduces frictional resistance, particularly through fluctuating pore-water pressures (Iverson & Denlinger, 2001). Fluid erosion of sediment is modeled as a function of excess shear stress, influenced by factors like slope gradient and fluid flux (Whipple, 2004; Davies & McSaveney, 2008). Sediment transport rates vary widely in mountains and are challenging to measure (Kirchner et al., 2001). Debris flows move rapidly on low slopes and can involve water-saturated debris with volumes (Plafker & Ericksen, 1978; Haeberli et al., 2004). Catastrophic events like natural dam failures can produce significant sediment pulses (Korup & Tweed, 2007; Hopfenblatt et al., 2021). Various processes like landslides, glaciers, and debris flows transport large blocks, while rivers are limited to gravel-sized material. Finally, wind transport is limited to smaller grain sizes.

Sediment storages, including moraine-dammed lakes, alluvial fans, and landslide deposits, significantly influence mountain river dynamics (Davies and Korup, 2010). Despite their importance, systematic quantification of sediment storage in large catchments remains lacking (Hinderer, 2001; Wasson, 2003). Methodological challenges hinder accurate volumetric estimates (Hoffmann & Schrott, 2002; Schrott et al., 2003). Floodplains and braidplains form due to river bed aggradation, with floodplains experiencing periodic inundation (Reinfelds & Nanson, 1993). Landslide deposits accumulate in various locations, affecting sediment delivery ratios and drainage system organization (Korup & Tweed, 2007). Moraines, glacial deposits, and alluvial fans play crucial roles in shaping mountain landscapes and influencing trunk-river dynamics. Deltas act as significant sediment traps, while lakes become rapidly infilled in tectonically active mountain belts. Sediment storages in mountain valleys influence sediment transfer rates and valley morphology (Clague & Evans, 2000), with storage failures leading to sudden sediment inputs downstream (Korup & Tweed, 2007). Despite their transient nature, these dynamics complicate long-term mountain belt evolution assumptions (Davies & Korup, 2007; Korup & Tweed, 2007).

#### 1.2.1.2. Weathering

Weathering is the initial process destabilizing surface layers (Carson & Kirkby, 1972; Perri, 2020). It is classified into mechanical, biological, and chemical processes, shaping landforms and landscapes (Fig. 1.12). Geochemistry, biochemistry, and laboratory studies have enriched our understanding of weathering processes (Hall et al., 2012).

Denudation, volcanism, and tectonics are interconnected processes shaping landscapes of Earth through weathering. Where climate is not the primary factor, the use of "rock decay" is suggested (Bruthans et al., 2018; Migoń, 2021). The relationship between weathering and denudation is complex, with denudation constrained by weathering ("weathering-limited denudation") or hindered by the transport of weathering-produced debris ("transport-limited denudation"). Thus, understanding weathering-limited and transport-limited systems enhances comprehension of weathering processes within the broader context of denudation (Carson & Kirkby, 1972).

Sediment cascades operate across various temporal scales, from individual storm events to geological epochs. Changes in vegetation cover and land management can impact geomorphological processes with delayed effects, making erosion and sediment yield predictions uncertain (Trimble, 1999; East et al., 2022). Trimble and Lund (1982) proposed a hysteresis model to explain lag effects in upland erosion due to land use changes, with further delays observed in floodplain-channel systems. Catchment erosion rates vary spatially due to factors such as soil erodibility and land management practices (Burt, 1989). Critical source areas, where runoff and erosion concentrate, are crucial (Heathwaite et al., 2000). Despite, detailed sediment budgets for

catchments remain limited, they are crucial for informing land and water management policies. This knowledge also aids in understanding large-scale landform development and smaller-scale processes like valley-side mass movements or terrace formation (Trimble, 1999).

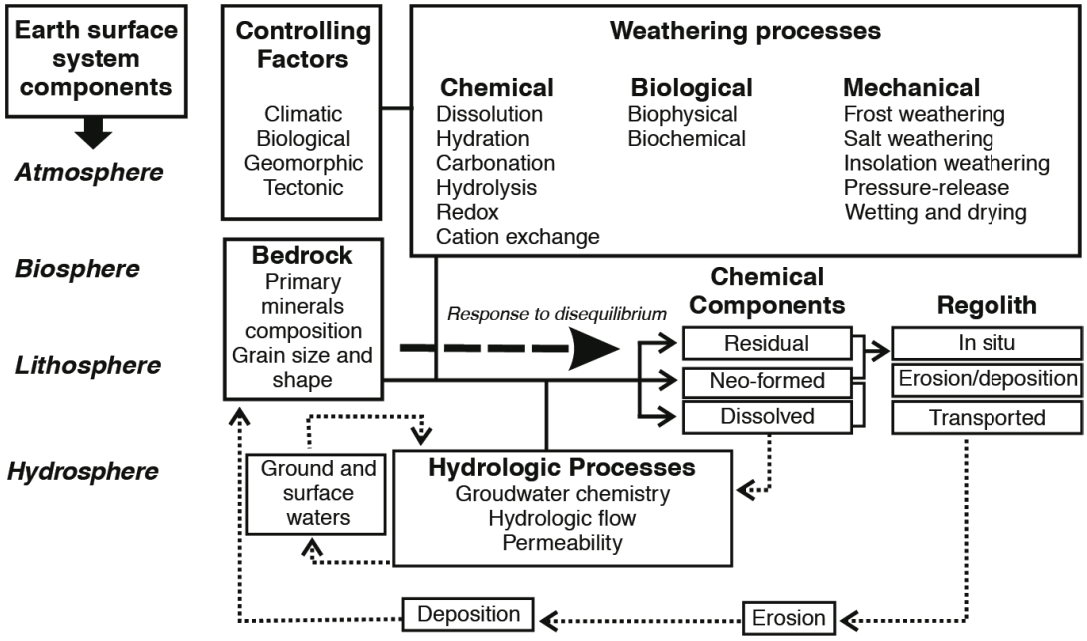


*Fig. 1.12: The foremost controls on weathering and the chemical composition of the regolith. Modified from McQueen (2009).*

### 1.2.1.3. Sediment sources

Streams in mountainous regions often originate on steep slopes characterized by shallow declivities or hollows (Fig. 1.13; Dietrich et al., 1986; Hack & Goodlett, 1960; Mani et al., 2023). These features collect water, forming seepage lines and springs, serving as starting points for surface drainage networks. Hollows also serve as deposition sites for soil, contributing to sediment transport downstream (Dietrich et al., 1986). Material mobilized from hillslopes can enter stream channels directly or move onto colluvial footslopes. Channels receiving direct sediment delivery from side slopes are termed "coupled" to hillslopes, while others are "buffered" or "uncoupled" (Fig. 1.14) Headward channels often experience direct sediment failure, evolving into debris flows, which are more like landslides than fluvial transport (Hungr et al., 2001). Debris flows are influenced by material characteristics and rainfall triggers, with varying flow speeds and volumes (Bovis and Jakob, 1999).

In montane channels, sediment transport operates under two regimes, primarily constrained by sediment supply. Steep channels rely on limited mobile material, preventing widespread export (Church, 2010). Debris flows stop where they can drain rapidly, influenced by debris texture and channel topography. Coarser materials halt on steeper gradients, while muddy slurries flow onto gentler slopes. Debris composition reflects source rocks (Fannin and Rollerson, 1993; Benda and Cundy, 1990), with confinement loss and flow path bends affecting stopping angles. Debris flow deposits are unsorted, containing boulders, cobbles, and finer soil, often with high organic content. During motion, large clasts and organic debris concentrate at the front, top, and sides, forming protective armour (Costa, 1984). Levees are left behind, leading to irregular mounded deposits near channels. Debris flows frequently deposit at steep tributary junctions, forming debris flow cones characterized by typical stopping angles.

Warburton (1992) proposed a three-phase model for bed material transport in steep channels, phases based on flow conditions and sediment mobilization. Phase 1 involves moderate flows where sand is primarily mobilized (Whiting et al., 1999), while Phase 2 at high flows entails the entrainment

of gravel (Wilcock and McArdell, 1993). Phase 3, rare but more frequent in steeper channels, involves the disruption of the bed structure, causing all sizes of material to move (cf. Batalla et al., 1999). The sequential mobilization establishes a correlation between flow and bed material transport, with sensitivity to flow changes near threshold conditions.

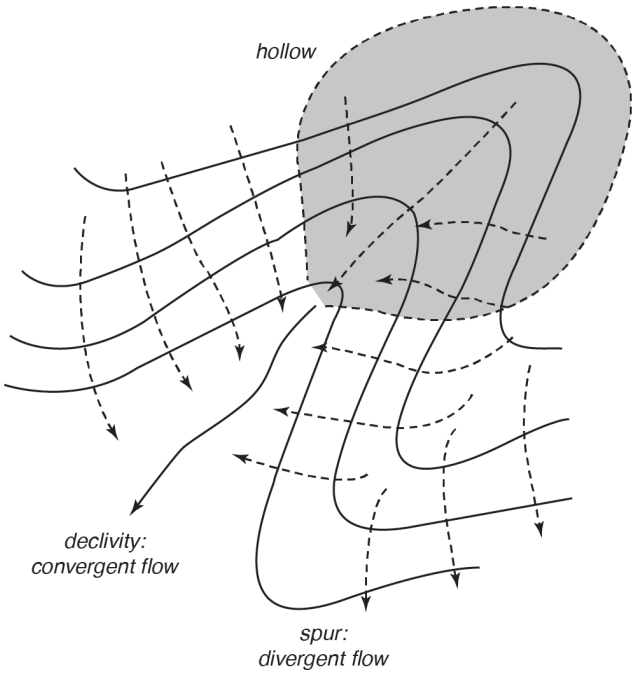


*Fig. 1.13: Drainage lines on a hillside slope. Note the convergence of flow into hollows (from Church, 2010).*

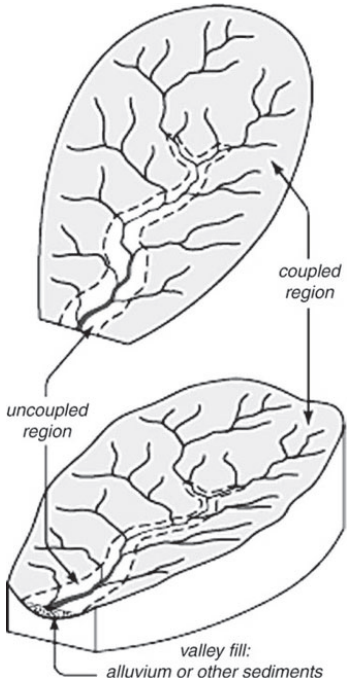


*Fig. 1.14: Sketch of a drainage basin depicting coupled and uncoupled sections (from Church, 2010).*

Wash material, consisting of sediment capable of travelling long distances in streams and not commonly found on the streambed, is typically composed of particles finer than 180 μm, with suspension velocity lower than entrainment velocity. Its occurrence depends on supply limitations, influenced by weather and geomorphological processes (Nistor and Church, 2005). Fine sediments in wash material originate from various sources such as mass wasting deposits, high stream banks, gully walls, temporary storage areas, and debris dams, with significant contributions from debris flow deposits and landslide scars (Beschta, 1981). Sediment delivery can be episodic, with high-magnitude, low-frequency events like debris flows causing sudden increases in sediment concentration, or part of the normal regime, with smaller, more frequent contributions from processes like dry ravel and surface wash (Nistor and Church, 2005).

In montane streams, forests contribute large organic debris such as limbs, roots, and whole trees exceeding 10 cm in diameter, significantly shaping channel morphology (Montgomery et al., 1995). This large wood debris plays a crucial role in sediment storage and transfer (Heede, 1972; Keller and Swanson, 1979). While smaller wood debris can be moved by high flows, debris flows can transport wood pieces of almost any size, leading to their accumulation into distinct jams along the channel, usually anchored by a stationary key piece.

#### 1.2.1.4. Steeplands

The term "steepland" lacks a universally accepted definition but it is usually defined as a terrain with hillslopes exceeding a gradient of 12% (approximately 7 degrees) and covered by shallow, immature soils supporting natural vegetation, forests, or pasture (Macklin et al., 2010). The depth and maturity of these soils are influenced by the frequency of mass movements, such as landslides triggered by

heavy rain or seismic activity, and the rate of recovery on scar surfaces (Dietrich et al., 1995; D'Odorico and Fagherazzi, 2003; Wakatsuki et al., 2005). Changes in sediment production and dispersal in steepland river systems during the Anthropocene are largely influenced by land cover (Kao and Liu, 2002; Kao and Milliman, 2008; Liu et al., 2008).

In regions like northern and southern California, as well as New Zealand, human activities such as timber harvesting, exotic grasslands, and deforestation have significantly increased erosion rates and sediment production in steepland river systems (Sommerfield and Wheatcroft, 2007; Kettner et al. 2007). Landslides, bank erosion, and lack of root reinforcement exacerbate natural instability, contributing to sediment loads. Reforestation efforts have shown promise in reducing sediment production, but challenges remain in areas susceptible to erosion (Marden et al., 2005). Steepland rivers play a vital role in transporting organic carbon to coastal oceans (Scott et al., 2006). Effective management strategies, including targeted restoration programs like erosion control treatments and reforestation, are crucial for mitigating sedimentation without resorting to controversial measures (Marden et al., 2005).

#### 1.2.1.5. Local buffers of the sediment cascade

The sediment pathway from its source to the sink is often described as a "jerky conveyor belt" due to frequent interruptions at different timescales, from small, transient deposition zones to larger, persistent landscape features (Ferguson, 1981). Sediment storage zones, such as debris cones and alluvial fans, occur at transitions in the sediment pathway, such as hillslopes-channel intersections or changes in valley-floor gradient, significantly impacting system dynamics (Harvey, 2010).

These zones affect sediment flux, responding to changes in flood power and sediment supply, reflecting critical stream power relationships. Alluvial fans, especially, are sensitive to stream power conditions. Excess power leads to sediment removal, increasing coupling through the system, while excess sediment supply results in deposition, reducing coupling (Fig. 1.15). These zones not only influence sediment flux but also preserve records of past critical power variations, providing insights into upstream sediment source area changes.

Alluvial fans and debris cones play crucial roles in paleoenvironmental reconstructions, especially in upland and mountain regions, offering insights into past environmental changes compared to downstream fluvial sites influenced by flood power variations.

1) Small-Scale, Ephemeral Gully-Mouth Debris-Flow Lobes form from sediment generated within gully systems during storms or other sediment-producing events. These flows may enter into streams directly or deposit as lobes at the base of the gully. Seasonal variations in sediment production and removal events, such as summer storms delivering sediment and late winter snowmelt floods flushing the system, result in cyclic sediment build-up and periodic removal. These features typically operate on timescales of decades or less.
2) Tributary-Junction Debris Cones, found at the base of large gully systems or steep tributaries, are too large to be removed by individual stream floods, preserving successive debris-flow deposits. They provide records of hillslope debris-flow activity over centuries during the late Holocene.
3) Tributary-Junction Fluvial Fans, similar to debris cones but at tributary-main river junctions, reflect interactions between main river flood power and tributary sediment supply. Operating over decades to centuries they are influenced by flood power and tributary sediment supply during the late Holocene.

Fan morphology is shaped by sediment transport processes and deposition mechanisms, with sediment transported to fans by debris flows or tractional processes in flowing water (Blair and

McPherson, 1994). Deposition occurs when transporting power falls below a minimum threshold, influenced by flow characteristics, surface roughness, and gradient (Fig. 1.15).

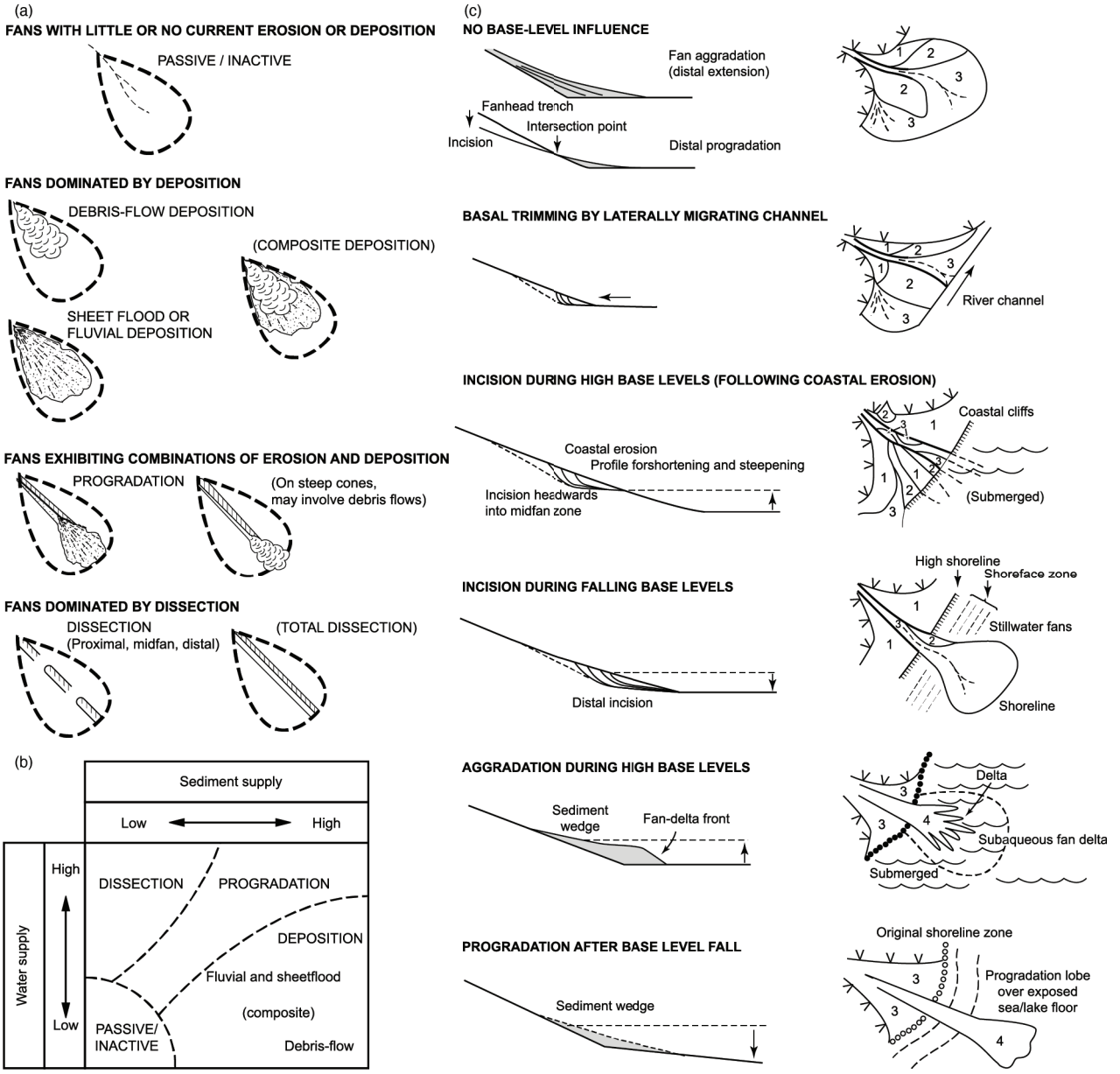


*1.15: (a) Fan style; (b) the impact of flood power and sediment supply on fan style; and (c) the influence of base-level conditions on fan profiles and plan views (figure adapted from Harvey, 2010).*

Catchment characteristics, like size and sediment supply rates, influence fan morphology, resulting in inverse relationships between drainage area and fan gradient (Harvey, 1997a). Morphometric analyses help identify factors affecting fan morphology.

Alluvial fans operate around critical stream power thresholds, sensitive to changes in water/sediment ratios that can switch between transport and depositional processes (Wells and Harvey, 1987). Changes in environmental conditions can lead to switches in depositional styles, preserving records of past environmental changes (Fig. 1.15).

Post-depositional processes, combined with absolute dating methods such as radiocarbon and luminescence, help to correlate fan segments and determine deposition phases, linking them to environmental changes (Harvey et al., 1981; Chiverrell et al., 2007). Cosmogenic nuclide dating is also a promising technique with potential applications in dating sedimentary surfaces (Harbor, 1999; Schaefer et al., 2022).

Base-level conditions significantly influence distal fan zones (Fig. 1.15). When fans extend to a stable base level, they are mainly controlled by proximal factors, preserving a climate-driven signal (Harvey, 2002). However, changes in base level, such as lateral migration of the axial stream or fluctuations in base level, can alter fan profiles and cause distal incision by toe-cutting (Leeder and Mack, 2001). Rising base levels may bury distal fan sediments or transform the fan into a delta, while falling base levels can lead to incision into distal fan surfaces (Harvey et al., 1999a; Bowman, 1988). Global sea levels and lake levels, responding to climate changes, also influence fan sediment regimes and base-level conditions. High base levels during times of limited sediment supply may coincide with proximally-driven dissection of fan upper parts, whereas falling sea levels during periods of increased sediment flux may result in fan progradation onto exposed sea floors (Harvey, 2002c; Harvey et al., 1999a).

Fans and cones play a key role in sediment dynamics, evident across various spatial and temporal scales. In some settings modern active gullies contribute debris flows to the stream system, forming debris-flow lobes or small debris cones (Harvey, 1997b). These gullies serve as primary sediment sources, with downstream sedimentation zones characterized by coarser sediment and braided reaches (Church and Jones, 1982). Over time, these gullies stabilize or disconnect from the stream, transitioning into single-thread channels (Harvey, 1992, 1997b, 2001). Similar phenomena occur on a larger scale along streams, where persistent braided sedimentation zones exist downstream of larger alluvial fans and debris cones (Harvey, 1986, 2007). These zones endure for over 50 years and experience significant sediment input during extreme flood events, leading to increased braiding (Harvey, 1986, 2007). The effectiveness of small-scale tributary junction fans in buffering sediment dynamics varies temporally, coupling with the system under rare, extreme flood conditions (Fryirs et al., 2007).

#### 1.2.1.6. Soil erosion

Soil erosion is a complex process involving soil particle detachment and movement, rainfall infiltration, pooling, and runoff (Borrelli et al., 2021). The intensity and frequency of these processes are influenced by climate, rainfall patterns, topography, soil properties, land management, and spatial scale. While soil resistance to erosion has been extensively studied, less attention has been given to soil dynamic properties and input factor variability. Interactions between climate, land use, and soil characteristics primarily influence soil erosion at the field scale, whereas runoff becomes the dominant factor at the catchment scale (Auzet et al., 2004). Furthermore, soil erosion, influenced by factors like soil properties and precipitation patterns, often mirrors water flow pathways. Research emphasizes scaling in understanding sediment dynamics (Trimble and Crosson, 2000), with the sediment delivery ratio (SDR) suggesting decreased sediment delivery downstream (Walling, 1983). However, complexities arise, studies have shown increased suspended sediment concentrations downstream but decreasing sediment yield in headwaters before rising in lower basins (Bull et al., 1995; Michaelides and Wainwright, 2002). Overland flow, which can manifest as small rills or sheets, is influenced by factors like rainfall intensity and soil resistance (Bull & Kirkby, 1997). Erodibility depends on surface permeability, soil properties, and vegetation, whereas shear stress is affected by raindrop impact and slope (Govers, 1991). Surface runoff can result from infiltration-excess or saturation-excess mechanisms, with the Variable Source Area (VSA) model explaining storm runoff from saturated areas (Anderson & Burt, 1990; Dunne & Black, 1970). Soil characteristics, hydraulic conditions and surface roughness also influence erosion and deposition rates. Accurate modeling of runoff and erosion processes relies on understanding these factors, with various equations employed to predict sediment transport rates (Abrahams et al., 1998; Borrelli et al., 2021).

Hence, erosion processes, such as rilling and gullying, are predominant, impacting agriculture and infrastructure and causing off-site effects on water quality and landscapes (Boardman, 2006; Valentin et al., 2005; Krause et al., 2003). Various approaches explain channel initiation, with models

integrating fluvial and slope processes elucidating landscape evolution. Gullying is influenced by diverse factors, including land use and climate change, though modeling its development is challenging due to morphological complexities (Sidorchuk, 2005). Badlands, extensively dissected areas devoid of vegetation, form from unchecked rill and gully erosion (Faulkner, 2008), exhibiting high drainage density and steep V-shaped channels. They encompass a mosaic of physiographic units, influenced by lithology, soil distribution, and weathering of bedrock (Gallart et al., 2002).

#### 1.2.1.7. Peatland erosion

Peat accumulations are widespread in humid temperate zones, influenced by relief and drainage conditions (Lourenco et al., 2023). Steep slopes limit peat to local accumulations, whereas gentler slopes and maritime locations can support extensive blanket peat formations (Lindsay, 1995). Given their sensitivity to climate change, understanding the erosional status of peatlands is crucial (Bragg and Tallis, 2001; Evans and Burt, 2010).

Classifying mires based on hydrology and topography helps elucidate their role in sediment cascades (Seminiuk and Seminiuk, 1995; Charman, 2002). Mires can be categorized as net sources or sinks of sediment, with subdivisions into mineral and organic sediment sources and sinks. Sediment delivery mechanisms vary based on mire position in the sediment cascade, highlighting the importance of mire position and erosional status in determining their function within the wider sediment system.

Over time, mire roles in sediment cascades change. Widespread upland mire formation shifted sites from mineral sediment sources to sinks thousands of years ago, whereas erosion in the last millennium transformed upland mires into major sediment sources (Evans and Burt, 2010). Recent studies show revegetation of eroded guilles with Sphagnum and Eriophorum, with rapid peat accumulation under favorable conditions (Clement, 2005; Crowe et al., 2008). Thus, eroded peat landscapes experience cyclic 'cut and fill' forming dynamic mosaics across upland surfaces and influencing mire system roles in the wider sediment cascade.

The limited geomorphological studies on upland mires have predominantly focused on degraded systems, partly due to the perception of eroding mires as environmental degradation sites. Intact mires surface morphology is mainly controlled by hydrological processes, with low drainage density but potential dissection by pre-existing stream systems, especially in blanket peatlands. They serve as sites of sediment accumulation and significant carbon sinks (Worrall et al., 2003), with organic sediment export occurring through downslope creep, bank collapse, or rapid mass movement events, such as peat slides (Bower, 1960). Peat slides, associated with high pore-water pressures, are low-frequency high-magnitude organic sediment transfer events, contributing significantly to the sediment budgets (Alison et al., 1998). Bower (1961) identified two main types of gullies in peat erosion and suggested fluvial incision as the primary cause. Weathering processes make surface peat easily mobilized during storms, but detailed understanding of erosion processes in peatlands remains nascent compared to mineral soil erosion systems.

### Peatland Sediment Cascades and Biogeochemical Cycling

#### Sediment-Related Mechanisms

The dynamic nature of sediment flux from peatland systems significantly impacts the role of peatlands in biogeochemical cycling (Mozafari et al., 2023). The effects of peat erosion on biogeochemical systems can be classified into two main classes: those directly associated with changes in sediment flux from eroding or recovering systems, and the effects on peatland function of morphological change in the peatland surface driven by erosional processes.

One of the most significant impacts of changing sediment flux from peatland systems is on peatland carbon budgets. Peatlands are crucial carbon sinks (Worrall et al., 2003), but erosion can shift them to carbon sources by removing carbon from catchments (Evans et al., 2006). Understanding how particulate carbon moves between source and sink is crucial for assessing feedbacks between the sediment system and climate change (Pawson, 2008).

#### Morphologically-Driven Biogeochemical Change

The impacts of peatland erosion, particularly gully formation, affects more than just sediment flux - it alters peatland function by lowering the water table adjacent to gully zones. Changes in the water table strongly influence carbon flux, with varying effects on the carbon balance depending on local soil conditions (Holden, 2005). Understanding peatland hydrology and geomorphology is essential for assessing carbon cycling broader ecosystem functions. The erosional status of peatlands plays a key role in sediment cascades and requires thorough study with ecological factors influencing peatland function.

The past two decades, there have been significant advancements in understanding sediment flux controls and internal dynamics within peatlands (Holden et al., 2006). Yet, there remain important gaps in understanding the broader role of peatlands in sediment cascades (McHugh et al., 2002). The shift from intact blanket peatlands to a degraded pattern over Holocene timescales likely involved significant changes in organic and mineral sediment flux magnitudes (Higgitt et al., 2001). Progress in this is crucial not only for understanding the sediment system but also because sediment from peatlands influences carbon losses and pollutant release (Higgitt et al., 2001).

### 1.2.2 Lakes

Lakes are inland enclosed and standing water. However, due to the diverse nature of such bodies, defining lakes can be somewhat arbitrary (Cohen, 2003; O'Sullivan and Reynolds, 2008). They are integral components of the terrestrial hydrosphere, formed through various geological and geographical processes, and act as essential links between the atmosphere, biosphere, and lithosphere. Their evolution is influenced by tectonic shifts, climatic changes, and human activities, resulting in intricate interactions between geological, physical, chemical, and biological processes, all of which are recorded in lacustrine sediment archives (Shen, 2013).

Lakes, though occupying just 1% of Earth's land surface and containing less than 0.02% of its water (Talbot and Allen, 1996; Wetzel, 2001; Verpoorter et al., 2014), are diverse and are classified by various characteristics such as origin, chemistry, and trophic state (Wetzel, 2001; Eugster and Hardie, 1978). Specifically, classification by formation triggers eight types: glacial, riverine, human-made, eolian, coastal, karstic, tectonic, and volcanic (Wetzel, 2001).

Lacustrine water bodies respond to external forces such as climate through physical, chemical, and biological processes, acting as important mediators for paleolimnological records (Cohen, 2003). Fluctuations in lake level, often associated with climate, can be used for climate reconstructions (Imboden and Wüest, 1995; Corella et al., 2013), whereas chemical cycles like CO2 dynamics reflect climate change (Cole et al., 2007). Lakes host complex biotas with diverse species and interactions, valuable for studying past environmental conditions and current global changes (Margalef, 1983; Adrian et al., 2009; Leland and Berkas, 1998). They play essential roles in ecosystem trophic chains (Margalef, 1983) and regional economies. Lakes function as independent watersheds, providing water, sediment, biomass, and chemicals, also acting as sinks for these materials (Shen, 2013).

#### 1.2.2.1. The physical environment of lakes

Physical processes, such as hydrology, light and heat penetration, and current dynamics, play crucial roles in filtering external climate signals in lakes. For instance, hydrological dynamics dictate lake

levels, recorded through ancient shoreline elevations, while light and heat influence organism distribution and water column mixing (Cohen, 2003).

### The hydrological cycle

The hydrological cycle governs water movement in and out of lakes, determining their levels through various inputs and outputs (Cohen, 2003). Inputs include precipitation, surface runoff, and groundwater discharge, while outputs comprise surface outflow, evaporation, evapotranspiration from plants, groundwater recharge, and hydration reactions with sediments (Fig. 1.16). In open basins, where inputs match outputs, lake levels remain stable despite increased precipitation or runoff (Gronewold et al., 2020). Conversely, in closed basins, changes in input-output ratios lead to significant level fluctuations, resembling rain gauges. Such closed lakes, common in arid regions, offer records of climate and human-induced changes through level shifts linked to precipitation, evaporation, or drainage diversion (Cohen, 2003).

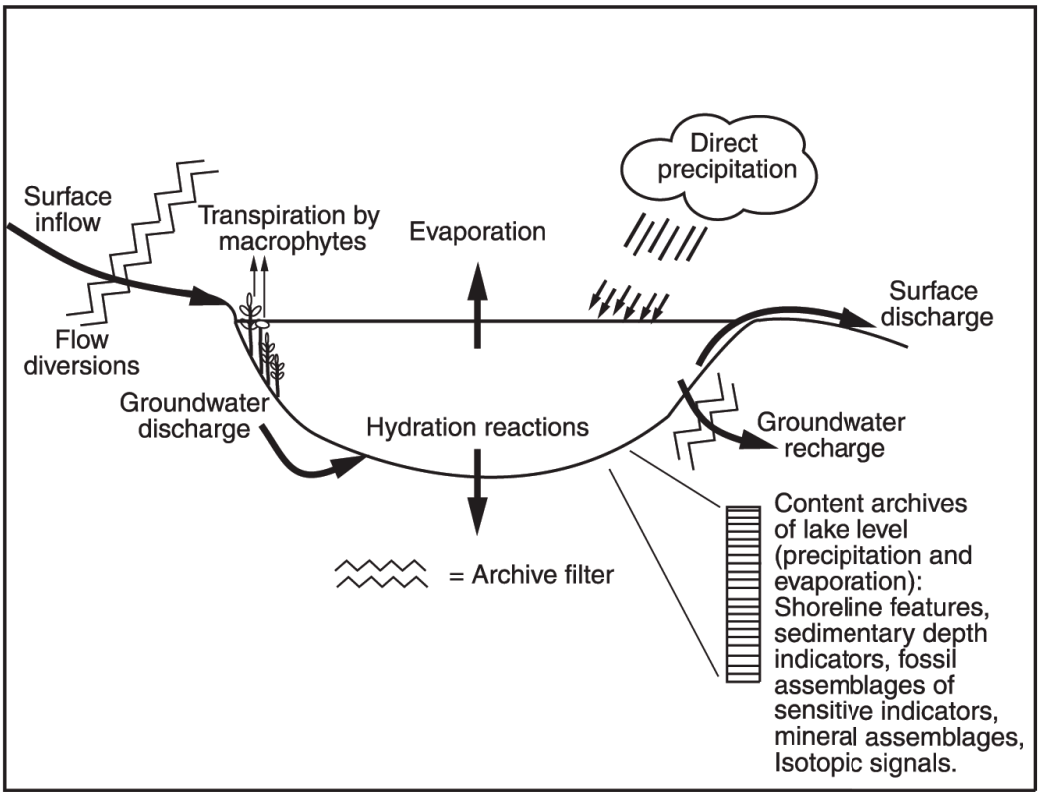


*Fig. 1.16: The hydrological cycle in lakes (from Cohen, 2003)*

### Light penetration, heat, mixing and stratification

The distribution of organisms such as diatoms and heat in lakes is heavily influenced by the depth and absorption of various light wavelengths in lake water (Hofmann et al., 2020). Lakes are categorized into photic zones, where photosynthesis occurs, and aphotic zones below. The littoral zone, within the photic zone, is inhabited by benthic organisms, while the profundal zone lies deeper (Fig. 1.17). Light penetration and growth of photosynthesizing organisms depend on factors like sediment, plankton, and water composition (Cohen, 2003).

The interplay of heat penetration, turbulence, and water column mixing in lakes is crucial for interpreting past climates and sedimentary records (Ragotzkie, 1978). Heat, mainly from solar radiation, affects mixing processes through wind, density instabilities, and turbulence (Imboden and Wüest, 1995). Stratification, influenced by factors like lake morphology and air temperature, varies among lakes (Hutchinson and Löeffler, 1956; Woolway et al., 2021). Different lakes exhibit diverse mixing patterns influenced by their geographical locations and thermal regimes (Lewis, 1987).

Meromictic lakes exhibit incomplete mixing, but exist various mixing patterns, from monomictic to amictic, which can result from seasonal and long-term mixing dynamics (Fig. 1.17) (Miller and Aiken, 1996). The presence or absence of vertical mixing influences oxygen distribution and primary productivity (Valero-Garcés and Kelts, 1995). Seasonal variations in primary productivity and endogenic mineral formation contribute to identifying mixing regimes from sedimentary records (Hilton, 1985). Understanding the interplay between heat penetration, turbulence, and water column mixing in lakes will be crucial for interpreting sedimentary records and reconstructing past climate dynamics, offering valuable insights into paleolimnological studies (Cohen, 2003).

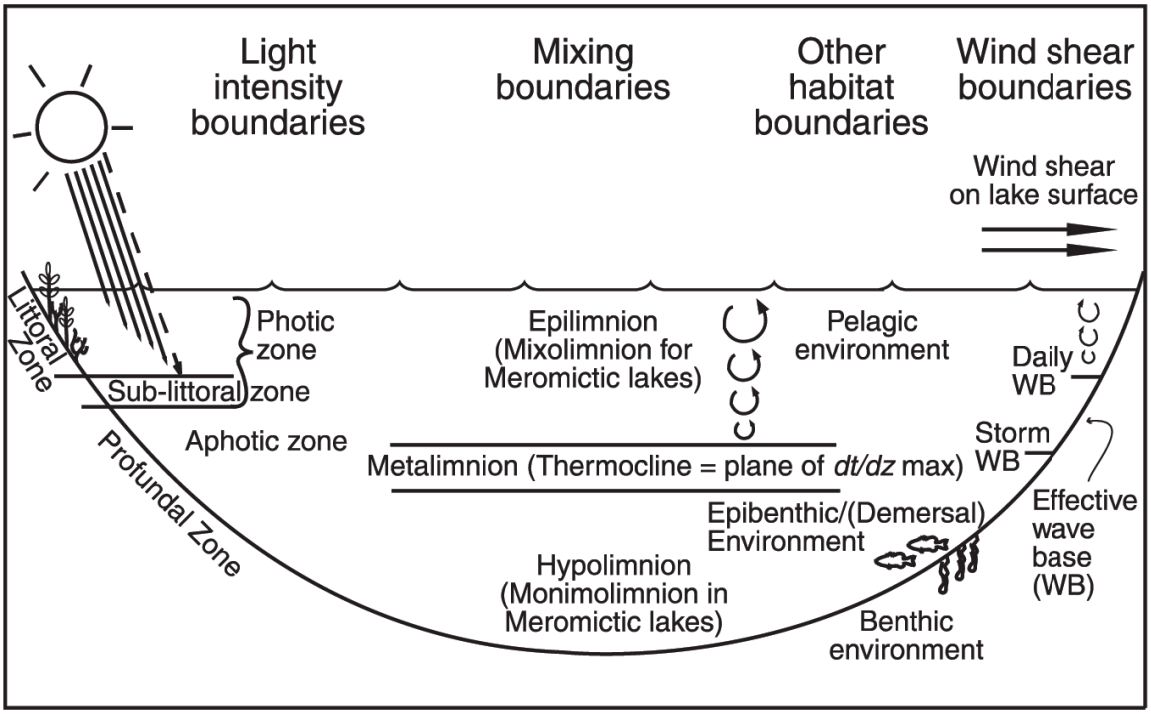


*Fig. 1.17: Zonation of the lake environment. The vertical positions of boundaries related to light, mixing, habitats, and wind shear are not fixed relative to each other (figure from Cohen, 2003).*

## Fluid flows

Fluid flows play a crucial role in moving and dispersing sediment within lakes (Cohen, 2003). Currents in lakes, characterized by unidirectional flows lacking wave oscillations, result from various factors such as wind, wave momentum, and gravity-driven density instabilities (Imboden and Wüest, 1995) (Fig. 1.18). Small-volume lakes are strongly influenced by through-flowing currents, with seasonal variations. Influent currents, influenced by temperature, salinity, or suspended load differences, may float, descend as interflows, or underflows into lakes, affecting sediment distribution (Rea et al., 1981; Carmack et al., 1986; Weirich, 1986; Okamoto et al., 1995). Overflows, interflows, and underflows demonstrate varying velocities and sediment transport capacities (Smith and Ashley, 1985; Weirich, 1984; Pickrill and Irwin, 1982). Gravity flows, including turbidity and debris flows, play crucial roles in sediment transport, forming distinct depositional features in lakes. Turbidity flows exhibit a predictable anatomy, while debris flows deposit massive, unstratified layers of debris (Giovanoli, 1990; Scholz et al., 1993).

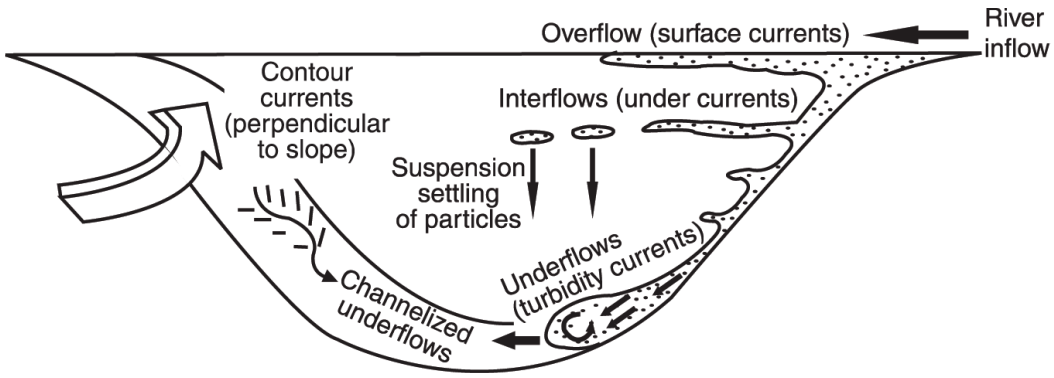


*Fig. 1.18: The interactions within lakes resulting from density-driven currents highlight the diverse range of processes occurring as water of different densities enters the lake (from Cohen, 2003).*

#### 1.2.2.2. The chemical environment of lakes

Understanding lake chemistry is crucial for accurately interpreting the geochemical records in lake deposits. Elemental and isotopic distributions are influenced by external climatic and watershed processes. Solute concentrations regulate organism distribution and mineral precipitation or dissolution. Sedimentary archives contain fossil and mineral remnants, allowing reconstructions of ancient water chemistry and associated paleoclimate or human activities. Interpreting isotopic records depends on understanding their behavior within lakes and their connections to external factors like rainfall and nutrient discharge.

##### Carbon

The carbon cycle in lakes involves diverse forms of carbon, both inorganic and organic, transitioning between particulate and dissolved states. Lakes serve as significant reservoirs of atmospheric carbon, impacted by human activities like fossil fuel combustion (Kling et al., 1991; Dean and Gorham, 1998). Lake ecosystems ability to sequester carbon is linked to their biological processes (Schindler et al., 1997). Carbon dioxide dynamics, influenced by pH, are central to lake carbon cycles, with processes like photosynthesis and respiration affecting carbon flux (Dean, 1999). Acidification from CO2 dissolution or industrial pollutants alters lake ecosystems. Organic carbon, including diverse molecules, influences lake processes (Meyers and Ishiwatari, 1993). Both autochthonous and allochthonous sources contribute dissolved and particulate organic carbon to lakes, impacting water quality and ecosystem structure (Wetzel, 2000). Variations in dissolved organic carbon affect lake acidity and transparency (Rasmussen et al., 1989; Fee et al., 1996). Particulate organic carbon, though a small fraction, provides insights into past community dynamics (Meyers and Ishiwatari, 1993). Factors like lake depth and mixing influence POC fluxes (Katz, 1990). Understanding these complexities is vital for interpreting lake sediment records accurately.

##### Solutes and particles

Solutes and particulates enter lakes through various pathways, including rivers, groundwater discharge, atmospheric gaseous exchange, air-borne particulate matter, and precipitation. The significance of these sources depends on factors like lake location, regional climate, and human activities (Smith et al., 2020). Rock weathering, primarily through mechanical degradation and biochemical decay processes, contributes most dissolved solids and particulates to lakes (Johnson & Brown, 2018). Weathering rates are influenced by factors such as bedrock type, climate, and human activities, affecting vegetation, soil types, and transport potential (Jones, 2019). Vegetation greatly accelerates hydrolysis weathering reactions, releasing alteration product particulates and dissolved ions. Industrial and agricultural runoff contribute nutrients and metals to lakes globally (Garcia et al., 2023). Atmospheric precipitation, including sea spray and acidic precipitation from industry, also plays a significant role in supplying particulates to lakes.

### Salinity

Global compilations of inland water composition reveal that a limited set of ions dominates the dissolved solid content of dilute rivers flowing into lakes, including $Na^+$, $K^+$, $Ca^{2+}$, $Mg^{2+}$, $Cl^-$, $HCO_3^-$, $CO_3^{2-}$, and $SO_4^{2-}$. These ions originate from various sources such as oceans, atmospheric deposition, and weathering of minerals (Finley and Drever, 1997). Salinity in lakes is determined by the net accumulation of salts from all sources, with outflow and mineralization contributing to salt loss. Hydrologically open lakes generally do not accumulate extremely high salinities unless influenced by factors like pre-existing evaporite deposits. Closed basin lakes, however, can experience increasing salinity over time due to the buildup of dissolved solids. Understanding changes in salinity in closed basin lakes is crucial for paleolimnologists as it is linked to precipitation, runoff, evaporation ratios, and climate fluctuations (Last, 1982).

### Nutrients

Nutrients play a vital role in the metabolic processes of lacustrine organisms, with phosphorus, nitrogen, silicon, and iron being key limiting nutrients (Dillon and Rigler, 1975; Schindler, 1974; Vollenweider, 1976). These elements are crucial for functions like nucleic acid formation and protein synthesis (Cowell and Dawes, 1991; Lebo et al., 1992). Nutrient availability influences species composition and productivity in lakes, with phosphorus typically limiting productivity in temperate lakes, while nitrogen, silica, and iron may be more critical in tropical and arid regions (Cowell and Dawes, 1991; Lebo et al., 1992). Seasonal variations in nutrient depletion patterns can lead to changes in phytoplankton communities, challenging the notion of a single limiting nutrient. Nitrogen serves as a vital nutrient for life, necessitating its conversion from inert gaseous $N_2$ to $NH_3$ by various bacteria and cyanobacteria through fixation. Fixed nitrogen enters watersheds and lakes, impacting their ecosystems profoundly (Schindler, 1977; Howarth et al., 1988). In lakes, nitrogen rules crucial reactions, including nitrification and denitrification, affecting its availability (Seitzinger, 1988). Bacterial activity in sediments further controls nitrogen cycling, affecting lake ecosystems (Seitzinger, 1988). Nitrogen signals in lake sediments provide insights into terrestrial watershed conditions and internal nitrogen cycling, discernible through C=N ratios (Meyers and Ishiwatari, 1993). Additionally, the dominance of nitrogen fixation in lake ecosystems can be inferred from chemical fossils and stable isotopic compositions of the accumulated organic matter, providing further insights into nitrogen cycling (Leavitt et al., 1994b; Talbot, 2001; Leng et al., 2006).

Silicon in lakes originates primarily from the weathering of silicate minerals transported into lakes via surface flow or groundwater (Finley and Drever, 1997). Silicon serves as a crucial nutrient for the growth of lacustrine organisms, particularly diatoms, and its depletion and cycling in lakes are intricately linked to diatom productivity cycles. Depletion of silica by diatom growth can lead to shifts in phytoplankton composition within lakes (Kilham, 1971). In lakes with meromictic characteristics, silica concentrations in the monimolimnion remain relatively high due to limited secondary consumption below the mixed layer, making sediments effective sinks for silica accumulation (Michard et al., 1994). However, in large, deep lakes, most settling diatoms are redissolved, contributing to silica recycling if retained in the upper water column (Johnson and Hecky, 1988).

### Stable isotopes and isotopic fractionation

Isotopes, varying in neutron numbers while maintaining constant proton and electron counts, exhibit distinct behaviours in physicochemical and biochemical processes due to their differing masses. Stable isotopes remain unchanged over time, while radiogenic isotopes decay into other forms. Physicochemical processes, like evaporation, and biological processes such as photosynthesis can lead to isotopic fractionation, enriching certain isotopes in products and depleting them in source materials (Cohen, 2003; Leng et al., 2006). Understanding stable isotope fractionation in lacustrine

environments is crucial, as it reflects environmental factors like evaporation rates and vegetation cover. The degree of fractionation in a physicochemical process is typically quantified by comparing the isotopic composition of the end products to that of a standard. Absolute isotopic quantities are challenging to measure directly; instead, isotopic ratios are determined relative to materials with known ratios. This is expressed as the deviation of an element in one sample from the standard, denoted by the delta (δ) value in per mil (‰) (Eq. 1.1):

$$\delta‰ = [(Rsample - Rstandard)/Rstandard] \cdot 1000$$

*(Eq. 1.1)*

Fractionation during chemical reactions is influenced by temperature, a characteristic noted early on in the potential applications of stable isotopes in paleoenvironmental reconstruction, such as inferring paleotemperatures from fossil material or authigenic minerals (Urey, 1947). Yet, a diverse range of inorganic equilibrium processes and biochemical kinetic processes also induce fractionation (Cohen, 2003; Leng et al., 2006).

The Earth hosts two primary stable isotopes of carbon, $^{12}C$ and $^{13}C$, with $^{12}C$ being much more abundant than $^{13}C$. Carbon cycling within lakes is complex, involving diverse forms preserved as organic matter and carbonate minerals (Cerling and Quade, 1993). Unlike oxygen, no single carbon reservoir dominates a lake budget universally. Various fractionation processes influence carbon isotopes in lakes (Herczeg and Fairbanks, 1987), including terrestrial plant debris and phytoplankton-derived organic matter (Street-Perrott et al., 1997). Long-term trends toward heavier $^{13}C$ values in lacustrine organic matter may result from productivity increases, especially in meromictic lakes (Talbot & Lærdal, 2000).

Nitrogen isotopes, primarily $^{14}N$ and $^{15}N$, are introduced into lakes from terrestrial and atmospheric sources (Talbot, 2001; Leng et al., 2006), with human activities altering fluxes globally (Minigawa & Wada, 1984; Zhang et al., 2020). Fractionation occurs at multiple points in the lacustrine nitrogen cycle, reflecting primary productivity and trophic levels (Peterson & Fry, 1987; Leng et al., 2006). Long-term trends toward more positive $^{15}N$ values in lacustrine organic matter often signify increased productivity (Talbot & Johannessen, 1992), serving as valuable indicators of environmental change over time.

#### 1.2.2.3. The biological environment of lakes

Biological processes serve as a valuable source of information, reflecting environmental variations through fossil abundances, evolutionary shifts, or extinctions. Fossils uniquely record changes in lake temperature or water chemistry, supplementing geochemical archives. A transect from shoreline to offshore typically reveals distinct habitat and organism changes. The littoral zone, near the shore, experiences abundant sunlight, hosting diverse autotrophic and heterotrophic life. Macrophytes, both emergent and submerged, provide substrates for various organisms, though wave-swept areas may lack them, instead hosting algae or photosynthetic bacteria attached to rocks or sand. Deeper sublittoral zones see reduced light penetration, with benthic primary production sustained by algae or bacteria. Profundal zones rely on detritus consumption and microbial resources for secondary productivity. Heterotroph communities are indirectly regulated by light gradients, along with factors like wave action and substrate variations in benthic habitats. The pelagic environment accommodates plankton, nekton (mainly fish), and picoplankton, with species diversity influenced by currents, nutrient levels, and predation. However, distinctions between benthic, planktonic, and nektonic organisms are somewhat arbitrary, as many move between these realms.

##### Phytoplankton

Phytoplanktonic communities encompass a diverse range of single-celled and colonial algae and bacteria, known as "algae," despite their varied origins (Canter-Lund and Lund, 1995). These organisms are ecologically and somewhat evolutionarily distinct to variations in their dominant pigments, crucial for photosynthesis. Chlorophyll-a is common among all blue–green bacteria and algae, whereas other chlorophylls and carotenoid pigments are specific to certain algal groups. Cyanobacteria, a monophyletic group, utilize chlorophyll for oxygen-producing photosynthesis and possess specialized cells called heterocysts for nitrogen fixation ($N_2$).

### Benthos

The diversity of planktonic and nektonic organisms spans both littoral and profundal zones of lakes. Benthic organisms, requiring robust body structures due to constant contact with hard surfaces, dominate the lacustrine fossil record over plankton. Cyanobacteria form mats and mounds in the littoral and sublittoral zones of many lakes, often comprising complex microbial communities. Macrophyte distributions are influenced by water chemistry, especially nutrient availability and salinity, with changes in nutrient loading significantly influencing community structure. Groundwater flow also affects macrophyte distribution patterns. Macrophytes are commonly preserved in lake fossils as fruits, seeds, spores, pollen, or emergent plant leaves, often containing lignin or silicified. However, submerged macrophytes typically lack a cuticle around leaves and stems, reducing their preservation probability, except in acidic bogs where preservation is enhanced (Schweingruber et al., 2020). Sponges (Porifera) are simple multicellular heterotrophs, with adult sponges being benthic filter feeders, while their gametes and larvae disperse in the plankton. Freshwater sponges belong mainly to the Spongillidae family, characterized by a skeletal meshwork of siliceous spicules and gemmules for reproduction. Spongillids vary in morphology, adapting to a range of substrate and water chemistry conditions (Harrison, 1990). Insect communities in lakes exhibit distinct habitat zonation influenced by vegetation and substrate. Aquatic insects are mainly found in the littoral zone, with diversity decreasing with depth. Well-vegetated littoral zones host diverse species, whereas rocky areas resemble stream beds (Ward, 1992). Chironomids, crucial benthic inhabitants, dominate the profundal zone and are valuable for paleolimnologists due to their fossil preservation characteristics (Walker, 2002).

## 1.3 Paleolimnology

Paleolimnology relies on archives, encompassing both the historical records within and the physical locations housing such records (Fig. 1.19). Lakes serve as dynamic repositories influenced by various external and internal factors, shaping their history over time. Sedimentary deposits, originating from catchment erosion and internal lake processes, offer resilient records of past climatic and environmental conditions. Analyzing sedimentary layers in lake cores allows deductions about changes over time, driven primarily by climate alongside tectonic events and human activities (Cohen, 2003; Bradley, 2015). Particularly, lakes exhibit diverse responses to climate change, including increased water temperatures and extended ice-free periods at mid and high latitudes (Schindler et al., 1996). Additionally, tropical lakes experience elevated surface temperatures, resulting in enhanced stability of the water column stratification (Plisnier et al., 1999).

Content archives in paleolimnology comprise several sediment inputs, including terrigenous, chemical, and biogenic sediments, as well as cosmogenic and volcanogenic particles, and both exogenous (e.g., pollen) and endogenous (e.g., diatoms) fossil materials. These archives serve as indicators of environmental conditions rather than complete representations; they undergo filtering that can distort or dampen the original record. Some filters may obscure meaning or aid interpretation by removing noise. Lag times between events and deposition, such as pollutants transported to lakes via groundwater, can occur (Smol, 2009). Paleolimnologists employ different sampling tools, each with unique strengths and weaknesses, to address research questions effectively (Cohen 2003).

Matter circulates between terrestrial and aquatic ecosystems, impacting both the biotope and biocenosis (Kuriata-Potasznik et al., 2020). Understanding the interaction between terrestrial and lacustrine archives requires integrating spatial and temporal paleoenvironmental data, including sediment cascade dynamics. Non-climatic factors like tectonics mainly shape lake basin morphology, whereas climatic influences such as glacial activity and lake-level fluctuations also play significant roles. Lake basins act as depocenters for sedimented particles, reflecting both terrestrial landscape dynamics and lacustrine processes over extended periods (Dietze et al., 2010).

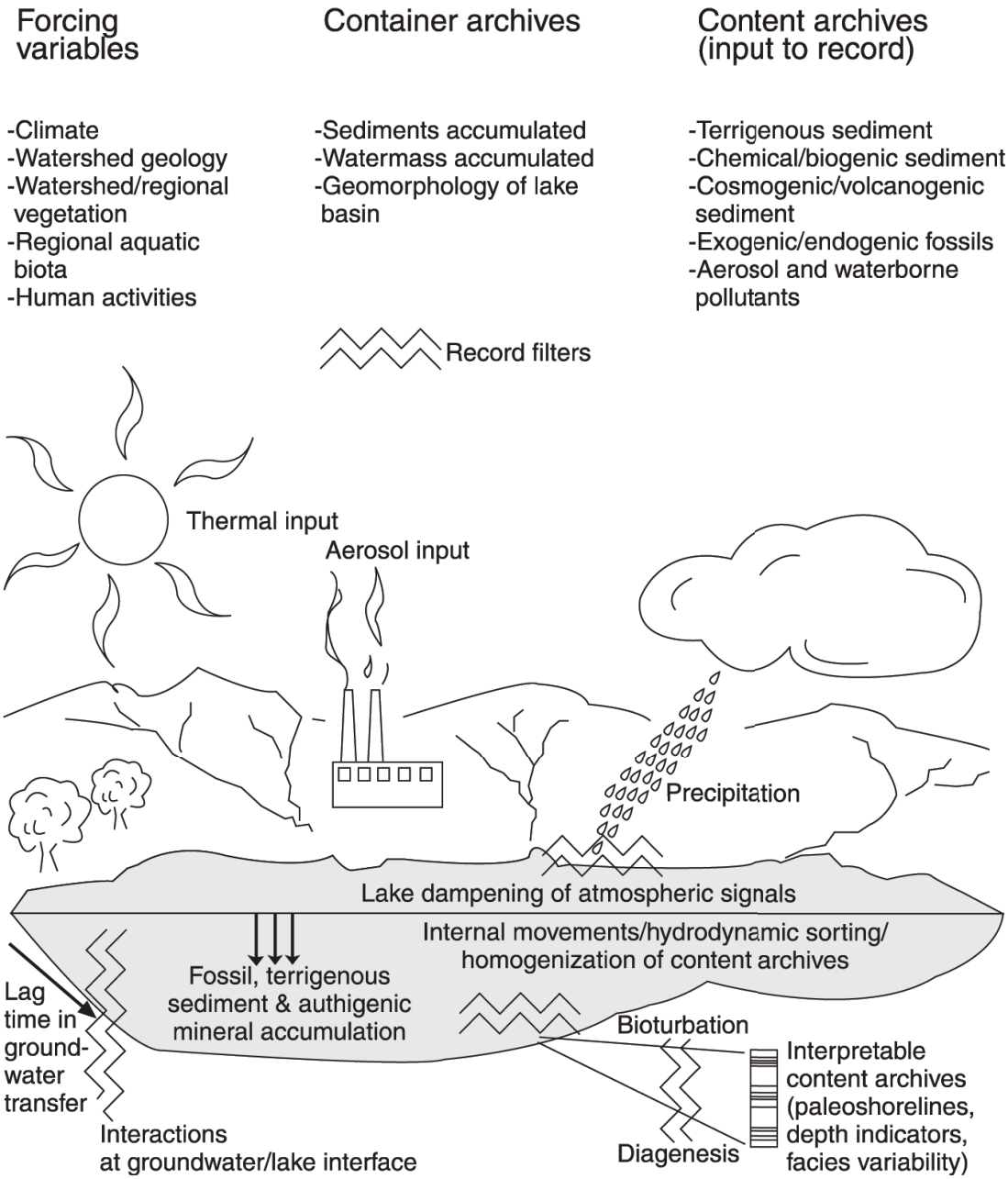


*1.19: A simple model explaining the factors influencing the creation of sedimentary records in lakes. External factors, known as forcing variables, regulate the formation, persistence, and characteristics of the lake. Container archives are the recording media that house the indicators of external environmental change. Content archives consist of physical records such as fossils, sediments, and geochemical data, essential for reconstructing paleolimnological histories. Zigzag lines highlight major points of record filtering. Adapted from Cohen, (2003).*

Investigating the history of lake basins has emerged as a significant area of study due to their role as local repositories of data pertaining to hydrological cycles, lake/catchment ecology, and sedimentary processes over time (Wünnemann et al., 2015). While lake-bottom sediment records

are commonly used to trace a lake evolution in response to climate change, recent research suggests that alterations in depositional environments may also stem from non-climatic factors such as tectonic activity, changes in catchment morphology, and human influence (Coulthard et al., 2005; Dietze et al., 2010; Zhang et al., 2012).

### 1.3.1. Limnogeology

Limnogeology delves into the dynamics of lake systems, largely drawing inspiration from advancements in marine geology (Kelts, 1988). Both Paleoceanography and Limnogeology, pertaining respectively to marine and continental environments, employ a multiproxy approach to unravel past environmental and climate fluctuations (Last and Smol, 2001a; Piovano et al. 2014). Sediment coring is the predominant method in Limnogeology research, drawing from diverse disciplines like agronomy, botany, climatology, chemistry, ecology, geography, geology, hydrology, physics, and zoology (Kelts, 1988; Cohen, 2003; Birks and Birks, 2006; Ariztegui et al., 2008). Since the 1970s, interest in lake geological processes and deposits has surged, covering topics from basin evolution to paleoecology (Kelts and Hsü, 1978; Anadón et al., 1991; Gierlowski-Kordesch and Kelts, 2000). Limnogeology growing importance in Earth sciences lies in its applications, including sources of industrial minerals and fossil fuels, Quaternary paleoclimate investigations, water resource management, and environmental research (Kelts, 1988; Last and Ginn, 2005; Davidson and Jeppesen, 2013).

### 1.3.2. Limnogeomorphology

Geomorphology, a significant branch of Quaternary science, explores the formation processes of landforms and associated sediments (Hughes et al., 2005; 2007). Traditionally, Quaternary sediment subdivision relied on morphostratigraphy for landform-based classification and lithostratigraphy for lithology-based classification (Hughes, 2010). Usually, both methods are employed together, forming the basis of geomorphological approaches. An alternative formal method, allostratigraphy, identifies stratigraphical units by their bounding discontinuities. Analyzing the sedimentary evolution alongside geomorphic characteristics revealing deposition forms in the landscape unveils the morphodynamics processes of sedimentation in the lake basin (Scheidegger, 1961). In other words, geomorphological and stratigraphic studies, as well as age modeling, help understand how depositional environments have changed over time in the studied systems, and how these changes are related to the way sediments are deposited and move within the lake basin.

Limnogeomorphology, focusing on lake-catchment systems, offers a unique perspective by using lacustrine sediments as recording media for past phenomena (Kashiwaya et al., 2004). This interdisciplinary approach combines present instrumental measurements with historical field observations, providing insights into both past and present environmental changes (Ahnert, 1987; Pelletier, 2009). By connecting proxy data with observational data, lake-catchment systems serve as proxy observatories for understanding earth-surface processes and environmental changes (Kashiwaya et al., 2015). Surficial processes get recorded in lake sediments. Therefore, lake sediments provide a temporal framework to understand the evolution of surficial processes (Dietze et al., 2010). However, challenges arise in extracting useful information from sedimentary records due to the need for precise filtering (Kashiwaya et al., 2004). The term "limnogeomorphology" describes this integrated approach (Kashiwaya, 2008).

To establish a continuous quantitative record from present to past, several steps are necessary. It is essential to understand the link between instrumental observations and sedimentary records, which involves establishing transfer functions (Shimada et al., 2002). Then, past environments are quantitatively reconstructed using sedimentary data and historical documents. Finally, long-term environmental changes are estimated, considering factors like cosmic-solar and orbital fluctuations (Kashiwaya, 2012).

Climatic and geomorphic forces continuously shape lake-catchment systems, impacting them over long periods and varying scales. These forces, including water flow and glacial movement, shape landforms and earth-surface systems, with solar insolation driving large-scale climatic changes. In the short term, climatic external forces affect geomorphology of lake catchment systems, particularly affecting lacustrine environments. Studying sediment records from lakes during the present instrumental period help researchers understand the link between sedimentary archives and meteorological conditions, offering insights into earth-surface processes (Kashiwaya, 2017).

Tectono-geomorphic forces have played a pivotal role in shaping lake-catchment systems, as evidenced by examples such as Lake Biwa and Lake Baikal (Kashiwaya, 2017). These examples highlight how tectonic activity has significantly influenced the evolution of lake-catchment systems over geological time scales (Meyers et al., 1993; Yokoyama, 1984). Tectonic activity has left its mark on sediments in Lake Baikal, albeit with lower resolution due to lower sedimentation rates (Mats and Perepelova, 2011). In turn, analysis of sedimentary data from Lake Biwa indicates a rapid decrease in mineral grain size during initial sedimentation, suggesting rapid subsidence and gradual aggradation of the lake, potentially indicating changes in water level (Meyers et al., 1993; Yokoyama, 1984).

Early human impacts on lake-catchment systems, particularly irrigation and reservoir construction, have had significant impacts on lake-environmental records (Kashiwaya et al., 2017). Ancient civilizations such as those in Egypt and Mesopotamia developed irrigation systems with reservoirs (Shanan, 1987), creating new lake-catchment systems whose sedimentary records deliver information of past environmental changes. However, continuous sedimentary records are rare due to natural disruptions and human activities at inflow and outflow sites. The fluctuating water levels of the Aral Sea throughout the Holocene, due to water overuse for irrigation, suggest that paleoenvironmental data can also aid in understanding recent anthropogenic land-use changes in a region (Boomer et al., 2000).

In recent years, Geographical Information System (GIS) platforms and high-resolution Digital Elevation Models (DEMs) have facilitated the application of geomorphometric techniques in terms of time-consumption and cost-effectiveness (Troiani et al. 2014, 2017). These techniques also allow studying large areas accurately and efficiently to produce geomorphological maps (Pike 2009).

Landscape analysis techniques are useful for different aims, including identifying recent geological processes such as active tectonics and landslides, local conditions including lithological contrasts, and past geomorphic processes like glacial erosion (e.g., Larue 2008; Pérez-Peña et al. 2010; Antón et al. 2014). These are often manifest in the drainage network, creating knickpoints or knickzones, which are abnormal increases in river gradient (Walsh et al. 2012). Knickpoints are localized, while knickzones affect longer river segments. Indexes like the Normalized Steepness Index (Ksn) quantify gradient changes, with knickzones showing higher values. Ksn is a computing tool based on the stream-power model, which relates the local channel slope and the contributing drainage area upstream (Perron and Royden 2013) (Eq. 1.2).

$$K_{sn} = \frac{S}{A^{\theta}}$$

*(Eq. 1.2)*

Where:

- *$K_{sn}$ is the normalized steepness index.*

- *S is the average slope of the hillside in degrees (°).*

- *A is the up-stream drainage area of the watershed in square meters (m²).*

*- θ is the concavity = 0,45 (averaged for global rivers, necessary for intercomparison).*

Linear regression in logarithmic area-slope river profiles is the conventional method for analysing ks and θ, but it presents challenges due to high autocorrelation in both parameters (Kirby and Whipple 2012). As θ does not vary widely, a solution is to use a fixed reference concavity (θref) to derive a Ksn. Perron and Royden (2013) proposed the most used method for deriving Ksn from a fixed reference concavity, integrating Eq. 1.2 and defining the Chi index (χ). This integration enables the calculation of Ksn through linear regression between the χ and elevation, with the slope of a Chi-elevation plot representing the Ksn index. These indexes have been successfully applied to detect landslides in several studies (Walsh et al. 2012; Gu et al. 2021; Troiani et al. 2014).

### 1.3.3. Lake sediments

Lakes serve as crucial repositories of environmental information storing sediments that accumulate over time (Cohen, 2003; Smol, 2009; Nichols, 2009). These sediments serve as comprehensive natural archives, offering detailed insights into the temporal evolution of a lake's chemical, physical, and biological characteristics, along with past climate variations of the region (Oldfield, 2005). Nevertheless, lake sediment records require careful assessment of catchment conditions and water properties due to individual lake variability (Birks, 2015). Sediments comprise allochthonous and autochthonous materials, sourced externally and internally, respectively, and are employed for paleoecological and paleoclimatic reconstructions (O'Sullivan and Reynolds, 2008; Bengtsson and Herschy, 2012; Nichols, 2009; Birks, 2015) (Fig. 1.20).

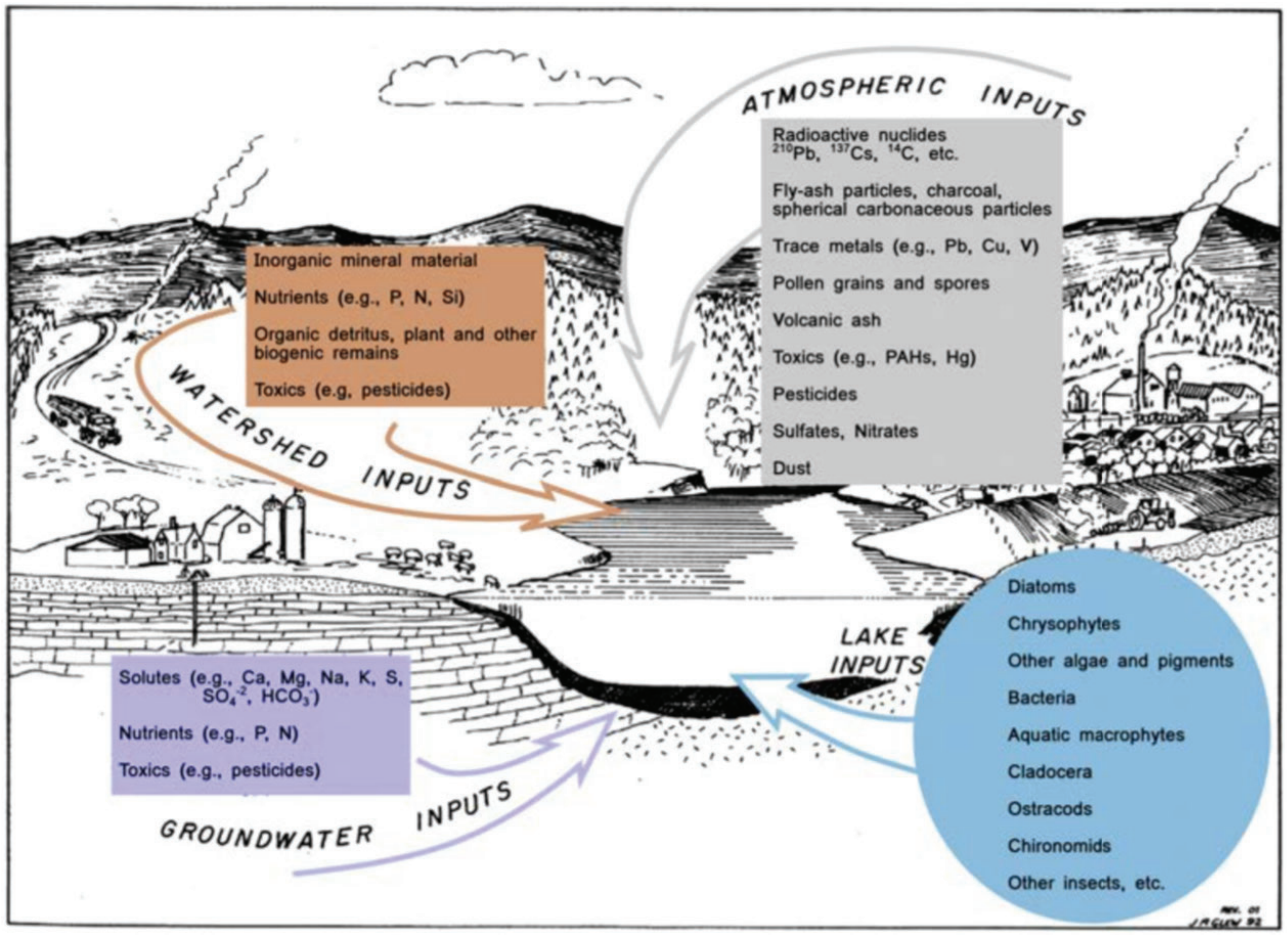


*Fig. 1.20: Schematic diagram illustrating the transfer of material from the atmosphere, the watershed and the groundwater to sediments in a lake (allochthonous input; rectangles) and from sources within the lake itself (autochthonous input; circle). Figure from Sánchez-López (2016) after modified from Smol et al. (2001).*

Lake sediment analysis provides valuable information about environmental changes by examining its composition (Birks, 2015). Techniques such magnetic susceptibility track glacier activity (Nesje et al., 2000; Polissar et al., 2005), whereas scanning X-ray fluorescence (XRF) enables high-resolution elemental data acquisition for understanding past conditions (Shanahan et al., 2008; Croudace and Rothwell, 2015; Bakke et al., 2010). Pollen, plant macrofossils, phytoliths, and organisms like ostracods and diatoms in the water column offer insights into climatic variability (Rull et al., 2011; Parnell et al., 2015; Hannon and Gaillard, 1997; Jackson et al., 1997; Barboni et al., 1999; Holmes, 2001; Schwalb, 2003; Battarbee et al., 2001). Isotopic values of oxygen ($\delta^{18}O$) and carbon ($\delta^{13}C$), along with biomarkers like glycerol dialkyl glycerol tetraethers (GDGTs), further enhance our understanding of past environmental and climatic dynamics (Leng and Marshall, 2004; Leng, 2006; Eglinton and Eglinton, 2008; Castañeda and Schouten, 2011; Powers et al., 2010).

#### 1.3.3.1. The organic fraction

##### Organic matter

Organic matter from lake sediments offers valuable clues for reconstructing past environments and climate changes within lake ecosystems and their surrounding areas (Meyers, 1997; Rullkötter, 2001). Although it represents a small fraction of sediment composition, this organic matter, comprising lipids, carbohydrates, proteins, and other components from lake organisms, serves as a source of proxies for understanding historical ecosystem dynamics (Meyers, 1997; Rullkötter, 2001). The organic matter content in lake sediments helps interpret natural and human-induced changes in local and regional ecosystems.

Origin of organic matter in lake sediments is mainly plants in and around the lake, categorized into non-vascular (e.g., phytoplankton and bacteria) and vascular (e.g., grasses, shrubs, macrophytes) groups. These plants retain their distinct biochemical compositions in sedimentary organic matter (Meyers, 1994).

The concentration of total organic carbon (TOC) in sediments is crucial for assessing organic matter abundance (Dean, 1974). Weight loss on ignition (LOI) was first used to estimate organic matter, whereas TOC spectrometric measurements are preferred due to potential LOI overestimations caused by volatile non-carbon sediment components (Dean, 1974). TOC concentrations offer a more accurate approximation of organic matter content, typically containing about 50% carbon (Meyers and Teranes, 2001).

TOC serves as a comprehensive measure reflecting the proportion of organic matter evading remineralization during sedimentation, influenced by various factors like biomass production, degradation, and depositional processes (cf., Tenzer et al., 1997). Spatial variability in sediment TOC concentrations within lakes is influenced by factors such as hydraulic sorting, clastic sediment addition, and carbonate dissolution (Thompson & Eglinton, 1978; Dean, 1999). Mass accumulation rates of organic carbon provide meaningful measures of organic matter delivery and preservation, aiding in identifying shifts in primary productivity, although post-burial degradation can obscure TOC accumulation rates (Hodell & Schelske, 1998). Microbial processing in oxic pore-waters can also impact sedimentary organic carbon records over time.

The distinction between sedimentary organic matter derived from aquatic versus land sources is discernible through the C/N ratio compositions of algae and vascular plants (Fig. 1.21). Phytoplankton-derived organic matter has C/N values ranging from 4 to 10, while organic matter from cellulose-rich, protein-poor vascular land plants usually presents C/N ratios of 20 or higher (Fig. 1.21). The carbon isotopic composition of organic matter ($\delta^{13}C$) in lake sediments serves multiple purposes, including assessing organic matter sources, reconstructing past productivity rates, and identifying changes in nutrient availability in surface waters (Hollander & McKenzie, 1991; Hollander

et al., 1992; Hodell & Schelske, 1998; Brenner et al., 1999). Increases in organic matter accumulation rates and its isotopic ratio indicate enhanced aquatic productivity in lakes. Sedimentation of algal organic matter leads to dissolved inorganic carbon (DIC) depletion in surface-water reservoirs, causing an increase in the isotopic values of remaining inorganic carbon and subsequently in newly produced organic matter. Changes in algal productivity, influenced by factors like pH, temperature, and nutrient limitation, affect the isotopic composition of organic matter (Takahashi et al., 1990; Fogel & Cifuentes, 1993) (Fig. 1.22).

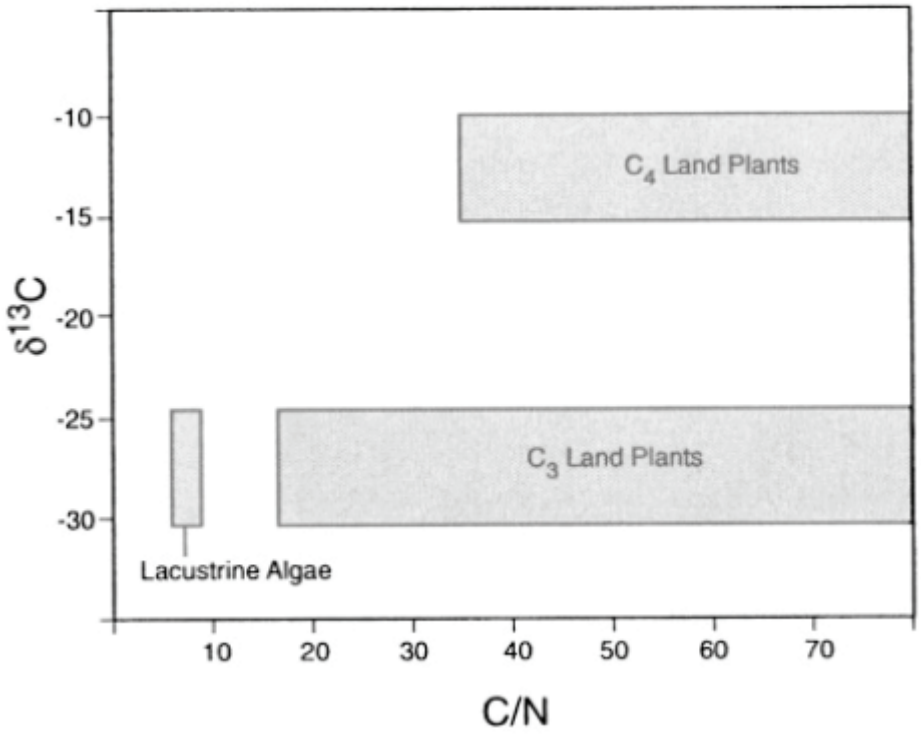


*Fig. 1.21: The typical elemental and carbon isotopic compositions of organic matter derived from algae in lakes, C3 and C4 land plants, which use CO2 as their source of carbon during photosynthesis. (from Meyers and Teranes, 2001)*

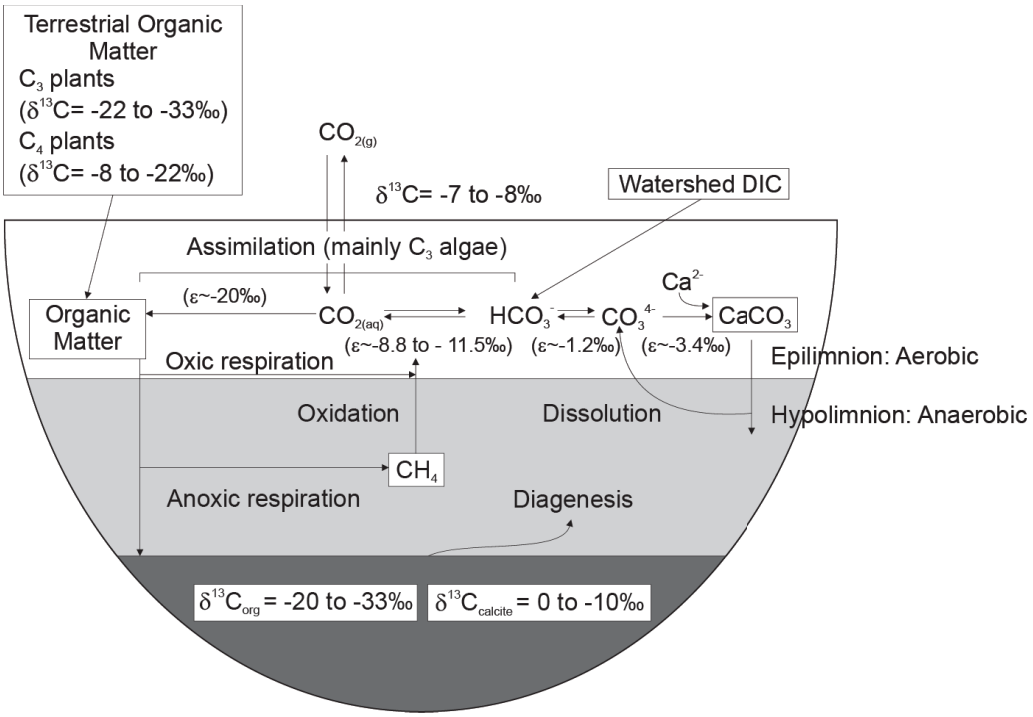

*Fig. 1.22: Idealised carbon isotope cycle in a small stratified lake. The isotopic composition of organic matter buried in sediments reflects a mix of terrestrial and lacustrine organic matter, the carbon isotopic composition of dissolved inorganic carbon (DIC), and the rates of primary production and respiration in the water column. Isotope enrichment factors (ε), showing the difference between the product and the substrate, vary depending on the form of DIC assimilated by lake algae (e.g. $CO_{2(aq)}$ or $HCO_3^-$). Inorganic carbonate ($CaCO_3$) typically forms in isotopic equilibrium with the DIC pool and thus indirectly reflects organic matter sources and primary production and respiration rates (figure from Hernandez, 2010, after modified from Meyers and Teranes, 2001).*

The nitrogen isotopic composition ($\delta^{15}N$) of sediment organic matter is a valuable proxy for identifying nitrogen sources to lakes and reconstructing past productivity rates (Bernasconi et al., 1997; Hodell & Schelske, 1998; Brenner et al., 1999). Algal utilization of dissolved inorganic nitrogen (DIN) in lake waters increases nitrate values, complicating reconstructions (Fogel & Cifuentes, 1993). Water column denitrification and shifts in phytoplankton composition further influence nitrogen isotopic composition (Fogel & Cifuentes, 1993) (Fig. 1.23).

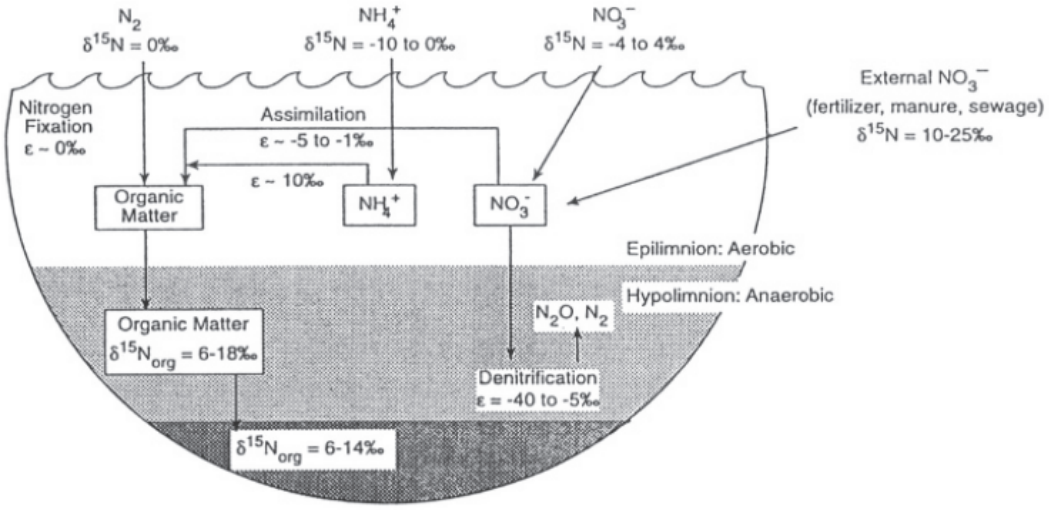


*Fig. 1.23: Idealized nitrogen isotope cycle in a small stratified lake. The isotopic signature of organic matter buried in sediments is influenced by nitrogen sources, rates of primary production and respiration, and the types of denitrification processes. Isotopic values for external sources of atmospheric and combined forms of nitrogen are from Kendall (1998). Isotope enrichment factors (ε) are from Fogel and Cifuentes (1993) and differ based on the form of inorganic nitrogen assimilated by lake algae. Note that Nitrogen isotopes are not fractionated by algal fixation of atmospheric $N_2$, and that the significance of nitrogen fixation can vary widely from lake to lake. Figure from Meyers and Teranes (2001).*

### Green algae and diatom remains

Green algae (Chlorophyta) encompass over 8000 recognized species with considerable morphological diversity, from unicellular to colonial forms (Fig. 1.24). Unicellular types are small (a few micrometers), whereas colonial, filamentous, and coccoid types can be macroscopic. Molecular genetic studies reveal the paraphyletic nature of the group, with certain green algae sharing an evolutionary lineage with higher plants (Kumar and Rzhetsky, 1996).

Diatoms, classified under Bacillariophyceae, are characterized by unique siliceous cell walls, featuring intricate valve patterning (Battarbee et al., 2001; Round, 1981a, 1984; Medlin et al., 1993). Ranging from 50 to 400 µm, they typically have a frustule formed by two overlapping valves (Fig. 1.25). Diatoms are divided into two main groups: the radially symmetrical centric diatoms and the axially symmetrical pennate diatoms. Pennate diatoms feature longitudinal subdivisions facilitated by a raphe, allowing gliding along substrates. Diatoms share common pigments such as chlorophyll-a and c2, as well as β-carotene, with accessory pigments like fucoxanthin, diatoxanthin, and diadinoxanthin giving many species a brownish hue. With diverse ecological lifestyles, diatoms

occupy planktonic, benthic, or meroplanktonic niches across various aquatic environments. They are particularly important in paleolimnology, serving as indicators of past environments due to their exceptional preservation and predictable distribution patterns in response to water chemistry (Hoek et al., 1995).


*Fig. 1.24: Light microscope photograph of green algae Desmodesmus sp. Arrow indicates an empty cell (from Demura et al., 2021).*

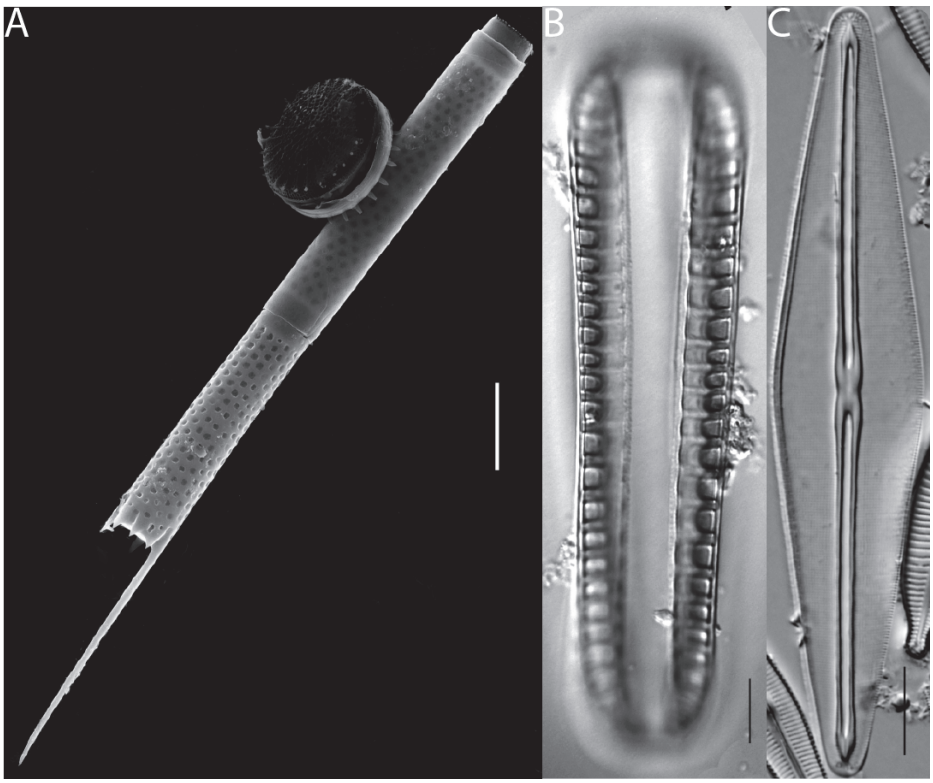


*Fig. 1.25: Scanning electron microscopy (SEM) images of the cell walls of three different diatom genera: A) Aulacoseira, B) Surirella, C) Frustulia. Scalebar = 10 µm.*

Diatoms are ubiquitous in aquatic environments worldwide, thriving in both planktonic and benthic habitats within lakes, shaping sediment records (Round, 1981c). Planktonic diatoms encompass holoplankton, meroplankton, and tychoplankton, with many species entering a resting phase to survive harsh conditions (Lund, 1954). Tychoplankton, originating from the benthos, are prevalent even in large lakes, cautioning against assuming all planktonic taxa are truly planktonic. Benthic diatoms reside in lake margins, their distribution into deeper water dependent on substrate availability and light penetration (Round, 1981c). Different communities, such as epilithon and epiphyton, share species but exhibit distinct dynamics influenced by substrate types and plant hosts. Epipsammon, adapted to dark, anoxic conditions, consists of small, firmly attached taxa capable of entering a resting phase until resuspended by wave activity (Jewson & Lowry, 1993). Epipelon, primarily composed of motile raphid taxa, thrives in low light conditions, navigating through mud interstitial waters to avoid burial. In shallow or clear lakes, sampling true epipelon can be challenging due to the presence of dead or resting cells from other habitats.

A significant physical factor controlling the distribution and composition of diatoms in lakes is temperature (Lotter et al., 1997; Weckström et al., 1997; Suzuki & Takahashi, 1995; Richardson et al., 2000). Studies suggest a potential for reconstructing past temperatures using diatom composition from sediment cores (Korhola et al., 2000). However, disentangling temperature specific influence from other lake variables remains challenging (Anderson, 2000). Light duration and intensity drive algal productivity and species composition in lakes (Reynolds, 1984; Maberly et al., 1994). Changes in light climate can impact plankton biomass and composition, with implications for benthic diatom communities (Schindler et al., 1996; Pienitz & Vincent, 2000). Turbulent mixing influences phytoplankton composition, especially during stratification periods controlled by temperature and wind (Reynolds, 1973; Bradbury & Dieterich-Rurup, 1993). Understanding these relationships is crucial for interpreting sediment records in paleolimnological studies.

Various chemical factors influence diatom composition, with nutrients, pH, and conductivity/salinity being significant. Specifically, nutrients, especially N, P, and silica, regulate diatom growth and species composition, with P often driving productivity changes (Tilman et al., 1982; Kilham et al., 1986; 1996). Furthermore, pH is crucial in freshwater systems, strongly influencing diatom species composition (Battarbee et al., 1999).

#### 1.3.3.2. The inorganic fraction

Chemical and mineralogical analyses of lake sediments provide insights into their history and characteristics (Last, 2001; Boyle, 2001). Chemostratigraphic approaches are useful to reconstruct erosion histories, pollution tracking, and nutrient dynamics. However, interpreting bulk elemental data alone is challenging without considering mineralogical composition (Prothero and Schwab, 2004). Describing sediments solely based on bulk chemistry can be misleading, limiting interpretive potential (Last, 2001). Integrating mineralogical data with elemental analysis is crucial for accurately reconstructing the lake history, offering genetic and paleolimnological details that chemical analysis alone cannot deliver. This integration enhances understanding of lacustrine sediment dynamics and history by distinguishing oxidation states and polymorphs (Boyle, 2001).

##### Minerals in lake sediments

The mineral composition of lake sediments is paramount for paleolimnologists, offering information related to sediment genesis, transport mechanisms, and past environmental conditions (Lewis, 1984). Three main mineral types—allogenic, endogenic, and authigenic—form lacustrine deposits. Allogenic minerals are brought into the lake from external sources, while endogenic minerals originate within the lake water and authigenic minerals form through diagenetic processes (Talbot & Allen, 1996). Detrital minerals reveal basin tectonics, sediment provenance, and climatic changes, aiding in reconstructing past drainage basin size and morphology (Olsen, 1990). Endogenic

minerals, like carbonates and sulfates, reflect past chemical and limnological conditions, while authigenic minerals such as sulphurs and iron oxides provide clues about environmental changes (Salvany and Orti, 1994).

Analytical methods such as X-ray diffractometry (XRD) and optical mineralogy are used to characterize lake sediment minerals (Last, 2001). Understanding these minerals enhances the interpretation of paleolimnological data, contributing to the reconstruction of past environmental conditions. Various studies emphasize the importance of mineral analysis in deciphering paleoenvironmental information, underlining its significance in paleolimnology.

#### Inorganic geochemical paleolimnology

Inorganic geochemical analysis of sediment has played a central role in palaeolimnology since its establishment as a research field (Boyle, 2001). Currently, inorganic geochemical methods complement general palaeolimnology studies, contributing significantly to multidisciplinary lake history research (Valero-Garcés et al., 1997). The common analytical method for elemental determination of lake sediments is XRF (Boyle, 2000). Combined with biological data, sediment chemical data offer comprehensive insights into long-term environmental change and recent human impact. Despite its speculative nature in the absence of biological methods, geochemical palaeolimnology remains valuable due to its cost-effectiveness and potential for preliminary data analysis and extrapolation.

An important objective of geochemical paleolimnology is to determine the provenances of the sedimentary components (Boyle, 2001). In palaeolimnology, understanding the origin and transport mechanisms of sediment components is essential. Multivariate analysis facilitates identification of end-member compositions, yet further research is needed to characterize potential source materials and account for particle size fractionation effects in the catchment/lake system (e.g., Birks et al., 2012). Data transformation and scaling help mitigate the influence of outliers, while Principal Component Analysis (PCA) provides a relatively objective assessment of relationships (Dean & Bhattacharya, 2008). Furthermore, mineralogical data can be used as a constraining variable of the geochemical composition by using Redundancy analyses (RDA). This provides further evidence on provenance analyses and delivery pathways (Giralt et al., 2008). Development of techniques in this area is crucial. Additionally, understanding how lake and catchment environments influence component concentrations is also of paramount importance.

Furthermore, geochemical paleolimnology has demonstrated to be a valuable indicator of human impacts through acidification, atmospheric pollution, exotic sediment introduction and anthropic erosion. Thus, inorganic geochemical paleolimnology also provides solid clues about the long-term catchment evolution. It is particularly useful for the assessment catchment weathering state. The interplay between weathering and sediment dynamics in catchment evolution underscores the complexity of environmental processes. Apparently, erosion enriches sediment with certain elements (K, Na, Mg) due to preservation within the mineral lattices prior to weathering, whereas depletion in such elements may indicate greater catchment stability due to enhanced leaching and destruction of alkali bearing minerals (Mackereth, 1966; Catalan et al., 2014). Furthermore, mineralogical fluctuations can also result from mechanical sorting of particle sizes or differences in source composition (Boyle, 2001). Therefore, significance of physical controls on element ratios highlights the need for comprehensive approaches in interpreting sediment records, incorporating both weathering processes and sedimentary dynamics (Moalla, 1997).

### 1.3.3.3. Facies models for lacustrine depositional systems

Facies models simplify transport, depositional, and diagenetic processes in lake sediments, aiding paleolimnologists in conceptualizing sediment sequences. However, heterogeneity among lakes

implies challenges, as models developed for one lake may not apply to others due to overlooked process differences. Sedimentologists analyze lacustrine facies at micro and macro scales, discerning variations in composition, texture, and structure reflecting local processes or larger-scale phenomena like infilling, climate change, or tectonic activity, crucial for understanding human impacts or long-term environmental changes (Cohen, 2003).

## Factors controlling lacustrine sedimentation

According to Cohen (2003), the sedimentation patterns in lakes are governed by six major factors, which include regional climate, geology, and human activities over the past millennia. These factors are intricately interconnected and often exhibit complex relationships. Understanding the interplay and feedback loops among these factors is a key challenge in paleolimnology. It is crucial to avoid overly simplistic interpretations that attribute observed deposition patterns solely to a single cause. Instead, recognizing the multifaceted nature of these interactions is essential for accurate paleolimnological interpretations (Fig. 1.26).

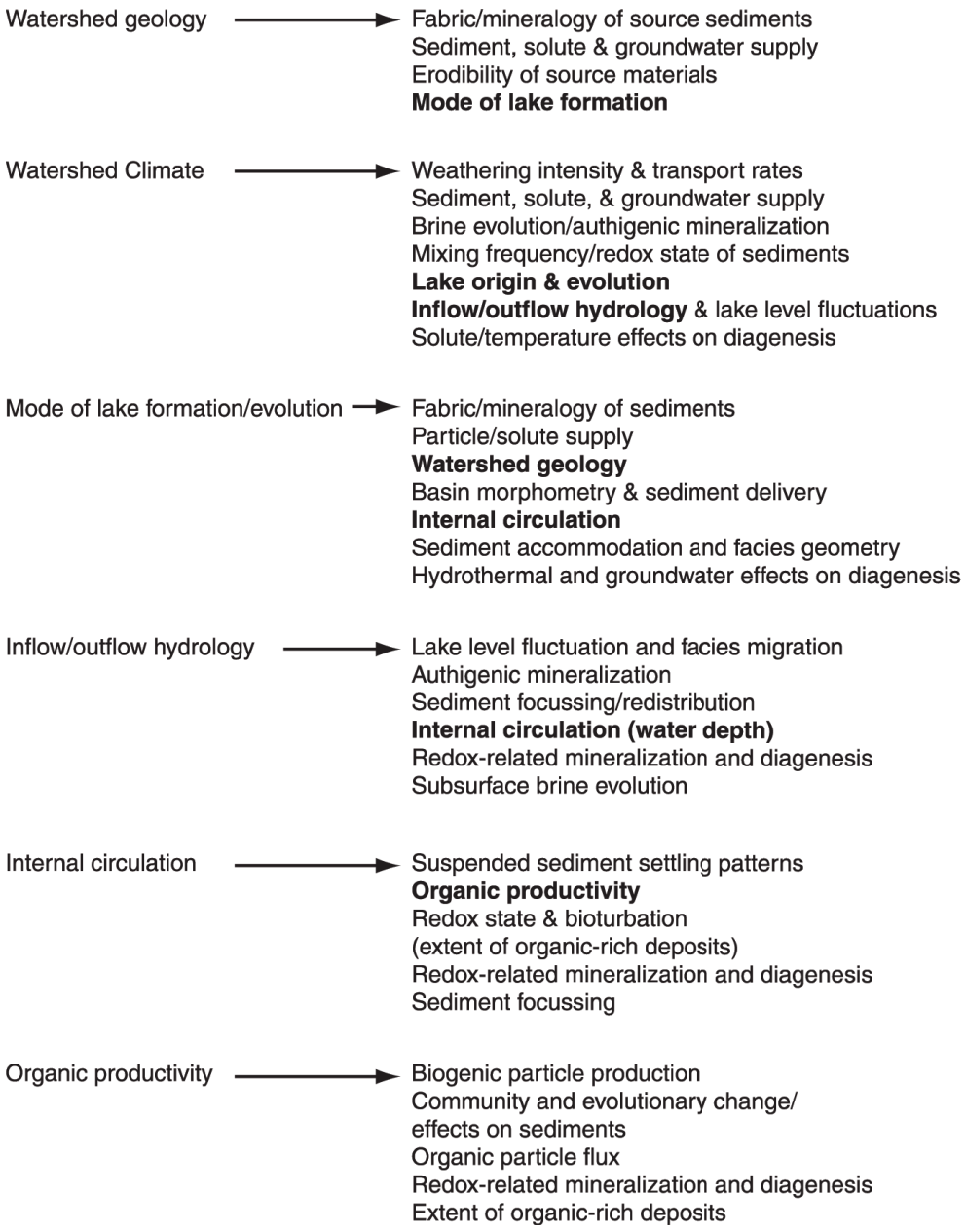


*Fig. 1.26: Key factors influencing the large-scale differences observed in lake sedimentation patterns, facies development, and facies geometry. These "major" factors are interconnected, influencing each other (in bold) through intricate interactions (figure from Cohen, 2003).*

### Watershed Geology

The topography, bedrock composition, and structure of a lake watershed greatly influence sediment input rates and geochemistry (Kalindekafe et al., 1996). Topography, affecting mass-wasting rates, leads to higher sediment accumulation downstream from mountainous areas. Geological characteristics like bedrock composition determine sediment texture and availability, impacting lakeshores differently based on rock type. Smaller lakes often have uniform geology, while larger ones show more complexity due to varied terrain and climate (Kalindekafe et al., 1996). Bedrock also influences water chemistry, affecting solute range, buffering capacity, and mineral formation, with certain types regulating runoff and sediment discharge rates in response to land clearing (Reid and Frostick, 1986).

### Watershed Climate

Local precipitation in a lake watershed affects vegetation, soil development, and erosion rates (Langbein & Schumm, 1958). These factors collectively influence sediment delivery rates and the chemical composition of particulate matter and dissolved solids entering the lake (Yemane et al., 1996; Yuretich et al., 1999). Climate-induced changes are evident in elemental concentrations and clay minerals deposited in lakes. For example, cold, dry climates favor chlorite-dominated clays, whereas warmer, wetter conditions promote kaolinite dominance (Yemane et al., 1996; Yuretich et al., 1999). In arid regions, sediment delivery is slower, dominated by wind-blown dust and chemical precipitates rather than clastic particles. Yet, transport accelerates with semi-arid precipitation levels of 300–400 mm $yr^{-1}$ (Langbein & Schumm, 1958). Vegetation growth seasonality in humid tropics can affect lake sediment yields more than mean annual precipitation (Walling & Kleo, 1979). Temperature also triggers sediment delivery patterns, influencing soil, vegetation, and ice development, with warmer temperatures generally leading to higher sedimentation rates (Itkonen & Salonen, 1994).

### Lake Formation and Evolution

The formation and maintenance of a lake basin play a crucial role in determining its sedimentary infill. Processes involved in creating and sustaining the basin, such as material excavation or elevation of depression margins, shape sedimentological variations (Pickrill and Irwin, 1983; Tiercelin et al., 1994). These differences stem from varying subaerial and subaqueous slopes linked to basin-forming processes, influencing basin morphometry. For example, steep lake margins from volcanic caldera collapse or glacial rock basins exhibit gravity flow deposits, while floodplain or wind deflation basins lack such deposits (Pickrill and Irwin, 1983; Tiercelin et al., 1994). In tectonic lakes, sediment composition often relates to basin structural contexts (Soreghan and Cohen, 1996). Long-term sediment accumulation rates in these basins are governed by underlying fault motion and subsidence rates, varying systematically across the lake floor.

### Inflow and outflow hydrology

The hydrological dynamics of lakes, influenced by upstream sources and downstream discharge, affect depositional patterns (Baker et al., 2009). Whether a lake is open or closed at its surface, determined by spillways, governs deposit variability. Open lakes with outlets experience minimal elevation changes due to balanced inflow and outflow. Conversely, closed lakes experience significant fluctuations, affecting sediment accumulation and environmental boundaries. These fluctuations lead to erratic delta shifts and shoreline erosion during low levels. Proglacial lakes, impacted by ice blockage and post-deglaciation rebound, show rapid level changes and sedimentary shifts. Climate influences lake persistence and groundwater dynamics, particularly in arid regions.

### Internal water circulation

Internal circulation and mixing play crucial roles in determining the redox state of sediments, their resuspension, and the accumulation of organic matter (Håkanson, 1982; Fillipi et al., 1998; Bloesch and Uelinger, 1986). Amictic and meromictic lakes offer finely resolved paleolimnological records due to limited resuspension and bioturbation (Håkanson, 1982). Sedimentary signals in such lakes can resolve monthly events, if not shorter durations (Håkanson, 1982). However, resuspension from bottom current activity diminishes sedimentary resolution, blurring seasonal signals and causing long-distance sediment transport (Bloesch and Uelinger, 1986). Vigorous circulation or slow accumulation can mix decades-old deposits, while fine particulate matter may remain suspended due to internal hydrodynamic mechanisms (Lee and Hawley, 1998). Horizontal transport and gravitational flows lead to sediment focusing, particularly in small lakes, where sediment accumulation rates vary based on sediment supply, settling, and resuspension (Davis and Ford, 1982; Ludlam, 1984).

#### Organic productivity

Changes in organic productivity within lakes have sedimentary consequences principally reflected in the accumulation rates of organic sediments, encompassing combustible organic matter, biogenic silica, and calcium carbonate precipitation (Hodell et al., 1998). Nonetheless, variations in heterotrophic consumption efficiency and organic matter solubility hinder direct interpretation of organic flux rates as productivity proxies (Hicks et al., 1994). Short-term productivity fluctuations are additionally influenced by phytoplankton debris settling rates, which are contingent upon factors like water depth, circulation, and particle dynamics (Haberyan, 1985; Pilskaln and Johnson, 1991). However, challenges in resolving short-term productivity changes solely from accumulation rate data persist due to particle degradation, resuspension, and grazing (Zohary et al., 1998).

### 1.3.3.4. Stratigraphy

#### Morphostratigraphy, lithostratigraphy and allostratigraphy

Stratigraphy involves categorizing rock bodies, including sediments, into distinct, mappable units based on their properties (Salvador, 1994). These properties encompass landform morphology, sediment characteristics, and sediment architecture. The organization of these units can be achieved through three approaches: morphostratigraphy, lithostratigraphy, and allostratigraphy.

Morphostratigraphy is the division of sedimentary units based on surface form. However, morphostratigraphical units often incorporate lithological criteria as well and, therefore, the spatial distribution of these units is typically depicted using geomorphological maps, which integrate both morphological and lithological aspects. This approach is extensively employed in Quaternary science, constituting a fundamental aspect of geomorphology (Hughes, 2007).

Terraced fluvial successions exemplify the widespread application of morphostratigraphy, where terrace surface age decreases with lower altitude due to fluvial aggradation and incision phases (Sancho et al., 2008). However, solely relying on surface morphology oversimplifies fluvial activity, obscuring terrace unit internal structure complexities. A more comprehensive understanding is achievable through three-dimensional alluvial stratigraphy, using spatial variability in surface form and lithological characteristics (Mackey and Bridge, 1995).

Lithostratigraphy involves classifying rock units based on observable lithological properties and relative stratigraphic positions (Salvador, 1994; Weerts and Westerhoff, 2007). Crucial for geological mapping, these units follow the Law of Superposition and require precise definitions and designated type sections (Salvador, 1994). Factors like sediment composition, texture, and sedimentary structures aid in their delineation. According to the International Stratigraphic Guide, type sections should encompass a range of geological features, including lithology, thickness, paleontology, mineralogy, structure, and geomorphic expression.

Allostratigraphy focuses on the correlation and interpretation of sedimentary deposits based on lithological characteristics and discontinuities. Unlike lithostratigraphy, which relies primarily on lithological similarities to define rock units, allostratigraphy emphasizes the significance of depositional breaks, such as unconformities or significant changes in sedimentary facies, in stratigraphic analysis (Rawson et al., 2002). These breaks represent periods of erosion, non-deposition, or changes in sedimentary environments, allowing the recognition of distinct packages of sedimentary layers known as alloformations or allosequences (Miall, 1997). Allostratigraphy aids in understanding the spatial and temporal relationships between sedimentary units (Salvador, 1994). Changes in lake levels over time are documented through palaeoshorelines, providing insights into moisture variations during the Quaternary period and allostratigraphy offers an objective means of grouping heterogeneous lacustrine deposits (Marx et al., 2009), facilitating the grouping of genetically related deposits within a single stratigraphic unit. Erosion events within lake basins, indicative of significant geomorphological changes, are associated with major lake level regressions or subaqueous debris flows. An allostratigraphic approach facilitates grouping heterogeneous deposits within a single unit based on discontinuities, favoring the understanding of the latter, while a lithostratigraphic approach divides deposits into separate units, facilitating the comprehension of gradual environmental changes. A combined approach may also prove beneficial for lacustrine sequences (Räsänen et al., 2009).

### Sequential stratigraphy in lakes

As defined by Catuneanu (2002), sequential stratigraphy is the most recent and perhaps the most revolutionary paradigm in sedimentary geology, revolutionizing methods of stratigraphic analysis. Unlike other more conventional types of stratigraphic analysis, such as biostratigraphy, lithostratigraphy, or magnetostratigraphy, which essentially involve data collection, sequential stratigraphy is built up by considering two key factors: the reconstruction of allochthonous control parameters at the time of sedimentation, and the prediction of facies architectures in areas not yet studied. Key principles of sequence stratigraphy include the recognition that sequence boundaries occur across various scales, indicative of both short-term and long-term base level adjustments. These adjustments control erosion and deposition processes throughout the depositional system, also known as a systems tract, spanning from upland areas to lake basins. Depositional styles within a systems tract are intricately linked to relative base level status, dictating sediment distribution patterns. It has become evident that large sediment bodies are typically demarcated by erosion or nondeposition surfaces, reflecting fluctuations in relative base level—a concept encompassing the elevation of a receiving basin (e.g., a lake) relative to sediment sources. These fluctuations can stem from various factors such as changes in lake level, tectonic uplift, subsidence, or other forcings. Such surfaces give rise to sedimentary sequences, studied under the discipline of sequence stratigraphy (Cohen, 2003). Although originally developed for marine sediments, sequence stratigraphy principles are also applicable to lacustrine settings. However, lakes differ notably from oceans due to their frequent and significant elevation changes, as well as the absence of a globally consistent eustatic pattern. The study of stratigraphic sequences in lake basins enables paleolimnologists to assess major shifts in relative lake level, aiding in the differentiation of factors such as sediment supply, subsidence, and climate impact on basin infilling. (Bohacs et al., 2000). Terraces are commonly found near or at the surface of lakes, formed by erosion and deposition processes (Adams and Wesnousky, 1998). During periods of falling lake levels, these terraces can become exposed, allowing for their elevation to be measured.

Sequence stratigraphy aims to understand and interpret the vertical and lateral relationships of sedimentary rocks in the context of water-level changes and related depositional processes. This scientific approach provides a framework for recognizing, correlating, and predicting the distribution of sedimentary successions, ultimately contributing to a comprehensive understanding of Earth's

dynamic geological history (Carrion-Torrente, 2023). The sequence stratigraphic methodology provides a genetic, process-based analytical approach to stratigraphic interpretation that necessarily involves conceptual depositional models (Catuneanu et al., 2011).

The sequence stratigraphy model integrates multiple types of data to improve interpretation of sequences. Sequences are hierarchical levels, ranging from second-order to lower ranks, ranging from allogenic such as eustatic, tectonic, and climatic, to autogenic processes like sediment supply. All sequences are bounded by sequence stratigraphic surfaces and can be subdivided into component systems of corresponding hierarchical rank (Catuneanu, 2019). Hence, the identification of these sequence stratigraphic surfaces (Fig. 1.27) is essential for understanding how sedimentary successions are structured. These surfaces act as boundaries between sequences, defining stratigraphic units that represent different sedimentary reactions to water-level fluctuations (Zecchin and Catuneanu, 2013).

Once sequence stratigraphic surfaces are identified, stratigraphic sequences can be subdivided into system tracts, which are linked to specific shoreline trajectories. Systems tracts, defined by Brown and Fisher (1977), represent distinct stratal units characterized by their stacking pattern and bounding surfaces, dividing a sequence. These tracts categorize sequences based on shoreline trajectories, including transgression, normal regression (lowstand or highstand), and forced regression. Types of systems tracts include: Transgressive Systems Tract (TST), Normal Regressive Systems Tract (comprising Highstand - HST, and Lowstand - LST), and Falling-Stage Systems Tract (FSST) (Fig. 1.27):

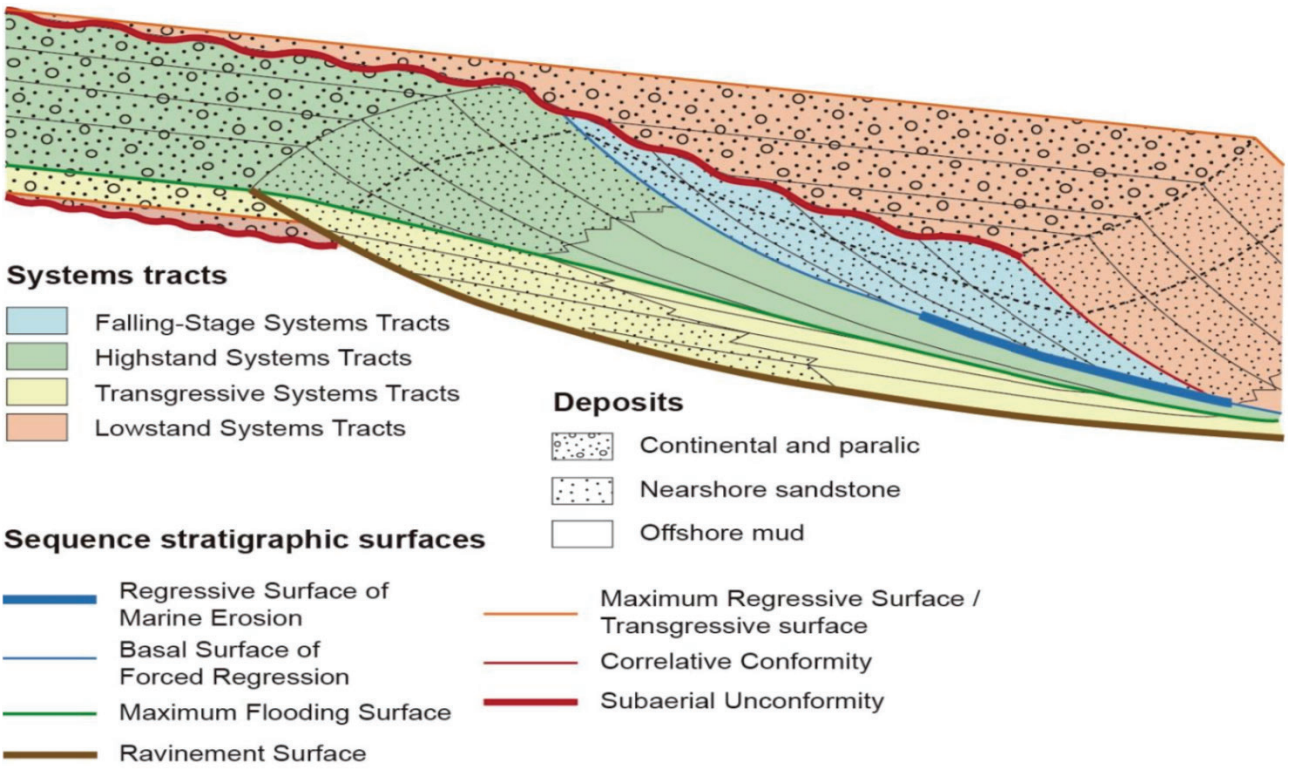


*Fig. 1.27: Sequence stratigraphic surfaces and systems tract beds, encompassing continental to offshore deposits. Figure from Carrion-Torrente (2023) after adapted from Zecchin and Catuneanu (2013).*

(1) Transgressive Systems Tract (TST): It is characterized by retrogradational stacking patterns, marked by the presence of the Maximum Regressive Surface (MRS) and/or Ravinement Surface (RS) at the base, and the Maximum Flooding Surface (MFS) at the top. This retrogradational architecture reflects conditions where accommodation creation rates exceed sediment supply rates

at the shoreline, often resulting in a deepening-upward trend in shallow environments (Catuneanu, 2002, 2006).

(2) Normal Regressive Systems Tract (Lowstand and Highstand): These deposits display both progradational and aggradational depositional trends (Fig. 1.27). The Lowstand Systems Tract (LST) lies between forced regressive strata below and transgressive strata above, or between two Falling-stage Systems Tract units. It is marked by the Subaerial Unconformity (SU) and Correlative Conformity (CC) at the base, and the Maximum Regressive Surface (MRS) and/or Ravinement Surface (RS) at the top. The Highstand Systems Tract (HST) starts at the Maximum Flooding Surface (MFS) and ends at the SU with the Basal Surface of Forced Regression (BSFR), or the MRS if the Falling-stage Systems Tract is absent, and/or the Regressive Surface of Marine Erosion (RSME). Normal regressions are driven by sediment supply, leading to shallowing-upward trends near the shoreline but may differ in deeper basin areas. They typically form sedimentary bodies with clinoforms, including continental, deltaic, shoreface/shelf, shelf margin, and deeper marine sediments (Catuneanu, 2006, 2019; Zecchin and Catuneanu, 2013)

(3) Falling-Stage Systems Tract (FSST): They comprise forced regressive deposits and display diagnostic progradational and downstepping stacking patterns. It is bounded by the BSFR, the RSME and the SU at the base and by the SU with its Correlative Conformity– CC at the top, potentially truncated by younger RS (Fig. 1.27).

### Rhythmites and varves

Rhythmites, characterized by alternating sediment types, such as couplets or more complex patterns like triplets, serve as valuable tools for reconstructing terrestrial climate records due to their high-resolution nature (Cohen, 2003). These sediment sequences, composed of clastic, chemical, and organic deposits, help to understand the diversity of processes influencing each rhythmite component (Shunk et al., 2009).

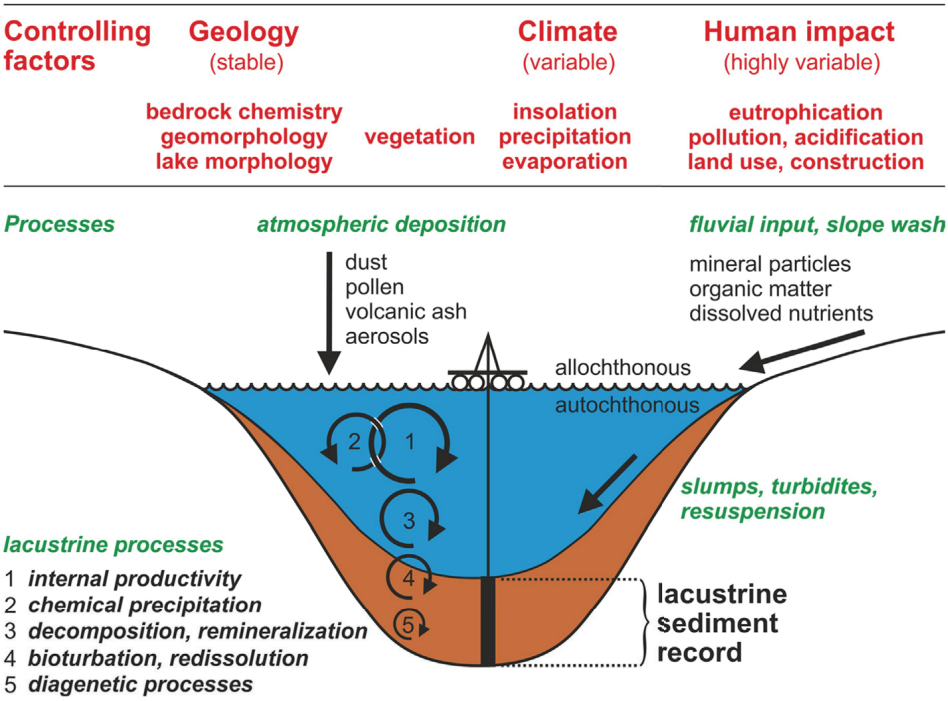


*Fig. 1.28: Formation of lacustrine varved sediments: controlling factors and processes. Adapted from Zolitschka et al. (2015).*

Annually laminated lake sediments, commonly referred to as varved sediments, provide distinct chronological records with data proxies resolved by seasons (e.g., Brauer et al., 1999; Czymzik et al., 2016; Martin-Puertas et al., 2012; Neugebauer et al., 2012; Zahrer et al., 2013; Zolitschka et al., 2015). The formation and preservation of varved sediments thrive under low-energy hypoxic to anoxic bottom water conditions, where oxygen depletion inhibits burrowing organism activity and minimizes post-depositional disturbances (Brauer, 2004; Zolitschka et al., 2015). These conditions are conditioned by lake stratification, mixing and productivity (Dragër et al., 2017) (Fig. 1.28). Varved sediment records facilitate quantitative reconstructions of past climates, assessments of ecosystem responses to climate change, evaluations of human impacts, and absolute calendar-year dating (Lotter and Birks, 1997; Van Daele et al., 2014; Nakagawa et al., 2012).

In temperate climates, well-developed soils and vegetation in the catchment area limit mineral influx into lakes. Chemical weathering in this environment produces clay minerals and releases nutrients employed by catchment area plants. Organic matter from litter or soil enters lakes, forming biogenic varves reflecting annual productivity cycles (Fig. 1.29). High lake productivity may induce eutrophication preserving biogenic varves. Dissolved oxygen fluctuations, especially in the hypolimnion, influence lake stratification, potentially causing meromixis and varve formation. Nutrient redistribution during mixing triggers algal blooms with diatoms prominent in sediment records. These diatoms contribute to varve composition with siliceous diatom frustules being well-preserved in sedimentary records (Fig. 1.29). Winter runoff events transport minerogenic and organic matter into lakes, contributing to varve formation. The composition of varves can vary over time depending on runoff intensity, reflecting fluctuations in environmental conditions. (Wehrli et al., 1997).

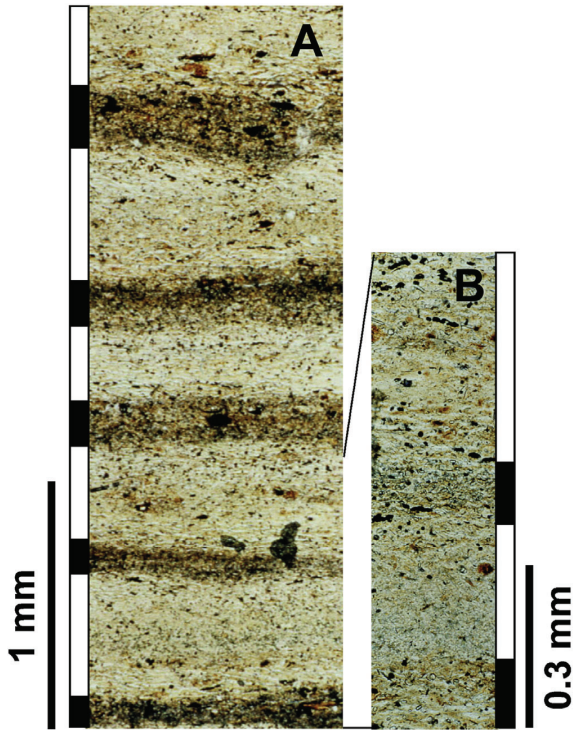


*Fig. 1.29. Example of biogenic varves from Lake Holzmaar in Germany (Zolitschka et al., 2000). (A) Macroscopic photograph of pale diatom laminae and dark organic detritus. (B) Microscopic photograph in normal light documents the internal structure of biogenic varves. Massive planktonic diatom blooms produce pale laminae, whereas dark laminae contain larger benthic and epiphytic diatoms as well as dark spots of organic matter and pyrite. The black and white bars on the left or right of the images indicate the dark and pale sublaminae of annual layers. (Adapted from Zolitschka et al. 2015).*

In the 1980s, known varved lakes were concentrated in specific regions such as the European Alps, northern Sweden, Finland, northeastern North America, and the East African Rift System (O'Sullivan, 1983). However, a recent global inventory of 143 varved lake chronologies, known as the updated Varves DataBase (VDB), shows a more evenly distributed availability of varve records worldwide (Ojala et al., 2012). Initially, the discovery of varved sedimentary records predominantly occurred in lakes across recently deglaciated terrains and was often serendipitous, but more recent findings have been guided by empirical considerations such as water depth and meromictic conditions (O'Sullivan, 1983; Anderson et al., 1985).

Research suggests that annually laminated sediments are commonly found in lakes with water depths exceeding 10 m and rarely occur between 5 m and 7 m (Ojala et al., 2000; Zillén et al., 2003). Moreover, laminated sediments are more likely to be found in relatively deep lakes with small surface areas compared to shallow lakes with large surface areas (Tylmann et al., 2013). Ideal conditions for the formation and preservation of varved sediments include a lake deeply incised into the catchment area and surrounded by elevated terrain and forests to limit wind-driven mixing (Tylmann et al., 2012).

The presence of an annual rhythm in varves allows for consecutive layer counting to establish their chronological sequence. With the inclusion of an absolute anchor, such as the topmost varve representing the year of coring, precise and continuous calendar-year chronologies can be established by counting back through time (Zolitschka et al., 2015). Even in the absence of an anchor point, a floating varve chronology still offers precise relative time control. This tight chronological precision provided by varve counting offers a significant advantage over other dating techniques like radiometric dating, which often rely on discrete sampling and interpolation methods (Zolitschka et al., 2015).

Various methods, including microstratigraphic analyses of thin sections (Brauer, 2004), digital image analysis (Francus, 2004), and μ-XRF-based techniques (Marshall et al., 2012), are used for this purpose, each with its advantages and disadvantages.

## 1.4 The North Atlantic region

### 1.4.1 Atmospheric patterns in the North Atlantic region

The large geographic variability of the vast North Atlantic confers this oceanic region with a wide range of interdependent climates, from tropical and subtropical to oceanic and arctic. The interannual and interdecadal variability of these climates is mainly controlled by the Tropical Atlantic Variability at low latitudes, whereas the NAO, stretchily related with the Arctic Oscillation, do at mid and high latitudes (Fig.1.30; Marshall et al., 2001). Therefore, a better understanding and a longer timescale perspective of the North Atlantic atmospheric dynamics can help to unmask future climate change impacts (Tierney et al., 2020) affecting Western Europe in the upcoming decades (e.g. extreme weather events associated with the weakening and/or migration of the jet stream; Mellado-Cano et al., 2019; Woollings and Blackburn, 2012; Francis and Vavrus, 2015; Guo et al., 2021; Osman et al., 2021; Kidston et al., 2015). These changes, partly induced by decadal-scale variations of atmospheric modes of variability, affect agricultural harvests, water management, energy supply and demand, primary activities over both land and sea, etc. (Hernández et al., 2020a; Trigo et al., 2002; 2004; Jerez et al., 2013; Costas et al., 2012; García Herrera et al., 2007), thereby affecting the welfare of millions of people and the equilibrium of numerous environmental cycles in the north Atlantic regions (Hurrell et al., 2003).

The NAO is widely acknowledged as the predominant mode of winter climate variability in the North Atlantic region, contributing significantly to year-to-year climate fluctuations in the Northern Hemisphere (Hurrell, 1995; Wanner et al., 2001; Hurrell and Deser, 2010). It explains around 40%

of the variability in winter sea-level pressure (SLP) in this area (Pinto and Raible, 2012). However, a more comprehensive understanding of regional SLP and climate variability requires consideration of other lesser-known modes of variability. The East Atlantic (EA) and Scandinavian (SCA) patterns have emerged as important contributors to winter climate in Europe (Fig 1.31; Comas-Bru and McDermott, 2014; Hall and Hanna, 2018), impacting the sensitivity of climate variables like temperature and precipitation to the NAO. The interaction between these modes has significant effects on climates across different spatial and temporal scales (Fig. 1.32), with implications for ecosystems and societies (e.g., Jerez and Trigo, 2013; Bastos et al., 2016), and potential consequences for resources such as wind energy (Zubiate et al., 2017).

The NAO involves the redistribution of air masses between the Arctic and the subtropical Atlantic, characterized by a north–south dipole of SLP anomalies associated with the Azores High and the Icelandic Low (Hurrell, 1995) (Fig. 1.30). The NAO influences the extratropical zonal flow and exhibits fluctuations between positive and negative phases, leading to significant changes in surface air temperature, winds, storminess, and precipitation across Eurasia, northern Africa, Greenland, and North America (Hurrell and Deser, 2010). Traditionally, the NAO is quantified using an index calculated as the difference in normalized SLP between specific locations such as Iceland and the Azores, Lisbon, or Gibraltar (Cropper et al., 2015; Rogers, 1984; Hurrell and van Loon, 1997). However, alternative methods like empirical orthogonal function analysis (EOF) offer robust alternatives for defining the NAO index (NAOi) (Folland et al., 2009).

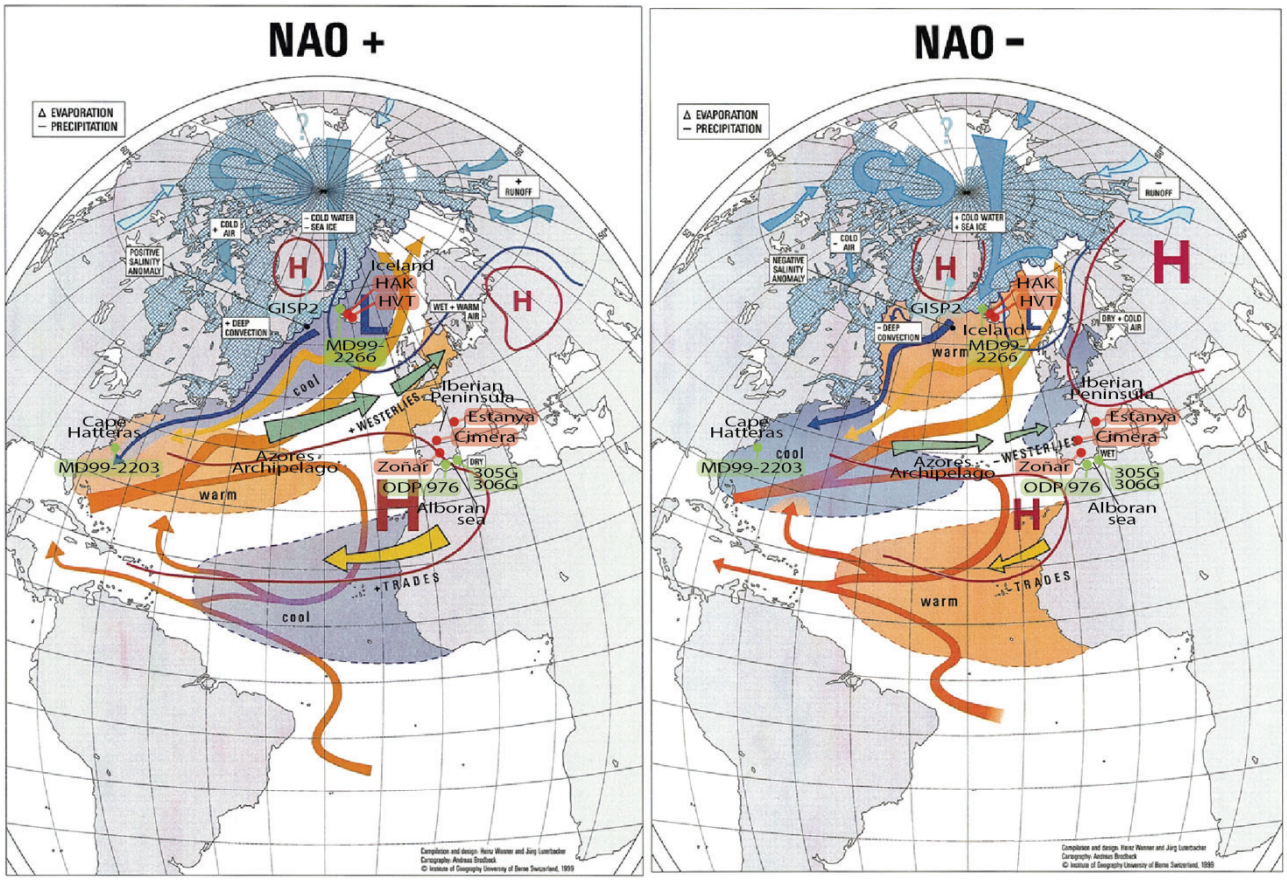


*Fig. 1.30: A visual representation of the two phases of the North Atlantic Oscillation (NAO): A) the positive phase ($NAO^+$) and B) the negative phase ($NAO^-$). Shading areas indicate sea surface temperatures (SSTs) outlined by dashed contours, and sea-ice extent. Arrows show the flow systems in the ocean (light red and blue), atmosphere (green and yellow arrows represent the westerly and trade winds, respectively) and rivers. Solid blue and red contours represent Sea Level Pressures (H=high, L=Low), and white rectangles denote characteristic climate conditions or important processes. The representation includes the location of*

*paleoclimatic records discussed in subsequent sections: lacustrine records (red dots), marine records (green dots) and ice records (blue dot). Figure adapted from Wanner et al. (2001).*

The EA pattern, recognized as a significant climate variability mode in the North Atlantic region Fig. 1.31), exhibits variability in its depiction across studies. It was initially identified by Barnston and Livezey (1987) through EOF analysis. However, the precise representation of its EOF loadings remains a subject of debate. Some researchers depict it as a north-south dipole of anomaly centers stretching across the North Atlantic (Bastos et al., 2016; Chafik et al., 2017), while others characterize it as a distinct SLP monopole near Iceland and Ireland (Josey and Marsh, 2005; Moore and Renfrew, 2012; Comas-Bru and McDermott, 2014; Zubiate et al., 2017; Comas-Bru and Hernandez, 2018). Despite this disparity, its primary center consistently aligns along the nodal line of the North Atlantic Oscillation (NAO), suggesting a southward shifted NAO with associated shifts in the North Atlantic storm track and jet stream towards lower latitudes (Woollings et al., 2010) (Fig. 1.32). Various methods are employed to derive an index for the EA (EAi), including EOF analyses (Barnston and Livezey, 1987; Comas-Bru and McDermott, 2014; Moore et al., 2013) or rotated principal component analysis. Additionally, the SLP instrumental series from Valentia Observatory, Ireland, has been used in a limited number of studies (Comas-Bru et al., 2016; Comas-Bru and Hernandez, 2018). The positive phase of the EA typically features robust positive SLP anomalies offshore Ireland, resulting in below-average surface temperatures in southern Europe, drier conditions over western Europe, and increased precipitation across much of eastern Europe and the Norwegian coast (Moore et al., 2011; Rodríguez-Puebla and Nieto, 2010). The EA, shifted southeastward from the NAO and with a more zonal disposition (Hernández et al., 2020a; Mellado-Cano et al., 2019), plays a key role in the modulation of the NAO southern centre of action (Comas-Bru and McDermott, 2014; Hernández et al., 2020a; Mellado-Cano et al., 2019) (Fig. 1.32). This modulation impacts weather patterns across Europe, influencing temperature and precipitation distributions. Understanding the dynamics and spatial characteristics of the EA pattern is essential for comprehending the broader climate variability in the North Atlantic region and its implications for regional climate conditions.

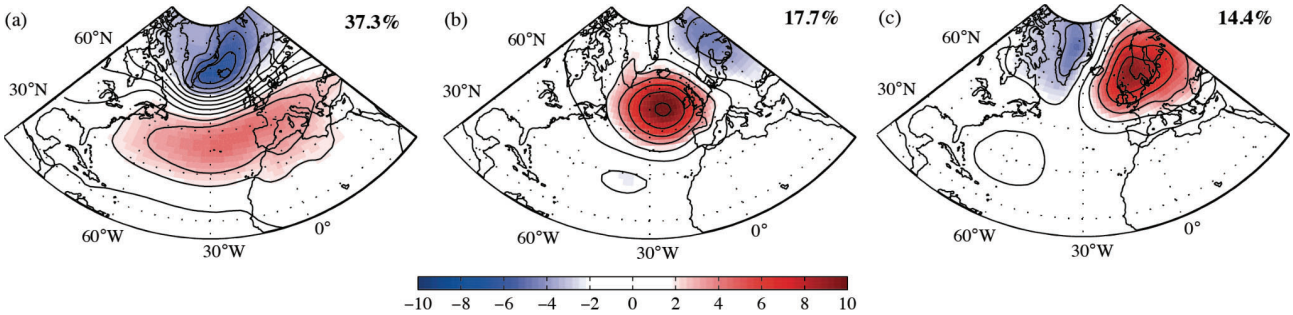


*Fig. 1.31: Spatial representation of the first three eigenvectors of the gridded winter (DJF) monthly sea-level pressure anomalies for the North Atlantic region (1872–2009) calculated using the 20CRv2 global dataset (Compo et al., 2011): (a) North Atlantic Oscillation (NAO), (b) East Atlantic pattern (EA) and (c) Scandinavian pattern (SCA). The empirical orthogonal function (EOF) was performed using the cross-correlation matrix. Percentage are the values of total variance explained by each eigenvector. (Adapted from Comas-Bru and McDermott, 2014).*

The SCA pattern, considered the third leading mode of winter SLP variability in Europe (Fig. 1.31), exhibits a center at 60-70° N, 25-50° E, equivalent to the Eurasia-1 pattern. To date, temporal indices of the SCA have primarily been derived using EOF analyses (Comas-Bru and McDermott, 2014; Crasemann et al., 2017; Moore et al., 2013) and rotated principal component analysis (Bueh and Nakamura, 2007; CPC, 2012). During the positive phase of the SCA (Comas-Bru and McDermott, 2014; Crasemann et al., 2017; Moore et al., 2013), higher-than-average pressure anomalies typically occur over Fennoscandia, western Russia, and, in some cases, northern Europe. This may lead to blocking situations, causing dry conditions over Scandinavia, below-average temperatures in central

Russia and western Europe, and increased precipitation in southern Europe (Bueh and Nakamura, 2007; Crasemann et al., 2017; Scherrer et al., 2006).

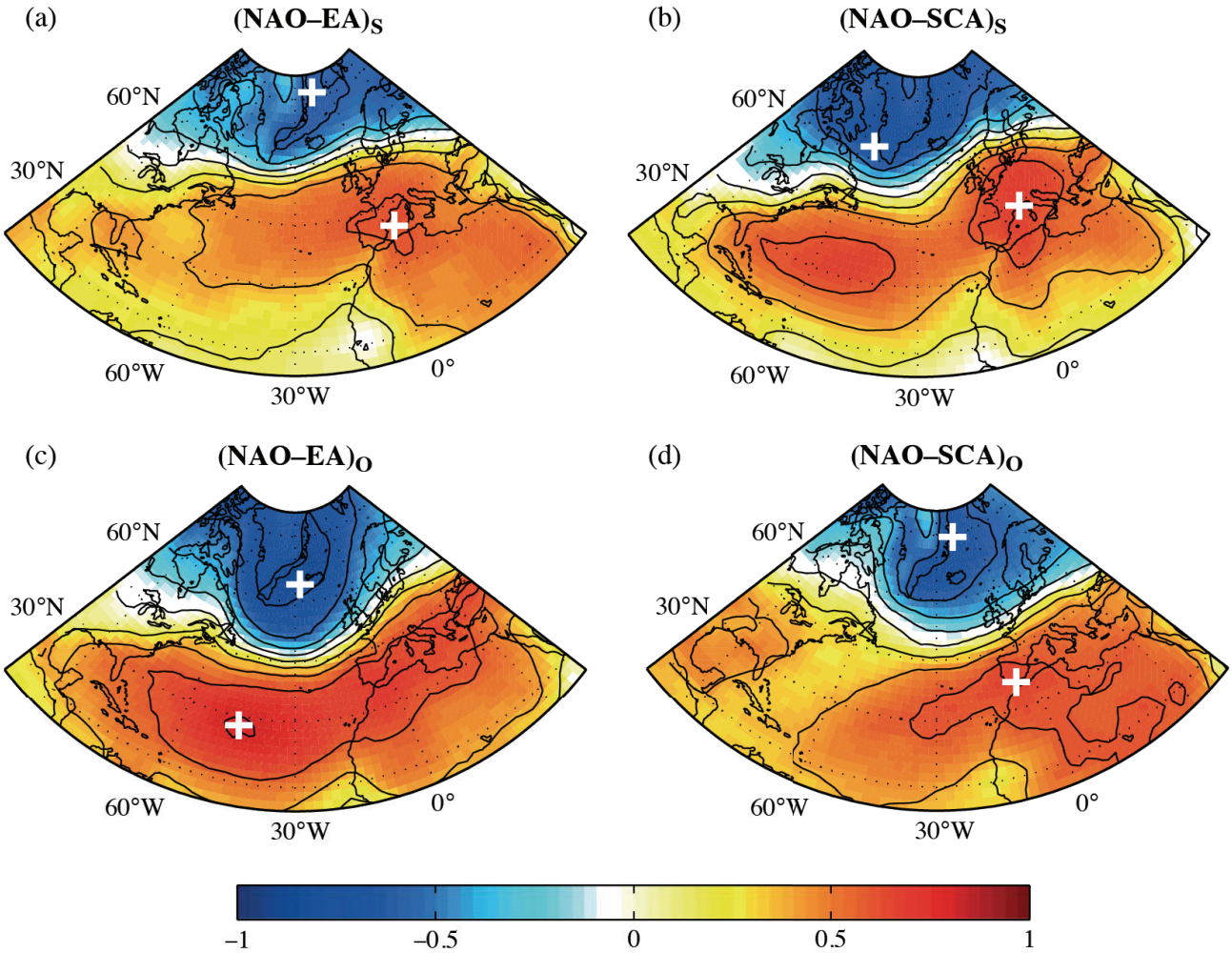


*Fig. 1.32: Spatial correlations between winter sea-level pressure and the NAOi for combinations of the other indices: (left) NAOi–EAi combinations based on (a) 51 winters of indices of the same sign, and (c) 57 winters of opposite sign; (right) NAOi–SCAi combinations based on (b) 56 winter of indices of the same sign, and (d) 52 winters of different sign. NAOI, North Atlantic Oscillation index; EAI, East Atlantic index; SCAI, Scandinavian index. White crosses indicate the location of the strongest correlated grid cells. (Adapted from Comas-Bru and McDermott, 2014)*

### 1.4.2 Oceanic Islands in the North Atlantic - The Macaronesia

Genuine islands are categorized into three groups: continental islands, continental fragments or microcontinents, and oceanic or volcanic islands. Oceanic islands, like those in the Macaronesian region, originate from volcanic activity, lacking continuous life from the ocean floor due to magma accumulation over millions of years. Their lifespans vary greatly, from short-lived instances to long-standing examples. These islands form through various processes, including volcanic arches above subduction zones, volcanic structures associated with central oceanic ridge systems, and mantle plumes within intra-plate settings. Despite their potential for significant height and size, oceanic islands typically remain relatively small (Fernández-Palacios, 2011).

Volcanic ocean islands grow and evolve by the action of several geological processes. Their present-day morphology is the result of the activity of volcanic, erosional, depositional, tectonic, isostatic, eustatic, and mass-wasting processes (Ramalho et al., 2013). Oceanic hotspot islands are prominent, dynamic geological features that rise from the deep seafloor. Volcanic edifices

architecture in oceanic islands, derive from a balance between constructive tectonovolcanic processes and destructive processes (Azevedo and Portugal Ferreira, 1999). This ongoing battle between construction and destruction shapes coastlines over time. The dynamics of this interaction vary across space and time, ruling the evolution of island edifices (Ramalho et al., 2013; Casalbore et al., 2015; Quartau et al., 2018a). The impact of these processes on the geomorphological features of the above-water sections of volcanic islands is thoroughly understood (e.g., Thouret, 1999; Ricchi et al., 2020).

Volcanic islands are predominantly formed underwater, making the study of their submarine areas crucial for gaining comprehensive insights, as they offer more information than above-water counterparts. Previous research focused on large-scale instability processes, but less on volcanism, erosion, tectonics, sediment supply variations, and climatic/oceanographic conditions on the surrounding shelves. High-resolution surveys in recent years revealed the importance of insular shelves for understanding geological history. These surveys emphasized the need for further research in this area (Masson et al., 2002; Mitchell et al., 2002; Ricchi et al., 2018; Romagnoli et al., 2018).

The Macaronesia constitutes a biogeographic region composed by four main archipelagos (Cabo Verde, Canary Islands, Madeira and Azores), which are distributed from tropical to subtropical latitudes within the eastern half of the north Atlantic Ocean (14º - 39º N and 13º - 31º W) (Fig. 1.33). These islands share similar geological and ecological characteristics due to their volcanic origins and isolation. The orography within these archipelagos is characterized by pronounced elevation gradients from the coastal lowlands to the interior highlands (Fig. 1.33). The Macaronesian climate varies from subtropical to tropical, with lush vegetation and diverse ecosystems, including cloud forests, laurel forests, and desert landscapes.

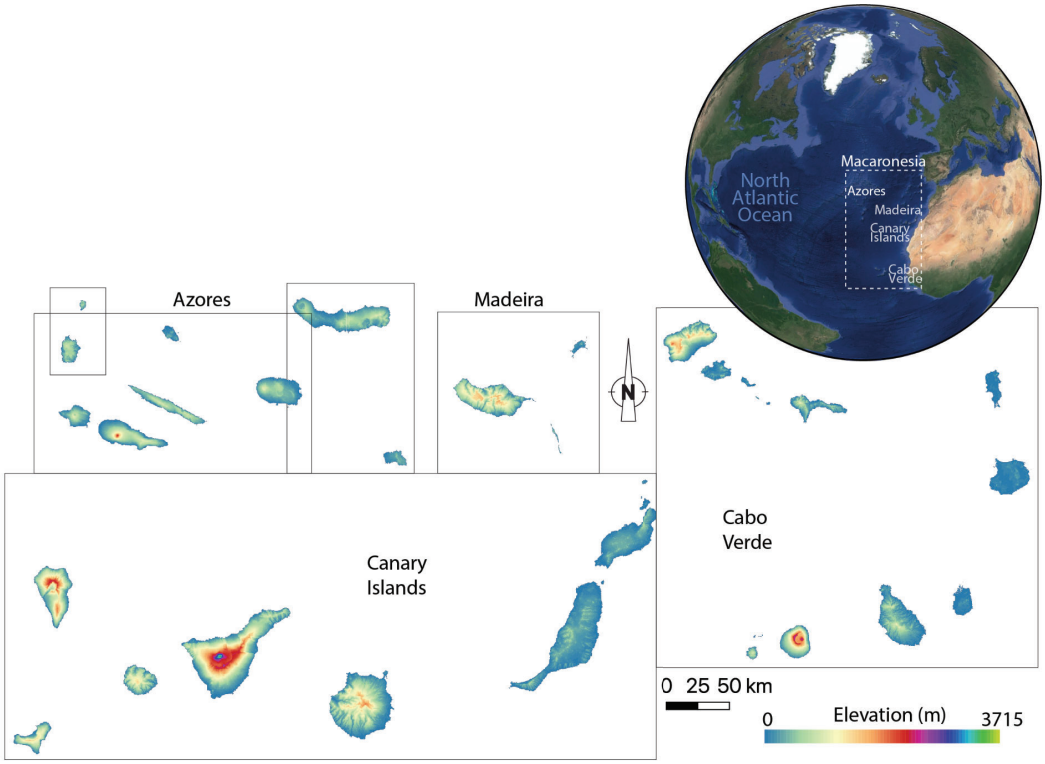


*Fig.1.33: The Macaronesia in the context of the North Atlantic Ocean. Azores, Madeira, Canary Islands and Cabo Verde are represented. Color scale shows the topography of each island.*

The Azores Archipelago, located west of Portugal, consists of nine major islands formed by volcanic activity along the Mid-Atlantic Ridge. Madeira island, situated southwest of Portugal, is composed of two inhabited islands and several smaller islets, all formed by volcanic eruptions. The Canary

Islands, located off the northwest coast of Africa, comprise seven main islands formed through volcanic activity associated with hotspots and rift zones. The Cape Verde Islands, situated off the coast of West Africa, consist of ten main islands formed by volcanic eruptions.

### 1.4.2.1. Sentinels of the Anthropocene onset and human environmental degradation

Human activities have profoundly impacted ecosystems globally, prompting debates on establishing pre-human baselines and defining the Anthropocene era (Barnosky et al., 2017). Archaeological and paleodata provide information about human impacts on continental systems (Malhi et al., 2016), and, in turn, recent colonization of remote oceanic islands provides precise records of ecosystem dynamics (Nogué et al. 2021). Island ecosystems facilitate quantifying the transition from prehuman to human-dominated states and assessing anthropogenic impacts within long-term ecological contexts.

Fossil pollen time series analysis from various islands reveals that human arrival systematically accelerated directional compositional changes, significantly surpassing natural perturbations (Nogué et al., 2021) (Fig. 1.34). Although the timing and magnitude of ecological changes vary among islands, general trends indicate substantial increases post-human colonization (Fig. 1.34). These findings show the effects of human arrival on island ecosystems, with irreversible ecological legacies persisting for centuries (Wilmshurst et al., 2014; Nogué et al. 2021).

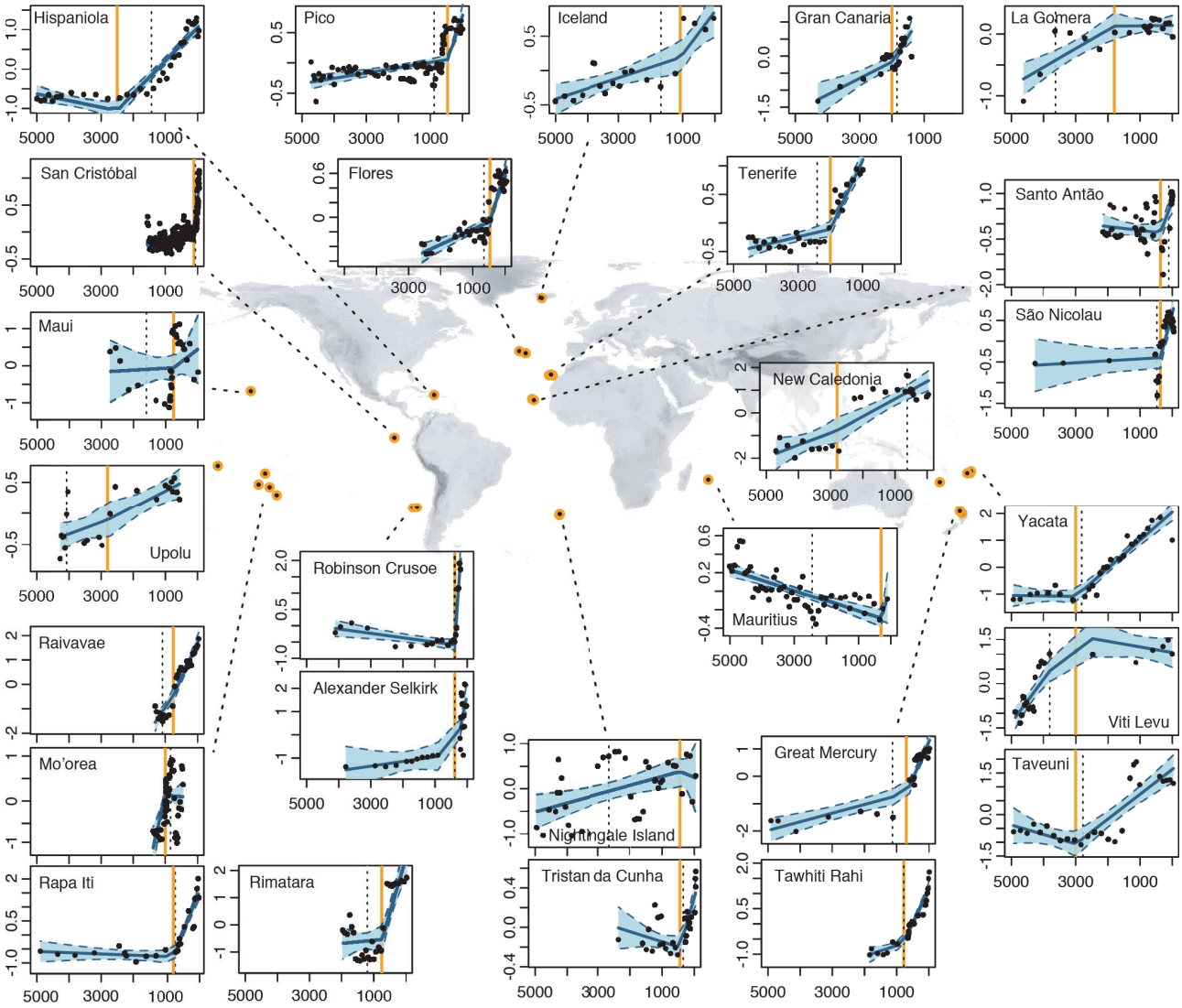


*Fig. 1.34: Human arrival accelerated compositional turnover on islands. Global analysis of rate of palynological and thus vegetation compositional turnover (slope of the line) for 27 representative fossil pollen records from*

*sedimentary sequences. The x-axes display calibrated years before present, whereas the y-axes represent the main gradient in pollen composition. These plots show results of breakpoint analyses of the rate of compositional turnover, with the date of human arrival indicated by the vertical orange lines. Scaling varies among panels. Shaded areas represent 95% confidence intervals, and optimized breakpoint, denoted by the vertical dashed black lines, indicate significant shifts in turnover rate. Adapted from Nogué et al. (2021).*

In addition to historical documents, lake sediment provides anthropogenic information from periods before historical records were available. However, it is generally difficult to discriminate anthropogenic information in sediment from natural information.

### *Rate of Change Analysis*

Quantifying spatiotemporal changes in biological composition or diversity is crucial for addressing the current biodiversity crisis and for disentangling underlying drivers, including climate change, land-uses, pollution, or introduction of invasive species (e.g., Steinbauer et al., 2018). Long-term observational studies spanning several decades to a century are increasingly valued for their ability to provide knowledge into these changes (Magurran et al., 2019). Such studies have revealed significant compositional shifts in recent decades and centuries, driven by human activities and climatic variations (Mottl et al., 2021; Seddon et al., 2015; Shuman et al., 2005). However, similar rates of change (RoC) have also been detected over longer geological time scales, suggesting complex interactions between natural and anthropogenic influences (Kemp et al., 2015). To understand the impacts of human activities on ecosystems, it is imperative to compare temporal changes in species composition and diversity through human history. This requires investigating whether observed changes are unique to the period of human influence or if they predate human-dominated systems (Birks et al., 2016; Mottl et al., 2021; Nogué et al., 2021). Paleontological data from terrestrial and marine proxies offer valuable information related to these changes, delivering a historical perspective that extends beyond the time frame of human observations.

RoC analysis has emerged as a valuable tool in paleoecology for quantifying temporal changes in compositional diversity. It measures the rate and magnitude of compositional change within a stratigraphic sequence, allowing the comparison of rates of change within and between sequences (e.g. Birks and Ammann, 2000; Birks and Birks, 2008; Correa-Metrio et al., 2012; Urrego et al., 2009). Despite its widespread use in paleoecology, there is a need for further exploration of the methodology underlying RoC analysis and its implications (see Birks, 2012).

Different approaches to estimate RoC (Bennett and Humphry, 1995; Birks, 2012) involve various techniques, such as transforming stratigraphical levels, smoothing data, and selecting dissimilarity metrics. However, these choices can lead to challenges, including sensitivity to temporal sampling variation, lack of standardization between studies, and the influence of intrinsic sequence properties (Birks, 2012). Consequently, although RoC analysis offers valuable insights into temporal changes in biological composition, interpreting and comparing RoC results across different studies or sequences can be challenging, as the expected patterns of RoC within a sequence are often unclear.

#### 1.4.2.2. Volcanic lake basins

Insular watersheds formed by volcanism are characteristically small, short and very steep with near vertical valley walls (Smith et al., 2003; Antunes & Carvalho, 2018). Streams within these watersheds exhibit rapid changes in altitude over short distances, resembling continental headwater streams with narrow, straight paths and turbulent, often seasonal flows. Substrates consist of coarse materials like bedrock, boulders, and gravel, though gradients may decrease in older, deeper catchments or coastal areas (Hughes and Malmqvist, 2005). According to the River Continuum Concept, headwater channels in Macaronesian islands are likely detritus-based systems dominated by shredder and collector feeding guilds. Middle sections may see increased algal production and biomass of scrapers and grazers due to higher light and nutrient levels. Lower floodplains are

generally absent, though some constrained ones exist in wider catchments. Limited spatial heterogeneity and habitat diversity compared to continental systems restrict the diversity of invertebrates able to inhabit these ecosystems (Malmqvist, 2002).

Lakes are prominent features of most volcanic terrains, however the nomenclature of volcanic lakes, rooted in geological terminology, may necessitate revisions due to contributions from tectonic, geomorphic, and volcanological processes to their formation (Christenson et al., 2015). Classification of volcanic lakes depends on the temporal connection to volcanic activity and the volcanic status of the region. The temporal link between volcanic events and lake formation serves as a defining parameter. Lakes may form within active craters, in satellite vents, or due to volcanic/geomorphic alterations in drainage patterns (Németh, 2020).

Volcanogenic, and especially crater lakes are often very deep, particularly in humid climates. Many of the world's deepest lakes fall into this category, despite their small surface areas. Great depth combined with the wind-sheltering provided by steep crater walls combine to inhibit wind-driven mixing of these lakes. Where this has led to anoxia in bottom waters, these lakes can provide exceptionally resolved and long paleolimnological records. Two broad categories of topographical closure encompass almost all volcanic lakes: lakes formed in craters, and lakes formed where volcanic dams of various types impound pre-existing rivers.

1) Crater lakes form in the topographical closure produced by volcanic crater formation. Because volcanism occurs in response to regional tectonic processes such as subduction or rifting, crater lakes tend to occur in geologically defined clusters (Newhall et al., 1987). Because of their small watershed areas and sensitivity to local surficial precipitation, cyclical climatic change or cyclical volcanism may produce large lake-level fluctuations in calderas (Chesner and Rose, 1991).
    a) Craters may develop on a relatively small scale following single explosive eruptions. Such craters, known as maars, are circular or semicircular features, typically only a few hundred meters to a few kilometers in diameter (Büchel, 1993). Compound craters are the landforms formed through multiple overlapping maars, independently whether such a crater formed during a single eruptive period or through several co-located eruptions occurring at different times. Raised ridges situated between low points within a compound crater are denominated "septum" (plural: septa) (Graettinger, 2018). Maars are normally excavated into the surrounding country rock, and are surrounded by a crater rim and walls of ash ejecta, which provides closure for subsequent lake formation. Maar lakes have been particularly important and fruitful subjects of paleolimnological research, far in excess of their abundance. Their small drainage areas make them particularly sensitive to local climate variations (Sime-Ngando et al., 2016).
    b) At the other extreme, crater formation may occur on top of large, stratified volcanoes, forming complex and very large calderas up to several tens of kilometers in diameter. Collectively, crater lakes are characterized by circular shapes and steep flanks, the result of a tendency of surficial rocks to collapse into the emptied magma chambers below the volcanic edifice following eruption. This produces a series of ring fractures, near-vertical faults that define the edges of the underlying cavity. Deeply collapsed calderas lying in humid climates are likely to be infilled by lakes that are very deep in comparison with their surface areas. By contrast, in arid or semihumid climates, small drainage basin areas lead to evaporitic conditions in closed basin caldera lakes, often strongly interacting with hydrothermal groundwater systems (Larson, 1989).

    Lakes formed within calderas are commonly hydrologically closed basins, at least for surface water flow. The combination of basin depth, limited drainage basin input, and ongoing subsidence makes volcanic crater lake basins potentially long-lived systems. Lakes in large collapsed calderas share many similarities with maars. ion.

2) River valleys can be dammed by a variety of volcanic obstructions, resulting in the formation of volcanic dam lakes. Lava flows, domes, or volcanoes can all block off valleys or create topographical closure between adjacent volcanic edifices. When pre-existing rivers are suddenly blocked in this fashion they are converted into elongate or dendritic lakes.

#### 1.4.2.3. Sediments in volcanic lakes

Volcanic lakes are particularly intriguing for palaeolimnological research, offering unique advantages due to their formation in volcanic areas less affected by glacial events, thus preserving sediment structures effectively and facilitating core sampling. Despite many volcanic lakes are relatively young, they provide historical records extending over 100,000 years (e.g., Valle di Castiglione, Lago Grande di Monticchio, Lac Ribains). Particularly sediment archives of volcanic lakes, help to decipher natural climate variability at seasonal to millennial scales, and help identifying causal mechanisms. Their importance includes their potential to provide precise and accurate inter-archive correlations (e.g., based on tephrochronology) and to record cyclicity and high frequency climate signals (Marchetto et al., 2015).

Studies on volcanic lakes delve into diverse areas including the impact of human activities like fish stocking and atmospheric deposition of pollutants (Skov et al., 2010; Schettler and Romer, 1988; Ruiz-Fernández et al., 2007). These small catchment areas unveil information of atmospheric processes and natural air-transported proxies, but human-induced changes in land use can significantly affect them, as seen even in ancient times (Guilizzoni et al., 2002). Its volcanic nature can influence palaeolimnological studies, with endogenous fluids affecting water temperature, pH levels, and rapid variations in water levels impacting both biota and sediment deposition (Funiciello et al., 2003). Additionally, submerged aquifer sources may introduce chemicals, altering biogeochemical cycling within the lake (Michard et al., 1994).

## 1.5 Hypothesis and aims

Lake sediment archives vary in their suitability for addressing specific research questions. Some regions, such as Macaronesia, offer ideal natural archives due to their environmental characteristics. The Azores Archipelago, with its remote location and complex geological setting, provides unique sedimentary records for paleoenvironmental studies. These sediments constitute an invaluable resource to investigate the dynamic evolution of the landscape, where it is hipothesized that the interaction between atmospheric, land and human processes might contribute to the sedimentary variability for three reasons:

1) The remote location of the Azores Archipelago in the North Atlantic Ocean can provide useful knowledge about regional climate evolution. Its location facilitates assessments of global circulation patterns, inaccessible elsewhere. This unique location should allow for comparative analysis with continental regions, aiding in establishing correlations between precipitation, temperature, and the spatial and temporal evolution of atmospheric patterns like the North Atlantic Oscillation (NAO) and East Atlantic (EA) dipoles.

2) The Azores Archipelago also should constitute a record of the beginning of the Anthropocene, since these islands were colonized in relatively recent times. Therefore, they should constitute a natural laboratory that allows us to analyse the effects on ecosystems derived from increasing anthropic pressure on local and scales into the natural systems.

3) The Azores should constitute an exceptional resource to identify the interactions between the climatic and anthropic system with the physical substrate. Since the archipelago is located in one of the areas with the most complex geodynamics on the planet, presenting a wide range of geological processes and derived landscape forms, it should give clues about the response of the different

systems (climate and ecological) to the interaction with the geological physical environment which operates at uncoupled time scales.

Hence, the main objective of this study is to characterize the processes that have dominated lacustrine sedimentary dynamics in the western (Flores and Corvo Islands) and central (Pico Island) sectors of the Azores Archipelago. Lithological, biogeochemical, mineralogical data obtained from sedimentary records of lake-catchment systems of Funda (Flores Island), Caldeirão (Corvo Island), and Caveiro (Pico Island) are used for this purpose.

More specific scientific objectives are:

- To establish the temporal framework when the processes controlling the sediment deposition occurred by constructing age-depth models derived from radiometric dating and varved sediments, as well as to reconstruct the evolution of the established depositional environments.
- To develop a limnogeomorphological approach to contrast content and container archives of the lacustrine basins to achieve a profound understanding of the spatial patterns of input, distribution, and deposition of the sediments. This aims to evaluate why there are differences in long-term climate reconstructions and understand how local and regional factors affect changes in biogeochemistry.
- To reconstruct the environmental evolution of the western and central sectors of the Azores Archipelago since the mid Holocene and to evaluate the relative contribution of local and regional forcings on sedimentation to establish a climatic reconstruction of the central North Atlantic for the last 5200 years.
- To compare the obtained paleoclimatic reconstruction with previous reconstructions from the North Atlantic sector (Europe, America and Greenland), thus characterizing the spatiotemporal evolution of atmospheric dynamics in the region, with special emphasis on the most prominent regional atmospheric modes of climate variability: the North Atlantic Oscillation (NAO) and the East Atlantic pattern (EA).

# 2. The Azores Archipelago

The Azores is the remotest and most septentrional archipelago within the Macaronesia, occupying subtropical latitudes of central north Atlantic Ocean (37°–40° N, 25°–31° W), located 1500 km away from the continental Europe and 3900 km from the North American coast (Fig. 2.1). This archipelago conforms part of Portugal and it is composed of nine main islands distributed in three different groups along a 600 Km long WNW-ESE stripe: a) the Azores Archipelago Western Group (WG) made up of Flores and Corvo islands, b) the central group (CG) with Faial, São Jorge, Graciosa, Terceira, and Pico islands, c) and the eastern group (EG) consisting of São Miguel and Santa Maria islands. The orography of the islands within the archipelago is typically characterized by pronounced elevation gradients from the coastal lowlands to the interior highlands (Fig. 2.1).

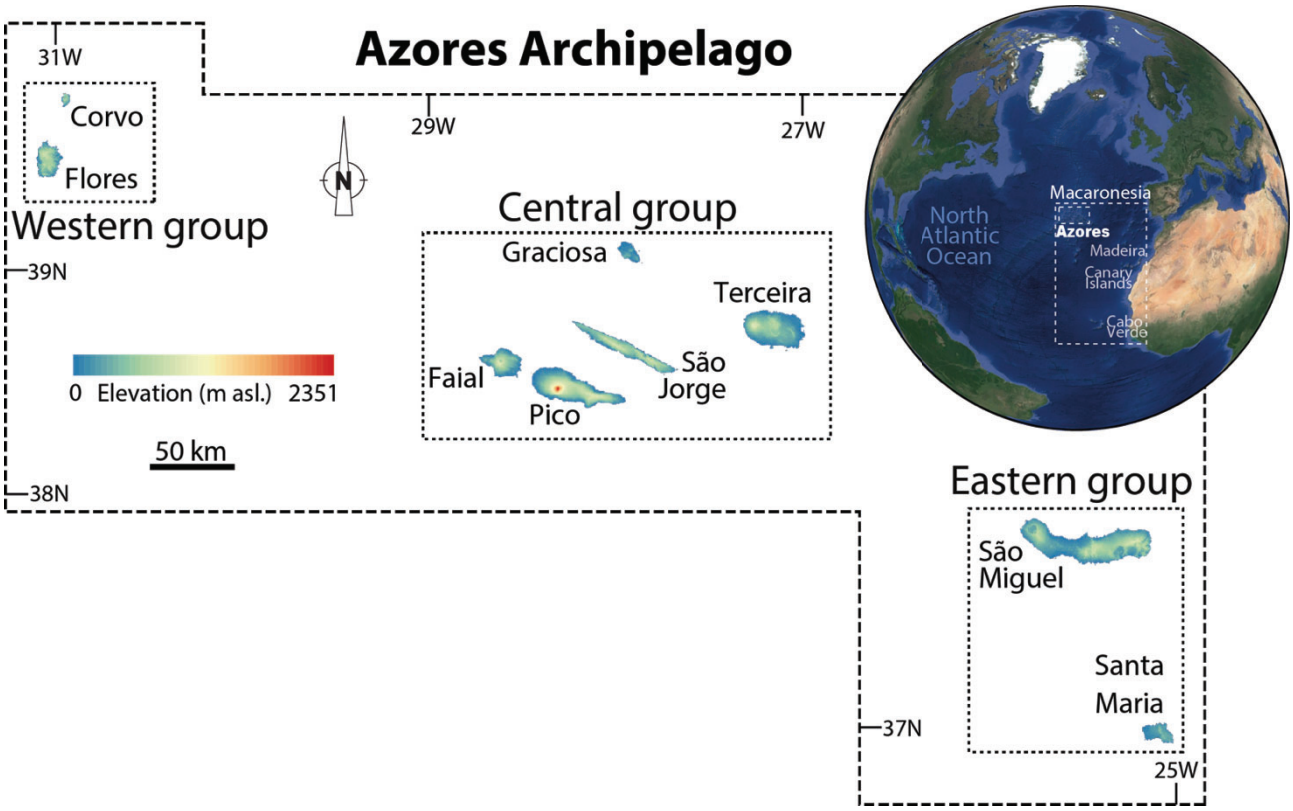


*Fig. 2.1: The Azores Archipelago within Macaronesia in the north Atlantic Ocean. All the islands from the Azores are indicated. Dashed rectangles include islands from the same group.*

## 2.1 Geological setting

The Archipelago has a tectono-volcanic origin (ca. 8 Ma.; Abdel-Monem et al., 1975), linked to a mantle melting anomaly (Métrich et al., 2014; Genske et al., 2016) and the tectonic confluence between the plates of North America, Eurasia, and Nubia at the Azores triple junction (ca. 39ºN, 29ºW) (Miranda et al., 2018) (Fig. 2.2).

### 2.1.1 Tectonic geodynamics

The northern and southern branches of the Azores triple junction imply a relatively simple geodynamic model, dominated by the Mid Atlantic Ridge (MAR) opening along an NNE-SSW trend (Fig. 2.2). The related orthogonal stresses provoke the Eurasia and Nubia divergence from the North American plate, affecting domains with different relative tectonic propagation (Merkouriev and DeMets, 2008; 2014a; b). However, the eastern branch of the Azores triple junction has undergone a more complex evolution than the MAR during the latest 20 Ma., making the interpretation of its

tectonic nature and exact location historically controversial. Nevertheless, the magnetic (Searle, 1980; Luis et al., 1994; Luis & Miranda, 2008) and bathymetric (Searle, 1980; Miranda et al., 2014) insights gathered by Miranda et al. (2018) allowed the interpretation of the Terceira Rift (TR) as the present-day configuration for this branch, which present an arcuate trend along a general WNW-ESE orientation (Fig. 2.2). Morphotectonic signs (Vogt & Jung, 2004; 2018; Miranda et al., 2014; Lourenço et al, 1998) revealed volcanic alignments (e.g., Faial-Pico and São Jorge Islands) corresponding with active segments of the Eurasia-Nubia boundary (Lourenço et al., 1998). This was interpreted as the result of the recent and progressive WNW migration of the triple junction (DeSousa, 2007) (Fig. 2.2). Furthermore, neo-tectonic and seismotectonic evidences (McKenzie, 1972; Laughton and Whitmarsh, 1974; Searle, 1980; Madeira & Ribeiro, 1990) allowed the interpretation of a leaky transform geodynamic model for this boundary. This model is characterized by trans-tensive stresses (Fernandes et al., 2006) generating prevalent co-axial oblique extension westward from Terceira Island. Although, non-coaxial distributed deformation dominates the inter-plate zone between the TR and the volcanic lineaments (DeSousa, 2007) (Fig. 2.1).

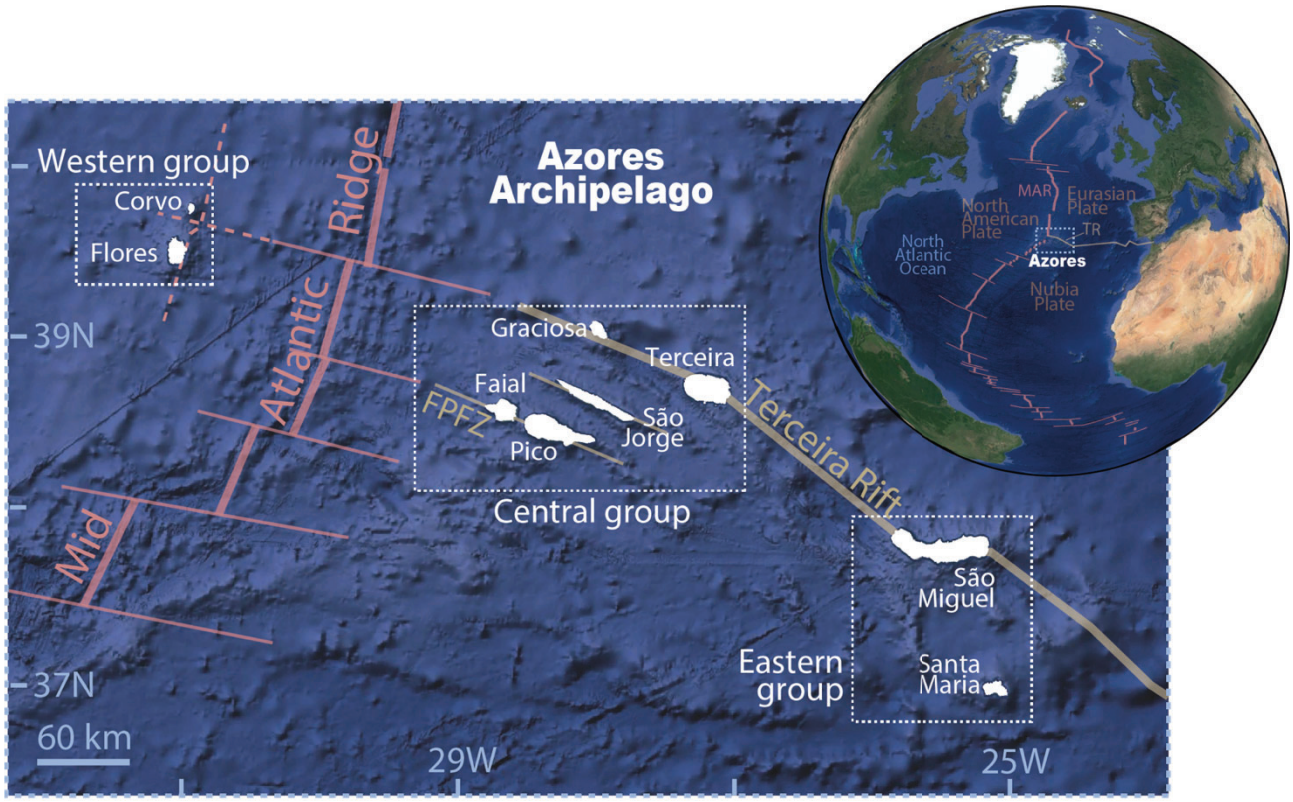


*Figure 2.2: Geologic setting of the Azores Archipelago, including a North Atlantic Ocean overview with the Azores triple junction tectonic scheme. Red colour indicates the tectonic structures related to the orthogonal geodynamics dominating at the Mid Atlantic Ridge, whereas brown colour indicates the position of the Terceira Rift and volcanic lineaments related to the leaky trans-tensive geodynamics of the Azores triple junction eastern branch. Dashed lines reveal the disposition of the prevalent tectonic lineations. MAR: Mid Atlantic Ridge, TR: Terceira rift, FPFZ: Faial-Pico Fracture Zone.*

### 2.1.2 Surface faulting

The tectonic geodynamics of the Azores result in two structural domains (Fig. 2.2). The geodynamics along the MAR generate a structural interference that accommodates the mantle uplift with N20-30ºE normal faults and the transform zones between the different tectonic domains with N140-150ºE dextral transfer faults (Azevedo and Ferreira, 2006). This structural pattern dominates the Azorean sector westwards from the MAR (Azevedo and Ferreira, 2006), which constitutes a stable tectonic setting within the north American plate, where relatively negligible instrumental seismicity has been recorded (Fontiela et al., 2018; Fernandes et al., 2006; Hildenbrand et al., 2018).

In contrast, the leaky transformant geodynamics along the arcuate Terceira Rift generates an interference between dextral N110ºE-N120ºE and sinistral N140ºE-N150ºE (relay zones) strike faults (DeSousa, 2007), which show high to moderately high activity in most cases. This activity corresponds with relatively high instrumental seismicity rates, composed by surficial earthquakes of relatively low magnitude (Fontiela et al., 2018) with a maximum expected varying from Mw 6 to 7. The associated slip-rates usually range from a few tenths of millimetres to a few millimetres per year (Madeira et al., 2015).

### 2.1.2 Tectono-volcanic architecture

Volcanism in the Azores is tectonically controlled, occurring along faults or at fault intersections (Madeira et al., 2015). Eruptive styles range from effusive to moderately explosive, depending on magma composition and water presence (Azevedo and Ferreira 1999). Tectono-volcanic activity involves constructive volcanic activity and tectonic uplift and destructive such as crater-forming volcanic explosions, caldera collapses and tectonic subsidence processes (Azevedo and Ferreira, 1999).

In structural domains with preferred orientations, effusive and strombolian styles induce volcanism along faults, typically forming monogenetic fissure systems composed of cone rows and associated with lava flows (Nunes, 2020; Pedrazzi et al., 2015). Within these domains, tectonic subsidence normally occurs as long graben structures (Madeira et al., 2015) (Fig. 2.2). In contrast, at structural domains dominated by fault intersections the installation of shallow magma reservoirs favours volcanic progradation forming central and polygenetic shield volcanoes and stratovolcanoes (Luis et al., 1998). This volcanic activity constitutes prominent edifices that reach up thousands of meters above sea level like the 2351 m of Pico Mountain in Pico Island (Madeira et al., 2015) (Fig. 2.1). However, within these domains, subsidence is more likely to occur in the form of collapsed calderas, especially when volcanic loads are high enough (Azevedo and Ferreira 2006; Andrade et al., 2022).

Phreatomagmatism is favoured at hydraulically charged islands leading to the formation of explosive subsurface activity (Andrade et al., 2021; 2022; 2023). This activity in the Azores can occur both along faults or at faults intersections, commonly forming rows of maars and tuff rings clusters composing fissure systems (Comprida maar) and central volcanic systems (Funda maars cluster). Furthermore, central vents like Negra maar are also common (Azevedo and Portugal Ferreira, 2006; Andrade et al; 2022; 2023).

## 2.2 Climatic setting

### 2.2.1 Oceanic circulation

The oceanographic conditions in the archipelago are dominated by the Azores current (Fig. 2.3), a branch of the Gulf Stream that gyres clockwise, transporting temperate waters from tropical latitudes and resulting in elevated Sea Surface Temperatures (SST) in the region (e. g. Klein and Siedler, 1989). The strength and position of this oceanic current play a crucial role controlling the climatic conditions of the archipelago. The WG and the CG are further affected by incoming meanders and filaments originating in the Gulf Stream, whereas the eastern island group is mostly affected by westward propagating eddies pinching off from the Azores Current (Caldeira and Reis, 2017).

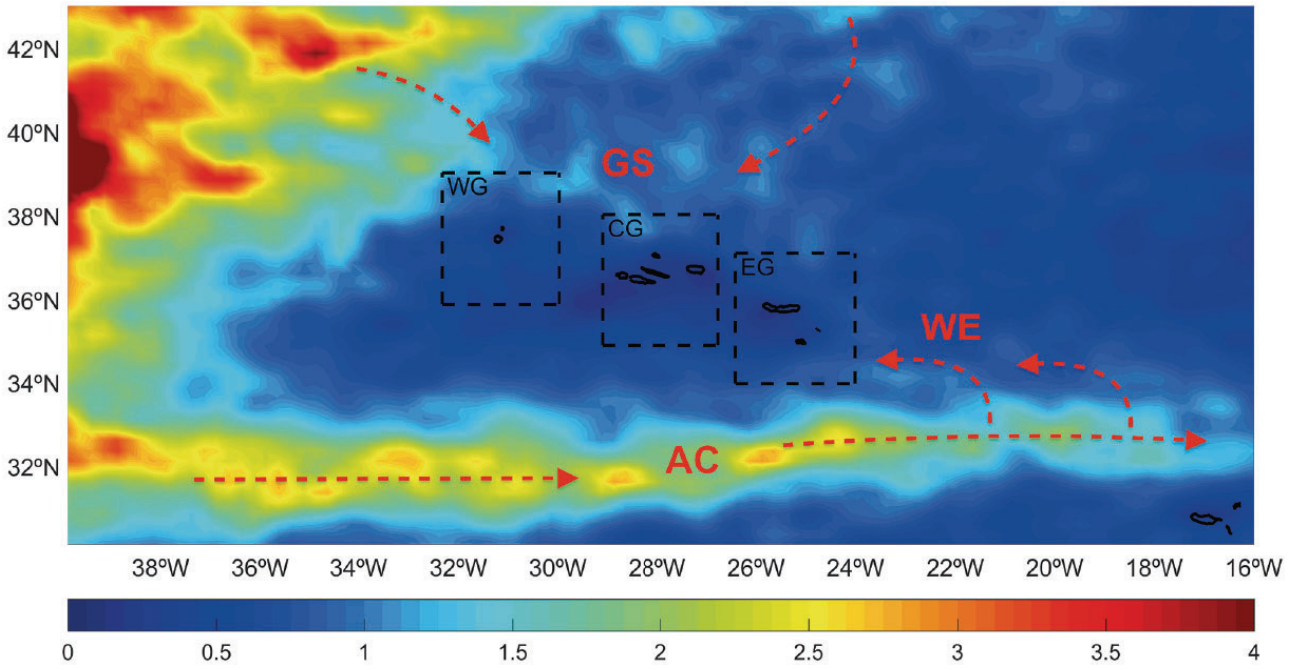


*Fig. 2.3: Overall mean (2004-2014) eddie kinetic energy ($cm^2\ s^{-2}$) at the Azores region (figure from Caldeira and Reis, 2017). Gulf Stream AC: Azores Current. WE: Western propagating Eddies.*

### 2.2.2 Atmospheric circulation

The Azores archipelago is exposed to the north-westernmost side of the subtropical high-pressure system (Azores anticyclone) between September and March, being mostly affected by the westerlies that transport moist and warm tropical air to the region (Fig. 1.30). This atmospheric configuration allows the North Atlantic storm-track to pass directly across the archipelago favouring the arrival of tropical cyclones, mainly storms, but with increasing influence of hurricanes (Hernández et al., 2016). Furthermore, during winters with weakened (strengthened) NAO, the southward (northward) migration of the westerlies from northern (southern) latitudes enhances (diminishes) the climatic effects of the storms track in the Azores (Fig. 1.30). Consequently, the Azores Archipelago is particularly vulnerable to the climatic impacts of the NAO during the winter (Barceló and Nunes, 2012; Hernández et al., 2016; Paredes et al., 2017).

Besides, during late spring and summer, the Azores are dominantly influenced by the Azores high-pressure system, creating anti-cyclonic conditions (Davis et al., 1997). In July and August, the Azores High commonly sits over the region and deflects polar depressions (Björck et al., 2006) (Fig. 1.30). Under these atmospheric conditions, the dominance of trades over the Azores increases, moving less humid and colder air masses than the westerlies. Furthermore, the northern migration of the trades during summer months favours the arrival of Saharan dust to north Atlantic subtropical latitudes, transported by northern branches of the Saharan air layer (Brust and Waniek, 2010). The mineral composition of this dust varies depending on the source region of the particles.

The atmospheric circulation in the Azores is further influenced by the pronounced elevation gradient of the archipelago (Fig. 2.1). The westerlies and trades, transporting heat and humidity throughout the North Atlantic, interact with the Azores, especially at the highlands of the islands with the most pronounced elevation gradients (Barceló and Nunes, 2012; Cropper and Hanna, 2014).

### 2.2.3 Climate

Oceanographic and atmospheric circulation in the Azores contribute to a predominantly temperate oceanic climate in the archipelago, with dry season in the lowlands and without dry season in the

highlands (Fig. 2.4). This climate is characterized by high relative air humidity, generally cloudy skies, and frequent strong winds (Barceló and Nunes, 2012; Hernández et al., 2016).

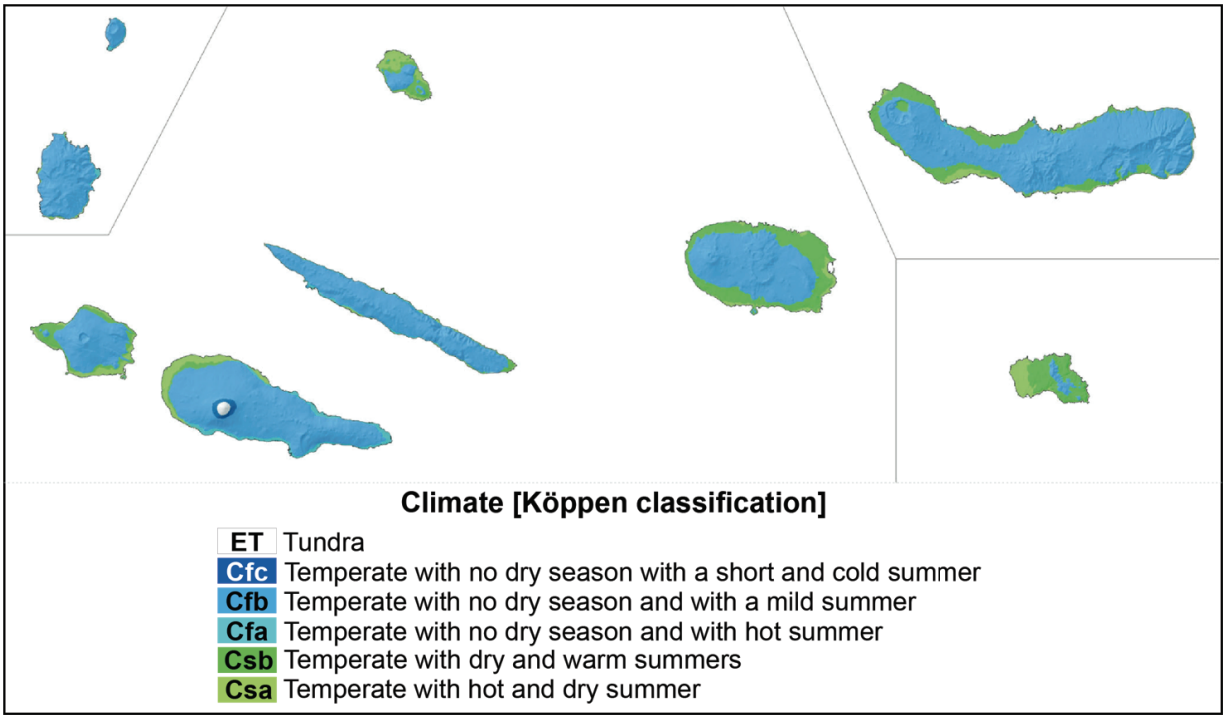


*Fig. 2.4: Climate (Köppen classification) distribution in the Azores Archipelago based on observational data obtained from daily meteorological observations for the period between 1971 and 2000 (modified from Barceló and Nunes, 2012).*

Rainfall is the most common form of precipitation in the Azores (average annual of 960.6 mm). This is favoured by the elevated terrains of the highest oceanic islands, creating convective precipitation patterns that especially impact the interior highland areas, particularly on the windward sides (Barceló and Nunes, 2012; Cropper and Hanna, 2014) (Fig. 2.5). Additionally, there is a longitudinal variation in the annual average precipitation across the archipelago, ranging from 730 mm year$^{-1}$ in Santa Maria (the east-most island) to 1666 mm year$^{-1}$ in the westernmost Flores Island (Paredes et al., 2017) (Fig. 2.5).

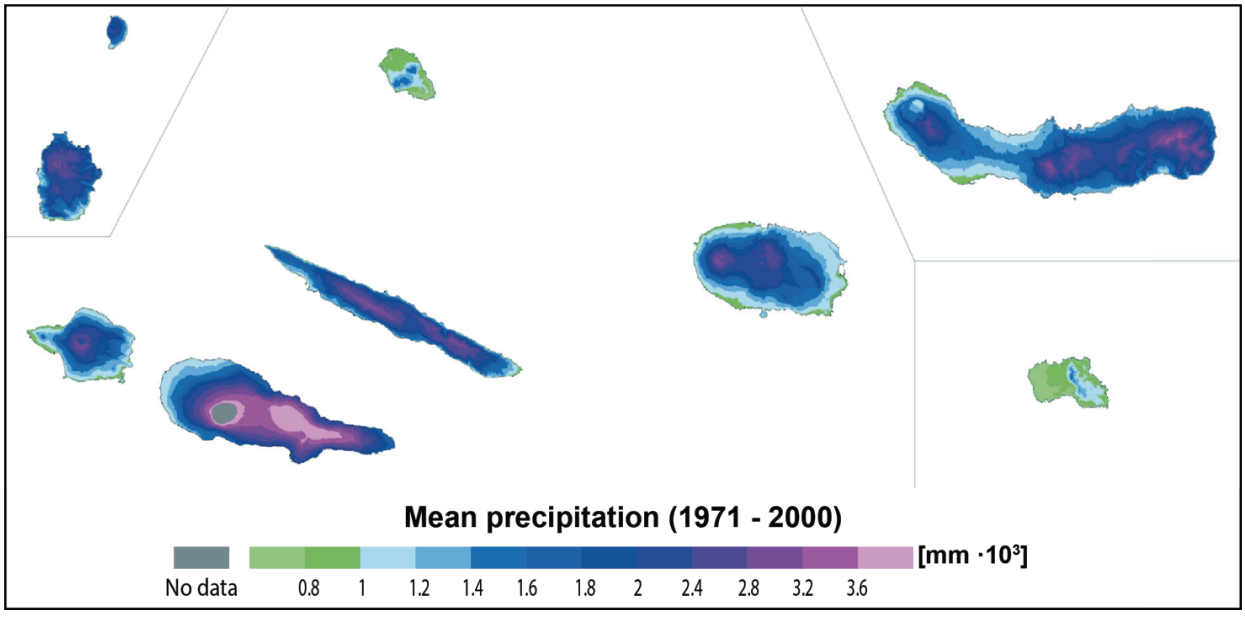


*Fig. 2.5: Precipitation distribution in the Azores Archipelago based on observational data obtained from daily meteorological observations for the period between 1971 and 2000 (modified from Barceló and Nunes, 2012).*

Furthermore, rainfall follows a strong seasonal cycle, with 75% of the total occurring between October and March (Fig. 2.6a). There is considerable interannual variability (Fig. 2.6b), leading to significant differences in the quantity and duration of rainfall episodes. Very wet years are characterized by longer episodes and higher precipitation, and very dry years characterized by shorter episodes and less precipitation. Wetter conditions in the Azores region correspond with negative values of the NAO index (NAOi) (Hernández et al., 2016).

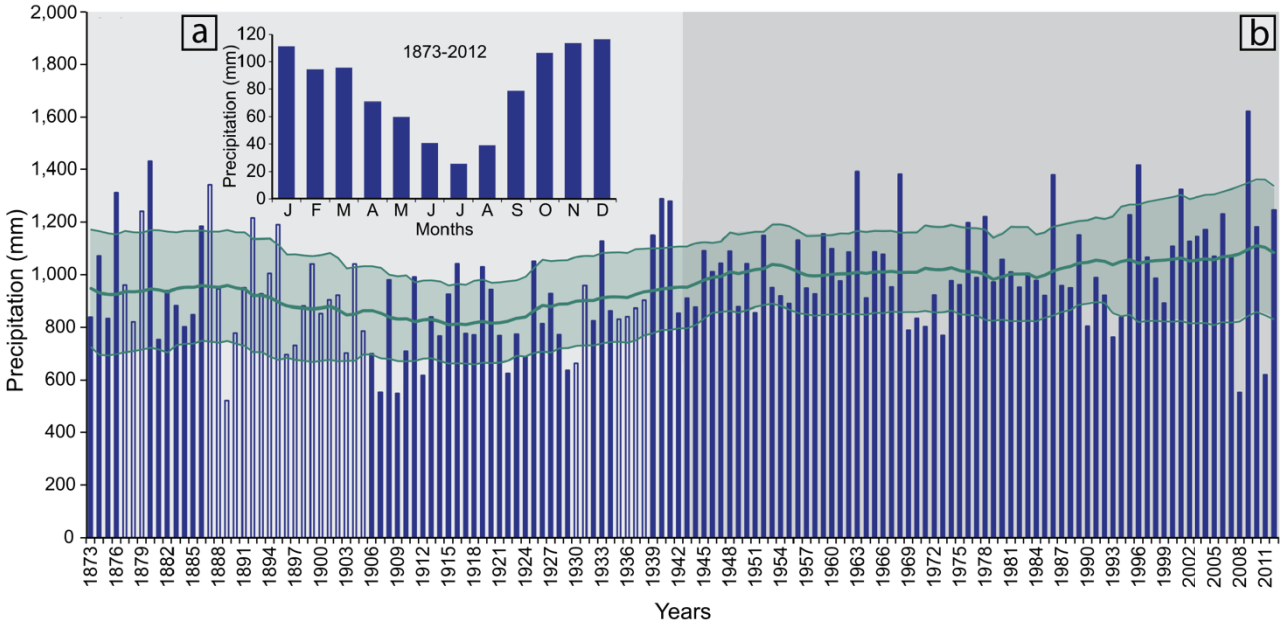


*Fig. 2.6: a) Annual mean precipitation (mm), 1873–2012. Annual precipitation series were computed by summing daily values if no more than two values per month were missing (solid bars). In cases where this occurred, series were completed using monthly datasets from previously digitised monthly series, which have been already used by other authors (e. g. Cropper and Hanna, 2014) covering this time period (open bars). The thick line represents a 31-point moving mean, emphasising the low-frequency variability of the annual precipitation series, and the shaded area indicates the corresponding 31-point moving standard deviation (modified from Hernández et al., 2016).*

Thermal conditions in the Azores are characterized by mild temperatures with average annual values of 17.4 ºC. Nevertheless, the steep orography of the archipelago (Fig. 2.1) contributes to the creation of pronounced temperature gradients, with milder temperatures in the lowland areas and prevailing colder conditions in the highlands (Barceló and Nunes, 2012; Cropper and Hanna, 2014) (Fig. 2.7). The temperature exhibits small annual variations, with the warmest conditions occurring during the summer (Cropper and Hanna, 2014) Warmer summers in the Azores region correspond to positive values of the EA index (EAi) at the decadal scale, likely due to higher solar irradiance (Hernández et al., 2021).

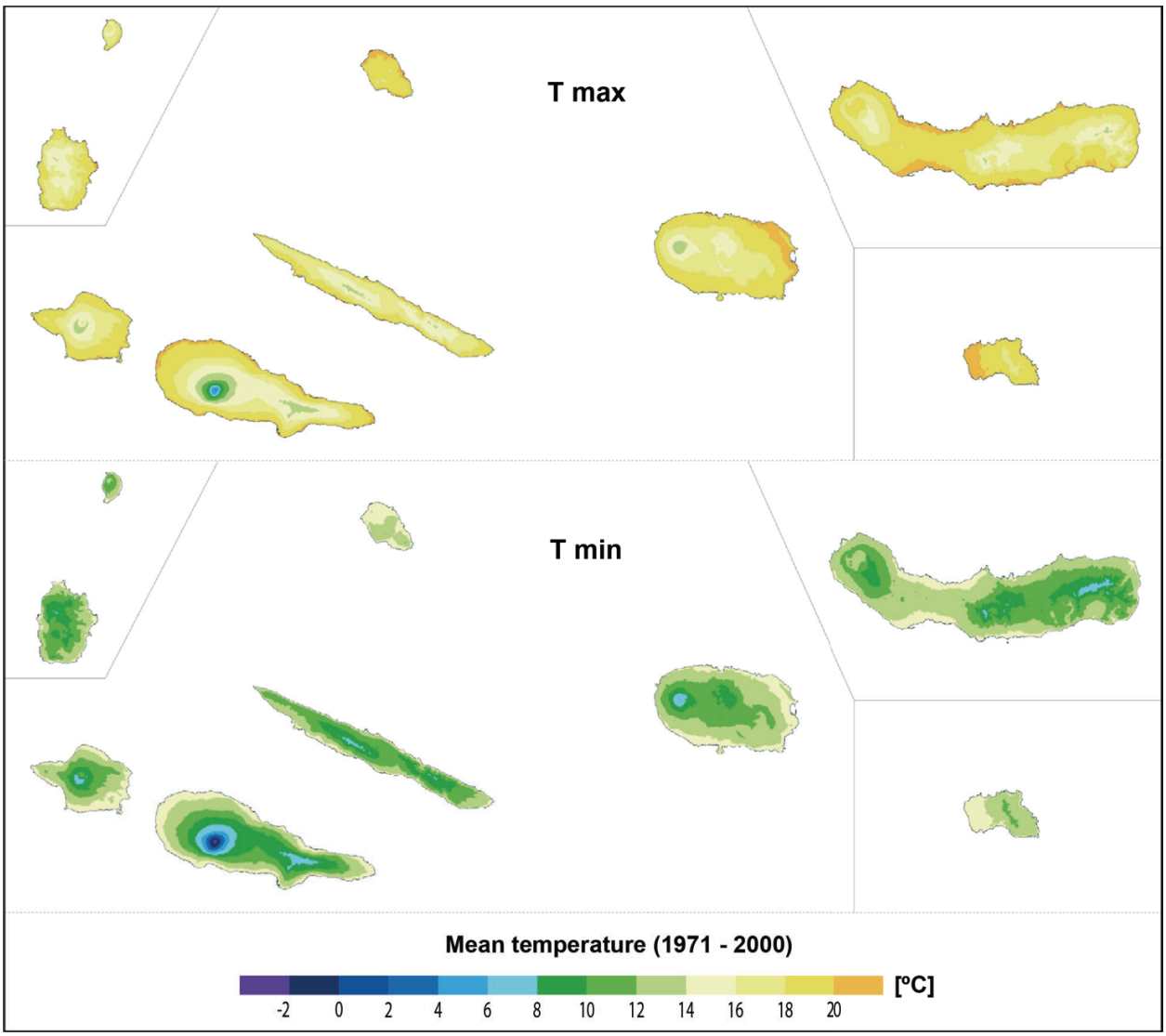


*Fig. 2.7: Maximum and minimum temperature distribution in the Azores Archipelago based on data obtained from daily meteorological observations for the period between 1971 and 2000 (modified from Barceló and Nunes, 2012). T max: maximum temperature. T min: minimum temperature.*

## 2.3 Landscape

### 2.3.1 Geomorphology

Tectono-volcanism shapes the island's morphology of the Azores (Azevedo and Ferreira, 1999) (Fig. 2.8). The landscape reflects the intricate dynamic interplay between volcanic activity and surface faulting (Madeira et al., 2015; Azevedo and Ferreira, 2006; França et al., 2003; Navarro et al., 2009) . Volcanic deposits often obscure the surface expression of faulting, yet fault locations can be identified by alignments of cones and crater rows (Madeira et al., 2015). The island's geomorphology clearly displays active tectonic processes through features such as fault scarps, displaced cones, streams, and volcanic alignments (Madeira et al., 2015). Additionally, the diverse landforms across the archipelago result from the ongoing interaction between volcanic growth and surface processes (Hevia-Cruz et al.,2024).

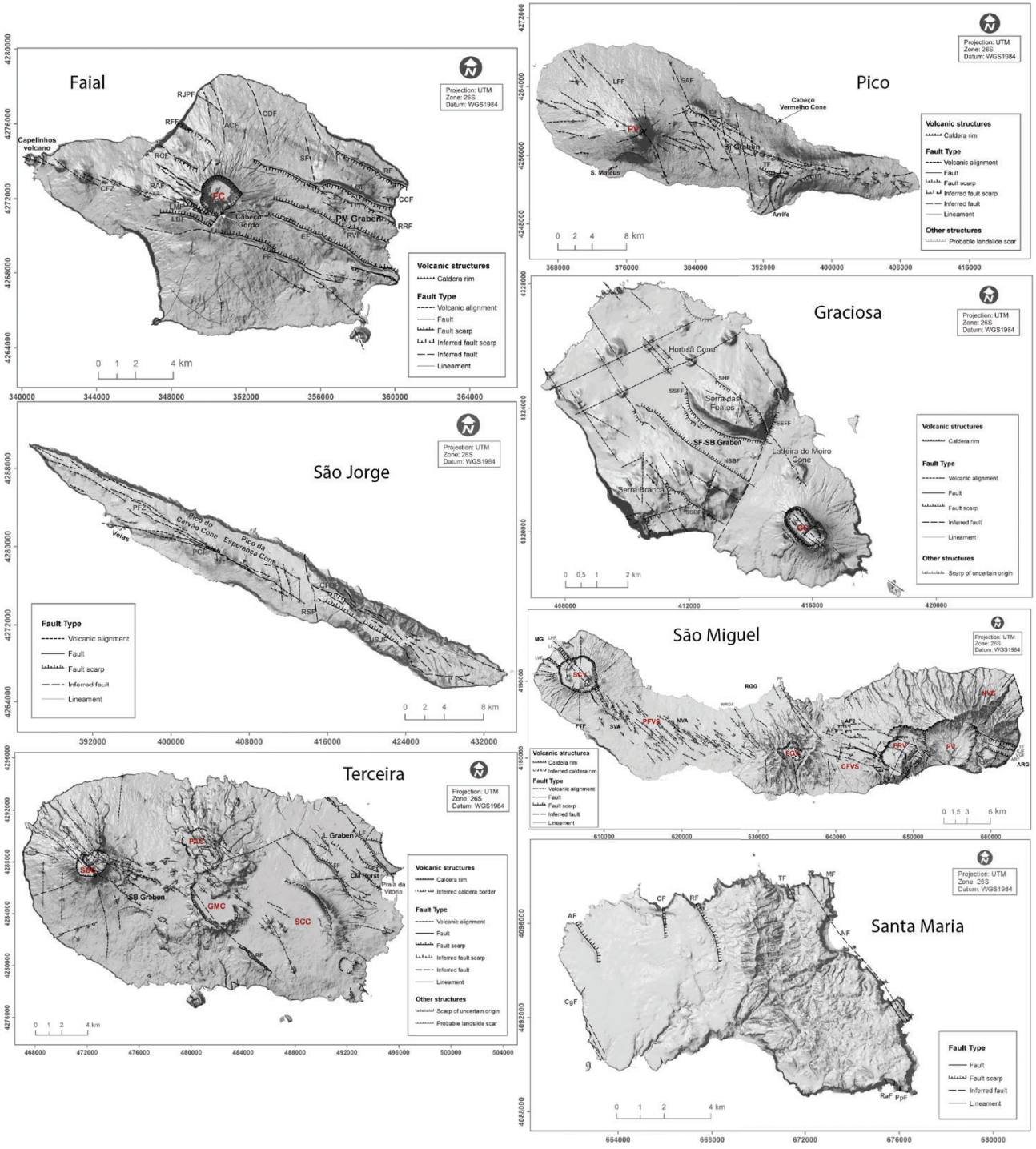


*Fig. 2.8: Neotectonic sketch of the Azores archipelago central and western groups, superimposed on a DTM (digital terrain model). Note the geomorphological expression of tectonovulcanism over the Azores Archipelago, reflected in the islands shorelines and reliefs, which align following tectonic lineations and show prominent depressions forming large basins and aligned volcanic structures. Modified from Madeira et al., (2015).*

### 2.3.2 Vegetation

The Azores Archipelago exhibits native flora species including Erica azorica, Ilex azorica, Juniperus brevifolia, Laurus azorica, Picconia azorica, among others. Many of these species have faced extinction or are now restricted to small relictic patches across the islands (Connor et al., 2012). Elias et al. (2016) modelled the natural potential vegetation of the Azores (Fig. 2.9) that refers to the most probable vegetation in an area assuming no significant human interference or major natural disasters using these flora bastions. This model is based on the environmental characteristics,

particularly climate and geology (Rull et al., 2017). The model exhibit eight vegetation zones, whose distribution is dominated by the altitudinal gradient of the archipelago (Fig. 2.1): 1) the *Erica Morella* coastal woodlands, 2) *Picconia Morella* lowland forest, 3) *Laurus* Submontanae forest, 4) *Juniperus Illex* Montanae forest, 5) *Juniperus* Montanae woodlands, 6) *Calluna-Juniperus* Altimontanae Scrublands, 7) *Calluna-Erica* Subalpine Scrublands and 8) *Calluna* Alpine Scrublands.

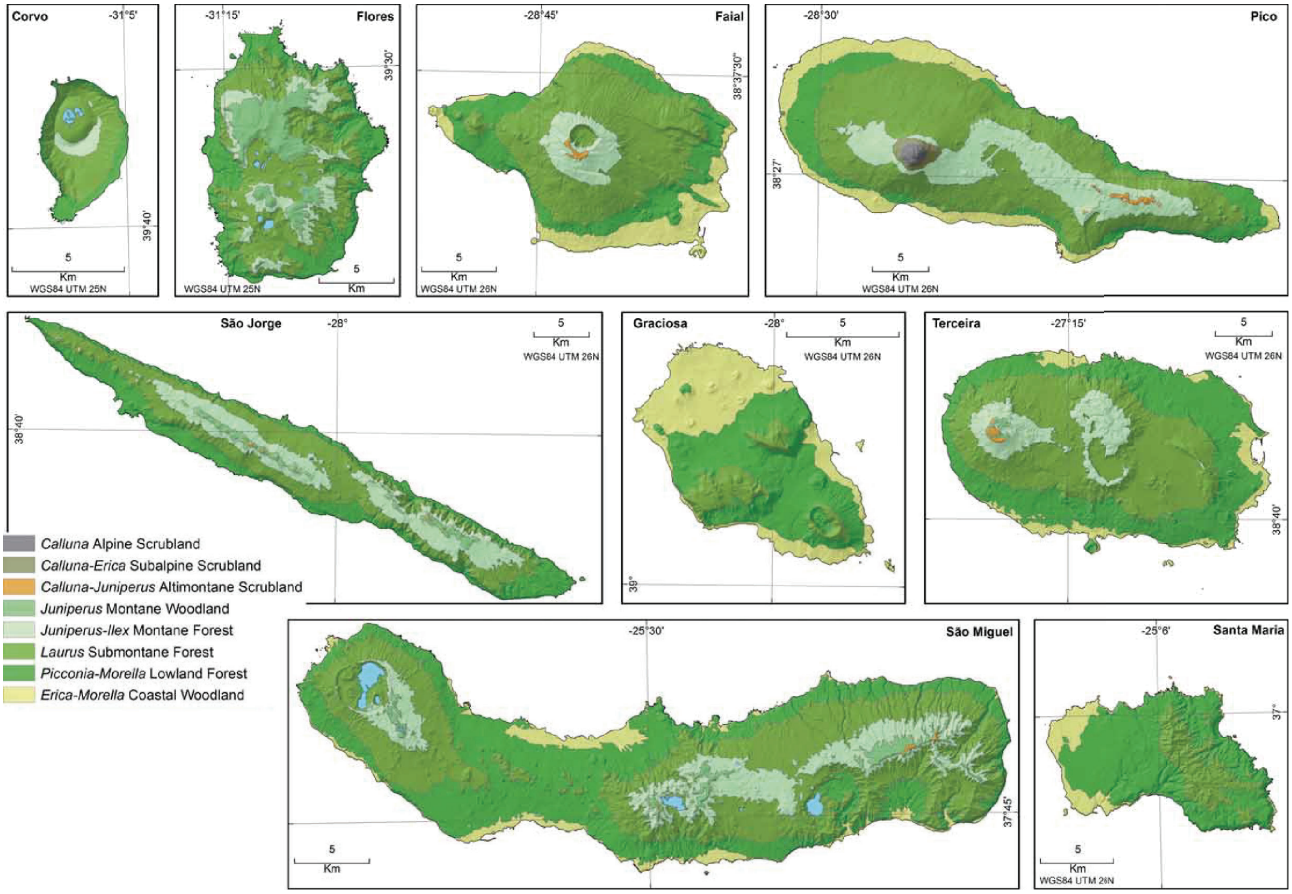


*Fig. 2.9: Potential distribution maps of the natural zonal vegetation types in the Azores Islands (Modified from Elias et al., 2016, see for further details).*

### 2.3.3 Hydrology

The hydrological dynamics of the Azores Archipelago are heavily influenced by its volcanic origin and geographical characteristics. Evaporation from the temperate ocean serves as the primary source for both surface water and groundwater recharge (Antunes and Carvalho, 2018).

The youth and limited dimensions of the Azores, confer them watersheds with short and steep valley walls, typically covering areas less than 30 $km^2$ and consisting of coarse substrates such as bedrock, boulders, and gravel (Hughes, 2003; Smith et al., 2003; Hughes and Malmqvist, 2005; DROTRH/INAG 2001). The volcanic eruptions and subsequent processes such as fracturing and weathering play significant roles in shaping the heterogeneity and anisotropy of groundwater occurrence, movement and storage (Antunes and Carvalho, 2018).

Rainwater in young basaltic formations, such as in the Azores Archipelago, rapidly infiltrate upon reaching the ground surface, showing high rates of infiltration. This infiltration either recharges aquifers or feeds streams, with drainage capacity being more pronounced at higher steeplands. Rainwater may also fill endorheic basins, typically found within volcanic craters (Antunes and Carvalho, 2018).

The Azores exhibit an average runoff rate of $322 \cdot 10^6$ $m^3$, with significant variations among islands, such as São Miguel Island recording the highest runoff ($1731 \cdot 10^6$ $m^3$) and Graciosa the lowest ($8 \cdot 10^6$

$m^3$) (Antunes and Carvalho, 2018; DROTRH/INAG 2001). Runoff has demonstrated to be < 1% of total rainfall under pasture, but increases sharply to near 20% of the rainfall when the soil is tilled and not protected by vegetation (Fontes et al., 2004). Additionally, the islands display an average annual evapotranspiration of 597 l/$m^2$ (Antunes and Rodrigues, 2014).

### Streams

Watersheds in the Azores, particularly those poorly developed, result in streams with low gradient profiles, descending from high altitudes over short distances (<10 km). Despite abundant precipitation, most streams exhibit a flashy flow regime, with high flows in winter and minimal flow in summer. Nevertheless, some islands in the Azores (i.e., Santa Maria, São Miguel, São Jorge, Faial, and Flores) host permanent streams. Chemical compositions of these permanent streams are influenced by atmospheric inputs from oceanic rainfall and the weathering of volcanic rocks (Louvat and Allègre, 1998; Hughes and Malmqvist, 2005; Antunes and Carvalho, 2018; DROTRH/INAG, 2001).

### Lakes

The humid temperate climate in the Azores region promotes high hydrological availability and intense chemical weathering of volcanic rocks, favouring the formation of about 88 small lakes within the diverse array of tectono-volcanic basins present in the archipelago (Fig. 2.8). The Azorean lakes are typically hosted inside collapsed calderas, cone craters, and maar craters, usually distributed above 250 m asl throughout the highlands of São Miguel, Terceira, Pico, Flores and Corvo islands. However, examples within lava caves, such as Furna do Enxofre lake in Graciosa Island, are also found at the lowlands (Porteiro, 2000; Antunes & Carvalho, 2018; Cruz et al., 2006) (Fig. 2.10).

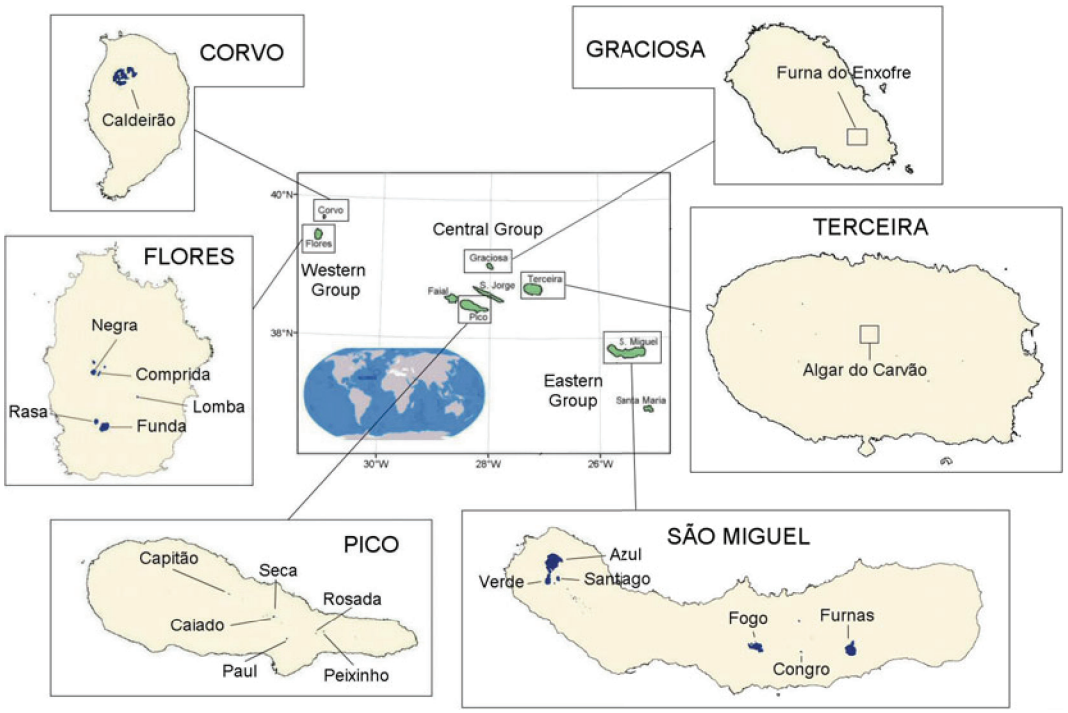


*Fig. 2.10: Lakes distribution within the Azores Archipelago (figure from Antunes and Carvalho, 2018).*

In general, lakes situated within calderas exhibit the largest surface areas and water volumes, reaching up to 3.6 $km^2$ and $47361 \cdot 10^3$ $m^3$, respectively (Lake Azul in São Miguel Island; Fig. 2.10). Nevertheless, greater depths are typically associated with lakes located inside maars, with maximum water depths of up to 120 m observed in Lake Negra on Flores Island (Fig. 2.10). Most of the lakes are relatively small and shallow, typically featuring surfaces below 1 $km^2$ and maximum depths of less than 10 m. These lakes are commonly found within scoria cone craters, such as Lake Rosada

in Pico Island (Fig. 2.10), with an area of 1.25 $hm^2$, 5.2 m of maximum water depth, and a volume of $27.3 \cdot 10^3$ $m^3$. Ninety-three percent of the total volume of lake waters is located at São Miguel Island, Flores contribute 5%, and Terceira, Pico, and Corvo 2% (Porteiro, 2000; Antunes and Carvalho, 2018; Cruz et al., 2006).

The temperature of the Azorean lake waters is generally low, ranging between 5.2 °C in winter and 23.5 °C in summer (Cruz et al., 2006; Antunes and Carvalho, 2018). The spring temperature rise promotes the formation of a thermocline within the deepest lakes inhibiting water circulation between the epilimnion and the hypolimnion. Some of these lakes exhibit a monomitic behaviour, typically overturning during fall (e. g. lakes Funda and Santiago; Fig. 2.10; Ritter et al., 2022; Vázquez-Loudeiro et al., 2023), whereas others are polymictic (e. g. Lake Empadadas in São Miguel Island; Hernández et al., 2017). In the Azores, lakes shallower than 12 m show small temperature changes with depth throughout the year and do not stratify, being more prone to holomictic behaviour (e. g. lakes Capitao, Caiado and Paul; Andrade et al., 2019; Fig. 2.10).

The hydrogeochemisytry of the Azorean lake waters is influenced by sea-salt spraying exhibiting compositions of the Na-Cl type. Additionally, some lakes are impacted by water-rock interactions and display compositions of the Na-$HCO_3$ type, while a limited group of lakes display a hydrogeochemistry influenced by volcanic fluids, showing the hydrogeochemical type of Mg-$HCO_3$. Dissolved silica ($SiO_2$) levels in the waters are relatively low in the majority of lakes, likely due to biological uptake by diatoms (Cruz et al., 2006; Antunes and Carvalho, 2018). Carbon dioxide ($CO_2$) concentration has a wide range of expression in the lakes of the Azores due to differences in water stratification, circulation, and volcanic fluid inputs. The lakes from São Miguel and Graciosa such as Furna do Enxofre Lake are located in active volcanos and fumarolic fields, usually showing higher $CO_2$ concentrations than other lakes in the Azores (Andrade et al., 2019; Antunes and Rodrigues, 2011).

The saturation state of the Azorean lake waters is highly dilute. Therefore, mineral precipitation does not significantly affect species concentration in the water (Cruz et al., 2006). The water quality of these systems exhibits significant variability, conditioned by volcanic influences and human activity.

### 2.3.4 Surficial processes

The hyper-humid climate prevalent in the Azores archipelago, coupled with dense vegetation, predominantly dictates subaerial denudation processes and the formation of landforms resulting from volcano-tectonic activity. When volcanic activity subsides for extended periods, ranging from thousands to tens of thousands of years, denudational processes unveil distinct faulting features, including fault scarps, tectonically controlled drainage patterns, displaced eruptive centers such as cones and domes, streams, interfluves, and sag ponds, attributable to accumulated surface ruptures (Madeira et al., 2015).

Dissolved elemental concentrations in river waters yield specific chemical denudation rates, while suspended loads reflect partial rock dissolution during weathering. Mechanical erosion rates in the Azores, ranging from 170 to 500 tons per square kilometer per year, significantly exceed the global average, underscoring the ease of erosion in basaltic terrains (Louvat and Allégre, 1998). Erosion in the volcanic soils of the Azores produces < 5 kg $ha^{-1}$ 1 $year^{-1}$ 1 of sediment under pasture cover, but increased to almost 15 ton. $ha^{-1}$ 1 during periods of soil disturbance by tillage and less protected by vegetation (Fontes et al., 2004).

Furthermore, mass-wasting events, including large-scale flank collapses and landslides, are significant in the Azores, influenced by hydroclimatic changes, marine erosion, and tectono-volcanic activity (Costa et al., 2015; Marques et al., 2008; Hildenbrand et al., 2018; Malheiro, 2006).

## 2.4 Lacustrine sedimentary infill

Sediments deposited in the Azorean lakes are commonly composed of a variable mixture of in-lake algal productivity remnants, allochthonous terrigenous and organic material, and tephra deposits. These lake sediments have been particularly useful to perform Holocene paleoenvironmental reconstructions of the first human arrival in the archipelago and progressive anthropic pressure increase after the Portuguese colonization (Raposeiro et al., 2021), with the consequent degradation of ecosystems (Ritter et al., 2022; Richter et al., 2022; Vázquez-Loureiro et al., 2019; Connor et al., 2012; Rull et al., 2017) as well to reconstruct the late Holocene paleoclimatic evolution and to infer atmospheric circulation spatiotemporal patterns in the central north Atlantic region with high temporal resolution (Björck et al., 2006; Hernández et al., 2017; Richter et al., 2022). Furthermore, tephra deposits hosted in these lakes have allowed the reconstruction of the eruptive styles and histories of the islands (Andrade et al., 2021; 2022; 2023).

### 2.4.2 Paleoclimatic evolution

Proxy-based studies have offered insights into the relationship between the lacustrine systems of the Azores Archipelago and the late Holocene evolution of the climatic system in the central north Atlantic. The NAO partly controls climatic conditions of the archipelago (Björck et al., 2006; Hernandez et al., 2017; Richter et al., 2022; Rubio-Ingles, 2016). Wetter conditions in the Azores region occur during negative phases of the NAO at inter-decadal time-scales. Furthermore, the EA seems to have some influence in the summer temperatures of the region (Rubio-Ingles, 2016). Oceanographic circulation modes have also been suggested as influencers on the Azorean climatic evolution over the last millennia. Hernández et al. (2017) discussed the effects of the Atlantic Multidecadal Oscillation over the biogeochemical composition of the sediments of Lake Empadadas in São Miguel Island during the last millennium. Björck et al., 2006 inferred Atlantic drift-ice variations as a possible source of climatic variability across the central north Atlantic further back in time (350 to 5100 cal yr BP).

### 2.4.3 Settlement and colonization

Despite the Azores already appearing in maps dating back to 1330 CE (anonymous), the Portuguese official discovery of the archipelago was pinpointed between 1427 CE (Santa Maria Island) to 1452 CE (Flores and Corvo islands). Raposeiro et al. (2021) used lake sediment proxy records (fecal sterols, macro-charcoal particles and PAH, vegetal macrofossils, pollen, diatoms and biogeochemical elements and isotopes), supported by climate model simulations and additional archeological and genetic evidence, to evidence a complex colonization pattern of the archipelago since the early medieval times (Fig. 2.11).

The occupation of the three groups of islands may have been simultaneous, but the colonization pattern was influenced by physical geographic gradients. The spatiotemporal variation of the atmospheric circulation in the north Atlantic led to varying climatic conditions that facilitated colonization pulses at different times from different latitudes of Europe. Furthermore, altitudinal gradients of the islands conditioned water resource availability, forcing the first inhabitants to occupy the highlands of steeper islands first (looking for the permanent lentic waterbodies) than in the flatter ones, which have better-developed hydrological systems with lotic systems supplying freshwater to coastal settlements. Climate changes may have forced the inhabitants of flatter islands to look for hydrological resources in the highland lakes only during prevalent dry and warm periods.

In this complex geographic setting, Azorean colonization has occurred in four different phases depending on the steadily increase of anthropic pressure: a) the pre-anthropogenic state (up to 800 CE); b) the first anthropogenic impacts which took place from 800 to 1070 CE through livestock introduction and local forest clearance, likely performed by the Norse, whose arrival from

Scandinavia would have been favored by weakened westerlies during the end of the EMA, when a $NAO^-/EA^-$ atmospheric configuration prevailed; c) widespread human presence, farming, and regional deforestation with the slash and burn method from 1070 to 1420 CE; d) consolidation of profound ecological transformation of terrestrial and lacustrine ecosystems from 1420 CE to the present through forest burning, cereal cultivation and animal husbandry, driven by the Portuguese, whose arrival from the Iberian Peninsula was favored by weakened westerlies during the LIA when $NAO^-/EA^+$ atmospheric configuration prevailed.

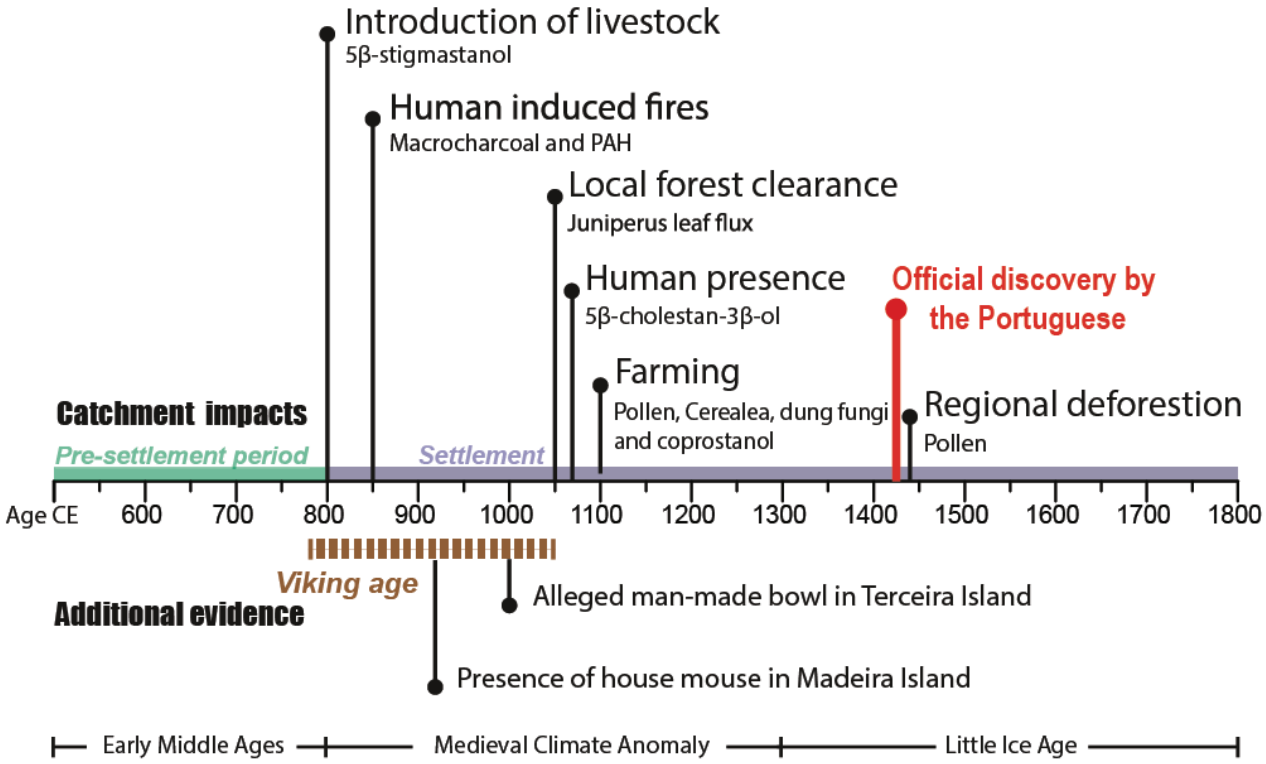


*Fig. 2.11: Summary of evidence for earlier human activities and the timing of the Portuguese arrival in the Azores Archipelago between 500 to 1800 CE (from Raposeiro et al., 2021).*

Thus, the increasing anthropogenic pressure has played a crucial role in driving diverse degrees of degradation in the waters of Azorean lakes. It has led to irreversible changes in the trophic state of the lakes through an increase of soil erosion after deforestation (Rull et al., 2017) and fish introduction promoting resuspension (Raposeiro et al., 2017). Furthermore, climatic and anthropic synergy effects on lacustrine sedimentation have occurred (Ritter et al., 2022). High nutrient inputs into some lakes due to fertilizers from agricultural practices result in their eutrophication (Gonçalves et al. 2006a, b; Antunes and Rodrigues 2011; Gonçalves, 2008). The most eutrophic aquatic systems are found in basins where the surrounding land is exploited by the livestock industry (Antunes and Rodriguez, 2011). In 2018, 39% of lakes were classified as eutrophic.

### 2.4.4 Paleoecology and ecosystems shifts

#### Vegetation

Rull et al., 2017 reconstructed the evolution of São Miguel Island flora in the EG using pollen from lake sediments of Lake Azul (Fig. 2.10). The pollen compositional shifts reveal three distinct vegetation zones, reflecting shifts in plant communities and human activities over time.

a) From 1273 CE±40 to 1358 CE±40, there was a dominance of native trees such as *Juniperus brevifolia* and *Morella faya*, indicative of the original laurisilva forests that covered the island before human settlement. However, a decline in *Juniperus pollen*, coupled with the

appearance of cereal pollen like *Secale cereale*, suggests human impact, possibly through forest burning and initial attempts at cereal cultivation.

b) From 1422 CE±40 to 1845 CE±21, the disappearance of *Juniperus brevifolia* and *Picconia azorica* pollen indicates the loss of native forests, likely due to deforestation by fire. Historical records support this, noting extensive forest use for charcoal and housing. The landscape transitioned to open vegetation dominated by *Erica azorica* and *Myrsine africana* shrubs, possibly for grazing, with sporadic cereal cultivation.
c) From 1848 CE±21 to 2010 CE±1, there was a significant shift characterized by the decline of *Erica azorica* and *Myrsine africana*, replaced by exotic trees like *Pinus pinaster* and *Cryptomeria japonica*, reflecting intensive forestry practices. The increase in ornamental plants like *Hydrangea macrophylla* further signifies landscape modification. Despite fluctuations, the dominance of imported trees indicates sustained human influence on the vegetation.

Besides, Connor et al. (2012) analyzed flora changes resulting from island colonization in the CG and WG, using a palynological approach with sediments from Lake Caveiro and Bog (Pico Island) and Lake Rasa (Flores island; Fig. 2.10). Environmental reconstructions were divided into statistically significant pre-human impact and post-human impact phases. The phase boundaries felt around 490 cal. yr BP for Lagoa Rasa, 410 cal. yr BP for Lagoa do Caveiro, and 385 cal. yr BP for Pico Bog, and they coincide with colonization history (Raposeiro et al., 2021).

### Freshwater habitats

Raposeiro et al. (2018) investigated the spatial distribution of sub-fossil diatom and chironomid assemblages in surface sediments of Lake Azul in São Miguel Island (Fig. 2.10). This study highlighted the effects of the spatial distribution of sedimentation and taphonomic processes inducing significant variability over the composition and distribution of the sub-fossil remains. Sedimentation processes, particularly the sand fraction, play a key role in shaping the distribution of diatom and chironomid assemblages in Lake Azul. The observed gradient of fossil assemblages from nearshore to offshore reflected the real living compositions close to their habitats, but taphonomic processes have a strong effect on spatial distribution, particularly in areas with steeper slopes. Thus, they demonstrated that working with biological proxies based on a single offshore deeper zone can lead to a loss of species diversity, highlighting the importance of multi-core and multi-site approaches in high depth-gradient lakes to improve the accuracy of environmental reconstructions.

Vázquez-Loureiro et al., (2019), in turn, emphasized the paleoecological evolution of Lake Azul, using diatom assemblages over the past approximately 720 years. They established 6 main phases: 1) an eruptive phase marking the beginning of the lake history after a volcanic eruption (Caldeira Seca P17 eruption); 2) a moderately shallow oligotrophic lake; 3) a deep oligotrophic lake; 4) an oligotrophic lake and transition to a new trophic state; 5) a deep mesotrophic lake; 6) a deep meso-eutrophic stratified lake.

The identified long-term drivers of trophic status changes were eruptive volcanism, external nutrient loads, changes in lake morphometry, trophic controls, changes in water column mixing regime, and artificial fertilization. The cataclysmic eruption of Caldeira Seca P17 played a primary role in configuring the lake ecology, with subsequent phases influenced by both natural and anthropogenic factors.

Furthermore, Vazquéz-Loureiro et al., (2023) provided a comprehensive analysis of the drivers influencing algal assemblage composition in the neighbor Lake Santiago (Fig 1.10), as well as the ecological history of the lake and its response to environmental forcing. They also defined a number of phases of ecological evolution: 1) an eutrophic lake due to an enhanced nutrient runoff from the catchment; 2) a shift to mesotrophic conditions due to changes in nutrient availability and light:P and

N:P ratios, with changes in the mixing regime of the lake; 3) a return to eutrophic conditions due to factors such as weakened summer stratification and prolonged reduction in spring and summer temperatures; 4) a probable regime shift with an enhanced stability of the water column, possibly related to increased spring and summer temperatures under global warming conditions. A comparison with Lake Azul highlights differences in ecological responses despite their proximity and similar climatic context. Factors such as volcanic eruptions, tephra deposition, catchment characteristics, and lake morphology contribute to divergent ecological histories between the two lakes.

The paleoecology and ecosystem shifts from the studied lakes here are developed in section 2.5.

## 2.5 Study area

Within the Azores Archipelago the present PhD Thesis encompasses the WG and the CG (Fig. 2.1), focusing on Flores (25 S 655404.67 m E 4367991.39 m N), Corvo (25 S 662203.07 m E 4396428.61 m N) and Pico (26 S 384584.00 m E 4257467.31 m N) islands (Fig. 2.1).

### 2.5.1 The Azores Archipelago Western Group

The sub-orthogonal structural pattern dominating westward of the MAR conditioned the volcanic nucleation and evolution of the WG islands within the North American plate, resulting in relative sub-isometric morphologies (Azevedo & Ferreira, 2006). The prevalent fractures related to the MAR favoured an approximately NNE-SSW preferred accretion of the WG to form a 4000 m high single volcanic edifice that connects at the base (Azevedo & Ferreira, 1999; 2006; França et al., 2006; Genske et al., 2012; Dias, 2001). The construction of the composed Azores Archipelago WG volcanic edifice involved a proto-insular stage characterized by submarine and emergent eruptions, which began forming 2.2 Ma ago, followed by an insular stage with subaerial eruptions that started 0.7 Ma ago (Azevedo & Portugal Ferreira, 2006; Azevedo, 1991; Genske et al., 2012; Dias, 2001). The products resulting from the insular volcanism of the WG mainly consist of lava flows and pyroclastic deposits (fall and surge deposits) with compositions ranging from alkali basalts to trachytes (Azevedo and Portugal Ferreira, 2006; Larrea et al., 2013). These rocks present porphyritic textures characterized by the presence of megacrysts of clinopyroxene (Ti-Augite), olivine, and plagioclase up to 2 cm, included in finely-crystalline plagioclase dominated groundmass (Genske et al., 2012; Larrea, 2014) (Fig. 2.12).

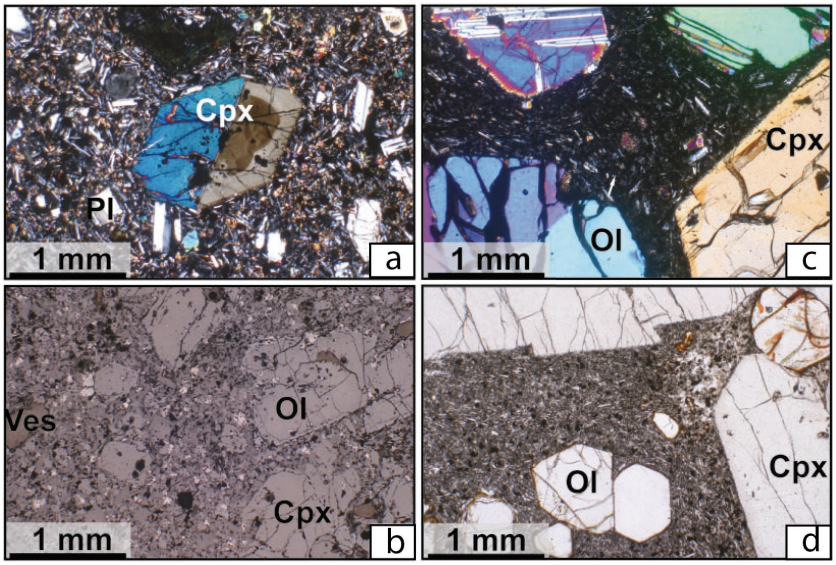


*Fig. 2.12: Representative photomicrographs of the WG alkali basatls: Left side Flores Island (sample location close to Santa Cruz; Fig. 2.13), right side Corvo island (sample from the inner Caldera; Fig. 2.17), up-side crossed polars, down-side reflected light. Cpx: clinopyroxene, Ol: olivine, Pl: plagioclase, Ves: vesuvianite.*

*Note the porphyritic textures and the megacrysts of Cpx and Ol. The reader is referred to the original source for further details of sample location (modified from Genske et al., 2012), corresponding the photomicrographs from Flores Island to FL-09 sample and the ones from Corvo Island to the C-09 sample.*

## Flores Island

Flores is the westernmost island of the Azores Archipelago (Fig. 2.2 and 2.13) with a surface of 143 km$^2$, maximum length of 16 km, and a width of up to 12 km (Fig 2.13). The peripheric lowlands are characterized by prominent incised valleys and cliffs. The highlands are composed by a central plateau with elevations above 500 m asl, where the island reaches a maximum altitude of 915 m asl at Morro Alto Peak. Within this central plateau, a 100 m relief depression dominates the southwesternmost sector, locally known as the "Caldeira das Sete Lagoas".

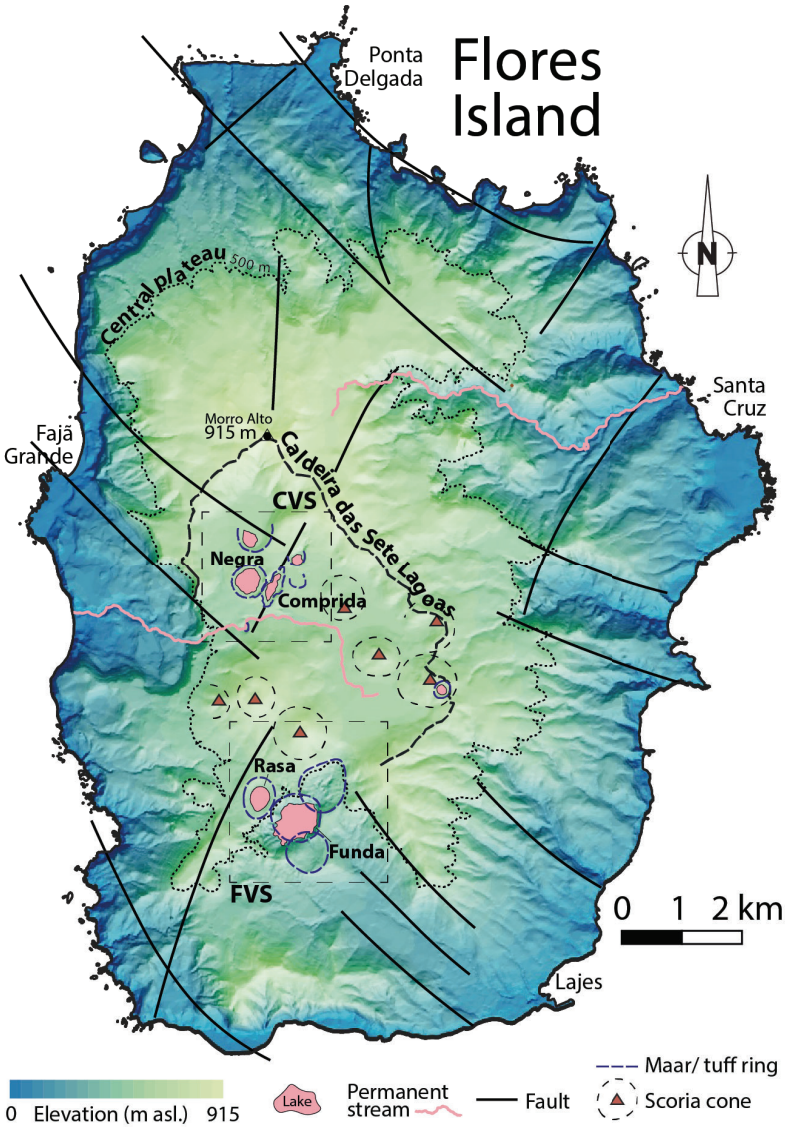


*Fig. 2.13: Digital Elevation Model of Flores Island including a tectono-volcanic map composed of faults identified by Azevedo and Portugal Ferreira, (2006) and the phreatomagmatic structures discussed by Andrade et al. (2022; 2023). CVS: Comprida Volcanic System. FVS: Funda Volcanic System. Geographic domains and surficial waters are also indicated.*

Flores Island morphology was shaped by the progradation of overlapping polygenetic volcanoes (composing a main central volcano), vertical tectonic movements, and mass-wasting episodes (Azevedo and Portugal Fereira, 1999; 2006; Hildenbrand et al., 2018). The insular tectonovolcanic architecture (Azevedo and Portugal Ferreira, 2006; Andrade et al., 2022; 2023) involved: 1) a first stage from 700 to 500 Ka of effusive and explosive volcanism that generated a massive production

of lava and pyroclastic deposits, corresponding in turn with a period of marked tectonic uplift (1000 to 550 ka); 2) a second stage of tectonic subsidence (550 to 400 ka) when isostatic compensation of the previous volcanic loads led to the main volcanic edifice collapse resulting in the formation of the Caldeira das Sete Lagoas within the central plateau (Andrade et al., 2022; 2023) (Fig. 2.13); 3) a second stage that occurred between 400 and 200 ka of effusive volcanism fed from small volcanic centres; and 4) the last stage of volcanism (<200 to 3 ka), composed by monogenetic effusive and explosive basaltic eruptions, some of them with violent phreatomagmatic activity, taking advantage of the MAR-related structural intersections (Morisseau and Traineau, 1985; Azevedo and Portugal Ferreira, 2006; Andrade et al., 2021; 2022; 2023). These eruptions mainly occurred within the Caldeira das Sete Lagoas, where the effusive activity led to the formation of strombolian scoria cones and lava flows infilling alluvial valleys towards the lowlands. The explosive volcanic activity generated eruptive centres, highlighting the Comprida Volcanic System (CVS) and the Funda Volcanic System (FVS) on the northern and southern sides, respectively. The CVS encompasses a cluster of five (probably six) maar craters formed in a single volcanic eruption ca. 3200 years ago, whereas the FVS includes a cluster of three, probably four, coalescent vents forming a compound maar crater and a tuff ring that formed between 3430 and 3250 years ago (Azevedo & Ferreira, 2006; Andrade et al., 2021; 2022; 2023) (Fig. 2.13).

Most of the lake systems in Flores are sited within the pronounced terrain depressions derived from the maars and tuff rings (Cruz et al., 2006; Antunes and Carvalho, 2018) formed during the last stage of volcanism in the island (Andrade et al., 2021; 2022; 2023) (Fig. 2.13). This configuration confers them with high topo-bathymetric gradients, featuring steep littoral margins and reduced shallow areas. These lakes exhibit thermal water stratification in the summer that does not affect hydrogeochemical composition in depth, which is dominated by Na-Cl in small lakes, while large ones exhibit Ca-HCO3 chemical facies. Generally, the lake waters are freshwater with low mineralization. Lakes in Flores Island do not interact with the seepage of magmatic fluids, instead, the organic matter degradation is the only source of $CO_2$ (Antunes and Rodrigues, 2014).

### Funda lake-catchment system

From Flores Island, the case study is the Funda lake-catchment system (Fig. 2.14), which develops with the Rasa Lake system. In this system, the Flores Island plateau meets the FVS at the structural intersection of the southernmost edge of the Caldeira das Sete Lagoas (Azevedo and Portugal Ferreira, 2006; Andrade et al., 2022).

The watershed of the Funda lake system (Fig. 2.13) covers 3.14 $km^2$ and is composed of volcanic rocks of the insular stage (Azevedo and Portugal Ferreira, 2006; Larrea et al., 2018; Geske., 2012) (Fig. 2.11). It comprises part of the Flores Island plateau at the west-to-north-western periphery, including the southwestern flank of a scoria cone at the north side of the watershed (Fig. 2.14 and 15f) and the southernmost edge of the Caldeira das Sete Lagoas at the northeast (Fig. 2.14). Also, the east-to-southwest periphery and the central sector are occupied by the compound crater formed by the maar cluster of the FVS. The northeastern sector of the crater is filled by the north-eastern maar, where the most prominent erosive scars within the watershed indicate an enhanced progression of alluvial incision (Figs. 2.14 and 15c). The southern sector contains the southern maar (Andrade et al., 2021), whereas the central sector contains the Funda maar, where the lake lays, surrounded by steep flanks. Funda maar has a peripheric rim incised in the transition to the central plateau (Figs. 2.14 and 15d). At the north-eastern drainage mouth, the topmost part of a subaquatic alluvial fan emerges from Lake Funda (Fig. 2.15e).

The vegetation within the watershed comprises introduced tree and herbaceous species such as *Cryptomeria japonica* distributed in patches dominating the southwestern and north-eastern sides (Fig. 2.15a and g) and *Hedychium gardneranum* widely and densely extended throughout the

watershed (Fig. 2.15), whereas native bushes such as *Erica azorica,* found at the southern side of the watershed, have resisted the increased anthropic pressure during the last centuries. Before regional deforestation, the vegetation in the Funda watershed should likely consist of *Laurus submontane* forests in the lower domain and Juniperus-Ilex montane forest and woodlands at higher elevations in the northern scoria cone (Elias et al., 2016; Fig. 2.9). The land uses of the surrounding areas of the lake are forestry production (0.18 km2) and cow grazing (0.41 km2), whereas bushes cover 2.1 km2 (DROTRH/INAG, 2001).

The Lake Funda system is endorheic, and most of the drainage is formed by ephemeral streams, however, a semipermanent/permanent stream flowing within the northeastern maar supplies detrital material and water to the lake (Fig. 2.14): a) the northeastern semipermanent stream flows through the prominent incised sector of the NE maar crater and drains most of the NE sector of the watershed, being the fastest flowing and most persistent; b) the northeastern stream, which is the steeper and drains the small northwestern sector of the basin; c) the southwestern one that flows along the western sector of the central maar, and d) the southern one that flows across the S maar. The b and c streams b and c correspond with the incised sectors of the Lake Funda rim and are likely fed by the groundwaters of Lake Rasa, lying at ca. 200 m above Lake Funda.

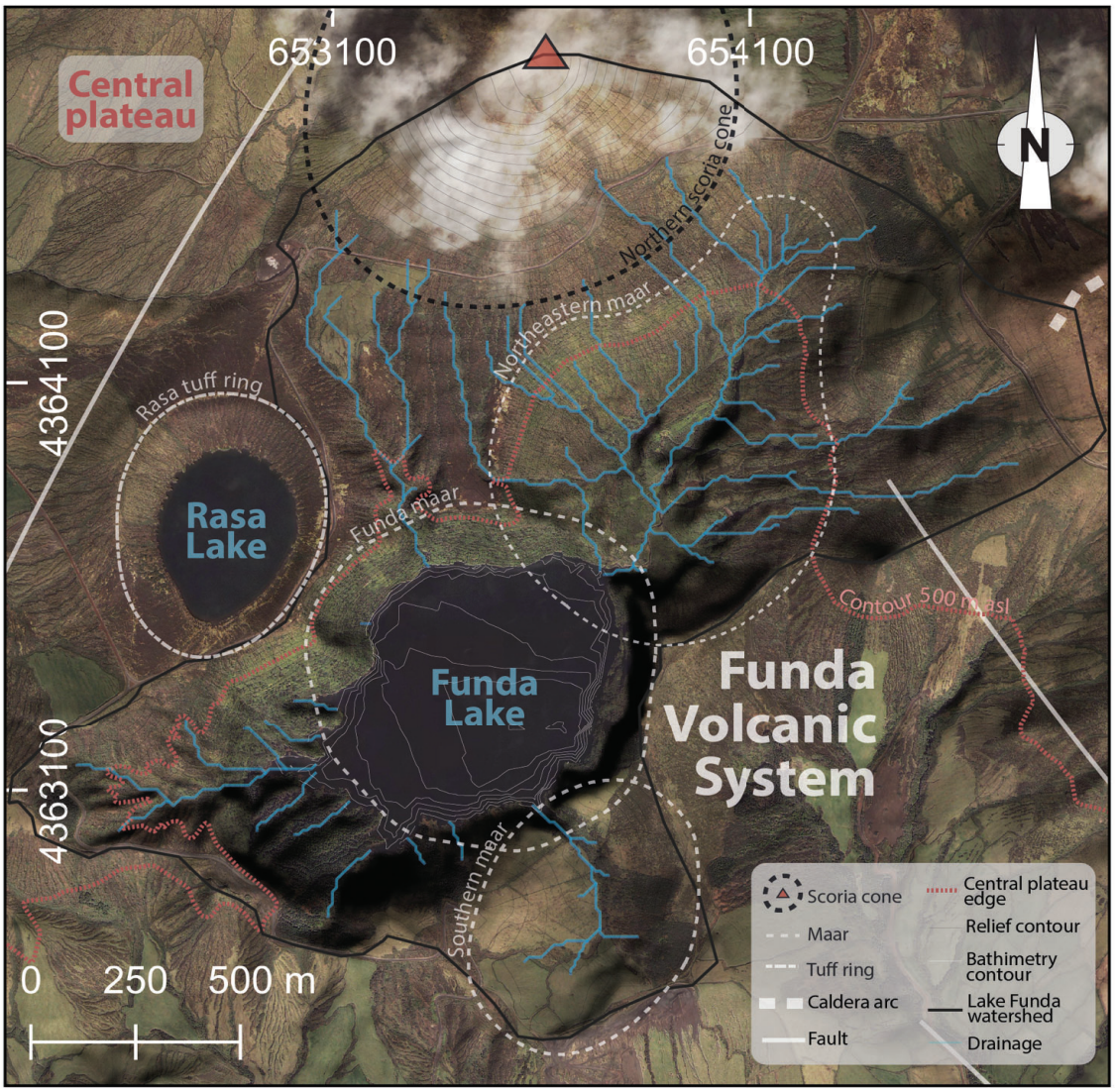


*Fig. 2.14: Funda Volcanic System. Geographic domains (central plateau) and tectono-volcanic features such as maars, tuff rings, scoria cones (Andrade et al., 2022;2023) and faults (Azevedo and Portugal Ferreira, 2006) are indicated. Relief contour: max = 470 m asl, min= 360 m asl, equidistance = 10 m. Bathymetry contour: max =360 m asl, min = 325 m asl, equidistance = 5 m.*

Lake Funda is a maar lake located at 360 m asl inside the central and largest vent of the FVS. It has a maximum water depth of 35.7 m, follows a monomictic thermal regime and it has a water volume of 7.93 x $10^6$ $m^3$. It occupies an area of 0.36 $km^2$ with an ellipsoidal perimeter 873 m long and 635 wide (Andrade et al., 2019; Antunes and Rodrigues, 2014) (Figs. 2.14 and 15).

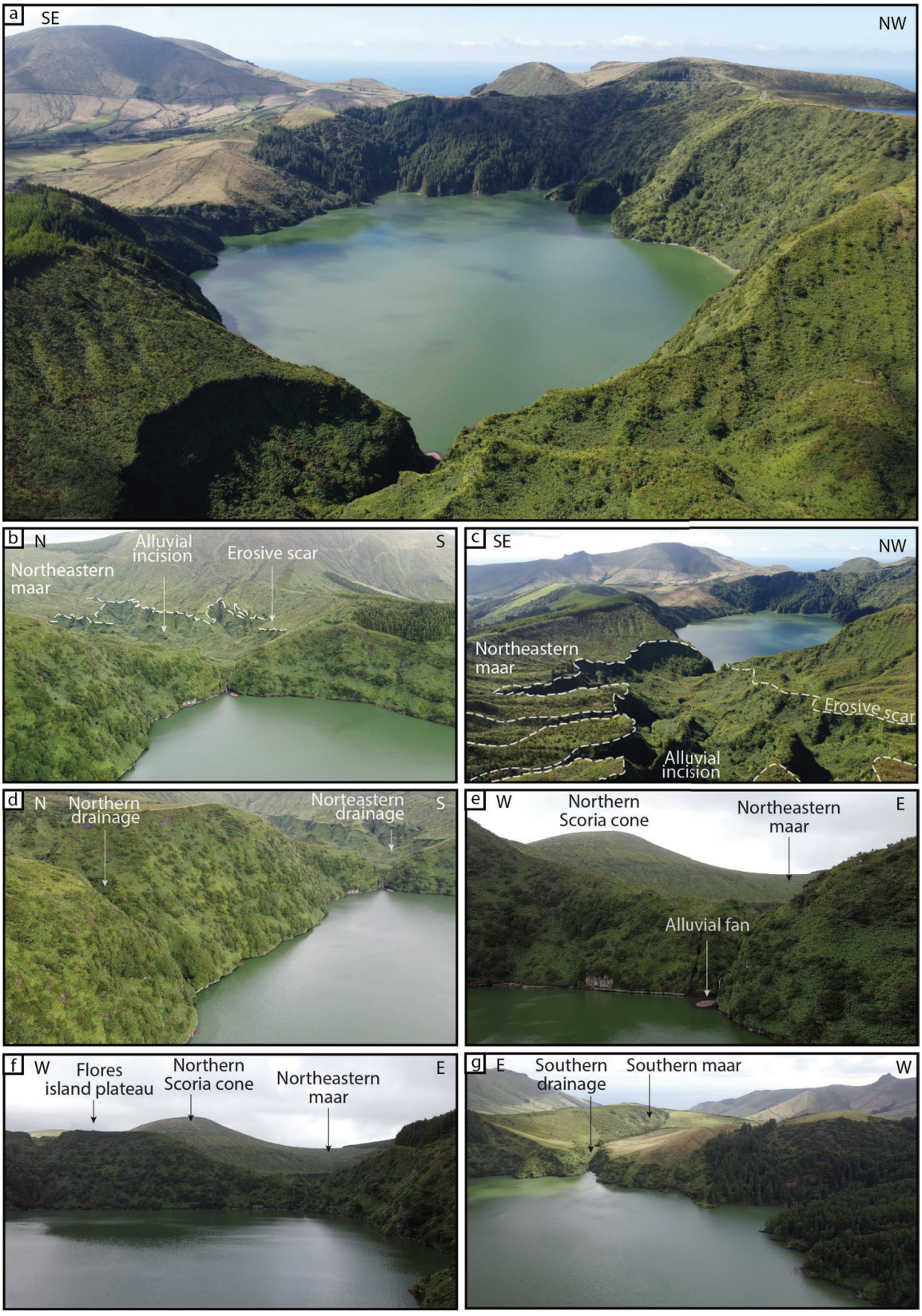


*Fig. 2.15: Photographs of Lake Funda System: a) general overview of Lake Funda, b) northeastern and c) southwestern perspectives of the northeastern maar, d) northern margin of Lake Funda, southwestern and north-eastern perspectives of the incised sector within the NE maar crater, respectively.*

The lake has a residence time of 2.7 years (Andrade et al., 2019). pH levels fluctuate between 6.71 and 9.94, with a mean of 7.54 and a median of 7.4 (Antunes et al., 2006). Electrical conductivity ranges from 76 to 148 µS·cm−1, with a mean of 106.4 µS·cm−1 and a median of 123 µS·cm−1 (Antunes et al., 2006). Temperature varies from 11.5°C in January to 26.6°C in August. Stratification typically begins around May/June and persists until November (Ritter et al., 2022; Gonçalves et al., 2009) (Fig. 2.16). During summer, the hypolimnion forms below approximately 15 meters depth, leading to a decrease in pH and oxygen levels, occasionally resulting in full anoxia, along with an increase in total CO2 (Antunes et al., 2006).

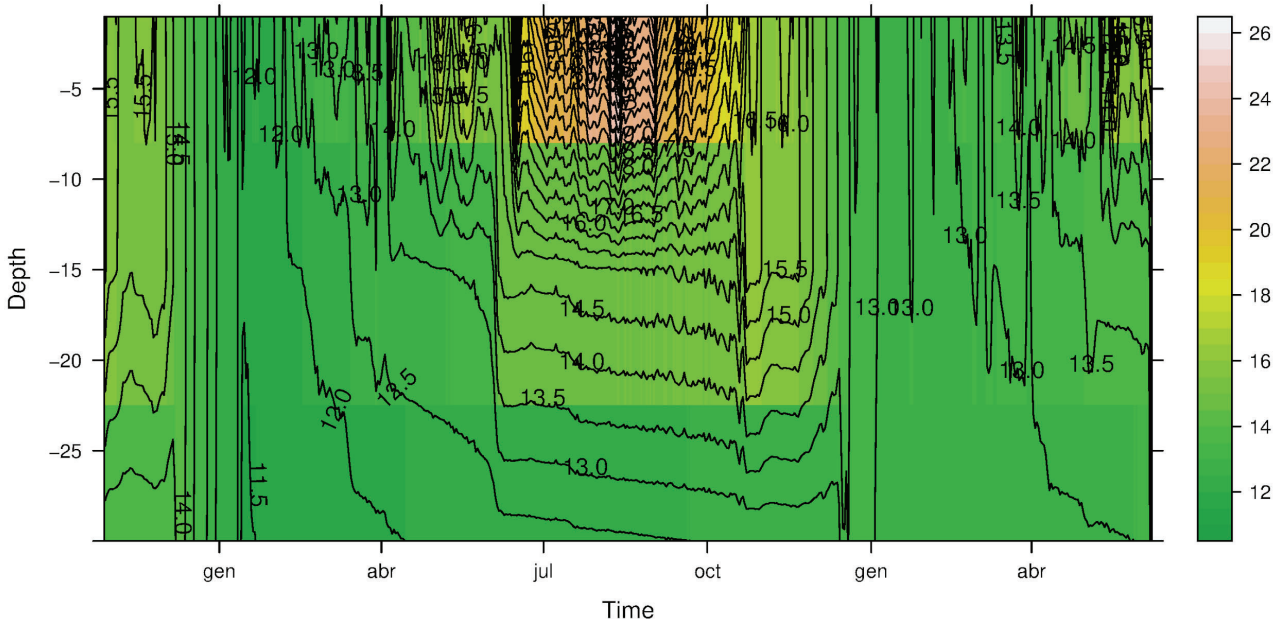


*Fig. 2.16: Lake Funda* continuous temperature (ºC) records from October 2015 to June 2017 in depth (Gonçalves et al., 2009).

Hydrogeochemistry of Lake Funda is characterized by Na-Cl type with influence of Na-Ca-$HCO_3$ chemical facies, resulting from sea salt contribution and water-rock interaction (Antunes and Rodrigues, 2014). The lake presents a bicarbonate sodium tendency at the bottom (Cruz et al., 2006). The total $CO_2$ content along the water column ranges from 24.76 to 38.32 mg·$L^{-1}$ (mean = 30.45 mg·$L^{-1}$). The seasonal effect on the total amount of $CO_2$ emitted into the atmosphere is present, and during summer is 0.36 t·d−1, and through winter, the emissions are expected to be higher due to full mixing (Andrade et al., 2019). Lake Funda has a significantly higher concentration of $CO_2$ in the hypolimnion compared to other lakes on Flores Island, consistent with the higher productivity of this lake (Antunes and Carvalho, 2018).

### Funda lake sediments

Ritter et al. (2022) applied partitioning RDA to pollen, diatoms and chironomids biotic assemblages of Lake Funda sediments, enabling the reconstruction of the main ecological phases. The δ15N served as an indicator of in-lake dynamics variability, reflecting changes in nutrient availability and the influence of climate and anthropogenic impacts on lake ecosystems. Three main phases of ecological evolution in Lake Funda and their relationships with human climate and internal factors over the last millennium were recognized (Fig. 2.17):

1) The mesotrophic phase A (from 950 ± 50 to 1330 ± 40 CE) characterized by the absence of coprophilous fungi and the presence of dense forest cover around the lake basin. During this period, the pollen record indicates the dominance of junipers at higher altitudes and laurel forests in lower areas (Elias et al., 2016; Fig. 2.9). Biological assemblages reflect climatic stability, with greater

variability better explained by climate than by deforestation or internal lake dynamics. However, around 1200 AD, changes in biological assemblages suggest water level oscillations due to frequent intense runoff episodes.

2) The transitional Phase B (from 1330 ± 40 to 1565 ± 10 CE), constituting an ecological shift developed during the transition from the Medieval Climate Anomaly to the Little Ice Age. It is characterized by high climate variability and the onset of anthropogenic disturbances in the catchment. Initial climate instability is reflected in extreme variability in all studied proxies. Human activities, such as deforestation and livestock farming, rapidly transform the ecosystem, increasing soil erosion and nutrient input to the lake. This change leads to rapid eutrophication of the lake and significant alteration in the biological community, especially among primary producers.

3) The eutrophic Phase C (from 1565 ± 10 to 2009 ± 5 CE), when the lake shows a decrease in biological diversity and an increase in eutrophication, associated with changes in lake dynamics and the presence of cattle. The effects of Portuguese colonization on Lake Funda after 1563 CE are evident in changes in vegetation and human activity in the surrounding area. Climatic factors, especially during the Little Ice Age, have been determining factors in lake variability, affecting productivity and species composition. Eutrophication intensifies in more recent phases, caused by phosphorus remobilization and increased nitrogen-fixing cyanobacteria.

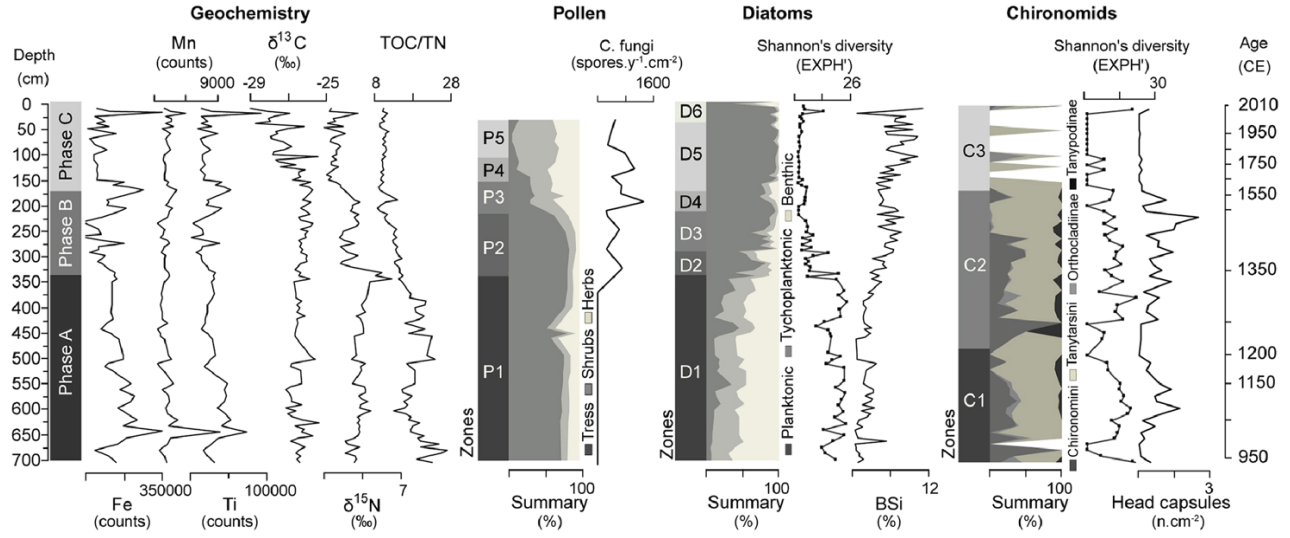


*Fig. 2.17: Stratigraphic profiles of geochemical and biological data from Lake Funda. From left to right: geochemistry stratigraphic zones, Fe, Mn, Ti, $\delta^{13}C$, $\delta^{15}N$ and TOC/TN profiles, pollen stratigraphic zones, major pollen groups, % of fungi, diatom stratigraphic zones, major diatom groups, diatom diversity profile, biogenic silica profile, chironomid stratigraphic zones, chironomid diversity and head capsules profiles (adapted from Ritter et al. 2023).*

Furthermore, Richter et al., (2022), used Lake Funda sediments to investigate the hydrogen isotope composition of leaf waxes (δDwax), which in higher terrestrial plants correlates with changes in precipitation isotopic composition (δDprecip) (Sachse et al., 2012). They reported early human presence on the Azores likely dating back to c. 700-850 CE based on paleoecological evidence, suggesting limited settlements existed before Portuguese colonization in the 15th century (Raposeiro et al., 2021). Between c. 1000-1400 CE, stable climatic conditions prevailed on Flores Island, evident from pollen and leaf wax records (Connor et al., 2012; Raposeiro et al., 2021). However, by c. 1300-1350 CE, changes in nitrogen isotopes indicated increased N-fixation likely due to livestock presence, impacting lake nutrient dynamics (Raposeiro et al., 2021). Human activities intensified around c. 1500 CE, evidenced by changes in sediment proxies like C/N ratios and biogenic silica, indicating increased nutrient inputs to Lake Funda (Raposeiro et al., 2021). Lake Funda response to human impacts suggested a shift to a new trophic state and loss of resilience

(Ritter et al., 2022). The 20th century saw further environmental changes, including reforestation efforts and fluctuations in precipitation, affecting lake ecosystems (Raposeiro et al., 2017; Borges et al., 2019). Despite reforestation, Lake Funda remained eutrophic, emphasizing the long-term impacts of human activities on lake ecosystems.

### Corvo Island

Corvo Island is located at 20 km to the NNE from Flores, making it the remotest island of the archipelago (Fig. 2.1). Moreover, is the smallest island, with 6.3 km long and 4 km wide, covering a surface of 17.1 km$^2$ (Fig 2.17). The tectono-volcanic evolution of Corvo insular stage was marked by the development of a polygenetic single shield volcano coronated by a collapsed summit caldera (Fig. 2.18). The most accepted volcanostratigraphy for Corvo Island is based on the relative chronology of the caldera formation (Fança et al., 2006; Larrea et al., 2013):

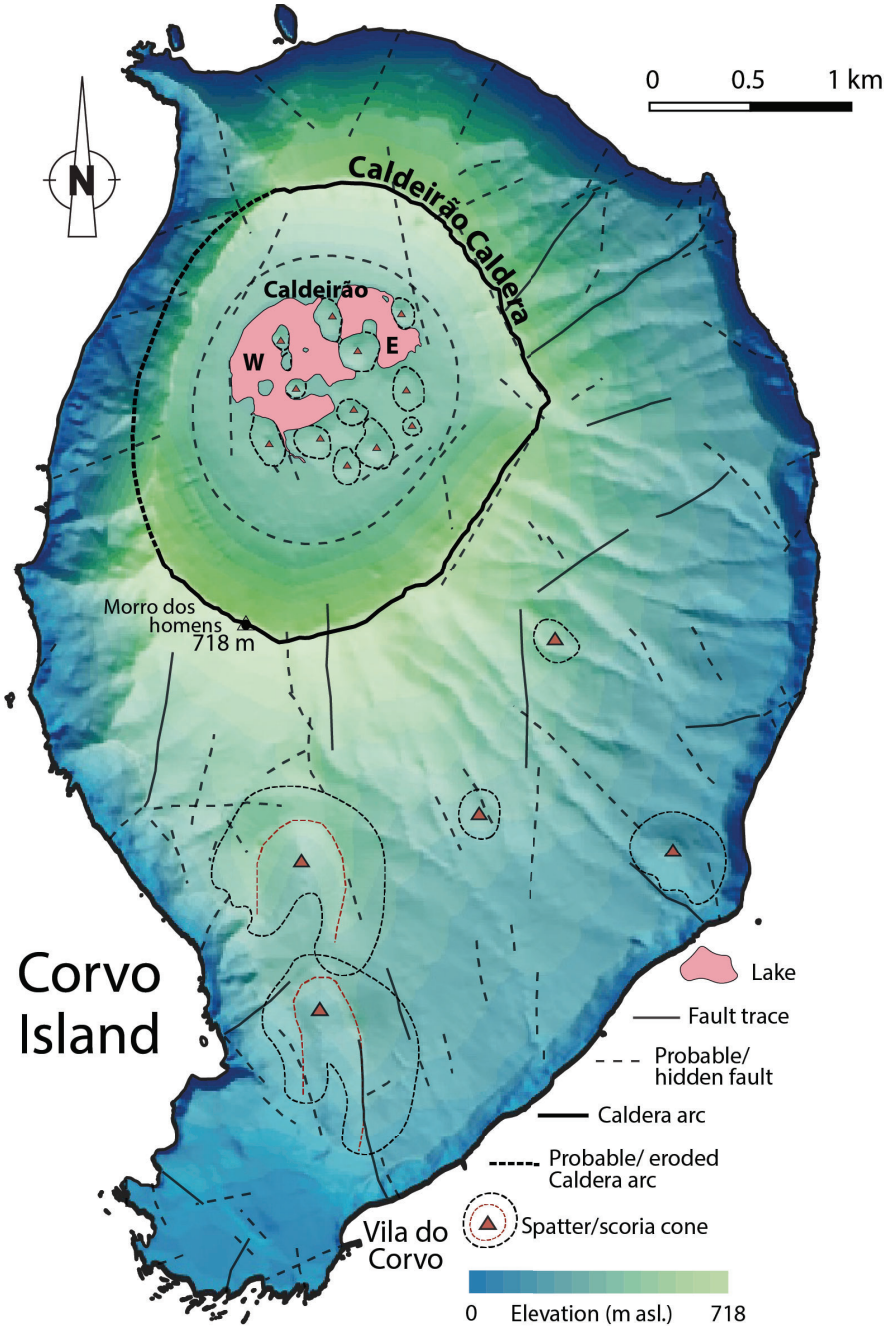


*Fig. 2.18: DEM of Corvo Island including a tectono-volcanic map composed by the faults identified by Dias (2001) and the volcanic structures from França et al. (2003). Surficial waters are indicated.*

1) The Pre-caldera stage comprises the first subaerial stages of the island, outcropping at the coastal cliffs where the oldest (1-1.5 Ma) lavas are found;

2) The syn-caldera stage is formed by pyroclastic deposits and lava flows associated with the stratovolcano collapse (Dias, 2001; Larrea, 2014) 0.43+/- 0.34 Ma ago (Pacheco et al., 2023). The caldera forming mechanism and date still remain a matter of active debate, however, no evidence has yet been found for deposits related to a major explosive eruption (Kueppers et al., 2018). Dias (2001) proposed a model based on tectonic collapse through ring-faulting;

3) The post-caldera stage, when the last volcanic activity in the island (Vila do Corvo flank eruption) took place ca. 80 ka ago (Zbyszwski, 1967; Dias, 2001; Genske et al., 2012; França et al., 2006). Within the inner part of the caldera, at the bottom, several strombolian phreatomagmatic cinder cones were formed after 370 ka (Beier et al. 2010) along the ring fault (Kueppers et al., 2018) (Fig. 2.18), whereas an alluvial and colluvial sedimentary infill occupies the peripheric sector smoothing the topography break derived from the ring fault (Dias, 2001).

According to Dias (2001), the fracturing of Corvo Island is composed of three families of faults covering highly varying orientations (Fig. 2.18): 1) between N010ºW and N090ºW; 2) between N010ºW and N010ºE; and 3) between N010ºE and N090ºE. However, the Vila do Corvo platform, the northeastern, and southwestern island sectors present more fracturing intensity related to the 1 and 2 fault families. Furthermore, in Corvo Island, the caldera ring fault imposes an annular trend, standing out over this structural pattern.

The highlands are characterized by a conic central mountain corresponding with the central volcano, and a 300-m-deep and 2-km-diameter landform depression corresponding to the caldera, locally known as "*Caldeirão*". This depressed relief is surrounded by an annular crest, where the maximum altitude of the island (718 m asl) is reached at "*Morro dos Homens*" peak in the southwesternmost part. The lowlands correspond to the central volcano base, where some side vents and related lava flows develop in the south, whereas prominent cliffs occupy the northern part of the island. Intense marine erosion affecting the northern and western cliffs led to the caldera western flank partial mass wasting (França et al., 2006) (Fig. 2.18).

Climate at the coastal southern lowland of Corvo Island shows a similar precipitation pattern as the one reconstructed from Ponta Delgada in Sao Miguel Island (Hernandez et al., 2016), though displaying wetter summers with a difference of ca. 20 mm. Temperatures are mild, displaying small annual variations, with the highest recorded during summer months with the peak in august (Fig. 2.19).

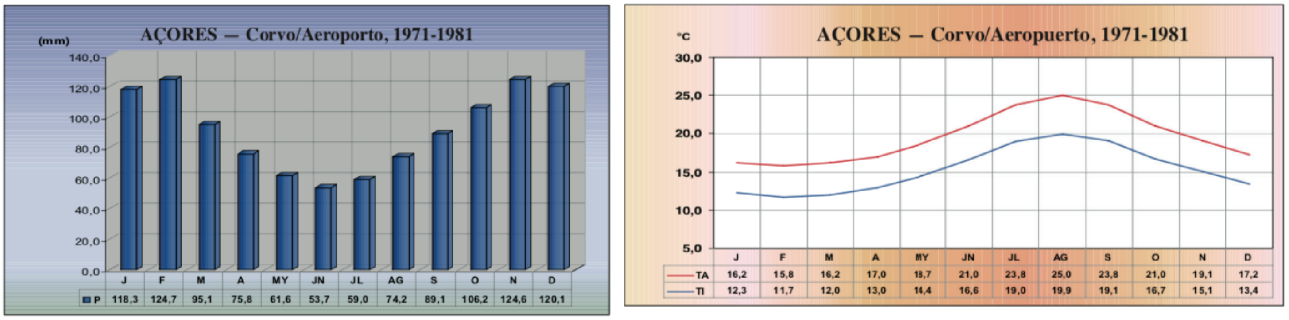


*Fig. 2.19: month climatic values of precipitation (left side) and air temperature (right side) in the Corvo Island airport (1971-2000). Modified from AEMET and IPMA (2012).*

### Caldeirão lake-catchment system

The only two lake systems of the island are located within the Caldera, forming Lake Caldeirão, an endorheic composed lake system. The watershed of Caldeirão W involves the western half and the southeastern quarter of the inner caldera, occupying an area of 2.31 km$^2$, whereas the watershed of Caldeirão E, locally known as "*Cachimbo*", extends the northeastern quarter, with an area of 0.97 km$^2$ (Fig. 2.20). The composed watershed is constituted by pyroclastic rocks (caldera flanks) and lava flows (caldera crests) of the insular stage (Dias, 2001; Larrea, 2014; Geske et al., 2012) (Fig. 2.11). The drainage within the composed watershed is centripetal at the caldera flanks, especially concentrated on the southwestern side. However, at the caldera bottom corresponding with the ring fault scarp, this drainage flow across alluvial fans coalescing to form the main river, which supplies siliciclastic material and water to a delta formed in the southern margin of Caldeirão W, commonly covered by macrophytes (Fig. 2.20 and 21a,c,g). Some of the steep post-caldera cinder cones are covered by the colluvial/alluvial infill and favour peatlands formation in the south-eastern part of the caldera bottom by retaining humidity in the watershed (Figs. 2.20 and 21e,f).

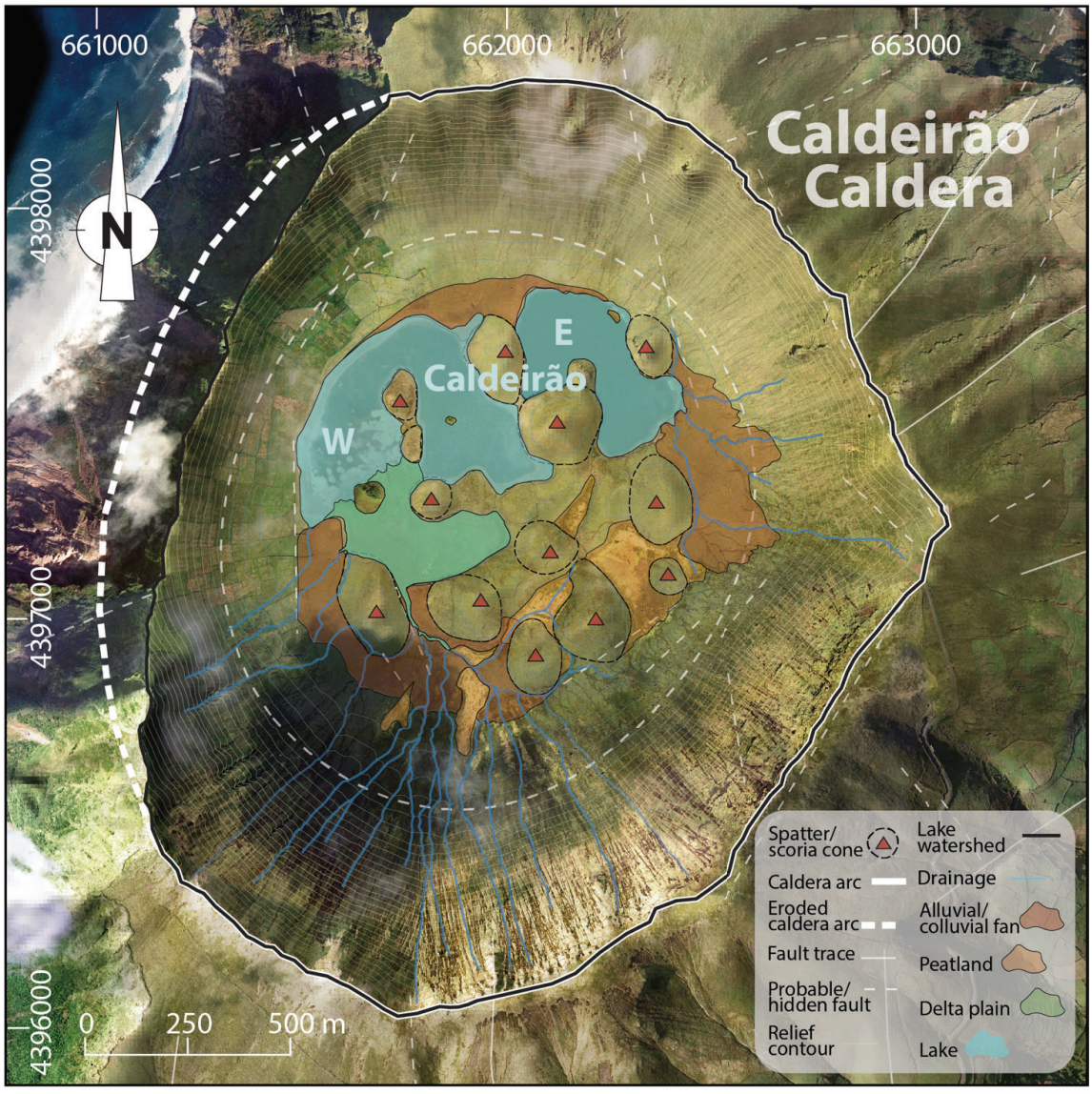


*Fig. 2.20: Caldeirão lake-catchment system within Corvo Caldera. Tectono-volcanic features such as faults (Dias, 2001), scoria cones and the caldera arc (França et al., 2003). Depositional environments such as alluvial fans (Dias, 2001) and peatlands are indicated.*

Nowadays, native vegetation is remnant at the inner part of the most prominent stream channels in the flat southern domain of the watershed, whereas the rest is mostly deforested. However, according to Elias et al., (2016), the natural potential vegetation within the caldera may have been

composed of Laurus submontane forest at the bottom sector, whereas Juniperus-Ilex montane forest would have been dominating the crest, especially the southernmost side (Fig. 2.9).

Land uses within the watershed are dominated by extensive cow grazing, covering 2.07 km$^2$ in the lake periphery, whereas 0.7 km$^2$ are occupied by bushes (DROTRH/INAG, 2001).

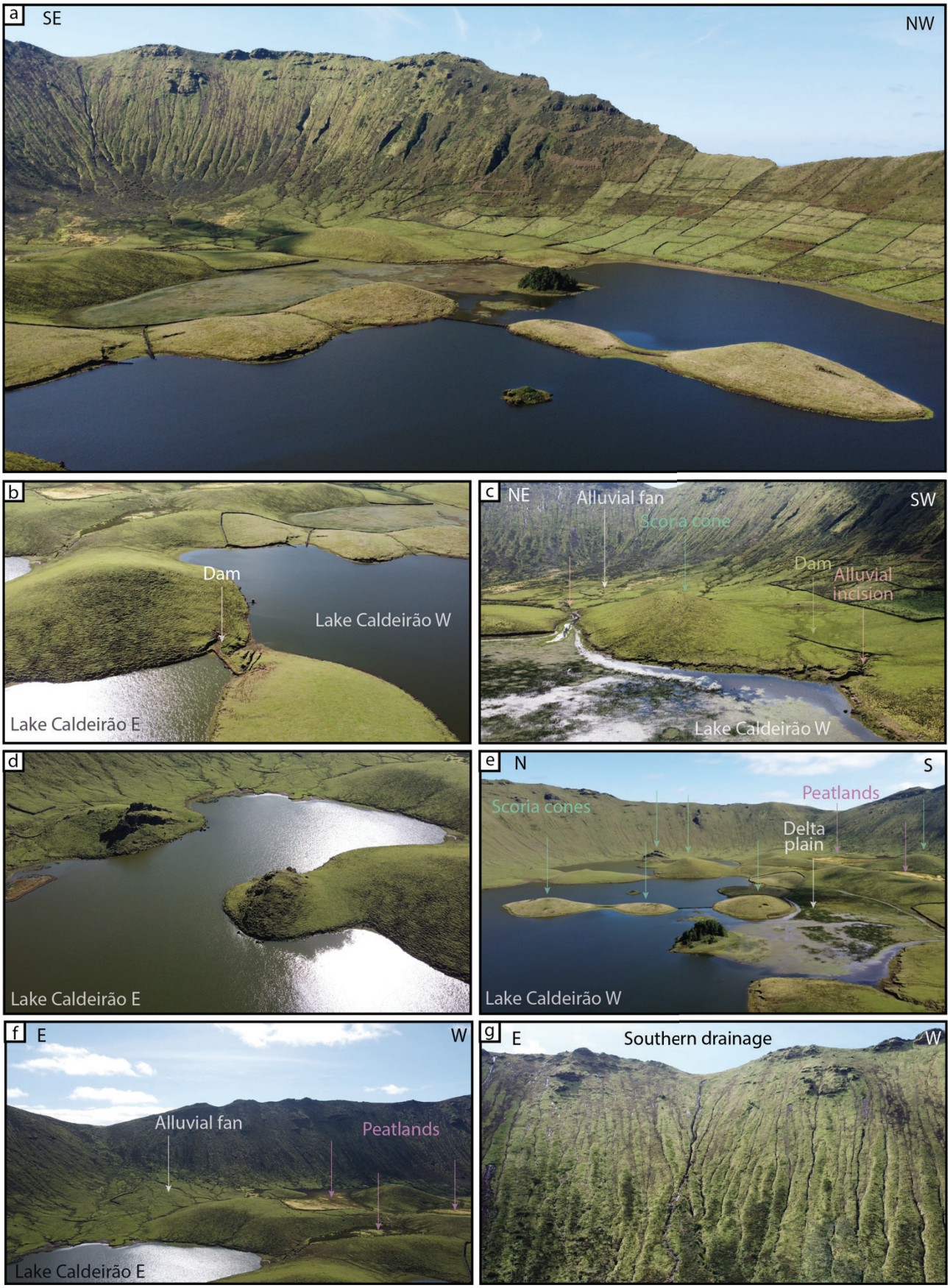

*Fig. 2.21: Photographs of Lake Caldeirão system: a) general overview of Caldeirão W and the southwestern sector of the caldera, b) anthropogenic dam separating Caldeirão W and E lakes, c) southern alluvial fan incised by the drainage and retained by dams, d) Lake Caldeirão E, e) general overview of the eastern sector from the western sector of the caldera. Note the Quaternary sedimentary infill and lakes adapted to the scoria cones, e) peatlands and g) parallel drainage pattern in the caldera southern flank.*

Caldeirão W and E (Fig. 2.20 and 21) are shallow polymictic lakes, sited on the Corvo caldera bottom, partially covering some of the post-caldera cinder cones, that conform little islands within them. During historical times, these two lakes have been separated through anthropogenic dam constructions (Fig. 2.21b,c). The water level of Caldeirão W (E) reaches 392 (398) m asl, with a surface of 0.12 (0.8) $km^2$ that extends 650 m long and 630 m wide, a relatively shallow maximum depth 2.8 (1.9) m and a volume of 16.29 x $10^4$ (9.02 x $10^4$) $m^3$ (Andrade et al., 2019).

The hydrogeochemistry of Lake Caldeirão W is of the Na-Cl type, revealing the dominance of marine contribution to the lake water from sea spray (Antunes and Carvalho, 2018). Averaged physicochemical parameters (2006 - 2018) obtained from the *Relatorio do Estado do Ambiente dos Açores* (REEA, 2019) indicate relatively clean (3.71 NTU), well-oxygenated (9.59 mg $L^{-1}$), slightly acidic (pH = 6.7), with medium conductivity (77.39 µS $cm^{-1}$) waters for Lake Caldeirão W (Samplig at: UTM 661696, 4397429, zone 25N; Fig. 2.20).

### 2.5.2 The Azores Archipelago Central Group

The Azores Archipelago CG lies eastwards from the MAR, ca. 250 km away from the WG, on the Eurasian-Nubia inter-plate diffuse boundary. Terceira and Graciosa are located over the TR, whereas São Jorge Faial and Pico islands form volcanic alignments that correspond with active segments of the plate boundary (Lourenço et al., 1998), where the dextral trans-tensive stresses of the transform leaky geodynamics induce dominant non-coaxial distributed deformation (DeSousa, 2007). Among these active segments highlights the Faial-Pico Fracture Zone (FPFZ), where Faial and Pico islands nucleate, composing a volcanic lineament dominated by the orientation of the dextral N110ºE-N120ºE faults (Fig. 2.2).

#### Pico Island

Pico Island is located 250 km to the ESE from the WG, being the largest island of the CG and the second most extensive of the Azores archipelago, with an area of approx. 447 $km^2$ (Fig. 2.1). Its nucleation started ca. 300 ka ago (being the youngest of the archipelago) at the interference with the subsidiary N140ºE-N150ºE sinistral faults, forming polygenetic volcanoes such as the shield volcano corresponding to the Lajes-Topo Volcanic Complex and the strombolian Pico volcano, corresponding to the Montanha Volcanic Complex, with the Pico Mountain reaching 2351 m asl at Piquinho summit, constituting the highest elevation of Portugal (Fig. 2.22).

Furthermore, the prevalent structural orientation dominates at the FPFZ (Fig. 2.2) favoured the formation of the fissural volcanic complex of São Roque-Piedade ca. 230 ka ago (Larrea et al., 2018) at the eastern side of Pico, overlying the polygenetic volcanoes, along a N110ºE-N120ºE preferent orientation (Lourenço et al, 1998; Madeira et al., 2015) (Fig. 2.22). The rocks composing the São Roque-Piedade Volcanic Complex are dominated by alkali basalts characterized by porphyritic, sometimes aphyric, textures with phenocrystals of clinopyroxene, plagioclase, olivine and minor oxides. The matrix is composed of the same mineral assemblage but with a higher fraction of oxides (Larrea et al., 2018).

The evolution of the São Roque-Piedade Volcanic Complex is driven by the Brejos Graben (Fig. 2.22), a normal dextral faults system defined northwards by the southern dipping Lagoa do Capitão fault and southwards by the northern dipping Topo Fault (Nunes et al., 2020; Madeira & Brum da Silveira, 2003; Madeira et al., 2015). The São Roque-Piedade Volcanic Complex is made up of lava

flows that generate the N and S steep flanks at the eastern side of the island and up to 170 small monogenetic scoria cones aligned along the graben structures at the crest. Moreover, the highlands are composed of a plateau disposed along a WNW-ESE ridge, standing above 800 m asl, locally known as “Planalto da Achada”.

The interaction between the Brejos Graben dextral faults activity and the related volcanic scoria cones provokes tectonic cone displacements, with “Cabeço do Caveiro” (Madeira and Brum da Silveira, 2003; Madeira et al., 2015), with its age estimated to be ca. 50 ka old based on geologic field relations (França, 2000) (Fig. 2.22).

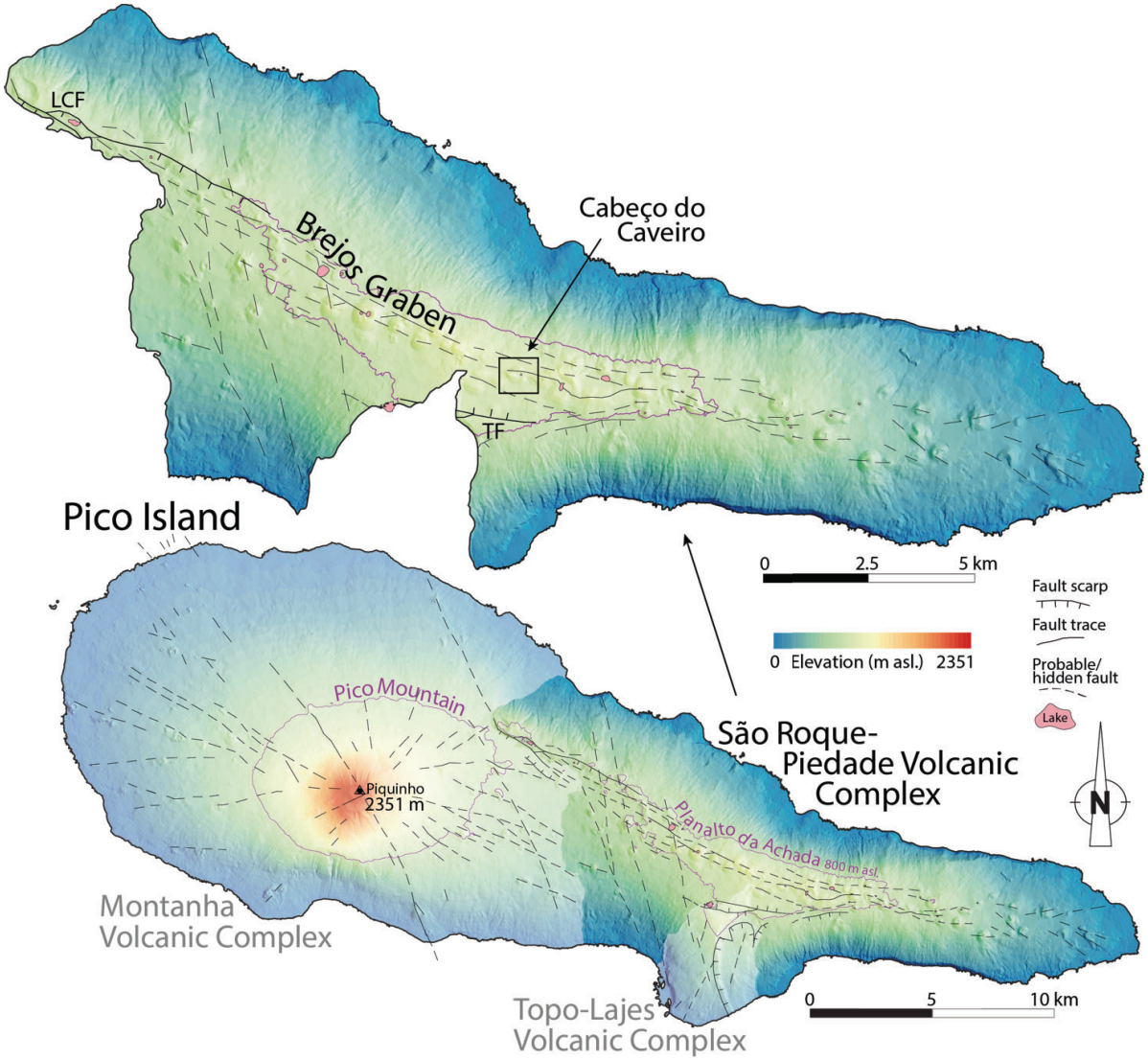


*Figure 2.22: DEM of Pico Island including a tectonic map composed by the faults interpreted by Madeira et al. (2003). The geographic domains and permanent surficial waters are as well indicated. TF: Topo fault; LCF: Lagoa do Capitão fault.*

Pico lakes dominantly distribute within the monogenetic scoria cone craters and tectonic depressions at the *Planalto da Achada* (Cruz et al., 2006; Antunes and Carvalho, 2018) (Fig. 2.22). These lakes present the lowest concentrations of $CO_2$ due to their small dimensions, which favors substantial water circulation throughout the year (Antunes and Carvalho, 2018).

Climate in Pico island western coastal lowlands precipitation pattern is similar to Ponta delgada in São Miguel Island (Hernandez et al., 2016), but with wetter summers with a difference of ca. 20 mm. Temperatures are mild, displaying small annual variations, with the highest temperature recorded during summer months (Fig. 2.23).

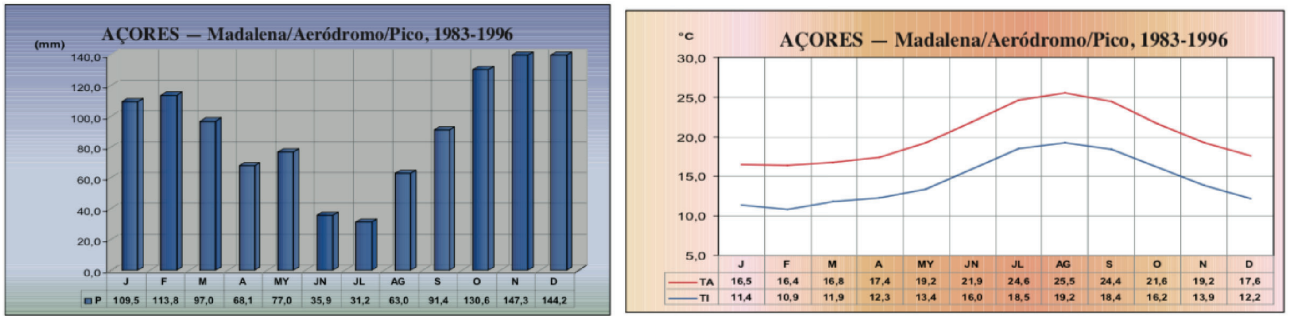


*Fig. 2.23: Monthly values of precipitation (left side) and air temperature (right side) from Madalena aerodrome in Pico Island (1971-2000). Modified from AEMET and IPMA (2012).*

### Caveiro lake-catchment system

From Pico Island, the studied system is Caveiro lake-catchment one (Fig. 2.24), which has a small watershed (0.05 km²) hydrologically open to the east, constituting most of Cabeço do Caveiro cone crater area. The cone crater flanks are composed of mafic volcanic scoria from the São Roque-Piedade Volcanic Complex, whereas the crater bottom is partially silted-up by a Holocene sedimentary infill composed by colluvial/alluvial deposits and a Sphagnum-built peatland that surrounds the western side of the lake (Figs. 2.24 and 25a,c). The drainage is composed of a tectonically controlled straight stream on the western side, which constitutes the only lake inlet (Figs. 2.24 and 25b), whereas on the eastern side, there is the only outlet that drains the lake to the southern flank of São Roque Piedade Volcanic Complex.

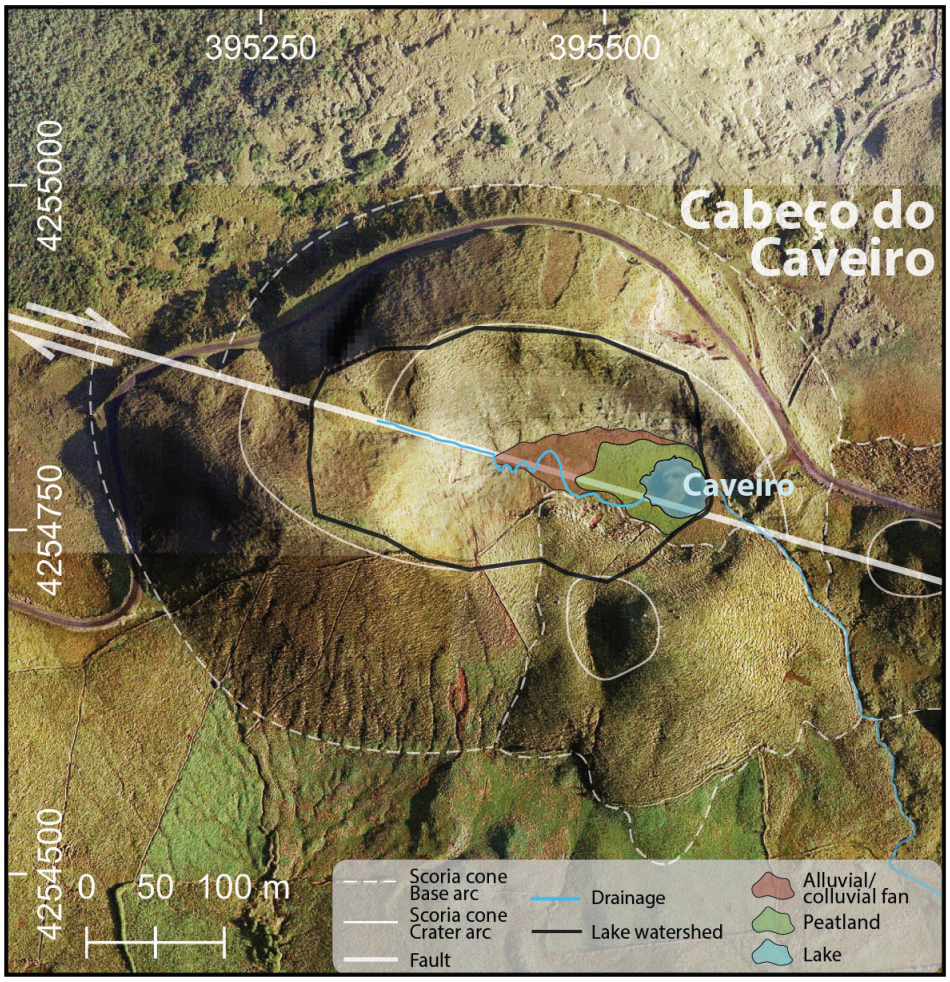


*Fig. 2.24: Caveiro lake-catchment system within Cabeço do caveiro scoria cone crater. Brejos Graben fault and scoria cones are indicated (Madeira and Brum da Silveira, 2003).*

Current vegetation is characterised by meadows dominated by grasses. However, the potential natural vegetation across the Planalto da Achada could have been Juniperus-Ilex montane forest (Elias et al., 2016) (Fig. 2.9). Apart from the Sphagnum-built peatland, the current aquatic macrophyte vegetation in the lake is predominantly dominated by Potamogeton polygonifolius. Besides, grazing cattle have a significant impact on the landscape of Planalto da Acaha and the small catchment of Caveiro (Björck et al., 2006).

Lake Caveiro is shallow (ca. 3.5 m max depth), small (0.00155 $km^2$), subrounded (ca. 45 m in diameter) and polymictic, located on the eastern side of Cabeço do Caveiro scoria cone carter at an elevation of 903 m asl (Figs. 2.24 and 2.25). The lake has relatively cold (11.1ºC), clean (0.79 NTU) and well oxygenated (10.8 mg $L^{-1}$) waters with neutral pH (7.0) and low conductivity (38 µS $cm^{-1}$). Nutrients are present in moderate concentrations (total nitrogen – 0.4 mg N $L^{-1}$; total phosphorus - 10µ $PL^{-1}$) (values measured during field coring campaign). Owing to its shallowness most probably the lake follows a thermal holomictic regime.

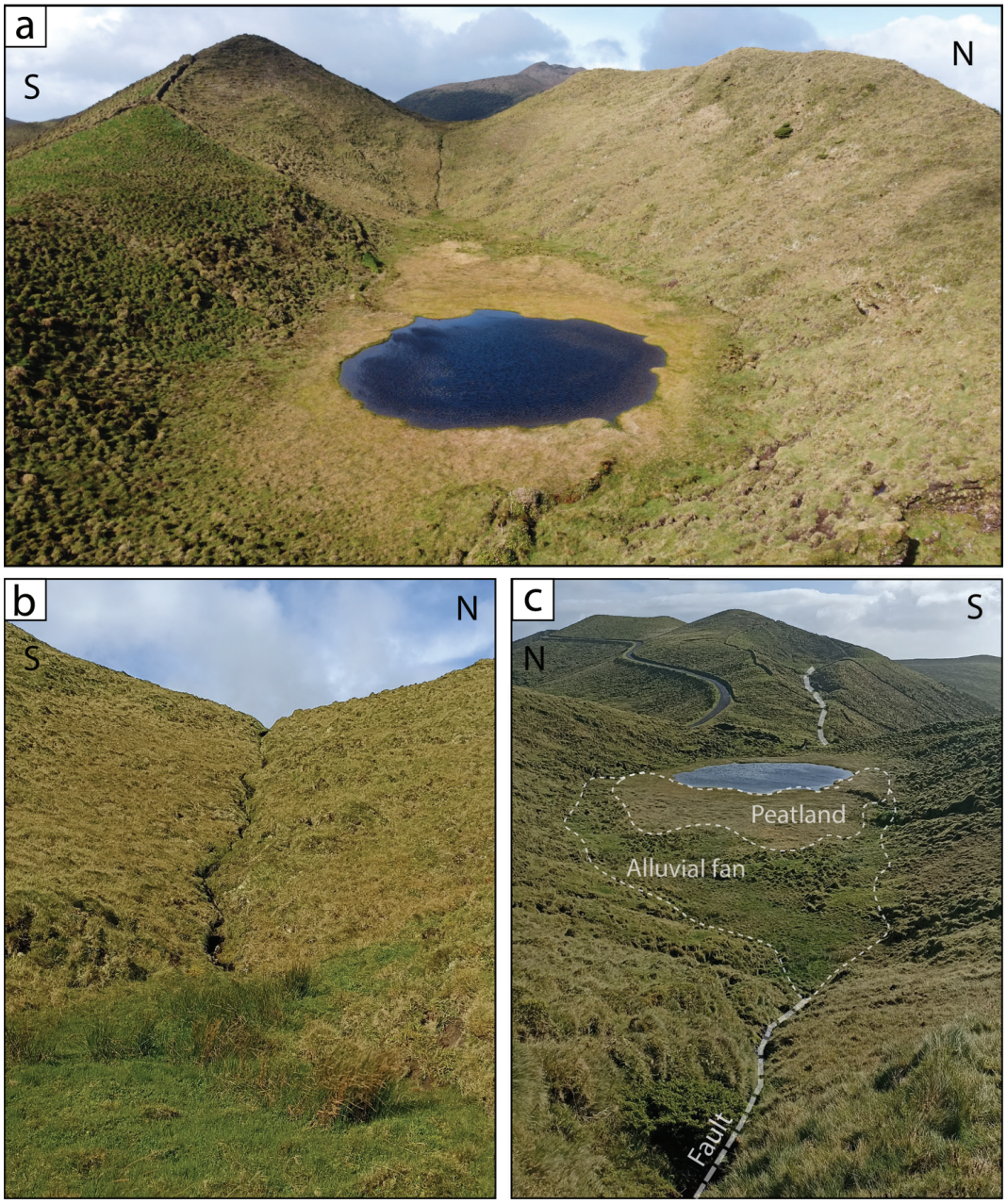


*Fig. 2.25: Photographs of Caveiro lake system: a) general overview of Cabeço do Caveiro cone crater, b) straight pattern of the drainage c) tectonic control of the Brejos graben structures over the drainage, alluvial fan, peatland and lake disposition.*

Lake Caveiro sediments have been used for paleoenvironmental reconstructions using variable proxy-based records (Björck et al., 2006; Connor et al., 2012; Marques; 2021). Besides the paleoclimatic inferences made by Björck et al. (2006), they identified up to 20 tephra deposits within Caveiro lacustrine sedimentary infill suggesting a sedimentary model highly impacted by volcanic activity. Fifteen of these tephras were inferred from macroscopic lithological changes, characterized by light brown tones, and other five through high XRF intensities.

Marques (2021) used diatom assemblages of Lake Caveiro sediments to reconstruct three main phases of environmental evolution during the last ca. 6000 years (Fig. 2.26), presumably linked to volcanic activity, climate changes and anthropic impacts due to deforestation, affecting the trophic status and pH of the lake:

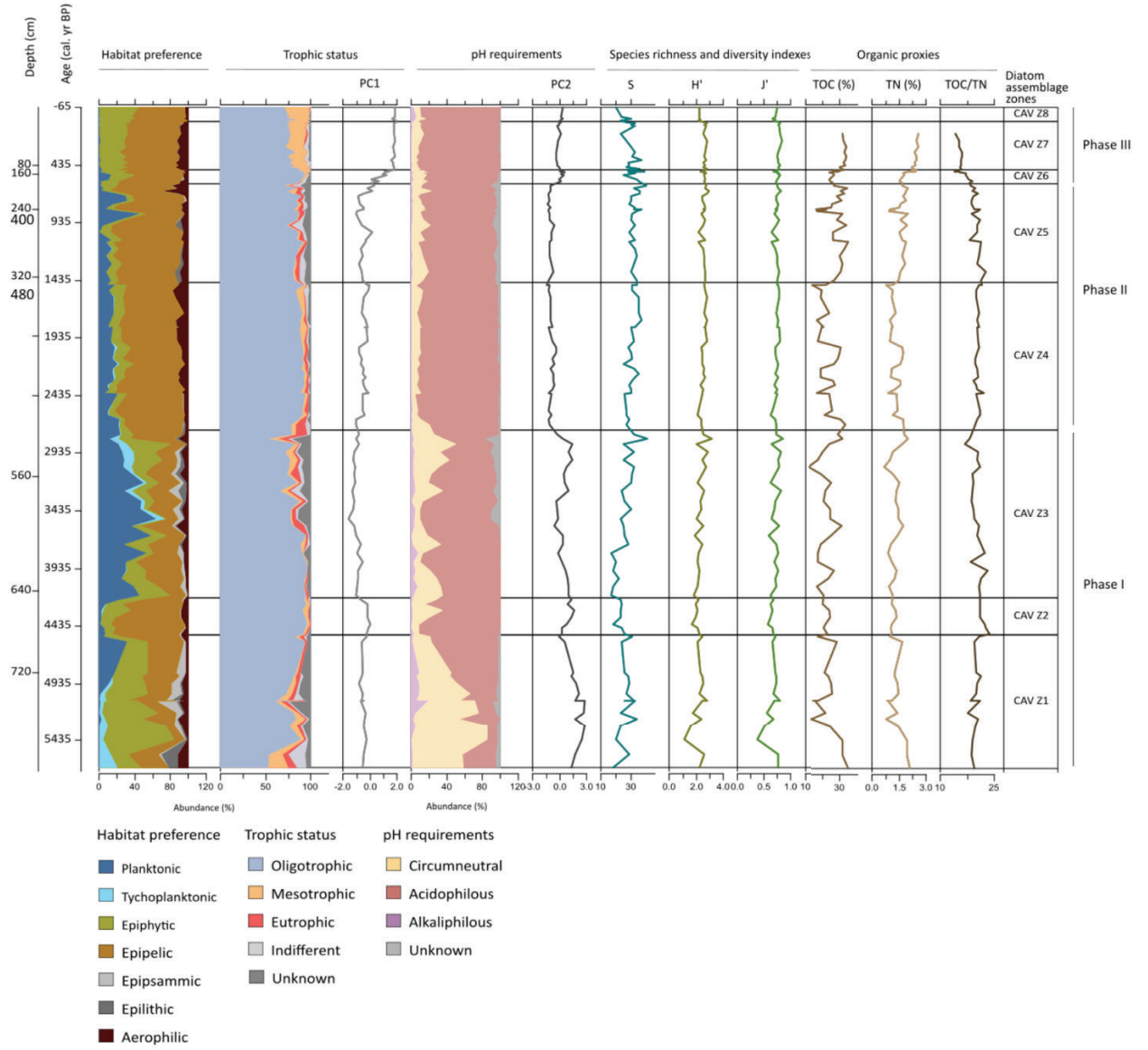


*Fig. 2.26: Diatom groups, first and second principal components (PC1 and PC2), species richness (S) and diversity indexes (Shannon's diversity (H') and Pielou's evenness (J')) and organic proxies (TOC, TN, TOC/TN) through Lake Caveiro sedimentary record. From Marques (2021).*

1) The Phase I (ca. 5670 – 2730 cal. yr BP), when the lake's formation followed major volcanic eruptions, leading to unstable conditions indicated by the abundance of opportunistic species like *A. minutissimum*. Cold and dry climate conditions prevailed, with occasional wet pulses, influencing the lake's water level. The dominance of circumneutral species reflects increased pH levels due to volcanic deposits, coinciding with a period of neoglaciation.

2) The Phase II (ca. 2730 – 600 cal. yr BP), increased acidity in the lake, likely due to reduced volcanic activity and the influence of humic acids from coniferous species in the catchment. Dry climate phases, including the 2800 BP cold event, led to a decline in lake water levels. Epipelic species expanded, indicating shallower conditions, while wet pulses during the Roman Warm Period temporarily affected the lake dynamics.
3) The Phase III (ca. 600 cal. yr BP – present), when anthropogenic disturbances, particularly deforestation, drove changes in this phase. Increased soil erosion led to higher nutrient loading and a shift towards oligo-mesotrophic conditions. Mesotrophic species proliferated, along with epiphytic species indicative of macrophyte presence. Acidophilus species increased due to pH decline from Sphagnum expansion, exacerbated by continued deforestation and sedimentation, resulting in shallower, silted lake conditions despite wetter climates.

# 3. Materials, methods and data

## 3.1 Geomorphic analysis

### 3.1.1 Relief

The morphology of Funda, Caldeirão, and Caveiro lake-catchment systems was analysed using QGIS 3.10 software and digital cartography provided by the *Instituto Geográfico do Exército* (IGeoE) in collaboration with the *Secretaria Regional dos Recursos Naturais* of the Azores government (2000) and the *Plano Regional da Água* (2003). Unlike for Funda and Caldeirão, limited spatial data were available for the Caveiro system. Therefore, catchment and lake perimeter polygons, as well as the drainage within the catchment, were manually delineated using the Pico Island contour elevation map and orthophotos. The spatial data were projected using zones 25N (for Flores and Corvo Islands) and 26N (for Pico Island) of the EPSG:32625 - WGS 84/UTM reference system.

The relief of Funda, Caldeirão, and Caveiro lake-catchment systems was analysed by generating Digital Elevation Models (DEMs) for their respective catchments. To achieve this, Triangulated Irregular Network (TIN) interpolations were applied to contour elevation maps (10 m equidistance) of Flores, Corvo, and Pico. Due to the reduced dimensions of Cabeço do Caveiro compared to the larger FVS and Caldeirão Caldera, higher spatial resolution was necessary. Therefore, looking for a balance between accuracy and reliability, grid sizes of 10 m were used for Flores and Corvo islands, while 5 m was used for Pico Island (Figs. 2.13, 2.17, and 2.20). The resulting datasets were clipped with the watershed perimeter polygons of their respective lakes after extracting the lake area. This process allowed the generation of DEMs that replicate the relief of the Funda ($_{R}DEM_{fun}$), Caldeirão ($_{R}DEM_{cald}$), and Caveiro ($_{R}DEM_{cav}$) catchments. Spatial comparisons between the drainage of the three lake systems were carried out by standarising, the absolute elevations of $_{R}DEM_{fun}$, $_{R}DEM_{cald}$, and $_{R}DEM_{cav}$ to their respective elevations above their base levels (abl), resulting in the relative relief of the study area ($_{R}DEM$).

The raster surface-to-volume analysis applied to $_{R}DEM_{fun}$, $_{R}DEM_{cald}$, and $_{R}DEM_{cav}$ was used to determine the floodable volume within the lake systems. Additionally, raster slope analyses were conducted to reveal slope distributions and average values, providing insights into the relative kinetic energy of surface waters. Furthermore, slope/area relationships of the mentioned datasets were established by calculating the $K_{sn}$ (Eq. 1.2) to unveil spatial trends of erosion. Using the 'landspy' library (Pérez-Peña et al., 2024), point maps with $K_{sn}$ values were generated, selecting a threshold value of 100 $m^2$ for the $_{R}DEM_{fun}$ and $_{R}DEM_{cald}$ and 25 $m^2$ form the $_{R}DEM_{cav}$ (1 pixel), to obtain the maximum spatial resolution. These point maps of $K_{sn}$ values were converted into raster maps using Inverse Distance Weighting (IDW) interpolation, to infer sediment cascading pattern across the study area, including the coupled and uncoupled region (Church, 2010; Fig. 1.14). $K_{sn}$ average values were established for each dataset.

#### Drainage

The drainage analysis of Lake Funda basin was used creating a hydrologically corrected DEM, applying the 'r.fill.dir' function with $_{R}DEM_{fun}$, to fill depressions and avoid atypical values. Subsequently, the 'r.watershed' tool was employed to generate flow direction and accumulation rasters, which were employed in the 'r.stream.extract' function to generate the drainage. The function ‘r.watershed.outlet’ allowed the delineation of drainage watersheds for the lake system by selecting the base level as outlet point. It is worth noting that the accuracy of the $_{R}DEM_{cald}$ and the $_{R}DEM_{cav}$ data in flat areas, where contour elevation data for TIN interpolations were limited, was insufficient for accurately identifying stream positions and drainage watersheds using the same methodology applied in Funda Lake-catchment system, where elevation gradients were more pronounced.

Consequently, the Corvo drainage polyline provided by IGeoE was adopted for further drainage analyses in Caldeirão lake basin after clipping it with the hydrological basin polygon. The most prominent streams of the study area were selected and the $K_{sn}$ rasters were subsampled along them to identify sediment cascading along the uncoupled region (Church, 2010). The Ksn profiles of the selected streams were projected using the $_{R}$DEM to analyse the distribution of elevations and relative erosive power, indicative of the hydrological processes at play along them.

### 3.1.2 Bathymetry

The lake bottom morphology of the three water bodies was analysed to gain insights into the sediment distribution and internal processes within. This analysis compares the bathymetries of Funda ($_{B}DEM_{fun}$) and Caldeirão ($_{B}DEM_{cald}$), whose absolute elevations were standardized into water depths to obtain the relative bathymetry of the study area ($_{B}$DEM). However, no bathymetry data was available for Lake Caveiro, and no edition was allowed for the $_{B}DEM_{cald}$. Therefore, only lake depths were used from $_{B}DEM_{cald}$ to determine the morphology of Lake Caldeirão whereas raster slope analysis was employed with the $_{B}DEM_{fun}$ to better characterize the morphology of Lake Funda bottom. Since Lake Caveiro presents a subrounded perimeter, an estimation of the water body volume was established by considering its shape as a spherical cap with 44.18 m Ø (averaged diametric measures along the shoreline) (Eq. 3.1). Lake/watershed area and lake area/volume ratios were calculated to compare the scales of the sedimentary processes and to determine their respective contributions.

$$Vcav = \frac{\pi \cdot h}{6}(3r^2 + h^2)$$

*(Eq. 3.1)*

Where:

- *$V_{cav}$ is the Lake Caveiro volume.*

- *h is the height of the spheric casquet (Lake Caveiro max. depth) = 3.5 m.*

- *r is the radius of the spheric casquet (Lake Caveiro area radius = 22.1 m).*

## 3.2 Fieldwork, lake sediments coring and core selection

In September 2022, in situ landscape analysis allowed for the identification of morphologies derived from surficial processes within Funda, Caldeirão and Caveiro lake-catchment systems. Erosive scars and peri-lacustrine depositional environments were characterized and mapped with the help of orthophotos. In June 2015, two cores from sedimentary infill of Cabeço do Caveiro cone crater were extracted using a six-cm-Ø UWITEC® piston corer installed in an UWITEC® platform raft. One 1170 cm long core was obtained from the peatland placed on the eastern part of the cone crater, while the other 930 cm long core was extracted from Lake Caveiro itself. In June 2017, four sediment cores up to 700 cm long were recovered from Lake Caldeirão, and two cores up to 990 cm long were obtained from Lake Funda using the same equipment (Fig.3.2). Additionally, seven cores up to 200 cm long were recovered using six-and-nine-cm-ø UWITEC® gravity corers from the floating platform to obtain backup cores of the topmost sediment sections of Lakes Funda and Caldeirão (Fig. 3.1). All the cores were immediately sealed, transported to Geosciences Barcelona (GEO3BCN-CSIC), and stored in a dark cold room at +4 ºC.

*Figure 3.1. Photographs of the field coring campaigns: on the left side Lake Caveiro, in June 2015. On the right side, Lake Caldeirão in June 2017. On the bottom, Lake Funda in June 2017. Photos by Santiago Giralt.*

For this PhD thesis, the most representative records of offshore facies were selected, as they contain the most suitable grain sizes for geochemical analyses, primarily fine-grained sediments. Moreover, piston cores were preferred due to their greater length, covering a more extended time period. Therefore, for subsequent analyses, the selected set of offshore piston cores includes the FN1702 (994 cm long) obtained from Lake Funda (UTM coordinates: 25S - 653462.6, 4363393.5), the CL1703 (580 cm long) obtained from Lake Caldeirão (UTM coordinates: 25S - 661917.0, 4397445.2) and the CVL1B (930 cm long) obtained from Lake Caveiro (UTM coordinates: 26S - 395555.5, 4254782.7) (Fig. 3.1). The uppermost section of Lake Funda sediments is characterised by a clear rhythmic laminated pattern. However, after previous samplings, there were not enough sediments in core FN1702 to make up thin sections. Then, the backup gravity core FN1704G (9 cm ø and 200 cm long) was used for this purpose, as it was the longest parallel core recovered from the same location.

## 3.3 Sediment records analyses

All the selected cores were longitudinally split into two halves. Sediment losses were identified and the core section depths were converted into composite decompacted depths, considering core catcher depths and applying the decompaction correction (Eq. 3.2):

$$D_D = \frac{100 - (D_R * 100)}{D_C}$$

*(Eq. 3.2)*

Where:

*$D_D$ is the decompacted depth*

*$D_R$ is the recovered depth*

*$D_C$ is the cored depth.*

### 3.3.1 Sediment characterization

#### Visual description

Visual lithological description facilitated the macroscopic characterization of the sediments that included observations of grain size, sedimentary structures and colour. This visual recognition process was complemented by high-resolution core images (Fig. 3.2). The images were acquired from the best-preserved halves of the cores with a high-resolution Charged Coupled Device (CCD) colour line-scan camera, mounted in an Avaatech® II X-Ray Fluorescence (XRF) core scanner from the CORELAB Laboratory of the Universitat de Barcelona (Spain). Furthermore, coarse sediments such as sands, microconglomerates, coarse ashes, and lapilli were sampled and dried at 60ºC for 48 hours for direct observations with a magnifying glass. The classification of epiclastic materials was determined utilizing the Wentworth scheme (1922), while the primary grain sizes of volcanic particles were assessed employing the Fisher scale (1961).

#### Microscopic analysis

The visual description was complemented by optical microscopic observations of smear slides and thin sections. Sediments for smear slides were sampled at intervals of 10 cm along the cores and at specific depths where macroscopic observations revealed colour, composition or texture changes. In total, a set of ca. 250 smear slides were prepared and analyzed. The smear slide technique involved extracting a minute sediment sample with a toothpick and depositing it onto a transparent glass microscope slide. A drop of distilled water was employed to disperse the sample, which was then spread out using the toothpick. The slide was left to air-dry for a period of 24 hours to allow the water to evaporate. A few drops of UV Loctite® 358 adhesive were applied to the sample, and a glass coverslip was affixed. The prepared smear slide was then exposed to UV light for 30 seconds to facilitate the curing of the adhesive (Rothwell, 1998). Furthermore, a composite sequence of samples (100 x 15 x 35 mm) was taken from the FN1704G core to make thin sections of Lake Funda laminated sediments (Fig. 3.3). The samples were freeze-dried using liquid nitrogen and subsequently impregnated with epoxy resin (Araldite®) under vacuum conditions (Brauer and Casanova, 2001) at MK Factory (Stahnsdorf, Germany). This process aimed to obtain a series of 25 overlapping (2 cm) thin sections, which were studied under optical microscope and correlated using the marker layers shared between thin sections. Microscopic observations of smear slides were carried out using the high-end polarization microscope Leica® DM4500 P with x630 magnification and located at GEO3BCN-CSIC, whereas thin sections were analysed using a using a Leica (M205C) stereo-zoom petrological microscope with plane- and cross-polarised light, at 80x. located at Royal Holloway University of London (UK).

The microscopic characterization included observations of mineral composition, biotic microremains, and organic matter. Semiquantitative average relative proportions of the micro-components were established, and the lithofacies were classified following the method proposed by Schnurrenberger et al. (2003). At least the genera of subfossil diatom assemblages were identified, whereas the biostratigraphic relative abundances and specie determinations from Ritter et al. (2022) (for FN1702 and FN1704G records), Raposeiro et al. (2021) (for CL1703 record) and Marques (2021) (for CVL1B record) were used to infer the stratigraphic evolution of environmental conditions within the lakes. The sediment records used for the aforementioned works were the same used in this study.

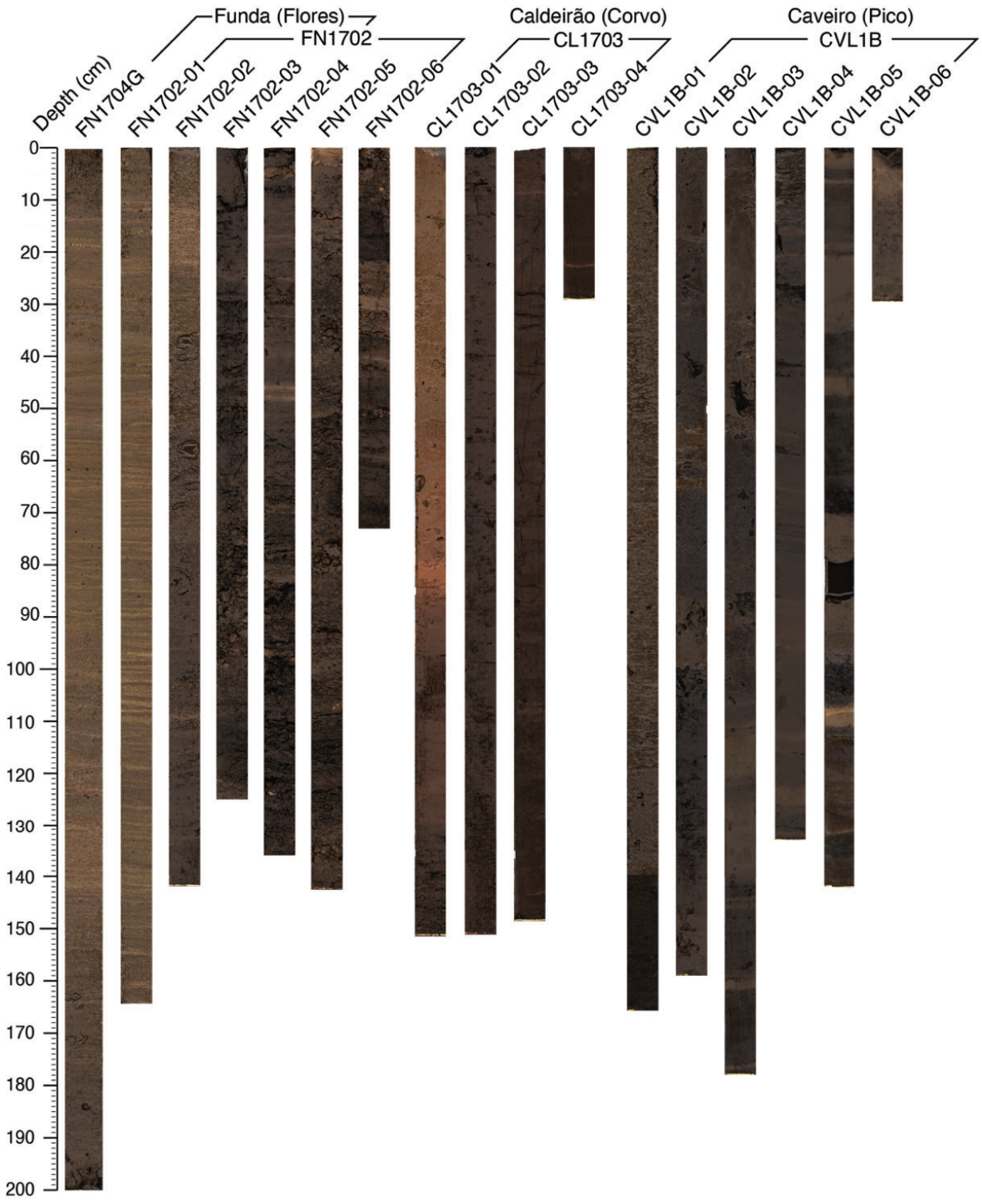


*Figure 3.2: High resolution images of the studied sediments.*

Furthermore, the distinct laminae compositions and stratigraphic organization patterns were characterized to identify rhythmic micro-lithofacies and to assess the sedimentation processes contributing to the formation of this laminated sedimentary pattern. Moreover, rhythmite counts were conducted to examine their sedimentation frequency by comparing the results with the independent radiometric chronology from the FN1702 record, after correlating marker layers between both sediment records. Finally, laminae and rhythmite thicknesses were measured to evaluate the rhythmic processes intensities and the varve quality index (VQI) was established. Rhythmite counts and laminae thickness measurements in core sections where lamination vanish (VQI=0) were interpolated from proximal sections.

*Fig. 3.3: Thin sections: a) Sampling sediments for thin sections. b) Laminated pattern and marker layers identified in the thin sections.*

### 3.3.2 Radiometric dating

#### $^{210}$Pb and $^{137}$Cs dates

Radiometric measurements of $^{210}$Pb, $^{226}$Ra and $^{137}$Cs were carried out every four centimetres for the section included in the uppermost 80 cm of FN1702 record. In the case of CL1703 record, $^{210}$Pb and $^{226}$Ra measurements were obtained every centimetre from the uppermost 20 cm (Raposeiro et al., 2021, Ritter et al., 2022, Richter et al., 2022), whereas for CVL1B record, measurements were obtained from the uppermost 130 cm. These analyses were conducted at the Isotopic Geochemistry and Geochronology Laboratory of the Universidad Nacional Autónoma de México (UNAM) located at Mazatlán (Mexico).

Gamma spectrometry was used to determine the $^{226}$Ra and $^{137}$Cs concentrations. About 1 g of dry and ground sample was placed into polyethylene calibrated geometries (length = 40 mm, diameter = 10 mm) sealed with rubber caps and Teflon tape. Samples were stored for 21 days to allow secular equilibrium between $^{226}$Ra and $^{214}$Pb. Then, samples were measured in a gamma spectrometry system with a high-resolution low-background Ortec-Ametek HPGe well-type detector for at least 48 hours.

Concentrations of $^{210}$Pb were determined through the analysis of its granddaughter $^{210}$Po by alpha-spectroscopy, assuming secular equilibrium of both radionuclides at the time of analysis (Sanchez-Cabeza et al., 1998). A known amount of $^{209}$Po was added to each sample as an internal tracer. Samples were acid digested using an analytical microwave, solutions were conditioned in HCl 1 N and polonium isotopes were plated onto silver discs. Alpha emissions were measured using Passivated Implanted Planar Silicon (PIPS) CANBERRA Mod. PD-450 18 AM detectors and the activities were quantified after corrections for background and reagent blanks. Supported $^{210}$Pb concentrations were determined by averaging the total $^{210}$Pb concentrations at the base of the $^{210}$Pb profile, verified with some measurements of $^{226}$Ra concentrations along the core carried out by gamma-spectroscopy using a high-purity germanium detector CANBERRA Mod. GCW3523. Sedimentation rates were determined using the Constant Flux:Constant Sedimentation (CF:CS) model (Robbins, 1978).

#### Accelerator Mass Spectroscopy (AMS) $^{14}$C dates

A total of 8 samples from sediments of CL1703 record and 7 samples from sediments of FN1702 record were dated by AMS $^{14}C$ from pollen-concentrated material after pre-treat them with acid digestion (Raposeiro et al., 2021, Ritter et al., 2022, Richter et al., 2022). Additionally, 11 samples from sediments of CVL1B record were dated using the same previous methodology. Radiocarbon dating was performed at Laboratoire de Radiochronologie (Université de Laval, Quebec, Canada). The radiocarbon ages were calibrated to calendar years (CE) using the CALIB 7.1 software (Stuiver and Reimer, 1993) and the INTCAL20 curve (Reimer et al., 2020), selecting the median of the 95.4% distribution (2σ probability interval).

### 3.3.3 X-Ray Fluorescence core scanning

The core halves used for imaging were also employed to determine the elemental composition of the clayish and silty sediments at intervals of 2 mm. This analysis was conducted at 10 kV (15 s acquisition time and 1000 μA for CL1703; 20 s acquisition time and 1200 μA for FN1702) and at 30 kV (45 s acquisition time and 1500 μA for both cores) using the XRF core scanner from the CORELAB laboratory of the Universitat de Barcelona (Spain). The incoherent/coherent (inc/coh) ratio, which corresponds to the Compton to Rayleigh scattering ratio, was calculated. This ratio is representative of the ratio between crystalline and amorphous material (Crowdace et al., 2006; Chawchai et al., 2016), providing information about the organic content in the sediment (Davies et al., 2015). Among the 32 chemical elements identified by XRF, only those with median values of at least 1500 cps (counts per second) were considered statistically significant for subsequent analyses.

### 3.3.4 Bulk X-Ray Diffraction (XRD)

Samples of 1-cm-thick every 5 cm only from sections with XRF measurements were dried at 60 °C for 48 h and manually ground, using an agate mill, for mineralogical identification. Mineralogical analyses were conducted using the XRD spectrometer Bruker D8-A25, equipped with a Cu tube (k lambda=1.5405 Å) and an ultrafast position sensitive detector (PSD) located at GEO3BCN-CSIC (Spain). XRD spectra were collected over the 2θ range between 4° and 60° with steps of 0.035° and an equivalent integration time of 96 s per step. A voltage (current) of 40 kV (40 mA) was applied to the x-ray generator. Standard procedures were used for the identification and relative abundance quantification of the minerals in the crystalline fraction (Chung, 1974a, 1974b).

### 3.3.5 Biochemical analyses

#### Bulk C and N elemental and stable isotopes

Same samples used for XRD analyses were also employed to determine the total carbon (TC) and total nitrogen (TN) and their respective stable isotopes ($\delta^{13}C$ and $\delta^{15}N$) (Raposeiro et al., 2021; Ritter et al., 2022). The organic chemistry analyses were conducted using a Finnigan delta Plus EA-CF-IRMS spectrometer at the Centres Científics i Tecnològics at Universitat de Barcelona (CCiTUB, Spain) and a Thermo Finnigan Flash- EA1112 elemental analyser at Servizos de Apoio á Investigación at Universidade da Coruña (Spain). Given the negligible carbonate content below the detection limit of the X-ray diffractometer, TC was considered equal to the total organic carbon (TOC). TOC and TN results are expressed as percentages of the sediment dry weight and their relative standard deviation is 0.05. The TOC/TN atomic ratio was calculated for all the samples. Isotopic values are reported in the conventional delta-notation (‰) relative to the Pee Dee Belemnite (PDB) carbon and atmospheric nitrogen ($N_2$) standards, respectively.

#### Biogenic Silica

Biogenic Silica (BSi) was extracted using the wet-alkaline leaching technique (Mortlock and Froelich, 1989), Carbonates and organic matter were removed by digestion with HCl 1M and hydrogen peroxide ($H_2O_2$). Then, BSi was leached with $Na_2CO_3$ 2M and the solution was separated from the

remaining sediment with centrifugation, whereas bicarbonate was neutralized with HCl. BSi, in the form of dissolved silicate, was measured by the molybdate blue colorimetric method (Hansen and Grashoff, 1983) with an AutoAnalyser Technicon II from the Instituto de Investigacións Mariñas (IIM-CSIC, Spain). BSi values are expressed in percentage with respect to dry sediment (% wt) and the precision of the method is about ± 0.2 (Bernárdez et al., 2005).

## 3.4 Statistical analyses

The statistical analyses were conducted using the R software and the latest versions of several packages (R Development Core Team, 2021).

### 3.4.1 Age-depth modelling

The age-depth models were constructed by combining the $^{137}$Cs only available for the FN1702 record and $^{210}$Pb profiles with the AMS $^{14}$C dates. Inconsistent reversal ages derived from reworked lithologies were excluded from age-depth modelling.

The age-depth models of FN1702 (Raposeiro et al., 2021, Ritter et al., 2022, Richter et al., 2022) and CL1703 (Raposeiro et al., 2021) records were constructed using the R 'clam' script (Blaauw, 2010) to find the best fitting. Unlike FN1702 and CL1303 records, the sediment characterisation of CVL1B revealed recurrent lithological changes along most of the record, suggesting differences in sedimentation rates. Therefore, the age-depth model was constructed using Bayesian statistics from the R 'bacon' script (Blaauw, 2010). Depths with different accumulation rates ('acc.mean') were considered based on sedimentological interpretations of CVL1B sediments. Lithofacies interpreted as instantaneous deposits due to flash floods of tephra fallout were taken into account when constructing the chronological model of a given sedimentary record. The obtained radiometric chronologies were expressed in calendar years Before Present (cal. yr. BP).

### 3.4.2 Multivariate statistics

Multivariate statistics were applied to the geochemical (XRF analyses), biochemical (organic analyses), and mineralogical (XRD analysis) datasets. The objective was to identify genetic and environmental sedimentary conditions, their stratigraphical patterns, as well as their rhythm of change and the main sedimentary drivers responsible for them.

#### Data structure

As one of the objectives of this PhD thesis is to reconstruct climatic conditions based on the signal present in the lake sediments. Core sections dominated by deposits with non-lacustrine origin were excluded. The discarded sections may constitute potential sources of undesirable biogeochemical and mineral noise not related with climate fluctuations. Since XRF data was originally at 2 mm resolution, median values within one centimetre were calculated with a regular spacing of 50 mm to obtain the same spatial resolution for all proxies.

The geochemical variables determined by XRF and the analysed biochemical variables compose the biogeochemical datasets. After removing rows with missing values, the biogeochemical and mineral datasets included eighteen variables (thirteen and five, respectively) and ninety-five samples for CL1703 record, twenty variables (fifteen and five, respectively) and one hundred and three samples for FN1702 record, and twenty-seven variables (seventeen and ten, respectively) with one hundred twenty-seven samples for CVL1B record. The 50 mm datasets were used to identify the main components of biogeochemical variability, through clustering, ordination and rate of change analyses.

In contrast, the 2 mm geochemical datasets were preferred for conducting correlations with observational records. These records typically display high frequencies (e. g. monthly-annual) but

span relatively short time periods (commonly limited to some decades or a few centuries). Therefore, after removing rows with missing values, these high-resolution geochemical datasets were composed of two thousand six hundred thirty-three (2633) samples and fifteen variables for the FN1702 record, two thousand four hundred forty-five (2445) samples and thirteen variables for the CL1703 record, and three thousand ninety-four (3094) samples and thirteen variables for the CVL1B record.

#### Clustering analyses

The k-means clustering algorithm ('stats' R-package; R Core Team, 2021) was applied to the 50 mm biogeochemical datasets after standardizing. The statistically significant number of centroids, selected to nucleate the biogeochemical groups of samples, was identified using the elbow method based on minimizing the total within-cluster sum of squares. Median values of the variables within the biogeochemical groups were used to characterize their specific biogeochemical and mineral compositions. Additionally, median values of TOC/TN atomic ratio and $\delta^{13}C$ were also calculated with 1 σ confidence intervals and plotted in TOC/TN - $\delta^{13}C$ diagrams (Meyers, 1994) to determine the organic matter origin of the biogeochemical groups.

Stratigraphically constrained cluster analyses were applied to both, 50- and 2-mm biogeochemical datasets after standardizing (CONISS; Grimm, 1987). The statistically significant groups were selected following the broken-stick model (Bennett, 1996) whenever the structure of the input data allowed it. Otherwise slope breaks of the sum of squares were considered.

#### Ordination analyses

The R-package 'vegan' was used to perform RDA using the 50 mm datasets (Oksanen et al., 2013). The mineral variables were employed as a constraining matrix (environment) of the biogeochemical variables (response), given that each mineralogical species represents a "compendium" of geochemical elements (Giralt et al., 2008). Both datasets were separately standardized (mean 0 and 1 σ interval), and the 'envfit' function was used to identify statistically significant mineral sources. These sources were related to the biogeochemical groups identified with the k-means algorithm based on the relationships revealed by the RDA. The main components of mineralogically constrained biogeochemical variability from the RDA significant axes were determined using the 'anova' function ('stats' R-package; R Core Team, 2021).

The Vegan package was also employed to conduct PCAs. After standardization, PCAs were applied to both, the biogeochemical dataset at a 50 mm resolution and the geochemical dataset at a 2 mm resolution. The number of significant PCA axes were determined using the broken-stick model (Bennett, 1996).

Trajectory analyses of samples across the significant eigenvectors of RDA and PCA were established in order to identify stratigraphic patterns of variability.

#### Rate of change analyses

Rate of Change (RoC) analyses ('R-Ratepol' R package; Mottl et al., 2021) were conducted on the 50 mm XRF geochemical datasets to identify periods of relatively accelerated compositional changes (Mottl et al., 2021). To pinpoint the ages of these changes, peak points were detected by identifying the RoC threshold from values above the sum of the median plus the 95th percentile of all RoC values.

### 3.4.3 Time series analyses

#### Proxy-based records.

The high-resolution proxy-based records were obtained by resampling the 2mm PCAs eigenvectors

at 50 mm using the 'approx' function ('stats' R-package; R Core Team, 2021) and by determining Pearson's rank correlation coefficients (ρ) and associated p-values between them and the 50mm RDAs and PCAs eigenvectors. These records were complemented with the ones obtained from the combination of rhythmite counts and laminae thickness measurements from the FN1704G record after demonstrating a similar temporal resolution. Smoothened signals were calculated with a 0.1 span value.

### Instrumental records

To identify the impact of climatic variability over the sedimentary infill of Lakes Funda, Caldeirão and Caveiro, the daily observational records based on daily median values for the period comprised between 1970 and 2017 CE of precipitation, maximum ($T_{max}$) and minimum temperature ($T_{min}$) from meteorological stations at Flores, Corvo and Pico airports were employed. In turn, monthly median values of the NAOi and EAi by Comas-Bru and Hernández (2018) were employed to analyse the atmospheric circulation influence on climate of the study area.

Climate seasonality, as revealed by previous studies on observational hydroclimatic (Hernandez et al., 2016) and temperature (Barceló and Nunes, 2012; Cropper and Hanna, 2014) variability in the Azores, helped identify the months of interest for subsequent correlation analyses. Furthermore, Lake Funda water temperatures, monitored by Gonçalves et al. (2009) using thermistors at the surface, at 15 m and at 30 m depth, every hour from November 2015 to May 2017 (Fig. 3.4), were also employed to determine the seasonal pattern of the thermocline, which is crucial for understanding the lamination formation of its topmost sediments. Precipitation datasets were smoothed into an annual time-scale using the months of the Azores regular season of precipitation (ONDJFM; Hernandez et al., 2016), whereas summer months (JJA) were selected for the temperature datasets.

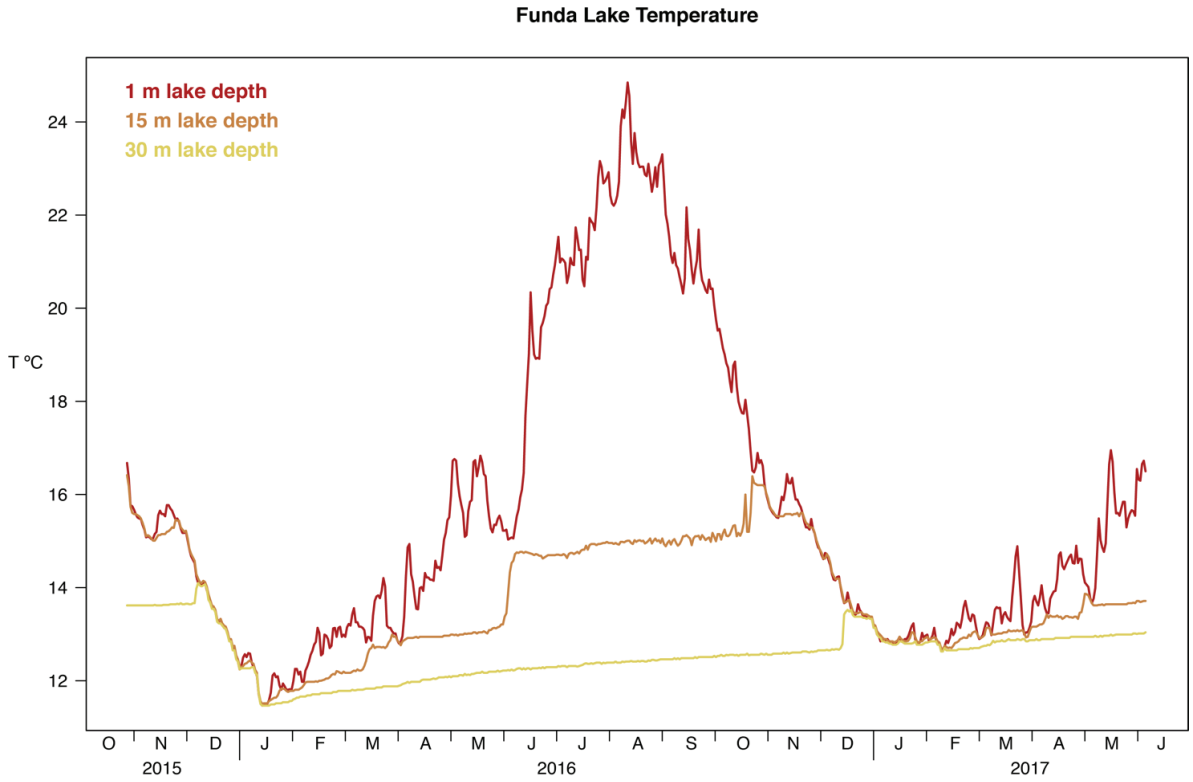


*Fig. 3.4: Lake Funda water temperature in depth (data from Gonçalves et al., 2009). J: January; F: February; M: March; April: April; M: May; J: June; J: July; A: August; S: September; O: October; N: November; D: December.*

### Pearson product-moment correlation coefficients

Pearson correlation coefficients (ρ) and associated p-values were established within atmospheric indexes, climatic variables and limnological records to evaluate the seasonal impact of the NAO and the EA on the regional climate fluctuations, and ultimately on the lacustrine sedimentary dynamics of the analysed lake systems. For the Azores regular wet season (ONDJFM) the monthly averaged precipitation and the NAOi were selected whereas for the summer months (JJA) $T_{max}$ and $T_{min}$ and the EAi were chosen.

Annually averaged climatic datasets were correlated with high-resolution proxy-based records using the same months as for the atmospheric indexes. To achieve this, the meteorological and limnological datasets were detrended. In addition, to identify and correct lag periods derived from age-depth modelling uncertainties and/or delayed sedimentary responses to climatic forcings, cross-covariance estimates were employed using the 'acf' function ('stats' R-package; R Core Team, 2021). The significance of ρ (p-value) is always discussed with a significance level set at $p < 0.05$.

# 4. Results

## 4.1 Limnogeomorphology

The morphometric analysis of the relief ($_{R}DEM_{fun}$, $_{R}DEM_{cald}$ and $_{R}DEM_{cav}$), combined with the available lake bathymetries ($_{B}DEM_{fun}$ and $_{B}DEM_{cald}$) and limnomorphometric parameters, has allowed a comparative characterization of the morphology of the Funda, Caldeirão and Caveiro lake-catchment systems (Table 4.1; Figs. 4.1 and 4.2).

The size of Funda and Caldeirão systems is very similar, covering relatively extensive areas compared to the Caveiro system, which is two orders of magnitude smaller (occupying only ca. 1.43% of their areas). The margins of the Funda and Caldeirão systems reach at least 82.8 m in elevation to reach their outlets, whereas the Caveiro system is hydrologically open on its eastern side. Therefore, the floodable volumes of the Funda and Caldeirão systems are relatively large, whereas it is negligible in the Caveiro system, which exhibits the lowest values of the lake/catchment area ratio (Table 4.1). Furthermore, the capacity for flooding within the Funda system is mainly expressed in the vertical dimension, whereas the Caldeirão system has sufficient space both vertically and horizontally.

### 4.1.1 Reliefs

The surfaces that reproduce the relief of Funda ($_{R}DEM_{fun}$), Caldeirão ($_{R}DEM_{cald}$) and Caveiro ($_{R}DEM_{cav}$) catchments are characterized by the combination of four different landforms:

Non-oriented:

1) Basin: concentric increase of elevations, from the central lowlands to the peripheric highlands.
2) Dome: concentric decrease of elevations, from the central highlands to the peripheric lowlands.

Oriented:

3) Valley: specular increasing of elevations, from the axial lowlands to the marginal highlands.
4) Slope: increase/decrease of elevations

The relief of Caldeirão is primarily defined by landform 1, which forms the inner shape of the caldera. The peripheric flanks constitute the highlands that exhibit the highest elevations along the uneroded section of the caldera arc, particularly on the SSW side. In contrast, lower elevations are notable on the WNW side, corresponding to the eroded/collapsed sector of the caldera. The resulting crest forms the interfluve that presents an ellipsoidal shape (AR = 1.33) trending NNE (interfluve major axis = N011ºE). The bottom of the caldera composes the lowlands, where landform 2 replicates up to 11 times, revealing scattered distributions corresponding to the post-caldera spatter cones. Most of the Caldeirão catchment surface corresponds to the lowlands. The alluvial/colluvial fans compose a smooth transition between the highlands and the lowlands.

The relief of Caveiro combines the western portion of landform 1 with landform 3. Landform 1 conforms the central geometry of the volcanic structure of Cabeço do Caveiro, whereas landform 3 corresponds to the intersection of the dextral fault of the Brejos Graben and the relief, displaying a WNW-ESE trend. The lower elevations correspond to the crater bottom, where landform 1 dominates the silted-up central-to-eastern sector, while the higher elevations align with the displaced crater flanks at the southwest and north-to-northwest sides, where landform 3 is imposed. The watershed interfluve aligning with the displaced crater arc exhibits a marked ellipsoidal shape (AR = 1.68) along the trend of the fault intersection (interfluve major axis = N105ºE) (Fig. 4.1).

The Funda catchment relief incorporates all the previously mentioned patterns. The catchment highlands include landform 4, corresponding with the Flores Island plateau (slightly sloping SSE) and the southernmost edge of the Caldeira das Sete Lagoas (strongly sloping westwards), in conjunction with the southern section of landform 2 at the southern flank of the northern scoria cone. The highlands within the Funda catchment constitute most of its surface. In the catchment lowlands, landform 1 repeats up to five times. Three of them correspond to the coalescent maars of the FVS (Andrade et al., 2022). Additionally, landform 1 is also present to the southwestern side of the Funda maar and to the northeastern side of the NE maar, likely indicating two additional maars. These landforms exhibit intersecting scattered distributions, combined with landform 3 (crater AR = 1.80) along a N020ºE trend (crater major axis). However, the intersection between the SW maar, the Funda and the S maars (including Rasa tuff ring) aligns along the orientation of the minor axis of the main crater (N110ºE). The intersections between all maars form four septa: 1) between the Funda maar and the S maar; 2) between the Funda maar and the SW maar (partially submerged); 3) between the Funda maar and the NE maar, and 4) between the NE maar and the small maar lying at its northwestern side. The intersections between maars (landform 1) and regional topography (landform 4) form the main crater rim (Graettinger, 2018), traversing the catchment longitudinally from SW to NE.

| **Tectono-volcanic basin** | | **FVS maars cluster** | **Caldeirão collapsed caldera** | | | **Cabeço do Caveiro scoria cone crater** |
|---|---|---|---|---|---|---|
| **Lake-catchment system** | | **Funda** | **Caldeirão east** | **Caldeirão west** | **Caldeirão Total** | **Caveiro** |
| Area [km2] | | 3.51 | 1.05 | 2.43 | 3.48 | 0.05 |
| Heigh [m] | | 445.7 | 261.9 | 312.8 | 312.8 | 63.5 |
| Outlet elevation [m] | | 100.7 | 1.9 | 82.8 | 82.8 | 3.5 |
| Floodable volume [km3] | | 0.3230 | 0.0000902 | 0.2203 | 0.2203 | 0.00000271 |
| Lake/ catchment area | | 0.12 | 0.08 | 0.05 | 0.06 | 0.03 |
| Major axis [m] | | NE maars: 2675 | - | - | Interfluve: 2318 | Interfluve: 299 |
| Major axis [º] | | NE maars: N011ºE | - | - | Interfluve: N011ºE | Interfluve: N105ºE |
| Minor axis [m] | | NE maars: 1479 | - | - | Interfluve: 1745 | Interfluve: 178 |
| Aspect ratio (AR) | | NE maars: 1.80 | - | - | Interfluve: 1.33 | Interfluve: 1.68 |
| **Catchment** | $_{R}$DEM | $_{R}$DEM$_{fun}$ | $_{R}$DEM$_{cald}$ | | | $_{R}$DEM$_{cav}$ |
| | Area [km2] | 3.14 | 0.97 | 2.31 | 3.28 | 0.05 |
| | Max. relative relief [m] | 410 | 260 | 310 | 310 | 60 |
| | Floodable volume [km3] | 0.32 | 0.22 | 0.22 | 0.22 | 0.00 |
| | Mean slope [º] | 21.515 | - | - | 21.473 | 19.695 |
| | Max slope [º] | 76.12 | - | - | 52.11 | 49.13 |
| | Mean Ksn | 0.90 | - | - | 0.70 | 0.76 |
| | Max Ksn | 16.16 | - | - | 3.24 | 2.17 |

| | | | | | | |
|---|---|---|---|---|---|---|
| | Max. drainage order | 3rd | - | - | 3rd | 1st |
| Lake | BDEM | BDEMfun | BDEMcald | | | - |
| | Area [km2] | 0.3689 | 0.0805 | 0.1236 | 0.2041 | 0.00155 |
| | Max depth [m] | 35.7 | 1.9 | 2.8 | 2.8 | 3.5 |
| | Volume (accommodation space) [km3] | 0.00793 | 0.0000902 | 0.0001629 | 0.0002531 | 0.00000271* |
| | Mean depth (volume / area) [m] | 21.49634 | 1.12050 | 1.31796 | 1.24008 | 1.74529 |
| | Area / volume | 47 | 892 | 759 | 806 | 573 |

*Table 4.1: Limnomorphometric parameters of the selected lake basins. * Estimated.*

### Slopes

The slope analysis derived from catchment relief reveals large differences between maximum values, with Funda catchment showing extreme values, whereas Caldeirão and Caveiro catchments have moderate values. Despite variations in elevation distributions and maximum slopes, Funda and Caldeirão catchments show similar mean slopes, with Caveiro having a slightly reduced value (Table 4.1).

The slope distribution (Fig. 4.1) in Funda catchment shows flat domains corresponding to 1) the bottom of the maars; 2) the bottom of the incised sectors developed on the bottom of the maars (on the NE maar); and 3) the basal part of the northern scoria cone southwestern flank in transition to Flores Island plateau. In Caldeirão catchment, low slopes correspond with the sedimentary infill of the post-caldera stage at the lowlands, with peatlands and alluvial/colluvial fans around the spatter scoria cones (Fig. 2.2). Likewise, the flat domain in Cabeço do Caveiro corresponds to the silted up central domain of the crater, where the colluvial fan and the peatland are asymmetrically disposed near Lake Caveiro (Fig. 2.2).

Besides, the steep domains within Funda catchment extend 1) towards the flanks of the northern scoria cone; 2) to the southernmost flank of the Caldeira das Sete Lagoas; 3) to the flanks of the maars, highlighting the max slopes at the eastern flank of the Funda maar; and 4) at the margins of the already incised valleys corresponding to erosive scars (Fig. 2.15b and c). In Caldeirão, the high catchment slopes mainly distribute on the scarps of the peripheric caldera flanks, isolated from the lake by the flat central domain. A similar distribution occurs in Cabeço do Caveiro, where the scarps are located in the displaced cone crater flanks, isolated from the lake by the flat central silted-up domain.

### Drainages

The drainage patterns within Funda, Caldeirão and Caveiro catchments reveal significant morphological contrasts arising from differences in system sizes and slope distributions. The large catchments of the Funda and Caldeirão systems feature multiple streams extending over kilometric distances, whereas only one stream, approximately 250 m length, is observed within the smaller Caveiro catchment (Figs. 4.1 and 4.2).

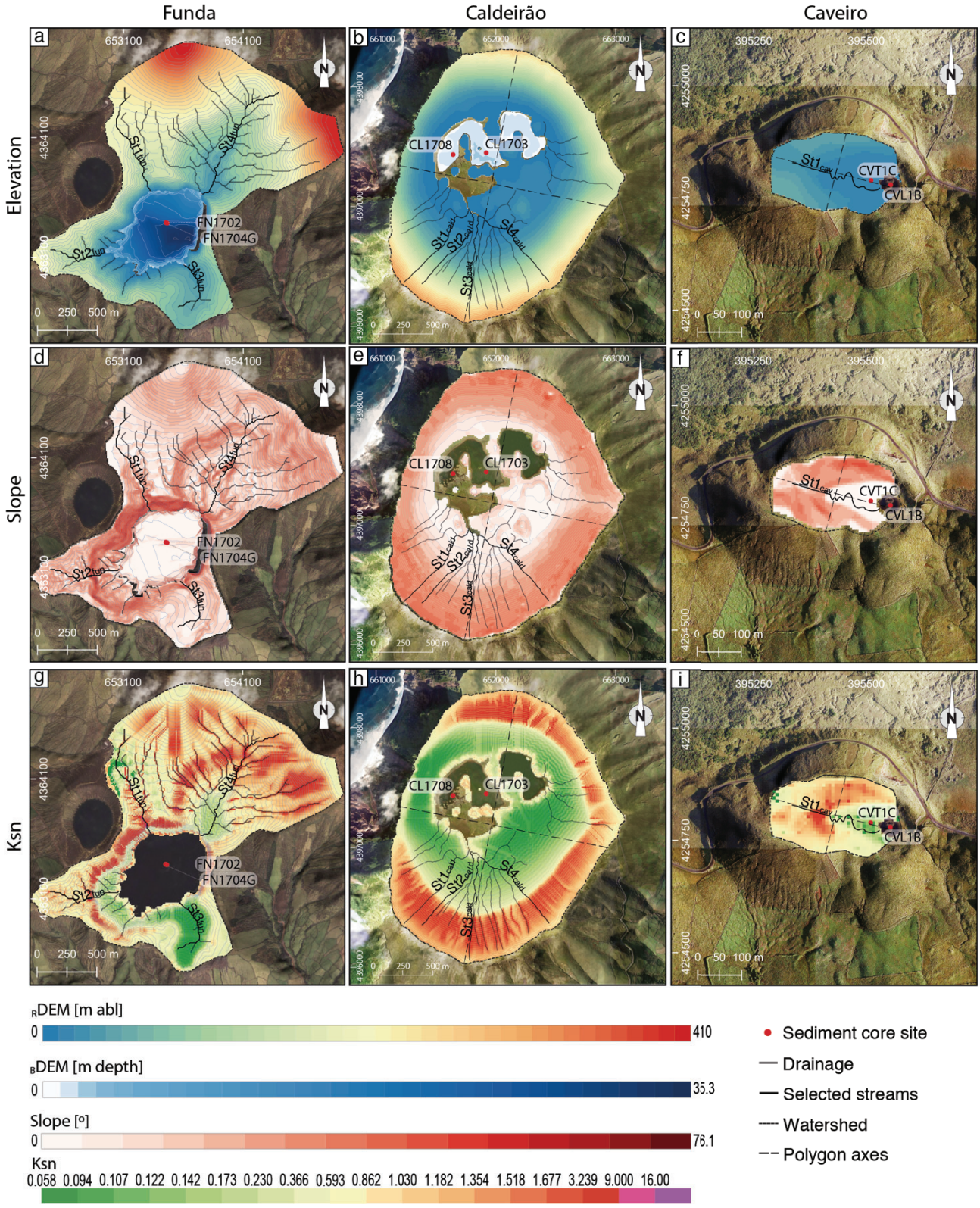


*Figure 4.1: Morphometric analysis of lake-catchment systems. a), d), g) Funda, b), e), h) Caldeirão and c), f), i) and Caveiro lake basins, including a), b), c) the available standardized elevation (RDEM and BDEM), d), e), f) slope angles and g), h) i) Ksn maps. The drainage, the streams selected for profile analysis and the position where the sedimentary cores were retrieved are indicated. Relief contour = 10 m. Bathymetry contour = 5 m.*

Furthermore, concentric landforms derived from the inner (landform 1) and outer (landform 2) flanks of central volcanic structures correspond, respectively, to centripetal and radial drainages characterized by low-order streams (mostly 1st order) draining limited areas. In the Funda catchment, this is evident around the maar crater flanks (especially at the SW maar) and the flanks

of the northern scoria cone. In the Caldeirão system, this pattern is observed on the steep flanks of the caldera (Fig. 2.19a, e and g).

In contrast, oriented elevation patterns correspond to drainages with preferential distribution, where streams coalesce to form dendritic drainages with higher order (up to 3rd order). Furthermore, fault intersections with the relief impose additional trends to the drainages, as seen in Caveiro (Fig. 2.22) and likely in the row of coalescent maars of the Funda catchment (Fig. 2.14).

Besides, lower-order stream sections are situated within steep domains, showing sub-parallel drainage patterns. This is observed at the southernmost edge of the Caldeira das Sete Lagoas and the southern flank of the Caldeirão caldera (Fig. 2.19g). In contrast, higher-order stream sections flow within flat domains, exhibiting higher sinuosity and dendritic distributions. This is evident on the southern side of the Caldeirão caldera bottom. Additionally, landform 2 at the caldera bottom contributes to the coalescence of streams.

### Potential erosion

Ksn mean and maximum values are the highest for the Funda catchment, whereas Caldeirão and, especially, Caveiro show relatively low maximum values. In contrast, the Ksn mean value is higher for Caveiro than for Caldeirão, but intermediate, below the value of Funda (Table 4.1). As expected, the Ksn distribution shows the highest values where steepness and/or drained area are maximum, whereas the lowest values are distributed where slopes and/or drained area are minimum. The distinct combinations between slope and drained area result in four domains of potential erosion:

- Domain 1: Low erosion domain (Ksn < 0.4). This domain extends to the flat domains of the study area.
- Domain 2: Intermediate erosion domain (0.4 < Ksn < 0.6): this domain covers most of the area of Funda and Caveiro catchments. In Funda catchment, it corresponds to 1) the Flores Island plateau and 2) with the S and NE maars flanks. In Caveiro catchment, it corresponds to 1) the alluvial fan, 2) most of the SW cone crater flank, and 3) the flat domain corresponding to the BG fault. In contrast, within Caldeirão catchment, this domain is limited to the peripheric lake rim, likely corresponding to an incipient incision wave, and to a narrow annular stripe corresponding to the transition from steep to flat domain.
- Domain 3: High erosion domain (0.6 < Ksn < 4). This domain fits the steepest domains and especially high Ksn values corresponding to most of the stream channels. In the Funda catchment, this domain fits the main maar crater rim and the septa between intersecting maars, composing incision waves. The most prominent erosive scars progress at the bottom of the NE maar (Fig. 2.15b and c). In the Caldeirão Catchment, this domain spans the steep caldera flanks, showing peak values when corresponding to streams channels. In the Caveiro Catchment, this domain sits on the slopes of the western side, concentrating at the fault intersection with topography.
- Domain 4: Extreme erosion domain (ksn > 4). This domain is only present in the Funda catchment and is limited to the steepest sections (crater arc) of alluvial channels draining extensive flat areas from the Flores Island plateau.

### Streams

The profile analysis of the most prominent streams within the $_{R}$DEM reveals considerably higher balance for Caldeirão and Caveiro drainages than for Funda (Fig 4.2). Funda drainage streams reveal prominent knickpoints distributed at diverse elevations at the intersection with maars septa and the main crater, where incision waves specially progress. In contrast, knickpoints at Caldeirão drainage distribute at the same elevations (ca. 5 m abl.), corresponding to the intermediate erosion

of the lake rim. Caveiro drainage shows only one knickpoint found at St1 stream head. The profiles of the most prominent streams cross the distinct erosion domains, which is indicative of the hydrological processes along them.

Funda catchment displays four main streams. Three of them drain the watershed sector of the Flores Island plateau at the north ($St1_{fun}$), west ($St2_{fun}$) and northwestern ($St4_{fun}$) sides (Fig. 4.1). Only two of them flow directly into Lake Funda from the plateau ($St1_{fun}$ and $St2_{fun}$). The $St1_{fun}$ flows across Domain 1 from ca. 750 to 550 m length, whereas upstream (from ca. 1000 to 750 m in length) and downstream (from ca. 550 m to the base level), it flows across Domain 3, reaching Domain 4 between 225 and 100 m abl., where incision reaches the highest Ksn values of the $_R$DEM (16.16) at the prominent knickpoint located on the main crater rim at 100 m abl. In its last 60 m length, $St1_{fun}$ descends 80 m in elevation gradient across domain 2 before reaching the base level. The $St2_{fun}$ reproduces the morphometry for the last 500 m length section of $St1_{fun}$, including the knickpoint sector that corresponds to the main crater rim, which reaches Ksn values of 9. The $St2_{fun}$ also crosses Domain 2 before reaching the lake base level in the already incised sector of the SW maar at the last ca. 100 m in length (Fig. 4.2).

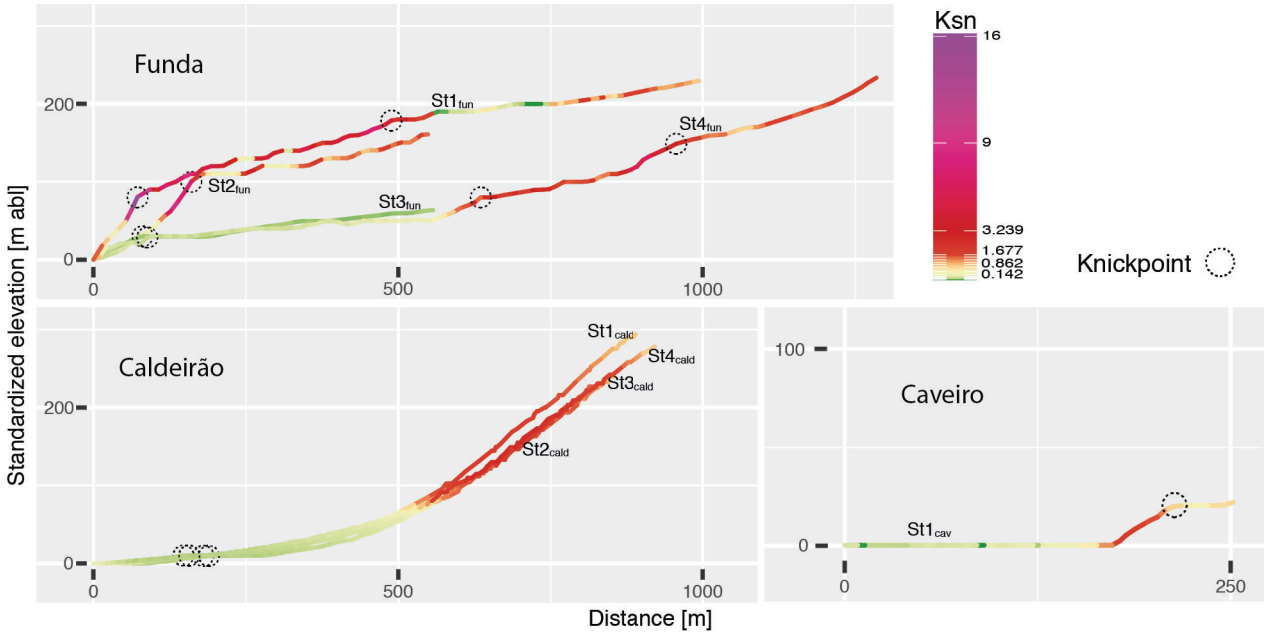


*Fig. 4.2: Profile analysis of the most prominent streams of Funda, Caldeirão and Caveiro catchments, indicating the Ksn values and the knickpoints identified.*

Furthermore, from Flores Island plateau, $St4_{fun}$ flows across the Northeastern maars before reaching Lake Funda (Fig. 4.1). This stream exhibits a straight disposition fitting the landform 3 axial orientation and the northeastern maar major axis (N020ºE). A prominent knickpoint (Ksn ≈ 3) at 625 m of length and at ca. 225 m abl. (Fig. 4.2) corresponds to the Funda-NE maar septum, where incision shows the highest progression within the $_R$DEM (Fig. 2.15b and c). This knickpoint divides $St4_{fun}$ profile into two distinct sections. The section comprised between 225 and 80 m abl. drains the Northeastern coalescent maars across Domain 3, where another knickpoint corresponds to the septa derived from the intersection between them at 900 m in length and 125 m abl. Furthermore, between 80 m abl. and the base level, $St4_{fun}$ flows through Domains 1 and 2, composed of the incised sector developed on the NE maar bottom, containing also a smooth knickpoint of 10 m height at the last ca. 10 m in length before reaching the lake (Fig. 4.2). In contrast, from outside of the plateau, a third stream ($St3_{fun}$) drains the S maar sector (Fig. 4.1), flows at low height (<70 m), crossing along Domain 1, with a low Ksn value (< 0.3) (Fig. 4.2).

The most prominent streams of Caldeirão drainage ($St1_{cald}$, $St2_{cald}$, $St3_{cald}$ and $St4_{cald}$) are located at the southern sector of the caldera reaching up to 300 m abl. They converge towards the lake while flowing through colluvial/alluvial fans and peatlands (Fig. 4.1). All these streams present similar morphometries derived from the concave morphology inherited from the caldera collapse and colluvial/alluvial infilling at the Domain 1 periphery (Fig. 4.2). The streams present sections above ca. 80 m abl. flowing through Domain 3, however, below ca. 80 m abl., the streams already flow through Domain 1, corresponding to diverse depositional environments. At this later domain and at ca. 200 m of the base level, all these streams show smooth knickpoints at the same height (ca. 5 m abl.) corresponding to Domain 2 and erosive scars of moderate progression (Fig. 2.19c). Similarly, the $St1_{cav}$ of Caveiro drainage flows through Domain 3 at the western margin of the lake basin, following the tectonic lineation to sharply reach Domain 1 at 100 m length, intersecting the alluvial fan and the peatland before reaching the base level (lake) through Domain 1 (Figs. 4.1 and 4.2).

#### Field landform analysis

In situ landforms analysis revealed the largest erosive scars within Funda lake-catchment system, which are composed of badlands incised at the young morphologies of the FVS inherited from subsurface explosive activity (Andrade et al., 2022). These bad-lands are especially prominent at the axial zone of the NE maar in correspondence with the Funda-NE maars septum (Fig. 2.15b,c) and at the intersection between the main crater rim in correspondence with the Funda maar and the plateau of Flores Island (Fig. 2.15d,f). In contrast, within Cadeirão catchment erosive scars are constituted by gullies, prevailing at the peripheric steeplands in correspondence especially with the most prominent streams (Fig. 2.21a), whereas the only remarkable rill in Caveiro corresponds with the tectonically controlled stream (Fig. 2.25). At the flatlands of both lake systems peri-lacustrine depositional landforms fill the depressed reliefs between scoria cones in Caldeirão and within the main crater in Caveiro conforming peatlands. Furthermore, alluvial fans install at the slopefoots, getting adapted to the scoria cones and overlying the peatlands in Caldeirão (Fig. 2.21a,c,f), whereas, sitting at the mouth of the tectonic rill in Caveiro (Fig. 2.25c). Incision progresses over them, in the form of gullies in Caldeirão (Fig. 2.21c) and rills in Caveiro (Fig. 2.25a). Lastly, within Lake Funda it is worth noting a depositional landform showing its topmost part over the lake level, that could correspond with a submerged alluvial fan (Fig. 2.15e).

### 4.1.2 Lakes

#### Volumetries

The lake area/volume ratio reveals the contrast between the morphologies of Funda, Caldeirão and Caveiro waterbodies (Table 4.1). Funda is a deep and extensive lake due to its conic-like lake bottom shapes, whereas Lake Caldeirão is a shallow and extensive lake because of the plate-like morphology of the bottom. It is noteworthy that despite the difference in lake volume between lakes Caldeirão and Caveiro, they present a relatively similar lake area/volume ratio, determining similar plate-like waterbody morphologies (Table 4.1). Therefore, Lake Funda is the most voluminous lake, exhibiting the deepest mean depths, whereas lakes Caldeirão and especially Caveiro display the lowest volumes, exhibiting similar mean depths but relatively extensive areas instead.

#### Bathymetries

The lake bottom morphologies derived from the bathymetric analyses of lakes Funda and Caldeirão reveal a strong morphological contrast, supporting results from volumetric analyses (Fig. 4.1):

Lake Caldeirão depths exhibit symmetric sedimentary wedges that gradually deepen, following a radial trend adapted to the scoria cones, from the periphery of the lake (A) towards the depocenter (B) located at the central part (Fig. 4.1b). A macrophyte patch identified in situ covers the area near the mouths of the most prominent streams at the southern side of Lake Caldeirão, revealing the

presence of a submerged delta plain (Fig. 2.15 c and e), where no bathymetric data are available. Given the reduced dimensions of Lake Caveiro (Table 4.1), the high area/volume estimated, its subrounded shoreline, and the dominance of landform 1 relief at the lake sector, a cap-like shape is inferred for its bottom, similar to that of Caldeirão but without the influence of landform 2 of the scoria cones.

In contrast, the depths and slopes of the Lake Funda show five different domains that indicate asymmetric distributions of sedimentary wedges and displaced depocenters (Fig. 4.1a and d): A) The peripheric lake rim, characterized by steep (25-35º slopes) and shallow (<15 m lake depth) areas; B) The western lake bottom sector, which is almost flat (<5º slopes) but gradually deepens (0-35 m depth) eastward from the $St2_{fun}$ mouth; C) The northern lake bottom sector is also flat (<5º slopes) and moderately deep (15-25 m lake depth), sloping south to southwest. This last sector lies close to $St1_{fun}$ and $St4_{fun}$ and exhibits shallow depths (<20 m) near $St4_{fun}$ mouth; D) The deep (> 30 m) depocenter, located to the southeast side of the lake, has a flat topography with slopes of less than 5º; and E) A steep (5-15º slopes) and deep (25-30 m lake depth) domain trending east-west between sectors c and d. Contrarily to the Caldeirão and Caveiro lake depocenters, it is worth noting that the lowest elevations of Lake Funda and the whole systems (depocenter) are within the Funda maar crater, below the regional topography (Flores island plateau).

### Sediment coring

Lake sediments coring (Fig. 4.1) in the most pelagic area of Lake Funda was performed over the steep and deep bathymetric domain (E), whereas in the most pelagic area of Lake Caldeirão, the sediments were recovered close to the central depocenter (B), as the sediments from Caveiro, where maximum depths were measured at the coring site. The topmost sediments of core section FN1702-01 (8 cm) and FN1704G (4 cm) were not recovered, and ca. 8 cm of sediment losses occurred at 80 cm of CVL1B-05 core section depth. The decompacted depth of the selected piston core sections (referred to as depth hereon) extends to: a) 990 cm for the composite record from cores FN1702 and FN1704G (Figs. 4.3 and 4.4), b) ca. 580 cm for CL1703 record (Fig. 4.5), and c) 930 cm for CVL1B record (Fig. 4.6).

## 4.2 Sedimentary lithofacies

The sediments of Lake Funda show a strong textural contrast with respect to their depth. While coarse terrigenous deposits dominate the base of FN1702 record (lowermost 665 cm depth), fine laminated sediments lie at the top (the uppermost 325 cm depth), which are replicated by the sediments of the parallel record FN1704G (Figs. 3.2 and 4.3).

In contrast, Lake Caldeirão sediments (core CL1703) are made up of fine massive deposits. These sediments are dark brown at the base of the record (the lowermost 440 cm depth), whereas reddish and light brown tones dominate at the top of the record (the uppermost 140 cm depth) (Figs. 3.2 and 4.4).

Lake Caveiro sediments (core CVL1B) consist of tephritic and coarse detritic deposits (lowermost 385 cm depth), interbedded with a dominant fine massive black and pale alternance of muds extending to the lowermost 730 cm depth. The topmost part of the record features a brown organic mud at the uppermost 200 cm depth (Figs. 3.2 and 4.5).

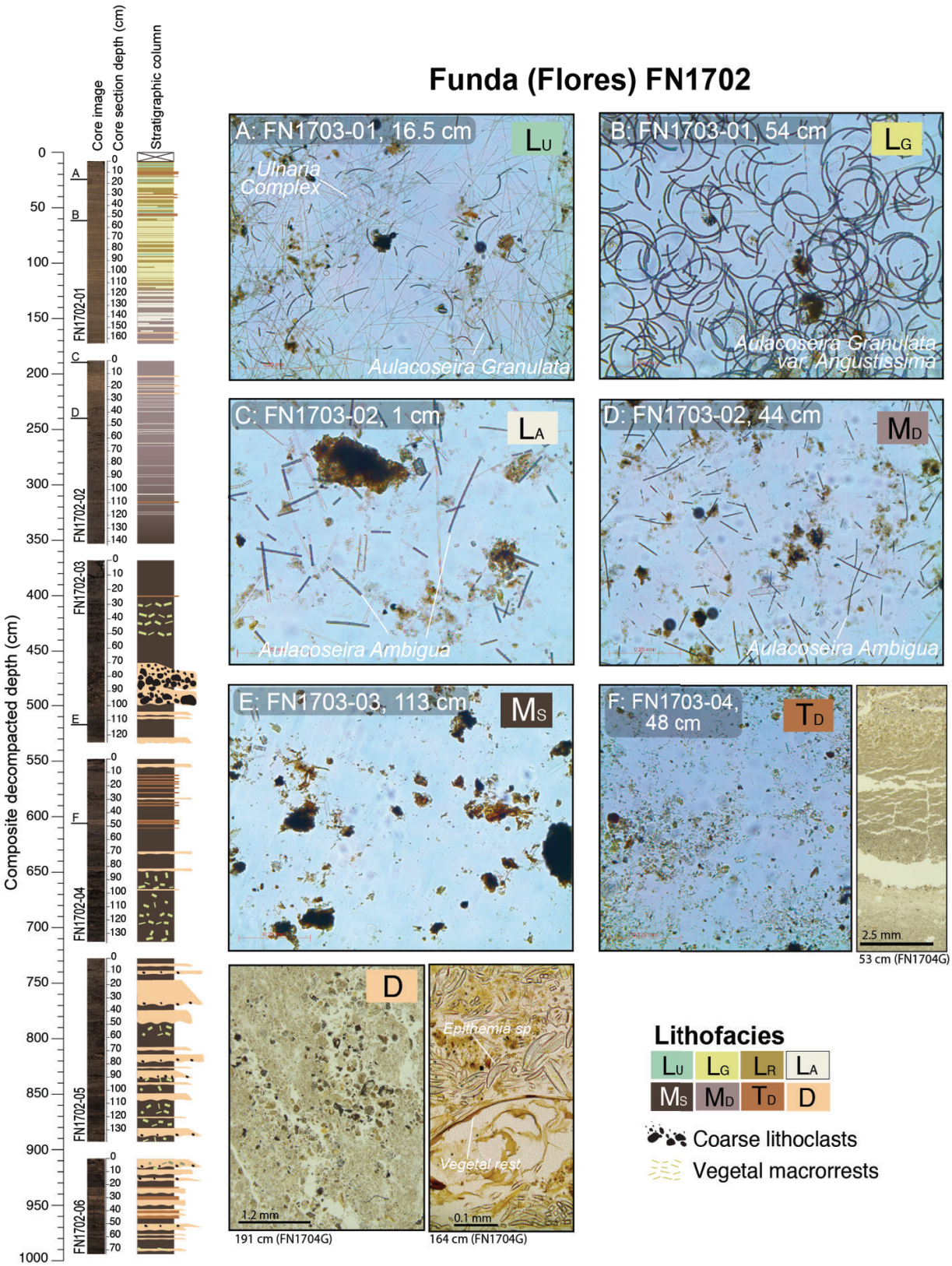


*Figure 4.3: Lithofacies of Lake Funda sediments (FN1702 and FN1704G records). Lithofacies: **$L_U$**: Greenish, massive, monospecific diatomaceous ooze of Ulnaria Complex, **$L_G$**: Yellowish, massive, multiespecific diatomaceous ooze with amorphous organic aggregates and silty clay, **$L_A$**: Yellowish, banded, diatomaceous ooze of Aulacoseira ambigua, with amorphous organic aggregates and silty clay, **$L_R$**: Brownish, massive, loose sapropel including silty clay and eutrophic planktonic diatoms. **$M_D$**: Brown-to-greyish, massive, silty sapropel with variable proportions of bioclasts, **$M_S$**: Dark-brown-to-black, massive silty mud with epilithic and epipsammic diatom oozes, **D**: Light-brown, reddish and black, centimetre-to-decimetre-thick, finning-up-to-*

*massive, erosive layers of sands-to-pebbles with terrestrial organic remains,* ***T$_D$****: Light-brown, millimetre-to-centimetre-thick thinning-up horizons of sandy silt with organic remain.*

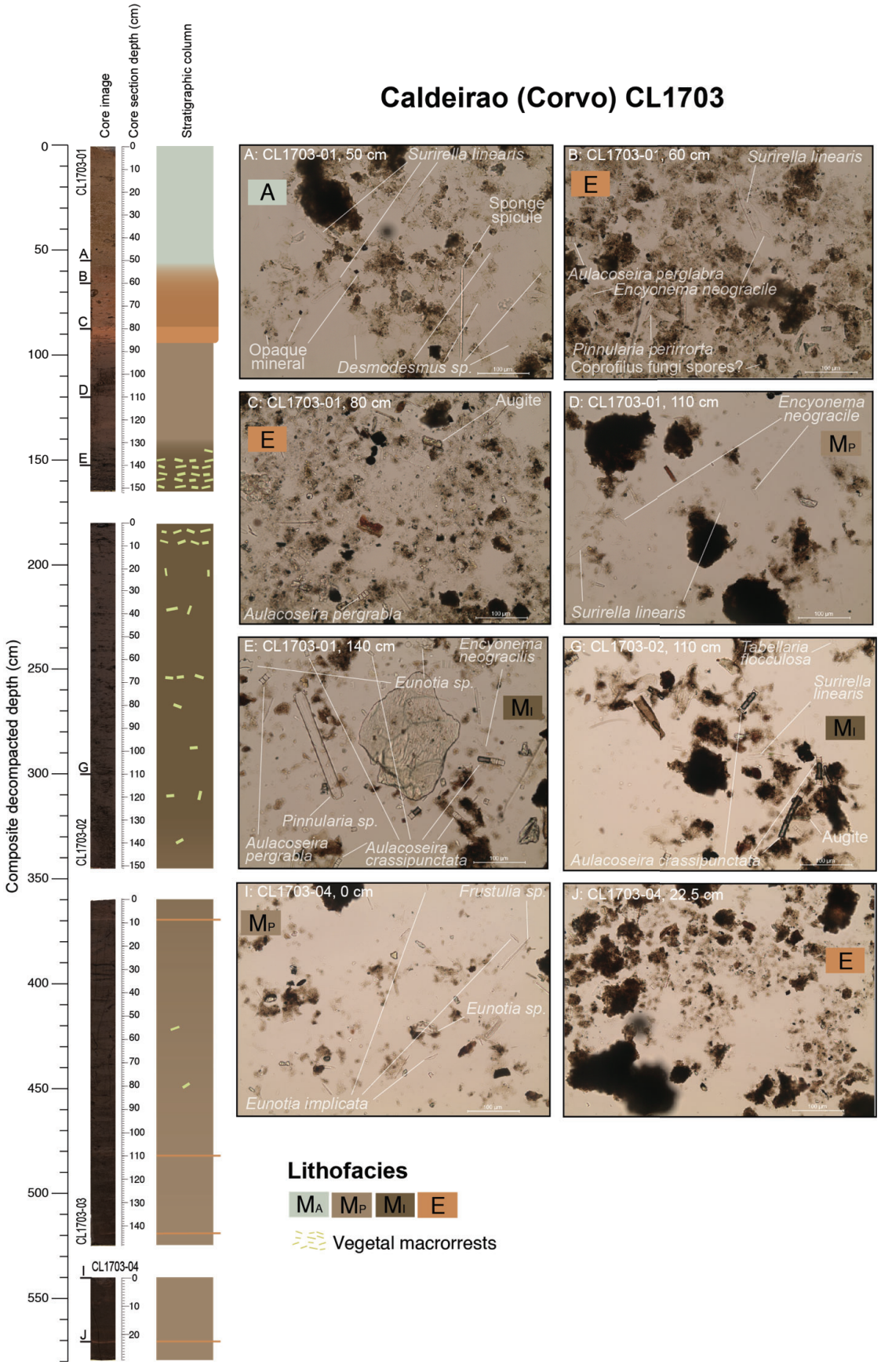


*Figure 4.4: Lithofacies of CL1703 (Lake Caldeirão)* ***M$_A$****:* Light-brown, massive, opaque minerals silt, with aquatic plants and green algae particulate remains ***M$_P$****: Dark-brown, massive, organic mud with terrestrial*

*vegetal remains.* ***MI:*** Dark-brown to greyish, massive, tychoplanktonic diatom ooze with terrestrial vegetal macrorests. ***E****: Reddish, massive, millimetre-to-decimetre layers of sand, silt and clay, with reddish amorphous organic aggregates*

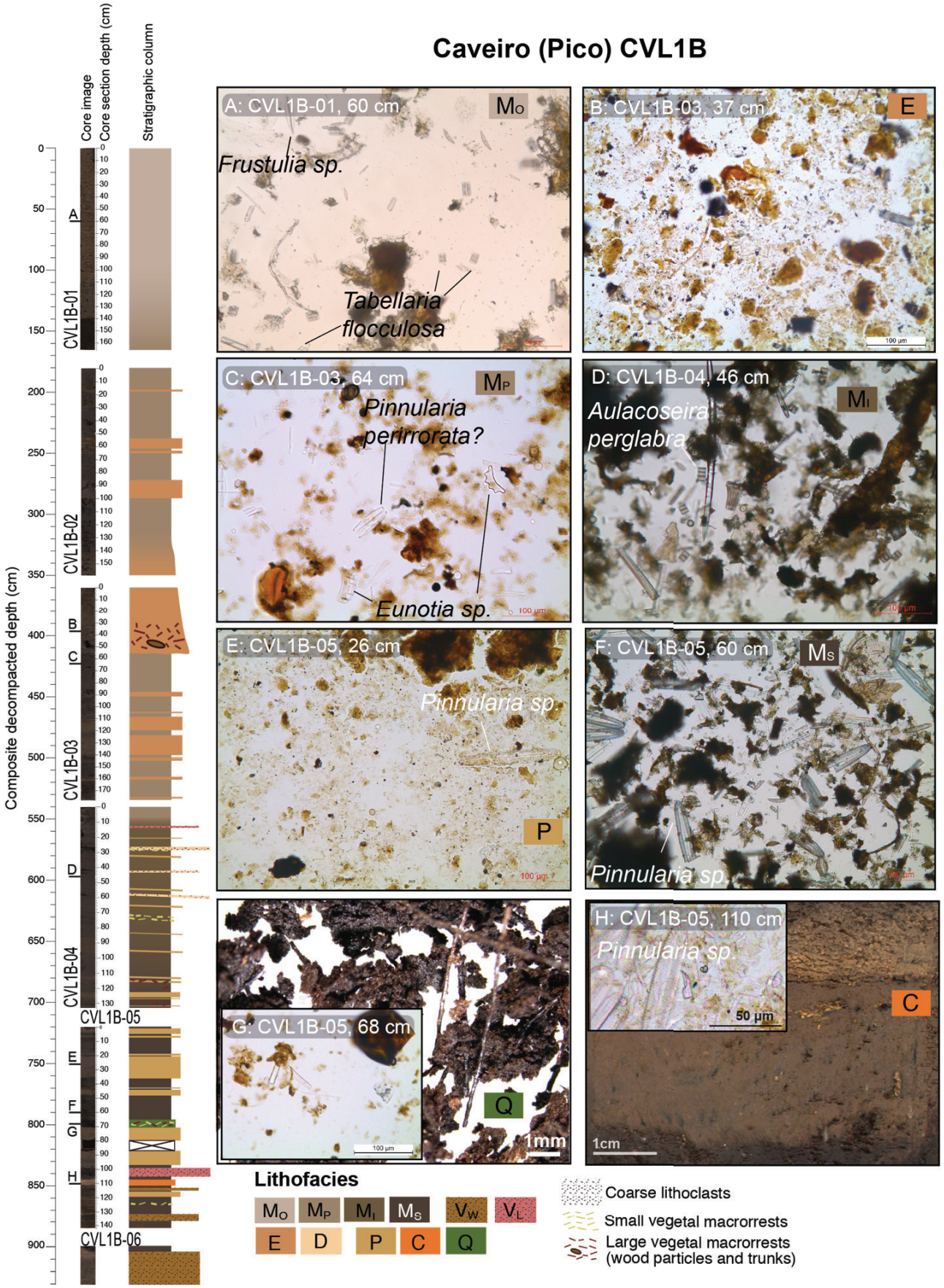

*Figure 4.5: Lithofacies of CVL1B (Lake Caveiro): **$M_D$**: Brown-to-greyish, massive, silty sapropel with variable proportions of bioclasts. **$M_O$**: Brown, massive, diatomaceous ooze with aquatic plant remains and black amorphous aggregates of organic matter. **$M_P$**: Dark-brown, massive, organic mud with terrestrial vegetal remains. **$M_I$**:* Dark-brown to greyish, massive, tychoplanktonic diatom ooze with terrestrial vegetal macrorests. ***$M_S$**: Dark-brown-to-black, massive silty mud with epilithic and epipsammic diatom oozes. **E**: Reddish, massive, millimetre-to-decimetre layers of sand, silt and clay, with reddish amorphous organic aggregates. **D**: Light-brown, reddish and black, centimetre-to-decimetre-thick, finning-up-to-massive, erosive layers of sands-to-pebbles with terrestrial organic remains. **Q**: Black, massive, peat with poorly matured silt and diatoms. **P**: Reddish, millimetric-to-decimetric massive layers of sapropel with iron (hydr)oxides and aerophilic diatoms. **C**: Light-orange, low-angle cross laminated centimetric diatomaceous ooze with reddish organic matter. **$V_W$**: Brownish, reddish and black, centimetric-to-decimetric, massive layers of coarse ash with reddish amorphous organic aggregates. **$V_L$**: Black, centimetric, massive layers of lapilli and coarse ash.*

The visual and microscopic sediment characterization has enabled the recognition of sixteen lithofacies. Table 4.2 provides a summary of the key components and characteristics at macro- (Fig. 3.2) and microscale (Figs. 4.3, 4.4 and 4.5) of the organic lithofacies and Table 4.3 of the lithoclastic lithofacies.

| Organic Lithofacies (acronym) | Lake (Record) | Macrofacies (Figure 3.2) | | Microfacies (Figures 4.3, 4.4 and 4.5) | | |
|---|---|---|---|---|---|---|
| | | Lithology | Sedimentary structure and bedding | Clastic component (%) | Subfossil biotic assemblage (%) | Organic matter (%) |
| **Greenish, massive, monospecific diatomaceous ooze of *Ulnaria Complex* ($L_U$)** | Funda (FN1702 and FN1704G) | Greenish ooze | Massive loose laminae. Diffuse to sharp bottom and sharp top | No present (0%) | Monospecific concentration of planktonic eutrophic diatoms *(Ulnaria Complex)* (95%) | Amorphous aggregates (5%) |
| **Yellowish, massive, multiespecific diatomaceous ooze with amorphous organic aggregates including silty clay ($L_G$)** | Funda (FN1702 and FN1704G) | Yellowish ooze | Massive loose laminae. Diffuse to sharp top and diffuse bottom | Fine subrounded clasts with good sorting (5%) | Dominated planktonic, eutrophic diatoms (*Aulacoseira Granulata*, 10%; *Aulacoseira Granulata var. Angustissima* 70 %; *Ulnaria Complex,* 5%*)* (85%) | Amorphous aggregates including part the mineral component (10%) |
| **Brownish, massive, loose sapropel including silty clay and eutrophic planktonic diatoms ($L_R$)** | Funda (FN1702 and FN1704G) | Brownish sapropel | Massive loose laminae. Diffuse top and diffuse to sharp bottom | Fine subrounded clasts with good sorting (25%) | Dominated by variable proportions of planktonic, eutrophic diatoms (*Aulacoseira Granulata*; *Aulacoseira Granulata var. Angustissima*) and *Ulnaria Complex* (15%) | Amorphous aggregates including part the mineral component (60%) |
| **Whiteish, banded, diatomaceous ooze of *Aulacoseira Ambigua*, with amorphous organic aggregates and silty clay ($L_A$)** | Funda (FN1702 and FN1704G) | Whiteish ooze | Banded loose laminae. Sharp bedding planes | Fine subrounded clasts with good sorting interspersed among diatom bioclasts forming bands (15%) | Dominated by mesotrophic and planktonic diatoms (*Aulacoseira Ambigua*) (70%) | Amorphous floccules interspersed among diatom bioclasts forming bands. The aggregates include most of the mineral component (15%) |
| **Brownish, massive to floccule-like aggregates of sapropel with planktonic, mesotrophic and** | Funda (FN1702 and FN1704G) | Brown clayey silt | Massive-to-laminated compact. Sometimes patchy floccules | Loose, poorly sorted and subangular clasts. (30%) | Dominated by planktonic, mesotrophic diatoms (*Ulnaria complex, A. granulata, A. ambigua*). Epiphitic (*Epithemia sp.*) and benthic (Pinnularia sp.) diatoms (30%) | Amorphous reddish patches. Bituminous coal particles (40%) |

| | | | | | | |
|---|---|---|---|---|---|---|
| **epiphytic diatoms ($M_D$)** | | | | | | |
| **Brown, massive, diatomaceous ooze with aquatic plant remains and black amorphous aggregates of organic matter ($M_O$)** | Caveiro (CVL1B) | Brown ooze | Massive | Fine subangular clasts (5%) | Dominated by acidophilic and saprophilic, benthic diatoms (*Tabellaria flocculosa*; abundant colonies, *Frustulia sp., Pinnularia sp.* and *Eunotia sp.*). Aquatic plant remains (60%) | Black amorphous aggregates (35%) |
| **Black, massive, peat with poorly matured silt and diatoms (Q)** | Caveiro (CVL1B) | Black peat | Massive | Silty subangular clasts (20%) | Diatoms (20%). Large plant remains (roots) (60%) | Well preserved particulate, low fragmentation |
| **Light-orange, low-angle cross laminated centimetric diatomaceous ooze with reddish organic matter (C)** | Caveiro (CVL1B) | Orange silty ooze | Centimetric layer with low-angle cross lamination and sharp bedding planes | Opaque minerals (5%) | Benthic diatom bioclasts (*Eunotia sp. and Pinnularia sp*.) and abundant sponge spicules, some of them fragmented. (65%) | Reddish amorphous aggregates (30%) |
| **Reddish, millimetric-to-decimetric massive layers of sapropel with iron (hydr)oxides (P)** | Caveiro (CVL1B) | Reddish sapropel | Centimetre to decimetre thick massive layers, sometimes presenting clinoforms. Sharp bedding planes | Granular aggregates including opaque heavy minerals and flakes of iron (Hydr)oxides. Some subangular sandy particles (pyroxene, plagioclase) (20%) | Benthic diatom bioclasts (*Pinnularia sp*.) and Sponge spicules (5-20%) | Patchy, amorphous, reddish aggregates including the mineral component. (60-75%) |
| **Dark-brown to greyish, massive, tychoplanktonic diatom ooze with terrestrial vegetal macrorests ($M_I$)** | Caldeirão (CL1703) | Dark-brown ooze | Massive | Variable proportions of fine subrounded well sorted clasts included in organic matter aggregates (0-15%) | Dominated by variable proportions of diatom oozes of tychoplanktonic (*Aulacoserira crassipunctata, A. perglabra*), aerophilus (*P. perirrorata*) and benthic acidophilus (*Eunotia paludosa, Eunotia implicata, Pinnularia sp.*) species. Sponge spicules. Variable concentrations of terrestrial vegetal rests. (40-60%) | Amorphous black-to-reddish aggregates (25%) |
| | Caveiro (CVL1B) | Greyish ooze | Massive | Loose, poorly sorted and weathered, subangular clasts. (10-50%) | Dominated by oligotrophic, planktonic and tychoplanctonik diatoms (*Aulacoseira perglabra,* Staurosira cf. venter and Staurosirella sp.). Benthic diatoms (*Pinnularia sp.*) and sponge spicules. Layers of terrestrial plant remains (woody particles). (10-30%) | Amorphous black aggregates. (20-30%) |
| **Dark-brown, massive, sapropel with silt and terrestrial vegetal rests ($M_P$)** | Caldeirão (CL1703) | Dark brown sapropel | Massive | Loose, poorly sorted and weathered, subangular clasts. Some sandy particles of olivine (10-40%) | Dominated by benthic, acidophilus and saprophilus diatoms (*Eunotia sp., E. Implicata, E. Paludosa, Frustulia sp., Pinnularia sp., Tabellaria flocculosa*). Sponge spicules and vegetal rests (10-20%) | Amorphous black aggregates. (40-80%) |
| | Caveiro (CVL1B) | Dark brown sapropel | Massive | Variable proportions of fine subrounded well | Dominated by diatom oozes of benthic, acidophilus (*Pinnularia sp., Eunotia sp., Frustulia sp.,* | Amorphous reddish aggregates (70%) |

| | | | | | | |
|---|---|---|---|---|---|---|
| | | | | sorted clasts included in organic matter aggregates (10%) | *Tabellaria flocculosa*) and aerophilic (*Pinnularia perirrorata*) species. Planktonic diatom oozes (*Aulacoseira sp*.). (20%) | |
| **Dark-brown-to-black, massive silty sapropel with epilithic and epipsammic diatom oozes ($M_S$)** | Funda (FN1702) | Dark brown sapropel | Massive | Loose, poorly sorted and weathered, subangular silty clasts. (30%) | Dominated by benthic circumneutral diatoms (*Epithemia sp., Achnanthidium minutissimum, Campylodiscus hibernicus*). Large vegetal rests (30%). | Amorphous black-to-reddish aggregates (40%) |
| | Caveiro (CVL1B) | Black sapropel | Massive | Loose, poorly sorted, poorly weathered, subangular silty clasts. (30%) | Dominated by circumneutral, oligotrophic and benthic diatoms with variable proportions of epipelic (*Encyonema gaeumannii, Eunotia incisa, Pinnularia sp.*), epiphytic (*Encyonema neogracile*) and epilithic opportunistic (*Achnanthidium minutissimum*) species. Sponge spicules. (30%) | Amorphous black aggregates. (20-40%) |

*Table 4.2: Organic lithofacies of the selected sedimentary records. The characterization includes macroscopic observations of lithology and sedimentary structures, alongside microscopic identification of components (Figs. 4.3, 4.4 and 4.5), with stablished semiquantitative average relative proportions that allowed the lithofacies classification following system proposed by Schnurrenberger et al. (2003). Diatom species determination and environmental constrains derive from Ritter et al., 2022 for FN1702 and FN1704G records, from Raposeiro et al. (2021) and Pla-Rabes (personal communication) for CL1703 record and from Marques (2021) for CVL1B.*

| **Lithoclastic Lithofacies (acronym)** | **Lake (Record)** | **Macrofacies (Figure 3.2)** | | **Microfacies (Figures 4.3, 4.4 and 4.5)** | | |
|---|---|---|---|---|---|---|
| | | **Lithology** | **Sedimentary structure and bedding** | **Clastic component (%)** | **Subfossil biotic assemblage (%)** | **Organic matter (%)** |
| **Light-brown, massive, opaque minerals silt, with aquatic plants and green algae particulate remains ($M_A$)** | Caldeirão (CL1703) | Light reddish silt | Massive | Poorly sorted, subrounded clasts with opaque minerals (50%) | Dominated by benthic diatoms (*Surirella linearis, Tabellaria flocculosa)* and particulate organic matter (aquatic plants remains and green algae; *Desmodesmus sp*.) (25%) | Amorphous reddish aggregates (25%) |
| **Reddish, massive, millimetre-to-decimetre layers of sand, silt and clay, with reddish amorphous organic aggregates (E)** | Caldeirão (CL1703) | Reddish sand silt and clay | millimetre-to-centimetre-thick massive layers | Poorly sorted, subrounded clasts Some sandy particles of plagioclase and pyroxene. (50%) | Dominated by benthic (*Frustrulia sp., Eunotia sp., encyonema neogracile, Pinnularia sp., Surirella linearis*) and aerophilic (*P. perirrorata*) diatom bioclasts. sponge spicules (15%) | Amorphous reddish aggregates (45%). Some particulate (5%), highlighting punctual coprophilous fungi spore concentrations. (35%) |
| | Caveiro (CVL1B) | Reddish sand silt and clay | Massive, sharp (bottom) and diffuse (top) bedding planes | Poorly sorted sand silt and clay subrounded augite and plagioclase grains. (60%) | Dominated by epipelic diatoms (*Pinnularia sp.*). Large vegetal rests (trunks) (10%) | Patchy, amorphous, reddish aggregates including the mineral component. (30%) |

| | | | | | | |
|---|---|---|---|---|---|---|
| **Light-brown, reddish and black, centimetre-to-decimetre-thick, finning-up-to-massive, erosive layers of sands-to-pebbles with terrestrial organic remains (D)** | Funda (FN1702) | Light brown, reddish and black sands to pebbles | Centimetre-to-decimetre-thick layers, with finning-up to massive disposition and erosive base. | Very poorly sorted. Subrounded and grain-supported sand to pebble. Reddish grains. (85%) | Epiphitic diatoms (*Epithemia sp.*), some of them attached to vegetal plant remains (0-10%) | Terrestrial plant macrorrests (0-5%) |
| | Caveiro (CVL1B) | Black sands and gravelly sands | Massive erosive layer. Macrophytes at the base. | Microconglomerate grains included in a fine sand matrix. Poorly sorted subrounded reddish particles. (80-100%) | Benthic (*Eunotia incisa, Pinnularia sp., encyonema neogracile*), planktonic (*Aulacoseira perglabra* and aerophilic (*Pinnularia perirrorata*) diatom bioclasts (0-10%). Macrophytes at the base. | Black amorphous aggregates (0-10%) |
| **Light-brown, millimetre-to-centimetre-thick thinning-up horizons of sandy silt with organic remains ($T_D$)** | Funda (FN1702 and FN1704G) | Light brown sandy silt | Millimetre-to-centimetre-thick thinning-up laminae. Subunits C, D and E of the Bouma (1962) sequence. Sharp bottom and flame structures at the top. | Very well sorted fine sand to sandy silt with subhedral rounded clasts (90%) | Epiphitic diatoms (*Epithemia sp.*) and sponge spicules (5%) | Amorphous aggregates and bituminous coal particles (5%) |
| **Black, centimetric, massive layers of lapilli and coarse ash ($V_L$)** | Caveiro (CVL1B) | Black lapilli and coarse ash | Centimetric massive layers | Volcanic glass with angular shapes and good sorting (100%) | No present (0%) | No present (0%) |
| **Brownish, reddish and black, centimetric-to-decimetric, massive layers of coarse ash with reddish amorphous organic aggregates ($V_W$)** | Caveiro (CVL1B) | Brownish, reddish and black coarse ash | Centimetric to decimetric massive layers | Well sorted reddish subangular clasts (95-100%) | No present (0%) | Reddish amorphous aggregates (0-5%) |

*Table 4.3: Lithoclastic lithofacies of the selected sedimentary records. The characterization includes macroscopic observations of lithology and sedimentary structures, alongside microscopic identification of components (Figs. 4.3, 4.4 and 4.5), with stablished semiquantitative average relative proportions that allowed the lithofacies classification following system proposed by Schnurrenberger et al. (2003). Diatom species determination and environmental constrains derive from Ritter et al., 2022 for FN1702 and FN1704G records, from Raposeiro et al. (2021) and Pla-Rabes (personal communication) for CL1703 record and from Marques (2021) for CVL1B.*

Since Lithofacies D, and $V_L$ revealed sampling limitations, and $V_W$ suggested a non-lacustrine origin, the sections of the records dominated by them (FN1702-05 and FN1702-06 and the bottommost 85 cm of core section CVL1B-05 and the core section CVL1B-06; Figs. 4.3 and 4.5) were excluded for biogeochemical and mineral characterization.

## 4.3 Biogeochemical composition and fluxes within the sediment records

The XRF analyses revealed the presence of Si, Cl, K, Ca, Ti, V, Mn, Fe, Sr, and Zr in the sediments of FN1702 (Fig. 4.6), CL1703 (Fig. 4.7) and CVL1B (Fig. 4.8) records. In addition, the FN1702 record also displayed statistically consistent XRF intensities of Cr and Al, the CL1703 record Al, and the CVL1B record Cr, Al and Rb.

From the bottom to the top, the biogeochemical values of FN1702 record (Fig. 4.6) display a decreasing trend for all chemical elements, except for Cl and BSi (alongside Inc/coh and Si), whose trend is increasing. Moreover, TC, TN and TOC/TN show an oscillating pattern which is opposite to that following Si. Besides, the Mn and $\delta^{13}C$ signals display a peaky pattern. In turn, the $\delta^{15}N$ and S exhibit abrupt changes. Furthermore, XRF intensities of most of the elements at the topmost sediments show oscillations fitting the lamination pattern.

The biogeochemical composition of the CL1703 record (Fig 4.7) displays more constant values than those from the FN1702 record. Specifically, all the elements (except Cl) show high values in the lower part (base up to 370 cm depth), A decrease between 350 and 150 cm depth and high values between 150 and 50 cm depth (except Br). Finally, from 50 cm to the top of the record, the values are low again. The TOC, TN, and Inc/coh ratio exhibit constant values with an excursion to minimum values at 90 cm depth, whereas TOC (TN) in the topmost 50 cm decreases (increases). Therefore, the TOC/TN ratio shows constant values with a progressive decreasing upwards trend from 90 cm, displaying the lowest values in the uppermost 50 cm. Conversely, $\delta^{13}C$, with minimum values at the bottom of the record, gradually increases from 150 cm depth upwards. Cl and BSi covariate positively showing the highest values between 500 and 200 cm and an abrupt decrease from 150 to 90 cm. Br and $\delta^{15}N$ display the same positive covariance with a sharp decrease in $\delta^{15}N$ at the top of the record.

The biogeochemical composition of CVL1B record (Fig. 4.8) exhibits values with abrupt changes for Al, K, Ca, Ti, V, Mn, Fe, Zr with a decreasing upwards trend from 640 cm to the top of the record. This pattern is similar for $\delta^{15}N$ and $\delta^{13}C$, whereas the TOC and TN display the opposite pattern. The Rb and Sr show low values with some peaks. The Br presents medium values through most of the record and high values at the top (100 cm to 45 cm depth), whereas Cl and Si show the lowest values in this section, and the highest at the bottom (up to 630 cm depth).

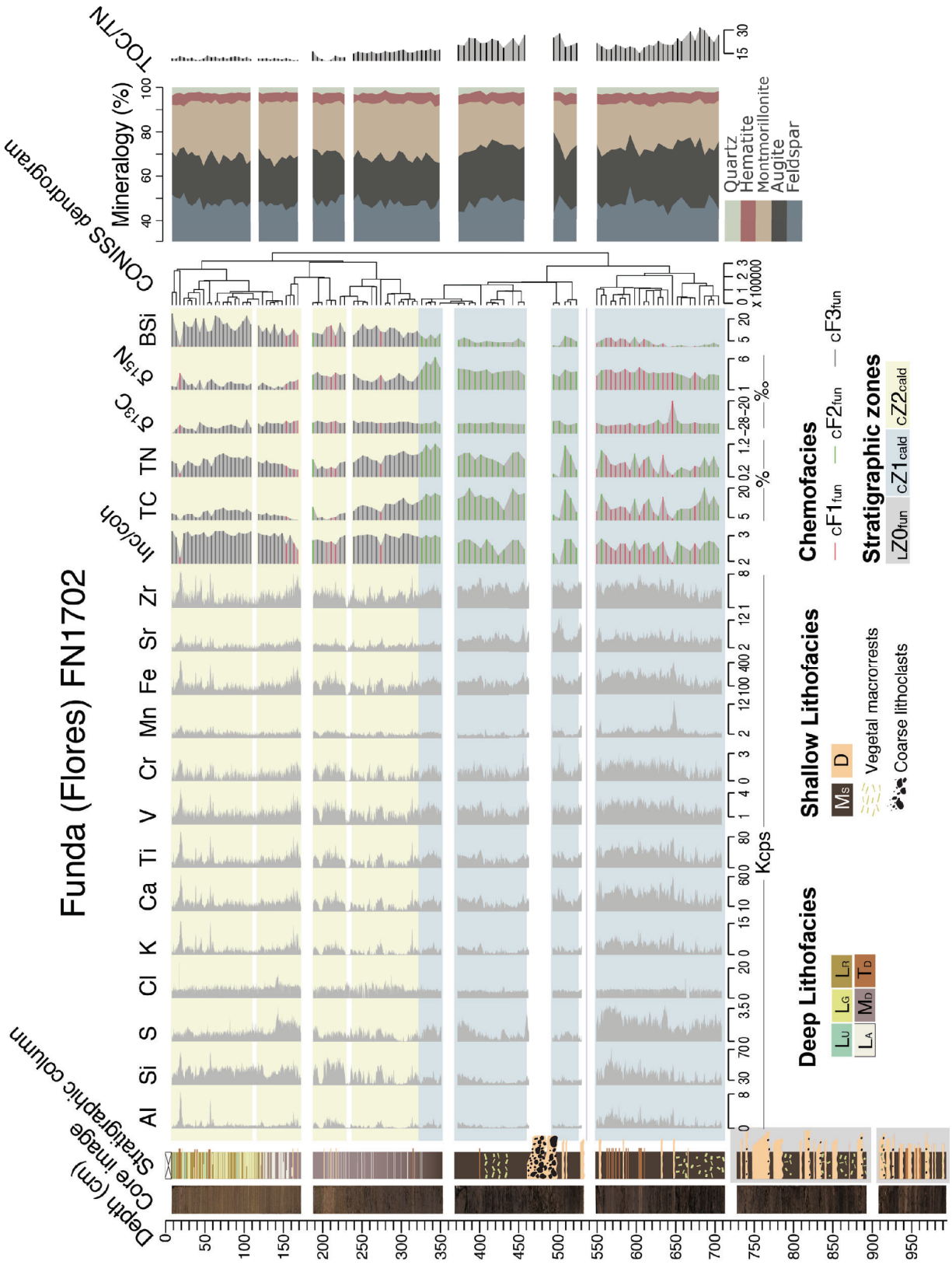


*Fig 4.6: Stratigraphic plot of FN1702 record and high-resolution core images with the relative content of organic elements and isotopes derived from the bulk organic matter analysis, the relative percentages of mineral species derived from the XRD analysis, and the element intensities derived from XRF analysis. The stratigraphic zones identified through lithofacies and statistical analyses of the FN1702 record are also indicated, including the CONISS dendrogram. Lithofacies:* ***L**U: Greenish, massive, monospecific diatomaceous ooze of Ulnaria Complex,* **L**G: Yellowish, massive, multiespecific diatomaceous ooze with amorphous organic aggregates and silty clay,* **L**A: Yellowish, banded, diatomaceous ooze of Aulacoseira ambigua, with amorphous organic aggregates and silty clay,* **L**R: Brownish, massive, loose sapropel including silty clay and eutrophic*

*planktonic diatoms.* ***M$_D$****: Brown-to-greyish, massive, silty sapropel with variable proportions of bioclasts,* ***M$_S$****: Dark-brown-to-black, massive silty mud with epilithic and epipsammic diatom oozes,* ***D****: Light-brown, reddish and black, centimetre-to-decimetre-thick, finning-up-to-massive, erosive layers of sands-to-pebbles with terrestrial organic remains,* ***T$_D$****: Light-brown, millimetre-to-centimetre-thick thinning-up horizons of sandy silt with organic remain.*

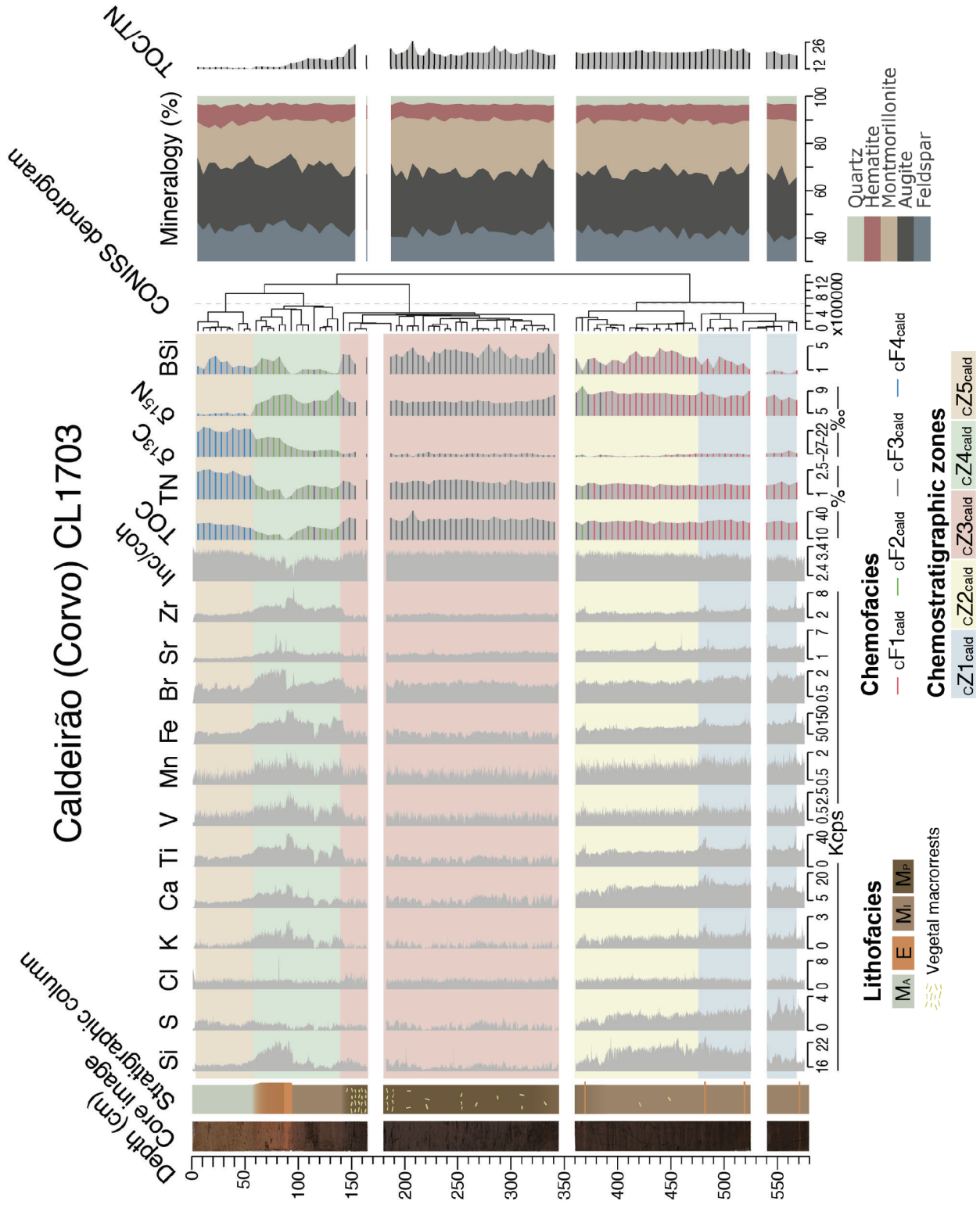


*Fig 4.7: Stratigraphic plot of CL1703 record and high-resolution core images with the relative content of organic elements and isotopes derived from the bulk organic matter analysis, the relative percentages of mineral species derived from the XRD analysis, and the geochemical elements intensities derived from XRF analysis.*

*The stratigraphic zones identified through lithofacies and statistical analyses of the CL1703 record are also indicated, including the CONISS dendrogram. Lithofacies:* ***MA:*** Light-brown, massive, opaque minerals silt, with aquatic plants and green algae particulate remains ***MP****: Dark-brown, massive, organic mud with terrestrial vegetal remains.* ***MI:*** Dark-brown to greyish, massive, tychoplanktonic diatom ooze with terrestrial vegetal macrorests. ***E****: Reddish, massive, millimetre-to-decimetre layers of sand, silt and clay, with reddish amorphous organic aggregates*

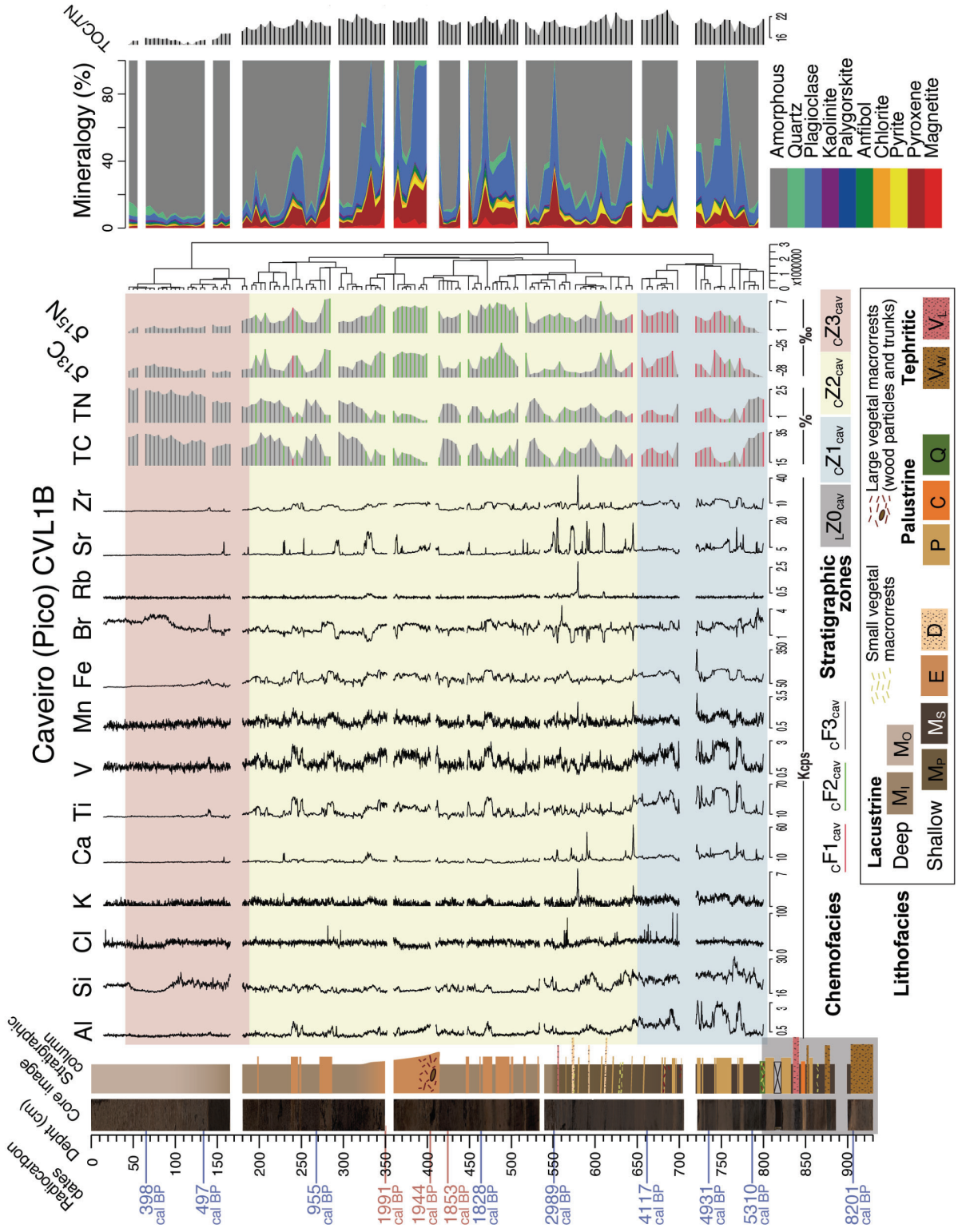


*Fig 4.8: Stratigraphic plot of CVL1B record and high-resolution core images with the relative content of organic elements and isotopes derived from the bulk organic matter analysis, the relative percentages of mineral species derived from the XRD analysis, and the geochemical elements intensities derived from XRF analysis. The stratigraphic zones identified through lithofacies and statistical analyses of CVL1B record are also*

*indicated, including the CONISS dendrogram. Radiometric ages are indicated in cal. yr. BP, red ones are reversals. Lithofacies: **$M_D$**: Brown-to-greyish, massive, silty sapropel with variable proportions of bioclasts. **$M_O$**: Brown, massive, diatomaceous ooze with aquatic plant remains and black amorphous aggregates of organic matter. **$M_P$**: Dark-brown, massive, organic mud with terrestrial vegetal rests. **$M_S$**: Dark-brown-to-black, massive silty mud with epilithic and epipsammic diatom oozes. **E**: Reddish, massive, millimetre-to-decimetre layers of sand, silt and clay, with reddish amorphous organic aggregates. **D**: Light-brown, reddish and black, centimetre-to-decimetre-thick, finning-up-to-massive, erosive layers of sands-to-pebbles with terrestrial organic remains. **Q**: Black, massive, peat with poorly matured silt and diatoms. **P**: Reddish, millimetric-to-decimetric massive layers of sapropel with iron (hydr)oxides and aerophilic diatoms. **C**: Light-orange, low-angle cross laminated centimetric diatomaceous ooze with reddish organic matter. **$V_W$**: Brownish, reddish and black, centimetric-to-decimetric, massive layers of coarse ash with reddish amorphous organic aggregates. **$V_L$**: Black, centimetric, massive layers of lapilli and coarse ash.*

### 4.3.1 Chemofacies

The application of the k-means clustering algorithm to the available biogeochemical datasets groups samples according to their biogeochemical composition (Fig. 4.9). The median values of the biogeochemical variables based on the selected centroids characterize the chemofacies (cF), which are sediments with distinctive biogeochemical budgets (Table 4.4). According to the applied k-means algorithm and the biogeochemical median values, three chemofacies compose FN1702 ($_cF1_{fun}$, $_cF2_{fun}$, and $_cF3_{fun}$) and CVL1B ($_cF1_{cav}$, $_cF2_{cav}$, and $_cF3_{cav}$) records, whereas four chemofacies compose the CL1703 ($_cF1_{cald}$, $_cF2_{cald}$, $_cF3_{cald}$ and $_cF4_{cald}$).

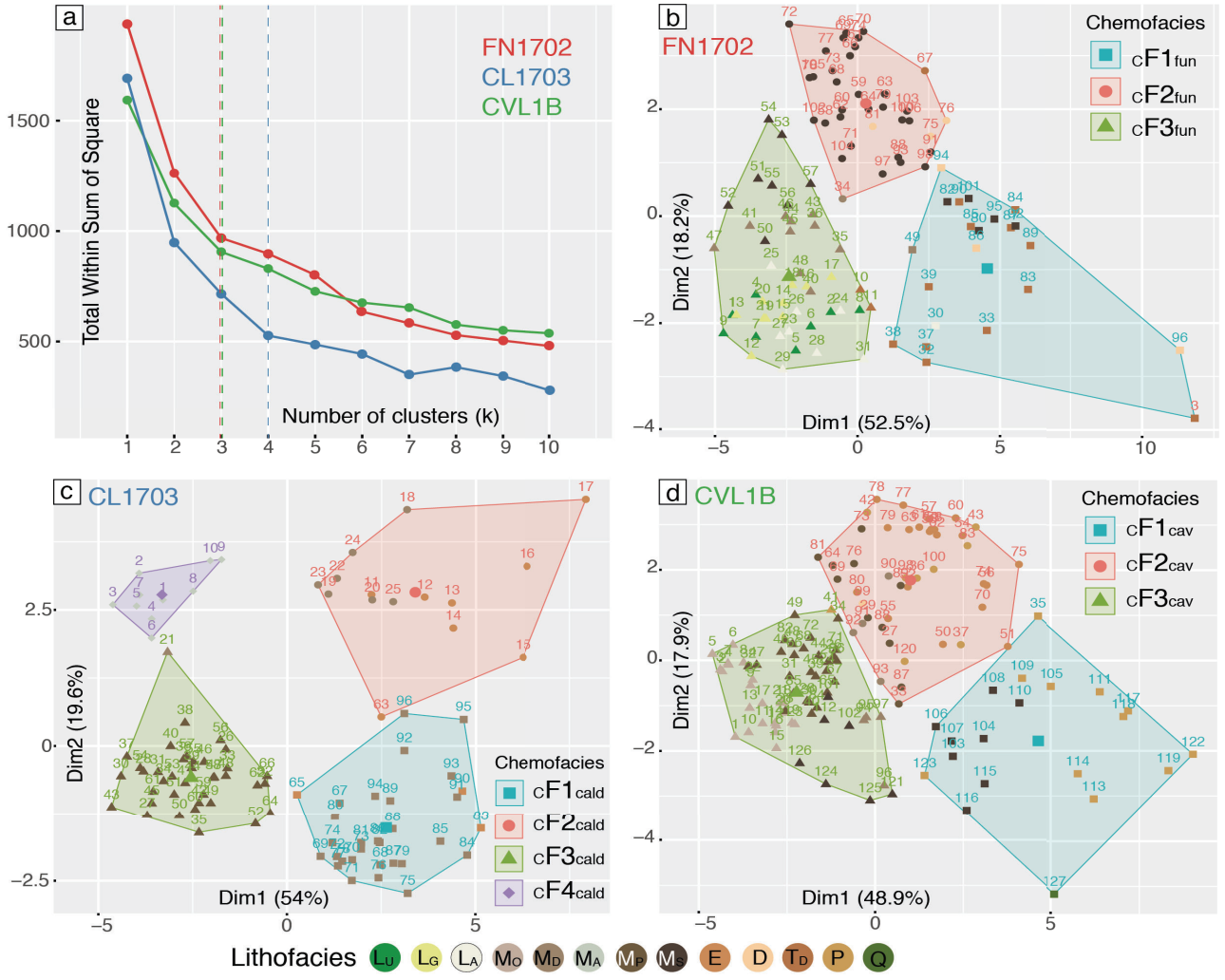


*Figure 4.9: Biogeochemical groups obtained through the K-means clustering algorithm that define the chemofacies: a) The elbow method applied to the total sum of squares within the clusters of FN1702, CL1703*

*and CVL1B biogeochemical datasets. The elbow method allows discerning the optimal number of clusters corresponding to the chemofacies of b) FN1702, c) CL1703, and d) CVL1B records. The clustered samples are represented in function of the lithofacies to which they belong.*

Within the FN1702 record and with respect to the rest of chemofacies, the $_{C}F1_{fun}$ has higher values of all the elements with the exception of the Cl, $_{C}F2_{fun}$ is richer in TOC, d15N and Sr, and $_{C}F3_{fun}$ presents higher values of Cl, BSi and Inc/coh. In the CL1703 record, $_{C}F1_{cald}$ and $_{C}F2_{cald}$ show the higher values in all the elements with the exception of the Cl and S for $_{C}F2_{cald}$. The $_{C}F3_{cald}$ has high values of BSi and TOC, contributing to the amorphous fraction (Inc/coh). Finally, $_{C}F4_{cald}$ shows the highest concentration of $\delta^{13}C$ and TN and the lowest of $\delta^{15}N$. In CVL1B record, $_{C}F1_{cav}$ has high values of all the elements with the exception of Rb, whereas high values of the organic (TC and TN) and isotopic ($\delta^{13}C$ and $\delta^{15}N$) fraction characterize the composition of $_{C}F3_{cav}$ and $_{C}F2_{cav,}$ respectively.

| | | | | Lake (record) | | | | | | | | | |
|---|---|---|---|---|---|---|---|---|---|---|---|---|---|
| | | | | Funda (FN1702) | | | Caldeirão (CL1703) | | | | Caveiro (CVL1B) | | |
| Facies | Lithofacies | | | $T_D$ D | $M_S$ | $L_U$ $L_G$ $L_A$ $M_D$ | $M_D$ | $M_D$ E | $M_P$ | $M_A$ | $M_S$ P Q | E | $M_O$ $M_D$ $M_P$ $M_S$ |
| | Chemofacies | K-means centroids | | $_{C}F1_{fun}$ | $_{C}F2_{fun}$ | $_{C}F3_{fun}$ | $_{C}F1_{cald}$ | $_{C}F2_{cald}$ | $_{C}F3_{cald}$ | $_{C}F4_{cald}$ | $_{C}F1_{cav}$ | $_{C}F2_{cav}$ | $_{C}F3_{cav}$ |
| | | Geochemical elements [Kcps] | Al | 2.09 | 0.58 | 0.55 | - | - | - | - | 1.23 | 0.40 | 0.27 |
| | | | Si | 46.24 | 29.49 | 40.52 | 20.08 | 18.15 | 16.08 | 16.49 | 23.25 | 17.28 | 18.36 |
| | | | S | 2.11 | 1.16 | 0.86 | 1.99 | 0.70 | 0.47 | 0.85 | - | - | - |
| | | | Cl | 5.76 | 4.74 | 6.06 | 2.77 | 2.30 | 2.42 | 2.30 | 2.49 | 1.80 | 1.93 |
| | | | K | 5.98 | 2.17 | 1.85 | 1.13 | 1.14 | 0.32 | 0.39 | 1.56 | 0.36 | 0.39 |
| | | | Ca | 32.87 | 18.80 | 13.98 | 12.94 | 8.20 | 5.18 | 4.13 | 12.38 | 4.99 | 3.62 |
| | | | Ti | 46.63 | 25.68 | 18.28 | 20.44 | 24.01 | 10.87 | 12.40 | 41.62 | 19.59 | 8.77 |
| | | | V | 2.63 | 1.88 | 1.48 | 1.12 | 1.46 | 0.73 | 0.96 | 2.02 | 1.52 | 1.09 |
| | | | Cr | 1.72 | 0.99 | 0.64 | 0.00 | - | - | - | - | - | - |
| | | | Mn | 2.96 | 2.32 | 2.38 | 1.33 | 1.25 | 0.91 | 0.85 | 1.47 | 1.18 | 0.96 |
| | | | Fe | 234.33 | 160.62 | 106.89 | 87.14 | 108.58 | 54.64 | 56.82 | 143.92 | 110.97 | 66.84 |
| | | | Br | - | - | - | 1.41 | 1.44 | 1.25 | 1.01 | 2.01 | 2.02 | 1.72 |
| | | | Rb | - | - | - | - | - | - | - | 0.16 | 0.19 | 0.17 |
| | | | Sr | 5.12 | 4.71 | 2.42 | 2.95 | 2.43 | 2.14 | 1.15 | 4.10 | 2.14 | 1.19 |
| | | | Zr | 5.61 | 4.69 | 2.84 | 3.35 | 4.57 | 2.69 | 2.79 | 10.06 | 8.05 | 2.50 |
| | | Biochemical proxies | Inc/ coh | 2.65 | 2.75 | 3.01 | 3.09 | 2.94 | 3.17 | 3.19 | - | - | - |
| | | | BSi | 2.83 | 1.93 | 6.23 | 2.68 | 1.10 | 3.61 | 1.69 | - | - | - |
| | | | TOC [%] | 7.27 | 14.54 | 7.93 | 28.83 | 17.93 | 31.23 | 25.63 | 21.20 | 18.96 | 29.01 |
| | | | TN [%] | 0.48 | 0.79 | 0.72 | 1.59 | 1.41 | 1.74 | 2.35 | 1.13 | 1.12 | 1.81 |
| | | | $\delta^{13}C$ [‰] | -26.29 | -26.50 | -26.45 | -27.17 | -25.98 | -27.06 | -21.82 | -27.12 | -26.21 | -27.80 |
| | | | $\delta^{15}N$ [‰] | 3.72 | 3.86 | 2.18 | 8.42 | 7.35 | 7.11 | 4.88 | 4.03 | 5.38 | 2.62 |

*Table 4.4: Facies of the selected sediment records, including the lithofacies and the chemofacies identified through sediment characterization and k-means clustering algorithm applied to the biogeochemical composition, which is specified using median values of the variables within each centroid, respectively. The table is arranged using the centroids identified with k-means clustering.*

## Organic matter sources

According to the chemofacies mean values of $\delta^{13}C$ and TOC/TN (Fig. 4.10), the organic matter origin of the FN1702 record exhibits a mainly lacustrine algae-derived origin within $_{C}F2_{fun}$, a predominantly C3 land plant-derived composition within $_{C}F3_{fun}$, and a mixed composition corresponding to $_{C}F1_{fun}$. In the CL1703 record, $_{C}F1_{cald}$ and $_{C}F3_{cald}$ show a C3 land plant-derived composition. $_{C}F4_{cald}$ is composed of lacustrine algae organic matter, whereas the $_{C}F2_{cald}$ has a combined origin of the organic matter, composed by algal and C3 land plats. In CVL1B record, the organic matter has a predominantly C3 land plant-derived origin for all the chemofacies.

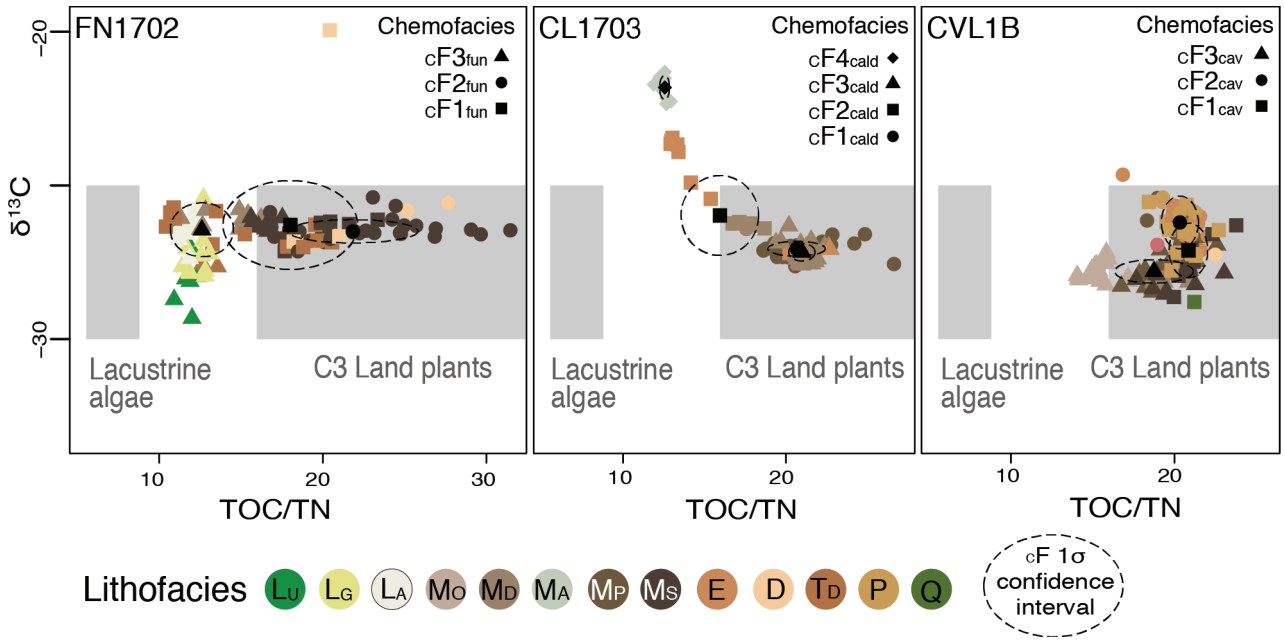


*Figure 4.10: Diagrams indicating the organic matter origin fields according to the δ13C and TOC/TN values (modified from Meyers and Teranes, 2003) for FN1702, CL1703 and CVL1B records. Lithofacies and chemofacies are indicated, as well as the median values and 1 σ confidence intervals of δ13C and TOC/TN for each chemofacies.*

## 4.4 Mineral composition and fluxes within the sediment records

The relative proportions of mineral species within FN1702 and CL1703 records demonstrate the dominance of feldspar over montmorillonite and augite, with hematite and quartz as minor components (Figs. 4.6 and 4.7 respectively). Conversely, the CVL1B record shows a broader range of mineral species, with a dominance of plagioclase, pyroxene, magnetite, and pyrite also containing smaller amounts of quartz, kaolinite, paligorskite, amphibole, and chlorite (Fig. 4.8).

The mineral signal of the FN1702 record is characterized by high relative concentrations of augite and feldspar at the lowermost section, showing an abrupt drop at ca. 400 cm depth. This drop corresponds to a relative rise in montmorillonite concentrations, reaching the highest values at the topmost section.

On the contrary, the mineral signal of the CL1703 record exhibits the opposite pattern to FN1702, showing low relative concentrations of augite and feldspar at the lowermost section, but an abrupt rise at ca. 150 cm depth at the expense of montmorillonite concentrations, which reach their lowest values at the topmost section.

Finally, the mineral signal of CVL1B displays an increasing trend of magnetite and pyroxene from the bottom of the record to ca. 415 cm depth, followed by a decrease from that depth to the top of the record. Pyrite and plagioclase reach the highest concentrations at the lowermost part of the record decreasing to the top, whereas chlorite, anfibol, paligorskite, and kaolinite present the opposite pattern. Quartz relative proportions are low along most of the record, displaying very high concentrations at the topmost section of the record (uppermost 100 cm depth).

## 4.5 Stratigraphy of the sediment records

### 4.5.1 Rhythmic microlithofacies

The microscopic analysis of thin sections from the FN1704G record provided stratigraphic information of the uppermost laminated sediments of Lake Funda (Fig. 4.11). From bottom to top, the succession of lithofacies composing the laminated pattern is as follows: 1) the light-brown

compact lamina of lithoacies $M_D$ composed of sapropel, which also appears loose including planktonic diatom remains to compose lithofacies $L_R$; 2) the yellowish multi-specific ooze of lithofacies $L_G$, which also appears as banded, composed of *Aulacoseira ambigua* (lithofacies $L_A$); and 3) the whitish ooze dominated by *Ulnaria Complex* of Lithofacies $L_U$ (Table 4.2). The stratigraphic patterns described by this succession form three rhythmic microlithofacies (rhythmites) as described below (Figs. 4.11):

- The rhythmic microlithofacies 1 ($_R$F1) shows a couplet of layers formed by the silty sapropel of Lithofacies $M_D$ and the banded ooze of *Aulacoseira ambigu*a (Lithofacies $L_A$). This succession presents sharp transitions between laminae. The concentration of vegetal terrestrial macro-remains in the light-brown layer is the highest of all the rhythmic mirolitofacies.
- The rhythmic microlithofacies 2 ($_R$F2) similarly to $_R$F1, includes a couplet of laminae but the transitions between the laminae are diffuse. The predominant diatom concentration is *Aulacoseira granulata var. angustissima*, which is concentrated in the Lithofacies $L_G$ pale layer. Whereas the dark lamina is constituted by Lithofacies $L_R$ layers, including the diatomitic concentrations of the pale layer, but diluted with organic matter.
- The rhythmic microlithofacies 3 ($_R$F3) adds the whiteish (greenish at macroscale; Fig. 4.4) lamina, dominated by diatom concentrations of *Ulnaria complex* (Lithofacies $L_U$), to the brown/yellow couple (lithofacies $L_R$/$L_G$). The whitish layer usually appears after the yellowish lamina, conforming a triplet ($_R$F3a), but sometimes it also appears after the light-brown, lacking the yellowish one ($_R$F3b).

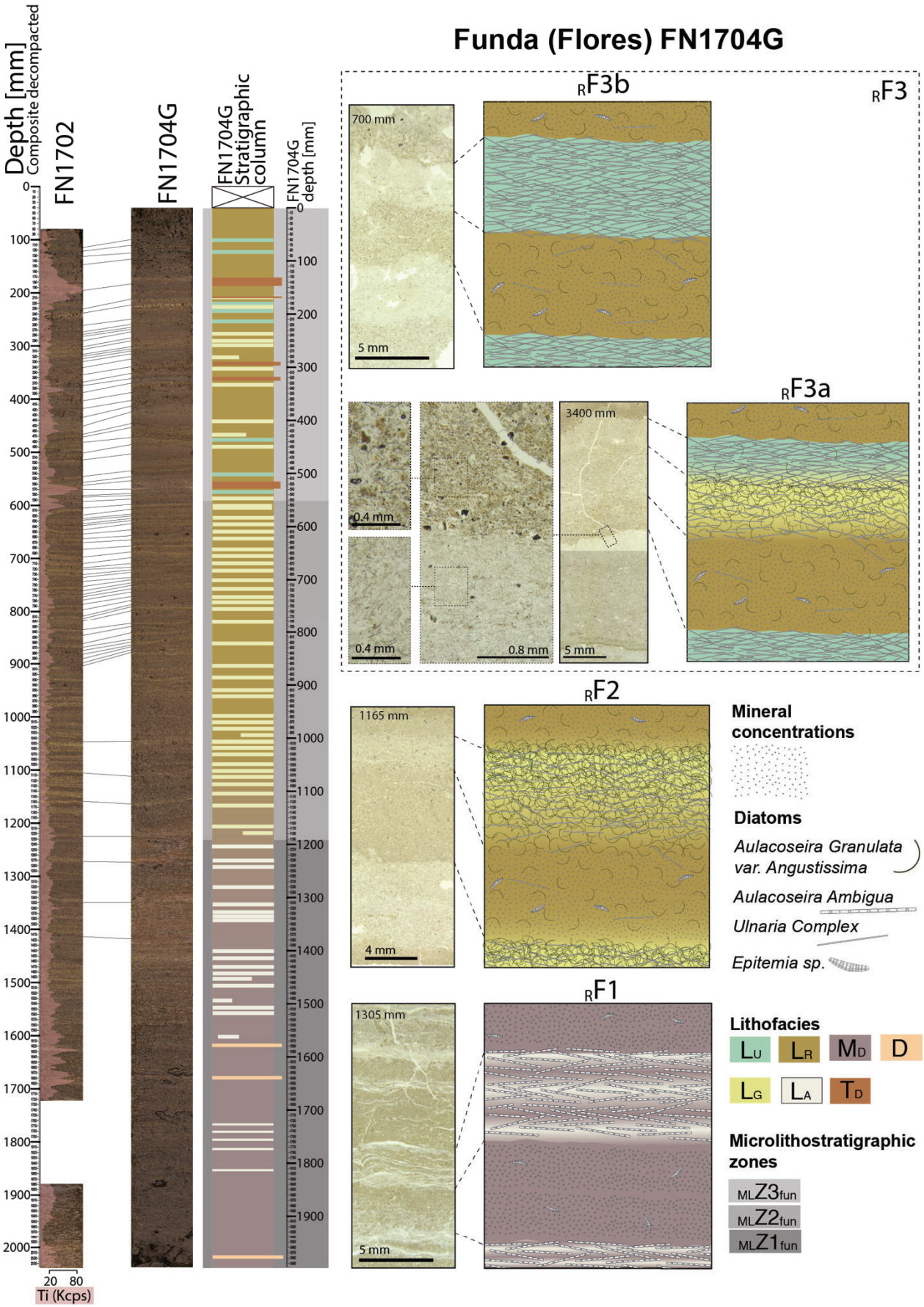


*Figure 4.11: Rhythmic microlithofacies of FN1704G record correlated with FN1702 record (Lake Funda sediments); RF1, RF2, RF3a and RF3b inferred from thin section analyses of FN1704G record and Microlithostratigraphic zones inferred from microscopic analyses are indicated. Ti flux within FN1702 record is indicated.*

### 4.5.2 Stratigraphic zones

Associations of lithofacies encompassing the rhythmic microfacies define microlithoestratigraphic zones ($_{ML}Z1_{fun}$, $_{ML}Z2_{fun}$ and $_{ML}Z3_{fun}$). Moreover, core sections composed of associations of lithofacies dominated by coarse lithic sediments, which are unable for geochemical characterization, constitute supplementary lithostratigraphic zones ($_{L}Z0_{fun}$ and $_{L}Z0_{cav}$). Lastly, the application of CONISS clustering algorithm to the available biogeochemical datasets grouped samples with stratigraphical proximity and biogeochemical affinity, conforming chemostratigraphic zones (chemozones), which are chemofacies associations. The CONISS algorithm applied to the biogeochemical datasets established two (k=3), five (k=6), and three (k=4) groups to conform the chemozones of FN1702 ($_{C}Z1_{fun}$ and $_{C}Z2_{fun}$), CL1703 ($_{C}Z1_{cald}$, $_{C}Z2_{cald}$, $_{C}Z3_{cald}$, $_{C}Z4_{cald}$ and $_{C}Z5_{cald}$) and CVL1B ($_{C}Z1_{cav}$, $_{C}Z2_{cav}$ and $_{C}Z3_{cav}$), respectively.

#### Funda lake sediments (FN1702 and FN1704G records)

Lithofacies $M_S$, punctually interbedded by Lithofacies $T_D$ (from 935 to 960 cm depth) and regularly by deposits of variable thickness (from cm to dm) and grain sizes (from fine sand to pebble) of lithofacies D constitute the $_{L}Z0_{fun}$ (Core bottom to 712 cm depth) (Fig. 4.6).

A chemofacies association composed by $_{C}F2_{fun}$, which is regularly interbedded by $_{C}F1_{fun}$ at the bottom of this unit (712 to 540 cm depth) and by decimetric proximal turbiditic deposits of lithofacies D between 460 to 500 cm depth, characterizes the $_{C}Z1_{fun}$ (712 to 325 cm depth).

The $_{C}F3_{fun}$, which is interbedded by $_{C}F1_{fun}$ at 20 cm, from 150 to 220 cm depth, and 275 cm depth, forms the $_{C}Z2_{fun}$ (325 cm depth to top). Punctually, the $_{C}Z2_{fun}$ includes a sample corresponding with $_{C}F2_{fun}$ at ca. 190 cm depth (Fig. 4.7). In turn, the $_{C}F3_{fun}$ is composed of the rhythmic lithofacies ($_{R}F1$, $_{R}F2$ and $_{R}F3$), forming association of lithofacies with the turbiditic deposits of lithofacies $T_D$ ($_{C}F1_{fun}$), allowing the distinction of three microlithostratigraphic zones (Fig. 4.11):

- The microlithostratigraphic zone 1 ($_{ML}Z1_{fun}$), composed of $_{R}F1$, frequently interbedded by Lithofacies $T_D$, showing relatively coarse and low-mature lithic particles (Fig. 4.3). This $_{ML}Z1_{fun}$ occurs from 119 to 200 cm of FN1704G core depth.
- The microlithostratigraphic zone 2 ($_{ML}Z2_{fun}$), composed of $_{R}F2$, was deposited between 55 and 119 cm depth. The $_{ML}Z2_{fun}$ is rarely interbedded by turbiditic deposits.
- The microlithostratigraphic zone 3 ($_{ML}Z3_{fun}$), composed of $_{R}F3$, is frequently interbedded by thick deposits of up to 3 amalgamated layers of lithofacies $T_D$. They present fine and mature lithic clasts, showing flame structures at the top (Fig. 4.3). The $_{ML}Z1_{fun}$ mostly appears in the uppermost 55 cm of the FN1704G record.

#### CL1703 record

The chemical composition of $_{C}Z1_{cald}$ (core bottom to 477 cm depth) and $_{C}Z2_{cald}$ (477 to 351 cm depth) are very similar, mainly composed of $_{C}F1_{cald}$ (Fig. 4.7). However, the uppermost section of $_{C}Z2_{cald}$ (from 390 to 351 cm depth) shows a transition from $_{C}F1_{cald}$ to $_{C}F3_{cald}$, corresponding with a punctual occurrence of $_{C}F2_{cald}$ at ca. 370 cm depth. The $_{C}Z3_{cald}$ (351 to 140 cm depth) is exclusively composed of sediments enriched in organic derivates of $_{C}F3_{cald}$, with the highest content of terrestrial plant remains at 150 to 190 cm depth. A succession of lithofacies $M_D$ (from ca. 140 to 93 cm depth) and E (from ca. 93 to 58 cm depth), dominated by the lithic enriched sediments of $_{C}F3_{cald}$, makes up the $_{C}Z4_{cald}$ (140 to 58 cm depth). The $_{C}Z5_{cald}$ (58 cm depth to core top) is exclusively composed of $_{C}F4_{cald}$.

#### CVL1B record

The lithofacies $M_S$, interbedded by a succession of centimetre to decimetre-thick deposits of lithofacies $V_W$, C and P, interrupted by a centimetre-thick deposit of Lithofacies $V_L$ at ca. 840 cm depth, forms $_{L}Z0_{cav}$ (930 to 800 cm depth) (Fig. 4.8). In its lower section (from 800 to 690 com depth),

an alternation of $_{C}F3_{cav}$ and $_{C}F1_{cav}$ makes up the $_{C}Z1_{cav}$ (800 to 650 cm depth). At its uppermost section (from 690 to 650 com depth) the boundary between the lithofacies $M_S$ (corresponding to $_{C}F3_{cav}$) and P (corresponding to $_{C}F1_{cav}$) blurs, replaced by Lithofacies $M_I$, forming a continuous sequence of $_{C}F1_{cav}$. Corresponding to this sequence, there also are layers of millimetre and centimetre-thick vegetal remains and lithofacies P presenting low-angle clinoforms (Fig. 3.2).

The $_{C}Z2_{cav}$ (from 650 to 190 cm depth) is composed of $_{C}F3_{cav}$ and regularly interbedded by $_{C}F2_{cav}$. The $_{C}Z2_{cav}$ is divided into two different sections according to the lithofacies:

- A basal section (from 650 to 540 cm depth), where the $_{C}F3_{cav}$ is composed of Lithofacies $M_D$, interbedded by millimetre-to-centimetre low-angle tilted layers of vegetal remains and lithofacies E and D ($_{C}F2_{cav}$). Furthermore, this section includes a centimetre-thick layer of volcanic coarse ash (Lithofacies $V_L$) at ca. 557 cm depth.
- A top section (from 550 to 190 cm depth), which includes an alternation of lithofacies $M_P$ and E corresponding to $_{C}F3_{cav}$ and $_{C}F1_{cav}$, respectively. There is also a thick, thinning-upwards deposit of the latter lithofacies (from 415 to 330 cm depth), with a thick level rich in large terrestrial plant remains (even trunks) at its base.

The $_{C}Z3_{cav}$ (190 to 40 cm depth) is exclusively composed of $_{C}F3_{cav}$ (lithofacies $M_O$).

## 4.6 Main components of biogeochemical and mineral variability

The RDA reveals relationships between the significative mineral species (environmental variables) and the identified chemofacies (response variables), allowing for the establishment of their geochemical sources (Fig. 4.12, 4.13 and 4.14). According to the 'envfit' function performed to the RDAs, the augite, hematite, montmorillonite, and quartz are the main minerals for FN1702 and CL1703 (including feldspar). However, the main minerals in CVL1B are the plagioclase, kaolinite, pyrite, pyroxene, magnetite, chlorite, palygorskite, and amorphous materials composed by variable proportions of opal from diatom remains, volcanic glass and organic matter.

### 4.6.1 FN1702 record

The RDA of the Lake Funda dataset ($RDA_{fun}$) shows that $_{C}F1_{fun}$ is associated with augite, $_{C}F2_{fun}$ is linked to hematite and quartz, and $_{C}F3_{fun}$ is related to montmorillonite (Fig. 4.12).

This $RDA_{fun}$ presents one significant eigenvector ($RDA1_{fun}$), explaining 83.6% of the total variance (Fig. 4.13), whereas the PCA of Lake Funda dataset ($PCA_{fun}$) presents two significant eigenvectors that explain 70.7% of the total variance (Fig. 4.14). The first eigenvector of $PCA_{fun}$ ($PC1_{fun}$) accounts for 52.5% of this variance, whereas the second eigenvector ($PC2_{fun}$) accounts for 18.2 % of the total variance (Fig. 4.12).

Samples belonging to $_{C}F1_{fun}$ and $_{C}F3_{fun}$ rule the $RDA1_{fun}$ and $PC1_{fun}$ at their positive and negative ends, respectively, and at the negative end of $PC2_{fun}$. Furthermore, $_{C}F2_{fun}$ lies at the positive end of $PC2_{fun}$, exhibiting no relationship with $PC1_{fun}$ (Fig. 4.12).

The trajectory analysis across the significant eigenvectors of $PCA_{fun}$ shows that the samples of $_{C}Z1_{fun}$ are dominantly located at the $PC1_{fun}$ and $PC2_{fun}$ positive quadrant, describing a trend that fits with a negative correlation line between both eigenvectors. However, from sample 103 to 58, there is no trend but a cloud of points at the positive end of $PC2_{fun.}$ The sample trajectory of $_{C}Z2_{fun}$ (from sample 57 to 1) imposes an additional trend over the one detected in $_{C}Z1_{fun.}$ It fits with a direct correlation line between $PC1_{fun}$ and $PC2_{fun}$, displacing the samples towards the $PC1_{fun}$ and $PC2_{fun}$ negative quadrant, except for samples 33 to 39 and 3, which follow the former trend, locating at the quadrant defined by the positive values of $PC1_{fun}$ and negative of $PC2_{fun}$ (Fig. 4.12).

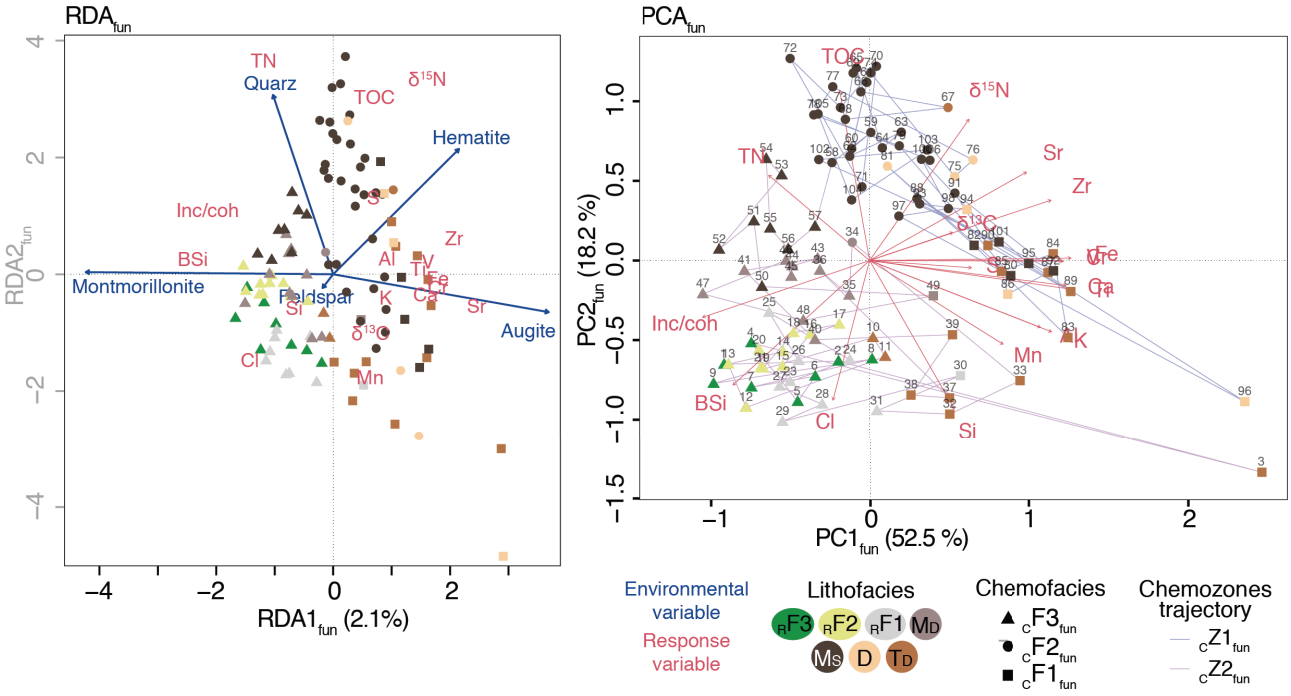


*Figure 4.12: RDA and PCA biplots showing the significant eigenvectors of the FN1702 record (RDA$_{fun}$ and PCA$_{fun}$, respectively), with samples differentiated by lithofacies and chemofacies. The biplots include the trajectory analysis of the chemostratigraphic zones. Shaded eigenvectors are not significant.*

### 4.6.2 CL1703 record

The RDA of Lake Caldeirão dataset (RDA$_{cald}$) shows $_{C}$F1$_{cald}$ and $_{C}$F2$_{cald}$ associated with augite and feldspar, with $_{C}$F1$_{cald}$ also related to montmorillonite. In contrast, $_{C}$F3$_{cald}$ and $_{C}$F4$_{cald}$ are associated with quartz and with montmorillonite and hematite, respectively (Fig. 4.13). The RDA$_{cald}$ presents one significant eigenvector (RDA1$_{cald}$), explaining 64.4% of the total variance (Fig. 4.13), whereas the PCA (PCA$_{cald}$) presents two significant eigenvectors that explain 75.4% of the total variance (Fig. 4.14). The first eigenvector of PCA$_{cald}$ (PC1$_{cald}$) accounts for 54.0% of this variance, whereas the PCA$_{cald}$ second eigenvector (PC2$_{cald}$) accounts for 19.5% of the total variance (Fig. 4.13).

The RDA1$_{cald}$ and PC2$_{cald}$ are ruled by the samples corresponding to $_{C}$F2$_{cald}$ and $_{C}$F4$_{cald}$ at their positive ends, whereas $_{C}$F1$_{cald}$ and $_{C}$F2$_{cald}$ lie at the negative one. The PC1$_{cald}$ is dominated at its positive end by $_{C}$F1$_{cald}$ and $_{C}$F3$_{cald}$, whereas $_{C}$F2$_{cald}$ and $_{C}$F4$_{cald}$ lie at the negative one (Fig. 4.13). Moreover, the trajectory analysis of $_{C}$Z1$_{cald}$ and $_{C}$Z2$_{cald}$ shows their samples occupying the right-down quadrant, whereas $_{C}$Z3$_{cald}$ samples lie on the PC1$_{cald}$ and PC2$_{cald}$ negative quadrant. Furthermore, $_{C}$Z4$_{cald}$ samples are located at the PC1$_{cald}$ and PC2$_{cald}$ positive quadrant, while $_{C}$Z5$_{cald}$ samples lie on the negative PC1$_{cald}$ and positive PC2$_{cald}$ quadrant. No trends are observed within the chemozones of CL1703. However, between $_{C}$Z1$_{cald}$, $_{C}$Z2$_{cald}$ and $_{C}$Z3$_{cald}$, the variability progresses steadily along PC1$_{cald}$, and transitions from $_{C}$Z3$_{cald}$ to $_{C}$Z4$_{cald}$ and from $_{C}$Z4$_{cald}$ to $_{C}$Z5$_{cald}$ show substantial displacements (Fig. 4.13).

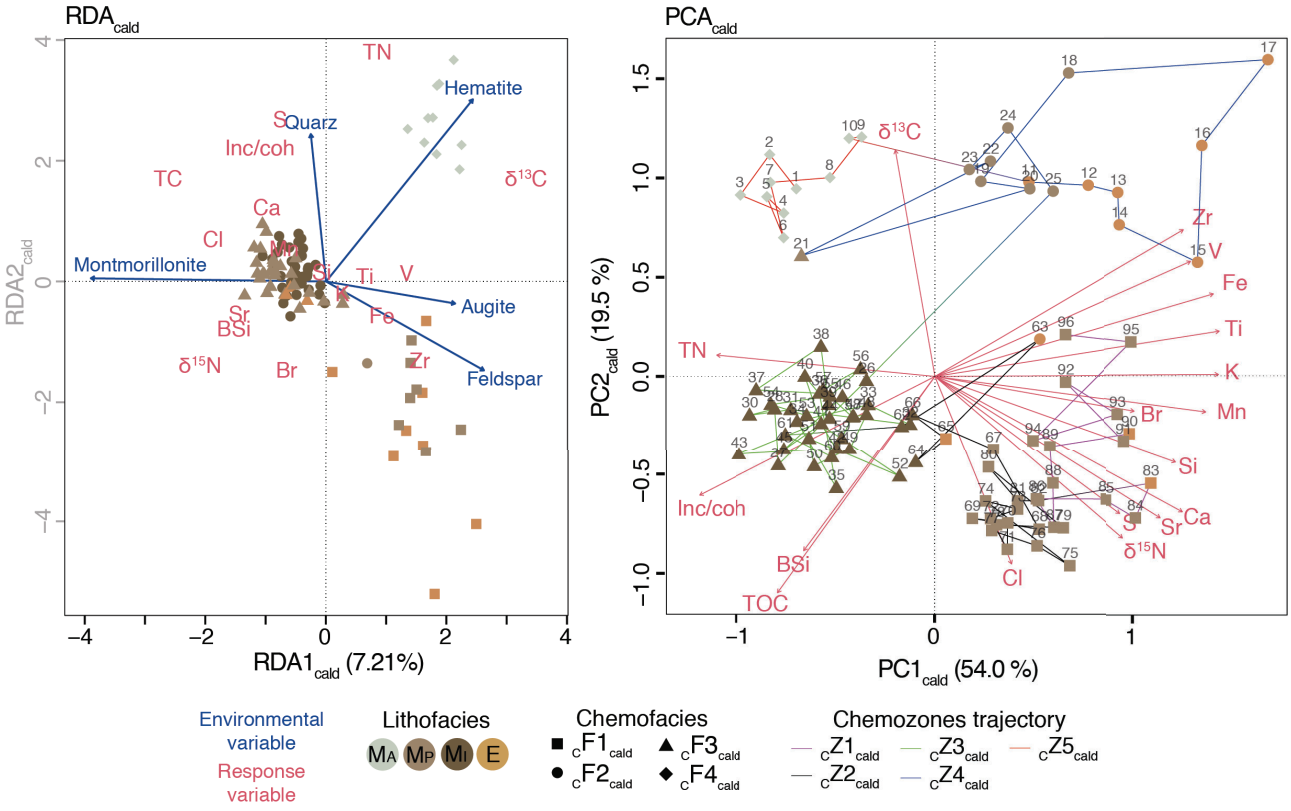


*Fig. 4.13: RDA and PCA biplots showing the significant eigenvectors of the CL1703 record ($RDA_{cald}$ and $PCA_{cald}$, respectively), with samples differentiated by lithofacies and chemofacies. The biplots include the trajectory analysis of the chemostratigraphic zones. Shaded eigenvectors are not significant.*

### 4.6.3 CVL1B record

The RDA of Lake Caveiro dataset ($RDA_{cav}$) shows $_{C}F1_{cav}$ associated with pyrite and plagioclase, $_{C}F2_{cav}$ with magnetite and pyroxene, and $_{C}F3_{cav}$ with amorphous material, kaolinite, chlorite, palygorskite, and quartz (Fig. 4.14).

The $RDA_{cav}$ presents three significant eigenvectors explaining 37.6% of the total variance (Fig. 4.13). The first eigenvector ($RDA1_{cav}$) accounts for 29.5% of this variance, whereas the $RDA_{cav}$ second eigenvector ($RDA2_{cav}$) accounts for 8%, and the $RDA_{cav}$ third eigenvector ($RDA3_{cav}$) for 3.4% of the total variance. The PCA of Lake Caveiro dataset ($PCA_{cav}$) presents two significant eigenvectors that explain 66.8% of the total variance (Fig. 4.14). The first eigenvector ($PC1_{cav}$) accounts for 48.9% of this variance, whereas the $PCA_{cav}$ second eigenvector ($PC2_{cav}$) accounts for 17.9% of the total variance (Fig. 4.14).

The $RDA1_{cav}$ and $PC1_{cav}$ are ruled by the samples corresponding with $_{C}F1_{cav}$ and $_{C}F2_{cav}$ at their positive ends, and the variables and samples belonging to $_{C}F3_{cav}$ at their negative sides. The $RDA2_{cav}$ and $PC2_{cav}$ are ruled by the samples corresponding to $_{C}F2_{cav}$ at their positive ends, whereas the negative ends are linked to samples corresponding to $_{C}F1_{cav}$. However, $_{C}F3_{cav}$ has low influence on $RDA2_{cav}$ and $PC2_{cav}$, except for the samples of lithofacies $M_S$ from $_{C}Z1_{cav}$, which weight the negative end of these axis. The $RDA3_{cav}$ is controlled by Br, TOC and TN, as well as quartz and pyrite, from lithofacies $M_O$ and P. At its negative end, it is ruled by Sr and Rb, as well as plagioclase and pyroxene, from lithofacies $V_L$ and D (Fig. 4.14).

The trajectory analysis of $RDA_{cav}$ on the plane containing $RDA1_{cav}$ and $RDA2_{cav}$ (Fig. 4.14) reveals that $_{C}Z1_{cav}$ is positioned in the quadrant defined by positive values of $RDA1_{cav}$ and negative values of $PC2_{cav}$ ($RDA2_{cav}$), apart from samples 126 to 124, which lie in the quadrant defined by negative values of both eigenvectors. $_{C}Z2_{cav}$ occupies the quadrant defined by positive values of $RDA1_{cav}$ and

RDA2$_{cav}$ when corresponding with $_{C}$F2$_{cav}$, whereas it evolves towards negative values of RDA1$_{cav}$ when corresponding with $_{C}$F3$_{cav}$. $_{C}$Z3$_{cav}$ exhibits variability along RDA2$_{cav}$ while remaining on the negative side of PC1$_{cav}$ (RDA1$_{cav}$). The trajectory analysis of PCA$_{cav}$ mirrors the variability of the plane containing the first two axes of RDA$_{cav}$ (RDA1$_{cav}$ and RDA2$_{cav}$).

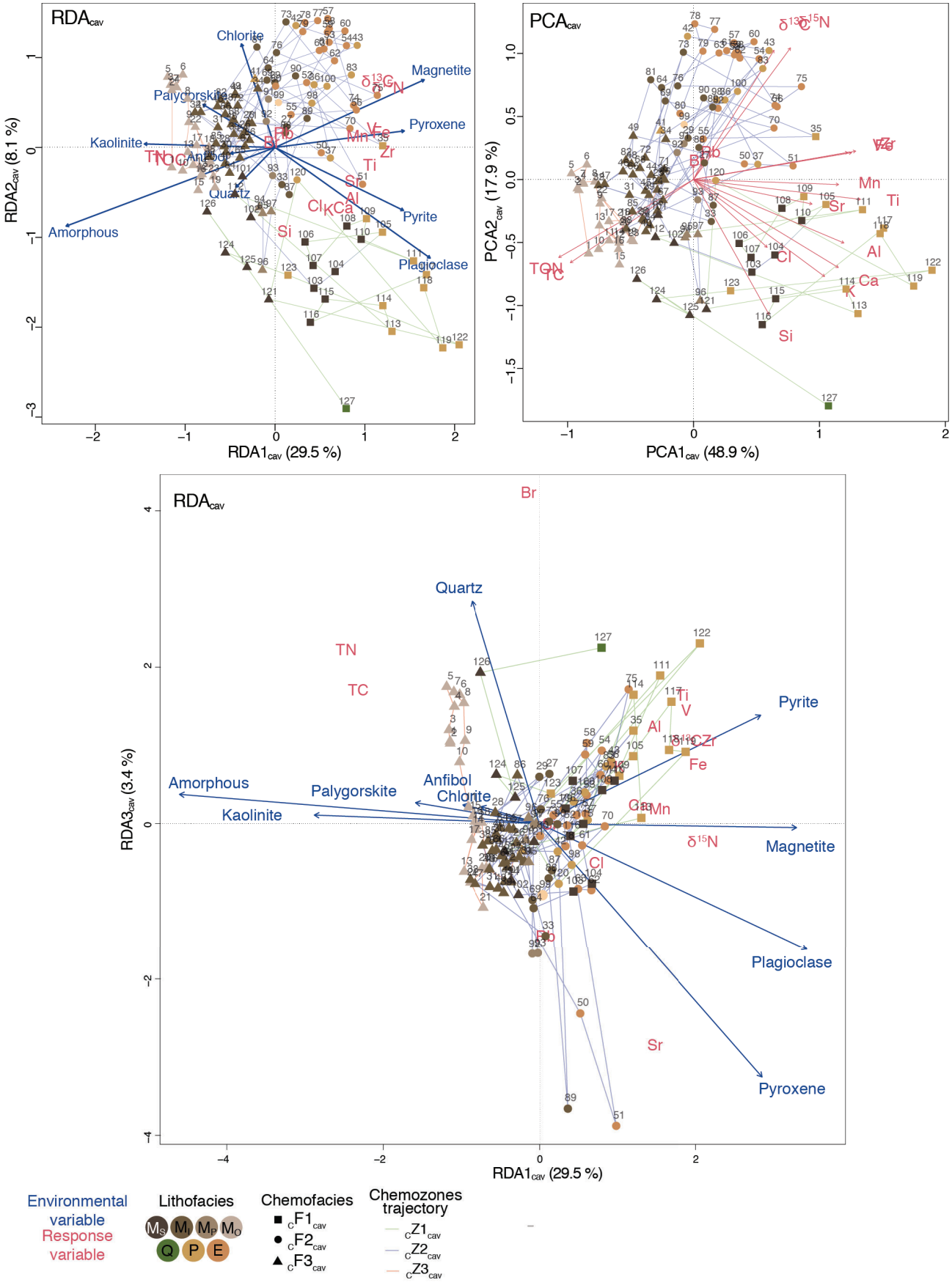

*Figure 4.14: RDA and PCA biplots showing the significant eigenvectors of the CVL1B record ($RDA_{fun}$ and $PCA_{fun}$, respectively), with samples differentiated by lithofacies and chemofacies. The biplots include the trajectory analysis of the chemostratigraphic zones.*

The trajectory analysis of $RDA_{cav}$ on the plane containing $RDA1_{cav}$ and $RDA3_{cav}$ (Fig. 4.14) reveals that ${}_{C}Z1_{cav}$ and ${}_{C}Z2_{cav}$ follow a positive correlation line between both eigenvectors, moving towards the quadrant defined by their positive values, especially corresponding to samples of facies P. Samples from ${}_{C}Z3_{cav}$, conversely, exhibit a trend from negative to positive values of $RDA3_{cav}$ at the negative side of $RDA1_{cav}$, whereas ${}_{C}Z2_{cav}$ has a low relationship with $RDA1_{cav}$ and $RDA3_{cav}$, apart from samples 89, 50, and 51, which strongly correlate with negative values of $RDA3_{cav}$.

## 4.7 Age-depth models of the sediment records

Since three of the ten measured AMS $^{14}C$ dates within FN1702 revealed reversal ages, the age-depth model for this record was constructed using the remaining six. The CVL1B record also revealed three AMS $^{14}C$ dates with reversal ages, therefore the Bayesian age-depth model was calculated with the remaining nine dates. Additionally, the model excluded three AMS $^{14}C$ dates: 1) the bottommost one and 2) the two topmost ones, selecting the $^{210}Pb$ dates instead, which revealed ca. 200 years younger ages. Conversely, for the age-depth model of CL1703 all the AMS $^{14}C$ dates were used since they exhibited stratigraphic coherence with no reversals (Table 4.5; Fig. 4.15).

| Lake | Sample ID | Université Laval # | $^{14}C$ age (yrs BP) | ± | cal. $^{14}C$ age (yrs BP) | 2 σ (cal. yr BP) |
|---|---|---|---|---|---|---|
| Funda | FN1702-01-52.8 | ULA- 774 | Modern | | 1955.6 | $^{+0.3}/_{-0.3}$ |
| | FN1702-01-154 | ULA- 5787 | 530 | 15 | 537 | $^{+10}/_{-10}$ |
| | FN1702-01-160 | ULA- 7747 | 1440 | 20 | 1330 | $^{+40}/_{-30}$ |
| | FN1702-02-34 | ULA- 7657 | 510 | 15 | 530 | $^{+10}/_{-10}$ |
| | FN1702-02-108 | ULA- 7745 | 550 | 20 | 550 | $^{+80}/_{-50}$ |
| | FN1702-03-67 | ULA- 7744 | 785 | 20 | 700 | $^{+30}/_{-20}$ |
| | FN1702-04-47 | ULA- 7738 | 1340 | 20 | 1280 | $^{+20}/_{-20}$ |
| | FN1702-04-135 | ULA- 7739 | 1100 | 20 | 1000 | $^{+60}/_{-40}$ |
| | FN1702-05-73 | ULA- 7737 | 1300 | 20 | 1250 | $^{+40}/_{-20}$ |
| | FN1702-06-71 | ULA- 7655 | 995 | 20 | 930 | $^{+30}/_{-30}$ |
| | | | | | | |
| Caldeirão | CL1703-01-78 | ULA-7752 | 350 | 20 | 390 | $^{+10}/_{-70}$ |
| | CL19-02G | ULA-8880 | 605 | 15 | 604 | $^{+40}/_{-20}$ |
| | CL1703-01-149 | ULA-8250 | 765 | 15 | 688 | $^{+20}/_{-20}$ |
| | CL1703-02-09 | ULA-8354 | 1045 | 15 | 950 | $^{+20}/_{-20}$ |
| | CL19-02G | ULA-8881 | 1115 | 15 | 1015 | $^{+45}/_{-40}$ |
| | CL1703-02-65 | ULA-7751 | 1225 | 20 | 1150 | $^{+30}/_{-80}$ |
| | CL1703-03-66 | ULA-8356 | 2295 | 20 | 2335 | $^{+15}/_{-25}$ |
| | CL1703-03-144 | ULA-8357 | 2905 | 15 | 3035 | $^{+40}/_{-70}$ |
| | CL1703-04-28 | ULA-7750 | 3540 | 20 | 3840 | $^{+50}/_{-20}$ |
| | | | | | | |
| Caveiro | CVL-1B-1-65-68 | ULA-5793 | 290 | 15 | 398 | $^{-22}/_{30}$ |
| | CVL-1B-1-132-133 | ULA-5713 | 420 | 20 | 497 | $^{-27}/_{17}$ |
| | CVL-1B-2-79-80 | ULA-5724 | 1055 | 20 | 955 | $^{-27}/_{28}$ |
| | CVL-1B-2-151-152 | ULA-6277 | 2040 | 15 | 1991 | $^{-46}/_{59}$ |
| | CVL-1B-3-63-64 | ULA-5715 | 1905 | 20 | 1853 | $^{-35}/_{41}$ |
| | CVL-1B-3-43-44 | ULA-5717 | 1995 | 20 | 1944 | $^{-48}/_{47}$ |
| | CVL-1B-3-103-104 | ULA-6278 | 1875 | 20 | 1828 | $^{-58}/_{46}$ |
| | CVL-1B-4-8-9 | ULA-5714 | 2870 | 20 | 2989 | $^{-63}/_{76}$ |
| | CVL-1B-4-82-83 | ULA-6290 | 3750 | 20 | 4117 | $^{-40}/_{39}$ |
| | CVL-1B-5-13-14 | ULA-5722 | 4380 | 25 | 4931 | $^{-68}/_{107}$ |
| | CVL-1B-5-53-54 | ULA-6289 | 4585 | 20 | 5310 | $^{-23}/_{12}$ |
| | CVL-1B-6-7-8 | ULA-5723 | 7380 | 25 | 8201 | $^{-39}/_{114}$ |

*Table 4.5: Radiocarbon dates of the sediment records.*

Funda lake sediments provide a record of the environmental history of Flores Island for the last 1200 years derived from the radiometric chronology of FN1702 record (Table 4.5; Fig. 4.15) and of 270 years from the varve chronology of FN1704G (Fig. 4.16). The CL1703 sediments cover the last 3700

years (Table 4.5; Fig. 4.15), whereas CVL1B sediments span the last 5200 years (Table 4.5; Fig. 4.15). The sedimentation rates derived from the FN1702 record indicate a first stage (from ca. 1000 to 525 yr cal BP) of rapid sedimentation of ca. 10 mm yr-1, with instantaneous deposits, followed by a later stage (from ca. 525 yr cal BP to the present) with lower sedimentation rates of ca. 5 mm yr-1 (Fig. 4.15), which are also found in the varve chronology of FN1704G during the period between 1860 and 1966 CE (Fig. 4.16). The FN1704G record also shows relatively higher sedimentation rates of 10.7 mm yr-1 corresponding with the first period, up to 1859 CE, and the last period, from 1967 CE onwards to the present. In contrast, the sedimentation rates obtained from CL1703 remain relatively constant, ranging from 0.35 to 1.38 mm yr-1 (Fig. 4.15). Lastly, the sedimentation rates of CVL1B demonstrates a first period (from ca. 5200 to 1000 cal yr BP) of relatively lower sedimentation rates of ca. 1.19 mm yr-1 and a second period (from ca. 1000 cal yr BP to the present) of relatively higher sedimentation rates of ca. 2.73 mm yr-1 (Fig. 4.15).

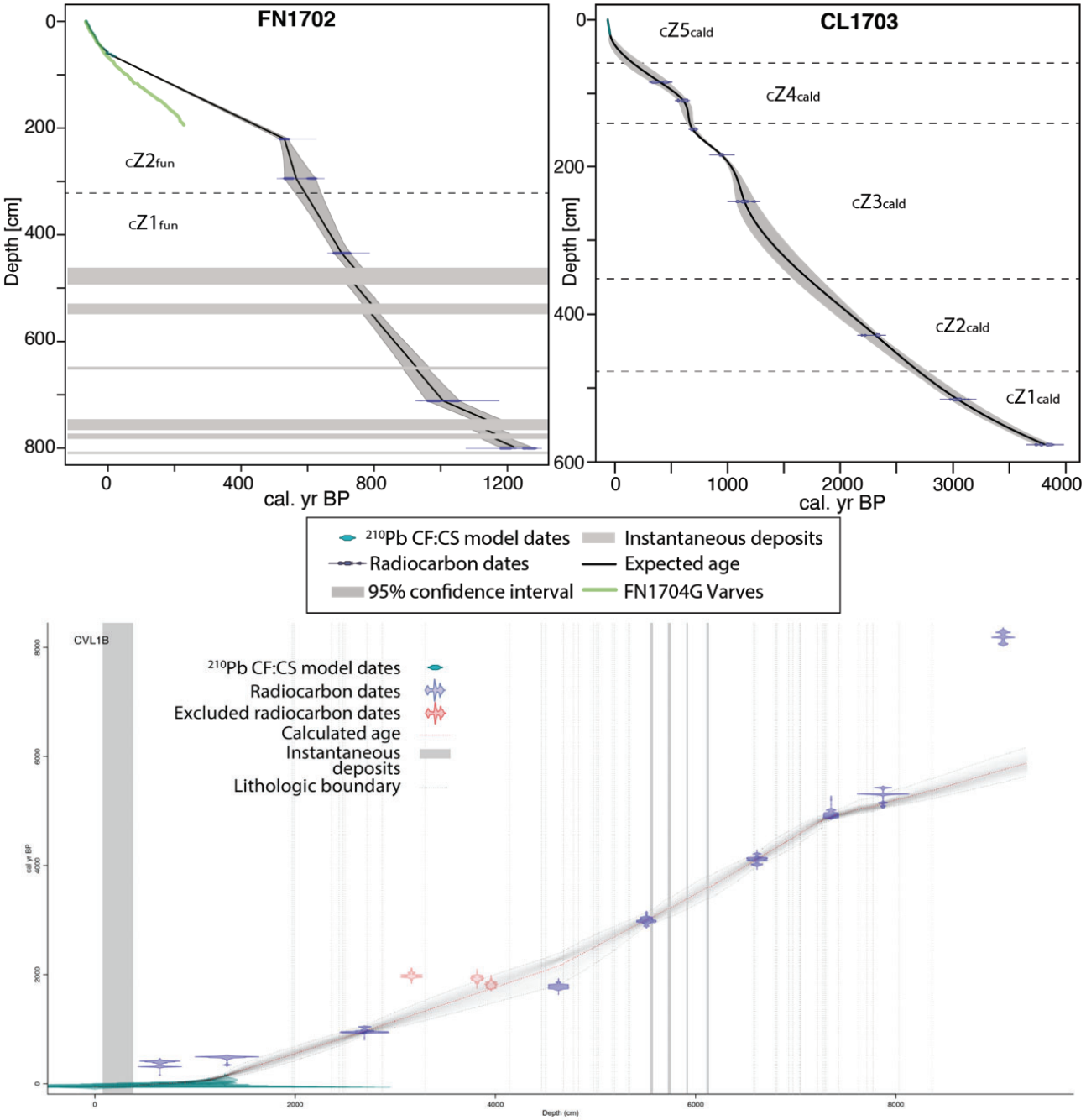


*Fig. 4.15: Radiometric age-depth models: up-left side FN1702 record, compared with the varve chronology obtained from FN1704G record and right up-side CL1703 record. The stratigraphic zones are indicated. Downside shows the Bayesian age-depth model performed on CVL1B record.*

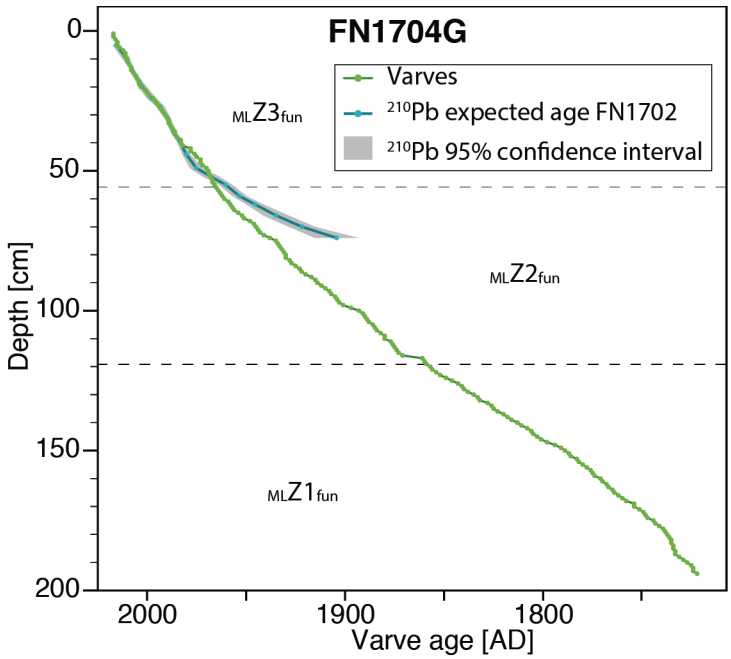


*Fig. 4.16: Varve-based age-depth model from FN1704G record. $^{210}$Pb dates from FN1704G are indicated.*

## 4.8 High resolution proxy-based records

The correlation between the main components of biogeochemical and mineral variability at a 50 mm resolution with the main components obtained from the PCA analysis conducted on the geochemical datasets at a 2 mm has enabled the identification of the main components of variability of FN1702 (Table 4.6), CL1703 (Table 4.7), and CVL1B (Table 4.8) for subsequent high-resolution analyses (Fig. 4.18). As expected, the $PC1_{fun}$ obtained from the 2 mm dataset captures the variability of $PC1_{fun}$ and $RDA1_{fun}$ from the 50 mm dataset, while $PC2_{fun}$ derived from the 2 mm delineates the variability of $PC2_{fun}$ of 50 mm one. The same occurs for $PC1_{cald}$ (2 mm) with $PC1_{cald}$ (50 mm), $PC2_{cald}$ (2 mm) with $PC2_{cald}$ and $RDA1_{cald}$ (50 mm), and $PC1_{cav}$ (2 mm) with $PC1_{cav}$ and $RDA1_{cav}$ (50 mm). However, it is noteworthy that $PC2_{cav}$ and $RDA2_{cav}$ (50 mm) become the third eigenvector $PC3_{cav}$ (2 mm) when mineral and biological data (50 mm??) are not considered. Conversely, $RDA3_{cav}$ (50 mm) is significant and agrees with $PC2_{cav}$ (2 mm) variability.

| n=103 | | 50 mm | | | 2 mm | |
|---|---|---|---|---|---|---|
| | | PC1 | PC2 | RDA1 | PC1 | PC2 |
| 50 mm | PC1 | 1.00 | | | | |
| | PC2 | **-0.26**** | 1.00 | | | |
| | RDA1 | **0.79***** | 0.06 | 1.00 | | |
| 2 mm | PC1 | **0.82***** | -0.15 | **0.74***** | 1.00 | |
| | PC2 | -0.06 | **-0.47**** | **-0.29**** | 0.06 | 1.00 |

*Table 4.6: Pearson correlation coefficients between the significant eigenvectors of FN1702 record at a 50 mm resolution and the eigenvectors of FN1702 PCA at a 2 mm resolution. Bold indicates p values below 0.05. *** values with a significance of p<0.001 and ** with a significance of p<0.01.*

| n=95 | | 50 mm | | | 2 mm | |
|---|---|---|---|---|---|---|
| | | PC1 | PC2 | RDA1 | PC1 | PC2 |
| 50 mm | PC1 | 1.00 | | | | |
| | PC2 | 0.00 | 1.00 | | | |
| | RDA1 | 0.00 | **0.98***** | 1.00 | | |
| 2 mm | PC1 | **0.93***** | -0.04 | -0.02 | 1.00 | |
| | PC2 | 0.03 | **-0.85***** | **-0.77***** | 0.07 | 1.00 |

*Table 4.7: Pearson correlation coefficients between the significant eigenvectors of CL1703 record at a 50 mm resolution and the eigenvectors of CL1703 PCA at a 2 mm resolution. Bold indicates p values below 0.05. *** values with a significance of p<0.001 and ** with a significance of p<0.01.*

| n=127 | | 50 mm | | | | | 2 mm | | |
|---|---|---|---|---|---|---|---|---|---|
| | | PC1 | PC2 | RDA1 | RDA2 | RDA3 | PC1 | PC2 | PC3 |
| 50 mm | PC1 | 1.00 | | | | | | | |
| | PC2 | 0.00 | 1.00 | | | | | | |
| | RDA1 | **0.98*** ** | 0.19* | 1.00 | | | | | |
| | RDA2 | -0.43 | **0.89*** ** | **-0.26** ** | 1.00 | | | | |
| | RDA3 | 0.21* | -0.13 | 0.16· | -0.14 | 1.00 | | | |
| 2 mm | PC1 | **0.93*** ** | -0.16· | **0.88*** ** | **-0.55*** ** | 0.20* | 1.00 | | |
| | PC2 | -0.09 | 0.08 | -0.07 | 0.10 | **-0.77*** ** | -0.10 | 1.00 | |
| | PC3 | -0.11 | **-0.73*** ** | **-0.23** ** | **-0.66*** ** | -0.19* | 0.01 | 0.01 | 1.00 |

*Table 4.8: Pearson correlation coefficients between the significant eigenvectors of CVL1B record at a 50 mm resolution and the eigenvectors of CL1B PCA at a 2 mm resolution. Bold indicates p values below 0.05. *** values with a significance of p<0.001 and ** with a significance of p<0.01*

The selected eigenvectors of $PCA_{fun}$, $PCA_{cald}$, $PCA_{cav}$ (at 2 mm resolution hereon), combined with their respective radiometric chronologies, have allowed the reconstruction of the environmental changes for 1) the Funda lake-catchment system ($PC1_{fun}$ and $PC2_{fun}$), 2) the Caldeirão system ($PC1_{cald}$ and $PC2_{cald}$), and 3) the Caveiro system ($PC1_{cav}$, $PC2_{cav}$ and $PC3_{cav}$), spanning the past 1000, 3800, and 5200 years, respectively (Fig. 4.17). Additionally, lamina and rhythmite thickness measurements, when combined with the chronology obtained through varve counting in the FN1704G, have allowed the annual reconstruction for the last 250 years for the Funda system (Fig. 4.17).

The application of the CONISS clustering algorithm to the obtained PCs identifies groups of samples responding to the environmental drivers of processes controlling sediment deposition within the lake systems of Funda, Caldeirão and Caveiro (Fig. 4.17). According to the CONISS algorithm analysis, the optimal number of groups to conform the environmental stages through time is: two groups for the Funda lake basin ($S1_{fun}$ and $S2_{fun}$); five groups for the Lake Caldeirão basin ($S1_{cald}$, $S2_{cald}$, $S3_{cald}$, $S4_{cald}$ and $S5_{cald}$); and three groups for the Caveiro lake basin ($S1_{cav}$, $S2_{cav}$ and $S3_{cav}$). Furthermore, CONISS applied to the rhythmic microlithofacies thicknesses from FN1704G record allowed the identification of three environmental substages for the Funda lake basin within $S2_{fun}$ ($S2a_{fun}$, $S2b_{fun}$ and $S2c_{fun}$).

### 4.8.1 Funda system

#### Biogeochemical changes (FN1702 record)

$S1_{fun}$ (1000 - 650 cal. yr BP) shows a first period (from 1000 to 800 cal. yr BP) of moderate to high increasing values of $PC1_{fun}$ and $PC2_{fun}$, dropping to moderate for $PC1_{fun}$ and reaching the lowest values of the entire record for $PC2_{fun}$ in the second period (from 800 to 650 cal. yr BP). During $S1_{fun}$, the Rate of Change (RoC) shows an oscillating trend with a noisy pattern, regularly exceeding the median threshold.

$S2_{fun}$ (650 cal yr BP – present) shows: 1) a first period (from 650 to 250 cal. yr BP) of increased values for both $PC1_{fun}$ and $PC2_{fun}$, 2) a second period (from 250 to 0 cal. yr BP) with decreased values for $PC1_{fun}$, whereas remaining stationary for $PC2_{fun}$, and 3) a third period (from 0 cal. yr BP to present) exhibiting peak values of $PC1_{fun}$ and a sharp drop for $PC2_{fun}$. The RoC analysis in $S2_{fun}$ shows very low and smooth values, interrupted by a peaky pattern centred at 550 cal yr. BP, 250 cal yr. BP, and the present. The RoC peak at 550 cal yr BP represents a prominent peak point with considerable amplitude, spanning from ca. 500 to 600 cal yr. BP, whereas the peaks found at 250 cal. yr. BP and the present span a few tens of years.

#### Rhythmic microlithofacies thicknesses (FN1704G record)

Within $S2_{fun}$, $S2a_{fun}$ (195 - 180 cal. yr BP) contains thick rhythmites (up to 20 mm) and laminae, both Lithofacies $M_D$ (ca.10 mm) and L (ca. 10 mm), corresponding to the end of the $S2_{fun}$ first period.

$S2b_{fun}$ (180 - 50 cal. yr BP) includes thin rhythmites (from ca. 5 to 10 mm) and laminae, for both Lithofacies $M_D$ (ca. 5 mm) and L (from ca. 2 to 5 mm), corresponding to the second period of $S2_{fun}$. $S2c_{fun}$ covers the last ca. 100 years, corresponding to the third period of $S2_{fun}$, presenting medium-to-thick rhythmites (from ca. 5 to 15 mm) and lithofacies $M_D$ laminae (up to ca. 10 mm), whereas Lithofacies L laminae are thinner (ca. 3 mm).

Furthermore, the turbiditic deposits of Lithofacies $T_D$ show the highest frequencies corresponding to $S2a_{fun}$ and $S2c_{fun}$, especially thick deposit (up to 20 mm) composed of up to 3 amalgamated layers coalescing at the latest period of $S2b_{fun}$ (ca. 1970 CE) and $S2c_{fun}$ (ca. 2006 CE).

### 4.8.2 Caldeirão system (CL1703 record)

$S1_{cald}$ (3800 - 2700 cal yr. BP) shows consistently high scores for $PC1_{cald}$, interrupted by peaky patterns at 3700, 3100 and 2750 cal yr BP, whereas $PC2_{cald}$ displays an increasing trend with low-amplitude oscillations.

$S2_{cald}$, (2700 - 2075 cal yr BP) presents a constant decreasing trend for $PC1_{cald}$ scores, while maintaining constant high values for $PC2_{cald}$. The RoC during $S1_{cald}$ and $S2_{cald}$ is negligible.

$S3_{cald}$ (2075 - 675 cal yr BP) shows low scores of $PC1_{cald}$ following a wavering pattern, with the peaky pattern found at $S1_{cald}$ reappearing in the first period (2000 cal yr BP). Similarly, $PC2_{cald}$ displays a wavering pattern oscillating around circumneutral scores. Despite presenting negligible scores along most of the stage, the RoC from $S3_{cald}$ presents higher scores from ca. 950 to 1050 cal yr BP and a prominent peak point, with amplitude of around 100 years, in the transition to $S4_{cald}$ at 675 cal yr BP.

$S4_{cald}$ (675 -250 cal yr BP) is characterized by a first period with an increasing trend for $PC1_{cald,}$ followed by a decreasing trend to circumneutral scores after 550 BP, whereas $PC2_{fun}$ presents the opposite pattern. The RoC scores remain low after the transitional peak from $S3_{cald}$. However, there is a slight score increase at the end of this stage in transition with $S5_{cald}$ at 250 cal yr BP.

Lastly, $S5_{cald}$ (250 cal yr BP - present) exhibits low scores for $PC1_{cald}$ with a first period of decrease (from 250 to 200 cal. yr BP) and a second period of increase after 1950 CE. $PC2_{cald}$, conversely, presents a stable pattern with circumneutral scores. The RoC replicates the pattern of $S4_{cald}$, showing a peak point at the present.

### 4.8.3 Caveiro system (CVL1B record)

$S1_{cav}$ (5200 - 3950 cal yr BP) is characterized by high scores for $PC1_{cav}$ and $PC3_{cav,}$ showing opposite oscillations in the first period (from 5200 to 4300 cal. yr BP), with considerable high amplitude in $PC1_{fun}$. The $PC2_{cav}$ displays low values and replicates the oscillating pattern of $PC3_{cav}$. The RoC scores present peak points corresponding to the highest amplitude oscillations at ca. 5200 and 5000 cal yr BP, whereas during the rest of the stage, they remain low.

$S2_{cav}$ (3950 - 1875 cal yr BP) displays decreasing trends with low and high amplitude wavering patterns for $PC1_{cav}$ and $PC3_{cav}$, respectively. $PC2_{cav}$ remains stationary, but it is interrupted by a prominent peaky pattern for the period between 3600 to 3000 cal yr BP. The RoC shows a first period of values hardly rising above the median threshold (from 3950 to 2800 cal. yr BP), but it also shows a second period of values regularly exceeding the median treshold (from 2800 to 1875 cal. yr BP).

$S3_{cav}$ (1875 - 1375 cal yr BP) is characterized by high values of $PC1_{cav}$, while low for $PC2_{cav}$ and $PC3_{cav,}$ with low RoC values.

The $S4_{cav}$ (1375 - 20 cal yr BP) displays a decreasing trend for $PC1_{cav}$ and $PC2_{cav}$, whereas increasing for $PC3_{cav}$. Furthermore, $PC1_{cav}$ shows a peaky pattern (from 1000 to 700 cal. yr BP), which is oppositely replicated by $PC2_{cav}$ and $PC3_{cav.}$ The RoC presents high values during the described peaky pattern, showing peak points corresponding to the highest amplitudes.

$S5_{cav}$ (20 cal yr BP - present) is characterized by low values in all the three PCs ($PC1_{cav}$, $PC2_{cav}$ and $PC3_{cav}$) corresponding to peak points of RoC at the beginning of the stage and at the present.

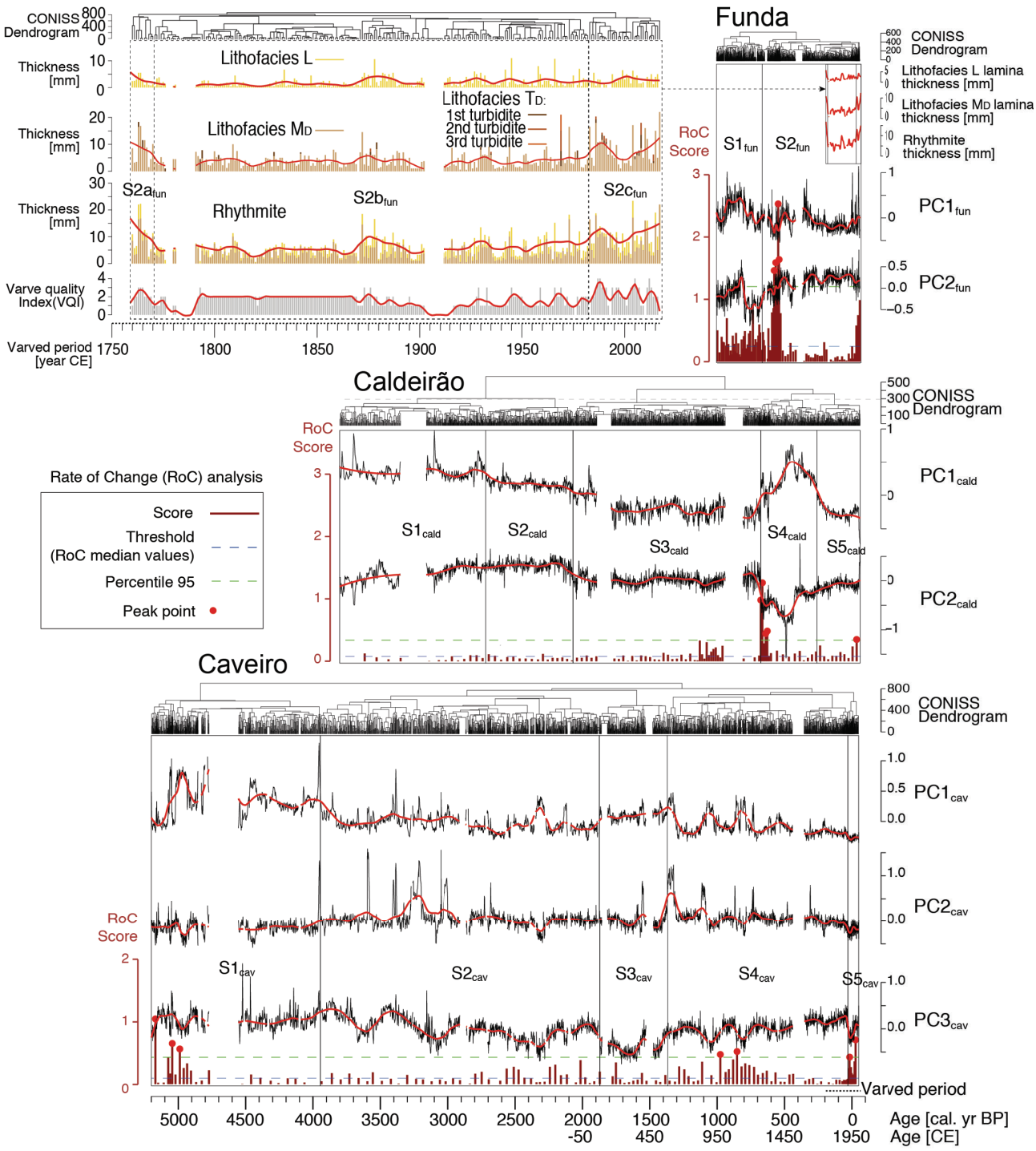


*Fig. 4.17: PCs values from the studied proxy-based records, FN1702 (Funda), CL1703 (Caldeirão) and CVL1B (Caveiro). The ordination analyses were applied to the 2 mm resolution XRF datasets and to the laminae and rhythmite thicknesses measurements performed on FN1704G record (Funda), using the available radiometric and varve chronologies. The paleoenvironmental stages revealed by CONISS and the Rate of Change (RoC) analyses for each dataset are indicated. VQI: Varve Quality Index. Red wiggles represent smoothen signals at 0.1 span value.*

### 4.8.4 Correlation with observational records

Time series correlation analysis performed between the precipitation and temperature observed in the study area and the main drivers of biogeochemical variability within Funda and Caldeirão

systems and laminae and rhythmite thicknesses show high significant effects between them. Pearson correlation coefficients (ρ) between significant PCAs eigenvectors and instrumental meteorological variables of the WG show that $PC1_{fun}$ is influenced by the WG wet season (ONDJFM) precipitation (ρ = 0.35, p-value = 0.05) two years after, whereas summer (JJA) temperatures influence (ρ = -0.31 p-value = 0.1) the $PC2_{fun}$ 3 years after, which in turn also exerts high significant effect over $PC1_{fun}$ (Table 4.10). Furthermore, summer air temperatures show strong significative effects over the thicknesses of the dark (ρ = 0.43, p-value = 0.05) and pale (ρ = 0.45, p-value = 0.01) laminae and over the complete rhythmites (ρ = 0.56, p-value = 0.001) 6 years after. In turn rhythmites show significant maximum effect over the dark (ρ = 0.93, p-value = 0.001) lamina and high over the pale one (ρ = 0.45, p-value = 0.01) laminae. In turn, $PC1_{cald}$ is positively correlated (ρ = 0.51, p-value =0.01) with the WG wet season precipitation 5 years later, whereas the summer temperatures are positively correlated (ρ = 0.40, p-value = 0.05) to $PC2_{cald}$ after 6 years (Table 4.10).

| *Lag period $PC1_{fun}$ = 2 years*<br>*Lag period $PC2_{fun}$ = 3 years* | *WG Precipitation (ONDJFM)* | *WG Air temperature (JJA)* | *$PC1_{fun}$* | *$PC2_{fun}$* |
|---|---|---|---|---|
| *WG Precipitation (ONDJFM)* | *1* | | | |
| *WG Air temperature (JJA)* | *0.058* | *1* | | |
| *$PC1_{fun}$* | ***0.35**** | *0.014* | *1* | |
| *$PC2_{fun}$* | *0.12* | ***-0.31·*** | ***0.46**** | *1* |

*Table 4.8: Pearson's correlation matrix: main drivers of biogeochemical variability of Funda system ($PCA_{fun}$) vs. WG climate variables. Significance codes: 0 '***' 0.001 '**' 0.01 '*' 0.05 '.' 0.1 ' ' 1. Lag period from auto-correlation function is indicated.*

| Lag period dark lamina = 6 years<br>Lag period pale lamina = 6 years<br>Lag period rhythmite = 6 years | WG Precipitation (ONDJFM) | WG Air temperature (JJA) | Dark lamina (Litofacies $M_D/L_R$) | Pale lamina (Litofacies LU/LG/LA) | Rhythmite (Dark lamina + Pale lamina) |
|---|---|---|---|---|---|
| WG Precipitation (ONDJFM) | 1 | | | | |
| WG Air temperature (JJA) | -0.059 | 1 | | | |
| Dark lamina (Litofacies $M_D/L_R$) | 0,07 | **0.43*** | 1 | | |
| Pale lamina (Litofacies $L_U/L_G/L_A$) | -0.20 | **0.45**** | 0.029 | 1 | |
| Rhythmite (Dark lamina + Pale lamina) | -0.027 | **0.56***** | **0.93***** | **0.40*** | 1 |

*Table 4.9: Pearson's correlation matrix: Lake Funda sediments laminae and rhythmite thicknesses vs. WG climate variables. Significance codes: 0 '***' 0.001 '**' 0.01 '*' 0.05 '.' 0.1 ' ' 1. Lag period from auto-correlation function is indicated.*

| Lag period $PC1_{cald}$ = 5 years<br>Lag period $PC2_{cald}$ = 6 years | WG Precipitation (ONDJFM) | WG Air temperature (JJA) | $PC1_{cald}$ | $PC2_{cald}$ |
|---|---|---|---|---|
| WG Precipitation (ONDJFM) | 1 | | | |
| WG Air temperature (JJA) | -0.12 | 1 | | |
| $PC1_{cald}$ | **0.51**** | -0.09 | 1 | |
| $PC2_{cald}$ | -0.14 | **0.39*** | -0.11 | 1 |

*Table 4.10: Pearson's correlation matrix: main drivers of biogeochemical variability of Caldeirão system ($PCA_{cald}$) vs. WG climate variables. Significance codes: 0 '***' 0.001 '**' 0.01 '*' 0.05 '.' 0.1 ' ' . Lag period from auto-correlation function is indicated.*

In turn, Pearson correlation coefficients (ρ) between the NAOi and EAi and the monthly average instrumental meteorological dataset of the WG (Table 4.11) reveal the influence of NAO and EA on precipitation and temperature. The NAO has a significant impact (ρ = -0.40, p-value = 0.01) on the humid season (ONDJFM) precipitation, whereas the EA influences the summer (JJA) air temperature (ρ = 0.55, p-value = 0.01).

| | WG Precipitation (ONDJFM) | WG Temperature (ONDJFM) | NAOi | EAi |
|---|---|---|---|---|
| WG Precipitation (ONDJFM) | 1 | | | |
| WG Temperature (JJA) | -0.19 | 1 | | |

| | | | | |
|---|---|---|---|---|
| NAOi | **-0.40*** ** | 0.018 | 1 | |
| EAi | 0.012 | **-0.55*** ** | 0.12 | 1 |

*Table 4.11: Pearson correlation matrix: WG climate variables vs. indexes of the North Atlantic atmospheric modes of circulation. Significance codes: 0 '***' 0.001 '**' 0.01 '*' 0.05 '.' 0.1 ' ' .*

# 5. Discussion: The sedimentary dynamics from source to sink and derived geomorphic imprints within the lake-catchment systems of Funda, Caldeirão, and Caveiro.

The sedimentologic and geomorphic evidence observed has enabled the inference of the sedimentary distribution and dynamics within Funda, Caldeirão and Caveiro lake-catchment systems. The main drivers of lacustrine sedimentation have been established determining the origins (Table 5.1) and processes involved (Table 5.2) in the facies deposition, alongside the provenances and delivery routes inferred from lake water volumes and erosive landforms.

## 5.1 Sedimentary origins and provenances

The composition of the lithofacies within FN1702, CL1703, and CVL1B records (Tables 4.2, 4.3 and 4.4) provides insights into the genesis of the sediments (Table 5.1) (Schnurrenberger et al., 2003). By correlating genetic associations of lithofacies with biogeochemical K-means clustering (Fig. 4.9), it was able to identify the sediment origin (Table 5.1). The origin has been inferred from genetic interpretations of sedimentary components from the lithofacies and the biogeochemical and mineral relationships established within ordination analyses (Figs. 4.12, 4.13 and 4.14). Moreover, the biochemical characterization of chemofacies has supported the biogenic genesis of the facies (Fig. 4.10) (Meyers, 1994). Allogenic, endogenic, and pedogenic origins have been inferred, and secondary contributions from external sources have also been detected. Besides, the domains of erodibility identified with Ksn analysis allowed the determination of the most plausible provenances of allogenic materials (Burt and Allison, 2010), whereas lake water volumes served to infer the provenances for endogenic ones.

| Record | Facies (F) (Fig. 4.9) | | | | | | |
|---|---|---|---|---|---|---|---|
| | Chemofacies ($_c$F) (Table 4.5) | | | | **Mineral facies (Table 4.6) association (RDA)** Provenance | **Genetic association of Lithofacies** Composition | **Acronym** Sediment provenance |
| | **Acronym (K-means groups)** | **Enrichment** | **Depletion** | **Biochemical Provenance** TOC/TN vs. d13C signature (Fig. 4.10) | | | |
| FN1702 (Funda) | $_c$**F1$_{fun}$** | Geochemical elements and biochemical isotopes | Biochemical proxies | Lacustrine algae and C3 land plants | **Augite** Catchment rock phenocrystals | **$T_D$ D** Lithoclastic | **F1$_{fun}$** Catchment rock |
| | $_c$**F2$_{fun}$** | TOC $\delta^{15}$N Sr Zr TN | BSi Inc/coh Cl Si | Predominantly C3 land plants | **Quart** Saharian **Hematite** Catchment soils | **$M_S$** Biogenic carbonaceous | **F2$_{fun}$** Catchment organic carbonaceous |

| | | | | | | | |
|---|---|---|---|---|---|---|---|
| | **$_cF3_{fun}$** | BSi Inc/coh Cl | Geochemical elements TOC and biochemical isotopes | Predominantly lacustrine algae | **Montmorillonite**<br>Resuspended clay from lake bottom | **$L_U$ $L_G$ $L_A$**<br>Endogenic organic within the photic zone<br>**$M_R$**<br>Resuspended material<br>**$M_D$**<br>Endogenic organic | **$F3_{fun}$**<br>Endogenic biomineralization from nutrient recycling |
| **CL1703 (Caldeirão)** | **$_cF1_{cald}$** | Geochemical elements, $\delta^{15}N$, TOC | $\delta^{13}C$ TN | $C_3$ land plants | **Montmorillonite**<br>Catchment rock weathering<br>**Augite Feldspar**<br>Catchment rock lithorelicts | **$M_D$**<br>Biogenic carbon | **$F1_{cald}$**<br>Catchment rock lithorelicts and soil derivates (weathered neo-formed clays and Organic leaching) |
| | **$_cF2_{cald}$** | Si K Ti V Mn Fe Br Zr $\delta^{13}C$ and $\delta^{15}N$ | Cl S biochemical proxies | $C_3$ land plant/ lacustrine algae | **Augite Feldspar**<br>Catchment rock lithorelicts<br>**Hematite**<br>Catchment soils | **$M_D$ E**<br>Biogenic carbon and lithoclastic | **$F2_{cald}$**<br>Catchment rock lithorelicts and reworked organic matter from the catchment |
| | **$_cF3_{cald}$** | Inc/coh BSi TOC | $\delta^{13}C$ $\delta^{15}N$ geochemical elements | $C_3$ land plants | **Montmorillonite**<br>Catchment rock weathering<br>**Quartz**<br>Saharian | **$M_P$**<br>Biogenic fossiliferous and plant debris | **$F3_{cald}$**<br>Endogenic organic (diatoms) |
| | **$_cF4_{cald}$** | $\delta^{13}C$ TN Inc/coh | $\delta^{15}N$ TOC Bsi geochemical elements | Lacustrine algae | **Hematite**<br>Endogenic<br>**Quartz**<br>Saharian | **$M_A$**<br>Biogenic carbon: Particulate algal remains | **$F4_{cald}$**<br>Endogenic organic (green algae) |
| **CVL1B (Caveiro)** | **$_cF1_{cav}$** | Geochemical elements | Biochemical elements | $C_3$ land plants | **Pyrite**<br>Endogenic in anaerobic peatland<br>**Plagioclase**<br>Soil parent rock | **Biogenic carbonaceous:**<br>**Q**<br>Black Particulate organic matter<br>**P**<br>Reddish amorphous organic matter | **$F1_{cav}$**<br>Pedogenic peat formed in situ (original and degraded) |
| | **$_cF2_{cav}$** | $\delta^{13}C$ $\delta^{15}N$ Ti V Mn Fe Br Rb Sr Zr | Biochemical elements | $C_3$ land plants | **Magnetite** | **E**<br>Lithoclastic, and Biogenic | **$F2_{cav}$**<br>Catchment rock lithorelicts and |

| | | | | | | | |
|---|---|---|---|---|---|---|---|
| | | | | | Catchment rock weathering<br>**Pyroxene**<br>Catchment rock | carbon: reddish organic matter | allochthonous peat (reworked) |
| | **$_{C}F3_{cav}$** | TOC TN | Geochemical elements and biochemical isotopes | $C_3$ land plants | **Kaolinite**<br>Catchment rock weathering<br>**Palygorskite Chlorite**<br>Interstitial hydrothermal fluids<br>**Quartz**<br>Saharian | **$M_O$ $M_P$ $M_D$ $M_S$**<br>Biogenic carbon and fossiliferous | **$F3_{cav}$**<br>Endogenic organic (carbon and silicic) |
| | - | - | - | - | - | **$V_L$**<br>Primary lapilli | External tephra from Pico Island volcanic eruptions |
| | - | - | - | - | - | **C**<br>Biogenic fossiliferous | Endogenic organic (bioclasts) |
| | - | - | - | - | - | **$V_W$**<br>Weathered epiclastic/lapilli | Minerogenic basement |

*Table 5.1: origin and provenance of the sediments based on biogeochemical budgets (chemofacies), organic chemical signature, mineral RDA associations and the composition of the genetic associations of lithofacies conforming the sedimentary facies identified through biogeochemical k-means clustering.*

### 5.1.1 Allogenic sediments

#### FN1702 record

The allochthonous fraction within FN1702 sediments is constituted by $F1_{fun}$ and $F2_{fun}$ (Table 5.1). The geochemically enriched composition of $_{C}F1_{fun}$ associated with augite indicates the minerogenic origin of $F1_{fun}$. The provenance of $F1_{fun}$ derives from the coarsest mineral fraction of the catchment, as augite is part of the rock phenocrystals of Flores Island (Genske et al., 2012; Larrea et al., 2018; Fig. 2.11). Moreover, $F1_{fun}$ is linked to lithofacies D and TD, which are mainly composed of lithoclasts, confirming the minerogenic origin of this Facies. The prevalent lithoclastic composition of this facies may indicate the reworking of alluvial material previously deposited elsewhere in the catchment and fractionated from light organic to fine material. The submerged alluvial fan identified in the field may have constituted the source of these materials (Fig. 2.15e). Nevertheless, the primary provenance may be constituted by the highly erodible domain 3 (section 4.1), where the most prominent erosive scars were observed (Fig. 2.15b,c). The correspondence between the highly erodible domain 3 and the maars septa and main crater scarps in Funda catchment (Fig. 4.1) indicate the provenance of $F1_{fun}$ allogenic deposits, which derive from the young volcanic inherited reliefs (maars septa and main crater) of the FVS (Andrade et al., 2022). This domain 3 constitutes an incipient incision wave, where poorly mature and thin soils may develop or even the bedrock could be exposed (Gomez et al., 2010).

Besides, the allochthonous fraction within FN1702 sediments also comprises most of the organic sediments of $F2_{fun}$ (Table 5.1). The carbonaceous organic composition of $_{C}F2_{fun}$ (Table 4.5), characterized by a biochemical signal dominated by C3 land plants (Fig. 4.10), indicates the allochthonous biogenic origin of $F2_{fun}$, probably derived from the forest cover of the catchment (Ritter et al., 2022; Raposeiro et al., 2021). The relationship of the allochthonous biochemical origin of $_{C}F2_{fun}$ (Table 4.5; Fig. 4.10) with lithofacies MS enriched in particulate organic matter and vegetal macro-rests supports this hypothesis. The organic matter derived from these forests would also have been responsible for enhanced generation of dissolved humic acids in the catchment soils, subsequently released into the lake through biodegradation activity (Meyers and Teranes, 2001). The partial relationships shown by d15N and d13C with $_{C}F2_{fun}$ are indicative of these degradation processes affecting the organic matter under oxidative conditions prior to burial (Lerch et al., 2011). Additionally, the partial relationships shown by $_{C}F2_{fun}$ with the Sr and Zr may indicate the influence of detrital inputs supplied alongside land-derived organic matter (Marshall et al., 2011). Besides domain 3, the provenance of $F2_{fun}$ sediments would rather imply domain 1, where the most prominent forests and thickest soils may easily install and develop (Schaetzl and Anderson, 2005).

### CL1703 record

The allochthonous fraction within CL1703 sediments dominates the facies $F1_{cald}$ and $F2_{cald}$ (Table 5.1). The dominant geochemical composition of $_{C}F2_{cald}$ associated with augite and feldspar, indicates the catchment rock provenance of $F2_{cald}$, derived from the large phenocrystals and feldspathic microcrystalline matrix (Genske et al., 2012; Larrea et al., 2018; Fig. 2.11). The geochemical budget composing $_{C}F1_{cald}$, associated with montmorillonite, indicates the influence of soil formation in the catchment in $F1_{cald}$, where neo-formed minerals are included into the resistant lithorelict fraction from the parent rock. Although $F1_{cald}$ and $F2_{cald}$ reveal minerogenic origins, the correspondence between the organic carbon lithofacies $M_P$ with these facies indicate organic contributions. The TOC, $d^{15}N$ and S enrichment of $_{C}F1_{cald}$ suggests enhanced release of organic derivates from catchment soils and preservation within $F1_{cald}$, that enriches in sulphur from organic matter leaching (Burnett et al., 2011; Hodell et al., 2012; Olsen et al., 2013). This organic enrichment is confirmed by the correspondence with black carbon biogenic components of lithofacies $M_P$. In contrast, the heavy isotopic enrichment of $d^{13}C$ from $_{C}F2_{cald}$, corresponding to the lithic reddish composition of lithofacies E, suggests the partial decomposition of the organic matter, where microbes assimilate light C isotopes (Lerch et al., 2011). The partial association of hematite with $F2_{cald}$ results from bacterial respiration processes that favour the precipitation of this mineral species, inducing the reddish tones of lithofacies E. Therefore, the composition of both facies reveals catchment provenances, but from different sources, primary from soils in $F1_{cald}$, and from degraded and reworked soils in $F2_{cald}$. This is confirmed by the lower TOC/TN ratio characterizing the biochemical signal of $_{C}F2_{cald}$, which indicates the minor contribution in $F2_{cald}$ of primary organic matter derived from land plants. The highly erodible domain 3 constituted by the peripheral steeplands of the Caldeirão catchment, particularly at the gullies and rills associated with the streams, may constitute the primary provenance of the coarse materials precursive of $F2_{fun}$ (Gomez et al., 2010). These materials accumulate concentrically constituting the alluvial fans at the slope break corresponding with the transitive domain 2 (Harvey, 2010). Once in the low erodible domain 1, pedogenetic processes may favour the transformation of these materials into the finer sediments precursive of $F1_{cald}$, that would form thick soils (Bracken, 2010) and favour peatland accretion and storage (Evans and Burt, 2010).

### CVL1B record

CVL1B sediments from the allochthonous fraction are derived from $F2_{cav}$ and lithofacies $V_W$ (Table 5.1). The geochemical enrichment of $_{C}F2_{cav}$ that associates with magnetite and pyroxene from the São Roque Piedade catchment rock composition (Larrea et el., 2018) suggests the minerogenic

nature of $F2_{cav}$. Likewise in $_{C}F2_{cald}$, the heavy isotopic carbon enrichment characterizing $_{C}F2_{cav}$ indicates the microbial fractionation of the organic matter (Lerch et al., 2011). Therefore, the $C_3$ land plant biochemical signal and the marked enrichment of carbon isotope values of $_{C}F2_{cav}$ might indicate the allochthonous contribution of biogenic materials partially decomposed from the peri-lacustrine peatland to form the sediments of $F2_{cav}$. The correspondence between the geochemical and heavy carbon isotopic compositions of the organic matter shown by $_{C}F2_{cav}$ with the lithoclasts and particulate organic matter from the reddish Lithofacies E confirms a mixed minerogenic-organic origin affected by partial decomposition for $F2_{cav}$. Besides, the reddish subangular lithoclasts of lithofacies $V_W$ correspond to weathered tephra that constitutes the basement of the lacustrine sedimentary infill of Lake Caveiro. Similarly, to Caldeirão catchment, the domain 3 composed by the western steeplands would constitute the primary source of $F2_{cav}$ minerogenic fraction, which may especially derive from the unique gully aligned with the Brejos graben fault intersection with the relief. The low erodible domain 1 constitute the flat central area prone to paralimnetic deposition, where pedogenesis transform these minerogenic materials, feeding the peatland, which grows in the transition to the lake (Fig. 2.25) contributing to the precursive materials of $F2_{cav}$ with biogenic derivates (Evans and Burt, 2010). Therefore, the precursive materials of $F2_{cav}$ mainly form at the western side of the catchment.

### 5.1.2 Endogenic sediments

#### FN1702 record

The endogenic fraction within FN1702 sediments is constituted by the $F3_{fun}$ (Table 5.1), where $_{C}F3_{fun}$ displays amorphous siliceous composition with lacustrine algal signal, indicating the diatom biosynthetic contribution to the origin of this facies. Diatoms sinthesize bioavailable silica from silicic acids for biomineralization within the photic zone (Bertrand et al., 2015). Silicic acids may derive from catchment rock weathering (e.g., Martin-Jezequel et al., 2000; Street-Perrott and Barker, 2008). In turn, microbes release nutrients within the hypolimnion using allochthonous mineral supply or biomineralized remains decanted from the epilimnion (Amblard et al., 1998). Therefore, the main sources of dissolved silica within the Lake Funda photic zone may derive either from catchment weathering or from the mineralized remains previously deposited in the lake bottom. The light montmorillonite associates with the endogenic organic $F3_{fun}$ and disposes opposite to the allochthonous minerogenic $F1_{fun}$, indicating resuspension as the most plausible source of bioavailable nutrients used by diatoms (Ritter et al., 2022; Gonçalves et al., 2013; 2009). The fall water column turnover (Gonçalves et al., 2009) redistributes the hypolimnetic materials into the photic zone constituting injections of nutrients through resuspension (Vázquez-Loureiro et al., 2023). These injections derive in planktonic diatom blooms that can reach up to 76% of the total biomass during winter and spring (Gonçalves et al., 2013), closing the positive feedback loop of productivity between algae and microbes (Ritter et al., 2022). The correspondence between the planktonic diatomites of lithofacies $L_U$, $L_G$, and $L_A$ with $F3_{fun}$ confirms the siliceous biosynthetic origin of $F3_{fun}$ performed by diatoms, whereas the lithofacies $L_R$ would correspond with the resettled materials derived from resuspension. The steep Funda maar crater flanks force Lake Funda vertical volumetric development (Table 4.1) to constitute the shallow bathymetric domain (a) (Fig. 4.1), which enables the formation of horizontal physicochemical barriers. Moreover, the volcanic morphology protects the epilimnion from wind erosion, favouring the installation of the thermocline during the summer months (Marchetto et al., 2015) (Fig. 2.16). The $F3_{fun}$ derives from this volumetric domain, where diatoms find light and nutrients from fall turnover, and from the resuspended material.

The $F2_{fun}$ also contributes to the endogenic sediments within the FN1702 record. As previously discussed, this facies is dominantly allochthonous. Though, the partial relationship of TN with $_{C}F2_{fun}$ and the amorphous organic matter found within lithofacies MS indicates the partial contribution of endogenic synthesis of biogenic carbon materials in $F2_{fun}$ (Meyers and Teranes, 2001). Bioavailable

forms of carbon for endogenic biosynthesis would mainly derive from the humic acids released by the soils generated in the catchment primarily corresponding with domain 1.

### CL1703 record

The endogenic fraction within CL1703 sediments is dominated by $F3_{cald}$ and $F4_{cald}$ (Table 5.1). The enrichment of $_{C}F3_{cald}$ in TOC and BSi may indicate the biogenic origin of $F3_{cald}$, favoured by a prominent forest cover which contributes to catchment soil formation (Connor et al., 2024, Raposeiro et al., 2021). Enhanced pedogenesis favours detrital storage in the watershed (Bracken, 2010) and leaching of dissolved nutrients from soils. Derived dissolved nutrients may supply organic matter (Meyers and Teranes, 2001) and siliceous acids to the lake, favouring productivity and diatom biomineralization within the lake (Martin-Jezequel et al., 2000; Street-Perrott and Barker, 2008). $_{C}F3_{cald}$ associates with montmorillonite, confirming the involvement of catchment weathering in the increased trophic state of the lake by releasing bioavailable nutrients. Furthermore, the correspondence of the diatomite from lithofacies $M_P$ with $F3_{cald}$ confirms the biogenic origin derived from biomineralization within the lake. Concentrations of vegetal macrorests support the forest contribution to $F3_{cald}$. Furthermore, the N-richness of $_{C}F4_{cald}$, showing in turn high d13C values, indicates algal productivity within the lake (Meyers and Teranes, 2001). The low isotopic values of d15N associated with $_{C}F4_{cald}$ demonstrate the isotopic fractionation of nitrogen performed by algal communities, assimilating light forms of nitrogen and fixing them into the sediments of $F4_{cald}$. This is further supported by the correspondence of $F4_{cald}$ with concentrations of particulate algal remains of *Desmodesmus sp*. within Lithofacies $M_A$. Besides, the correlation of $F4_{cald}$ with hematite may suggest endogenic precipitation of this mineral species, likely resulting from oxidized conditions, triggered by the extensive photosynthetic activity of green algae, which releases oxygen into the water column. Thick soils deducted from $_{C}F1_{cald}$ extensively occupying the low erodible domain 1, may have constituted the source of nutrients for endogenic biosynthesis of $_{C}F3_{cald}$ and $_{C}F4_{cald}$.

### CVL1B record

The endogenic fraction within CVL1B sediments is composed of $F3_{cav}$ and Lithofacies C (Table 5.1). The enrichment of $_{C}F3_{cav}$ in organic elements, associated with fine kaolinite clays and amorphous materials, suggests the endogenic organic origin of $F3_{cav}$. Likewise $F3_{cald}$, the association with kaolinite and amorphous material association with $F3_{cav}$ indicates the supply of allochthonous bioavailable silica forms and clays derived from weathering, which diatoms uptake for biomineralization (Bertrand et al., 2015). Furthermore, the biochemical signal of $_{C}F3_{cav}$, dominated by C3 land plants, supports the influence of allochthonous dissolved humic substances contributing to organic matter biosynthesis within the lake to form $F3_{cav}$ (Meyers and Teranes, 2001). The correspondence between $F3_{cav}$ and the organic carbonaceous and fossiliferous derivates composing lithofacies $M_O$, MD, MP and MS supports this scenario. Additionally, the bioclastic composition of Lithofacies C also indicates endogenic organic origin. Once the peripheric peatland is installed at domain 1, the organic supply within the lake to constitute $_{C}F3_{cav}$ may be ensured (Fig. 2.25).

## 5.1.3 Pedogenic fraction

Within the CVL1B record, the $F1_{cav}$ composes the pedogenic fraction of the sediments, found in their original position of formation (Table 5.1). The enrichment of $_{C}F1_{cav}$ in geochemical elements, which in turn is associated with plagioclase, indicates the primary minerogenic contribution of $F1_{cav}$. The correspondence of $_{C}F1_{cav}$ with organic matter from lithofacies P and Q indicates a double minerogenic and organic origin for $F1_{cav}$. The presence of dark peaty particulate components dominating Lithofacies Q, coupled with the light isotopic composition of the carbon present in the organic elements of $_{C}F1_{cav}$, indicate peat formation through paludification, retaining partially decomposed mineral particles from the parent rock and catchment. Furthermore, the association of $_{C}F1_{cav}$ with pyrite indicates authigenic precipitation of sulphurs derived from organic matter in

anaerobic conditions within Lithofacies Q (Bertrand et al., 2015). In contrast, the heavy carbon isotopic composition of $_{C}F1_{cav}$, corresponding with the reddish organic aggregates dominating Lithofacies P, suggests the accumulation of partially decomposed organic matter under subaerial oxygenic conditions, where the partial decomposition of the organic matter by bacteria induces the isotopic fractionation of the organic matter (Lerch et al., 2011). Therefore, the minerogenic-organic origin of $F1_{cav}$, constituted by varying organic matter compositions, indicates water lamina fluctuations in the lake margin controlling the catchment pedogenesis. These conditions may have been favoured by flat relief configurations, like those corresponding with domain 1 at the central part of the Caveiro system.

### 5.1.4 External contributions

Quartz, palygorskite and chlorite detected through XRD within these sediment records do not align with the common composition of Flores, Corvo and Pico Island rock mineralogy (Genske et al., 2012; Larrea et al., 2018; Fig. 2.11). Ordination relationships established between the mentioned mineral components and the allochthonous ($F1_{fun}$, $F2_{fun}$, $F1_{cald}$, $F2_{cald}$ and $F2_{cav}$), endogenic ($F3_{fun}$, $F3_{cald}$, $F4_{cald}$ and $F3_{cav}$) and pedogenic ($F1_{cav}$) Facies reveal exogenous contributions to the systems. These external contributions constitute secondary components of the sedimentary facies (Table 5.1).

The marked inverse relationships shown by quartz with primary allochthonous facies derived from the catchments ($F1_{fun}$, $F2_{cald}$ and $F2_{cav}$) and the partial relationships with endogenic facies ($F2_{fun}$, $F3_{fun}$, $F3_{cald}$, $F4_{cald}$, $F1_{cav}$ and $F3_{cav}$) suggest an aeolian provenance of this mineral specie. Quartz may have been transported by trade winds as suspended airborne particles within dust plumes from the Sahara Desert into the three studied systems (Brust and Waniek, 2010), accumulating within facies formed with low sedimentation rates as may be the endogenic ones.

The lack of palygorskite and chlorite within the São Roque-Piedade Volcanic Complex rock composition (Larrea et al., 2018) suggests the authigenic precipitation of these mineral species within the interstitial pores of the São Roque-Piedade Volcanic Complex rocks from Mg rich fluids, derived from ferromagnesic minerals solution (Galán and Pozo, 2011). Fluid overpressure within the rocks would mobilize palygorskite and chlorite into the systems, due to the water lamina fluctuations as deducted for the origin of $F1_{cav}$, which shows an inverse relationship with them.

Moreover, the halogen elements Cl and Br, although not contributing to the rock mineral composition in the catchment area (Genske et al., 2012; Larrea et al., 2018; Fig. 2.11), could accumulate in the lake waters through atmospheric inputs, transported as dissolved salts within marine spray particles (Mackereth, 1966; Sturges and Harrison, 1986). This aligns with the prevalent chlorinated hydrogeochemical facies observed in the lakes of the archipelago (Cruz et al., 2006; Antunes and Rodrigues 2014; 2018). The contribution of dissolved halogens to the lake waters in the three systems may be linked to stormy conditions (Unkel et al., 2010), which are common in the Azores (Hernandez et al., 2016), intensifying both marine spraying and catchment delivery to the lake. In fact, Cl and Br exhibit relationships with the facies derived from the catchments (Fig. 4.12, 4.13 and 4.14).

Furthermore, the primary lapilli of lithofacies $V_L$ constitutes tephra contributions from Pico Island volcanic activity, reaching Lake Caveiro directly from the atmosphere as fallout into the lake. The Rb and Sr contribution to CVL1B record may be related with atmospheric contributions of crypto-tephra associated with this volcanic activity (Vogel et al., 2010; Guyard et al., 2017; Damaschke et al., 2013). Moreover, rhythmic micro-lithofacies constitute stratigraphic patterns genetically related to resuspension, which induces time-uncoupled sedimentary deliveries within Lake Funda (Ritter et al., 2022).

## 5.2 Sedimentary processes

The facies provenance indicates the main sedimentary processes responsible for delivering sedimentary components within the three lake systems. Furthermore, the grain size and mineral associations within RDAs have provided further insights into the physical constraints imposed by the detected mineral species (Figs. 4.6, 4.7 and 4.8) on the biogeochemical mobilisation. Accordingly, it has been deduced that alluvial mobilisation and organic accumulation are the main pathways for delivering sedimentary components within the three systems.

| **Lake-catchment system (Sediment Record)** | **Facies** | **Genetic association of lithofacies**<br>Sedimentary process | **Mineral**<br>Physical constraints | **Sedimentary process** |
|---|---|---|---|---|
| **Funda (FN1702)** | **$F1_{fun}$** | **D**<br>Traction erosive deposition<br>**$T_D$**<br>Turbidity currents decantation | **Augite**<br>Alluvial remobilization of coarse and dense detritics | **Debris flows** |
| | **$F2_{fun}$** | **$M_S$**<br>Organic matter accumulation | **Quart**<br>Fine aeolian fallout<br>**Hematite**<br>Authigenic precipitation in soils and alluvial mobilisation | **Organic matter accumulation** |
| | **$F3_{fun}$** | **$_RF1$ ($M_D$ + $L_A$)**<br>High organic matter accumulation in sublittoral area. Flashy turnover triggering shallow lakebed partial erosion in sublittoral area and slight resuspension. Quick decantation of $M_D$ heavy dense organic floccules and lagged decantation of derived diatom blooms remains ($L_A$) | **Montmorillonite**<br>Fine detrital resuspension (chlorine sequester through adsorption/absorption) | **Organic remains accumulation through early decantation of resuspended materials and lagged decantation of derived biomineralized remains** |
| | | **$_RF2$ ($L_R$ + $L_G$)**<br>Flashy-to-progressive turnover, driving pelagic resettlement of resuspended material derived from lake margins bottom ($L_R$). Delayed decantation of derived diatom blooms remains ($L_G$) | | |
| | | **$_RF3$ ($L_R$ + $L_G$/$L_U$)**<br>Flash turnover, driving pelagic resettlement of resuspended material derived from lake margins bottom ($L_R$). Delayed decantation of diatom remains, derived from blooms with partial ($L_G$) and complete ($L_U$) water column circulation restriction. | | |
| **Caldeirão (CL1703)** | **$F1_{cald}$** | **$M_D$**<br>Organic matter accumulation<br>**E**<br>Alluvial mobilization | **Montmorillonite**<br>Neoformation of fine detrital material (chlorine sequester through adsorption/absorption) | **Alluvial mobilisation and soils formation** |

| | | | | |
|---|---|---|---|---|
| | | | **Augite Feldspar**<br>Coarse and dense detrital lithorelicts | |
| | **$F2_{cald}$** | **$M_D$**<br>Organic matter accumulation<br>**E**<br>Organic alluvial reworking | **Augite Feldspar**<br>Coarse and dense detrital lithorelicts | **Alluvial mobilisation and soils degradation** |
| | **$F3_{cald}$** | **$M_P$**<br>Accumulation of diatoms remains | **Montmorillonite**<br>Neoformation of fine detrital material | **Accumulation of biomineralized remains** |
| | **$F4_{cald}$** | **$M_A$**<br>Accumulation of green algae remains | **Hematite**<br>Oxidizing authigenic precipitation<br>**Quartz**<br>Fine aeolian fallout | **Organic matter accumulation** |
| **Caveiro (CVL1B)** | **$F1_{cav}$** | **P**<br>Accumulation of partially degraded organic matter<br>**Q**<br>Peatland accretion | **Pyrite**<br>Anaerobic endogenic precipitation<br>**Plagioclase**<br>In situ parent rock lithorelicts | **Pedogenesis** |
| | **$F2_{cav}$** | **E**<br>reworking of peri-lacustrine organic deposits | **Magnetite**<br>Neoformation of fine detrital material<br>**Pyroxene**<br>Coarse and dense detrital lithorelicts | **Peatland alluvial reworking** |
| | **$F3_{cav}$** | **$M_D$ $M_P$ $M_O$ $M_S$**<br>Accumulation of organic matter and diatoms remains | **Kaolinite**<br>Alluvial supply of fine clays<br>**Palygorskite Chlorite**<br>Lixiviated<br>**Quartz**<br>Aeolian fallout | **In-lake organic accumulation** |
| | - | **$V_W$**<br>Alluvial/subaerial reworking of tephra | - | **-** |
| | - | **C**<br>Accumulation of diatom remains by littoral longshore currents | - | **-** |
| | - | **$V_L$**<br>Volcanic fallout | - | **-** |

*Table 5.2: sedimentary processes mobilizing the sedimentary components within Funda, Caldeirão and Caveiro lake-catchment systems.*

### 5.2.1 Alluvial mobilization

Within the Funda system, the dominance of catchment-derived minerogenic material of $F1_{fun}$ demonstrates that the allochthonous supply in FN1702 sediments is mainly driven by the reworking of alluvial material, which mobilizes resulting in debris flows. This is evidenced by the prevalent coarse and subangular lithic composition of the conglomeratic Lithofacies D, transitioning to the sandy silts of Lithofacies $T_D$ that compose $F1_{fun}$ (Shanmugam, 2013). The light values of δ13C characterizing $_CF1_{fun}$ may be attributed to algal productivity (Meyers and Teranes, 2001) due to flows supplying nutrients that fertilize the lake. Additionally, the partial association of δ15N with $_CF1_{fun}$ confirms the dominance of external lake dynamics in sedimentation (Ritter et al., 2022). In turn, the partial contribution of S may indicate organic matter, preserved under anaerobic conditions (Burnett et al., 2011; Hodell et al., 2012; Olsen et al., 2013) due to rapid burial by debris flows. The Mn enrichment in $_CF1_{fun}$ may result from biological oxidation of Mn, favouring the formation of concretions around sediment grains and pebbles in the original environments of debris flows before reaching the lake bottom (e.g., Bertrand et al., 2015; Moreno et al., 2008).

Within the Caldeirão system, the allochthonous mineral composition of $F1_{cald}$ dominated by montmorillonite indicates the alluvial mobilisation through suspension of previously weathered volcanic catchment rocks (Bracken, 2010). The alluvial mobilisation of the finest fraction composed by the suspended smectites produces the hydrogeochemical fractionation of the dissolved chlorine ions concentrated in the lake waters (Cruz et al., 2006; Antunes and Rodrigues 2014; 2018) through absorption and/or adsorption, which finally incorporate into $F1_{cald}$ through decantation. In contrast, in the mineral facies of $F2_{cald}$ prevail coarser lithorelictic fraction, presenting higher relative resistance to alluvial action, mobilising through bedload drifting (Bracken, 2010). The coarse mineral composition of the lithoclastic Lithofacies E confirms this mechanism. Furthermore, the alluvial reworking of partially decomposed organic matter would explain the heavy carbon isotopic composition of $_CF2_{cald}$ (Lerch et al., 2011) corresponding to the reddish tones of Lithofacies E, whereas the Br associated with reddish laminae (sample 63) may correspond to exceptional floodings related to storms (Unkel et al., 2010).

Within the Caveiro system, the organic composition of the allochthonous $F2_{cav}$ indicates the reworking of the previously deposited peri-lacustrine peatland ($F1_{cav}$). The reddish tones and dual composition of Lithofacies E, dominated by large vegetal rest and poorly sorted detrital materials, indicate this reworking. Furthermore, the partial decomposition of the reworked organic sediments deduced from the heavy carbon isotopic composition of $_CF2_{cav}$ suggests a water level drop leaving the peatland subaerially exposed, which would die and its vegetal remains would be reworked and incorporated within the lake sediments.

### 5.2.2 Organic accumulation

Within the Funda system, the endogenic biomineral origin of $F3_{fun}$ indicates the organic accumulation of diatom bloom remains through decantation from the photic zone (Apolinarska et al., 2020; Ritter et al., 2022). Furthermore, the inclusion of Cl in $_CF3_{fun}$, associated with montmorillonite, indicates resuspension enhancing chlorine sequester performed by the lightest sedimentary fraction. During resuspension smectite re-adsorbs chlorine, fixing it into $F3_{fun}$ when decanting. Furthermore, organic matter may be also adsorpted by clays conforming the organo-mineral complexes (Chilom and Rice, 2009) and the flocculated/colloidal-like aggregates found in Lithofacies $M_D$ / $L_R$ in correspondence with $F3_{fun}$. This organic matter in turn may halogenate, enhancing chlorine sequester and resettling alongside diatom remains into $F3_{fun}$ when decanting. The independence shown by the two endmembers of allochthonous supply, $F1_{fun}$ (alluvial fluxes) and $F2_{fun}$ (soils leaching), with respect $_CF3_{fun}$, confirms the resettlement of resuspended material as the main mechanism of organic matter accumulation within $F3_{fun}$.

Moreover, the $F2_{fun}$ also contributes to organic accumulation within the Funda system. The inverse relationship shown by the $F2_{fun}$ from the allochthonous minerogenic $F1_{fun}$ and the endogenic diatomitic $F3_{fun}$ indicates the concentration of carbonaceous biogenic material in absence of debris flows and biomineralization. Furthermore, the relationship established between $F2_{fun}$ and quartz may indicate the low sedimentation rates of this facies due to this lack of alluvial and biomineral remains, allowing the accumulation of saharan dust (Brust and Wainiek, 2010). The forest cover deducted for the allochthonous biogenic origin of $F2_{fun}$ would have contributed with large amounts of vegetal remains to the lake sediments. Furthermore, leaching of humic substances from the derived soils would have contributed to the endogenic biosynthesis, subsequently decanted and accumulated.

The rhythmic lithological organization of the microlithofacies composing $F3_{cav}$ suggests the accumulation of biogenic varves, following the annual cycle of organic productivity (Brauer, 2004; Zolitschka et al., 2015) within Lake Funda (Gonçalves et al., 2013). This cycle is triggered by turnover convective resuspension during fall (Gonçalves et al., 2009; Fig. 2.16) inducing a decantation pattern in successive phases during the rest of the year (Vázquez-Loureiro et al., 2023). The varves composition and disposition has demonstrated variable processes implied in the annual rhythmic organic accumulation, expressing in three different ways:

- The $_{R}$F1couplet, where: 1) the Lithofacies $M_D$ constituting the dark laminae, with relatively compact texture and dominated by benthic and littoral biotic assemblages, indicates prevalent organic accumulation through a yearly constant influx from the catchment of detrital material and carbon organic matter ($F2_{fun}$). These may especially accumulate at the relatively shallow bathymetric domain C, constituting the delta plain where organic matter may easily accumulate in flatter conditions (Fig. 4.1). In these conditions the source of littoral derivates may be explained by the partial exposition of the submerged alluvial fan (Fig. 2.15e). The flocculated disposition of the organic aggregates in Lithofacies $M_D$, more noticeable in the transition to the pale laminae, indicates partial disaggregation induced by bottom shear stresses during fall turnover (Gonçalves et al., 2009; Fig. 2.16). 2) The centric planktonic diatom remains in the banded Lithofacies $L_A$ constituting the pale laminae indicates the dilution of organic matter accumulation ($F2_{fun}$) due to diatom blooms remains decantation and accumulation ($F3_{fun}$), alongside the resettling of the organic material partially resuspended from the dark laminae.
- The $_{R}$F2 couplet, where: 1) Lithofacies $L_R$ constituting the dark laminae, with small colloid-like organic aggregates with loose disposition and dominated by centric planktonic diatom remains, indicates the organic accumulation ($F3_{fun}$) through focussed resettlement of the heaviest resuspended fraction after fall turnover (Bloesch, 1995) and during winter mixing period (Gonçalves et al., 2009; Fig. 2.16). Therefore, it is assumed that the Lithofacies $L_R$ derives from the resuspended lightest sedimentary fraction, constituted by the organic matter of Lithofacies $M_D$ previously accumulated in shallower marginal areas ($F2_{fun}$) (e.g., Apolinarska et al., 2020; Evans, 1994). 2) The Lithofacies $L_G$ constituting the pale laminae, and composed by diatom remains accumulated with loose disposition, indicates diatom blooms decantation alongside the resettlement of resuspended organic material. The smooth transition from the dark to the pale laminae indicates the lag period between nutrient injection and the steady depletion in the photic zone, controlled by the progressive restriction of convective circulation during the progressive thermocline installation in spring and early summer (Gonçalves et al., 2009; Fig. 2.16). The steady depletion of nutrients may lead to increasing diatom mortality and decantation of the biosynthetic derivates diffusely concentrating after a certain lag period above the dark laminae, to finally constitute the pale laminae. Nevertheless, whenever the transition to the pale laminae is sharp indicates the flashy turnover, probably triggered by alluvial floods.

- The $_{R}$F3 triplet/couplet, where: 1) The Lithofacies $L_R$ conforming the dark laminae, includes epiphytic diatom assemblages, indicating catchment detrital supply while resuspended materials resettle. 2) The inclusion of Lithofacies $L_U$, exclusively constituted araphidic diatoms, above Lithofacies $L_G$ to conform the $_{R}$F3a triplet, indicates the complete restriction of convection during late summer and early fall (Gonçalves et al., 2009; Fig. 2.16). These conditions favoured the replacement of *Aulacoseira granulata* var. *angustissima*, adapted to turbulence, with Ulnaria Complex and *Aulacoseira granulata*, more adapted to strengthened stratification of the water column (Vázquez-Loureiro et al., 2023). 3) The lack of Lithofacies $L_G$ in $_{R}$F3b indicates the sharp transition from convection, probably derived from turnover due to inflows derived from alluvial floods, to stratification, in exceptional hot summer conditions (Gonçalves et al., 2009; Fig. 2.16).

Therefore, the rhythmic pattern indicates that the positive feedback loop established between diatoms and microbes through convective circulation and decantation, effectively guaranties the organic matter accumulation that conform the sediments of $F3_{fun}$ (Ritter et al. 2022; Vázquez-Loureiro et al., 2023). Due to wind protection within Funda maar crater flanks (domain A) wind-driven advection may be minimal (Marchetto et al., 2015), allowing a relatively regular distribution of decanting remains across the lake bottom.

Within the Caldeirão system, the biogenic origin of $F3_{cald}$ and $F4_{cald}$, with prevalent endogenic provenance, represents the accumulation of organic materials within Lake Caldeirão. Vegetal macrorrests composing Lithofacies $M_P$ would reach the lake through wind, contributing to the organic accumulation in $F3_{cald}$ sediments. The reddish tones of Lithofacies $M_A$, corresponding with $d^{13}C$ enrichment in $F4_{cald}$, suggest inputs of eroded soil material towards the lake. Therefore, negligible supply of bioavailable forms of silica would prevent diatom thrive (Mackereth, 1966), probably conferring green algae with a competitive advantage. Both the partial and strong association of quartz with $F3_{cald}$ and $F4_{cald}$, respectively, suggest the cessation of alluvial supply from the catchment, allowing the settlement of endogenic and aeolian materials. The positive relationship between hematite and $F4_{cald}$ confirms the accumulation of endogenic remains due to the cessation of catchment detrital input.

The $F1_{cav}$, $F3_{cav}$, and Lithofacies C constitute the sediments derived from organic accumulation within the Caveiro system. The pedogenic origin of $F1_{cav}$ in the Caveiro system suggests in situ accretion of soils derived from accumulation of peat (Lithofacies Q) and partially decomposed organic matter (Lithofacies P). Organic matter accretion retains the partially weathered mineral particles from the catchment rocks. In contrast, the organic origin of $F3_{cav}$ indicates organic accumulation and preservation within Lake Caveiro. This accumulation would be favoured by detritic buffering exerted by pedogenetic accretion deduced from $F1_{cav}$ formation in the lake surroundings. The partial association of paligorskite and chlorite with $_{C}F3_{cav}$ indicates the concentration of lixiviated materials into the $_{C}F3_{cav}$ through diffusion in absence of catchment detrital material. The correspondence of organic derivates from lithofacies series M supports the organic accumulation that conforms to $F3_{cav}$. The partial relationship of aeolian quartz with $F1_{cav}$ and $F3_{cav}$ indicates catchment detrital buffering by soil retention. Lastly, the partial relationship of Br with $F1_{cav}$ and $F3_{cav}$ indicates the accumulation of this element with organic matter through halogenation processes. The cross-lamination observed in Lithofacies C may indicate lacustrine beach deposits delivered from longshore wind-driven currents that accumulated fragmented biomineralized remains along a paleo shoreline.

## 5.3 Sedimentary delivery pathways and drivers

Erodibility domains (Fig. 4.1), alongside field analysis (Figs. 2.14, 2.20 and 2.24) of erosive landforms, including badlands, gullies and rills (Figs. 2.15 2.21 and 2.25), show the most probable delivery routes followed by the allochthonous sediments, whereas the depositional landforms

inferred from the elevation distribution within the systems provide insights into the sediment sinking patterns (Fig. 4.1). Therefore, the allochthonous Facies (Table 5.1) have been related to the erodibility domains (Figs. 4.1) enabling to identify the provenance areas and sedimentary processes mobilising the allochthonous sediments (Table 5.1), including both the coupled (Fig. 4.1) and uncoupled regions (Fig. 1.14 and 4.2). Highly erodible domains supported by erosive scars identified in field (Figs. 2.15, 2.21 and 2.25) indicate the primary sedimentary provenances, whereas, low erodibility domains reveal areas prone to soil development, peatland installation and paralimnetic alluvial storage prior to lake sedimentation (Burt and Allison, 2010). Additionally, the low erodible domains indicate the most probable areas for coupled mobilization through leaching, whereas the streams erodibility (Fig. 4.2) reveal sediment cascading through the uncoupled region (Fig. 1.14) that constitutes the most prominent delivery route for alluvial mobilization (Table 5.2: Fig. 4.2). The endogenic facies have been related to the lake volumes inferred from bathymetric domains revealing spatial patterns of endogenic sediments production, convective and advective mobilization and accumulation (Fig. 4.1).

In turn, the significant eigenvectors of the RDAs and PCAs reveal the main components of biogeochemical and mineral variability within FN1702 (Fig. 4.13), CL1703 (Fig. 4.14) and CVL1B (Fig. 4.15) sediment records. The sedimentary facies identified (Fig. 4.9) provide insights into sediment origins, sources, processes, and delivery pathways. Finally, the correlation between the significant eigenvectors with the sedimentary facies, allow the elucidation of the primary sedimentary drivers within Funda, Caldeirão and Caveiro lake-catchment systems.

### 5.3.1 Funda system

The low seismicity rates recorded in Flores Island (Fontiela et al., 2018) since formation of the FVS (Andrade et al., 2022) indicate negligible contribution of tectonic movements to alluvial incision. The scattered altitudinal distribution of knickpoints is attributed to alluvial incision responding to the young volcanic inherited reliefs (maars septa and main crater) of the FVS (Andrade et al., 2022). The alluvial incision belongs to the extremely erodible domain 4 where the draining extensive areas of the streams from Flores Island plateau cross the steeplands of domain 3 (Burt and Allison, 2010) (Fig. 4.1). In fact, the most prominent erosive scars correspond to these intersections, highlighting this between the Funda-NE maar septum and $St4_{fun}$. There, the landscape with badlands indicates the largest volume within the Funda system obliterated by erosion (Fig. 2.15b,c,d). Since the age of formation of these landforms is relatively similar (Andrade et al., 2022), relatively advanced erosive evolution has been inferred at the last 500 m of $St4_{fun}$ (Fig. 4.2). Therefore, alluvial incision has prominently progressed along $St4_{fun}$, whereas kept relatively moderate at $St1_{fun}$ and $St2_{fun}$ and negligible at $ST3_{fun}$. Furthermore, the steep crater flanks of Funda maar agreeing with the erodible domain 3 and the shallow bathymetric domain (A) would have favoured sediment cascading by preventing the development of paralimnetic depositional environments, and hampering the weathering in the catchment (Gomez et al., 2010). This combination allowed the mobilization of debris flows, whose most distal parts are recorded by $F1_{fun}$. Beside the alluvial supply through the uncoupled region, leaching across the coupled region (Fig. 1.14), especially in correspondence with domain 1 (Fig. 4.1) where the thickest soils form, might also have implied the delivery pathway of $F2_{fun}$. In contrast, the dominance of domain 1 at the southern maar indicates negligible alluvial mobilisation at $St3_{fun}$, although this area likely contributed to lake sedimentation through soil leaching.

Hence, since the origins of the FVS at ca. 3200 ago (Andrade et al., 2022) different volume inputs of alluvial material reached the lake. The accumulation of alluvial inputs within the lake have advanced significantly at $St4_{fun}$ mouth, whereas, at $St1_{fun}$ and $St2_{fun}$ sediment mouths display a of $St4_{fun}$ mouth with the landforms constituted by domains C and E may indicate a submerged delta fan. Whereas the flat bathymetric domain C located at ca. 20 m depth would have constituted a delta

plain, the steep and deep domain E may have constituted the delta front. In turn the slight slopes of domain B in correspondence with $St2_{fun}$ mouth may indicate an incipient delta formation with relative lower progress in the western side. Therefore, the flat deep bathymetric domain D located at the southwestern side of the lake corresponds with the displaced depocenter due to alluvial mobilization progress from Flores Island plateau and especially from the northeastern maar's alignment inducing the most prominent debris flows of $F1_{fun}$. Besides, the shallow steep bathymetric domain (A) corresponds to the zone of the lake where resuspension injects nutrients in the photic zone. This volumetric domain constitutes the location where there are living diatoms and they accumulate once they die, likely homogeneously, throughout the lake bottom.

Hence, the high negative correlation between the variability of $RDA1_{fun}$ and $PC1_{fun}$ (Fig. 4.12) represents the mineralogy and chemical composition within the Funda system responding to the same sedimentary driver that is interpreted as variation in erosion rates. This is because the dominance of debris flows from $F1_{fun}$ at the positive ends indicates enhanced erosion rates due to alluvial mobilization. However, materials with endogenic origin from $F3_{fun}$ and $F2_{fun}$ dominating at the negative ends indicate decreased erosion rates, thereby highlighting the organic accumulation derived from resuspension episodes, allochthonous organic matter leaching and endogenic biosynthesis. Thus, the sedimentary drivers deducted from Lake Funda catchment system are the result of the verticalized and oriented morphology within Funda lake basin (Fig. 4.1), which provokes an enhanced runoff that impulses sediment cascading (Burt and Allison, 2010).

The $PC2_{fun}$ is interpreted as an indicator of lake level fluctuations. At the positive side, the dominance of allochthonous organic matter accumulated in $F2_{fun}$ indicates extended and dense forests in the catchment (Ritter et al., 2022) contributing to evapotranspiration, driving the water removal from the system (Rosenmeier et al., 2002; Sun et al., 2008; Zhang et al., 2015), thereby leading to lower lake level. Conversely, the influence of eroded materials of $F1_{fun}$ at the negative side of $PC2_{fun}$ indicates enhanced erosion, evidencing higher runoff rates that may have contributed with water supply to raise lake level. Since the lake-catchment system is hydrologically closed and presumably well sealed, its elevation distribution also induces lake volumetric changes in depth rather than in area, amplifying lake level fluctuations. Finally, the $F3_{fun}$, also exerting influence at the negative end, evidences the summer thermocline installation and the accumulation of the organic material derived from fall resuspension. This is because high enough lake levels probably enabled the creation of a temperature gradient within the lake, allowing for the $F3_{fun}$ formation.

The thickness of the dark laminae (Fig. 4.18) during autumn/winter might be influenced by allochthonous input into the lake ($F2_{fun}$), however should be primarily driven by redeposition from shallow water sediments near the shoreline due to sediment focusing (e.g., Bloesch, 1995). This is evidenced by $F3_{fun}$ corresponding with the laminated sediments, lying on the negative end of $PC1_{fun}$ that indicates low erosion rates. On the other hand, the thickness of the pale sub-layer (Fig. 4.18) during spring/summer is closely tied to the intensity of diatom blooms, which in turn depends on nutrient input in the photic zone during resuspension (Martín-Puertas et al., 2012). This nutrient input is influenced by the intensity of remobilization (Vázquez-Loudeiro et al., 2023). The varve thickness (Fig. 4.18), is interpreted as the intensity of mixing of the water column, remobilizing sediment from the deeper waters to the epilimnion enhancing diatom productivity remains decantation to conform the pale lamina and sediment focusing and resettling into deeper waters conforming the dark lamina (Cohen, 2003).

### 5.3.2 Caldeirão system

Conversely to Funda catchment there are no badlands in Caldeirão landscape, where ephemeral streams are related to rills and gullies especially at the southern side of the catchment (Fig. 2.21a,g). Furthermore, the scattered distribution of the scoria cones at domain 1 may favour the retention of

debris flow and water. Therefore, domain 1, especially at the gaps between the scoria cones, constitutes a flat area prone to accumulate alluvial sediments (Harvey, 2010), pedogenesis processes (Bracken, 2010) and paludification (Evans and Burt, 2010), by constituting paralimnetic depositional environments that buffer sediment cascading (Burt and Allison, 2010). Since the hidro-sedimentary conditions prevent from the generation of prominent alluvial floodings at domain 2 and favours the alluvial sediments deposition at domain 1, the alluvial mobilization in Caldeirão catchment needs pedogenesis until its deposition. Therefore, the alluvial supply for the allochthonous fraction involves materials derived from soils and peri-lacustrine deposits formed at domain 1 (Gomez et al., 2010; Harvey, 2010), evidencing that alluvial mobilisation in Caldeirão involves two steps. The dual organo-minerogenic origin and catchment-derived provenance of $F1_{cald}$ and $F2_{cald}$ indicates evidence of this double contribution. Nevertheless, the correspondence of $F2_{cald}$ with coarser lithoclastic contributions from Lithofacies E indicates exceptional hydrological conditions allowing for the bedload alluvial mobilisation. Since the relatively flat disposition of domain 1 may have favoured prominent lake area fluctuations with hydrological cycles, the occurrence of Lithofacies E might be related with the erosive domain 2 at the lake rim (Fig. 4.1). Although contour elevation data was scarce at this location, field analysis showed incision forming prominent gullies at the scoria cones bases (Fig. 2.21c). Therefore, the knickpoints found at ca. 5 m abl in agreement with these erosive features in all the analysed streams may indicate the effects of base level fluctuations, leaving an abandoned lacustrine terrace, detected at ca. 150-200 m length southwards from the lake (Fig. 4.2). Contrary to Funda, the horizontal volumetric development of Caldeirão system favour base level fluctuation of streams and by pass as the main mechanism of alluvial mobilization through the incision of the peri-lacustrine deposits. Although the bathymetry indicates relatively regular alluvial accumulation surrounding the lake, the southern macrophite patch reveals the position of a gentle delta plain probably derived from enhanced soil erosion corresponding with this southern catchment sector.

The dominance of allochthonous facies $F1_{cald}$ and $F2_{cald}$ at the positive end of $PC1_{cald}$ indicates increased runoff triggering soil erosion (Bracken, 2010) and lake water volume changes. The inclusion of fine smectites within $F1_{cald}$ indicates alluvial mobilization dominated through suspension, which might be favoured by high weathering rates. In contrast, the dominance of lithorelicts within $F2_{cald}$ indicates a mobilization dominated by bedload drifting favoured by low soil retention. This may depend on pedogenesis or soil cohesion, hydroclimatic variability and changes in stream equilibrium profile. In contrast, the dominance of the endogenic facies $F3_{cald}$ and $F4_{cald}$ at the negative end of $PC1_{cald}$ indicates absence of detrital supply due to low runoff, favouring endogenic organic accumulation. Consequently, the $PC1_{cald}$ is interpreted as an indicator of runoff rates.

The high correspondence between the variability of $RDA1_{cald}$ and $PC2_{cald}$ indicates that the mineralogy and the chemical composition within the Caldeirão system respond to the same sedimentary driver that is interpreted as an indicator of pedogenesis. At the negative ends of these axes, the dominance of $F1_{cald}$, composed by weathering products, alongside $F3_{cald}$, which its endogenic origin is favoured by leaching of dissolved nutrients from soils, is indicating enhanced pedogenesis in the watershed. These conditions might be favoured during high hydrological recharge, retaining water and storing alluvial materials from domain 3 in the flat domain 1 resulting in wetlands forming soil and peatlands. Conversely, at the positive ends, the dominance of $F2_{cald}$ and $F4_{cald}$ indicates soil degradation through dissection and by-pass processes as indicated by the intermediate erodible domain 2. This is evidenced by the depletion of $F2_{cald}$ in fine clay minerals indicating a negligible weathering. The $F2_{cald}$, which is rich in degraded organic matter, indicates soil erosion drifting dead soil remains. Furthermore, the endogenic biosynthesis performed by green algae to compose $F3_{cald}$ indicate relatively low turbidity conditions due to reduced clay formation in soils. The reduced soil activity is evidenced by the prevalence of green algae as the main endogenic

producer within the lake due to diminished release of nutrients, thereby hampering the leaching of silicic acids. These conditions may confer green algae a competitive advantage over diatoms.

### 5.3.3 Caveiro system

The Caveiro system sedimentary processes are in accordance with the small size of the basin (Table 4.1), where the drainage is reduced, limiting the supply of allogenic materials. Instead, organic matter accumulation and reworking prevail accounting with recurrent compositional changes driven by accommodation space limitations (Björck et al., 2006). Nevertheless, alluvial supply within Caveiro catchment is localized at the western side of the catchment from where most of the clastic sediments should derive due to the confinement of the steeplands in this sector. Conversely, soil leaching might have dominated the allochthonous contribution to lake sedimentation, especially from the paralimnetic area constituted by domain 1 close to the lake at its western side (Fig. 4.1).

The high correlation between the variability of $RDA1_{cav}$ and $PC1_{cav}$ indicates that the mineralogy and chemical composition of the Caveiro system responds to the same sedimentary driver that is interpreted as variations of accommodation space. The negative ends of both axes are dominated by $F1_{cav}$, indicating paludification, and $F2_{cav}$, indicating the reworking of the soils formed in $F1_{fun}$, revealing reduced accommodation space. Whereas $F1_{fun}$ forms through peat aggradation in relative balance with the water lamina, $F2_{fun}$ does through detritic progradation due to water lamina drop. On the negative ends of the axes the dominance of the endogenic materials of $F3_{cav}$ indicates the creation of accommodation space, diminishing detrital progradation, thereby allowing for the accumulation of endogenic organic materials, fine detritic, and aeolian mineral particles.

The high correlation between the variability of $RDA2_{cav}$ and $PC2_{cav}$ indicates that the mineralogy and the chemical composition of the Caveiro system respond to the same sedimentary driver, which is interpreted as erosion rate fluctuations. The dominance of the $F1_{cav}$ and $F2_{cav}$ at their negative ends is indicative of low erosion rates allowing for the accumulation and preservation of organic matter, both lacustrine and palustrine (peatland accretion), whereas the dominance of $F2_{cav}$ at the positive ends of $RDA2_{cav}$ and $PC2_{cav}$ is indicative of high erosion rates, favouring the accumulation of lixiviates and especially reworked organic matter derived from peatland incision.

The $RDA3_{cav}$ is interpreted as the variation of organic matter accumulation. The positive end of the axis indicates high organic matter accumulation, both allogenic from $F1_{cav}$ and endogenic from $F3_{cav}$. In contrast, the dominance of $F2_{cav}$ at the negative end of this axis indicates detritic supply, diminishing the concentration of organic matter accumulated in the sediments

# 6. Discussion: Depositional environments within Funda, Caldeirão and Caveiro lake basins and their late Holocene evolution

The stratigraphic configuration of the ordination trajectory analyses and sedimentary facies, alongside age-depth modelling, has offered insights into the evolution of depositional environments within the three studied systems during the late Holocene. The inferred sedimentary evolution and geomorphological features revealing depositional forms in the landscape defined the depositional sedimentary morphodynamics within the lake basins.

## 6.1 Chronology

The sedimentation rates observed from the radiometric chronologies of FN1702, CL1703 and CVL1B sediment records (Figs. 4.15 and 4.17) are consistent with the sedimentary dynamics inferred from the facies identified (Tables 5.1 and 5.2), whereas lag periods derived from cross-correlation analysis between limnological data and instrumental meteorological datasets reveal the accuracy of age determination (Tables 4.8, 4.9 and 4.10). The rhythmite counts performed using thin sections throughout the profile of FN1704G match with the first ca. 40 years of the chronology obtained from the 210Pb and 137Cs profiles of FN1702 at annual time scale resolution (Fig. 4.16). This supports the seasonal frequency of deposition identified from the rhythmic succession of lithofacies and the stratigraphic relationships between them, confirming the formation of varves. Therefore, the rhythmite counts from FN1704G were used as an independent varve chronology (Fig. 4.16). However, the presence of 6-year time lags between summer temperatures and fall water column turnover strength, winter resuspension, and diatom productivity in Lake Funda suggests that the varved chronology of the FN1704G record is likely a floating chronology, possibly resulting from the absence of the topmost 4 cm of sediment.

### Funda lake sediments

The three AMS 14C dates of the FN1702 record showing reversal ages were considered inconsistent. The most plausible reason for these reversal ages is that they were analysed from samples located close to allochthonous coarse terrigenous sediments of lithofacies $T_D$ and D. This proximity likely resulted in the inclusion of reworked organic matter previously deposited in the catchment as demonstrated by the presence of plant debris in Lithofacies D at the sampling position of these radiocarbon dates (Fig. 4.3 and 6.1).

Sedimentation rates of the FN1702 record are consistent with macroscale observations (Fig. 5.1). The first stage shows relatively rapid sedimentation (from ca. 1000 to 525 yr cal BP) corresponds to the inferred shallow deltaic depositional environment of $Z1_{fun}$, where alluvial supply, including instantaneous deposits of debris flows from $F1_{fun}$, would have dramatically increased the sediment accumulation. The second stage displays relatively slow sedimentation rates (from ca. 525 yr cal BP to the present) corresponding to the deep pelagic scenario dominating the sedimentation of $Z2_{fun}$, where most of the alluvial supply remains relegated to proximal areas. These conditions would have partially prevented allochthonous contribution to sediment accumulation in pelagic areas. However, the decrease in the sedimentation rates do not match the change between depositional scenarios, occurring ca. 100 yr. later. The 100 years covering the biogeochemical RoC peak found at 600 BP

corresponds with the decrease in the sedimentation rate between $Z1_{fun}$ and $Z2_{fun}$, suggesting accelerated changes from that point with a response lag period of 100 years.

The correlation between the varves and temperature shows a 6-year lag, which could mean that it is a floating chronology due to the lack of the topmost 4 cm of FN1704G record (Table 4.9). The correspondence of $Z2c_{fun}$ with the period of high sedimentation rates found within FN1704G is explained by the high resuspension rates of $_{R}F3$ and the flashy deposits of Lithofacies $T_D$ (Fig. 4.4). In contrast, the correspondence between $Z2a_{fun}$ and $Z2b_{fun}$ with the period of relatively lower sedimentation rates is explained by the reduced resuspension. The correspondence with flashy Lithofacies D from $Z2a_{fun}$ would explain the relatively higher sedimentation rates shown at the lowermost 25 cm of FN1704G record (Fig. 4.15). However, previously to 1970 CE the compared chronologies ($^{210}$Pb dates from FN1702 and varve counts from FN1704G) mismatch (Figs. 4.15 and 4.16). This mismatch is interpreted as a result of a lack of inventory of the lowermost section of the unsupported 210Pb (Appleby, 1998) which in turn led to the aged chronology of the FN1702 record with respect to FN1704G, when establishing the CF:CS model.

During the time period within $Z2_{fun}$, the rapid sedimentation rates of the first substage of FN1704G chronology (from ca. 1750 to 1859 varve yr CE) corresponds with $Z2a_{fun}$ because this zone was dominated by a depositional scenario with relatively higher influence of catchment runoff. The relatively slow sedimentation rates of the second substage (from ca. 1860 to 1966 varve yr CE) corresponds with $Z2b_{fun}$ that likely was a depositional scenario dominated by relatively weakened thermocline and diminished catchment runoff, hampering the sediment accumulation in pelagic areas through alluvial supply and resuspension. The relatively high sedimentation rates observed in the third substage (from ca.1967 varve yr CE to the present) correspond with the depositional scenario dominated by relatively increased flooding state in the catchment and strengthen thermocline, promoting sediment accumulation through resuspension and turbidites derived from debris flows.

### Lake Caldeirão sediments

The relatively constant sedimentation rates during the ca. 3700 years within the CL1703 record reflects the homogeneous composition of the sediments mostly made up of massive muds. The broadly constant sedimentation rates of Caldeirão sediments are indicative of a deposition following relatively low frequency (low order) cycles of sedimentation within CL1703 (Fig. 4.4 and 4.15). The lack of reversal dates supports the dominance of primary sedimentation. However, slight sedimentation rate fluctuations corresponding with the last 1000 years of the CL1703 record correspond with a steady increase of the biogeochemical RoC, suggesting some rapid changes affecting the sedimentary dynamics within the Caldeirão lake-catchment system.

### Lake Caveiro sediments

Likewise, the excluded radiocarbon dates from Lake Funda sediments, the correspondence between the three reversal dates of CVL1B with Lithofacies E confirm the reworked nature of this lithofacies, derived from organic matter previously deposited in the catchment (Fig. 4.5). Furthermore, the lowermost excluded date was obtained from sediments of Lithofacies $V_W$ from $_{C}Z3_{cav}$ with a non-lacustrine origin. The two topmost dates were probably obtained from peaty reworked remains as from the peatland presence due to detrital buffering conditions of sedimentation deducted within $_{C}Z3_{cav}$.

The first stage of lower sedimentation rates of CVL1B chronology (from ca. 5200 to 1000 cal yr BP) corresponds with $_{C}Z1_{cav}$ and the lowermost section of $_{C}Z2_{cav}$ (up to 450 cm depth), which is composed of lithofacies P, $M_S$ $M_P$, and Q, characterized by low alluvial supply. A second stage of high sedimentation rates (from ca. 1000 cal yr BP to the present) corresponds to the topmost section of

$_{C}Z2_{cav}$ (from 450 cm depth) where Lithofacies E indicates higher alluvial supply, and with $_{C}Z3_{cav}$, composed of Lithofacies $M_{O}$, characterized by increased in-lake productivity.

## 6.2 Evolution of the depositional environments during the late Holocene

The textures, sedimentary structures and subfossil biotic assemblages shown by the lithofacies of FN1702, CL1703, and CVL1B records (Tables 4.2, 4.3 and 4.4) provide insights into the depositional environments (Table 5.3) (Last, 2001; Battarbee et al., 2001). Furthermore, the microlithozones composed by the rhythmic association of lithofacies (rhythmic microlithofacies) from the FN1704G record indicate higher frequency sedimentary responses to the processes associated with Lake Funda monomictic cycle. The biogeochemical CONISS applied to the fluxes of FN1702 (Fig. 4.6), CL1703 (Fig. 4.7), and CVL1B (Fig. 4.8) records (chemozones) correspond with the environmental associations of lithofacies, revealing the successions of depositional environments (Table 5.3). These depositional environments are discussed with previous interpretation of the aquatic habitats performed by Ritter et al (2022) for Lake Funda, by Raposeiro et al., (2021) for Lake Caldeirão, and by Marques et al., (2021) for Lake Caveiro.

Furthermore, ordination trajectory analyses indicate the evolution and intensity of the processes driving the sedimentation. Hereon, whenever the variability of PCA replicates the variability of RDA, only the former will be taken into account since they demonstrate to respond to the same sedimentary drivers and PCA explains more variability. Therefore, the correlation between lithozones, biozones and the inferred depositional scenarios (interplay between sedimentary drivers) into the stratigraphic zones offers insights into the physicochemical and biological conditions of the depositional environment (Table 5.3). Depositional stages corresponding with the stratigraphic zones are determined according to the chronology. The derived rate of compositional change (RoC) reveals accelerated depositional shifts. This combination allows the deduction of subaerial, transitional, and lacustrine environments. Additionally, it becomes possible to differentiate between shallow and deep lacustrine environments, further categorizing three deep sub-environments within the Funda system (Table 5.3).

Finally, the geomorphological analysis of recent depositional landforms, constituted by the catchment reliefs (Fig. 4.1) streams profiles (Fig. 4.2), the lake bathymetries (Fig. 4.1) and field analysis of Funda (Figs. 2.14 and 2.15), Caldeirão (Figs. 2.20 and 2.21) and Caveiro (Figs. 2.24and 2.25) systems revealed peatlands, lacustrine terraces abandoned in the catchments, and submerged alluvial and delta fans. These depositional landforms, in relation to the stratigraphic zones (Kashiwaya, 2017), constitute recent morphostratigraphic surfaces (e. g., Hugues, 2024), indicative of the three-dimensional sedimentary evolution. The derived spatiotemporal patterns of sedimentation reveal the sedimentary budgets released within the lakes through time, whereas the morphostratigrapic surfaces reveal the recent aftermath of morphodynamical patterns of sedimentation in the three systems.

| **Sediment record** | **Chemozone**<br>Environmental association of chemofacies | **Lithozone**<br>Lithofacies environmental association | **Depositional conditions** | |
|---|---|---|---|---|
| | | | **Sub-environment** | **Environment** |

<table>
<tr><td rowspan="5">FN1702 and FN1704G (Funda)</td><td rowspan="3">$_{C}Z2_{fun}$<br>$_{C}F1_{fun}$<br>(Debris flows)<br>$_{C}F2_{fun}$<br>(Organic matter accumulation)<br>$_{C}F3_{fun}$<br>(Resuspension)</td><td>$_{ML}Z2c_{fun}$<br>$_{R}F3$<br>(Diatom blooms decantation during strengthen and persistent summer thermocline rapidly eroded (commonly by alluvial floodings) provoking deep resuspension during fall turnover)<br>$T_{D}$<br>(Turbidity currents)</td><td>Warmer and deep epilimnion with intense runoff</td><td rowspan="3">Deep pelagic lacustrine</td></tr>
<tr><td>$_{ML}Z2b_{fun}$<br>$_{R}F2$<br>(Rapid-to-progressive deep fall turnover triggered by thermal decrease and diatom blooms decantation during summer)</td><td>Warm and deep summer epilimnion and low runoff</td></tr>
<tr><td>$_{ML}Z2a_{fun}$<br>$_{R}F1$<br>(Rapid and shallow fall turnover triggered by persistent runoff and diatom blooms decantation during summer)<br>D<br>(Distal debris flows)</td><td>Cold and shallow summer epilimnion with persistent winter runoff</td></tr>
<tr><td>$_{C}Z1_{fun}$<br>$_{C}F1_{fun}$<br>(Debris flows)<br>$_{C}F2_{fun}$<br>(Organic matter accumulation)</td><td>$_{L}Z1_{fun}$<br>$M_{S}$<br>(Organic matter accumulation during lake installation)<br>D<br>(Distal and proximal debris flows with erosive traction)</td><td colspan="2">Relatively shallow lacustrine delta front in sublittoral area dominated by in-lake processes</td></tr>
<tr><td>-</td><td>$_{L}Z0_{fun}$<br>D<br>(Proximal debris flows with erosive traction)<br>$M_{S}$<br>(Organic matter accumulation during lake installation)</td><td colspan="2">Shallow lacustrine delta plain in littoral area dominated by alluvial processes</td></tr>
</table>

| | | | |
|---|---|---|---|
| **CL1703 (Caldeirão)** | **$_{C}Z5_{cald}$** $F4_{cald}$ | **$_{L}Z5_{cald}$** $M_A$ | Shallow lacustrine and pelagic relatively proximal. Relatively low turbidity |
| | **$_{C}Z4_{cald}$** $F2_{cald}$ | **$_{L}Z4_{cald}$** $M_A + E + MP$ | Relatively shallow to deep lacustrine and pelagic distal to proximal. Relatively low turbidity. Aerophilic influence |
| | **$_{C}Z3_{cald}$** $F3_{cald}$ | **$_{L}Z3_{cald}$** MI | Shallow lacustrine and pelagic relatively proximal. Lake margin instability exposed margins. |
| | **$_{C}Z2_{cald}$** $F2_{cald} + F1_{cald}$ | **$_{L}Z2_{cald}$** E + MP | Transition from pelagic distal ($_{C}Z1_{cald}$) to proximal ($_{C}Z3_{cald}$). Relatively high turbidity |
| | **$_{C}Z1_{cald}$** $F1_{cald}$ | **$_{L}Z1_{cald}$** E + MP | Relatively shallow lacustrine and pelagic relatively distal. Saprobic and acid influence (Peatlands) |
| **CVL1B (Caveiro)** | **$_{C}Z3_{cav}$** $F3_{cav}$ | **$_{L}Z3_{cav}$** $M_O$ | Shallow lacustrine in pelagic area. Acid and saprobic with consolidated peripheric peatland |
| | **$_{C}Z2_{cav}$** $F3_{cav} + F2_{cav}$ | **$_{L}Z2_{cav}$** $MI + M_P + E$ | Shallow lacustrine in lake margin. Acid and saprobic with degrading peripheric peatland |
| | **$_{C}Z1_{cav}$** $F3_{cav} + F1_{cav}$ | **$_{L}Z1_{cav}$** $M_S + P + Q$ | Sublittoral shallow lacustrine to palustrine and peaty in lake margin. Poorly sealed basin. |
| | **-** | **$_{L}Z0_{cav}$** $V_W + V_L + C + M_S$ | Alluvial/colluvial and/or volcanic basement during incipient lake installation |

*Table 5.3: Depositional environments inferred from facies associations within stratigraphic zones.*

### 6.2.1 The Funda lake-catchment system

In summary the Lake Funda bathymetry constitutes a morphostratigraphic indicator (e. g., Hugues, 2024) of the most recent morphologic evolution of the sedimentary wedges within the lake. The delta plain morphology revealed by the bathymetric domain B may have corresponded with $Z0_{fun}$ before 1000 cal yr BP, whereas, the delta front morphology constituted by the steep bathymetric sector (E) could match the relatively deeper sedimentation of $Z1_{fun}$ (Fig. 4.1). The intermediate lake level deducted for the first subperiod of $Z1_{fun}$ may have reached a depth around ca. 20 m below the current water lamina, as indicates the slope break composing the delta (Fig.4.1). After profundization, in $Z2_{fun}$, alluvial supply gets relegated to the $St4_{fun}$ mouth to compose the steeper alluvial fan, crystalizing the deltaic morphology under a mantle of decanted material derived from $F3_{fun}$. During the deposit of the deep $Z2_{fun}$ after 600 cal yr BP. A first stage of relatively shallower lake levels may

have left exposed the alluvial fan (Fig. 2.15e). There a coastal environment could have been the responsible of the growth of the epiphitic diatoms and macrophytes, reworked into Lithofacies $M_D$ and especially within Lithofacies D, where diatoms still conserve the life disposition attached to the macrophyte rests (Fig. 4.3).

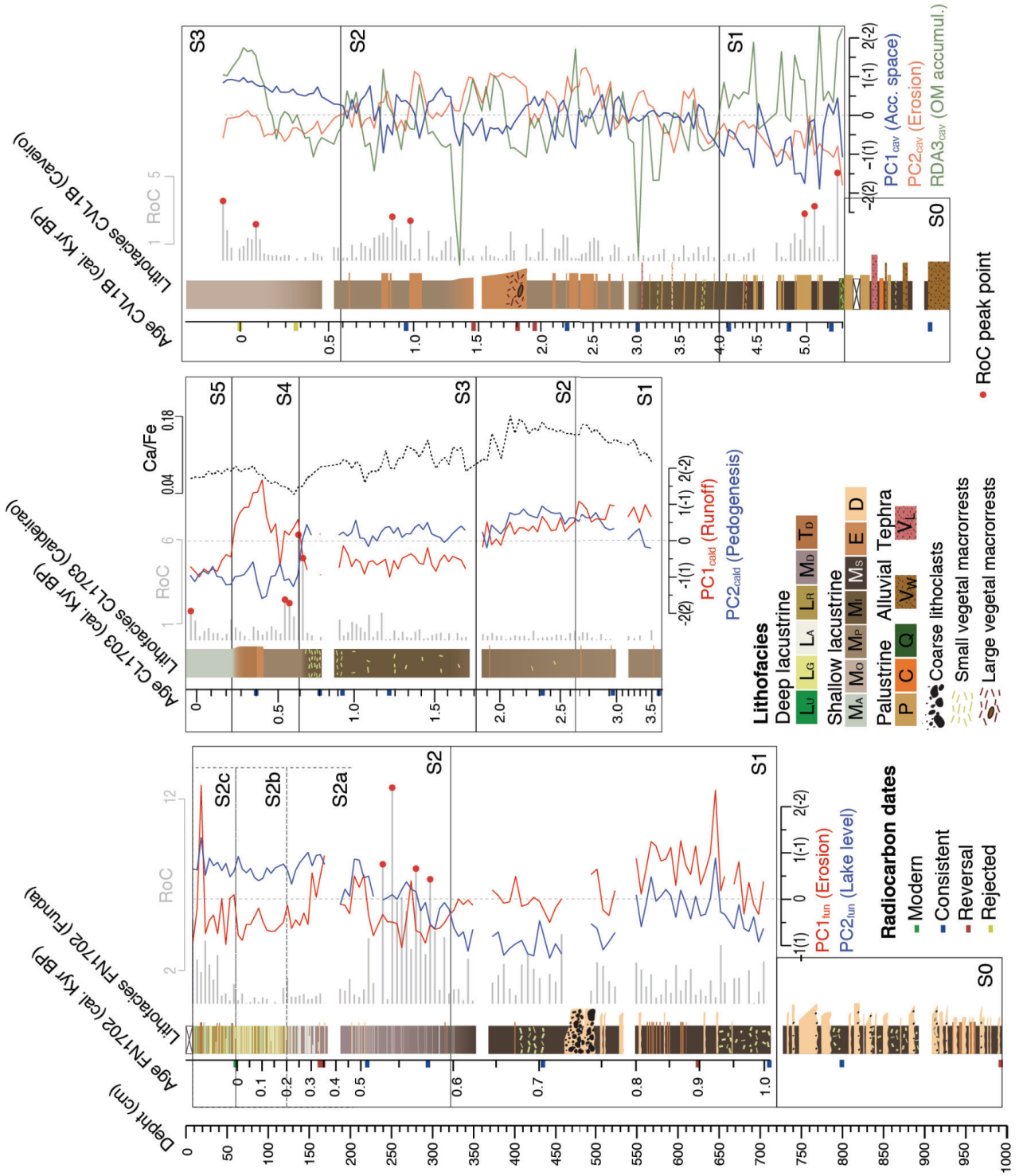


*Fig. 6.1: Interpretation of the sedimentary stages, indicating the lithofacies, radiocarbon dates, RoC and ordination trajectory analyses of the interpreted sedimentary drivers and identified along the depth profile of FN1702, CL1703 and CVL1B records.*

### Stage 0 (before 1000 cal. yr BP) – Littoral shallow lacustrine environment.

The lithozone $Z0_{fun}$ corresponding with this stage 0 (before 1000 cal yr BP) indicates a shallow lacustrine depositional environment strongly affected by alluvial supply in the littoral zone. Within

$Z0_{fun}$, the dominance of normal graded and erosive deposit of Lithofacies D indicates the deposition in littoral zone, since debris flows rapidly lose the kinetic energy when entering into the lake due to the plastic rheology of the tractive bedload frictioning the lakebed (Shanmugam, 2013) (Fig. 1.18). The inclusion of Lithofacies $M_S$, containing (D1 from Ritter et al., 2022; Fig. 2.17) opportunistic diatoms remains (*Achnanthidium minutissimum*; Marques, 2021), may indicate the renewing conditions of benthic habitats during stable sedimentation after debris flow events. These conditions are indicative of littoral sedimentation in proximity to alluvial streams mouth, probably corresponding to a submerged delta plain (Tye and Coleman, 1989). The proximal depositional environment dominating the sedimentation during this stage is supported by the flat bathymetric domain C, whose edge lies close to FN1702 and FN1704G core recovery location. This bathymetric domain is interpreted as the most recent expression of an old delta plain submerged at ca. 20 m depth (Fig. 4.1), which could have been dominating sedimentation at FN1702 core position before 1000 cal yr BP. Delta plain sedimentation may have induced the littoral depositional environment widely affected by alluvial supply during this stage. Consequently, before 1000 BP, lake levels could have been ca. 20 m lower than the current water lamina height.

### Stage 1 (from ca. 1000 to 600 cal yr BP) – Sublittoral shallow lacustrine environment

The trajectory analysis of $PCA_{fun}$ showing coupled fluctuations between erosion rates ($PC1_{fun}$), and lake level ($PC2_{fun}$) indicates runoff fluctuations supplying sediments and water to the lake. These fluctuations may have been driven by hydroclimate prior to the anthropic landscape transformation. Similar lake environmental conditions were interpreted by Ritter et al. (2022), corresponding with the named pre-shift phase A when runoff in littoral conditions, and high supply of allochtonous organic matter was released, affecting the biotic assemblages of diatoms and chironomids. These biotic assemblages mainly responded to climate changes rather than anthropic forcings and/or lake internal dynamics (Ritter et al., 2022).

Two subperiods are recognized during this stage 1. Intermediate to high erosion rates and low to intermediate lake levels dominated the first subperiod (from ca. 1000 to 800 cal yr BP) indicating high runoff. The distal alluvial Lithofacies $T_D$ dominates the environmental association of lithofacies, showing increased frequency of deposition to the end of the subperiod associated with high runoff This indicates more deposition of turbidity currents triggered by debris flows. The picnal plumes derived from turbidity currents travel longer distances in suspension than debris flows (Fig. 1.18) decanting at more distal positions (Shanmugam, 2013). Therefore, in comparison to the proximal littoral sedimentation inferred for stage 0, distal alluvial sedimentation during this stage 1 may have been favoured by relatively deeper conditions in the sublittoral zone. Therefore, the lithofacies deposited during this stage likely indicates a lake deepening due to increased runoff water supply, leading to a transition from distal alluvial to delta front depositional environments (Lemons and Chan, 1999). At the end of this subperiod (around 1200 CE), the diatom and chironmid assemblages described by Ritter et al. (2022) indicate water level oscillations due to frequent and intense runoff episodes, supporting the enhanced alluvial supply. Furthermore, the identification of Chironomus anthracinus-type and Psectrocladius sordinellus-type taxa, which typically associate with lake littoral zones, supports this hypothesis (Ritter et al., 2022; Raposeiro et al., 2018; Fig. 2.17).

During the second subperiod (from ca. 800 to 600 cal yr BP), low lake levels ($PC2_{fun}$) independently evolving from intermediate erosion rates ($PC1_{fun}$) indicate the cease of high runoff, leading to the prevalent organic accumulation of Lithofacies $M_S$ driven by leaching and endogenic biosynthesis. Mesotrophic conditions were revealed by diatoms and chironomid assemblages during this subperiod confirming the low influence of catchment runoff and the related erosion (Ritter et al., 2022). The deposit of the coarsest and thickest layer of the record of Lithofacies D occurring at ca. 750 cal yr BP under low runoff rates might be explained by reduced interstitial pressure within sedimentary wedge leading to landslides (daCosta, 2015), however further evidence is needed to

confirm this. Although low runoff rates are deducted, under lowstand conditions alluvial incision and distal progradation are favoured over the exposed delta plain where isolated runoff episodes could have triggered these thick coarse deposits.

In general, this stage indicates sublittoral deposition with alluvial influence that might correspond to the recent delta front geomorphology deducted from the steep and deep bathymetric domain E, in correspondence with the location of FN1702 (Fig. 4.1). The sedimentation in this depositional environment during the first subperiod (from ca. 1000 to 800 cal yr BP) was dominated by distal alluvial supply due to increased runoff inducing higher catchment erosion rates, modulated by the partial submersion of the flat delta plain under higher lake levels. In contrast, the delta plain exposition during lower lake levels of the second subperiod (from ca. 800 to 600 cal yr BP) may have favoured the alluvial incision of the delta plain leading to the deposition of thick debris flows.

### Stage 2 (from ca. 600 cal yr BP to the present) – Pelagic deep lacustrine environment

During this stage 2 (from ca. 600 cal yr BP to the present) (Fig. 6.1), the sedimentary composition of $Z2_{fun}$ indicates deep pelagic environment dominating Lake Funda sedimentation. The Lithofacies $M_D$ in correspondence with $F2_{fun}$ includes a mix of planktonic, benthic and littoral epiphytic diatom remains that indicate allochthonous organic accumulation in transitory lake deep conditions. In turn, the prevalent organic accumulation of $F3_{fun}$, dominated by planktonic diatom remains of the laminated sediments of Lithofacies L, indicates resuspension, and resettlement through decantation, with the derived diatom blooms remains, in a deep and pelagic lacustrine environment (Fig. 4.6 and 6.1).

The trajectory analysis of $PCA_{fun}$ reveals the lake deepening which induced the buffering of erosion rates. The orthogonal trend imposed in $Z2_{fun}$ over the one detected in $Z1_{fun}$ (Fig. 4.12) indicates the uncoupling between erosion rates and lake level fluctuations, becoming the lake level the main sedimentary driver. These depositional conditions may indicate the response of the system to deforestation (Raposeiro et al., 2021; Ritter et al., 2022). This is evidenced by the accelerated compositional changes shown by RoC analysis at a first subperiod (from ca. 600 to 500 cal yr. BP) that reveal four peak points reaching values of up to 12. Since the system is hydrologically closed and presumably well sealed, the orthogonal trend imposed in the trajectory analysis in stage 2, to the one dominating stage 1 when runoff dominated erosion, indicates increased water balance derived from a different forcing mechanism. This mechanism is interpreted as reduced evapotranspiration due to reduced vegetal cover (Ritter et al., 2022). Positive water balances trigger the progressive decrease of erosion rates due to deepening conditions as lake level increases. A transitional depositional environment during this 100 yr. matches the ecological shift evidenced by Phase B in Ritter et al. (2022), where human impact is dominating the variability of the biotic assemblages (Fig. 2.17). This variability shows the reduction of the forest cover suggested by a reduction of arboreal pollen and the lake level rise evidenced by the shift from benthic to planktonic diatom species (Fig. 2.17). Since proximal deltaic conditions were inferred in the previous stages 1 and 0, the lake deepening might be related with a prominent shoreline migration due to the delta plain flooding. The retrogradation facies evidences this retreatment, leading to pelagic conditions lasting up to the recent times, inducing the sedimentary cascading buffering (Burt and Allison, 2010).

Furthermore, deep conditions drive the formation of a thermocline, establishing the feedback loop between microbes and diatoms which induces the sedimentary model dominated by resuspension episodes triggered by fall turnover (Ritter et al., 2022). Specifically, the varves composition, texture and bedding reflect the sedimentary response to the seasonal environmental fluctuations driven by the interplay between Lake Funda monomictic cycle and the wet season catchment organic supply. The materials provenance and disposition within the dark laminae indicate variable accumulation of organic matter, driven either by catchment supply ($F2_{fun}$) or by the resuspension of this supply ($F3_{fun}$).

The disposition of the dark laminae has variable expression depending on the mobilization process: 1) resuspension, directly related to thermal distribution within Lake Funda during the summer and 2) catchment leaching and alluvial supply during the wet season, restoring the budget of light sediments in shallow proximal areas for resuspension. During fall turnover, the summer thermocline depth determines the lakebed extension and depth affected by resuspension. The strength of the thermocline determines the shear stresses affecting lakebed disaggregation, further dependent on the lakebed sediments cohesion (e.g., Bloesch, 1995). The disposition and composition of the pale laminae indicate variable conditions conditioning the competitive advantages of specific diatom species over the rest from lithofacies L. Depending on turbulence, turbidity, trophic state, and light penetration, among other factors, diatom remains composition in the pale laminae varies with time gradients in the environmental conditions. Moreover, the varves preservation may indicate the meromictic conditions of the lake, with partial or totally anoxic bottom waters (Anderson and Dean, 1988).

The varved sequence is episodically interrupted by distal lithoclastic deposits of lithofacies $F1_{fun}$. These deposits have been interpreted as exceptional runoff events. The interplay between summer stratification and catchment materials mobilisation is recorded in three different ways revealing three distinct depositional sub-environments within the $Z2_{fun}$. The lower RoC values of ca. 1 during this stage after the peaky pattern (Fig. 6.1), in comparison with the stage 1 which was alluvially dominated (enhanced erosion interrupting endogenic sedimentation due to storms) evidences the alluvial buffering and the regular influx of endogenic material. Conversely, this buffering points to a new sedimentary condition that corresponds to the eutrophic ecological state that Ritter et al (2022) defined as a travel with no return ticket covering the subsequent substages:

> Substage 2a (from ca. 500 to 200 cal yr BP) – Cold and shallow summer epilimnion with persistent winter runoff.

During this substage (from ca. 500 and 200 cal yr. BP) lake deepening relegated alluvial supply to the Funda maar crater walls, where water cascades derived from catchment streams might have supplied with coarse materials prominent alluvial fans. This is evidenced by the depositional landforms observed in field analysis at the mouth of $St4_{fun}$ which nowadays is almost submerged (Fig. 2.15e). The excursion shown by samples 33 to 39 to the quadrant defined by high lake level and erosion rates (right-down), following in turn the former trend observed in $Z1_{fun}$ (Fig. 4.12), evidences this paralimnetic depositional scenario. From there, alluvial floods rework the coarse materials stored in the alluvial fans to compose the distal debris flows/turbidites within the lake (Lithofacies $T_D$ and D; Fig. 4.3). This excursion supports the enhanced runoff conditions during all the stage 2a that might correspond to the partial recovery of prominent driving catchment floodings. In fact, this subperiod corresponds to the LIA, which in the Azores region is evidenced as a humid period (Björck et al. 2006). Ritter et al., (2022) also reported high climatic variability, leading to rapid changes in the ecosystem during this substage. Furthermore, within $Z2a_{fun}$, the distal debritic composition of $F1_{fun}$ in agreement with $_RF1$ within $Z2a_{fun}$ aligns with the deducted runoff enhancement in the catchment, further allowing to infer flooding events driving littoral reworking. This is shown by the concentrations of epiphytic diatom remains with relatively large vegetal rests indicating nearshore turbulence (Fischer and Eckmann, 1997; Cohen, 2003) (Fig. 4.11).

In the $Z2a_{fun}$, the $_RF1$ pattern varves indicate the seasonal interplay between catchment runoff and weak lake water column turnover in a depositional sub-environment dominated by intermediate depth (ca. 15 m) in a proximal environment. In the dark laminae, the littoral provenance of the epiphytic diatoms and macrophyte remains within Lithofacies $M_D$ indicates the accumulation of allochthonous organic matter derived from catchment alluvial processes in a relatively shallow sublittoral environment during the wet season ($F2_{fun}$). Furthermore, the compact flocculated

disposition of the sediments within Lithofacies $M_D$ indicates partial disaggregation of the allochthonous organic material accumulated in the lakebed, induced by fall resuspension. The inability to induce complete lakebed disaggregation, may derive either from slight shear stresses derived from weaker summer thermocline or relatively enhanced compaction from primary organic matter accumulation, and more likely from a combination of both factors. The dark lamina is also indicative of colder lake waters during the summer, by inducing a relatively weakened and shallower thermocline. These conditions would prevent from the loss of organic matter previously accumulated during the wet season, by inducing low shear stresses and removal towards deeper parts of the lake during fall turnover. The dominance of *Aulacoseira ambigua* diatom remains in Lithofacies $L_A$, which composes the pale laminae of $_R$F1, confirms the colder lake waters conditions during the summer (Denise, 2016). his diatom species has competitive advantage in mesotrophic, low lighten, mixed waters (Houk, 2003; Taylor et al., 2007; Denise, 2016), what could be favoured by the partial disaggregation of the organic matter, that retains nutrients within the suspended floccules observed in the dark laminae, limiting the bioavailability in the photic zone during the growing season.

### Substage 2b (from ca. 200 to 0 cal yr BP) – Warm and deep summer epilimnion with low runoff.

In the $Z2b_{fun}$, the $_R$F2 pattern of the varves indicate organic accumulation in a deep pelagic depositional environment. In the dark lamina, the planktonic diatoms dominate the subfossil biotic assemblage of Lithofacies $L_R$, which has an untied layout and is made up of fine organic matter flakes, indicating thereby resuspended shallower and proximal materials focusing into pelagic areas during the resettlement (e.g., Bloesch, 1995). The loose dispositions and diffuse top transition of Lithofacies $L_R$ indicate the resettlement of the particulate material derived from resuspension during winter mixing and spring progressive stratification. Contrarily to *A. ambigua*, *Aulacosira Granulata var. angustissima* prefers eutrophic and turbulent conditions (Taylor et al., 2007; Denise et al., 2006; Vázquez-Loudeiro et al., 2023). Therefore, the accumulation of *A. Granulata var. angustissima* of Lithofacies $L_G$ in the pale laminae of $_R$F2 would indicate enhanced resuspension due to stronger water mixing during fall turnover. These conditions may have occurred in a deep environment and a warm summer epilimnion, due to a strengthened summer thermocline, by inducing higher lake bottom shear stresses in marginal areas during fall turnover and higher turbulence due to enhanced convection during winter mixing period.

### Substage 2c (from ca. 0 cal yr BP to present) – Warmer and deep epilimnion with intense runoff:

In the $Z2c_{fun}$, the $_R$F3 pattern of the varved sequence indicate the presence of a deep and persistent thermocline due to hot epilimnion waters in summer and an increase of floodings within the catchment. The inclusion of the Ulnaria complex araphidic diatoms of Lithofacies $L_U$, over Lithofacies $L_G$ in the pale laminae of $_R$F3a, would indicate longer persistence of summer stratification than in $Z2b_{fun}$. In these conditions water column turbulence may become minimal, what may confer araphidic diatoms a competitive advantage over *Aulacoseira ambigua var. angustissima* which has preference for turbulent environments (Taylor et al., 2007; Denise et al., 2006; Vázquez-Loudeiro et al., 2023). The persistence of summer stratification means higher summer epilimnetic temperatures. Thus, when the Lithofacies $L_G$ lacks in the pale laminae ($_R$F3b) may indicate exceptional rapid summer stratification due to warmer conditions promoting storminess. Futhermore, the normal graded deposits with sharp bottom and diffuse top of Lithofacies $T_D$, constituting the transition between lithofacies L and M, would indicate the thermocline breakdown tiggered by alluvial floods and associated debris flows This would result in the turbidites recorded within $Z2c_{fun}$, confirming the distal pelagic conditions of sedimentation, evidencing the stormy conditions.

### 6.2.2 The Caldeirão lake-catchment system

Within the Caldeirão system, the lithofacies of CL1703 record (MP, MI, MA and E) are dominated by benthic diatom assemblages, indicating prevalent shallow lacustrine conditions dominating the sedimentation. Nevertheless, distinct biotic associations allowed inference of different benthic habitats with variable shallow conditions. The trajectory analysis (Fig. 6.1) reveals the interplay between surface runoff and pedogenesis affecting the lake ecosystems through controlling the water table and the dissolved nutrients release from soils. Furthermore, the horizontalized topo-bathymetric domain constituted by the flat bottom of the caldera, including the low erodible domain 1 and the plate-like bathymetry of Lake Caldeirão (Fig. 4.1) may favour benthic habitats diversity. This morphologic configuration is one of the main environmental factors controlling sediment cascading within Lake Caldeirão (Fig. 4.13) and, consequently, the environmental evolution within this lake catchment system has been discussed using the Ca/Fe ratio, which is indicative of pedogenetic inputs into the lake (Elbert et al., 2013). The $PC2_{cald}$, interpreted as pedogenesis, shows very high correspondence with Ca/Fe ratio during the evolution of the Lake Caldeirão sedimentation, confirming the sedimentary model proposed for Lake Caldeirão, where soil formation is highly involved in lake sedimentation, through the reduction of the grain size prior to alluvial mobilization on the flat subaerially exposed areas of domain 1.

#### Stage 1 (from ca. 3700 to 2700 cal yr BP) – High runoff and pedogenesis

During this stage 1 (from ca. 3700 to 2700 cal yr BP), the trajectory analysis of $PCA_{cald}$ indicates very high runoff and intermediate to high pedogenesis. The recurrent occurrence of thin laminae of Lithofacies E composed of degraded organic matter and high mineral content (Fig. 4.4), in turn related to Br (samples 83 and 90; Fig. 4.13), suggests frequent stormy conditions (Unkel et al., 2010) prevailing over the WG during this time period. These conditions might have favoured very high runoff, occasionally provoking soil instability. For this time period, Björck et al. (2006) provide evidence of partially wet conditions in an overall unstable climate, which might be related to the stormy conditions interpreted from high runoff rates and tempestites of the Caldeirão system. This higher hydrological availability corresponding to high runoff rates would have also favoured soil formation through hydrolysis (Schaetzl and Anderson, 2005; Depetris et al., 2014) and the dominance of the dense and extended *Juniperus brevifolia* forests reported by Raposeriro et al. (2021) and Connor et al. (2024). This vegetal cover would also have contributed to higher pedogenetic rates through organic matter supply, humidity and soil particles retention, and roots biodegradation (Schaetzl and Anderson, 2005; Depetris et al., 2014). Furthermore, high runoff rates might have favoured higher lake levels flooding the flat domain 1 and forming marshes. These marshes induced peatland formation between the scoria cones, and mineral soils elsewhere, covering the alluvial fans and scoria cones (Fig. 2.19).

The organic fraction dominated by acidophilic diatom remains within Lithofacies $M_P$ indicates a depositional environment under the influence of catchment mineral soil formation and peatland leaching, supplying silicic and humic acids, and resulting in acidic lake waters (Schaetzl and Anderson, 2005). Furthermore, the prevalent accumulation of sapropel and saprophilous diatom remains in Lithofacies $M_P$ suggests a distal pelagic depositional environment associated with extended coastal benthos and enhanced organic supply into the lake, derived from enhanced soil formation. This might be favoured by the lake water level rise extending across flat domain 1. Despite the arrival of acidic waters into the lake, the exposed conditions would have prevented detrital inputs, favouring a prevalent organic accumulation in distal pelagic zones. It can be interpreted that high runoff rates, inducing a well-recharged hydrological system, favoured frequent interactions between the soil and the surrounding forests during this stage. Occasionally, extraordinary and very high runoff rates resulting from storm events could threaten soil stability. However, the root system of the

forests played a key role in the soil stability through processes such as pedogenesis and soil retention.

### Stage 2 (from ca. 2700 to 1800 cal yr BP) – High to low runoff and pedogenesis

During the stage 2, the trajectory analysis of $PCA_{cald}$ shows a high-to-intermediate decreasing trend for runoff rates, but the highest pedogenesis rates for a first substage (from ca. 2700 to 2100 cal yr BP). For a second substage (from ca. 2100 to 1800 cal yr BP) runoff rates are intermediate and pedogenesis sharply drops to intermediate rates as well. In more detail, at ca. 1900 cal yr BP, a peaky pattern of runoff, corresponding with low pedogenetic rates may be revealing a storm event triggering increased runoff provoking soil erosion. The organic composition dominated by acidophilic diatom remains of Lithofacies $M_P$ and $M_I$ indicates a depositional environment under the influence of catchment soil formation and peat accretion, acidifying the lake waters through leaching. However, the composition of these two lithofacies blurring during the transition between the two exposed substages suggest ecological changes derived from a lake water level drop exposing the highest areas of the lake margins. This transition to drier conditions is also evidenced by the aridification determined by Björck et al., (2006). However, the same authors proposed a wet excursion roughly corresponding with the stormy event at ca. 1900 cal yr. BP in Caldeirão, indicating a tie point between both records. This tie point may correspond with tropical cyclonic conditions affecting the complete Azorean region. Hence, this stage corresponds with a progressive environmental transition where the first substage is dominated by similar conditions to stage 1, whereas the second substage evidences the reduction of the hydrological recharge of the system.

### Stage 3 (from ca. 1800 to 600 cal yr BP) – Low runoff and intermediate pedogenesis

During this stage, pedogenesis dominates the sedimentation over runoff, both remaining constant during the whole time period. At ca. 1000 cal yr BP the slight increase of RoC (Fig. 6.1) may correspond to the first inhabitant arrival into the archipelago performing the first landscape transformation (Raposeiro et al. 2021).

In contrast, the accumulation of tychoplanctonic and aerophilic diatom ooze (Lithofacies $M_I$) suggests a pelagic depositional environment associated with reduced coastal benthos. The accumulation of the Fragilaria sp. would indicate lake margins instability, whereas the aerophilic *Pinnularia perirrorata* may indicate exposed lake margins and enhanced bypass. In turn, the dominant accumulation of *Aulacoseira pergrabla* indicates enhanced mixing of the lake waters. Moreover, high concentration of vegetal rests in Lithofacies $M_I$ would support a depositional environment dominated by a fall of the lake water level allowing for vegetal cover growth closer to pelagic environments. Furthermore, the association of these lithofacies with fine clay particles in $F1_{cald}$ and $F3_{cald}$ may indicate deposition under relatively turbid lake waters.

### Stage 4 (from ca. 600 to 250 cal yr BP) – High runoff and soil degradation

During this stage 4, the trajectory analysis performed on $PCA_{cald}$ indicates increased runoff rates corresponding with a prominent drop of pedogenesis revealing soil degradation. The onset of this stage also corresponds with RoC peak points at ca. 600 cal yr BP, indicating that this sedimentary stage responds to the aftermath of the profound ecological shift performed by Portuguese colonizers through deforestation (Raposeiro et al., 2021, Connor et al., 2024). In more detail, a first substage, from ca. 600 to 450 cal. yr BP, shows intermediate runoff rates and a prominent drop of pedogenesis. Soil degradation reached the highest values of the record due to the rapid loss of vegetal cover, which may indicate the system responses to a positive feedback between human and climate.

Coupling with the humid conditions of the LIA (Bjorck et al., 2006; Hernandez et al., 2017; Raposeiro et al. 2024) may have provoked a positive water balance in the system due to diminished evapotranspiration and increased recharge, causing a prominent lake level rise (Raposeiro et al.,

2021). The trajectory analysis in $PCA_{cald}$ dominated by runoff indicate that the flat morphology revealed by Lake Caldeirão bathymetry and the low erodible domain 1 may have favoured lake area changes rather than water column depth as the response to increased water balance. Lake water level changes in the Caldeirão system therefore may have flooded the domain 1, where soils are predominantly located on this system. Afterwards, the second substage, from ca. 450 up to 250 cal yr BP, corresponds to extreme runoff rates and the highest soil loss of the record. In these conditions the detrital supply by reduced soil retention would prevail as  indicates the association of these lithofacies with $F2_{cald}$ and $F4_{cald}$ which are depleted in montmorillonite and enriched in feldspar and augite lithorelicts. Moreover, the dominance of lithic compositions and reddish tones within Lithofacies $M_A$ and E indicate proximal pelagic depositional environments affected by catchment soil degradation.

#### Stage 5 (from ca. 250 cal yr BP to present) – Low runoff and soil degradation

During this last stage low runoff and pedogenesis prevailed. This is attributed to the persistence of soil degradation with the complete loss of forest cover (Raposeiro et al., 2021; Connor et al., 2024) further favoured by arid conditions (Bjorck et al. 2006). Higher RoC values at the onset of this stage, corresponding with CONISS stage change at ca. 250 cal yr BP, and the occurrence of Lithofacies $M_A$ until the present may be attributed to streams damming (Fig. 2.19b; c; e). With the onset of the dry conditions, lake water level dropped and it may have led the lake floor to subaereal exposure at the flat topobathymetric domain of the caldera bottom.  These environmental conditions may have unbalanced the profile of the streams, enhancing the bypass and soil erosion (Fig. 1.15a,b). Soils might be already unconsolidated due to the poor root retention and pedogenesis on the lake margins and exacerbated soil erosion occurring since deforestation throughout the watershed due to base level changes. This association also indicates a decrease of suspended particles and dissolved silica release into the lake waters. Therefore, clearer lake waters with lower bioavailable silica contents favours green algae thrive, which would have found competitive advantage in detriment of diatoms. Green algae photosynthetic activity may have released large amounts of oxygen into the water column leading to the endogenic precipitation of hematite as a consequence of oxygen release, as indicated by the association of Lithofacies $M_A$ with hematite in $F4_{cald}$ condition. Therefore, $F4_{cald}$ indicates organic accumulation in clear oxygenated waters.

### 6.2.3 The Caveiro Lake-catchment system

The lithofacies analysis revealed variable concentrations of oxidised organic matter and no glass shards concentrations in the light brown to reddish lithofacies P and E (Fig. 4.5; Table 4.2), which likely correspond to the assumed tephras identified by Bjorck et al. (2006). However, they did not perform a microlithofacies analysis. The reddish tones induced by partially decomposed and oxidized organic matter were likely macroscopically described as light-brown facies and interpreted as ash deposits by Björck et al. (2006). Nevertheless, the detailed lithofacies analysis carried out here revealed tephra contributions which would derive from Pico Island volcanic activity, but in the form of primary lapilli (Lithofacies $V_L$) and much less frequent as previously suggested (Björck et al., 2006). Therefore, the impact of volcanic activity in Lake Caveiro sedimentation may have had less influence than previously thought. A PhD thesis and several congress publications from different paleolimnological perspectives have addressed paleoenvironmental reconstructions using the Caveiro system sedimentary infill (Marques, 2021; Raposeiro et al., 2017; 2018; Hernandez et al., 2018; Benavente-Marín et al., 2022; Giralt et al., 2017: Cabral, 2018; Johansson, 2015). However, publications following the large contribution of tephra deposits to the sedimentary model proposed by Björck et al. (2006) are scarce (Connor et al., 2012).

The $PC1_{cav}$ constitutes the chemical signal of changes in the accommodation space and $PC2_{cav}$ of detrital allochthonous supply, therefore the interplay between both sedimentary drivers has been

interpreted in terms of sequential chemostratigraphy. The interpretations have been supported by biostratigraphic clues from lithofacies analysis and lithostratigraphic evidence from the adjacent sedimentary record obtained from a peatland (CVT1C; Sáez et al., in preparation). Furthermore, hydroclimatic inferences from Björck et al., (2006) and the biostratigraphic zones and phases determined by Marques, 2021 (Fig. 2.23) further contributed to the discussion of the evolution of the proposed depositional environments.

### Stage 0 (before ca 5200 cal. yr BP) – Alluvial sedimentation.

Within the Caveiro system, the environmental association of lithofacies composing $_{L}Z0_{cav}$ indicates subaerial to lacustrine depositional conditions (Table 5.3). The Lithofacies $V_W$, consisting in both the weathered scoria fallout from the of São Roque Piedade volcanic Complex eruptions and the alluvial reworking of these materials, corresponds to the Cabeço do Caveiro crater basement where the lacustrine sedimentary infill lies. The alternance of subaerially altered scoria from lithofaces $V_W$ with organic deposits of Lithofacies $M_S$ is interpreted as depositional environment in permeable (low sealed) conditions that hardly allowed the accumulation of water for long time periods. In fact, Lithofacies $M_S$ includes opportunistic diatoms (*Achnanthidium minutissimum;* Marques, 2021) that could respond to incipient lake formation conditions. Besides, the coastal environment suggested by Lithofacies C corresponding with $V_W$ and $M_S$ supports the subaerial to lacustrine transitional conditions, where piezometric fluctuations close to the topography might occur. Furthermore, the lapilli from Lithofacies $V_L$ indicates volcanic activity in Pico Island during lake formation (Sabatier et al., 2022). The adjacent peatland record (CVT1C) also reveals the basement at ca. 12 m depth, constituted by weathered lapilli that may correspond to Lithofacies $V_W$ from CVL1B. Spatial relationships between the catchment elevations distribution (Fig. 4.1), the position of the Lithofacies $V_W$ and CVL1B and CVT1C records evidence the sub-surficial shape of Cabeço do Caveiro crater. This crater is at least ca. 12 m deep at the CVT1C position and ca. 9.30 m at CVL1B location, with 3,5 m of the lake water column (Fig. 6.2). The association of lithofacies of $Z0_{cav}$ revealing the incipient formation of the lake, combined to the spatial distribution of these lithofacies may indicate their correspondence with a Lowstand System Track (LST), where alluvial sedimentation prevails due to insufficient accommodation space.

### Stage 1 (from ca. 5200 to ca. 4000 cal. yr BP) – Shallow lacustrine to palustrine sedimentation

The onset of stage 1 is marked by peatland formation, as indicated by the occurrence of Lithofacies Q, composed by roots and large vegetal fragments and the highest values of organic matter accumulation of the whole record (Fig. 6.1). These conditions were sharply substituted by an alternation of shallow lacustrine and palustrine depositional conditions in correspondence with the RoC peak point at 5200 cal yr BP, to conform the $Z1_{cav}$ (Fig. 4.9) during the rest of stage 1 (Fig. 6.1). This transition indicates the installation of lacustrine conditions. The $PCA_{cav}$ trajectory analysis reveals a consistent trend of increasing accommodation space, against organic matter accumulation, which supports the persistent flooding conditions. In this context of peatland burying, erosion rates remain minimal, suggesting a gradual basin sealing rather than the influx rates of alluvial water, as responsible for the hydrological overflow. Therefore, lake deepening is primarily attributed to heightened weathering facilitating lake formation. Lithofacies $M_S$ composed of subangular sandy silts and black muds, coupled with increased accommodation space and reduced paludification, evidenced flooding conditions and a sublittoral sedimentary environment.

Nevertheless, while overall deepening conditions contribute to peatland drowning, the occurrence of accommodation space losses coupled with an increased accumulation of organic matter and Lithofacies P reveal water lamina drops, also creating favorable conditions for the accumulation of organic matter in palustrine conditions. Furthermore, the aerophilic diatom content, reddish tones and (oxy)hydroxide iron precipitation dominating Lithofacies P, indicating episodic oxygenic

subaerial exposition in a palustrine environment, support episodic lake water lamina drops and re-flooding cycles (Fig. 6.1). The $PCA_{cav}$ trajectory analysis shows significant abrupt drops in lake levels against paludification. This confirms the intermittent episodes of drastic reductions in water levels resulting in peatland conditions and potentially restarting the peatland formation.

The alternance between Lithofacies P and MS is characterized by a RoC peak point at 5000 cal yr BP corresponding to Lithofacies P and the occurrence of opportunistic diatoms in Lithofacies $M_S$, which might be indicating sudden water level drop events and the hydrological recovery afterwards. During these cycles high lake levels hamper paludification, due to peatland drowning and the installation of sublittoral environments as interpreted from Litofacies MS. Conversely, low lake levels and high paludification suggest palustrine sedimentation affected by the dead peatlands re-exposition, as inferred from Lithofacies P.

Masques (2021) reports the dominance of circumneutral species of diatoms associated with increased pH levels due to volcanic activity (Fig. 2.26). However, as previously discussed, volcanic activity is not a primary driver of sedimentation during this stage 1, which in contrast was dominated by incipient lake conditions affected by drought-flooding cycles. In these conditions peatland formation was limited, preventing the generation of humic acids that contribute to pH drops. Therefore, higher pH levels during stage 1 in comparison with other stages were likely caused by the absence of the peatland inwash supplying acidic fluids to the lake (Halsey et al., 1997).

Moreover, the biostratigraphic changes corresponding to the progressive transition from Lithofacies $M_S$ to $M_I$, which is enriched in planktonic and tychoplanktonic diatom remains (Marques, 2021), may indicate water column instability due to deepening conditions during the deposit of $Z1_{cav}$. In general, chemostratigraphic, lithostratigraphic and biostratigraphic indicators suggest the deposition of higher order sedimentary episodes during the deposit of a lower order TST, where despite episodic reduction of accommodation space, the general trend suggests its creation (Fig. 6.2).

### Stage 2 (from ca. 4000 to ca. 600 cal. yr BP) – high soil erosion and low organic matter accumulation under intermediate steady water level

The stage 2 (from ca. 4000 to ca. 600 cal. yr BP) (Fig. 6.1) in correspondence with $Z2_{cav}$ (from 650 to 190 cm depth) (Fig. 4.8) is characterized by a cyclic pattern of peatland erosion dominating the sedimentary processes. This cyclic pattern is constituted by increasing erosion rates during a first subperiod (from ca. 4000 to 1900 cal yr BP) and decreasing rates during the second subperiod (from ca. 1900 to 600 cal yr BP). Increased erosion periods correspond with periods with the lowest values of in-lake organic matter accumulation, and, consequently, the accumulated organic matter would have an external origin being introduced into the lake by erosional pulses.Besides, accommodation space fluctuates at an intermediate steady state, displaying an opposite pattern to soil erosion and paludification.

This depositional scenario is interpreted as a Regressive System Tract (RST), where water lamina fluctuations control sedimentation by inducing changes of accommodation space. In general, the intermediate accommodation space indicates normal regression where punctual water lamina drops induce palustrine conditions favouring organic matter influx from increased leaching, whereas water lamina rises drown peatlands and prevent soil leaching. The correspondence of regressive conditions is confirmed by saprophylic diatom remains of Lithofacies $M_P$, which indicate the influence of the peripheral peatland installed in the paralimnion supplying organic compounds to the lake. This is also confirmed by the increase of acidophilic diatom remains during this stage 2 (Marques, 2021; Fig. 2.26).

Specifically, the onset of stage 2 (from ca. 4000 to ca. 3000 cal. yr BP) (Fig. 6.1), corresponding to the basal section of $Z2_{cav}$ (from 650 to 550 cm depth) (Fig. 4.8), is characterized by the stabilization

of accommodation space at an intermediate steady state. However, peatland erosion rates ($PC2_{cav}$) increased, displaying an oscillating pattern with a diminishing of the organic matter accumulation. This sedimentary scenario may correspond to the early stage of a Highstand System Tract (HST), where accommodation space creation progressively stabilizes, whereas there was an increase of the sediment supply. This caused a normal regression that induced incipient subaerial exposition of the sedimentary wedge, inducing the peatland development at the paralimnion, which in turn contributed with organic lixiviated compounds within the lake. The occurrence of punctual debris flows, evidenced by three layers of Lithofacies D at ca. 575 cm depth (Fig. 6.1) and a tephra layer of Lithofacies $V_L$ at ca. 570 cm depth, indicates also an alluvial incision and a volcanic fallout occurring at the end of this first subperiod (ca. 3000 cal yr BP), hampering the perilacustrine development of soils. This is evidenced by the extreme reduction of organic matter accumulation during these events. Furthermore, the angular foresets shown by the lithofacies deposited during this subperiod, likely indicate the record of the distal part of the sedimentary wedge during conditions of high accommodation space just after a maximum flooding state (Fig. 1.27), corresponding with the MFS that constitutes the transition from stage 1 to stage 2. The biotic assemblage, rich in planktonic species, composing Lithofacies $M_I$ (Fig. 4.5; Fig. 2.23) (Marques, 2021), confirms the early HST during the first subperiod of this stage 2 (from ca. 4000 to ca. 3000 cal. yr BP) and the transitive state of maximum flooding. These deeper conditions in Lake Caveiro (Pico Island) coexisted with high runoff and pedogenesis rates in Lake Caldeirão (Corvo Island), evidencing similar hydroclimatic conditions driving sedimentation in both locations (Fig. 6.1).

Peatland installation occurred from 3000 to 1900 cal yr BP, corresponding with late HST conditions, where increased sediment supply and steady creation of accommodation space induced progradation with the consequent exposition of the proximal part of the sedimentary wedge, creating a paralimnetic area for peatland installation. This is evidenced by the occurrence of Lithofacies $M_P$ in CVL1B record, constituted by acidophilic and saprophilous diatom remains (Marques, 2021), which agree with peaty facies found in CVT1C sediment record at relatively similar height, relative to Cabeço do Caveiro basement (Fig. 6.2).

Furthermore, a prominent drop of the accommodation space, corresponding with low organic matter accumulation and the highest rates of soil erosion (Figs. 6.1 and 6.2) at ca. 1900 cal yr BP and lasting ca. 200 years (Fig. 6.1), indicates a forced regression causing peatland erosion and bypass. This is evidenced by the presence of an erosive surface, previously interpreted as the base of the slumpized deposits found in CVT1C, which would correspond with the peatland incision corresponding with a SU. The reduction of accommodation space during the forced regression induced the formation of a FSST at CVL1B under- and over- lied by its correspondent BSFR and CC, respectively. These surfaces correspond with the SU found in the CVT1C record. This forced regression corresponds to Lithofacies E, including the coarsest lithoclasts, plant debris and accumulation of trunks, which derive from paralimnetic erosion. These erosive conditions correspond to the three reversal ages found in CVL1B record (Fig. 6.1), evidencing the inclusion of older organic matter previously deposited in the catchment. Besides, these erosive conditions have occurred under a dry period causing a persistent lake water level drop. The aridity index reconstructed by Bjorck et al. (2006) shows the highest aridity conditions since the mid-Holocene corresponding with this period of forced regression. A decrease in runoff rates in Lake Caldeirão (Corvo Island) also coeval with this stage 3 from Lake Caveiro (Pico Island). This suggests that aridification was the cause of the forced regression during stage 2, due to decreased hydrological balance in the Caveiro system, causing drainage instability, which incises the peatland, as recorded at the CVT1C record leaving the FSST deposits at the CVL1B record location.

Then, sedimentary conditions were dominated by fluctuations in the accommodation space during the last subperiod of stage 2 (from ca 1700 to 600 cal yr BP), driving higher order cycles of soil

erosion and organic matter supply, similar to conditions before the exceptional erosive event. This is interpreted as LST deposits during the progressive creation of accommodation space due to a lake water level rise. Corresponding with this subperiod, the second ecological phase from Marques (2021) (2730 to 600 cal yr BP) evidences diatom assemblages responding to acid conditions, which were related to volcanic activity. However, as previously discussed, volcanic activity may have had minimal effect on Caveiro environment. The in-wash of degraded peatland rests, controlled by fluctuating water lamina, after exposure during the previous subperiod (1900 to 1700 cal yr BP) is a more plausible explanation (Halsey et al., 1997). Besides, RoC peak points at ca 1000 and 900 cal yr BP indicate lake water level drops triggering soil erosion, likewise during the stage 1. The correspondence of lithofacies E with these RoC peak points at ca. 300 and 250 cm depth, respectively, indicate accelerated water level drops induced by faster process than hydroclimatic fluctuations dominating the deposition of the FSST (at ca. 400 cm depth), where no RoC peak points were detected.

### Stage 3 (from ca. 600 cal. yr BP to present) – Shallow lacustrine sedimentation in pelagic zone

The onset of stage 3 is characterised by a first subperiod (from ca. 600 to 100 cal yr BP) of progressive increase of the accommodation space, whereas soil erosion decreases and paludification remains low (Fig. 6.1). However, Marques (2021) interpreted a shift from oligotrophic to mesotrophic conditions from diatom assemblages for this time subperiod, triggered by higher nutrient loads derived from increased soil erosion due to deforestation. Both interpretations are not necessarily incompatible, since biogeochemical inferences are dependent on the sedimentary morphodynamics and nutrients released within the small Lake Caveiro are not. Due to the small size of Caçbeço do Caveiro crater, this is interpreted as a TST phase that induced the lake depocenter migration. This migration created accommodation space by descending the lake bottom at the location of the core CVL1B. The sedimentary wedge prograded from the highly erodible domain 3 at the WNW, where $St1_{cav}$ operates along the fault intersection with relief (Fig. 2.24 and 2.25), towards the ESE inducing the lake depocenter migration following the tectonic lineation up to install pelagic conditions at the CVL1B coring site (Fig. 6.2).

A second subperiod (from ca. 100 cal yr BP to 50 CE) is characterized by 1) the highest lake levels of the entire record of Lake Caveiro, which then remains steady, 2) increased soil erosion and 3) the dominance of organic matter accumulation over the 1) and 2). This subperiod is interpreted as the last stage of Lake Caveiro ontogeny, because of the lake reached the spilling point of the outlet and consequently the basin siltation and the peatland reinstallation. These conditions do not allow for accommodation space creation, even with positive hydrological balances, therefore, HST conditions prevail during this second sub-period of stage 3. RoC peak points at ca. 100 cal yr BP might be indicative of this change in the sedimentary conditions. The ecological conditions deducted by Marques (2021) support this interpretation since acidophilus species were dominant, evidencing sphagnum expansion, and mesotrophic and epiphytic diatom species also evidenced higher nutrient loadings and the current peatland establishing at the CVT1C position (Fig. 6.2).

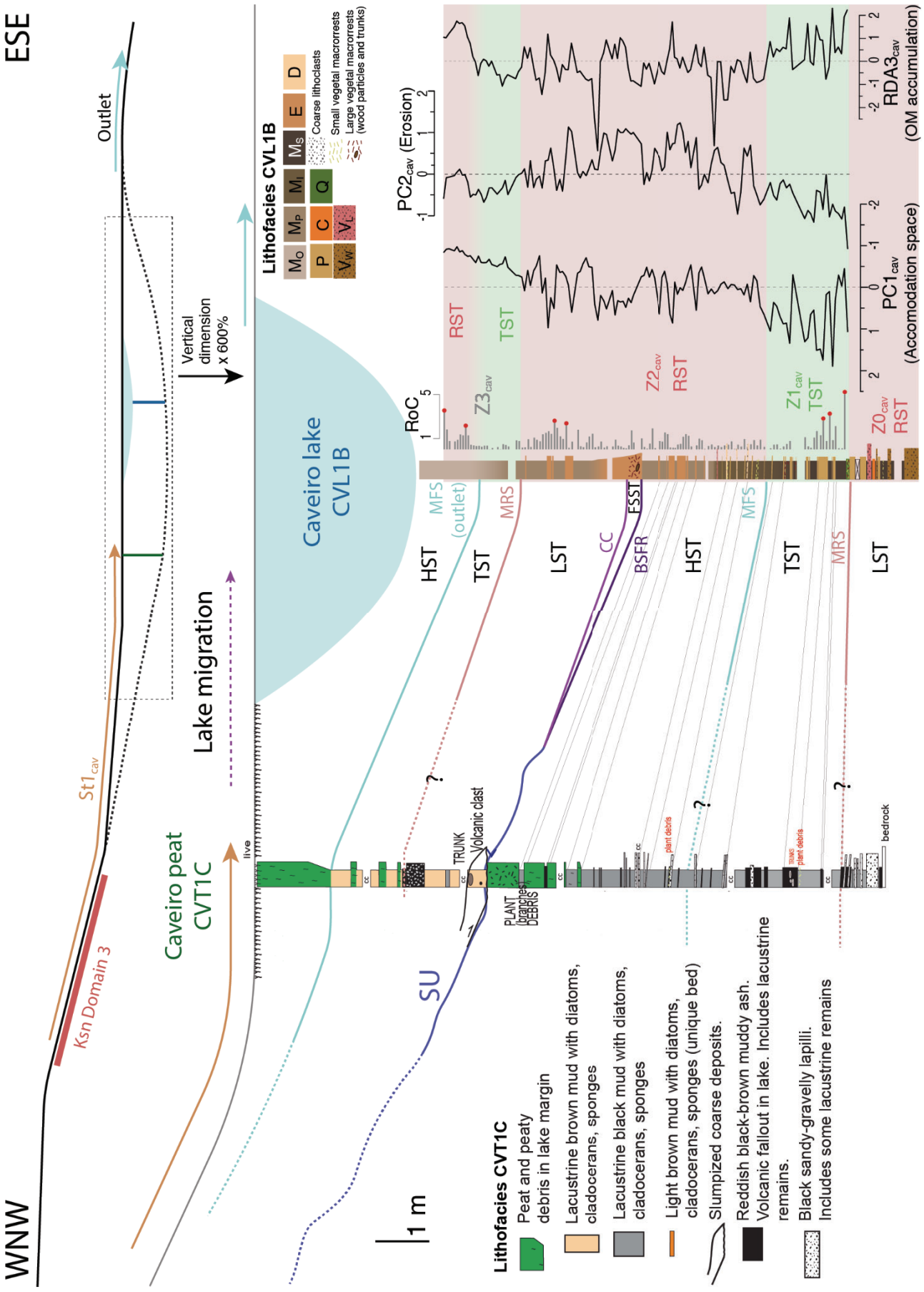


*Fig. 6.2: Cross section of Cabeço do Caveiro scoria cone crater along the prevalent WNW – ESE tectonic lineation (Fig. 2.21 and 2.22), showing a correlation panel between the available sedimentary records from its lacustrine sedimentary infill (CVL1B from the lake and CVT1C from the peatland). The figure details the*

*sequential stratigraphic analysis including systems tracks and surfaces. System tracks:* ***HST****: Highstand System Track,* ***LST****: Lowstand System Track,* ***TST****: Transgresive System Track,* ***FSST****: Falling Stage System Track. Surfaces:* ***MFS****: Maximun Flooding Surface,* ***MRS****: Maximun Regression Surface,* ***CC****: Correlative Conformity,* ***BSFR****: Basal Surface of Forced Regresion,* ***SU****: Subaerial Unconformity. Furthermore, lithostratigraphic analysis contributes to the interpretations. Lithofacies of CVL1B (Lake Caveiro):* $\boldsymbol{M_D}$*: Brown-to-greyish, massive, silty sapropel with variable proportions of bioclasts.* $\boldsymbol{M_O}$*: Brown, massive, diatomaceous ooze with aquatic plant remains and black amorphous aggregates of organic matter.* $\boldsymbol{M_P}$*: Dark-brown, massive, organic mud with terrestrial vegetal remains.* $\boldsymbol{M_S}$*: Dark-brown-to-black, massive silty mud with epilithic and epipsammic diatom oozes.* ***E****: Reddish, massive, millimetre-to-decimetre layers of sand, silt and clay, with reddish amorphous organic aggregates.* ***D****: Light-brown, reddish and black, centimetre-to-decimetre-thick, finning-up-to-massive, erosive layers of sands-to-pebbles with terrestrial organic remains.* ***Q****: Black, massive, peat with poorly matured silt and diatoms.* ***P****: Reddish, millimetric-to-decimetric massive layers of sapropel with iron (hydr)oxides and aerophilic diatoms.* ***C****: Light-orange, low-angle cross laminated centimetric diatomaceous ooze with reddish organic matter.* $\boldsymbol{V_W}$*: Brownish, reddish and black, centimetric-to-decimetric, massive layers of coarse ash with reddish amorphous organic aggregates.* $\boldsymbol{V_L}$*: Black, centimetric, massive layers of lapilli and coarse ash.*

# 7. Discussion: Environmental forcings controlling the lacustrine sedimentary evolution

The time series analysis derived from the biogeochemical data obtained from the sediments of lakes Funda, Caldeirão and Caveiro shows notable discrepancies (Fig. 4.17). Despite the islands share a relatively similar climate (AEMET and IPMA, 2012) (Figs. 2.4, 2.5 and 2.7), the correlations obtained between these signals and the observational precipitation and temperature data of the study area (Tables 4.8, 4.9 and 4.10), although significant, leaves parts of the biogeochemical variability unexplained (Fig. 7.1). Moreover, the combination between stratigraphic (Fig. 6.1) and morphometric analyses (Fig. 4.1 and 4.2) revealed spatial trends of hydro-sedimentary evolution inducing morpho-dynamical patterns of sedimentation (Fig. 7.2). Furthermore, RoC analysis shows peak points that reveal the impact of geologic processes and human activities on sedimentary evolution. Therefore, the effect induced by the morphological variations of the lake basins (Madeira et al., 2015; Azevedo and Portugal Ferreira, 2006), the eventual geologic (Madeira and Brum da Silveira 2009) (Fig. 7.3) and anthropic (Raposeiro et al., 2021; Ritter et al., 2022; Richter et al., 2022) (Fig. 7.4) impacts and climatic evolution (Björck et al., 2006; Hernández et al., 2017) (Fig. 7.5) over the biogeochemical signals recorded in the lake sediments of the three studied basins is discussed.

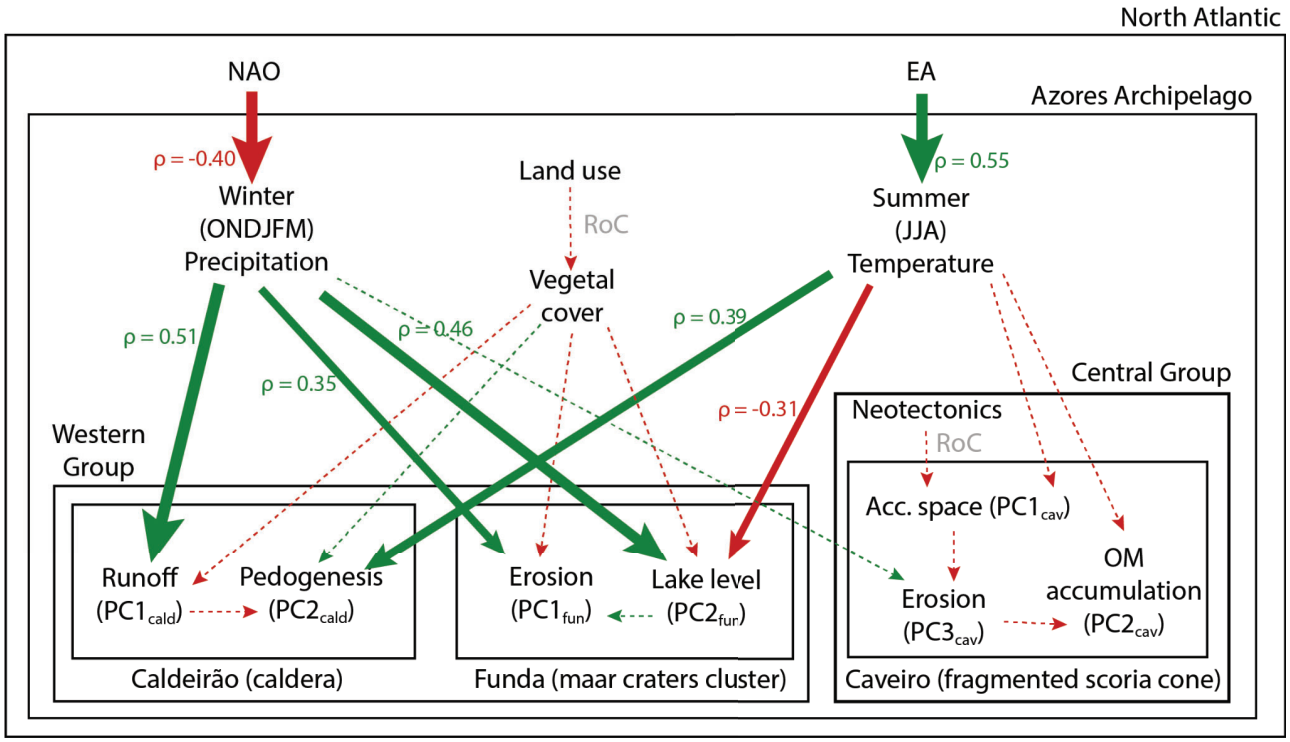


*Fig. 7.1: Conceptual model of the environmental forcings affecting the lacustrine sedimentary dynamics within Funda, Caldeirão and Caveiro lake-catchment systems. The model shows the relationships deducted from ordination analyses between lacustrine sedimentation processes and climatic, geologic, atmospheric and anthropic forcings affecting these mechanisms. Relationships deducted by RoC analysis are indicated. When available, Pearson rank correlation coefficients (ρ) and associated p-values are included. The arrows represent different relationships between conceptual model elements: direct (green), indirect (red), qualitative (dashed) and quantitative (solid) relationships. The thicknesses of the solid arrows are linked to the degree of correlation between the elements.*

## 7.1 The tectono-volcanic influence

The geomorphic features derived from the generation (Table 5.1), mobilization (Table 5.2) and deposition (Table 5.3) of sediments constitute the morphosedimentary systems. These systems offer insights into the three-dimensional hydro-sedimentary dynamics within the study area (e.g., Castanet et al., 2022). The association between the erosive landforms, evidenced by the scars (Figs. 2.15, 2.21, 2.25) corresponding with erodible domains (Fig. 4.1) that host the most prominent streams (Fig. 4.2), and the depositional sedimentary landforms (Fig. 4.1) conform the morphosedimentary systems (e.g., Valenzano et al., 2018; Castanet et al.,2022) of the study area. The study of these morphosedimentary systems shed light on the erosive-depositional morpho-dynamics (Wünnemann et al., 2015) within the studied lake-catchment systems, which has been related to the geological configuration of their corresponding lake basins (Cohen, 2003). The inferred hydro-sedimentary evolution within the studied lake-catchment systems is determined by the morphology of the lake basins, which in the Azores is dominated by the tectono-volcanic configuration (Madeira et al., 2015; Azevedo and Portugal Ferreira, 2006) of the plates triple junction (Miranda et al., 2018) (Fig. 2.2).

The differences in the relative sizes between the Funda Caldeirão and Caveiro lake-catchment systems (Fig. 4.1) are attributed to the prevailing structural domains where they establish (Fig. 2.2). The WG, dominated by the orthogonal structural domain resulting from MAR geodynamics, facilitates tectono-volcanic activity constrained to fault intersections. This process leads to the creation of relatively scarce, large, and deep tectono-volcanic basins within Flores (Fig. 2.14) and Corvo (Fig. 2.17) islands, where the extensive and deep systems of Funda and Caldeirão develop. In contrast, the TR trans-tensive stresses induce a structural domain with preferential orientations at the São Roque Piedade Volcanic Complex. This structural pattern promotes diffuse volcanic activity along fault planes, resulting in the formation of numerous small tectono-volcanic basins in Pico Island (Fig. 2.20), where the Caveiro system is situated. Furthermore, the structural lineation's of the dominant tectonic domains correspond with the orientation of morphometric elements of the lake-catchment systems (streams, major axes of watersheds and escarpments) and the spatial variability revealed by the morpho-sedimentary systems (most prominent erosive scars and direction of accretion of sedimentary wedges). Therefore, the tectonic configuration and the associated eruptive styles determine the distribution of elevations within the lake-catchment systems studied, inducing a variable hydro-sedimentary evolution in each of them:

### 7.1.1 The Funda volcanic system

The Funda lake-catchment system is located within the maars cluster of the FVS (Andrade et al., 2022) (Fig. 2.14) in correspondence with a tectonic domain in structural intersection (Fig. 2.2) (Azevedo and Portugal Ferreira, 2006). This tectono-volcanic setting favoured sub-surface explosive activity of a poly-genetic nature (Andrade et al., 2022) and localized in a single point (Madeira et al., 2015), creating large depressions in the terrain with very pronounced scarps connected to each other (Fig. 7.2). This morphology configured a relatively large basin where a broad, low-balance and low entropy alluvial network develops (Figs. 2.14, 4.1 and 4.2), favouring domains of high erodibility that drive in alluvial sedimentary cascades (Burt and Allison, 2010). This morphology also favours the volumetric development of the lake vertically and the formation of horizontal physical barriers such as the summer thermocline (Ritter et al., 2022). This induces high-frequency sedimentary patterns, derived from organic production triggered by resuspension events during mixing periods.

#### Morphological controls over catchment drainage

The mobilization of the alluvial material constituting the deposits of $F1_{fun}$ is highly favoured by alluvial floodings, which are facilitated by the steep and oriented landforms of the Funda system (Fig. 4.1). The eruptive style of the FVS favoured the generation of crater bottoms below the regional topography constituted by the Flores island plateau. The partial exposition of the FVS to the slope

of this plateau induced the formation of relatively large sub-basins within the northern side of Funda catchment sinking into the main crater. These large and steep drainages, corresponding with $St1_{fun}$, $St2_{fun}$ and $St4_{fun}$ streams (Figs. 4.1 and 4.2), maximize the flow accumulation by inducing the formation of the relatively large and dendritic high order sub-basins to constitute the extremely erodible domain 4 at the steeplands of the main crater. Therefore, enhanced hydrological connectivity boosting flow accumulation in $St1_{fun}$ and $St2_{fun}$, and especially in $St4_{fun}$ (Fig. 7.2) promoted higher sediment connectivity (Heckmann and Schwanghart, 2013; Najafi et al., 2021). The low spatial entropy dominating Funda lake-catchment system induces higher runoff at the northern side of the catchment and especially at the northeastern maars, which becomes relatively prevalent over infiltration by focussing the fluxes and promoting relatively energetic and fast flows. Whereas at the southern sector floodings may be limited. This jeopardized the spatial entropy of the morphosedimentary systems during accretion, provoking lake Funda depocentrer migration to the southeast side of Funda maar (Fig. 7.2). The most prominent one constitutes the delta fan submerged ca. 800 yr ago, when the lake level was 20 m below current position, where FN1702 record lies presenting a preferential direction along the $St4_{fun}$. On the other hand, the hydrological availability for $St3_{fun}$ is relatively restricted since it is unlinked to the plateau receiving less water from hydrological recharge.

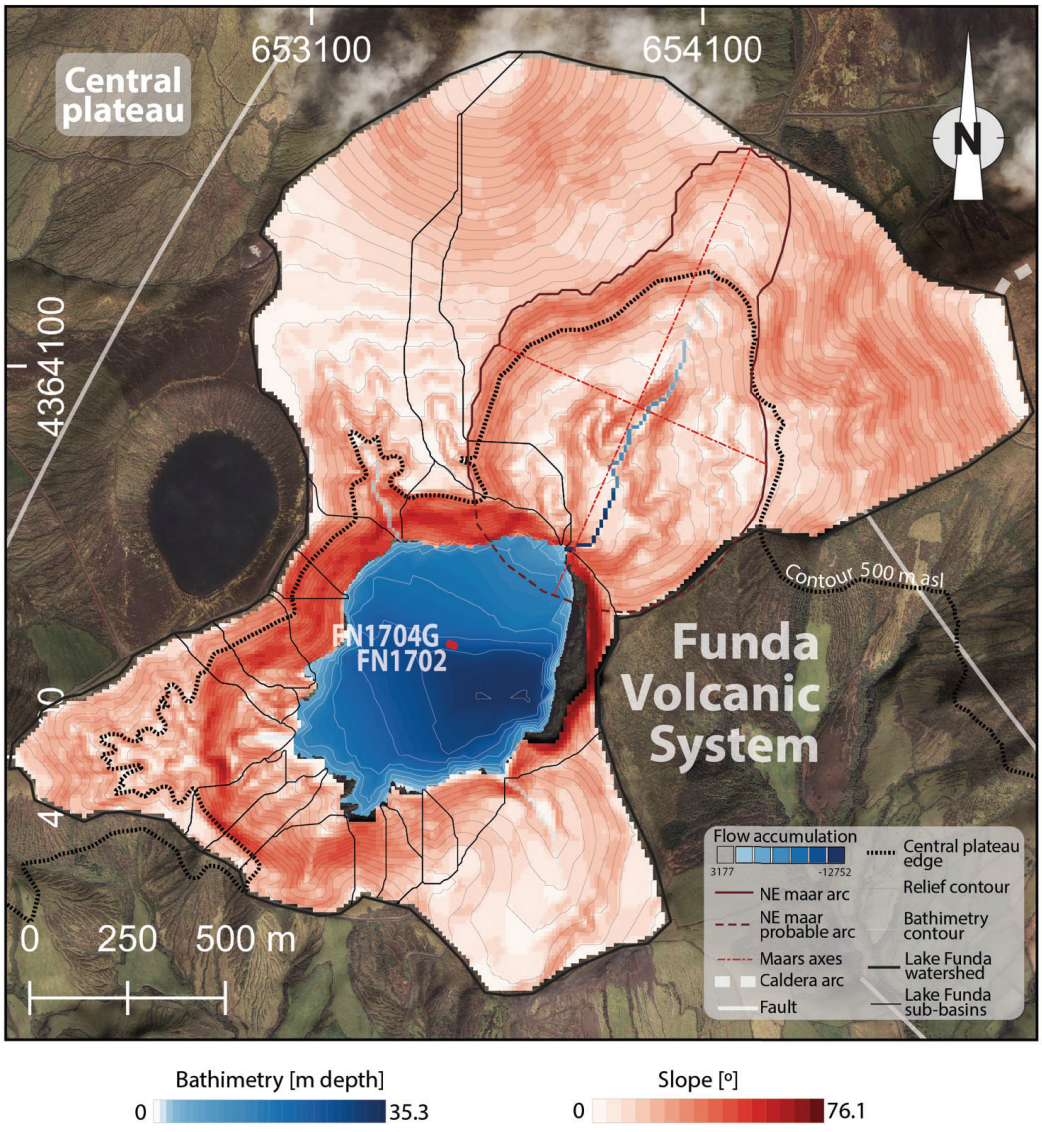


*Fig. 7.2: Funda lake-catchment system hydrology in relation with the prevalent tectono-volcanic structures conforming to the lake basin. Faults correspond with the prevalent tectonic lineation (Azevedo and Portugal Ferreira, 2006).*

Furthermore, the prevalent tectonic lineation N020ºE dominates the distribution of FVS craters (Azevedo and Portugal Ferreira, 2006), which aligns (Madeira et al., 2015) emphasizing hydrological connectivity (Fig. 4.1) boosting flow accumulation along this orientation (Fig. 7.2). The orientation of the major axis of the polygon composed by the north-easterns and Funda maars (Table 4.1), as well as of the straight disposition of $St4_{fun}$ and of the eastern scarp of Funda maar (Table 4.1) correspond with the regional tectonic lineation (Azevedo and Portugal Ferreira, 2006) (Fig. 7.2). This reveals the position of a fault related to the N020ºE family found within Flores Island (Azevedo and Portugal Ferreira, 2006) (Fig. 2.13), crossing the NE sector of the watershed (Fig. 2.14). Therefore, the fault intersection with relief (Azevedo and Portugal Ferreira, 2006; Madeira et al., 2015) constituting the water course of $St4_{fun}$ favouring the relative enhancement of flow accumulation with respect the rests of main streams within Funda catchment by constituting the less energetic pathflow and the promotion of dendritic drainage (Fig. 2.14). In contrast, the dominance of non-oriented and relatively flat landforms at the southern maar sector limit the flow accumulation of $St3_{fun}$. This is evidenced by the higher channel entrenchment at $St4_{fun}$, where incision experienced enhanced progress (Fig. 2.14 and 2.15b,c) relative to the other streams, despite sharing similar age of landform formation (Andrade et al., 2022). Therefore, the prevalent tectonics redirecting the flows along preferred orientations reinforced a positive feedback loop established between morphodynamics and erosion (Fig. 1.2) (Beechie et al., 2008). Whereas incision progress induced higher flow accumulation and sediment connectivity performing higher erosion, higher erosion induced higher accumulation flow through higher incision recruiting further tributaries. This results in a sedimentary state of low entropy within the system, which is reflected on the sediment samples collapsed into one dimension in the ordination analyses, corresponding with the fists sedimentary stage of Funda system (Fig. 4.12).

#### Morphological controls over in-lake deposition

Since the lake-catchment system is hydrologically closed and presumably well sealed, the eruptive style of the FVS configured distribution of elevations that induce lake long-term volumetric changes in depth rather than in area, amplifying (Fig. 1.2) lake level fluctuations. The generation and accumulation of the endogenic materials of $F3_{fun}$ is highly favoured by water system recharge through runoff and groundwater.

Water column increase facilitates the installation of the thermocline by creating a temperature gradient between the uppermost and the deepest parts of the lake. Thus, as climate-induced fluctuations in lake water level and long-term changes in the intensity and duration of overturn and stratification periods are more intense in in steep, deep lakes with limited shallow water areas like Lake Funda (Woolway et al., 2021; Ritter et al., 2022), significantly influence sedimentation patterns in the lake over the long term.

### 7.1.2 The Caldeirão caldera

The Caldeirão system is installed inside a caldera collapsed by ring faulting (Pacheco et al., 2013) (Fig. 2.18 and 2.20), sharing the intersecting structural domain with Funda (Azevedo and Portugal Ferreira, 2006) (Fig. 2.2). This tectono-volcanic setting probably favored polygenetic activity, forming Corvo stratovolcano and the subsequent collapse of its summit (Madeira et al, 2015) (Fig. 2.18). This activity generated a basin with a relatively broad morphology (Fig. 2.21), steep concentric flanks (Fig. 2.20) and a central domain of low erodibility (Fig. 4.1), which enhances the alluvial mobilization as the main driver of sedimentation, although buffered (Fig.4.2), thereby enhancing the effect of water supply over sediment. This geomorphic context adds stages to the chain of processes involved in the sedimentary cascade where pedogenesis, paludification and paralimnetic deposition of alluvial materials occur prior to the lacustrine deposition (Burt and Allison, 2010). Furthermore, the annular

fault confers a chaotic elevation distribution to the system (Fig. 2.20), inducing high spatial entropy to the morphosedimentary system, although it maintains the position of its depocenter over time.

#### Morphological controls over drainage and in-lake deposition

The chaotic distribution of the elevation within the Caldeirão system induces larger sub-basins multiplicity at domain 3, where the radial drainage favours infiltration over runoff due to the kinetic energy dispel by distributing hydrological budgets between numerous low order small sub-basins. This is evidenced by the closeness and straight dispositions of the erosive scars within the Caldeirão catchment (Fig. 2.21g). The lake-catchment system is hydrologically closed and presumably well sealed. Therefore, the flat distribution of elevations across Lake Cadeirão bottom and domain 1 induces lake volumetric changes in extension rather than in depth. Thus, this topobathymetric disposition would favour rapid soil development and drowning and paralimnetic sediment deposition and bypass due to lake water oscillations with occasional flooding of the flat domain 1. These effects are evidenced by incision (Fig. 2.21c) corresponding with the domain 2 of moderate erosion at the lake rim (Fig. 4.1) and the lacustrine terrace revealed by knickpoints at ca. 5 m abl in stream profiling analysis (Fig. 4.2).

### 7.1.3 The Cabeço do Caveiro scoria cone crater

The Lake Caveiro system is installed inside the crater of one of the 170 cinder cones of a fissure volcanic complex, and it is associated with a structural graben that favors diffuse polygenetic volcanism (Nunes, 2020; Madeira et al., 2015). The dominant transtensive tectonic activity in the central sector of the Azores Archipelago induces the formation of the graben and the fragmentation of the cinder cones (Madeira and Brum da Silveira, 2009). This complex tectono-volcanic scenario causes the formation of small and numerous lake basins with reduced drainage. That is why in the Lake Caveiro system the variation in the accommodation space and the accumulation of organic matter were the main drivers of sedimentation. Furthermore, tectonics has been responsible for the formation of oriented morphological patterns, favoring localized erosion domains and the hydrological opening of the lake system. This configuration induces a minimum entropy to the morphosedimentary system, which is forced into a rapid evolution between successive depositional scenarios. In its initial stages, sedimentation was similar to inLake Funda, with enhanced sedimentary cascade processes. However, in its final stages, when the system reached the overflow threshold, it evolved towards a behavior similar to Lake Caldeirão system, where sedimentary buffering prevails through the peri-lacustrine deposit. During this transition, the tectonic lineation dominated the migration of the depocenter.

#### Morphological controls over drainage and in-lake deposition

The tectonic controls over the drainage are evidenced by the fault intersection with relief, causing the basin hydrological opening to the ESE (Fig. 2.22) and determining the disposition of the only stream of the basin at the WNW. The localized disposition of the highly erosive domain 3 responds to this asymmetrical oriented disposition.

The biogeochemical imprint left by the evolution of the lake water level in the Caverio basin (PC1cav) increased during the last ca. 5200 years. This evolution is controlled by cyclical fluctuations in the hydrological balance, as it is shown by the agreement with the hydroclimatic record by Björck et al., (2006) and the runoff in Caldeirão (Corvo Island). The trend of this biogeochemical imprint throughout the entire evolution of the lake can be considered cumulative (Fig. 6.1). This cumulative evolution is attributed to a morphosedimentary effect caused by the accumulation of sediment (Fig. 1.1) and the consequent sedimentary wedge accretion following a preferential direction (Fig. 2.24). This direction of accretion would be marked by the dominant tectonic lineation, as shown by the erosional distribution of domain 3 (Fig. 4.1) that is linked to the only current coming from WNW

(Fig.4.2) along the intersection of the fault with the relief (Fig. 2.24 and 2.25). Thus, the depocenter of the Lake Caveiro has migrated from WNW to ESE following the tectonic lineation (Fig. 6.2). Consequently, the transgressions that occurred during stages 1 and 3 of Lake Caveiro1 increased the accommodation space in the position that CVL1B currently occupies, while the lacustrine transition from stage 0 of Lake Funda would have occurred from the WNW when the lake occupied a more central position in the crater.

In general, accommodation space in Lake Caveiro shows an increasing trend that indicates the effect of the morphodynamic evolution of the sedimentary wedge during its ontogeny. Accommodation space is the limiting factor for the Lake Caveiro sedimentation due to the small dimensions of Cabeço do Caveiro crater. The sedimentary wedge progrades from the WNW, as indicates domain 3 localized at the northwestern side of the catchment. This accretion constitutes a linear process (Fig.1.1) that induces the progressive migration of the depocenter towards the ESE, following the tectonic lineation imposed by the underlying fault, corresponding to the Brejos graben. The stage 1 was dominated by littoral and sublittoral conditions during the lake formation. Higher sediment supply from the WNW induced the progradation of the sedimentary wedge towards the ESE during the RST of stage 2. This oriented progradation might have resulted in shallower conditions at the WNW side of the lake, but deeper at the the opposite side due to the depocenter migration. Therefore, the CVL1B core location might have experienced a deepening. This evidence shows the migration of the lake inducing higher accommodation space at CVL1B location, which is related to the descent of the lake floor instead of a higher water lamina. Slumping deducted from 210Pb dates (ca. 8 to 38 cm depth) evidences the formation of the sedimentary WNW prograding wedge, eventually supplying with instantaneous deposits at CVL1B core location due to wedge instabilities.

### Neotectonics impact on sediment deposition

RoC peak points at ca. 5000 cal yr BP in correspondence with the palustrine conditions of Lithofacies P during stage 1, and at ca. 900 cal yr. BP matching with Lithofacies E during the last subperiod of stage 2, indicate rapid changes of the hydrological conditions. Whereas runoff does not show response to these rapid changes, lake levels drop and organic matter accumulates (Fig. 6.1) Therefore, the lake water level drops was a process independent from runoff. The two rapid changes can be attributed to the tectonic reactivation of the fault which Cabeço do Caveiro is associated with. Consequently, rapid infiltration events trigger prominent lake level drops inducing the marsh sedimentation in palustrine conditions, recorded by accumulated organic matter of Lithofacies P (Fig. 6.1). At the northern sector of the Brejos graben (Fig. 2.22), Madeira and Brum da Silveira (2009) defined colluvial wedges dating back from ca. 6200 to 800 cal yr BP and intersected by fault planes at the Lagoa do Capitao Fault Zone (Fig. 7.3). This match in the timing of the lake Caveiro rapid changes and the colluvial wedges of the Berjos graben suggests that the tectonic activity mobilizing the Brejos Graben could have also affected the southern side of the graben where Lake Caveiro overlies one the related faults. Open cracks may have caused the partial infiltration of the system causing dramatic drops in lake levels and the interruption of the stream flow along the fault intersection with the relief (Fig. 2.22), which is the unique one within the lake system. Consequently, minimal runoff and shallow water lamina promote the accumulation of organic matter in palustrine conditions after tectonic reactivation events, as evidenced by Lithofacies P, persisting until the system is impermeabilized with fine materials from weathering. Therefore, tectonic reactivation of the fault could have triggered strong impacts over local hydrology by altering infiltration patterns.

The RoC peak points at ca. 900 yr cal BP and ca. 5000 cal yr BP shown by the Lake Caveiro sediments are not observable at the sediment records from Lakes Funda and Caldeirão (Fig. 6.1). The former is likely due to the relative tectonic stability of the WG located on the North American plate (Fontiela et al, 2018), whereas the latter is older than the recovered sediments of Lakes Funda and Caldeirão.

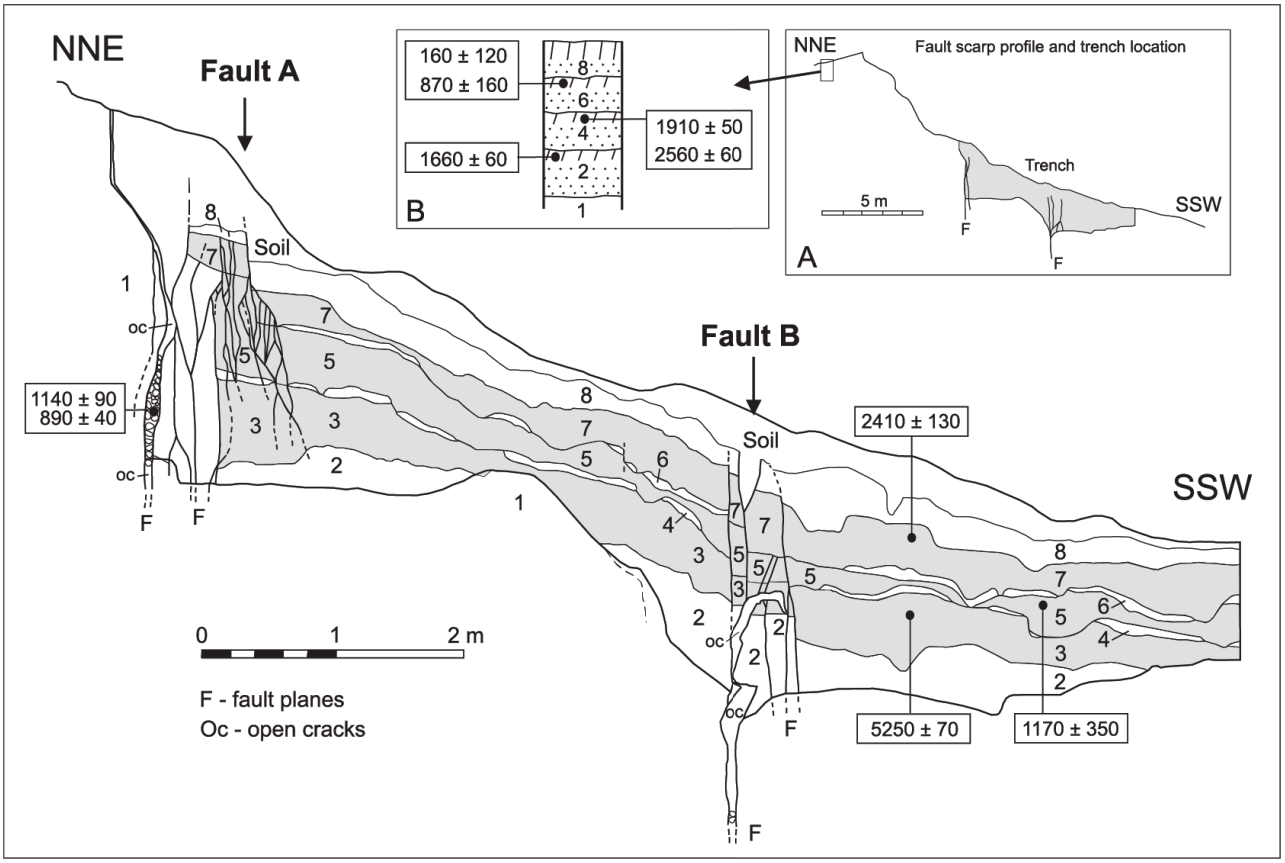


*Fig. 7.3. Simplified and reduced (originally at the 1/10 scale) map of the Lagoa do Capitão trench west wall showing two faults (A and B) associated to LC Fault Zone. The fault scarp, slightly degraded, is related to the northern fault. Stratigraphic sequence is composed of alternating layers of basaltic pyroclastic fall deposits (2, 4, 6, 8) and colluvial wedges (3, 5, 7; in grey), overlying a basement of basaltic lava flows (1); the sequence ends with present topsoil. All contacts are erosional. Inset A: slope profile across the fault and location of trench. Inset B: pyroclastic sequence (2, 4, 6, and 8), separated by dated paleosols and overlying lava flow 1, observed in up-thrown block. Radiocarbon dated deposits indicated (in years BP). Figure from Madeira and Brum da Silveira (2009).*

The last stage of sedimentation within Lake Caveiro (last ca. 1000 years) is characterized by constant pelagic lake conditions evidenced by Lithofacies $M_O$ and with no palustrine facies interruptions. This suggests the tectonic stabilization of the Graben. In fact, the previously faulted colluvial materials at the Lagoa do Capitao Fault Zone are overlaid by an undisturbed soil (Fig. 7.3) dating similar ages that the stability period suggested by Lithofacies $M_O$ in Lake Caveiro (Fig. 6.1), likely indicating the cessation of tectonic activity. In summary, the presence of lacustrine sedimentary infill in Lake Caveiro suggests the tectonic stabilization of the Brejos Graben over the last millennia. The gradual decrease in fault activity may have allowed the basin seal, leading to the formation of the lake.

## 7.2 Human colonization

The CONISS and RoC analyses applied to the biogeochemical fluxes of FN1702, CL1703 and CVL1B records indicate compositional shifts with variable acceleration rate on each study site (Fig. 7.4). Some of these shifts match the timing of the most significant events of human colonization across the Azores archipelago (Raposeiro et al., 2021). Therefore, variable responses of the lacustrine sedimentary dynamics to the impacts derived from colonization history of the archipelago

has been deducted. Furthermore, RoC peak points time lags between sites are indicative of the coloniztion pattern influenced by the variable orography across the archipelago.

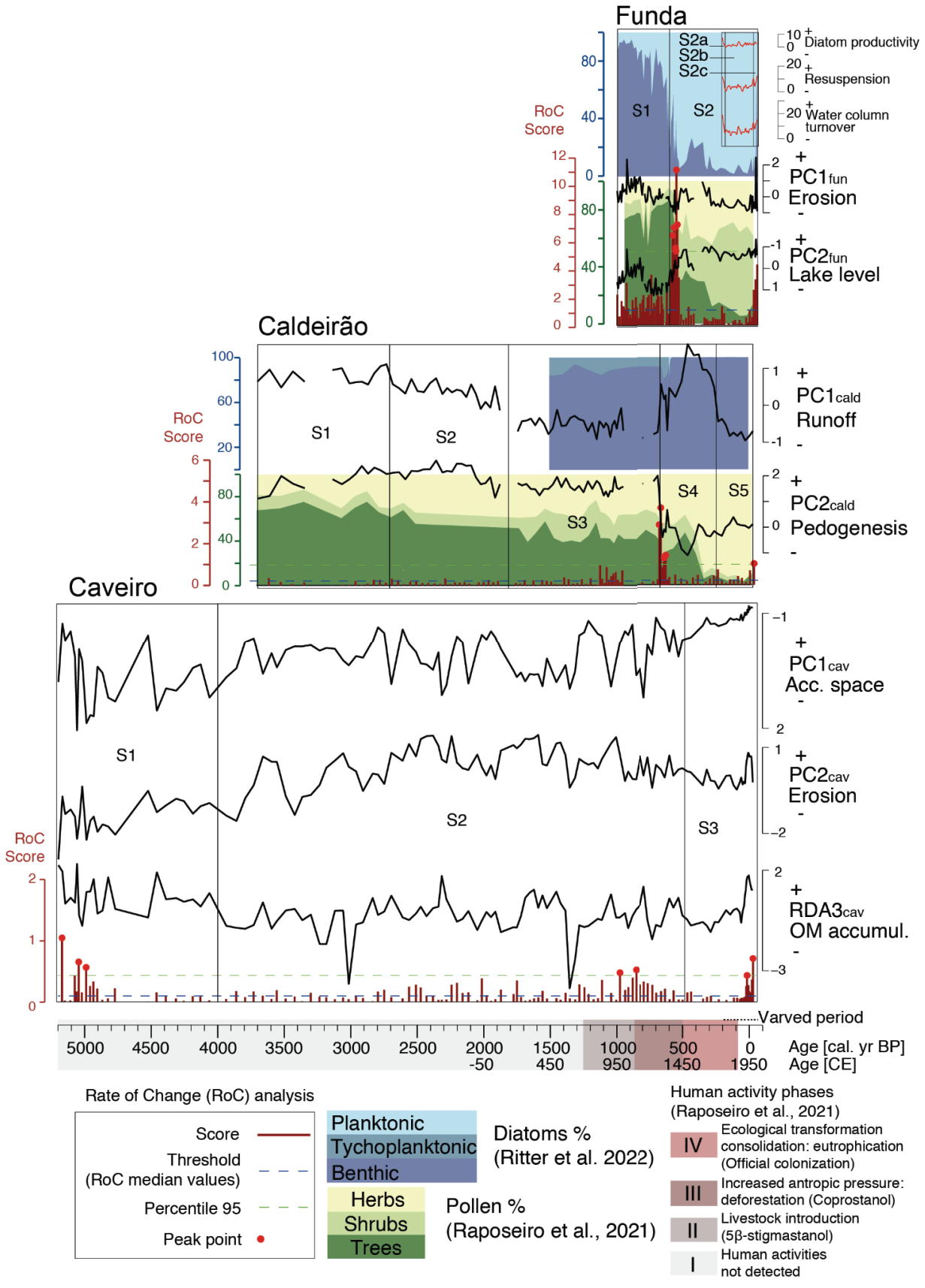


*Fig. 7.4: Evolution of the sedimentary dynamics within Funda, Caldeirão and Caveiro systems associated with the phases of ecological transformation performed on the Azores Archipelago (Raposerio et al., 2021), indicative of changes induced by human forces in the sedimentation.*

### 7.2.1 Pre-anthropogenic phase (before 700/850 CE)

RoC values close to 0 detected during the millenia subsequent to the neotectonic impact occurred in Lake Caveiro (ca. 5000 to 900 cal yr BP) in CVL1B and CL1703 records indicate a steady sedimentary evolution, either in lakes Caveiro and in Caldeirão. This evidence shows the pre-anthropogenic phase of the archipelago (Raposeiro et al., 2021; Fig. 2.11) (Fig. 7.4), when sedimentary conditions in pristine landscape exclusively responded to natural environmental forcings, such as climate and geology. Under these conditions negative feedbacks would have kept the steady state of Caldeirão and Caveiro systems (Fig. 1.2). During this pre-anthopogenic phase (ca. 5000 to 900 cal yr BP), the absence of increased RoC values corresponding with most of the Lithofacies P and E layer in CVL1B (Fig. 6.1) indicate steady conditions of deposit, probably due to water lamina fluctuation associated with hydroclimate, rather than to neotectonics impact.

### 7.2.2 Early settlement (Since 700/850 CE)

Increased RoC values in CL1703 record of ca. 1.5 at ca. 900 cal yr BP correspond with the first appearance of 5B-stigmastanol (850 ± 60 CE), which is indicative of livestock introduction in the archipelago (Raposeiro et al., 2021). This correspondence might stem from the effect of the first anthropogenic impacts detected within the Caldera of Caldeirão, which included human induced fires evidenced by increased macrochacoal particles and PAH influx (Raposeiro et al., 2021). Probably norse communities affected soil erosion and pedogenesis rates with partial forest clearance, looking for better conditions for cattle pasture and access to the lake (Raposeiro et al., 2021). Furthermore, RoC peak points found at similar age (ca. 900 cal yr BP) has been also detected in CVL1B record. This correspondence might indicate the same effect occurred in the Caldeirão Caldera within cabeço do Caveiro crater. Partial deforestation might have affected accommodation space by increased soil erosion, which in turn might have diminished organic matter accumulation rates within the crater. In turn, Pico island presents similar verticalized orography as Corvo island, which might have forced the first inhabitants to look for permanent water bodies in the island's uplands at the early stages of their arrival in both locations (Raposeiro et al., 2021). However, this is not entirely clear, since the peak points at 900 cal yr BP found in CVL1B record also correspond with discrete layers of Lithofacies P (Fig. 6.1) which might be generated by infiltration due to tectonic activity as previously discussed for the sedimentary stage 1 of Lake Caveiro. Furthermore, livestock presence in Peixinho catchment, which is located at 2 km from Lake Caveiro, were detected 200 years earlier (Raposeiro et al., 2021). The small size of Caveiro catchment might have buffered anthropogenic impacts derived from deforestation due to reduced influence on allochthonous sedimentation, which is rather dominated by the lake's rapid ontogeny due to reduced accommodation space. Nevertheless, further evidence is needed to shed light on this.

### 7.2.3 Regional deforestation (since 1070/1280 CE)

The highest RoC peak points of CL1703 (up to 6 at 1288 CE) and FN1702 (up to 12 at 1380 CE) records at ca. 600 cal yr BP corresponds with the third phase of human activity deducted by Raposeiro et al., (2021) determined through the first appearance of coprostanol (since ca. 1070-1280). Furthermore, this phase corresponds with the onset of the sedimentary stages 2 in Lake Funda, 4 in Lake Caldeirão and stage 3 in Lake Caveiro, marked by CONISS biogeochemical breaks (Fig. 7.4). The appearance of coprostanol in the lake sediments of the archipelago is indicative of widespread human presence, farming, and regional deforestation with the slash and burn method, further evidenced by increased *Juniperus* leaf influxes and B5-stigmastanol and prominent diminution drops of arboreal pollen (Raposeiro et al., 2021; Fig. 2.11). Therefore, increased anthropic pressure reflected in extensive and intense regional deforestation might have modulated the intensities of the processes involved in the sedimentation of the studied sites (Fig. 7.4), by inducing homeorhetic states that drove the lake sedimentation into new steady states (Fig. 1.2) (Ritter et al.,

2022). The effects of regional deforestation over soils was a reduction of cohesion, thereby increasing erosion (Raposeiro et al., 2021; Ritter et al., 2022; Richter et al., 2022). Furthermore, regional deforestation effects over hydrology induced higher hydrological availability due to reduced evapotranspiration (Ritter et al., 2022), as indicated by diatom habitat shifts corresponding with the vegetal cover reduction (Fig. 7.4). However, the variable morphology of the lake basins has induced contrasting sedimentary responses to regional deforestation (Raposeiro et al., 2021) and consequent hydrological superhabit (Ritter et al., 2022), by selectively amplifying some processes over others in the studied lake systems:

### Funda system

RoC peak points corresponding with deforestation at 600 BP in FN1702 record (Fig. 7.4) indicate the sedimentary response of the Funda system to increased hydrological availability derived from deforestation, which resulted in the lake deepening due to the verticalized distribution of elevations within Funda maar, by amplifying the increase of water column rather than the area (Ritter et al., 2022). This is evidenced by the ecological shift shown by diatom communities (phase B from Ritter et al., 2022; Fig. 7.4 and 2.17). Benthic species dominate before 600 cal yr BP whereas planktonic species do afterwards (Fig. 7.4). Lake deepening modulated the processes involved in Lake Funda sedimentation by limiting alluvial mobilization and by inducing the conditions for the installation of a strong and persistent summer thermocline (Ritter et al., 2022; Richter et al., 2022).

Erosion diminution at 600 cal yr BP corresponds with the transition between the sedimentary stages 1 to 2 indicates the buffering of alluvial mobilization into Lake Funda (Fig. 7.4). This is counterintuitive, since deforestation normally enhances soil erosion, and it does, however in Funda system reduced evapotranspiration induces a morphodynamic effect due to transgression (Fig. 1.15c). The delta fan submersion with the water lamina rise provoking the shoreline migration closer to the Funda maar crater walls, imposing a pelagic sedimentary state. Therefore, the alluvial mobilization derived from the positive feedback established between morphodynamics and erosion dominating at the sedimentary stage 1 buffers by getting relegated to more distal positions, closer to the Funda maar crater walls, where detrital deposits compose the alluvial fan associated to $St4_{fun}$ mouth.

Furthermore, lake level increase at 600 cal yr BP in the transition between the sedimentary stages 1 to 2 indicate the installation of the pelagic sedimentary conditions dominated by the thermocline seasonal cycle (Fig. 7.4). Therefore, deepening derived from reduced evapotranspiration and the verticalized Funda maar crater walls induce the establishment of the positive feedback between diatoms and microbes at the water volume within the bathymetric domain A. Resuspension, sediment focussing (Bloesch, 1995) and the derived exacerbated production of diatom remains during blooms (Ritter et al. 2022) impose in Lake Funda to dominate sedimentation (Fig. 7.4).

Therefore, the relatively high RoC values during the stage 1 indicate a steady sedimentary state In Funda system dominated by alluvial sedimentation. Then deforestation forced homoeopathic conditions through the reduction of evapotranspiration and lake deepening, inducing the establishment of the positive feedback loop between microbes and diatoms. This homeorhetic state drove the transition to a new steady sedimentary state characterized by buffered alluvial supply and steady pelagic sedimentation, as indicated by decreased RoC values at the sedimentary stage 2 (Fig. 7.4 and 1.2). This transition to a new steady state was referred to by Ritter et al. (2022) as the anthropogenic impact with no return ticket, which reflects in the sedimentary dynamics and evolution of the system (Fig. 7.4).

Therefore, human driven transition through deforestation and reduced evapotranspiration induced low ergodic biogeochemical signals to the lake sediments deposited in the Funda system, by

modulating the morphodynamic effects over erosion and organic production and accumulation. Therefore, the lake level rise derived from reduced evapotranspiration due to deforestation. A second feedback loop overimposed to the one rising sedimentary entropy of the system, which is evidenced in $PCA_{fun}$ by increased dispersal of $Z2_{fun}$ samples deposited during stage 2, with respect to the ones of $Z1_{fun}$ (Fig. 4.12). This enhancement of the system's sedimentary entropy resulted in biogeochemical signals closer to the imprint left by the climatic variability.

#### Caldeirão system

RoC peak points corresponding with deforestation at 600 cal yr BP in CL1703 record (Fig. 7.4) indicate the sedimentary response of the Caldeirão system to deforestation. This response is reflected in a drastic drop of pedogenesis in the watershed due to: 1) reducing mechanical weathering exerted by tree roots, by reducing chemical weathering exerted by humic acids derived from arboreal organic matter and 3) by diminishing soil cohesion deriving in lower residence time of soil lithorelicts in the catchment (Depetris et al., 2014) (Fig. 7.4 and 1.12). Reduced BSi values in $Z4_{cald}$ and $Z5_{cald}$ of CL1703 record correspond with the stages subsequent to deforestation. This evidence shows the effects of soil degradation on lake ecology, by reducing the release of silicic compounds within, affecting diatom thrive and biomineralization (e.g., Martin-Jezequel et al., 2000; Street-Perrott and Barker, 2008). Despite strong first-order geological controls on erosion, deforestation had such a profound impact on the suspended sediment loads of some rivers because it lowered the threshold of landscape sensitivity to erosion and destabilized the drainage basin mass balance system, impacting sediment production and dispersal (Gomez, Carter and Trustrum, 2007; Phillips and Gomez, 2007)

Furthermore, the response of the Caldeirão system to increased water availability is reflected in runoff enhancement. Since the flat domain 1 in the bottom of the caldera amplifies the increase of water area rather than the column, enhanced runoff might have resulted in a prominent lake expansion. This is evidenced by the ecological shift characterized by the transition from tychoplanctonic to benthic species (Raposeiro et al., 2021; Fig. 7.4), probably due to the generation of new benthic habitats. Furthermore, the occurrence of planktonic species corresponding with the impact reinforce the increased water availability. Moreover, Historical documents report the existence of seven islands within the lake during the period right after the impact (Fructuoso, 1522-1591). The scoria cones located within the caldera (Figs. 2.20 and 2.21) might have constituted these islands with levels ca. 20 m above the current water lamina.

Furthermore, the occurrence of the thick deposit of Lithofacies E during the sedimentary stage 4 (Fig. 6.1) indicates the dramatic loss of soil through erosion and enhanced bypass at the flat domain 1, due to diminished soil cohesion during the regressive phase of the lake. Runoff decreases at ca. 300 cal yr BP may correspond with limited hydrological availability in the system favouring the regressive phase responsible for soil erosion (Fig. 7.4). The incision of alluvial fans observed in field (Fig. 2.21c) in correspondence with the erosive domain 2 (Fig.4.1) might correspond with this period of exacerbated erosion.

### 7.2.4 Profound landscape transformation (since 1430/1450 CE)

Increased RoC values of ca. 1 in CL1703 record, corresponding with the onset of the sedimentary stage 5 in the Caldeirão caldera detected through a biogeochemical CONISS break, might indicate streams damming (Fig. 2.21b,c) during the profound landscape transformation occurred during the fourth phase of ecological transformation (Raposeiro et al., 2021). Since Portuguese inhabitants used the inner caldera for cow grazing since historical times (Raposerio et al., 2021), stream damming was probably motivated by the pasteure loss due to out-of-control soil erosion since the previous stage of landscape transformation was dominated by deforestation. Stream damming may

have resulted in dramatic consequences for nutrients released into the lake, hampering diatom thrive due to reduced silicic supply. This might have conferred a competitive advantage to green algae which thrived to compose the Lithofacies $M_A$, which evidences the transition to eutrophic conditions (Raposeiro et al., 2021), probably due to the alteration of the nutrients release pattern into the lake.

## 7.3 Climatic evolution

Pearson's rank correlation coefficients between the meteorological data of precipitation and temperature and the sedimentary drivers of the Funda and Caldeirão systems reveal the transmission mechanisms of the climatic signal to their lake sediments (Tables 4.8, 4.9 and 4.10). The WG lake sediments climatic imprints allow to discuss the paleoclimatic evolution of the Azores Archipelago (Björck et al., 2006; Hernandez et al., 2017) during the last 3700. However, further research is needed to determine the role of paleoclimate in the sedimentary infill of Lake Caveiro sediments.

The correlation analysis between Funda sedimentary dynamics and the climatic variables of the study area reveal the transmission mechanism of the climatic signal to Lake Funda sediments (Table 4.8 and 4.9; Fig. 7.1). The high correlation shown between catchment erosion ($PC1_{fun}$) and the humid season precipitation (ONDJFM) indicates the effect of runoff over the catchment denudation. The strong correlation shown by erosion ($PC1_{fun}$) and lake level ($PC2_{fun}$), indicates runoff driving both processes. Although displaying relatively high effect, the limited significance (p-value = 0.1) of the correlation between hydrological recharge ($PC2_{fun}$) and air summer (JJA) air temperatures, may indicate the multiple effects affecting lake level fluctuations within the Funda system. These effects could be attributed to: 1) water lamina fluctuations through lake waters direct evaporation and evapotranspiration performed by the vegetal cover, 2) over thermocline strength and depth during highstand conditions after 600 cal yr BP through lake waters temperatures and 3) over erosion during the lowstand before 600 cal yr BP, through enhanced runoff driven by sea surface water evaporation. Nevertheless, high significant correlations establish between summer temperatures and the varve thicknesses records revealing the influence of summer temperatures over summer thermocline depth, strength and persistence. The high correlation between summer temperatures and water column turnover, resuspension and diatom productivity indicates the sharpher, deeper and more persistent summer thermocline. These three parameters trigger more energetic fall turnover inducing higher lake bottom shear stress, convection and turbulence. Energetic fall turnover provokes enhanced resuspension episodes during winter and long-lasting resettlement, probably up to late summers, favouring diatom productivity and accumulation of derived fossil remains.

The correlation analysis between Caldeirão sedimentary dynamics and the climatic variables of the study area reveal the transmission mechanism of the climatic signal to Lake Caldeirão sediments (Table 4.10; Fig. 7.1). The strong effect shown by wet season (ONDJFM) precipitation over runoff ($PC1_{cald}$) indicates the effect of runoff over Caldeirão system catchment, delivering soil materials and water into the lake. In contrast, the high effect displayed by summer air temperatures over the pedogenetic conditions within the catchment indicates the effect over the catchment material reactivity through hydrolysis (Depetris et al., 2014) and bacteria decomposition (Lerch et al., 2011). Therefore, the interplay between particle size reduction forced by air thermal conditions in the catchment and particle mobilisation forced by precipitation indicate that the sedimentary dynamics within the Caldeirão system is dominated by denudation. Summer (JJA) temperatures raise weathering rates in Caldeirão watershed rocks, since higher temperature enhances the hydrolysis of primary minerals for a short time scale (Catalan et al., 2014).

The summer temperatures are transferred to Lake Funda sediments through the influence that air temperature and solar irradiation have on lake waters, inducing the formation of a thermocline, which eventually breaks to conform the laminated sedimentary pattern through resuspension. In contrast,

in Caldeirão, air temperatures signal is transmitted into lake sediments through an increase of the reactivity of the materials during pedogenesis due to higher temperatures (Catalan et al., 2014). This is why temperatures are recorded in a different way in each lake. In Lake Funda, temperature might be buffered by the hydroclimatic filter of the lake water (Fig. 1.19). However, the Caldeirão system records thermal conditions directly through summer air temperature variations, showing a noisier pattern.

Sediment cascading plays a pivotal role concerning precipitation signals recorded in Funda and Caldeirão systems. Precipitation is recorded in the sediments through erosion in the Funda system, but it does through runoff in Caldeirão, due to the distinct morphology of the basins. The verticalized distribution of elevation impulses sediment cascading in Funda system, whereas the flat paralimnion at the bottom of the caldera in Caldeirão system buffer detrital release into the lake, dominantly contributing with water supply, fine particles and dissolved compounds. Thus, the precipitation signal in Lake Funda is noisier, recording higher order cycles of precipitation such as severe storms and probably hurricanes (Hernandez et al., 2016), responsible for the delivery into the lake of deposits corresponding with $F1_{fun}$. In contrast, the Caldeirão system records lower order climatic signals of precipitation derived from long-term variability.

Time lags deduced from cross-correlation analyses might be indicating filtering effects (Fig. 1.19) of the climatic signal through the variable sedimentary dynamics within each lake system (Cohen, 2003). The sedimentary response of the Funda system to winter precipitation delays two years, whereas increased winter precipitation in the Caldeirão system takes five years (Tables 4.8 and 4.10). Furthermore, the effect of summer temperature over lake level in the Funda system delays three years, whereas it takes six years to influence in the Caldeirão system pedogenesis. Besides age-depth model uncertainties, variable time lags might be evidencing the effect of enhanced sedimentary cascading in the Funda system due to the verticalized distribution of elevations, and the buffering effect of the flat domain 1 over Lake Caldeirão sedimentation. In summary, for Lake Caldeirão sediments, high (low) runoff and low (high) weathering rates promote the input of larger (smaller) grain sizes. Moreover, the responsible for higher grain sizes in Lake Funda are extreme runoff events and lowstands, and viceversa. High (Low) and extreme (weak) runoff, is favoured during humid (dry) climate, while enhanced (reduced) weathering rates and lowstands (highstands) during warm (cold) climate.

### 7.3.1 Climatic evolution of the Azores Archipelago western group (Lakes Funda and Caldeirão) during the late Holocene

Despite being widely forced by the complex geological configuration of the underlying basins (Fig. 7.2) and the anthropic colonization history of the archipelago (Fig. 7.4), the sedimentary dynamics within Funda and Caldeirão systems has demonstrated to transfer climatic imprints to the biogeochemical signal recorded in their lacustrine sedimentary infill (Fig. 7.1), as detailed below:

Stage 1 (S1; ca. 3700 to 2700 cal. yr BP), only recorded in Lake Caldeirão sediments (Corvo Island), coincides with the Late Bronze Age (LBA) and the onset of the Iron Age (IA) (3700-2700 cal. yr BP) and it is characterized by a dominance of cold and humid conditions (Fig 7.5). These prevailing humid conditions also affected the CG (Fig. 7.5; Björck et al., 2006). However, from 3200 cal. yrs BP to the end of this period, a decreasing runoff trend in the CG reveals a progressive transition to more arid conditions (Fig. 7.5; Björck et al., 2006). This transition to drier conditions was also recorded in the WG, but ca. 200 years later (Fig. 7.5). These discrepancies might be related to the omission of time periods in the age-depth modelling of Lake Caveiro by Björck et al., (2006) due to tephra deposits interpretation.

Stage 2 (S2; ca. 2700 to 1800 cal. yr BP), which coincides with almost all the Iron Age (IA; 2700-2050 cal. yr BP) and the onset of the Roman Period (RP; 2050-1800 cal. yr BP), is also only recorded

in Corvo island, and it was characterized by a predominant humid and warm climate becoming progressively more arid and colder (Fig. 7.5). This decreasing trend in humid conditions was also recorded by diminishing runoff rates in the CG (Björck et al., 2006; Fig. 7.5)

Stage 3 (S3; ca. 1800 to 650 cal. yr BP) corresponds to the late RP (1800 - 1350 cal. yr BP), the Early Middle Ages (EMA; 1350 – 950 cal. yr BP), and the Medieval Climate Anomaly (MCA; 950 – 650 cal. yr BP) climatic periods, with the latest (MCA) being recorded in Lakes Funda and Caldeirão sediment records (Fig. 7.5). During this stage, Lake Caldeirão sediments recorded prevalent dry and warm conditions corresponding with the RP and the EMA (from 1800 to 1100 cal yr BP), reflected in decreased runoff and pedogenesis, respectively.

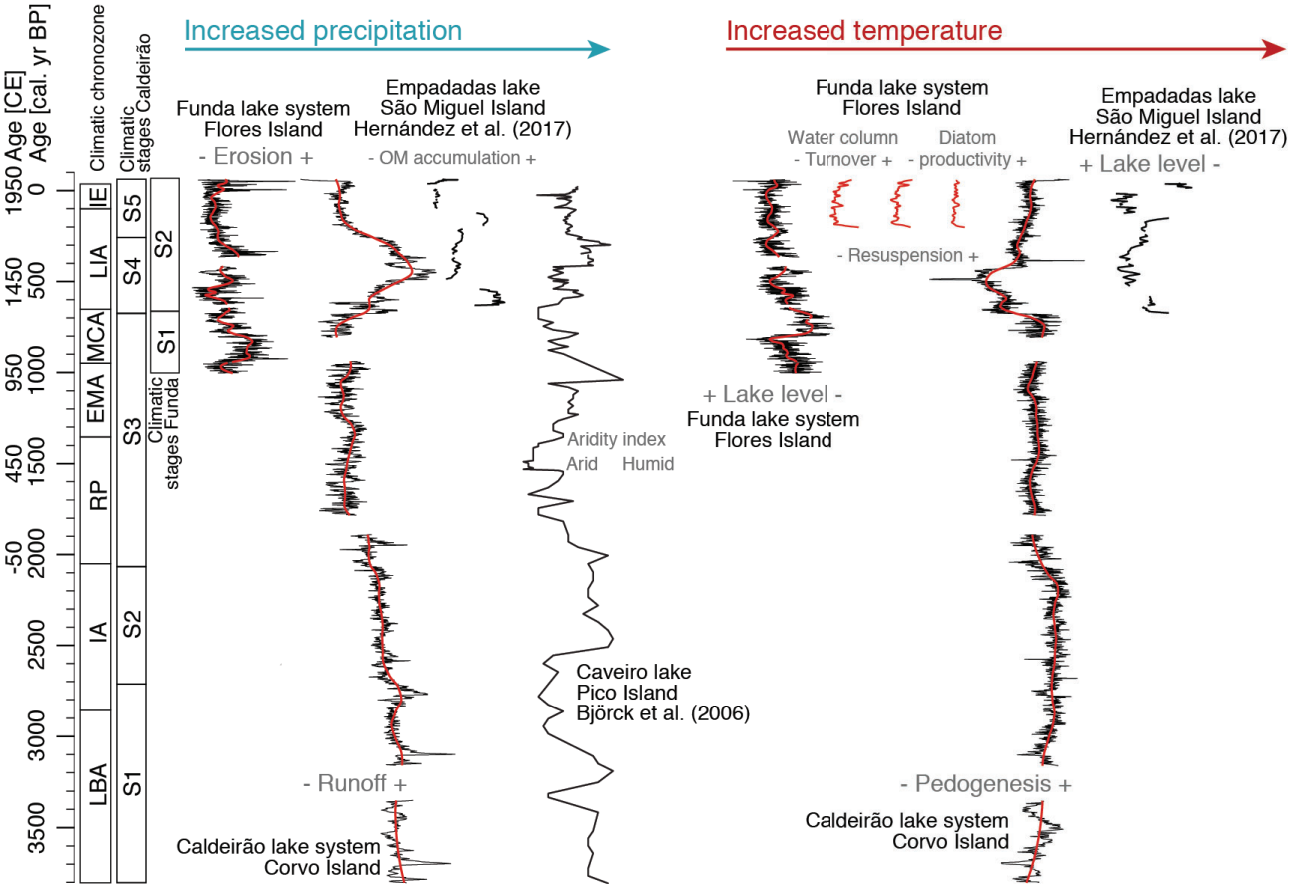


*Fig. 7.5: The climatic evolution in Funda and Caldeirão lake systems compared with the azorean paleoclimatic context. IE: industrial Era, LIA: Little Ice Age, MCA: Medieval Climate Anomaly, EMA: Early Middle Ages, RP: Roman Period. IA: Iron Age, LBA: Late Bronze Age.*

Lake Funda sediments recorded prevalent humid and cold conditions during the EMA-MCA transition (ca. 1100 – 900 cal. yr BP). However, this pattern does not replicate in the proximal Caldeirão system, which displays moderate to high rates of weathering and the lowest rates of runoff of the entire record, indicating prevalent dry and mild conditions. Since the dominant depositional conditions governing Lake Funda during this subperiod were characterized by the lacustrine delta prior to submersion, the abnormally wet and cold climate inferred for the Lake Funda system may be exacerbated due to the modulation of erosion intensity by the dominant geomorphic configuration. Alluvial processes might be more intense than in successive substages due to the geomorphological development during lake deepening conditions. This would induce a pattern of low ergodicity, misleading a proper climatic interpretation, which might be closer to that of Lake Caldeirão, which did not experience any morphosedimentary effect during this time period. Therefore, dry and mild climate conditions may have dominated the WG during the late MCA. Although, a drive change during the core extraction of Lake Caldeirão obscured the characterization of the climatic conditions

from ca. 950 to 850 cal yr BP. Finally, Lake Funda sediments recorded progressive aridification and warming during the late MCA (ca. 800 – 650 cal. yr BP) by decreasing erosion and lake levels.

Besides, in the CG, Björck et al. (2006) reconstructed low runoff rates during the late RP and the late MCA but higher during the EMA-MCA transition (Fig. 7.5) and low runoff rates during the unrecorded subperiod of Caldeirão system confirming the suggested arid conditions. Therefore, the same precipitation pattern (arid-to-humid and humid-to-arid) could be assigned to the WG and likely to the entire Azores Archipelago.

Stage 4 (S4; ca. 650 to 250 cal. yr BP) corresponds to the early Little Ice Age (LIA; 650 – 250 cal. yr BP). High runoff rates, high lake water levels, and very low weathering rates recorded in Corvo and Flores lake systems reveal the dominance of humid and cold climate conditions in the WG during this period. Increased precipitation was also reconstructed in the CG via enhanced runoff rates (Björck. et al., 2006; Fig. 7.5) and in the EG via increased nutrient supply triggering higher OM accumulation (Hernández et al., 2017; Fig. 7.5).

Stage 5 (S5; ca. 250 cal. yr BP to present) coincides with the late LIA (250 – 100 cal. yr BP) and the Industrial Era (IE; 100 cal. yr BP - present). During this stage, low runoff rates in Corvo and Flores islands reveal dominating arid conditions in the WG. Decreased runoff and OM accumulation reconstructed in other lakes from the Azores Archipelago suggest that these arid conditions prevailed in the rest of Azores Archipelago (Björck et al., 2006; Hernández et al., 2017). However, the IE shows a precipitation rising in the WG that extended to the rest of the archipelago during the late IE (ca. 0 cal. yr BP - present) (Björck et al., 2006; Hernández et al., 2017).

# 8. Discussion: The North Atlantic climatic evolution and atmospheric modes of climate variability impact on the Azores Archipelago during the late Holocene

The high significant correlation between the wet season (ONDJFM) precipitation in the WG and the NAOi reveals the effect of the north Atlantic storm track migration through time (Tabla 4.11). The negative correlation indicates that the Azores Archipelago is highly impacted by winter precipitation due to the Azores High weakening (negative NAOi), allowing the north Atlantic storm track to cross directly through the Archipelago (Table 4.11). These wetter conditions are reflected in the paleoclimatic evolution recorded in the sediments of Lake Funda (Table, 4.8) and Lake Caldeirão (Table, 4.10) (Section 7). Besides, the high significant correlation between the WG summer (JJA) temperatures and the EAi (Table. 4.11) is probably evidencing higher solar irradiance affecting atmospheric thermal condition globally (Moffa-Sanchez et al. 2014; Hernández et al. 2021). The WG lacustrine sediments evidence this climatic effect through increased catchment pedogenesis in Lake Caldeirão basin and through a partial contribution over lake level changes in Lake Funda. Thus, the environmental stages identified within the CL1703 record, supported by those from FN1702, allowed the identification of 5 main climatic stages. The reconstructed climatic evolution has been compared with other climate records (Fig. 7.5) of the North Atlantic sector (Fig. 1.30). Therefore, the interplay between the winter NAO and summer EA phases control a significant part of the climatic conditions in the WG. Dry winters and warm summers would predominate during winter positive NAO and summer positive EA atmospheric configuration, while wet winters and cold summers would predominate during winter negative NAO and summer negative EA phases.

### Stage 1 (S1; ca. 3700 to 2700 cal. yr BP) - negative winter NAO and negative summer EA

The dominant humid conditions for this stage revealed by the increased runoff rates in Corvo Island (Fig 8.1a) mismatch the low riverine discharge found in the Alboran sea (Nieto-Moreno et al., 2011; Fig. 8.1c) and the low water levels in lakes of the Iberian Peninsula (IP) (Martín-Puertas et al., 2008; Fig. 8.1d) (Fig. 1.30), arid conditions dominated the whole LBA period (3700-2850 cal. yr BP) in SW Europe. Conversely, in northwest Iceland the marine sediments of the MD99-2266 core from Isafjarðardjúp Fjord recorded high average chain lengths of leaf waxes, high global ice volume and low soil pH, indicating humid climatic conditions for this period (Moossen et al., 2015; Figs. 8.1g and 1.30).

The regional cold conditions reconstructed from Corvo Island are also recorded by the foraminifera assemblages from this period in the MD99-2203 core from Cape Hatteras (North Carolina coast; Fig. 1.30) (Cleroux et al., 2012), indicating cold subtropical SST (Fig. 8.1m). In the Pyrenees (northern IP), these colder conditions but for winter/spring temperatures are also recorded, with a rapid temperature rise at the end of this period (Pla and Catalan, 2005). Thus, according to the temperature reconstruction, progressive regional warming occurred, as well as an aridity enhancement in Azores Archipelago shown at the end of the LBA period (Björck et al., 2006; Fig. 7.5). This aridity enhancement in the central North Atlantic was likely triggered by low Total Solar Irradiance (TSI; Steinhilber et al., 2009; Fig. 8.1q). However, the increased biologic activity of lakes Haukadalsvatn (HAK) and Hvítárvatn (HVT) in western Iceland (Geirsdóttir et al., 2013; Figs. 8.1n

and 1.30) and changes in $\delta^{18}O$ of GISP2 ice core (Grootes and Stuiver, 1997; Figs. 8.1p and 1.30) suggests an opposite temperature pattern with warm climatic conditions in northwestern Europe and Greenland for all this stage.

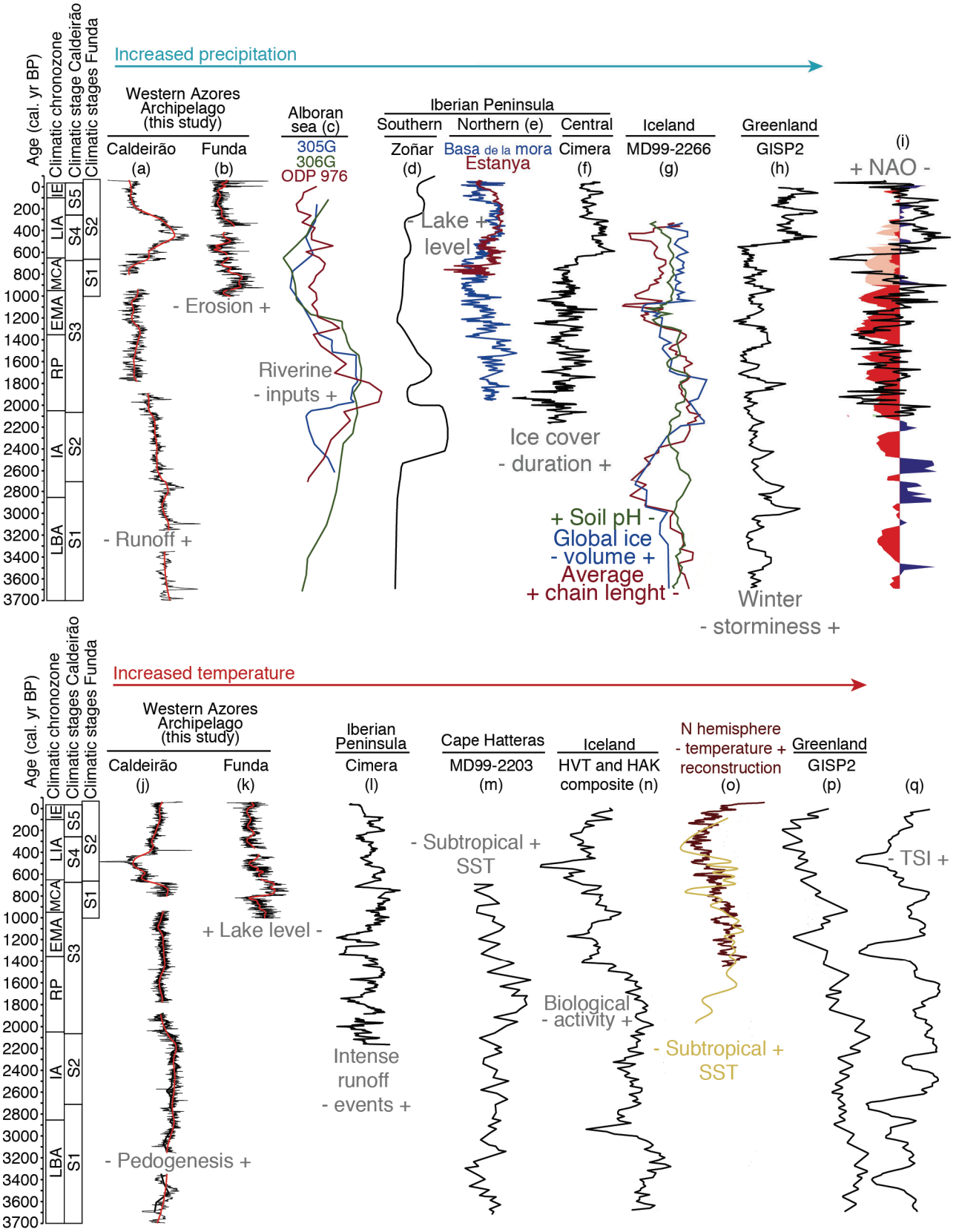


*Fig. 8.1. Regional climatic records comparison. The upper part shows records related to the precipitation of the North Atlantic sector: a) $PC1_{cald}$ and b) $PC1_{fun}$ from this work; c) 305G and 306G records from Nieto-Moreno et al., 2011; ODP 976 record from Martín-Puertas et al., 2010; d) 2008; e) Morellón et al., 2011; Moreno et al.,*

*2012; f) Sánchez-López el al., 2016; g) Moossen et al., 2015), h) storminess (Mayewsky et al., 1997) and i) NAO (Olsen et al., 2012; Hernández et al., 2020; Ortega et al., 2015). The lower part shows records related to Temperature of the North Atlantic sector: j) $PC2_{cald}$ and k) $PC2_{fun}$ from this work; l) Sánchez-López et al., 2016; m) MD99-2203 record from Cleroux et al., 2012; n) Geirsdóttir et al., 2013; o) deMenocal et al., 2000 and Mann et al., 2009; p) Grootes and Stuiver, 1997) and q) TSI (Steinhilber et al., 2009). IE: industrial Era, LIA: Little Ice Age, MCA: Medieval Climate Anomaly, EMA: Early Middle Ages, RP: Roman Period. IA: Iron Age, LBA: Late Broce Age, HAK: Haukadalsvatn, HVT: Hvítárvatn.*

This climatic scenario results from the prevalent negative winter NAO atmospheric configuration for this period (Olsen et al., 2012; Fig. 8.1i). These winter conditions would favour oceanic humid and warm westerlies following a meridional route, directly crossing through Azores Archipelago, towards southwestern Europe. Little is known about the summer EA role over the European Atlantic sector. Comas-Bru and Hernández (2018) suggested a weak influence of the summer EA over Europe displaying negative correlations with temperature, however Hernandez et al. (2015) showed a strong impact of the summer EA on Iberian temperatures, with warmer summers during EA positive phases. Thus, the reconstructed humid and overall cold climatic conditions of the WG for this period and the relationships established between instrumental winter precipitation and NAO, as well as instrumental summer temperatures and EA suggest a predominant combination of winter NAO and summer EA negative phases ($NAO^-$ - $EA^-$).

### Stage 2 (S2; ca. 2700 to 1800 cal. yr BP) - negative winter NAO and positive summer EA

The warm and humid conditions for this stage, becoming progressively more arid and colder found in the Azores (Fig. 7.5) corresponds with lowering lake levels in the southern IP at the end of this stage (Martin-Puertas et al., 2008; Fig. 8.1d). However, this trend contrasts with the high riverine inputs at the Alboran sea indicating predominant humid conditions during this period (Nieto-Moreno et al., 2011; Martín-Puertas et al., 2010; Fig. 8.1c). Furthermore, northwest Iceland recorded a progressive shift from arid to humid conditions (Mossen et al., 2015; Fig. 8.1g). This climatic evolution of the North Atlantic sector during the IA suggests that the same humid conditions present in Azores Archipelago extended towards southwestern Europe, while predominantly arid conditions dominated northwestern Europe.

The beginning of the RP (2050-1800 cal. yr BP) shows a reverse pattern with more arid conditions in Azores Archipelago (Fig. 8.1a,c) and the IP (Fig. 8.1d), and wetter conditions in northwest Iceland (Fig. 8.1g). The early RP lower weathering rates in Corvo island correspond to less intense and frequent runoff events in the central mountains of the IP (Sánchez-López et al., 2016; Fig. 8.1l) and enhanced biological activity in HVT and HAK lakes in northwestern Iceland (Geirsdóttir et al., 2013; Fig. 8.1n).

This North Atlantic European sector picture suggests a humidity gradient between southwestern and northwestern Europe that migrated towards northern positions during the RP, shifting the humid and warm westerlies route from southern to northern Europe. This precipitation gradient was also recognized at the IP for this period (Sánchez-López et al., 2016), with prevailing wet conditions in southeastern IP and dry conditions in northwestern Iberia.

The warm conditions prevailing at the WG during the IA (2850-2050 cal. yr BP) were also recorded in the Tagus prodelta sediments (Abrantes et al., 2005; Rodrigues et al., 2009) and the Northeast of IP for winter spring temperatures (Pla and Catalan, 2005). They were most probably caused by the enhancement of the subtropical SST (Cleroux et al., 2012; Fig. 8.1m) likely triggered by increased TSI (Steinhilber et al., 2009; Fig. 8.1q). This indicates a decreasing trend of temperature in southeastern Europe and increasing in northwestern Europe to the end of this stage, which is also observed in the NE of the IP (Pla and Catalan 2005).

These humid and warm climate conditions in the WG are linked to a prevalent negative winter NAO and positive summer EA ($NAO^-$ - $EA^+$). Negative NAO for this time period was also reconstructed by Olsen et al. (2012) (Fig. 8.1i) in the central north Atlantic. Similar to Stage 1, this atmospheric configuration led westerlies to a more meridional route. Moreover, the switching of climatic conditions during this stage, from wet and warm to dry and cold in Azores Archipelago and southwestern Europe (Pla and Catalan 2005; Björck et al., 2006; Martín-Puertas et al., 2008; Nieto-Moreno et al., 2011) and from dry and cold to wet and warm in northwestern Europe (Moossen et al., 20015; Geirsdóttir et al., 2013) suggest the migration of the precipitation gradient northwards.

### Stage 3 (S3; ca. 1800 to 650 cal. yr BP) - positive winter NAO and negative summer EA

The dominantly arid conditions in the Azores Archipelago for this stage correspond with predominant arid conditions reconstructed by Martín-Puertas et al. (2008) in the southern IP through decreasing lake levels during the late RP and lowstand lake conditions during the EMA and MCA (Fig. 8.1d). Furthermore, during the EMA and the MCA, a reduction in the ice cover duration of the mountain lakes of central IP (Sánchez-López et al., 2016; Figs. 8.1f and 1.30), a period of decreasing runoff floods in the northern IP (Moreno et al., 2012; Figs. 8.1e and 1.30) and the Alboran sea (Nieto-Moreno et al., 2011; Martín-Puertas et al., 2010; Figs.8.1e and 1.30) were recorded. Therefore, the entire IP and SW Europe were under generalised arid conditions. Conversely, in Northwestern Iceland, Moossen et al. (2015) found lower average chain lengths of n-alkanes derived from leaf waxes, lower soil pH and an increase in global ice volume during the late RP, the onset of the EMA and the MCA (from ca. 1800 to 1100 and from 950 to 650 cal. yr BP) linked to the predominance of humid conditions. However, a reverse pattern of these parameters was recorded during the late EMA (ca. 1100 – 950 cal. yr BP). Thus, an opposite precipitation pattern (humid-to-arid-to-humid) to that recorded in the Azores Archipelago dominated northwestern Europe between 1800 and 600 cal. yr BP (Stage 3; Fig. 8.1g).

The cold prevalent climate conditions reconstructed for the WG during this stage (1800 to 600 cal. yr BP) were also recognized in the IP, where a decrease of intense runoff floods was recorded (Sánchez-López et al., 2016; Fg. 10o) and higher temperatures in NE of Iberian Peninsula (Pla and Catalan 2005). However, the progressive warming recorded during the late MCA (ca. 800 – 650 cal. yr BP) in Flores Island was also recorded 150 years earlier in the IP. Meanwhile, a decrease in lake primary productivity in Iceland (Geirsdóttir et al., 2013) suggests a decreasing trend in temperatures from ca. 1800 to 600 cal. yr BP (Fig. 8.1n). Furthermore, low $\delta^{18}O$ values recorded in GISP2 ice core for this period (ca. 1800 - 600 cal. yr BP) indicate the same cold conditions in Greenland (Grootes and Stuiver, 1997; Fig. 8.1p). These generalized cold conditions in the North Atlantic Ocean were coherent with an overall decrease in SST (Cleroux et al., 2012; Fig. 8.1m), which reflects the cooling trend that affected the Northern Hemisphere (Mann et al., 2009; Fig. 8.1o). These cold conditions were also concurrent with a decrease in solar activity (Steinhilber et al., 2009; Fig. 8.1q).

The generalised arid and cold climatic conditions found in the North Atlantic European sector for this stage (ca. 1800 to 600 cal. yr BP) are associated with a winter positive NAO dominance and summer negative EA phases ($NAO^+$-$EA^-$). Positive NAO conditions were also reconstructed by Hernández et al. (2020b) and Olsen et al. (2012) for this period (Fig. 8.1i). This configuration points to a septentrional route for humid air masses preventing them from crossing the Azores Archipelago and transporting them directly to northwestern Europe. Nevertheless, a deflection to lower latitudes of westerlies likely occurred during the EMA-MCA transition (ca.1100 – 900 cal yr BP), as indicated by the increase of precipitation recorded in Azores Archipelago (Björck et al., 2006) and the decrease of precipitation recorded in Iceland (Moossen et al., 2015).

### Stage 4 (S4; ca. 650 to 250 cal. yr BP) - negative winter NAO and negative summer EA

High runoff rates, high lake water levels, and very low weathering rates were recorded in Corvo and Flores lake systems for this period, revealing the dominance of humid and cold climate conditions in the WG during this period. These humid conditions were also recorded in the central IP, through increasing ice cover duration in mountain lakes (Sánchez-López et al., 2016; Oliva et al. 2018) (Fig. 8.1f), low spring/winter temperatures (Pla and Catalan, 2005) and higher lake levels in the northern IP (Moreno et al., 2012; Morellón et al., 2011; Fig. 8.1e). However, lower lake levels at the southern IP (Martín-Puertas et al., 2008; Fig. 8.1d) and lower riverine inputs in the Alboran sea (Martín-Puertas et al., 2010; Nieto-Moreno et al., 2011; Fig. 8.1c) were also recorded during this period. In turn, in northwest Iceland high soil pH, longer average chain length of leaf wax derived n-alkanes and decreased global ice volume suggest an arid climate dominating Northwestern Europe (Moossen et al., 2015; Fig. 8.1g). Additionally, the highest salt concentrations found in GISP2 ice core for the last 3700 years reveal enhanced storminess during this period (Mayewsky et al., 1997; Fig. 8.1h).

The IP and Iceland also recorded low temperatures during this period (Pla and Catalan, 2005; Sánchez-López et al., 2016; Geirsdóttir et al., 2013; Oliva et al. 2018) triggered by low TSI (Steinhilber et al., 2009) (Fig. 8.1). These cold temperatures were recorded in Central Greenland (Grootes and Stuiver, 1997) as well by the SST of the North Atlantic (Mann et al., 2009; Cleroux et al., 2012; deMenocal et al., 2000; Fig. 8.1m,o) indicating regional cold conditions during the LIA.

This climatic scenario over the European North Atlantic region, similar to the one found during the LBA (3700 - 2800 cal. yr BP), would correspond to a negative winter NAO and summer EA ($NAO^-$ - $EA^-$). This NAO configuration was already reconstructed in previous works (Ortega et al., 2015; Olsen et al., 2012; Hernández et al., 2020b; Fig. 8.1i).

### Stage 5 (S5; ca. 250 cal. yr BP to present) - positive winter NAO and positive summer EA

During this stage, low runoff rates in Corvo and Flores islands reveal dominating arid conditions in the WG (Fig. 7.5). These overall arid conditions were also present in southeastern Europe, and they were reflected in the lower riverine inputs reconstructed in the Alboran Sea (Martín-Puertas et al., 2010; Fig. 8.1c), lower lake levels in the northern (Moreno et al., 2012; Morellón et al., 2011; Fig. 8.1e) and southern IP (Martín-Puertas et al., 2008; Fig. 8.1d), and shorter ice cover duration of central IP mountain lakes (Sánchez-López et al., 2016; Fig. 8.1f).

Enhanced weathering rates in Corvo island indicate the dominance of warm climate conditions in the WG which can be attributed to the current global warming trend. Changes in weathering rates have been linked to changes in temperatures at short time scales (Catalan et al. 2014). However, predominantly highstand lake level reconstructed in Lake Funda (Flores) would correspond to cold conditions in the WG. This discrepancy in temperature records could be attributed to the increasing precipitation trend found in Azores Archipelago due to enhanced runoff rates (Björck et al., 2006; Hernández et al., 2017; Fig. 8.1c,d). The increasing trend of precipitation during the late IE (ca. 0 cal. yr BP - present) reconstructed for Corvo, Pico, and Sao Miguel islands (Hernández et al., 2017), could also be affecting Flores Island (Fig. 8.1b). The central IP described these temperature discrepancies, attributing them to increasing OM contents, provoked by the growing anthropic pressure, what diluted the inorganic fraction of the sediments, thereby lowering the signal of almost all XRF geochemical elements (Sánchez-López et al., 2016). This could also be the case of Lake Funda, where anthropic activities induced permanent highstand conditions through forest clearance that resulted in a surplus of water in the lake system and promoted in-lake production. Therefore, although it would be masked in Lake Funda, the temperature records of Corvo and Sao Miguel islands (Hernández et al., 2017) suggest that warm conditions dominate the whole Azores Archipelago during this stage. In northwestern Europe, warmer temperatures were also recorded through increased lake biological activity in Iceland (Geirsdóttir et al., 2013; Fig. 8.1n) and changes

in $\delta^{18}O$ of ice in Greenland (Grootes and Stuiver, 1997; Fig. 8.1p). The generalised rising of Noth Atlantic SST (Cleroux et al., 2012; deMenocal et al., 2000; Fig. 8.1m,o) might be linked to the overall temperature increase that affected the Northern Hemisphere (Mann et al., 2009; Fig. 8.1o), most likely associated with both the increase in the TSI (Steinhilber et al., 2009; Fig. 8.1q) and the current anthropogenic global warming (Mann et al., 2009).

This climatic scenario was led by dominating positive winter NAO and summer EA (NAO+/EA+). Similar to Stage 3 (1800 - 600 cal. yr BP) the dominant NAO positive conditions provoked the northwards migration of humid and warm westerlies. Furthermore, positive EA values identified in the WG would correspond with the generalised warmer temperatures found in the North Atlantic European sector (Fig. 8.1).

Furthermore, the RoC peak point detected in the CL1703 record at present times, corresponding in turn with peak values in the FN1702 record and the establishment of stage 2c deducted from the FN1704G record indicate accelerated sedimentary changes attributable to global warming. Increased frequency and intensity of turbiditic deposits in Lake Funda (Fig. 4.18) might be related to enhanced stormines due to the jet stream weakening, provoking extreme weather events across the central North Atlantic region (Mellado-Cano et al., 2014).

# 9. Conclusions

The lake sediments within the tectono-volcanic basins of lakes Funda, Caldeirão and Caveiro have demonstrated their suitability to conduct paleoenvironmental research on landscape evolution. The biogeochemical characteristics of these sediments unrevealed the complex interaction between the landscape dynamics and the geologic configuration of the Azores Archipelago during the last four millennia, leading to the following specific conclusions:

- The use of K-means has enabled the quantitative characterization of facies based on distinct biogeochemical signatures, constituting chemofacies. Moreover, employing k-means partitioning on the stratigraphic sequences has facilitated the correlation between sedimentary sequences and the geomorphic evidence of the lake-catchment systems, thereby developing process-response models indicative of the morphosedimentary dynamics within these systems.

- The combined analysis of chemofacies with the identification of Ksn limnogeomorphic domains represents a new advancement in paleolimnology research. This advancement presents an opportunity to develop modern training or calibration datasets through transfer functions that bridge geomorphology and geochemical paleolimnology. These datasets enable the assessment of spatiotemporal erosive histories within lake-catchment systems.

- Age-depth model construction presented challenges due to discrepancies between different methodological approaches, emphasizing the significance of sedimentological analysis for accurately interpreting sedimentary processes and accumulation rates.

- Limnogeomorphology analysis of surficial processes have provided the needed knowledge to understand the spatial distribution of environmental changes. Additionally, sequential chemostratigraphy, coupled with lithostratigraphic evidence, revealed the sedimentation pattern within the Lake Caveiro system.

- Analysis of Ksn erodibility, field observations, and sediment cascading, using lithologic, geochemical, and biological data from proxy-based records, revealed sediment delivery pathways and system deposits. This identification showed their role in biogeochemical cycling from source to sink. Erosive domains identified the sources and delivery routes of allochthonous sedimentary facies, which varied within the three systems according to their elevation gradients and water volumes of the lake basins.

- The definition of spatiotemporal sedimentation patterns and morphostratigraphic surfaces have demonstrated that lakes Funda and Caldeirão represent two contrasting morphometric extremes such as low- and high-gradient lake basins ruling the sediment accumulation, whereas Lake Caveiro has rapidly evolved from high-gradient to low one due to its limited accommodation space.

- Microlithofacies analysis challenged the existing sedimentary model for Lake Caveiro, known for frequent tephra deposition. The previous model may have led to inaccurate interpretations and age constraints. The new model suggests hydrological decline due to neotectonic reactivation processes, thus offering a more accurate explanation.

- During the last ca. 1000 years, Lake Funda has shown homeorhetic behavior, driven by its steep basin gradient. This has led to positive feedback mechanisms that strengthen the cascading of alluvial sediment and in-lake productivity. In contrast, during the last ca. 3700 years, Lake Caldeirão has shown homeostatic behaviour due to its relief distribution. Consequently, the

biogeochemical variability of Lake Funda has been controlled by the alluvial sediment cascading and in-lake productivity, whereas in Lake Caldeirão hydroclimatic fluctuations have played a dominant role, making this lake more suitable for paleoclimatic reconstructions.

- Caveiro lake-catchment system has had a short ontogeny due to its small size during the last ca. 5200 years. This evolution demonstrates the transition from homeorhetic behaviour of the system to homeostatic during the last stage marked by siltation. This evolution was strongly affected by lineal morphosedimentary processes and modulated by cyclic hydroclimatic fluctuations.

- The complex tectono-volcanic configuration of the Azores triple junction rules the sedimentary dynamics of the lacustrine ecosystems by exerting long-term morphodynamic effects on their evolution. The morphology of the lake basins, largely modulated by the tectonic and volcanic setup of the Azores Archipelago plays a significant role in determining the morphosedimentary evolution within these systems. This governs the sedimentary entropy within the systems, leaving variable biogeochemical imprints in the lake sediments.

- The oriented relief of the Funda and Caveiro basins favor selective sediment accretion, modulating the intensity of the recorded drivers and resulting in low ergodicity in biogeochemical signals. Conversely, the chaotic relief of the Caldeirão basin promotes a morphosedimentary evolution with higher spatial stationarity resulting in high ergodicity in sediment-derived time series.

- Lake basins with more verticalized configurations, such as Funda and Caveiro basins in their early stages, promote sediment cascading and summer thermocline establishment. Both factors favor high-frequency sedimentary patterns reflecting low-order biogeochemical signals linked to the north Atlantic hurricane season and fall turnover. In contrast, basins like Caldeirão and late stages of Caveiro basins, with more horizontal configurations, buffer sediment cascading and primarily record higher-order biogeochemical signals, reflecting the NAO-EA interplay evolution.

- Rate of Change analyses allowed the identification of rapid biogeochemical shifts, aiding in identifying multidecadal climate fluctuations and human impacts on catchments. Correlations of rapid changes between the studied locations have disentangled local and regional contributions to the biogeochemical variability.

- Analysis of thin sections revealed varved sediments in Lake Funda, characterized by annual patterns influenced by fall resuspension and diatom productivity, showed the deposition of couplets and triplets of varying thickness. The recognition of varved sediments in Lake Funda offers high-resolution data for establishing correlations with observational records. These sediments are particularly valuable due to their location in subtropical latitudes, where studies on lake sediment studies are scarce compared to tropical and polar regions.

- Human disturbances in the Azores Archipelago have paradoxically provided an opportunity to enhance the understanding of North Atlantic climatic changes over the past 600 years. Despite these disturbances present challenges for natural conservation, ecosystem management, and environmental restoration efforts, they have simplified the transmission mechanisms of climatic signals to sedimentary archives. This simplification arises from the reduction in environmental complexity within lake-catchment systems.

- The reconstruction of the atmospheric, climatic and environmental changes in the European Atlantic sector reveals the significant impact of the summer EA on the North Atlantic climate.

This delivers new insights into atmospheric circulation patterns, essential for addressing the new challenges related to the current global change.

- The new knowledge of local and regional morphosedimentary evolution will facilitate the development of a more coherent regional paleoclimatic reconstruction. This deeper comprehension of sedimentary dynamics, particularly concerning alluvial mobilization processes associated with lacustrine sediments, will greatly benefit paleoenvironmental reconstructions.
- The obtained paleoclimatic dataset allowed the identification of the prevalent atmospheric patterns for the last 3700 years in the North Atlantic European sector. Five main stages have been established: Stage 1 (ca. 3700 to 2700 cal. yr BP) - negative winter NAO and negative summer EA; Stage 2 (ca. 2700 to 1800 cal. yr BP) - negative winter NAO and positive summer EA; Stage 3 (ca. 1800 to 650 cal. yr BP) - positive winter NAO and negative summer EA; Stage 4 (ca. 650 to 250 cal. yr BP) - negative winter NAO and negative summer EA; Stage 5 (ca. 250 cal. yr BP to present) - positive winter NAO and positive summer EA

### Future research

- The varved sediments of Lake Funda offer the opportunity of studying how global warming affects the central North Atlantic. Laminated sedimentary patterns in other lakes of the Azores Archipelago constitute promising records to aid in this purpose. By analyzing turbidite deposits alongside historical hurricanes, we can pinpoint the floating chronology of these sediments to understand how the jet stream weakening contributes to extreme weather events in the region.
- The integrated assessment of chemofacies and limno-geomorphology represents an opportunity for modern training or calibration datasets (transfer functions) that bridge the gap between limno-geomorphology and geochemical paleolimnology. This integration could enhance the spatio-temporal assessment of erosive histories within lake catchment systems, constituting a great advance for both disciplines, geomorphology and paleolimnology.
- The observed relationship between neotectonics and lacustrine sedimentation in Lake Caveiro highlights the potential of lake sediments in the Central Group of the Azores Archipelago, specifically, and tectono-volcanic lake basins, generally, for paleoseismicity research. This linkage might also represent an advancement for both disciplines, neotectonics and limnology.

## References


Abdel-Monem, A. A., Fernandez, L. A., & Boone, G. M. (1975). *K-Ar ages from the eastern Azores group (Santa Mafia, Miguel and the Formigas Islands)*.

Abrahams, A. D., Li, G., Krishnan, C., & Atkinson, J. F. (1998). Predicting sediment transport by interrill overland flow on rough surfaces. *Earth Surface Processes and Landforms: The Journal of the British Geomorphological Group*, *23*(12), 1087-1099.

Abrantes, F., Lebreiro, S., Rodrigues, T., Gil, I., Bartels-Jónsdóttir, H., Oliveira, P., Kissel, C., & Grimalt, J. O. (2005). Shallow-marine sediment cores record climate variability and earthquake activity off Lisbon (Portugal) for the last 2000 years. *Quaternary Science Reviews*, *24*(23–24), 2477–2494. https://doi.org/10.1016/j.quascirev.2004.04.009

ACIA. 2004. Impacts of a warming Arctic: Arctic climate impact assessment. Cambridge Univ. Press.

Adams, K. D., & Wesnousky, S. G. (1998). Shoreline processes and the age of the Lake Lahontan highstand in the Jessup embayment, Nevada. *Geological Society of America Bulletin*, *110*(10), 1318-1332.

Adrian, R., O'Reilly, C. M., Zagarese, H., Baines, S. B., Hessen, D. O., Keller, W., Livingstone, D. M., Sommaruga, R., Straile, D., Van Donk, E., Weyhenmeyer, G. A., & Winder, M. (2009). Lakes as sentinels of climate change. *Limnology and Oceanography*, *54*(6part2), 2283–2297. https://doi.org/10.4319/lo.2009.54.6_part_2.2283

Agencia Estatal de Meteorología (España) & Instituto de Meteorología (Portugal). (2012). *Atlas climático de los archipiélagos de Canarias, Madeira y Azores*. Agencia Estatal de Meteorología. https://doi.org/10.31978/281-12-006-X

Ahnert, F. (1987). Approaches to dynamic equilibrium in theoretical simulations of slope development. *Earth Surface Processes and Landforms*, *12*(1), 3-15.

Allison, R. J., Higgitt, D. L., Kirk, A. J., Warburton, J. E. F. F., Al-Homoud, A., Sunna, B., & White, K. E. V. I. N. (1998). Geology, geomorphology, hydrology, groundwater and physical resources. *Arid land resources and their management, Jordan desert margin*, 21-46.

Amasi, A., Wynants, M., Blake, W., & Mtei, K. (2021). Drivers, Impacts and Mitigation of Increased Sedimentation in the Hydropower Reservoirs of East Africa. *Land*, *10*(6), 638. https://doi.org/10.3390/land10060638

Amblard C, Boisson J-C, Fontvielle D, Gayte X, Sime-Ngando T (1998) Microbial ecology in aquatic systems: a review from viruses to protozoa. Rev Sci Eau N_ Special: 145–162.

Anadón, P., Cabrera, L., Julia, R., & Marzo, M. (1991). Sequential arrangement and asymmetrical fill in the Miocene Rubielos de Mora Basin (northeast Spain). *Lacustrine facies analysis*, 257-275.

Anderson, M. G., & Burt, T. P. (1990). Subsurface runoff. *Process studies in hillslope hydrology.*, 365-400.

Anderson, N. J. (2000). Diatoms, temperature and climatic change. *European Journal of Phycology*, *35*(4), 307-314.

Anderson, R. Y., & Dean, W. E. (1988). Lacustrine varve formation through time. palaeogeography, Palaeoclimatology, palaeoecology, 62(1-4), 215-235.

Anderson, R. Y., Nuhfer, E. B., & Dean, W. E. (1985). Sedimentation in a blast-zone lake at Mount St. Helens, Washington—implications for varve formation. *Geology*, *13*(5), 348-352.

Andrade, C., Cruz, J., Viveiros, F., & Coutinho, R. (2019). CO2 Flux from Volcanic Lakes in the Western Group of the Azores Archipelago (Portugal). *Water*, *11*(3), 599. https://doi.org/10.3390/w11030599

Andrade, M., Pimentel, A., Ramalho, R., Kutterolf, S., & Hernández, A. (2022). The recent volcanism of Flores Island (Azores): Stratigraphy and eruptive history of Funda Volcanic System. *Journal of Volcanology and Geothermal Research*, *432*, 107706. https://doi.org/10.1016/j.jvolgeores.2022.107706

Andrade, M., Ramalho, R. S., Pimentel, A., Hernández, A., Kutterolf, S., Sáez, A., Benavente, M., Raposeiro, P. M., & Giralt, S. (2021). Unraveling the Holocene Eruptive History of Flores Island (Azores) Through the Analysis of Lacustrine Sedimentary Records. *Frontiers in Earth Science*, *9*, 738178. https://doi.org/10.3389/feart.2021.738178

Andrade, M., Ramalho, R., Pimentel, A., Kutterolf, S., & Hernández, A. (2023). The recent volcanism of Flores Island (Azores), Part II: Stratigraphy and eruptive history of the Comprida Volcanic System. *Journal of Volcanology and Geothermal Research*, *438*, 107806. https://doi.org/10.1016/j.jvolgeores.2023.107806

Anselmetti, F. S., Ariztegui, D., Hodell, D. A., Hillesheim, M. B., Brenner, M., Gilli, A., McKenzie, J. A., & Mueller, A. D. (2006). Late Quaternary climate-induced lake level variations in Lake Petén Itzá, Guatemala, inferred from seismic stratigraphic analysis. *Palaeogeography, Palaeoclimatology, Palaeoecology*, *230*(1–2), 52–69. https://doi.org/10.1016/j.palaeo.2005.06.037

Antón, L., De Vicente, G., Muñoz-Martín, A., & Stokes, M. (2014). Using river long profiles and geomorphic indices to evaluate the geomorphological signature of continental scale drainage capture, Duero basin (NW Iberia). *Geomorphology*, *206*, 250-261.

Antunes, P., & Rodrigues, F. C. (2011). *Azores volcanic lakes: Factors affecting water quality*.

Antunes, P., & Rodrigues, F. C. (2014). Hydrogeochemistry assessment of volcanic lakes in the Flores Island Protected Areas (Azores, Portugal). *Revista de Gestão Costeira Integrada*, *14*(2), 321–334. https://doi.org/10.5894/rgci494

Antunes, P., & Rosário Carvalho, M. (2018). Surface and Groundwater in Volcanic Islands: Water from Azores Islands. In U. Kueppers & C. Beier (Eds.), *Volcanoes of the Azores* (pp. 301–329). Springer Berlin Heidelberg. https://doi.org/10.1007/978-3-642-32226-6_13

Antunes, P.C., Cruz, J.V., Freire, P. (2006). Caracterização Hidrogeoquímica de Lagos Vulcânicos da Ilha das Flores (Açores, Portugal).

Apolinarska, K., Pleskot, K., Pełechata, A., Migdałek, M., Siepak, M., & Pełechaty, M. (2020). The recent deposition of laminated sediments in highly eutrophic Lake Kierskie, western Poland: 1 year pilot study of limnological monitoring and sediment traps. Journal of Paleolimnology, 63(4), 283-304.;

Appleby, P. G., Flower, R. J., Mackay, A. W., & Rose, N. L. (1998). Paleolimnological assessment of recent environmental change in Lake Baikal: sediment chronology. Journal of Paleolimnology, 20, 119-133.

Ariztegui, D., Anselmetti, F. S., Gilli, A., & Waldmann, N. (2008). Late Pleistocene environmental change in Eastern Patagonia and Tierra del Fuego–A limnogeological approach. *Developments in Quaternary Sciences*, *11*, 241-253.

Arneth, A., Harrison, S. P., Zaehle, S., Tsigaridis, K., Menon, S., Bartlein, P. J., Feichter, J., Korhola, A., Kulmala, M., O'Donnell, D., Schurgers, G., Sorvari, S., & Vesala, T. (2010).

Terrestrial biogeochemical feedbacks in the climate system. *Nature Geoscience*, *3*(8), 525–532. https://doi.org/10.1038/ngeo905

Auzet, A. V., Poesen, J., & Valentin, C. (2004). Soil surface characteristics: dynamics and impacts on soil erosion. *Earth Surface Processes and Landforms: The Journal of the British Geomorphological Research Group*, *29*(9), 1063-1064.

Azevedo, J. M. M., & Ferreira, M. R. P. (1999). Volcanic gaps and subaerial records ofpalaeo-sea-levels on Flores Island (Azores): Tectonic andmorphological implications. *Journal of Geodynamics*, *28*(2–3), 117–129. https://doi.org/10.1016/S0264-3707(98)00032-5

Azevedo, J. M. M., & Ferreira, M. R. P. (2006). The volcanotectonic evolution of Flores Island, Azores (Portugal). *Journal of Volcanology and Geothermal Research*, 13.

Azevedo, J. M. M., Ferreira, M. R., & Martins, J. Á. (1991). The Emergent Volcanism of Flores Islands, Azores (Portugal). *Arquipélago-Life and Earth Sciences*, *9*, 37-46.

Baker, C., Thompson, J. R., & Simpson, M. (2009). Hydrological dynamics I: surface waters, flood and sediment dynamics. *The wetlands handbook*, *2*, 120-168.

Bakke, J., Dahl, S. O., Paasche, Ø., Riis Simonsen, J., Kvisvik, B., Bakke, K., & Nesje, A. (2010). A complete record of Holocene glacier variability at Austre Okstindbreen, northern Norway: An integrated approach. *Quaternary Science Reviews*, *29*(9–10), 1246–1262. https://doi.org/10.1016/j.quascirev.2010.02.012

Barboni, D., Bonnefille, R., Alexandre, A., & Meunier, J. D. (1999). Phytoliths as paleoenvironmental indicators, west side Middle Awash Valley, Ethiopia. *Palaeogeography, Palaeoclimatology, Palaeoecology*, *152*(1-2), 87-100.

Barnosky, A. D., Hadly, E. A., Gonzalez, P., Head, J., Polly, P. D., Lawing, A. M., ... & Zhang, Z. (2017). Merging paleobiology with conservation biology to guide the future of terrestrial ecosystems. *Science*, *355*(6325), eaah4787.

Barnston, A. G., & Livezey, R. E. (1987). Classification, seasonality and persistence of low-frequency atmospheric circulation patterns. *Monthly weather review*, *115*(6), 1083-1126.

Bastos, A., Janssens, I. A., Gouveia, C. M., Trigo, R. M., Ciais, P., Chevallier, F., Peñuelas, J., Rödenbeck, C., Piao, S., Friedlingstein, P., & Running, S. W. (2016). European land CO2 sink influenced by NAO and East-Atlantic Pattern coupling. *Nature Communications*, *7*(1), 10315. https://doi.org/10.1038/ncomms10315

Batalla, R. J., De Jong, C., Ergenzinger, P., & Sala, M. (1999). Field observations on hyperconcentrated flows in mountain torrents. *Earth Surface Processes and Landforms*, *24*(3), 247–253. https://doi.org/10.1002/(SICI)1096-9837(199903)24:3<247::AID-ESP961>3.0.CO;2-1

Battarbee, R. W. (1999). The importance of palaeolimnology to lake restoration. In *The Ecological Bases for Lake and Reservoir Management: Proceedings of the Ecological Bases for Management of Lakes and Reservoirs Symposium, held 19–22 March 1996, Leicester, United Kingdom* (pp. 149-159). Springer Netherlands.

Battarbee, R. W., Cameron, N. G., Golding, P., Brooks, S. J., Switsur, R., Harkness, D., ... & McGovern, A. (2001). Evidence for Holocene climate variability from the sediments of a Scottish remote mountain lake. *Journal of Quaternary Science: Published for the Quaternary Research Association*, *16*(4), 339-346.

Battarbee, R. W., Jones, V. J., Flower, R. J., Cameron, N. G., Bennion, H., Carvalho, L., & Juggins, S. (2001). *Diatoms* (pp. 155-202). Springer Netherlands.

Beechie, T. J., Pollock, M. M., & Baker, S. (2008). Channel incision, evolution and potential recovery in the Walla Walla and Tucannon River basins, northwestern USA. *Earth Surface Processes and Landforms*, *33*(5), 784–800. https://doi.org/10.1002/esp.1578

Beguería, S., Vicente-Serrano, S. M., Tomás-Burguera, M., & Maneta, M. (2016). Bias in the variance of gridded data sets leads to misleading conclusions about changes in climate variability. *International Journal of Climatology*, *36*(9), 3413–3422. https://doi.org/10.1002/joc.4561

Beier, C., Turner, S., Plank, T., & White, W. (2010). A preliminary assessment of the symmetry of source composition and melting dynamics across the Azores plume. *Geochemistry, Geophysics, Geosystems*, *11*(2), 2009GC002833. https://doi.org/10.1029/2009GC002833

Benda, L.E. and Cundy, T.W. (1990) Predicting deposition of debris flows in mountain channels. Canadian Geotechnical Journal, 27, 409–417.

Bengtsson, L., Herschy, R. W., & Fairbridge, R. W. (2012). Encyclopedia of lakes and reservoirs. *Monographiae Biologicae*, *53*, 10-26.

Benito, G., Macklin, M. G., Zielhofer, C., Jones, A. F., & Machado, M. J. (2015). Holocene flooding and climate change in the Mediterranean. *CATENA*, *130*, 13–33. https://doi.org/10.1016/j.catena.2014.11.014

Bennett, K. D. (1996). Determination of the number of zones in a biostratigraphical sequence. *New Phytologist*, *132*(1), 155–170. https://doi.org/10.1111/j.1469-8137.1996.tb04521.x

Bennett, K. D., & Humphry, R. W. (1995). Analysis of late-glacial and Holocene rates of vegetational change at two sites in the British Isles. *Review of Palaeobotany and Palynology*, *85*(3-4), 263-287.

Beres, M., Gilli, A., Ariztegui, D., & Anselmetti, F. S. (2008). The Lago Cardiel Basin, Argentina (49°S): Origin and evolution revealed by high-resolution multichannel seismic reflection studies. *Journal of South American Earth Sciences*, *25*(1), 74–85. https://doi.org/10.1016/j.jsames.2007.08.001

Bernárdez, P., Prego, R., Francés, G., & González-Álvarez, R. (2005). Opal content in the Ría de Vigo and Galician continental shelf: Biogenic silica in the muddy fraction as an accurate paleoproductivity proxy. *Continental Shelf Research*, *25*(10), 1249–1264. https://doi.org/10.1016/j.csr.2004.12.009

Bernasconi, S. M., Barbieri, A., & Simona, M. (1997). Carbon and nitrogen isotope variations in sedimenting organic matter in Lake Lugano. *Limnology and Oceanography*, *42*(8), 1755-1765.

Bertrand, S., Hughen, K., & Giosan, L. (2015). Limited influence of sediment grain size on elemental XRF core scanner measurements. Micro-XRF Studies of Sediment Cores: Applications of a non-destructive tool for the environmental sciences, 473-490.

Beschta, R. L., Jackson, W. L., & Knoop, K. D. (1981). Sediment transport during controlled reservoir release 1. *JAWRA Journal of the American Water Resources Association*, *17*(4), 635–641. https://doi.org/10.1111/j.1752-1688.1981.tb01270.x

Bhattacharjee, S., Bookhagen, B., Sinha, R. 2022. Sediment-transport rates from decadal to millennial timescales across the Indo-Gangetic Plain: Impacts of tectonics, climatic processes, and vegetation cover. Earth-Science Reviews, 233: 104165. doi: 10.1016/j.earscirev.2022.104165

Birks, H. H. (2003). The importance of plant macrofossils in the reconstruction of Lateglacial vegetation and climate: Examples from Scotland, western Norway, and Minnesota, USA. *Quaternary Science Reviews*, *22*(5–7), 453–473. https://doi.org/10.1016/S0277-3791(02)00248-2

Birks, H. H. (2015). South to north: Contrasting late-glacial and early-Holocene climate changes and vegetation responses between south and north Norway. *The Holocene*, *25*(1), 37-52.

Birks, H. H., & Ammann, B. (2000). Two terrestrial records of rapid climatic change during the glacial–Holocene transition (14,000–9,000 calendar years BP) from Europe. *Proceedings of the National Academy of Sciences*, *97*(4), 1390-1394.

Birks, H. H., & Birks, H. J. B. (2006). Multi-proxy studies in palaeolimnology. *Vegetation history and Archaeobotany*, *15*, 235-251.

Birks, H. J. B. (2012). Analysis of stratigraphical data. *Tracking environmental change using lake sediments: Data handling and numerical techniques*, 355-378.

Birks, H. J. B., & Birks, H. H. (2008). Biological responses to rapid climate change at the Younger Dryas—Holocene transition at Kråkenes, western Norway. *The Holocene*, *18*(1), 19-30.

Birks, H. J. B., Felde, V. A., & Seddon, A. W. (2016). Biodiversity trends within the Holocene. *The Holocene*, *26*(6), 994-1001.

Birks, J. B., Lotter, A. F., Juggins, S., & Smol, J. P. (Eds.). (2012). *Tracking environmental change using lake sediments: data handling and numerical techniques* (Vol. 5). Springer Science & Business Media.

Björck, S., Rittenour, T., Rosén, P., França, Z., Möller, P., Snowball, I., Wastegård, S., Bennike, O., & Kromer, B. (2006). A Holocene lacustrine record in the central North Atlantic: Proxies for volcanic activity, short-term NAO mode variability, and long-term precipitation changes. *Quaternary Science Reviews*, *25*(1–2), 9–32. https://doi.org/10.1016/j.quascirev.2005.08.008

Blaauw, M. (2010). Methods and code for 'classical' age-modelling of radiocarbon sequences. *Quaternary Geochronology*, *5*(5), 512–518. https://doi.org/10.1016/j.quageo.2010.01.002

Bloesch, J. (1995). Mechanisms, measurement and importance of sediment resuspension in lakes. *Marine and Freshwater Research*, *46*(1), 295-304.

Bloesch, J., & Uehlinger, U. (1986). Horizontal sedimentation differences in a eutrophic Swiss lake. *Limnology and Oceanography*, *31*(5), 1094-1109.

Boardman, J. (2006). Soil erosion science: Reflections on the limitations of current approaches. *Catena*, *68*(2-3), 73-86.

Bohacs, K. M., Carroll, A. R., Neal, J. E., & Mankiewicz, P. J. (2000). Lake-basin type, source potential, and hydrocarbon character: An integrated sequence-stratigraphic–geochemical framework.

Boomer, I., Aladin, N., Plotnikov, I., & Whatley, R. (2000). The palaeolimnology of the Aral Sea: a review. *Quaternary Science Reviews*, *19*(13), 1259-1278.

Borges, P. A. V., Lamelas-Lopez, L., Amorim, I. R., Danielczak, A., Boieiro, M., Rego, C., ... & Hochkirch, A. (2019). Species conservation profiles of cave-dwelling arthropods from Azores, Portugal. *Biodiversity Data Journal*, *7*.

Borrelli, P., Alewell, C., Alvarez, P., Anache, J. A. A., Baartman, J., Ballabio, C., ... & Panagos, P. (2021). Soil erosion modelling: A global review and statistical analysis. *Science of the total environment*, *780*, 146494. doi: https://doi.org/10.1016/j.scitotenv.2021.146494

Bovis, M. J., & Jakob, M. (1999). The role of debris supply conditions in predicting debris flow activity. *Earth Surface Processes and Landforms*, *24*(11), 1039–1054. https://doi.org/10.1002/(SICI)1096-9837(199910)24:11<1039::AID-ESP29>3.0.CO;2-U

Bower, M. M. (1961). The distribution of erosion in blanket peat bogs in the Pennines. *Transactions and Papers (Institute of British Geographers)*, (29), 17-30.

Bowman, D. (1988). The declining but non-rejuvenating base level—The Lisan lake, the Dead Sea area, Israel. *Earth Surface Processes and Landforms*, *13*(3), 239–249. https://doi.org/10.1002/esp.3290130305

Boyle, J. F. (2000). Rapid elemental analysis of sediment samples by isotope source XRF. *Journal of Paleolimnology*, *23*, 213-221.

Boyle, J. F. (2001). Inorganic geochemical methods in palaeolimnology. *Tracking environmental change using lake sediments: physical and geochemical methods*, 83-141.

Bracken, L. J. (2010). Overland flow and soil erosion. Sediment Cascades: An Integrated Approach, 181-216.

Bradbury, J. P., & Dieterich-Rurup, K. V. (1993). Holocene diatom paleolimnology of Elk Lake, Minnesota.

Bradley, R. S. (1999). *Paleoclimatology: reconstructing climates of the Quaternary*. Elsevier.

Bradley, R.S. (2015). Chapter 1 - Paleoclimatic Reconstruction. In: Bradley, R.S. (Ed.), Paleoclimatology, Third edition. Academic Press, San Diego, pp. 1–11. https://doi.org/10.1016/B978-0-12-386913-5.00001-6.

Bradley, R.S. (2015). Paleoclimatology: reconstructing climates of the Quaternary. Academic Press, Amsterdam.

Bragg, O. M., & Tallis, J. H. (2001). The sensitivity of peat-covered upland landscapes. *Catena*, *42*(2-4), 345-360.

Brauer, A. (2004). Annually laminated lake sediments and their palaeoclimatic relevance. *The climate in historical times: towards a synthesis of Holocene proxy data and climate models*, 109-127.

Brauer, A., & Casanova, J. (2001). Chronology and depositional processes of the laminated sediment record from Lac d'Annecy, French Alps. *Journal of Paleolimnology*, *25*(2), 163–177. https://doi.org/10.1023/A:1008136029735

Brauer, A., Endres, C., & Negendank, J. F. (1999). Lateglacial calendar year chronology based on annually laminated sediments from Lake Meerfelder Maar, Germany. *Quaternary International*, *61*(1), 17-25.

Brenner, M., Whitmore, T. J., Curtis, J. H., Hodell, D. A., & Schelske, C. L. (1999). Stable isotope ($\delta^{13}C$ and $\delta^{15}N$) signatures of sedimented organic matter as indicators of historic lake trophic state. *Journal of Paleolimnology*, *22*, 205-221.

Brooks, S. J., Udachin, V., & Williamson, B. J. (2005). Impact of copper smelting on lakes in the southern Ural Mountains, Russia, inferred from chironomids. *Journal of Paleolimnology*, *33*(2), 229–241. https://doi.org/10.1007/s10933-004-3936-x

Brosius, L. S., Anthony, K. M. W., Treat, C. C., Lenz, J., Jones, M. C., Bret-Harte, M. S., & Grosse, G. (2021). Spatiotemporal patterns of northern lake formation since the Last Glacial Maximum. *Quaternary Science Reviews*, *253*, 106773. https://doi.org/10.1016/j.quascirev.2020.106773

Brown Jr, L. F., & Fisher, W. L. (1977). Seismic-stratigraphic interpretation of depositional systems: examples from brazilian rift and pull-apart basins: section 2. Application of seismic reflection configuration to stratigraphic interpretation.

Brust, J., & Waniek, J. J. (2010). Atmospheric dust contribution to deep-sea particle fluxes in the subtropical Northeast Atlantic. *Deep Sea Research Part I: Oceanographic Research Papers*, *57*(8), 988–998. https://doi.org/10.1016/j.dsr.2010.04.011

Bruthans, J., Filippi, M., Slavík, M., & Svobodová, E. (2018). Origin of honeycombs: Testing the hydraulic and case hardening hypotheses. *Geomorphology*, *303*, 68–83. https://doi.org/10.1016/j.geomorph.2017.11.013

Büchel, G. (2007). Maars of the Westeifel, Germany. *Paleolimnology of European maar lakes*, 1-13.

Bueh, C., & Nakamura, H. (2007). Scandinavian pattern and its climatic impact. *Quarterly Journal of the Royal Meteorological Society: A journal of the atmospheric sciences, applied meteorology and physical oceanography*, *133*(629), 2117-2131.

Bull, L. J., & Kirkby, M. J. (1997). Gully processes and modelling. *Progress in physical geography*, *21*(3), 354-374.

Bull, L. J., Lawler, D. M., Leeks, G. J. L., & Marks, S. (1995). Downstream changes in suspended-sediment fluxes in the River Severn, UK. *IAHS Publications-Series of Proceedings and Reports-Intern Assoc Hydrological Sciences*, *226*, 27-38.

Burls, N. J., & Fedorov, A. V. (2017). Wetter subtropics in a warmer world: Contrasting past and future hydrological cycles. *Proceedings of the National Academy of Sciences*, *114*(49), 12888–12893. https://doi.org/10.1073/pnas.1703421114

Burnett, A. P., Soreghan, M. J., Scholz, C. A., & Brown, E. T. (2011). Tropical East African climate change and its relation to global climate: a record from Lake Tanganyika, Tropical East Africa, over the past 90+ kyr. *Palaeogeography, Palaeoclimatology, Palaeoecology*, *303*(1-4), 155-167.

Burt, T. P. (1989). Forest hydrology and ecology at Coweeta edited by W. T. Swank and D. A. Crossley, Springer-Verlag, Ecological studies volume 66, 1987, no. of pages: 469. *Hydrological Processes*, *3*(3), 289–293. https://doi.org/10.1002/hyp.3360030308

Burt, T. P., & Allison, R. J. (2010). Sediment cascades in the environment: An integrated approach. Sediment cascades: An integrated approach, 1-15.

Burt, T. P., & Allison, R. J. (2010). *Sediment Cascades: An Integrated Approach.*

Caldeira, R. M. A., & Reis, J. C. (2017). The Azores Confluence Zone. *Frontiers in Marine Science*, *4*. https://doi.org/10.3389/fmars.2017.00037

Camuera, J., Jiménez-Moreno, G., Ramos-Román, M. J., García-Alix, A., Jiménez-Espejo, F. J., Toney, J. L., & Anderson, R. S. (2021). Chronological control and centennial-scale climatic subdivisions of the Last Glacial Termination in the western Mediterranean region. *Quaternary Science Reviews*, *255*, 106814. https://doi.org/10.1016/j.quascirev.2021.106814

Canter-Lund, H., & Lund, J. W. (1995). *Freshwater algae: their microscopic world explored* (Vol. 582). Bristol: Biopress.

Carmack, E. C., Wiegand, R. C., Daley, R. J., Gray, C. B., Jasper, S., & Pharo, C. H. (1986). Mechanisms influencing the circulation and distribution of water mass in a medium residence-time lake. *Limnology and oceanography*, *31*(2), 249-265.

Carpenter, S. R., Benson, B. J., Biggs, R., Chipman, J. W., Foley, J. A., Golding, S. A., Hammer, R. B., Hanson, P. C., Johnson, P. T. J., Kamarainen, A. M., Kratz, T. K., Lathrop, R. C., McMahon, K. D., Provencher, B., Rusak, J. A., Solomon, C. T., Stanley, E. H., Turner, M. G., Vander Zanden, M. J., … Yuan, H. (2007). Understanding Regional Change: A Comparison of Two Lake Districts. *BioScience*, *57*(4), 323–335. https://doi.org/10.1641/B570407

Carrión-Torrente, A. (2023). Incised valleys of end-member fluvial systems in the gulf of Cadiz shelf: constraining the role of controlling factors. Universidad de Granada. 201 pp.

Carson, M.A., and Kirkby, M.J., 1972, Hillslope form and process: New York, Cambridge University Press, 475 p.

Casalbore, D., Romagnoli, C., Pimentel, A., Quartau, R., Casas, D., Ercilla, G., ... & Chiocci, F. L. (2015). Volcanic, tectonic and mass-wasting processes offshore Terceira Island (Azores) revealed by high-resolution seafloor mapping. *Bulletin of Volcanology*, *77*, 1-19.

Castanet, C., Purdue, L., Testé, M., Garnier, A., Develle-Vincent, A. L., Mokadem, F., ... & Nondédéo, P. (2022). Multi-millennial human impacts and climate change during the Maya early Anthropocene: implications on hydro-sedimentary dynamics and socio-environmental trajectories (Naachtun, Guatemala). *Quaternary Science Reviews*, *283*, 107458.

Castañeda, I. S., & Schouten, S. (2011). A review of molecular organic proxies for examining modern and ancient lacustrine environments. *Quaternary Science Reviews*, *30*(21-22), 2851-2891.

Casty, C., Handorf, D., & Sempf, M. (2005). Combined winter climate regimes over the North Atlantic/European sector 1766–2000. *Geophysical Research Letters*, *32*(13), 2005GL022431. https://doi.org/10.1029/2005GL022431

Catalan, J., Pla-Rabés, S., García, J., & Camarero, L. (2014). Air temperature-driven CO2 consumption by rock weathering at short timescales: Evidence from a Holocene lake sediment record. *Geochimica et Cosmochimica Acta*, *136*, 67–79. https://doi.org/10.1016/j.gca.2014.04.005

Catuneanu, O. (2002). Sequence stratigraphy of clastic systems: concepts, merits, and pitfalls. *Journal of African Earth Sciences*, *35*(1), 1-43.

Catuneanu, O. (2019). Scale in sequence stratigraphy. *Marine and Petroleum Geology*, *106*, 128-159.

Catuneanu, O., 2006. Principles of Sequence Stratigraphy. Elsevier, Amsterdam. 375 pp.

Catuneanu, O., Galloway, W. E., Kendall, C. G. S. C., Miall, A. D., Posamentier, H. W., Strasser, A., & Tucker, M. E. (2011). Sequence stratigraphy: methodology and nomenclature. *Newsletters on stratigraphy*, *44*, 173-245.

Cerling, T. E., & Quade, J. (1993). Stable carbon and oxygen isotopes in soil carbonates. *Geophysical Monograph Series*, *78*, 217-231.

Chafik, L., Nilsen, J. E. Ø., & Dangendorf, S. (2017). Impact of North Atlantic teleconnection patterns on Northern European sea level. *Journal of Marine Science and Engineering*, *5*(3), 43.

Charman, D. (2002). *Peatlands and environmental change* (pp. 301).

Chawchai, S., Kylander, M. E., Chabangborn, A., Löwemark, L., & Wohlfarth, B. (2016). Testing commonly used X-ray fluorescence core scanning-based proxies for organic-rich lake sediments and peat. *Boreas*, *45*(1), 180–189. https://doi.org/10.1111/bor.12145

Chenggao, G., & Renaut, R. W. (1994). The effect of Tibetan uplift on the formation and preservation of Tertiary lacustrine source-rocks in eastern China. *Journal of Paleolimnology*, *11*(1), 31–40. https://doi.org/10.1007/BF00683269

Chesner, C. A., & Rose, W. I. (1991). Stratigraphy of the Toba tuffs and the evolution of the Toba caldera complex, Sumatra, Indonesia. *Bulletin of Volcanology*, *53*, 343-356.

Chilom, G., & Rice, J. A. (2009). Organo-clay complexes in soils and sediments. Biophysico-chemical processes involving natural nonliving organic matter in environmental systems, 111-145.

Chiverrell, R. C., Harvey, A. M., & Foster, G. C. (2007). Hillslope gullying in the Solway Firth — Morecambe Bay region, Great Britain: Responses to human impact and/or climatic deterioration? *Geomorphology*, *84*(3–4), 317–343. https://doi.org/10.1016/j.geomorph.2005.12.014

Christensen, M. W., Stephens, G. L., & Lebsock, M. D. (2013). Exposing biases in retrieved low cloud properties from CloudSat: A guide for evaluating observations and climate data. *Journal of Geophysical Research: Atmospheres*, *118*(21). https://doi.org/10.1002/2013JD020224

Christenson, B., Németh, K., Rouwet, D., Tassi, F., Vandemeulebrouck, J., & Varekamp, J. C. (2015). Volcanic lakes. *Volcanic lakes*, 1-20.

Chung, F. H. (1974a). Quantitative interpretation of X-ray diffraction patterns of mixtures. I. Matrix-flushing method for quantitative multicomponent analysis. *Journal of Applied Crystallography*, *7*(6), 519–525. https://doi.org/10.1107/S0021889874010375

Chung, F. H. (1974b). Quantitative interpretation of X-ray diffraction patterns of mixtures. II. Adiabatic principle of X-ray diffraction analysis of mixtures. *Journal of Applied Crystallography*, *7*(6), 526–531. https://doi.org/10.1107/S0021889874010387

Church, M. (2010). Mountains and Montane Channels. In T. P. Burt & R. J. Allison (Eds.), *Sediment Cascades* (1st ed., pp. 17–53). Wiley. https://doi.org/10.1002/9780470682876.ch2

Church, M. (2010). The trajectory of geomorphology. *Progress in Physical Geography: Earth and Environment*, *34*(3), 265–286. https://doi.org/10.1177/0309133310363992

Church, M.J. and Jones, D. (1982) Channel bars in gravel-bed rivers, in Gravel-Bed Rivers (eds R.D. Hey, J.C. Bathurst and C.R. Thorne), John Wiley and Sons, Chichester, pp. 238–291.

Clague, J. (2000). A review of catastrophic drainage of moraine-dammed lakes in British Columbia. *Quaternary Science Reviews*, *19*(17–18), 1763–1783. https://doi.org/10.1016/S0277-3791(00)00090-1

Clement, S. (2005). *The future stability of upland blanket peat following historical erosion and recent re-vegetation* (Doctoral dissertation, Durham University).

Cléroux, C., Debret, M., Cortijo, E., Duplessy, J., Dewilde, F., Reijmer, J., & Massei, N. (2012). High-resolution sea surface reconstructions off Cape Hatteras over the last 10 ka. *Paleoceanography*, *27*(1), 2011PA002184. https://doi.org/10.1029/2011PA002184

Cohen, A. S. (2003). *Paleolimnology: The history and evolution of lake systems*. New York : Oxford University Press.

Cole, J. J., Prairie, Y. T., Caraco, N. F., McDowell, W. H., Tranvik, L. J., Striegl, R. G., ... & Melack, J. (2007). Plumbing the global carbon cycle: integrating inland waters into the terrestrial carbon budget. *Ecosystems*, *10*, 172-185.

Colman, S. M. (2006). Acoustic stratigraphy of Bear Lake, Utah–Idaho—Late Quaternary sedimentation patterns in a simple half-graben. *Sedimentary Geology*, *185*(1–2), 113–125. https://doi.org/10.1016/j.sedgeo.2005.11.022

Colman, S. M., Kelts, K. R., & Dinter, D. A. (2002). Depositional history and neotectonics in Great Salt Lake, Utah, from high-resolution seismic stratigraphy. *Sedimentary Geology*, *148*(1–2), 61–78. https://doi.org/10.1016/S0037-0738(01)00210-X

Comas-Bru, L., & Hernández, A. (2018). *Reconciling North Atlantic climate modes: Revised monthly indices for the East Atlantic and the Scandinavian patterns beyond the 20th century*. 16.

Comas-Bru, L., & McDermott, F. (2014). Impacts of the EA and SCA patterns on the European twentieth century NAO-winter climate relationship: Impacts of EA and SCA patterns on NAO-winter climate relationship. *Quarterly Journal of the Royal Meteorological Society*, *140*(679), 354–363. https://doi.org/10.1002/qj.2158

Comas-Bru, L., McDermott, F., & Werner, M. (2016). The effect of the East Atlantic pattern on the precipitation δ 18 O-NAO relationship in Europe. *Climate dynamics*, *47*, 2059-2069.

Connor, S. E., Lewis, T., van Leeuwen, J. F., Schaefer, H., Porch, N., Gomes, A. I., ... & Elias, R. B. (2024). Original plant diversity and ecosystems of a small, remote oceanic island (Corvo, Azores): Implications for biodiversity conservation. Biological Conservation, 291, 110512.

Connor, S. E., van Leeuwen, J. F. N., Rittenour, T. M., van der Knaap, W. O., Ammann, B., & Björck, S. (2012). The ecological impact of oceanic island colonization - a palaeoecological perspective from the Azores: Palaeoecology of human colonization of the Azores. *Journal of Biogeography*, *39*(6), 1007–1023. https://doi.org/10.1111/j.1365-2699.2011.02671.x

Connor, S. E., van Leeuwen, J. F., Rittenour, T. M., van der Knaap, W. O., Ammann, B., & Björck, S. (2012). The ecological impact of oceanic island colonization–a palaeoecological perspective from the Azores. Journal of Biogeography, 39(6), 1007-1023.

Cook E. R., Seager R., Cane M. A., Stahle D. W. (2007). North American drought: Reconstructions, causes, and consequences. Earth Sci. Rev. 81, 93 .

Cook, B. I., Shukla, S. P., Puma, M. J., & Nazarenko, L. S. (2015). Irrigation as an historical climate forcing. *Climate Dynamics*, *44*(5–6), 1715–1730. https://doi.org/10.1007/s00382-014-2204-7

Cook, E. R., Palmer, J. G., & D'Arrigo, R. D. (2002). Evidence for a 'Medieval Warm Period' in a 1,100 year tree-ring reconstruction of past austral summer temperatures in New Zealand. *Geophysical Research Letters*, *29*(14). https://doi.org/10.1029/2001GL014580

Cooper, M. J., Lamberti, G. A., Moerke, A. H., Ruetz, C. R., Wilcox, D. A., Brady, V. J., ... & Uzarski, D. G. (2018). An expanded fish-based index of biotic integrity for Great Lakes coastal wetlands. *Environmental monitoring and assessment*, *190*, 1-30.

Corella, J. P., Stefanova, V., El Anjoumi, A., Rico, E., Giralt, S., Moreno, A., ... & Valero-Garcés, B. L. (2013). A 2500-year multi-proxy reconstruction of climate change and human activities in northern Spain: the Lake Arreo record. *Palaeogeography, Palaeoclimatology, Palaeoecology*, *386*, 555-568.

Correa-Metrio, A., Bush, M. B., Cabrera, K. R., Sully, S., Brenner, M., Hodell, D. A., ... & Guilderson, T. (2012). Rapid climate change and no-analog vegetation in lowland Central America during the last 86,000 years. *Quaternary Science Reviews*, *38*, 63-75.

Costa, A. C. G., Hildenbrand, A., Marques, F. O., Sibrant, A. L. R., & Santos de Campos, A. (2015). Catastrophic flank collapses and slumping in Pico Island during the last 130 kyr (Pico-Faial ridge, Azores Triple Junction). *Journal of Volcanology and Geothermal Research*, *302*, 33–46. https://doi.org/10.1016/j.jvolgeores.2015.06.008

Costa, J.E. (1984) Physical geomorphology of debris flows, in Developments and Applications of Geomorphology (eds J.E. Costa and P.J. Fleisher), Springer-Verlag, Berlin, pp. 268–317.

Costas, S., Jerez, S., Trigo, R. M., Goble, R., & Rebêlo, L. (2012). Sand invasion along the Portuguese coast forced by westerly shifts during cold climate events. *Quaternary Science Reviews*, *42*, 15-28.

Coulthard, T. J., Lewin, J., & Macklin, M. G. (2005). Modelling differential catchment response to environmental change. *Geomorphology*, *69*(1–4), 222–241. https://doi.org/10.1016/j.geomorph.2005.01.008

Cowell, B. C., & Dawes, C. J. (1991). Nutrient enrichment experiments in three central Florida lakes of different trophic states. *Hydrobiologia*, *220*, 217-231.

Crasemann, B., Handorf, D., Jaiser, R., Dethloff, K., Nakamura, T., Ukita, J., & Yamazaki, K. (2017). Can preferred atmospheric circulation patterns over the North-Atlantic-Eurasian region be associated with arctic sea ice loss?. *Polar Science*, *14*, 9-20.

Cropper, T. E., & Hanna, E. (2014). An analysis of the climate of Macaronesia, 1865-2012: THE CLIMATE OF MACARONESIA, 1865-2012. *International Journal of Climatology*, *34*(3), 604–622. https://doi.org/10.1002/joc.3710

Cropper, T., Hanna, E., Valente, M. A., & Jónsson, T. (2015). A daily Azores–Iceland North Atlantic Oscillation index back to 1850. *Geoscience Data Journal*, *2*(1), 12–24. https://doi.org/10.1002/gdj3.23

Croudace, I. W., & Rothwell, R. G. (Eds.). (2015). *Micro-XRF Studies of Sediment Cores: Applications of a non-destructive tool for the environmental sciences* (Vol. 17). Springer Netherlands. https://doi.org/10.1007/978-94-017-9849-5

Croudace, I. W., Rindby, A., & Rothwell, R. G. (2006). ITRAX: Description and evaluation of a new multi-function X-ray core scanner. *Geological Society, London, Special Publications*, *267*(1), 51–63. https://doi.org/10.1144/GSL.SP.2006.267.01.04

Crowe, S. K., Evans, M. G., & Allott, T. E. H. (2008). Geomorphological controls on the re-vegetation of erosion gullies in blanket peat: implications for bog restoration. *Mires & Peat*, *3*.

Cruz, J. V., Antunes, P., Amaral, C., França, Z., & Nunes, J. C. (2006). Volcanic lakes of the Azores archipelago (Portugal): Geological setting and geochemical characterization. *Journal of Volcanology and Geothermal Research*, *156*(1–2), 135–157. https://doi.org/10.1016/j.jvolgeores.2006.03.008

Cuenca-Cambronero, M., Courtney-Mustaphi, C. J., Greenway, R., Heiri, O., Hudson, C. M., King, L., ... & Matthews, B. (2022). An integrative paleolimnological approach for studying evolutionary processes. *Trends in ecology & evolution*, *37*(6), 488-496.

Czymzik, M., Dreibrodt, S., Feeser, I., Adolphi, F., & Brauer, A. (2016). Mid-Holocene humid periods reconstructed from calcite varves of the Lake Woserin sediment record (north-eastern Germany). *The Holocene*, *26*(6), 935-946.

D'Agostino, K., Seltzer, G., Baker, P., Fritz, S., & Dunbar, R. (2002). Late-Quaternary lowstands of Lake Titicaca: Evidence from high-resolution seismic data. *Palaeogeography, Palaeoclimatology, Palaeoecology*, *179*(1–2), 97–111. https://doi.org/10.1016/S0031-0182(01)00411-4

D'Odorico, P., & Fagherazzi, S. (2003). A probabilistic model of rainfall-triggered shallow landslides in hollows: A long-term analysis. *Water Resources Research*, *39*(9), 2002WR001595. https://doi.org/10.1029/2002WR001595

da Costa, A. C. G. (2015). *Mass-wasting episodes in the geological evolution of the Azores islands: timing, recurrence, mechanisms and consequences* (Doctoral dissertation, Université Paris Sud-Paris XI; Universidade de Lisboa. Faculdade de ciências).

Damaschke, M., Sulpizio, R., Zanchetta, G., Wagner, B., Böhm, A., Nowaczyk, N., ... & Hilgers, A. (2013). Tephrostratigraphic studies on a sediment core from Lake Prespa in the Balkans. Climate of the Past, 9(1), 267-287.

Dansgaard, W., Johnsen, S. J., Clausen, H. B., Dahl-Jensen, D., Gundestrup, N. S., Hammer, C. U., ... & Bond, G. (1993). Evidence for general instability of past climate from a 250-kyr ice-core record. nature, 364(6434), 218-220.

Dätwyler, C., Neukom, R., Abram, N. J., Gallant, A. J. E., Grosjean, M., Jacques-Coper, M., Karoly, D. J., & Villalba, R. (2018). Teleconnection stationarity, variability and trends of the Southern Annular Mode (SAM) during the last millennium. *Climate Dynamics*, *51*(5–6), 2321–2339. https://doi.org/10.1007/s00382-017-4015-0

Davidson, T. A., & Jeppesen, E. (2013). The role of palaeolimnology in assessing eutrophication and its impact on lakes. *Journal of Paleolimnology*, *49*, 391-410.

Davies, S. J., Lamb, H. F., & Roberts, S. J. (2015). Micro-XRF Core Scanning in Palaeolimnology: Recent Developments. In I. W. Croudace & R. G. Rothwell (Eds.), *Micro-XRF Studies of Sediment Cores: Applications of a non-destructive tool for the environmental sciences* (pp. 189–226). Springer Netherlands. https://doi.org/10.1007/978-94-017-9849-5_7

Davies, T. R. H., & Korup, O. (2007). Persistent alluvial fanhead trenching resulting from large, infrequent sediment inputs. *Earth Surface Processes and Landforms*, *32*(5), 725–742. https://doi.org/10.1002/esp.1410

Davies, T. R. H., & Korup, O. (2010). Sediment Cascades in Active Landscapes. In T. P. Burt & R. J. Allison (Eds.), *Sediment Cascades* (1st ed., pp. 89–115). Wiley. https://doi.org/10.1002/9780470682876.ch4

Davies, T. R., & McSaveney, M. J. (2008). Principles of sustainable development on fans. Journal of Hydrology (New Zealand), 47(1), 43-65.

Davis, M. B., & Ford, M. S. (1982). Sediment focusing in mirror lake, New Hampshire 1. *Limnology and oceanography*, *27*(1), 137-150.

Davis, R. E., Hayden, B. P., Gay, D. A., Phillips, W. L., & Jones, G. V. (1997). The North Atlantic Subtropical Anticyclone. *Journal of Climate*, *10*(4), 728–744. https://doi.org/10.1175/1520-0442(1997)010<0728:TNASA>2.0.CO;2

De Batist, M., Klerkx, J., Van Rensbergen, P., Vanneste, M., Poort, J., Golmshtok, A. Y., Kremlev, A. A., Khlystov, O. M., & Krinitsky, P. (2002). Active hydrate destabilization in Lake Baikal, Siberia? *Terra Nova*, *14*(6), 436–442. https://doi.org/10.1046/j.1365-3121.2002.00449.x

de Sousa Lourenço, J. N. V. (2007). *Tectono-magmatic processes at the Azores triple junction* (Doctoral dissertation, Universidade do Algarve (Portugal)).

Dean, W. E. (1974). Determination of carbonate and organic matter in calcareous sediments and sedimentary rocks by loss on ignition; comparison with other methods. *Journal of Sedimentary Research*, *44*(1), 242-248.

Dean, W. E. (1999). The carbon cycle and biogeochemical dynamics in lake sediments. *Journal of paleolimnology*, *21*, 375-393.

Dean, W. E., & Gorham, E. (1998). Magnitude and significance of carbon burial in lakes, reservoirs, and peatlands. *Geology*, *26*(6), 535-538.

Dearing, J. A. (1991). Lake sediment records of erosional processes. In *Environmental History and Palaeolimnology: Proceedings of the Vth International Symposium on Palaeolimnology, held in Cumbria, UK* (pp. 99-106). Springer Netherlands.

Deaton, M., & Winebrake, J. J. (1999). *Dynamic modeling of environmental systems*. Springer Science & Business Media.

deMenocal, P. (2000). Coherent High- and Low-Latitude Climate Variability During the Holocene Warm Period. *Science*, *288*(5474), 2198–2202. https://doi.org/10.1126/science.288.5474.2198

Demura, M., Noma, S., & Hayashi, N. (2021). Species and fatty acid diversity of Desmodesmus (Chlorophyta) in a local Japanese area and identification of new docosahexaenoic acid-producing species. *Biomass*, *1*(2), 105-118.

Depetris, P. J., Pasquini, A. I., & Lecomte, K. L. (2014). *Weathering and the Riverine Denudation of Continents*. Springer Netherlands. https://doi.org/10.1007/978-94-007-7717-0

Deser, C., Phillips, A., Bourdette, V., & Teng, H. (2012). Uncertainty in climate change projections: The role of internal variability. *Climate Dynamics*, *38*(3–4), 527–546. https://doi.org/10.1007/s00382-010-0977-x

Dias, J.L.F. (2001). Geologia e tectónica da ilha do Corvo (Açores, Portugal). Contributos para o ordenamento do espaço físico. PhD thesis. DCT-FCT-Universidade de Coimbra. 102 p.

Dietrich, W. E., & Dunne, T. (1978). Sediment budget for a small catchment in a mountainous terrain.

Dietrich, W. E., Reiss, R., Hsu, M., & Montgomery, D. R. (1995). A process-based model for colluvial soil depth and shallow landsliding using digital elevation data. *Hydrological Processes*, *9*(3–4), 383–400. https://doi.org/10.1002/hyp.3360090311

Dietrich, W.E., Wilson, C.J. and Reneau, S.L. (1986) Hollows, colluvium, and landslides in soilmantled landscapes, in Hillslope Processes (ed. A.D. Abrahams), Allen and Unwin, Boston, pp. 361–388.

Dietze, E. (2012). *Water level cahnges and related sedimentary environments at Lake Donggi Cona, north-eastern tibetan plateau, China*.

Dietze, E., Wünnemann, B., Diekmann, B., Aichner, B., Hartmann, K., Herzschuh, U., IJmker, J., Jin, H., Kopsch, C., Lehmkuhl, F., Li, S., Mischke, S., Niessen, F., Opitz, S., Stauch, G., & Yang, S. (2010). Basin morphology and seismic stratigraphy of Lake Donggi Cona, north-eastern Tibetan Plateau, China. *Quaternary International*, *218*(1–2), 131–142. https://doi.org/10.1016/j.quaint.2009.11.035

Dillon, P. J., & Rigler, F. H. (1975). A simple method for predicting the capacity of a lake for development based on lake trophic status. *Journal of the Fisheries Board of Canada*, *32*(9), 1519-1531.

DiNezio, P. N., Tierney, J. E., Otto-Bliesner, B. L., Timmermann, A., Bhattacharya, T., Rosenbloom, N., & Brady, E. (2018). Glacial changes in tropical climate amplified by the Indian Ocean. *Science Advances*, *4*(12), eaat9658. https://doi.org/10.1126/sciadv.aat9658

Dräger, N., Theuerkauf, M., Szeroczyńska, K., Wulf, S., Tjallingii, R., Plessen, B., ... & Brauer, A. (2017). Varve microfacies and varve preservation record of climate change and human impact for the last 6000 years at Lake Tiefer See (NE Germany). *The Holocene*, *27*(3), 450-464.

Drake, N.A., Candy, I., Breeze, P., Armitage, S.J., Gasmi, N., Schwenninger, J.L., Peat, D., Manning, K. (2022). Sedimentary and geomorphic evidence of Saharan megalakes: A synthesis, Quaternary Science Reviews, 276: 107318. doi: 10.1016/j.quascirev.2021.107318

DROTRH/INAG (2001). *Plano Regional da Água. Relatório Técnico. Versão para Consulta Pública*. Direcção Regional do Ordenamento do Território e dos Recursos Hídricos e Instituto da Água, Ponta Delgada.

Dunne, T., & Black, R. D. (1970). Partial area contributions to storm runoff in a small New England watershed. *Water resources research*, *6*(5), 1296-1311.

Dunning, S. A., Rosser, N. J., Petley, D. N., & Massey, C. R. (2006). Formation and failure of the Tsatichhu landslide dam, Bhutan. *Landslides*, *3*(2), 107–113. https://doi.org/10.1007/s10346-005-0032-x

East, A. E., Warrick, J. A., Li, D., Sankey, J. B., Redsteer, M. H., Gibbs, A. E., Coe, J. A., & Barnard, P. L. (2022). Measuring and Attributing Sedimentary and Geomorphic Responses to Modern Climate Change: Challenges and Opportunities. *Earth's Future*, *10*(10), e2022EF002983. https://doi.org/10.1029/2022EF002983

Egler, F. E. (1964). Pesticides—in our ecosystem. *American Scientist*, *52*(1), 110-136.

Eglinton, T. I., & Eglinton, G. (2008). Molecular proxies for paleoclimatology. *Earth and Planetary Science Letters*, *275*(1-2), 1-16.

Elbert, J., Wartenburger, R., von Gunten, L., Urrutia, R., Fischer, D., Fujak, M., ... & Grosjean, M. (2013). Late Holocene air temperature variability reconstructed from the sediments of Laguna Escondida, Patagonia, Chile (45 30′ S). Palaeogeography, Palaeoclimatology, Palaeoecology, 369, 482-492.

Elias, R. B., Gil, A., Silva, L., Fernández-Palacios, J. M., Azevedo, E. B., & Reis, F. (2016). Natural zonal vegetation of the Azores Islands: Characterization and potential distribution. *Phytocoenologia*, *46*(2), 107–123. https://doi.org/10.1127/phyto/2016/0132

Eugster, H. P., & Hardie, L. A. (1978). Saline lakes. In *Lakes: chemistry, geology, physics* (pp. 237-293). New York, NY: Springer New York.

Evans, M. G., & Burt, T. P. (2010). Erosional Processes and Sediment Transport in Upland Mires. *Sediment Cascades: An Integrated Approach*, 217-239.

Evans, M. N., Tolwinski-Ward, S. E., Thompson, D. M., & Anchukaitis, K. J. (2013). Applications of proxy system modeling in high resolution paleoclimatology. *Quaternary Science Reviews*, *76*, 16–28. https://doi.org/10.1016/j.quascirev.2013.05.024

Evans, M., Warburton, J., & Yang, J. (2006). Eroding blanket peat catchments: global and local implications of upland organic sediment budgets. *Geomorphology*, *79*(1-2), 45-57.

Evans, R. D. (1994). Empirical evidence of the importance of sediment resuspension in lakes. Hydrobiologia, 284, 5-12.

Fagan, B., (2009). The long summer: how climate changed civilization. Basic books, New York.

Fannin, R.J. and Rollerson, T.P. (1993) Debris flows: some physical characteristics and behaviour. Canadian Geotechnical Journal, 30, 71–81.

Faulkner, H. (2008). Connectivity as a crucial determinant of badland morphology and evolution. *Geomorphology*, *100*(1-2), 91-103.

Fee, E. J., Hecky, R. E., Kasian, S. E. M., & Cruikshank, D. R. (1996). Effects of lake size, water clarity, and climatic variability on mixing depths in Canadian Shield lakes. *Limnology and oceanography*, *41*(5), 912-920.

Ferguson, R.I. (1981) Channel forms and channel changes, in British Rivers (ed. J. Lewin), Allen and Unwin, London, pp. 90–125.

Fernandes, R. M. S., Bastos, L., Miranda, J. M., Lourenço, N., Ambrosius, B. A. C., Noomen, R., & Simons, W. (2006). Defining the plate boundaries in the Azores region. *Journal of Volcanology and Geothermal Research*, *156*(1–2), 1–9. https://doi.org/10.1016/j.jvolgeores.2006.03.019

Fernández-Palacios, J. M. (2011). The islands of Macaronesia.

Filippi, M. L., Lambert, P., Hunziker, J. C., & Kübler, B. (1998). Monitoring detrital input and resuspension effects on sediment trap material using mineralogy and stable isotopes (δ18O and δ13C): The case of Lake Neuchâtel (Switzerland). *Palaeogeography, Palaeoclimatology, Palaeoecology*, *140*(1-4), 33-50.

Finley, J. B., & Drever, J. I. (1997). Chemical mass balance and rates of mineral weathering in a high-elevation catchment, west glacier lake, wyoming. *Hydrological Processes*, *11*(7), 745-764.

Finnegan, N. J., Hallet, B., Montgomery, D. R., Zeitler, P. K., Stone, J. O., Anders, A. M., & Yuping, L. (2008). Coupling of rock uplift and river incision in the Namche Barwa-Gyala Peri massif, Tibet. *Geological Society of America Bulletin*, *120*(1–2), 142–155. https://doi.org/10.1130/B26224.1

Fischer, P., & Eckmann, R. (1997). Seasonal changes in fish abundance, biomass and species richness in the littoral zone of a large European lake, Lake Constance, Germany.

Fisher, R.V. (1961). Proposed classification of volcaniclastic sediments and rocks: Geological Society of America Bulletin, v. 72, p. 1409–1414, doi: 10.1130/0016-7606(1961)72[1409:PCOVSA]2.0.CO;2.

Fogel, M. L., & Cifuentes, L. A. (1993). Isotope fractionation during primary production. In *Organic geochemistry: principles and applications* (pp. 73-98). Boston, MA: Springer US.

Folland, C.K., Knight, J., Linderholm, H.W., Fereday, D., Ineson, S., Hurrell, J.W., 2009. The summer North Atlantic Oscillation: past, present, and future. Journal of Climate 22(5), 1082–1103.

Fontes, J. C., Pereira, L. S., & Smith, R. E. (2004). Runoff and erosion in volcanic soils of Azores: Simulation with OPUS. *CATENA*, *56*(1–3), 199–212. https://doi.org/10.1016/j.catena.2003.10.011

Fontes, J. Ch., & Gasse, F. (1991). PALHYDAF (Palaeohydrology in Africa) program: Objectives, methods, major results. *Palaeogeography, Palaeoclimatology, Palaeoecology*, *84*(1–4), 191–215. https://doi.org/10.1016/0031-0182(91)90044-R

Fontiela, J., Sousa Oliveira, C., & Rosset, P. (2018). Characterisation of Seismicity of the Azores Archipelago: An Overview of Historical Events and a Detailed Analysis for the Period 2000–2012. In U. Kueppers & C. Beier (Eds.), *Volcanoes of the Azores* (pp. 127–153). Springer Berlin Heidelberg. https://doi.org/10.1007/978-3-642-32226-6_8

Foster, G. L., Royer, D. L., & Lunt, D. J. (2017). Future climate forcing potentially without precedent in the last 420 million years. *Nature Communications*, *8*(1), 14845. https://doi.org/10.1038/ncomms14845

Foster, I. D. L. (2010). Lakes and Reservoirs in the Sediment Cascade. In T. P. Burt & R. J. Allison (Eds.), *Sediment Cascades* (1st ed., pp. 345–376). Wiley. https://doi.org/10.1002/9780470682876.ch12

França, Z., Cruz, J. V., Nunes, J. C., & Forjaz, V. H. (2003). Geologia dos Açores: uma perspectiva actual. *Açoreana*, *10*(1), 11-140.

França, Z., Lago, M., Nunes, J.C., Galé, C., Forjaz, V.H., Pueyo, O. (2006). Geochemistry of alkaline basalts of Corvo Island (Azores, Portugal): preliminary data 4.

França, Z.T., Nunes, J.C., Cruz, J.V., Duarte, H.F. y Forjaz, V.H. (2003). En: Procceedings da 3a Assembleia Luso- Espanhola de Geodesia e Geofisica, Valencia (España). Univ. Politécnica de Valencia (España), II, 727-730

Francis, J. A., & Vavrus, S. J. (2015). Evidence for a wavier jet stream in response to rapid Arctic warming. *Environmental Research Letters*, *10*(1), 014005.

Francus, P., & Pirard, E. (2004). Testing for sources of errors in quantitative image analysis. *Image analysis, sediments and paleoenvironments*, 87-102.

Freire Luis, J., Miranda, J. M., Galdeano, A., Patriat, P., Rossignol, J. C., & Mendes Victor, L. A. (1994). The Azores triple junction evolution since 10 Ma from an aeromagnetic survey of the Mid-Atlantic Ridge. *Earth and Planetary Science Letters*, *125*(1–4), 439–459. https://doi.org/10.1016/0012-821X(94)90231-3

Friedrich, O., Norris, R. D., & Erbacher, J. (2012). Evolution of middle to Late Cretaceous oceans—A 55 m.y. Record of Earth's temperature and carbon cycle. *Geology*, *40*(2), 107–110. https://doi.org/10.1130/G32701.1

Fructuoso, G., (1522-1591) Saudades da Terra. In: Fructuoso G, (ed). Saudades da terra. – Instituto cultural da Ponta Delgada, Ponta Delgada.

Fryirs, K. A., Brierley, G. J., Preston, N. J., & Spencer, J. (2007). Catchment-scale (dis)connectivity in sediment flux in the upper Hunter catchment, New South Wales, Australia. *Geomorphology*, *84*(3–4), 297–316. https://doi.org/10.1016/j.geomorph.2006.01.044

Funiciello, R., Giordano, G., & De Rita, D. (2003). The Albano maar lake (Colli Albani Volcano, Italy): recent volcanic activity and evidence of pre-Roman Age catastrophic lahar events. *Journal of Volcanology and Geothermal Research*, *123*(1-2), 43-61.

Galán, E., & Pozo, M. (2011). Palygorskite and sepiolite deposits in continental environments. Description, genetic patterns and sedimentary settings. In Developments in clay science (Vol. 3, pp. 125-173). Elsevier.

Gallart, F., Solé, A., & Puigdefábregas, J. (2002). AND ROBERTO LÁZARO Estación Experimental de Zonas Aridas (CSIC), Almeria, Spain. *Dryland Rivers: Hydrology and Geomorphology of Semi-arid Channels*, 299.

García-Herrera, R., Hernández, E., Barriopedro, D., Paredes, D., Trigo, R. M., Trigo, I. F., & Mendes, M. A. (2007). The outstanding 2004/05 drought in the Iberian Peninsula: associated atmospheric circulation. *Journal of Hydrometeorology*, *8*(3), 483-498.

Garcia, F., Paz-Vinas, I., Gaujard, A., Olden, J. D., & Cucherousset, J. (2023). Multiple lines and levels of evidence for avian zoochory promoting fish colonization of artificial lakes. *Biology Letters*, *19*(3), 20220533.

Gasse, F., 1990, Tectonic and climatic controls on lake distribution and environments in Afar from Miocene to present. In Katz, B.J. (ed.), Lacustrine Basin Exploration—Case Studies and Modern Analogues. Amer. Assoc. Petrol. Geol. Mem. 50:19–41.

Geirsdóttir, Á., Miller, G. H., Larsen, D. J., & Ólafsdóttir, S. (2013). Abrupt Holocene climate transitions in the northern North Atlantic region recorded by synchronized lacustrine records in Iceland. *Quaternary Science Reviews*, *70*, 48–62. https://doi.org/10.1016/j.quascirev.2013.03.010

Genske, F. S., Beier, C., Stracke, A., Turner, S. P., Pearson, N. J., Hauff, F., Schaefer, B. F., & Haase, K. M. (2016). Comparing the nature of the western and eastern Azores mantle. *Geochimica et Cosmochimica Acta*, *172*, 76–92. https://doi.org/10.1016/j.gca.2015.08.019

Genske, F. S., Turner, S. P., Beier, C., & Schaefer, B. F. (2012). The Petrology and Geochemistry of Lavas from the Western Azores Islands of Flores and Corvo. *Journal of Petrology*, *53*(8), 1673–1708. https://doi.org/10.1093/petrology/egs029

Ghimire, S., & Higaki, D. (2015). Dynamic river morphology due to land use change and erosion mitigation measures in a degrading catchment in the Siwalik Hills, Nepal. *International Journal of River Basin Management*, *13*(1), 27–39. https://doi.org/10.1080/15715124.2014.963860

Gierlowski-Kordesch, E. H., & Kelts, K. R. (2000). *Lake basins through space and time*. American Association of Petroleum Geologists.

Giovanoli, F. (1990). Horizontal transport and sedimentation by interflows and turbidity currents in Lake Geneva. In *Large lakes: Ecological structure and function* (pp. 175-195). Berlin, Heidelberg: Springer Berlin Heidelberg

Giralt, S., Moreno, A., Bao, R., Sáez, A., Prego, R., Valero-Garcés, B. L., Pueyo, J. J., González-Sampériz, P., & Taberner, C. (2008). A statistical approach to disentangle environmental forcings in a lacustrine record: The Lago Chungará case (Chilean Altiplano). *Journal of Paleolimnology*, *40*(1), 195–215. https://doi.org/10.1007/s10933-007-9151-9

Giralt, S., Rico-Herrero, M. T., Vega, J. C., & Valero-Garcés, B. L. (2011). Quantitative climate reconstruction linking meteorological, limnological and XRF core scanner datasets: The

Lake Sanabria case study, NW Spain. *Journal of Paleolimnology*, *46*(3), 487–502. https://doi.org/10.1007/s10933-011-9509-x

Goddéris, Y., Donnadieu, Y., Le Hir, G., Lefebvre, V., & Nardin, E. (2014). The role of palaeogeography in the Phanerozoic history of atmospheric CO2 and climate. *Earth-Science Reviews*, *128*, 122–138. https://doi.org/10.1016/j.earscirev.2013.11.004

Gomez, B., Carter, L., & Trustrum, N. A. (2007). A 2400 yr record of natural events and anthropogenic impacts in intercorrelated terrestrial and marine sediment cores: Waipaoa sedimentary system, New Zealand. *Geological Society of America Bulletin*, *119*(11-12), 1415-1432.

Gomez, B., Page, M. J., & Trustrum, N. A. (2010). Pacific rim steeplands. *Sediment cascades: An integrated approach*, 117-151.

Gómez, J. A., Taguas, E. V., Vanwalleghem, T., & Pérez-Alcántara, R. (2010, May). Effect of large rainfall events on runoff and soil losses in two small experimental agricultural catchments in Southern Spain. In EGU General Assembly Conference Abstracts (p. 6021).

Gonçalves, V., Costa, A. C., Raposeiro, P., Marques, H., Ramos, J., Cunha, A., ... & Vilaverde, J. (2013). Monitorização das massas de água interiores da Região Hidrográfica Açores. Relatório Anual de 2012

Gonçalves, V., P. M. Raposeiro, J. Porteiro, M. H. Alves & M. C. Medeiros, (2006a). Proposta de definição de ecótipos e classificação preliminar do estado ecológico das lagoas dos Açores. Associação Portuguesa dos Recursos Hídricos 8.

Gonçalves, V., Raposeiro, P., & Costa, A. C. (2008). Benthic diatoms and macroinvertebrates in the assessment of the ecological status of Azorean streams. *Limnetica*, *27*(2), 317–328. https://doi.org/10.23818/limn.27.25

Gonçalves, V., Raposeiro, P., Costa, A. C., Marques, H., Malhão, V., Micael, J., & Cunha, A. (2009). Caracterização Ecológica das Massas de Água Interiores das ilhas de Pico, Faial, Flores e Corvo. Definição de ecótipos de Lagoas e Ribeiras. CCPA, Departamento de Biologia, Universidade dos Açores, Ponta Delgada.

Goosse, H., Barriat, P. Y., Loutre, M. F., & Zunz, V. (2010). *Introduction to climate dynamics and climate modeling*. Centre de recherche sur la Terre et le climat Georges Lemaître-UCLouvain.

Gornitz, V., 2009. Paleoclimate Proxies, An Introduction. In: Gornitz, V. (Ed.), Encyclopedia of Paleoclimatology and Ancient Environments. Springer Netherlands, Dordrecht, pp. 716–721. https://doi.org/10.1007/978-1-4020-4411-3_171.

Govers, G. (1991). Time-dependency of runoff velocity and erosion the effect of the initial soil moisture profile. *Earth Surface Processes and Landforms*, *16*(8), 713-729.

Graettinger, A. H. (2018). The shape and distribution of Maar craters using the MaarVLS database.

Grimm, E. C. (1987). CONISS: A FORTRAN 77 program for stratigraphically constrained cluster analysis by the method of incremental sum of squares. *Computers & Geosciences*, *13*(1), 13–35. https://doi.org/10.1016/0098-3004(87)90022-7

Gronewold, A. D., Smith, J. P., Read, L. K., & Crooks, J. L. (2020). Reconciling the water balance of large lake systems. *Advances in Water Resources*, *137*, 103505.

Grootes, P. M., & Stuiver, M. (1997). Oxygen 18/16 variability in Greenland snow and ice with $10^{-3}$—To $10^{5}$ -year time resolution. *Journal of Geophysical Research: Oceans*, *102*(C12), 26455–26470. https://doi.org/10.1029/97JC00880

Gu, Z. K., Yao, X., Yao, C. C., & Li, C. G. (2021). Mapping of geomorphic dynamic parameters for analysis of landslide hazards: A case of Yangbi river basin on the upper Lancang-Mekong of China. *Journal of Mountain Science*, *18*(9), 2402-2411.

Guilizzoni, P., Lami, A., Marchetto, A., Jones, V., Manca, M., & Bettinetti, R. (2002). Palaeoproductivity and environmental changes during the Holocene in central Italy as recorded in two crater lakes (Albano and Nemi). *Quaternary International*, *88*(1), 57-68.

Guo, X., Kossin, J. P., & Tan, Z. M. (2021). Impact of seasonality in the North Atlantic jet stream and storm migration on the seasonality of hurricane translation speed changes. *Journal of climate*, *34*(18), 7409-7419.

Guyard, H., Chapron, E., St-Onge, G., & Labrie, J. (2013). Late-Holocene NAO and oceanic forcing on high-altitude proglacial sedimentation (Lake Bramant, Western French Alps). The Holocene, 23(8), 1163-1172.

Haberyan, K. A. (1985). The role of eopepod fecal pellets in the deposition of diatoms in Lake Tanganyika 1. *Limnology and Oceanography*, *30*(5), 1010-1023.

Hack, J. T., & Goodlett, J. C. (1960). Geomorphology and forest ecology of a mountain region in the central Appalachians (No. 347). United States Government Printing Office.

Haeberli, W., Huggel, C., Kääb, A., Zgraggen-Oswald, S., Polkvoj, A., Galushkin, I., Zotikov, I., & Osokin, N. (2004). The Kolka-Karmadon rock/ice slide of 20 September 2002: An extraordinary event of historical dimensions in North Ossetia, Russian Caucasus. *Journal of Glaciology*, *50*(171), 533–546. https://doi.org/10.3189/172756504781829710

Håkanson, L. (1982). Bottom dynamics in lakes. In *Sediment/Freshwater Interaction: Proceedings of the Second International Symposium held in Kingston, Ontario, 15–18 June 1981* (pp. 9-22). Springer Netherlands.

Hall, K., Thorn, C., & Sumner, P. (2012). On the persistence of 'weathering'. *Geomorphology*, *149–150*, 1–10. https://doi.org/10.1016/j.geomorph.2011.12.024

Hall, R. J., & Hanna, E. (2018). North Atlantic circulation indices: links with summer and winter UK temperature and precipitation and implications for seasonal forecasting. *International Journal of Climatology*, *38*, e660-e677.

Halsey, L. A., Vitt, D. H., & Trew, D. O. (1997). Influence of Peatlands on the acidity of lakes in northeastern Alberta, Canada. *Water, Air, and Soil Pollution*, *96*(1–4), 17. https://doi.org/10.1007/BF02407194

Hannachi, A., Jolliffe, I. T., & Stephenson, D. B. (2007). Empirical orthogonal functions and related techniques in atmospheric science: A review. *International Journal of Climatology*, *27*(9), 1119–1152. https://doi.org/10.1002/joc.1499

Hannon, G. E., & Gaillard, M. J. (1997). The plant-macrofossil record of past lake-level changes. *Journal of Paleolimnology*, *18*, 15-28.

Hansen, H.P., Grashoff, K., 1983. Automated chemical analysis. In: Grashoff, M., Ehrhardt, M., Kremlin, K. (Eds.), Methods of Seawater Analysis. Verlag Chemie, Weinheim, pp. 368e376.

Harbor, J. (1999) Cosmogenic isotopes in Geomorphology. Geomorphology (Special Issue), 27, 1–172.

Hartmann, D. L. (2015). Global physical climatology (Vol. 103). Newnes.

Harvey, A. M. (1992). Process interactions, temporal scales and the development of hillslope gully systems: Howgill Fells, northwest England. *Geomorphology*, *5*(3–5), 323–344. https://doi.org/10.1016/0169-555X(92)90012-D

Harvey, A. M. (1997). Coupling between hillslope gully systems and stream channels in the Howgill Fells, northwest England: Temporal implications/Le couplage des systèmes de ravins et des lits fluviaux dans les Howgill Fells, nord-ouest de l'Angleterre : signification temporelle. *Géomorphologie Relief Processus Environnement*, *3*(1), 3–19. https://doi.org/10.3406/morfo.1997.897

Harvey, A. M. (2001). Coupling between hillslopes and channels in upland fluvial systems: Implications for landscape sensitivity, illustrated from the Howgill Fells, northwest England. *CATENA*, *42*(2–4), 225–250. https://doi.org/10.1016/S0341-8162(00)00139-9

Harvey, A. M. (2002a). Effective timescales of coupling within fluvial systems. *Geomorphology*, *44*(3–4), 175–201. https://doi.org/10.1016/S0169-555X(01)00174-X

Harvey, A. M. (2002b). The role of base-level change in the dissection of alluvial fans: Case studies from southeast Spain and Nevada. *Geomorphology*, *45*(1–2), 67–87. https://doi.org/10.1016/S0169-555X(01)00190-8

Harvey, A. M. (2007). Differential recovery from the effects of a 100-year storm: Significance of long-term hillslope–channel coupling; Howgill Fells, northwest England. *Geomorphology*, *84*(3–4), 192–208. https://doi.org/10.1016/j.geomorph.2006.03.009

Harvey, A. M. (2010). Local buffers to the sediment cascade: debris cones and alluvial fans. Sediment cascades: An integrated approach, 153-180.

Harvey, A. M. (2010). Local Buffers to the Sediment Cascade: Debris Cones and Alluvial Fans. In T. P. Burt & R. J. Allison (Eds.), *Sediment Cascades* (1st ed., pp. 153–180). Wiley. https://doi.org/10.1002/9780470682876.ch6

Harvey, A. M., Oldfield, F., Baron, A. F., & Pearson, G. W. (1981). Dating of post-glacial landforms in the central howgills. *Earth Surface Processes and Landforms*, *6*(5), 401–412. https://doi.org/10.1002/esp.3290060502

Harvey, A. M., Silva, P. G., Mather, A. E., Goy, J. L., Stokes, M., & Zazo, C. (1999). The impact of Quaternary sea-level and climatic change on coastal alluvial fans in the Cabo de Gata ranges, southeast Spain. *Geomorphology*, *28*(1–2), 1–22. https://doi.org/10.1016/S0169-555X(98)00100-7

Harvey, A.M. (1986) Geomorphic effects of a 100-year storm in the Howgill Fells, northwest England. Zeitschrift fur Geomorphologie, 30, 71–91.

Harvey, A.M. (1997a) The role of alluvial fans in arid zone fluvial systems, in Arid Zone Geomorphology: Process, Form and Change in Drylands (ed. D.S.G. Thomas), John Wiley and Sons, Chichester, pp. 231–259.

Heathwaite, A. L., & Dils, R. M. (2000). Characterising phosphorus loss in surface and subsurface hydrological pathways. *Science of The Total Environment*, *251–252*, 523–538. https://doi.org/10.1016/S0048-9697(00)00393-4

Heckmann, T., & Schwanghart, W. (2013). Geomorphic coupling and sediment connectivity in an alpine catchment—Exploring sediment cascades using graph theory. *Geomorphology*, *182*, 89–103. https://doi.org/10.1016/j.geomorph.2012.10.033

Heede, B. H. (1972). INFLUENCES OF A FOREST ON THE HYDRAULIC GEOMETRY OF TWO MOUNTAIN STREAMS1. *JAWRA Journal of the American Water Resources Association*, *8*(3), 523–530. https://doi.org/10.1111/j.1752-1688.1972.tb05174.x

Henehan, M. J., Ridgwell, A., Thomas, E., Zhang, S., Alegret, L., Schmidt, D. N., Rae, J. W. B., Witts, J. D., Landman, N. H., Greene, S. E., Huber, B. T., Super, J. R., Planavsky, N. J., & Hull, P. M. (2019). Rapid ocean acidification and protracted Earth system recovery followed the end-Cretaceous Chicxulub impact. *Proceedings of the National Academy of Sciences*, *116*(45), 22500–22504. https://doi.org/10.1073/pnas.1905989116

Herczeg, A. L., & Fairbanks, R. G. (1987). Anomalous carbon isotope fractionation between atmospheric CO2 and dissolved inorganic carbon induced by intense photosynthesis. *Geochimica et Cosmochimica Acta*, *51*(4), 895-899

Hernández, A., Cachão, M., Sousa, P., Trigo, R. M., Luterbacher, J., Vaquero, J. M., & Freitas, M. C. (2021). External forcing mechanisms controlling the North Atlantic coastal upwelling regime during the mid-Holocene. *Geology*, *49*(4), 433–437. https://doi.org/10.1130/G48112.1

Hernández, A., Kutiel, H., Trigo, R. M., Valente, M. A., Sigró, J., Cropper, T., & Santo, F. E. (2016). New Azores archipelago daily precipitation dataset and its links with large-scale modes of climate variability. International Journal of Climatology, 36(14), 4439-4454. https://doi.org/10.1002/joc.4642

Hernández, A., Martin-Puertas, C., Moffa-Sánchez, P., Moreno-Chamarro, E., Ortega, P., Blockley, S., ... & Xu, G. (2020). Modes of climate variability: Synthesis and review of proxy-based reconstructions through the Holocene. *Earth-Science Reviews*, *209*, 103286.

Hernández, A., Sáez, A., Bao, R., Raposeiro, P. M., Trigo, R. M., Doolittle, S., Masqué, P., Rull, V., Gonçalves, V., Vázquez-Loureiro, D., Rubio-Inglés, M. J., Sánchez-López, G., & Giralt, S. (2017). The influences of the AMO and NAO on the sedimentary infill in an Azores Archipelago lake since ca. 1350 CE. *Global and Planetary Change*, *154*, 61–74. https://doi.org/10.1016/j.gloplacha.2017.05.007

Hernández, A., Sáez, A., Santos, R. N., Rodrigues, T., Martin-Puertas, C., Gil-Romera, G., Abbott, M., Carballeira, R., Costa, P., Giralt, S., Gomes, S. D., Griffore, M., Ibañez-Insa, J., Leira, M., Moreno, J., Naughton, F., Oliveira, D., Raposeiro, P. M., Trigo, R. M., … Ramos, A. M. (2023). The timing of the deglaciation in the Atlantic Iberian mountains: Insights from the stratigraphic analysis of a lake sequence in Serra da Estrela (Portugal). *Earth Surface Processes and Landforms*, *48*(2), 233–242. https://doi.org/10.1002/esp.5536

Hernández, A., Sánchez-López, G., Pla-Rabes, S., Comas-Bru, L., Parnell, A., Cahill, N., Geyer, A., Trigo, R. M., & Giralt, S. (2020). A 2,000-year Bayesian NAO reconstruction from the Iberian Peninsula. *Scientific Reports*, *10*(1), 14961. https://doi.org/10.1038/s41598-020-71372-5

Hernández, A., Trigo, R. M., Pla-Rabes, S., Valero-Garcés, B. L., Jerez, S., Rico-Herrero, M., Vega, J. C., Jambrina-Enríquez, M., & Giralt, S. (2015). Sensitivity of two Iberian lakes to North Atlantic atmospheric circulation modes. *Climate Dynamics*, *45*(11–12), 3403–3417. https://doi.org/10.1007/s00382-015-2547-8

Hevia-Cruz, F., Hildenbrand, A., Sheldon, N. D., Hren, M. T., Zanon, V., Marques, F. O., ... & Haurine, F. (2024). Weathering pulses during glacial-interglacial transitions: Insights from well-dated paleosols in the Azores volcanic province (Central North Atlantic). *Quaternary Science Reviews*, *324*, 108438.

Hicks, R. E., Owen, C. J., & Aas, P. (1994). Deposition, resuspension, and decomposition of particulate organic matter in the sediments of Lake Itasca, Minnesota, USA. *Hydrobiologia*, *284*, 79-91.

Higgitt, D. L., & Lu, X. X. (2001). Sediment delivery to the three gorges:: 1. Catchment controls. *Geomorphology*, *41*(2-3), 143-156.

Hildenbrand, A., Marques, F. O., & Catalão, J. (2018). Large-scale mass wasting on small volcanic islands revealed by the study of Flores Island (Azores). *Scientific Reports*, *8*(1). https://doi.org/10.1038/s41598-018-32253-0

Hilton, J. (1985). A conceptual framework for predicting the occurrence of sediment focusing and sediment redistribution in small lakes. *Limnology and Oceanography*, *30*(6), 1131-1143

Hinderer, M. (2001). Late Quaternary denudation of the Alps, valley and lake fillings and modern river loads. *Geodinamica Acta*, *14*(4), 231–263. https://doi.org/10.1080/09853111.2001.11432446

Hodell, D. A., & Schelske, C. L. (1998). Production, sedimentation, and isotopic composition of organic matter in Lake Ontario. *Limnology and Oceanography*, *43*(2), 200-214.

Hodell, D. A., Channell, J. E. T., Curtis, J. H., Romero, O. E., & Röhl, U. (2008). Onset of "Hudson Strait" Heinrich events in the eastern North Atlantic at the end of the middle Pleistocene transition (~640 ka)? *Paleoceanography*, *23*(4), 2008PA001591. https://doi.org/10.1029/2008PA001591

Hodell, D. A., Schelske, C. L., Fahnenstiel, G. L., & Robbins, L. L. (1998). Biologically induced calcite and its isotopic composition in Lake Ontario. *Limnology and Oceanography*, *43*(2), 187-199.

Hodell, D. A., Turchyn, A. V., Wiseman, C. J., Escobar, J., Curtis, J. H., Brenner, M., ... & Brown, E. T. (2012). Late Glacial temperature and precipitation changes in the lowland Neotropics by tandem measurement of δ18O in biogenic carbonate and gypsum hydration water. *Geochimica et Cosmochimica Acta*, *77*, 352-368.

Hoek, C., Mann, D. G., & Jahns, H. M. (1995). *Algae: an introduction to phycology*. Cambridge university press.

Hoffmann, T., & Schrott, L. (2002). Modelling sediment thickness and rockwall retreat in an Alpine valley using 2D-seismic refraction (Reintal, Bavarian Alps). Zeitschrift für Geomorphologie / Supplementary Issues, 153-173.

Hofmann, A. M., Geist, J., Nowotny, L., & Raeder, U. (2020). Depth-distribution of lake benthic diatom assemblages in relation to light availability and substrate: implications for paleolimnological studies. *Journal of Paleolimnology*, *64*(3), 315-334.

Hofmann, M. H., Hendrix, M. S., Moore, J. N., & Sperazza, M. (2006). Late Pleistocene and Holocene depositional history of sediments in Flathead Lake, Montana: Evidence from high-resolution seismic reflection interpretation. *Sedimentary Geology*, *184*(1–2), 111–131. https://doi.org/10.1016/j.sedgeo.2005.09.019

Holden, J. (2005). Controls of soil pipe frequency in upland blanket peat. *Journal of Geophysical Research: Earth Surface*, *110*(F1).

Holden, J., Evans, M. G., Burt, T. P., & Horton, M. (2006). Impact of land drainage on peatland hydrology. *Journal of Environmental Quality*, *35*(5), 1764-1778.

Hollander, D. J., & McKenzie, J. A. (1991). CO2 control on carbon-isotope fractionation during aqueous photosynthesis: A paleo-pCO2 barometer. *Geology*, *19*(9), 929-932.

Hollander, D. J., McKenzie, J. A., & Haven, H. L. T. (1992). A 200 year sedimentary record of progressive eutrophication in Lake Greifen (Switzerland): implications for the origin of organic-carbon-rich sediments. *Geology*, *20*(9), 825-828.

Holmes, J. A. (2001). Ostracoda. *Tracking Environmental Change Using Lake Sediments: Volume 4: Zoological Indicators*, 125-151.

Hopfenblatt, J., Geyer, A., Aulinas, M., Álvarez-Valero, A. M., Gisbert, G., Kereszturi, G., Ercilla, G., Gómez-Ballesteros, M., Márquez, A., García-Castellanos, D., Pedrazzi, D., Sumino, H., Höskuldsson, A., Giralt, S., & Angulo-Preckler, C. (2021). Formation of Stanley Patch volcanic cone: New insights into the evolution of Deception Island caldera (Antarctica). *Journal of Volcanology and Geothermal Research*, *415*, 107249. https://doi.org/10.1016/j.jvolgeores.2021.107249

Houk, V., Klee, R., & Passauer, U. (2007). Observations on taxa of Melosira sensu lato among the slides from the Grunow diatom collection in Vienna (Austria). Part 1. Diatom research, 22(1), 57-80.

Howarth, R. W., Marino, R., & Cole, J. J. (1988). Nitrogen fixation in freshwater, estuarine, and marine ecosystems. 2. Biogeochemical controls. *Limnology and Oceanography*, *33*(4), 688-701.

Hughes S. J., 2003. A study of the freshwater macroinvertebrate fauna of Madeira and their application in a regional ecological monitoring system. [dissertation] PhD thesis, KingÕs College Division of Life Sciences, University of London, UK.

Hughes, P. (2024). Morphostratigraphy/allostratigraphy. In Encyclopedia of Quaternary Science, 3rd Edition (pp. 243-249). Elsevier BV.

Hughes, P. D. (2010). Geomorphology and Quaternary stratigraphy: The roles of morpho-, litho-, and allostratigraphy. *Geomorphology*, *123*(3–4), 189–199. https://doi.org/10.1016/j.geomorph.2010.07.025

Hughes, P. D., & Elias, S. (2007). Allostratigraphy/morphostratigraphy. In *Encyclopedia of Quaternary Sciences*. Elsevier BV.

Hughes, P. D., Gibbard, P. L., & Woodward, J. C. (2005). Quaternary glacial records in mountain regions: a formal stratigraphical approach. *Episodes Journal of International Geoscience*, *28*(2), 85-92.

Hughes, S. J., & Malmqvist, B. (2005). Atlantic Island freshwater ecosystems: Challenges and considerations following the EU Water Framework Directive. *Hydrobiologia*, *544*(1), 289–297. https://doi.org/10.1007/s10750-005-1695-y

Hungr, O., Evans, S.G., Bovis, M.J. and Hutchinson, J.N. (2001) A review of the classification of landslides of the flow type. Environmental and Engineering Geoscience, 7, 221–238.

Huntington, E., & Brooks, C. E. P. (1922). The Evolution of Climate in North-Western Europe: A Review. *Geographical Review*, *12*(1), 126. https://doi.org/10.2307/208661

Hurrell, J. W. (1995). Decadal trends in the North Atlantic Oscillation: Regional temperatures and precipitation. Science, 269(5224), 676-679.

Hurrell, J. W., & Deser, C. (2010). North Atlantic climate variability: the role of the North Atlantic Oscillation. *Journal of marine systems*, *79*(3-4), 231-244.

Hurrell, J. W., & Van Loon, H. (1997). Decadal variations in climate associated with the North Atlantic Oscillation. *Climatic change*, *36*(3), 301-326.

Hurrell, J. W., Kushnir, Y., Ottersen, G., & Visbeck, M. (2003). An overview of the North Atlantic oscillation. *Geophysical Monograph-American Geophysical Union*, *134*, 1-36.

Hutchinson, G. E., & Löffler, H. (1956). The thermal classification of lakes. *Proceedings of the National Academy of Sciences*, *42*(2), 84-86.

Hutchison, G. E. 1957. A treatise on limnology, v. 1. Wiley, New York. 1015 p.

Imboden, D. M., & Wüest, A. (1995). Mixing mechanisms in lakes. In *Physics and chemistry of lakes* (pp. 83-138). Berlin, Heidelberg: Springer Berlin Heidelberg.

Ionita, M., Lohmann, G., Rimbu, N., Chelcea, S., & Dima, M. (2012). Interannual to decadal summer drought variability over Europe and its relationship to global sea surface temperature. *Climate Dynamics*, *38*(1–2), 363–377. https://doi.org/10.1007/s00382-011-1028-y

IPCC, 2023: Summary for Policymakers. In: Climate Change 2023: Synthesis Report. Contribution of Working Groups I, II and III to the Sixth Assessment Report of the Intergovernmental Panel on Climate Change [Core Writing Team, H. Lee and J. Romero (eds.)]. IPCC, Geneva, Switzerland, pp. 1-34, doi: 10.59327/IPCC/AR6-9789291691647.001

Itkonen, A., & Salonen, V. P. (1994). The response of sedimentation in three varved lacustrine sequences to air temperature, precipitation and human impact. *Journal of Paleolimnology*, *11*, 323-332.

Ivanochko, T. S., Calvert, S. E., Thomson, R. E., & Pedersen, T. F. (2008). Geochemical reconstruction of Pacific decadal variability from the eastern North Pacific during the HoloceneThis article is one of a series of papers published in this Special Issue on the theme *Polar Climate Stability Network* . *Canadian Journal of Earth Sciences*, *45*(11), 1317–1329. https://doi.org/10.1139/E08-037

Iverson, R. M., & Denlinger, R. P. (2001). Flow of variably fluidized granular masses across three-dimensional terrain: 1. Coulomb mixture theory. *Journal of Geophysical Research: Solid Earth*, *106*(B1), 537–552. https://doi.org/10.1029/2000JB900329

Jackson, S. T., Overpeck, J. T., Webb-III, T., Keattch, S. E., & Anderson, K. H. (1997). Mapped plant-macrofossil and pollen records of late Quaternary vegetation change in eastern North America. *Quaternary Science Reviews*, *16*(1), 1-70.

Japan Geomorphol Union 23:415–431 (in Japanese with English abstract).

Jerez, S., & Trigo, R. M. (2013). Time-scale and extent at which large-scale circulation modes determine the wind and solar potential in the Iberian Peninsula. *Environmental Research Letters*, *8*(4), 044035.

Jerez, S., Montavez, J. P., Jimenez-Guerrero, P., Gomez-Navarro, J. J., Lorente-Plazas, R., & Zorita, E. (2013). A multi-physics ensemble of present-day climate regional simulations over the Iberian Peninsula. *Climate Dynamics*, *40*(11–12), 3023–3046. https://doi.org/10.1007/s00382-012-1539-1

Jerez, S., Trigo, R. M., Sarsa, A., Lorente-Plazas, R., Pozo-Vázquez, D., & Montávez, J. P. (2013). Spatio-temporal complementarity between solar and wind power in the Iberian Peninsula. *Energy Procedia*, *40*, 48-57.

Jewson, D. H., & Lowry, S. (1993). Cymbellonitzschia diluviana Hustedt (Bacillariophyceae): habitat and auxosporulation. *Hydrobiologia*, *269*, 87-96.

Johnson, T. C., & Hecky, R. E. (1988). A silica budget for Lake Mala,~ i: net fluvial input, biogenic opal preservation and burial. *Eos*, *69*, 1144.

Jones, B.M., Grosse, G., Farquharson, L.M., Roy-Léveillée, P., Veremeeva, A., Kanevskiy,, M.Z., Gaglioti, B.V., Breen, A.L., Parsekian, A.D., Ulrich, M., Hinkel, K.M. 2022. Lake and drained lake basin systems in lowland permafrost regions. Nature Reviews Earth & Environment, 3: 85-98. doi: 10.1038/s43017-021-00238-9

Jones, D. S., Walker, G. M., Johnson, N. W., Mitchell, C. P., Coleman Wasik, J. K., & Bailey, J. V. (2019). Molecular evidence for novel mercury methylating microorganisms in sulfate-impacted lakes. *The ISME journal*, *13*(7), 1659-1675.

Jones, P. D. (Ed.). (2001). History and Climate. Springer Science & Business Media.

Jones, P. D., & Mann, M. E. (2004). Climate over past millennia. *Reviews of Geophysics*, *42*(2), 2003RG000143. https://doi.org/10.1029/2003RG000143

Jones, P. D., Briffa, K. R., Osborn, T. J., Lough, J. M., Van Ommen, T. D., Vinther, B. M., Luterbacher, J., Wahl, E. R., Zwiers, F. W., Mann, M. E., Schmidt, G. A., Ammann, C. M., Buckley, B. M., Cobb, K. M., Esper, J., Goosse, H., Graham, N., Jansen, E., Kiefer, T., … Xoplaki, E. (2009). High-resolution palaeoclimatology of the last millennium: A review of current status and future prospects. *The Holocene*, *19*(1), 3–49. https://doi.org/10.1177/0959683608098952

Jones, R. G., Murphy, J. M., Noguer, M., & Keen, A. B. (1997). Simulation of climate change over europe using a nested regional-climate model. II: Comparison of driving and regional model responses to a doubling of carbon dioxide. *Quarterly Journal of the Royal Meteorological Society*, *123*(538), 265–292. https://doi.org/10.1002/qj.49712353802

Josey, S. A., & Marsh, R. (2005). Surface freshwater flux variability and recent freshening of the North Atlantic in the eastern subpolar gyre. *Journal of Geophysical Research: Oceans*, *110*(C5).

Jouzel, J., Stiévenard, M., Johnsen, S. J., Landais, A., Masson-Delmotte, V., Sveinbjornsdottir, A., Vimeux, F., Von Grafenstein, U., & White, J. W. C. (2007). The GRIP deuterium-excess record. *Quaternary Science Reviews*, *26*(1–2), 1–17. https://doi.org/10.1016/j.quascirev.2006.07.015

Juggins, S., & Birks, H. J. B. (2012). Quantitative Environmental Reconstructions from Biological Data. In H. J. B. Birks, A. F. Lotter, S. Juggins, & J. P. Smol (Eds.), *Tracking Environmental Change Using Lake Sediments* (Vol. 5, pp. 431–494). Springer Netherlands. https://doi.org/10.1007/978-94-007-2745-8_14

Kalindekafe, L. S. N., Dolozi, M. B., & Yuretich, R. (2019). Distribution and origin of clay minerals in the sediments of Lake Malawi. In *Limnology, Climatology and Paleoclimatology of the East African Lakes* (pp. 443-460). Routledge.

Kao, S. J., & Milliman, J. D. (2008). Water and Sediment Discharge from Small Mountainous Rivers, Taiwan: The Roles of Lithology, Episodic Events, and Human Activities. *The Journal of Geology*, *116*(5), 431–448. https://doi.org/10.1086/590921

Kao, S., & Liu, K. (2002). Exacerbation of erosion induced by human perturbation in a typical Oceania watershed: Insight from 45 years of hydrological records from the Lanyang-Hsi

River, northeastern Taiwan. *Global Biogeochemical Cycles*, *16*(1). https://doi.org/10.1029/2000GB001334

Kashiwaya, K. (2008). Studies on lake-catchment systems: an introduction to limno-geomorphology (Oral Session, Abstracts of the Taiwan and Japan Joint Symposium:" Geomorphological Hazards and Management" held on 17-18 March, 2008, at Taipei). 地形, *29*(2), 205.

Kashiwaya, K. (2012). Earth surface processes and environmental changes in lake-catchment systems. *Trans Jpn Geomorphol Union*, *33*, 121-136.

Kashiwaya, K. (2017). *Geomorphology of Lake-Catchment Systems*. Springer Singapore. https://doi.org/10.1007/978-981-10-5110-4

Kashiwaya, K., Shen, J., & Kim, J. Y. (Eds.). (2015). *Earth Surface Processes and Environmental Changes in East Asia: Records From Lake-catchment Systems*. Springer Japan. https://doi.org/10.1007/978-4-431-55540-7

Kashiwaya, K., Tsuya, Y., & Okimura, T. (2004). Earthquake-related geomorphic environment and pond sediment information. *Earth Surface Processes and Landforms*, *29*(6), 785–793. https://doi.org/10.1002/esp.1069

Katz, B. J. (1990). *Lacustrine basin exploration: Case studies and modern analogs*. American Association of Petroleum Geologists.

Keller, E.A. and Swanson, F.J. (1979) Effects of large organic material on channel form and fluvial processes. Earth Surface Processes and Landforms, 4, 361–380.

Kelts, K. (1988). Environments of deposition of lacustrine petroleum source rocks: an introduction. *Geological Society, London, Special Publications*, *40*(1), 3-26.

Kelts, K., & Hsü, K. J. (1978). Freshwater carbonate sedimentation. In *Lakes: chemistry, geology, physics* (pp. 295-323). New York, NY: Springer New York.

Kemp, A. L. W., & Harper, N. S. (1976). Sedimentation Rates and a Sediment Budget for Lake Ontario. *Journal of Great Lakes Research*, *2*(2), 324–339. https://doi.org/10.1016/S0380-1330(76)72296-2

Kemp, A. L. W., Dell, C. I., & Harper, N. S. (1978). Sedimentation Rates and a Sediment Budget for Lake Superior. *Journal of Great Lakes Research*, *4*(3–4), 276–287. https://doi.org/10.1016/S0380-1330(78)72198-2

Kemp, D. B., Eichenseer, K., & Kiessling, W. (2015). Maximum rates of climate change are systematically underestimated in the geological record. *Nature communications*, *6*(1), 8890.

Kettner, A. J., Gomez, B., & Syvitski, J. P. M. (2007). Modeling suspended sediment discharge from the Waipaoa River system, New Zealand: The last 3000 years. *Water Resources Research*, *43*(7), 2006WR005570. https://doi.org/10.1029/2006WR005570

Kidston, J., Scaife, A. A., Hardiman, S. C., Mitchell, D. M., Butchart, N., Baldwin, M. P., & Gray, L. J. (2015). Stratospheric influence on tropospheric jet streams, storm tracks and surface weather. *Nature Geoscience*, *8*(6), 433-440.

Kilham, P. (1971). A hypothesis concerning silica and the freshwater planktonic diatoms 1. *Limnology and Oceanography*, *16*(1), 10-18.

Kilham, P., Kilham, S. S., & Hecky, R. E. (1986). Hypothesized resource relationships among African planktonic diatoms. *Limnology and Oceanography*, *31*(6), 1169-1181.

Kilham, S. S., Theriot, E. C., & Fritz, S. C. (1996). Linking planktonic diatoms and climate change in the large lakes of the Yellowstone ecosystem using resource theory. *Limnology and Oceanography*, *41*(5), 1052-1062.

Kirby, E., & Whipple, K. X. (2012). Expression of active tectonics in erosional landscapes. *Journal of structural geology*, *44*, 54-75.

Kirchner, J. W., Finkel, R. C., Riebe, C. S., Granger, D. E., Clayton, J. L., King, J. G., & Megahan, W. F. (2001). Mountain erosion over 10 yr, 10 k.y., and 10 m.y. Time scales. *Geology*, *29*(7), 591. https://doi.org/10.1130/0091-7613(2001)029<0591:MEOYKY>2.0.CO;2

Klein, B., & Siedler, G. (1989). On the origin of the Azores Current. *Journal of Geophysical Research: Oceans*, *94*(C5), 6159–6168. https://doi.org/10.1029/JC094iC05p06159

Kling, G. W., Kipphut, G. W., & Miller, M. C. (1991). Arctic lakes and streams as gas conduits to the atmosphere: implications for tundra carbon budgets. *Science*, *251*(4991), 298-301.

Knutti, R., & Sedláček, J. (2013). Robustness and uncertainties in the new CMIP5 climate model projections. *Nature Climate Change*, *3*(4), 369–373. https://doi.org/10.1038/nclimate1716

Korhola, A., Weckström, J., Holmström, L., & Erästö, P. (2000). A quantitative Holocene climatic record from diatoms in northern Fennoscandia. *Quaternary research*, *54*(2), 284-294.

Korup, O. (2002). Recent research on landslide dams—A literature review with special attention to New Zealand. *Progress in Physical Geography: Earth and Environment*, *26*(2), 206–235. https://doi.org/10.1191/0309133302pp333ra

Korup, O. (2005). Geomorphic imprint of landslides on alpine river systems, southwest New Zealand. *Earth Surface Processes and Landforms*, *30*(7), 783–800. https://doi.org/10.1002/esp.1171

Korup, O., & Tweed, F. (2007). Ice, moraine, and landslide dams in mountainous terrain. *Quaternary Science Reviews*, *26*(25–28), 3406–3422. https://doi.org/10.1016/j.quascirev.2007.10.012

Koutavas, A., & Joanides, S. (2012). El Niño–Southern Oscillation extrema in the Holocene and Last Glacial Maximum. *Paleoceanography*, *27*(4), 2012PA002378. https://doi.org/10.1029/2012PA002378

Krause, A. K., Franks, S. W., Kalma, J. D., Loughran, R. J., & Rowan, J. S. (2003). Multi-parameter fingerprinting of sediment deposition in a small gullied catchment in SE Australia. *Catena*, *53*(4), 327-348.

Kueppers, U., Beier, C., Genske, F. S., & Caetano, D. (2018). Where to Go? A Selection and Short Description of Geological Highlights in the Azores. *Volcanoes of the Azores: Revealing the Geological Secrets of the Central Northern Atlantic Islands*, 331-355.

Kumar, S., & Rzhetsky, A. (1996). Evolutionary relationships of eukaryotic kingdoms. *Journal of Molecular Evolution*, *42*, 183-193.

Kuriata-Potasznik, A., Szymczyk, S., & Skwierawski, A. (2020). Influence of cascading river–lake systems on the dynamics of nutrient circulation in catchment areas. *Water*, *12*(4), 1144.

Lan, J., Wang, T., Chawchai, S., Cheng, P., Zhou, K., Yu, K., Yan, D., Wang, Y., Zang, J., Liu, Y., Tan, L., Ai, L., & Xu, H. (2020). Time marker of 137Cs fallout maximum in lake sediments of Northwest China. *Quaternary Science Reviews*, *241*, 106413. https://doi.org/10.1016/j.quascirev.2020.106413

Langbein, W. B., & Schumm, S. A. (1958). Yield of sediment in relation to mean annual precipitation. *Eos, Transactions American Geophysical Union*, *39*(6), 1076-1084.

Langbein, W. B., & Schumm, S. A. (1958). Yield of sediment in relation to mean annual precipitation. *Eos, Transactions American Geophysical Union*, *39*(6), 1076-1084.

Larrea, P., França, Z., Lago, M., Widom, E., Galé, C., & Ubide, T. (2013). Magmatic Processes and the Role of Antecrysts in the Genesis of Corvo Island (Azores Archipelago, Portugal). *Journal of Petrology*, *54*(4), 769–793. https://doi.org/10.1093/petrology/egs084

Larrea, P., França, Z., Widom, E., & Lago, M. (2018). Petrology of the Azores Islands. *Volcanoes of the Azores: revealing the geological secrets of the Central Northern Atlantic Islands*, 197-249.

Larson, G. L. (1989). Geographical distribution, morphology and water quality of caldera lakes: A review. *Hydrobiologia*, *171*(1), 23–32. https://doi.org/10.1007/BF00005721

Larue, J. P. (2008). Tectonic influences on the Quaternary drainage evolution on the north-western margin of the French Central Massif: The Creuse valley example. *Geomorphology*, *93*(3-4), 398-420.

Last, W. M. (1982). Holocene carbonate sedimentation in Lake Manitoba, Canada. *Sedimentology*, *29*(5), 691-704.

Last, W. M. (2001). Mineralogical analysis of lake sediments. *Tracking Environmental Change Using Lake Sediments: Physical and Geochemical Methods*, 143-187.

Last, W. M., & Ginn, F. M. (2005). Saline systems of the Great Plains of western Canada: an overview of the limnogeology and paleolimnology. *Saline systems*, *1*, 1-38.

Last, W. M., & Smol, J. P. (2001). An introduction to basin analysis, coring, and chronological techniques used in paleolimnology. In *Tracking environmental change using lake sediments: Basin analysis, coring, and chronological techniques* (pp. 1-5). Dordrecht: Springer Netherlands.

Laughton, A. S., & Whitmarsh, R. B. (1974). The Azores-Gibraltar Plate Boundary. In L. Kristjansson (Ed.), *Geodynamics of Iceland and the North Atlantic Area* (pp. 63–81). Springer Netherlands. https://doi.org/10.1007/978-94-010-2271-2_5

Lauretano, V., Zachos, J. C., & Lourens, L. J. (2018). Orbitally Paced Carbon and Deep-Sea Temperature Changes at the Peak of the Early Eocene Climatic Optimum. *Paleoceanography and Paleoclimatology*, *33*(10), 1050–1065. https://doi.org/10.1029/2018PA003422

Lawrence, J., Blackett, P., & Cradock-Henry, N. A. (2020). Cascading climate change impacts and implications. *Climate Risk Management*, *29*, 100234. https://doi.org/10.1016/j.crm.2020.100234

Leavitt, P. R., Fritz, S. C., Anderson, N. J., Baker, P. A., Blenckner, T., Bunting, L., Catalan, J., Conley, D. J., Hobbs, W. O., Jeppesen, E., Korhola, A., McGowan, S., RÜhland, K., Rusak, J. A., Simpson, G. L., Solovieva, N., & Werne, J. (2009). Paleolimnological evidence of the effects on lakes of energy and mass transfer from climate and humans. *Limnology and Oceanography*, *54*(6part2), 2330–2348. https://doi.org/10.4319/lo.2009.54.6_part_2.2330

Leavitt, P. R., Hann, B. J., Smol, J. P., Zeeb, B. A., Christie, C. E., Wolfe, B., & Kling, H. J. (1994). Paleolimnological analysis of whole-lake experiments: an overview of results from Experimental Lakes Area Lake 227. *Canadian Journal of Fisheries and Aquatic Sciences*, *51*(10), 2322-2332.

Lebo, M. E., Reuter, J. E., Rhodes, C. L., & Goldman, C. R. (1992). Nutrient cycling and productivity in a desert saline lake: observations from a dry, low-productivity year. *Hydrobiologia*, *246*, 213-229.

Lee, C. H., & Hawley, N. (1998). The response of suspended particulate material to upwelling and downwelling events in southern Lake Michigan. *Journal of sedimentary research*, *68*(5), 819-831.

Leeder, M. R., & Mack, G. H. (2001). Lateral erosion ('toe-cutting') of alluvial fans by axial rivers: Implications for basin analysis and architecture. *Journal of the Geological Society*, *158*(6), 885–893. https://doi.org/10.1144/0016-760000-198

Leland, H. V., & Berkas, W. R. (1998). Temporal variation in plankton assemblages and physicochemistry of Devils Lake, North Dakota. *Hydrobiologia*, *377*(1), 57-71.

Lemons, D. R., & Chan, M. A. (1999). Facies architecture and sequence stratigraphy of fine-grained lacustrine deltas along the eastern margin of late Pleistocene Lake Bonneville, northern Utah and southern Idaho. AAPG bulletin, 83(4), 635-665.

Leng, M. J., & Marshall, J. D. (2004). Palaeoclimate interpretation of stable isotope data from lake sediment archives. *Quaternary Science Reviews*, *23*(7-8), 811-831.

Leng, M.J., Lamb, A.L., Heaton, T.H.E., Marshall, J.D., Wolfe, B.B., Jones, M.D., Holmes, J.A., Arrowsmith, C. (2006). Isotopes in lake sediments. In: Leng, M.J. (Ed.). Isotopes in Palaeoenvironmental Research. Developments in Paleoenvironmental Research, 10: 147-184.

Lerch, T. Z., Nunan, N., Dignac, M. F., Chenu, C., & Mariotti, A. (2011). Variations in microbial isotopic fractionation during soil organic matter decomposition. *Biogeochemistry*, *106*, 5-21.

Leroy, S.A.G., Henry, P., Peyron, O., Rostek, F., Kende, J., Bard, E., Tachikawa, K. 2023. Palynology, palaeoclimate and chronology from the Saalian Glacial to Saint-Germain II interstadial from two long cores at the limit between the Mediterranean and Euxinian regions. Quaternary Science Reviews, 311: 108145. doi: 10.1016/j.quascirev.2023.10814.

Leverington, D. W., & Teller, J. T. (2003). Paleotopographic reconstructions of the eastern outlets of glacial Lake Agassiz. *Canadian Journal of Earth Sciences*, *40*(9), 1259–1278. https://doi.org/10.1139/e03-043

Lewis, D. W., 1984. Practical Sedimentology. Hutchinson Ross Publishing Company, New York, 227 pp.

Lewis, W. M. (1987). Tropical limnology. *Annual review of ecology and systematics*, 159-184.

Li, Y., Kino, K., Cauquoin, A., Oki, T. 2023. Contribution of lakes in sustaining the Sahara greening during the mid-Holocene, Climate of the Past, 19: 1891–1904. doi: 10.5194/cp-19-1891-2023

Lindsay, R. (2016). Peatland classification.

Liu, J. P., Liu, C. S., Xu, K. H., Milliman, J. D., Chiu, J. K., Kao, S. J., & Lin, S. W. (2008). Flux and fate of small mountainous rivers derived sediments into the Taiwan Strait. *Marine Geology*, *256*(1–4), 65–76. https://doi.org/10.1016/j.margeo.2008.09.007

Lotter, A. F., & Birks, H. J. B. (1997). The separation of the influence of nutrients and climate on the varve time-series of Baldeggersee, Switzerland. *Aquatic Sciences*, *59*, 362-375.

Lotter, A. F., Birks, H. J. B., Hofmann, W., & Marchetto, A. (1997). Modern diatom, cladocera, chironomid, and chrysophyte cyst assemblages as quantitative indicators for the

reconstruction of past environmental conditions in the Alps. I. Climate. *Journal of Paleolimnology*, *18*, 395-420.

Lourenco, M., Fitchett, J. M., & Woodborne, S. (2023). Peat definitions: A critical review. *Progress in Physical Geography: Earth and Environment*, *47*(4), 506-520.

Lourenço, N., Miranda, J. M., Luis, J. F., Ribeiro, A., Victor, L. A. M., Madeira, J., & Needham, H. D. (1998). *Morpho-tectonic analysis of the Azores Volcanic Plateau from a new bathymetric compilation of the area*.

Louvat, P., & Allègre, C. J. (1998). Riverine erosion rates on Sao Miguel volcanic island, Azores archipelago. *Chemical Geology*, *148*(3–4), 177–200. https://doi.org/10.1016/S0009-2541(98)00028-X

Lu, C., Liu, Z., Jia, H., Dai, Q., Li, M., Ren, M., Xia, S., Li, L., & Wang, S. (2018). The controls of geomorphology and sediment supply on sequence stratigraphic architecture and sediment partitioning of the lacustrine rift basin in the Es $_3$ of Liuzan area, Nanpu Sag, Bohai Bay Basin, China. *Australian Journal of Earth Sciences*, *65*(2), 275–301. https://doi.org/10.1080/08120099.2018.1413594

Ludlam, S. D. (1984). Fayetteville Green Lake, New York, USA: VII. Varve chronology and sediment focusing. *Chemical geology*, *44*(1-3), 85-100.

Luis, J. F., & Miranda, J. M. (2008). Reevaluation of magnetic chrons in the North Atlantic between 35°N and 47°N: Implications for the formation of the Azores Triple Junction and associated plateau. *Journal of Geophysical Research*, *113*(B10), B10105. https://doi.org/10.1029/2007JB005573

Luis, J. F., Miranda, J. M., Galdeano, A., & Patriat, P. (1998). *Constraints on the structure of the Azores spreading center from gravity data*.

Lund, J. W. G. (1954). The seasonal cycle of the plankton diatom, Melosira italica (Ehr.) Kutz. subsp. subarctica O. Mull. *The Journal of Ecology*, 151-179.

Luterbacher, J., Rickli, R., Xoplaki, E., Tinguely, C., Beck, C., Pfister, C., & Wanner, H. (2001). *THE LATE MAUNDER MINIMUM (1675–1715) – A KEY PERIOD FOR STUDYING DECADAL SCALE CLIMATIC CHANGE IN EUROPE*.

Luterbacher, J., Schmutz, C., Gyalistras, D., Xoplaki, E., & Wanner, H. (1999). Reconstruction of monthly NAO and EU indices back to AD 1675. *Geophysical Research Letters*, *26*(17), 2745–2748. https://doi.org/10.1029/1999GL900576

Luterbacher, J., Werner, J.P., Smerdon, J.E., Fernández-Donado, L., González-Rouco, F.J., Barriopedro, D., Ljungqvist, F.C., Büntgen, U., Zorita, E., Wagner, S., Esper, J., McCarroll, D., Toreti, A., Frank, D., Jungclaus, J.H., Barriendos, M., Bertolin, C., Bothe, O., Brázdil, R., Camuffo, D. (2016). European summer temperatures since Roman times. Environmental Research Letters 11, 024001.

Luterbacher, J., Xoplaki, E., Dietrich, D., Rickli, R., Jacobeit, J., Beck, C., Gyalistras, D., Schmutz, C., & Wanner, H. (2002). Reconstruction of sea level pressure fields over the Eastern North Atlantic and Europe back to 1500. *Climate Dynamics*, *18*(7), 545–561. https://doi.org/10.1007/s00382-001-0196-6

Maberly, S. C., Hurley, M. A., Butterwick, C., Corry, J. E., Heaney, S. I., Irish, A. E., ... & Roscoe, J. V. (1994). The rise and fall of Asterionella formosa in the South Basin of Windermere: analysis of a 45-year series of data. *Freshwater Biology*, *31*(1), 19-34.

Mackereth, F. J. (1966). Some chemical observations on post-glacial lake sediments. Philosophical Transactions of the Royal Society of London. Series B, Biological Sciences, 250(765), 165-213.

Mackey, S. D., & Bridge, J. S. (1995). Three-dimensional model of alluvial stratigraphy; theory and applications. *Journal of Sedimentary Research*, *65*(1b), 7-31.

Macklin, M. G., Tooth, S., Brewer, P. A., Noble, P. L., & Duller, G. A. T. (2010). Holocene flooding and river development in a Mediterranean steepland catchment: The Anapodaris Gorge, south central Crete, Greece. *Global and Planetary Change*, *70*(1–4), 35–52. https://doi.org/10.1016/j.gloplacha.2009.11.006

Madeira, J. & Brum da Silveira, A. (2009). Active tectonics and first paleoseismological results in Faial, Pico and S. Jorge islands (Azores, Portugal). *Annals of Geophysics*, *46*(5). https://doi.org/10.4401/ag-3453

Madeira, J., & Ribeiro, A. (1990). Geodynamic models for the Azores triple junctiun: A contribution from tectonics. *Tectonophysics*, *184*(3–4), 405–415. https://doi.org/10.1016/0040-1951(90)90452-E

Madeira, J., Brum da Silveira, A., Hipólito, A., & Carmo, R. (2015). Chapter 3 Active tectonics in the central and eastern Azores islands along the Eurasia–Nubia boundary: A review. *Geological Society, London, Memoirs*, *44*(1), 15–32. https://doi.org/10.1144/M44.3

Magnuson, J. J., Robertson, D. M., Benson, B. J., Wynne, R. H., Livingstone, D. M., Arai, T., Assel, R. A., Barry, R. G., Card, V., Kuusisto, E., Granin, N. G., Prowse, T. D., Stewart, K. M., & Vuglinski, V. S. (2000). Historical Trends in Lake and River Ice Cover in the Northern Hemisphere. *Science*, *289*(5485), 1743–1746. https://doi.org/10.1126/science.289.5485.1743

Magurran, A. E., Dornelas, M., Moyes, F., & Henderson, P. A. (2019). Temporal β diversity—A macroecological perspective. *Global Ecology and Biogeography*, *28*(12), 1949-1960.

Malheiro, A. (2006). Geological hazards in the Azores archipelago: Volcanic terrain instability and human vulnerability. *Journal of Volcanology and Geothermal Research*, *156*(1–2), 158–171. https://doi.org/10.1016/j.jvolgeores.2006.03.012

Malhi, Y., Doughty, C. E., Galetti, M., Smith, F. A., Svenning, J. C., & Terborgh, J. W. (2016). Megafauna and ecosystem function from the Pleistocene to the Anthropocene. *Proceedings of the National Academy of Sciences*, *113*(4), 838-846.

Malmqvist, B., & Rundle, S. (2002). Threats to the running water ecosystems of the world. *Environmental conservation*, *29*(2), 134-153.

Mani, P., Allen, S., Evans, S. G., Kargel, J. S., Mergili, M., Petrakov, D., & Stoffel, M. (2023). Geomorphic Process Chains in High-Mountain Regions—A Review and Classification Approach for Natural Hazards Assessment. *Reviews of Geophysics*, *61*(4), e2022RG000791. https://doi.org/10.1029/2022RG000791

Mann, M. E. (2007). Climate Over the Past Two Millennia. *Annual Review of Earth and Planetary Sciences*, *35*(1), 111–136. https://doi.org/10.1146/annurev.earth.35.031306.140042

Mann, M. E., Zhang, Z., Rutherford, S., Bradley, R. S., Hughes, M. K., Shindell, D., Ammann, C., Faluvegi, G., & Ni, F. (2009). Global Signatures and Dynamical Origins of the Little Ice Age and Medieval Climate Anomaly. *Science*, *326*(5957), 1256–1260. https://doi.org/10.1126/science.1177303

Marchetto, A., Ariztegui, D., Brauer, A., Lami, A., Mercuri, A. M., Sadori, L., ... & Guilizzoni, P. (2015). Volcanic lake sediments as sensitive archives of climate and environmental change. Volcanic lakes, 379-399.

Marcott, S. A., Shakun, J. D., Clark, P. U., & Mix, A. C. (2013). A Reconstruction of Regional and Global Temperature for the Past 11,300 Years. *Science*, *339*(6124), 1198–1201. https://doi.org/10.1126/science.1228026

Marden, M., Arnold, G., Gomez, B., & Rowan, D. (2005). Pre- and post-reforestation gully development in Mangatu Forest, East Coast, North Island, New Zealand. *River Research and Applications*, *21*(7), 757–771. https://doi.org/10.1002/rra.882

Margalef, R. (1983). Algas de una laguna salobre mediterranea (Lago di Patria, Napoles).

Marques, H. M. A. D. S. (2021). Reconstruction of past environmental changes in the Azores based on lacustrine diatom sedimentary records. Universidad dos Açores. 264 pp.

Marques, R., Zêzere, J., Trigo, R., Gaspar, J., & Trigo, I. (2008). Rainfall patterns and critical values associated with landslides in Povoação County (São Miguel Island, Azores): Relationships with the North Atlantic Oscillation. *Hydrological Processes*, *22*(4), 478–494. https://doi.org/10.1002/hyp.6879

Marshall, J., Kushnir, Y., Battisti, D., Chang, P., Czaja, A., Dickson, R., ... & Visbeck, M. (2001). North Atlantic climate variability: phenomena, impacts and mechanisms. *International Journal of Climatology: A Journal of the Royal Meteorological Society*, *21*(15), 1863-1898.

Marshall, M. H., Lamb, H. F., Huws, D., Davies, S. J., Bates, R., Bloemendal, J., ... & Bryant, C. (2011). Late Pleistocene and Holocene drought events at Lake Tana, the source of the Blue Nile. *Global and Planetary Change*, *78*(3-4), 147-161.

Marshall, M., Schlolaut, G., Nakagawa, T., Lamb, H., Brauer, A., Staff, R., ... & Tada, R. (2012). A novel approach to varve counting using μXRF and X-radiography in combination with thin-section microscopy, applied to the Late Glacial chronology from Lake Suigetsu, Japan. *Quaternary Geochronology*, *13*, 70-80.

Martín-Chivelet, J., Muñoz-García, M. B., Edwards, R. L., Turrero, M. J., & Ortega, A. I. (2011). Land surface temperature changes in Northern Iberia since 4000yrBP, based on δ13C of speleothems. *Global and Planetary Change*, *77*(1–2), 1–12. https://doi.org/10.1016/j.gloplacha.2011.02.002

Martin-Puertas, C., Brauer, A., Dulski, P., & Brademann, B. (2012). Testing climate–proxy stationarity throughout the Holocene: an example from the varved sediments of Lake Meerfelder Maar (Germany). *Quaternary Science Reviews*, *58*, 56-65.

Martín-Puertas, C., Jiménez-Espejo, F., Martínez-Ruiz, F., Nieto-Moreno, V., Rodrigo, M., Mata, M. P., & Valero-Garcés, B. L. (2010). Late Holocene climate variability in the southwestern Mediterranean region: An integrated marine and terrestrial geochemical approach. *Climate of the Past*, *6*(6), 807–816. https://doi.org/10.5194/cp-6-807-2010

Martin-Puertas, C., Matthes, K., Brauer, A., Muscheler, R., Hansen, F., Petrick, C., ... & Van Geel, B. (2012). Regional atmospheric circulation shifts induced by a grand solar minimum. Nature Geoscience, 5(6), 397-401.

Martín-Puertas, C., Valero-Garcés, B. L., Pilar Mata, M., González-Sampériz, P., Bao, R., Moreno, A., & Stefanova, V. (2008). Arid and humid phases in southern Spain during the last 4000 years: The Zoñar Lake record, Córdoba. *The Holocene*, *18*(6), 907–921. https://doi.org/10.1177/0959683608093533

Martin-Jézéquel, V., Hildebrand, M., & Brzezinski, M. A. (2000). Silicon metabolism in diatoms: implications for growth. *Journal of phycology*, *36*(5), 821-840.

Masson, D. G., Watts, A. B., Gee, M. J. R., Urgeles, R., Mitchell, N. C., Le Bas, T. P., & Canals, M. (2002). Slope failures on the flanks of the western Canary Islands. *Earth-Science Reviews*, *57*(1-2), 1-35.

Mats, V. D., & Perepelova, T. I. (2011). A new perspective on evolution of the Baikal Rift. *Geoscience frontiers*, *2*(3), 349-365.

McHugh, M., Harrod, T., & Morgan, R. (2002). The extent of soil erosion in upland England and Wales. *Earth Surface Processes and Landforms: The Journal of the British Geomorphological Research Group*, *27*(1), 99-107.

McMichael, A. J., Woodruff, R. E., & Hales, S. (2006). Climate change and human health: Present and future risks. *The Lancet*, *367*(9513), 859–869. https://doi.org/10.1016/S0140-6736(06)68079-3

McQueen KG (2009) Regolith geochemistry. In: Scott KM, Pain CF (eds) Regolith science. Springer, Dordrecht.

McSaveney, M., & Davies, T. (2007). Rockslides and Their Motion. In K. Sassa, H. Fukuoka, F. Wang, & G. Wang (Eds.), *Progress in Landslide Science* (pp. 113–133). Springer Berlin Heidelberg. https://doi.org/10.1007/978-3-540-70965-7_8

Medina-Elizalde, M., Burns, S. J., Lea, D. W., Asmerom, Y., Von Gunten, L., Polyak, V., Vuille, M., & Karmalkar, A. (2010). High resolution stalagmite climate record from the Yucatán Peninsula spanning the Maya terminal classic period. *Earth and Planetary Science Letters*, *298*(1–2), 255–262. https://doi.org/10.1016/j.epsl.2010.08.016

Medlin, L. K., Williams, D. M., & Sims, P. A. (1993). The evolution of the diatoms (Bacillariophyta). I. Origin of the group and assessment of the monophyly of its major divisions. *European Journal of Phycology*, *28*(4), 261-275.

Meek, N., 1999. New discoveries about the Late Wisconsinan history of the Mojave River: San Bernardino County Museum Association Quarterly, 46(3), p. 113-117.

Meinshausen, M., Nicholls, Z. R. J., Lewis, J., Gidden, M. J., Vogel, E., Freund, M., Beyerle, U., Gessner, C., Nauels, A., Bauer, N., Canadell, J. G., Daniel, J. S., John, A., Krummel, P. B., Luderer, G., Meinshausen, N., Montzka, S. A., Rayner, P. J., Reimann, S., … Wang, R. H. J. (2020). The shared socio-economic pathway (SSP) greenhouse gas concentrations and their extensions to 2500. *Geoscientific Model Development*, *13*(8), 3571–3605. https://doi.org/10.5194/gmd-13-3571-2020

Mellado-Cano, J., Barriopedro, D., García-Herrera, R., Trigo, R. M., & Hernández, A. (2019). Examining the North Atlantic Oscillation, East Atlantic pattern, and jet variability since 1685. *Journal of Climate*, *32*(19), 6285-6298.

Merkouriev, S., & DeMets, C. (2008). A high-resolution model for Eurasia-North America plate kinematics since 20 Ma. *Geophysical Journal International*, *173*(3), 1064–1083. https://doi.org/10.1111/j.1365-246X.2008.03761.x

Merkouriev, S., & DeMets, C. (2014a). High-resolution estimates of Nubia–North America plate motion: 20 Ma to present. *Geophysical Journal International*, *196*(3), 1281–1298. https://doi.org/10.1093/gji/ggt463

Merkouriev, S., & DeMets, C. (2014b). High-resolution Neogene reconstructions of Eurasia-North America Plate motion. *Geophysical Journal International*, *198*(1), 366–384. https://doi.org/10.1093/gji/ggu142

Métrich, N., Zanon, V., Créon, L., Hildenbrand, A., Moreira, M., & Marques, F. O. (2014). Is the 'Azores Hotspot' a Wetspot? Insights from the Geochemistry of Fluid and Melt Inclusions in Olivine of Pico Basalts. *Journal of Petrology*, *55*(2), 377–393. https://doi.org/10.1093/petrology/egt071

Meyers, P. A. (1994). Preservation of elemental and isotopic source identification of sedimentary organic matter. *Chemical Geology*, *114*(3–4), 289–302. https://doi.org/10.1016/0009-2541(94)90059-0

Meyers, P. A., & Ishiwatari, R. (1993). Lacustrine organic geochemistry—an overview of indicators of organic matter sources and diagenesis in lake sediments. *Organic geochemistry*, *20*(7), 867-900.

Meyers, P. A., & Ishiwatari, R. (1993). The early diagenesis of organic matter in lacustrine sediments. In *Organic geochemistry: Principles and applications* (pp. 185-209). Boston, MA: Springer US.

Meyers, P. A., & Takemura, K. (1997). Quaternary changes in delivery and accumulation of organic matter in sediments of Lake Biwa, Japan. *Journal of Paleolimnology*, *18*(3), 211-218.

Meyers, P. A., & Teranes, J. L. (2001). Sediment organic matter. Tracking environmental change using lake sediments: physical and geochemical methods, 239-269.

Miall, A. D., & Miall, A. D. (1997). Time in sequence stratigraphy. *The Geology of Stratigraphic Sequences*, 273-279.

Michaelides, K., & Wainwright, J. (2002). Modelling the effects of hillslope–channel coupling on catchment hydrological response. *Earth Surface Processes and Landforms: The Journal of the British Geomorphological Research Group*, *27*(13), 1441-1457.

Michard, G., Viollier, E., Jézéquel, D., & Sarazin, G. (1994). Geochemical study of a crater lake: Pavin Lake, France—Identification, location and quantification of the chemical reactions in the lake. *Chemical Geology*, *115*(1-2), 103-115.

Migoń, P. (2021). Sandstone geomorphology – Recent advances. *Geomorphology*, *373*, 107484. https://doi.org/10.1016/j.geomorph.2020.107484

Miller, L. G., & Aiken, G. R. (1996). Effects of glacial meltwater inflows and moat freezing on mixing in an ice-covered Antarctic lake as interpreted from stable isotope and tritium distributions. *Limnology and Oceanography*, *41*(5), 966-976.

Minagawa, M., & Wada, E. (1984). Stepwise enrichment of 15N along food chains: further evidence and the relation between δ15N and animal age. *Geochimica et cosmochimica acta*, *48*(5), 1135-1140.

Miranda, J. M., Luis, J. F., & Lourenço, N. (2018). The Tectonic Evolution of the Azores Based on Magnetic Data. In U. Kueppers & C. Beier (Eds.), *Volcanoes of the Azores* (pp. 89–100). Springer Berlin Heidelberg. https://doi.org/10.1007/978-3-642-32226-6_6

Miranda, J. M., Luis, J. F., Lourenço, N., & Goslin, J. (2014). Distributed deformation close to the Azores Triple "Point". *Marine Geology*, *355*, 27–35. https://doi.org/10.1016/j.margeo.2014.05.006

Mitchell, N. C., Masson, D. G., Watts, A. B., Gee, M. J., & Urgeles, R. (2002). The morphology of the submarine flanks of volcanic ocean islands: A comparative study of the Canary and Hawaiian hotspot islands. *Journal of Volcanology and Geothermal Research*, *115*(1-2), 83-107.

Moalla, S. M. N., Awadallah, R. M., Rashed, M. N., & Soltan, M. E. (1997). Distribution and chemical fractionation of some heavy metals in bottom sediments of Lake Nasser. *Hydrobiologia*, *364*, 31-40.

Moffa-Sánchez, P., Born, A., Hall, I. R., Thornalley, D. J. R., & Barker, S. (2014). Solar forcing of North Atlantic surface temperature and salinity over the past millennium. *Nature Geoscience*, *7*(4), 275–278. https://doi.org/10.1038/ngeo2094

Molnar, P., Anderson, R. S., & Anderson, S. P. (2007). Tectonics, fracturing of rock, and erosion. *Journal of Geophysical Research: Earth Surface*, *112*(F3), 2005JF000433. https://doi.org/10.1029/2005JF000433

Montgomery, D.R., Buffington, J.M., Smith, R.D. et al. (1995) Pool spacing in forest channels. Water Resources Research, 31, 1097–1105.

Moore, G. W. K., & Renfrew, I. A. (2012). Cold European winters: interplay between the NAO and the East Atlantic mode. *Atmospheric Science Letters*, *13*(1), 1-8.

Moore, G. W. K., Pickart, R. S., & Renfrew, I. A. (2011). Complexities in the climate of the subpolar North Atlantic: a case study from the winter of 2007. *Quarterly Journal of the Royal Meteorological Society*, *137*(656), 757-767.

Moore, G. W. K., Renfrew, I. A., & Pickart, R. S. (2013). Multidecadal Mobility of the North Atlantic Oscillation. *Journal of Climate*, *26*(8), 2453–2466. https://doi.org/10.1175/JCLI-D-12-00023.1

Moossen, H. (2015). North Atlantic Holocene climate evolution recorded by high-resolution terrestrial and marine biomarker records. *Quaternary Science Reviews*, 17.

Morellón, M., Valero-Garcés, B., González-Sampériz, P., Vegas-Vilarrúbia, T., Rubio, E., Rieradevall, M., Delgado-Huertas, A., Mata, P., Romero, Ó., Engstrom, D. R., López-Vicente, M., Navas, A., & Soto, J. (2011). Climate changes and human activities recorded in the sediments of Lake Estanya (NE Spain) during the Medieval Warm Period and Little Ice Age. *Journal of Paleolimnology*, *46*(3), 423–452. https://doi.org/10.1007/s10933-009-9346-3

Moreno, A., Pérez, A., Frigola, J., Nieto-Moreno, V., Rodrigo-Gámiz, M., Martrat, B., González-Sampériz, P., Morellón, M., Martín-Puertas, C., Corella, J. P., Belmonte, Á., Sancho, C., Cacho, I., Herrera, G., Canals, M., Grimalt, J. O., Jiménez-Espejo, F., Martínez-Ruiz, F., Vegas-Vilarrúbia, T., & Valero-Garcés, B. L. (2012). The Medieval Climate Anomaly in the Iberian Peninsula reconstructed from marine and lake records. *Quaternary Science Reviews*, *43*, 16–32. https://doi.org/10.1016/j.quascirev.2012.04.007

Moreno, A., Valero-Garcés, B. L., González-Sampériz, P., & Rico, M. (2008). Flood response to rainfall variability during the last 2000 years inferred from the Taravilla Lake record (Central Iberian Range, Spain). Journal of paleolimnology, 40, 943-961.

Morisseau, M., & Traineau, H. (1985). Mise en évidence d'une activité hydromagmatique holocène sur l'île de Flores (Açores). *Comptes rendus de l'Académie des sciences. Série 2, Mécanique, Physique, Chimie, Sciences de l'univers, Sciences de la Terre*, *301*(18), 1309-1314.

Mottl, O., Grytnes, J.-A., Seddon, A. W. R., Steinbauer, M. J., Bhatta, K. P., Felde, V. A., Flantua, S. G. A., & Birks, H. J. B. (2021). Rate-of-change analysis in paleoecology revisited: A new approach. *Review of Palaeobotany and Palynology*, *293*, 104483. https://doi.org/10.1016/j.revpalbo.2021.104483

Mozafari, B., Bruen, M., Donohue, S., Renou-Wilson, F., & O'Loughlin, F. (2023). Peatland dynamics: A review of process-based models and approaches. *Science of The Total Environment*, *877*, 162890.

Najafi, S., Dragovich, D., Heckmann, T., & Sadeghi, S. H. (2021). Sediment connectivity concepts and approaches. *CATENA*, *196*, 104880. https://doi.org/10.1016/j.catena.2020.104880

Nakagawa, T., Gotanda, K., Haraguchi, T., Danhara, T., Yonenobu, H., Brauer, A., ... & Lamb, H. (2012). SG06, a fully continuous and varved sediment core from Lake Suigetsu, Japan: stratigraphy and potential for improving the radiocarbon calibration model and understanding of late Quaternary climate changes. *Quaternary Science Reviews*, *36*, 164-176.

Navarro, A., Lourenço, N., Chorowicz, J., Miranda, J. M., & Catalão, J. (2009). Analysis of geometry of volcanoes and faults in Terceira Island (Azores): Evidence for reactivation tectonics at the EUR/AFR plate boundary in the Azores triple junction. *Tectonophysics*, *465*(1–4), 98–113. https://doi.org/10.1016/j.tecto.2008.10.020

Németh, K., & Kósik, S. (2020). Review of explosive hydrovolcanism. *Geosciences*, *10*(2), 44.

Nesje, A., Lie, Ø., & Dahl, S. O. (2000). Is the North Atlantic Oscillation reflected in Scandinavian glacier mass balance records?. *Journal of Quaternary Science: Published for the Quaternary Research Association*, *15*(6), 587-601.

Neugebauer, I., Brauer, A., Dräger, N., Dulski, P., Wulf, S., Plessen, B., ... & Brande, A. (2012). A Younger Dryas varve chronology from the Rehwiese palaeolake record in NE-Germany. *Quaternary Science Reviews*, *36*, 91-102.

Neukom, R., Steiger, N., Gómez-Navarro, J. J., Wang, J., & Werner, J. P. (2019). No evidence for globally coherent warm and cold periods over the preindustrial Common Era. *Nature*, *571*(7766), 550–554. https://doi.org/10.1038/s41586-019-1401-2

Newhall, C. G., Paull, C. K., Bradbury, J. P., Higuera-Gundy, A., Poppe, L. J., Self, S., ... & Ziagos, J. (1987). Recent geologic history of Lake Atitlán, a caldera lake in western Guatemala. *Journal of volcanology and geothermal research*, *33*(1-3), 81-107.

Nichols, G. (2009). *Sedimentology and stratigraphy*. John Wiley & Sons.

Niessen, F., Ebel, T., Kopsch, C., & Fedorov, G. B. (1999). High-Resolution Seismic Stratigraphy of Lake Sediments on the Taymyr Peninsula, Central Siberia. In H. Kassens, H. A. Bauch, I. A. Dmitrenko, H. Eicken, H.-W. Hubberten, M. Melles, J. Thiede, & L. A. Timokhov (Eds.), *Land-Ocean Systems in the Siberian Arctic* (pp. 437–456). Springer Berlin Heidelberg. https://doi.org/10.1007/978-3-642-60134-7_35

Nieto-Moreno, V., Martínez-Ruiz, F., Giralt, S., Jiménez-Espejo, F., Gallego-Torres, D., Rodrigo-Gámiz, M., García-Orellana, J., Ortega-Huertas, M., & de Lange, G. J. (2011). Tracking climate variability in the western Mediterranean during the Late Holocene: A multiproxy approach. *Climate of the Past*, *7*(4), 1395–1414. https://doi.org/10.5194/cp-7-1395-2011

Nistor, C. J., & Church, M. (2005). Suspended sediment transport regime in a debris-flow gully on Vancouver Island, British Columbia. *Hydrological Processes*, *19*(4), 861–885. https://doi.org/10.1002/hyp.5549

Nogué, S., Santos, A. M., Birks, H. J. B., Björck, S., Castilla-Beltrán, A., Connor, S., ... & Steinbauer, M. J. (2021). The human dimension of biodiversity changes on islands. *Science*, *372*(6541), 488-491.

Nunes, J. C. (2020). Geology and Volcanology of Pico Island (Azores, Portugal): A Field Guide. In F. Fernandes, A. Malheiro, & H. I. Chaminé (Eds.), *Advances in Natural Hazards and Hydrological Risks: Meeting the Challenge* (pp. 183–192). Springer International Publishing. https://doi.org/10.1007/978-3-030-34397-2_35

O'sullivan, P. E. (1983). Annually-laminated lake sediments and the study of Quaternary environmental changes—a review. *Quaternary Science Reviews*, *1*(4), 245-313.

O'Sullivan, P., & Reynolds, C. S. (Eds.). (2008). *The lakes handbook, volume 1: limnology and limnetic ecology* (Vol. 1). John Wiley & Sons.

O'Reilly, C. M., Alin, S. R., Plisnier, P.-D., Cohen, A. S., & McKee, B. A. (2003). Climate change decreases aquatic ecosystem productivity of Lake Tanganyika, Africa. *Nature*, *424*(6950), 766–768. https://doi.org/10.1038/nature01833

O'Sullivan, P., & Reynolds, C. S. (2005). *The lakes handbook. 1: Limnology and limnetic ecology* ([Nachdr.]-2005). Blackwell Science.

Ochiai, S., & Kashiwaya, K. (2003). A Conceptual Model of Sedimentation Processes for a Hydrogeomorphological Study in Lake Baikal. In K. Kashiwaya (Ed.), *Long Continental Records from Lake Baikal* (pp. 297–312). Springer Japan. https://doi.org/10.1007/978-4-431-67859-5_19

Ojala, A. E. K., & Alenius, T. (2005). 10000 years of interannual sedimentation recorded in the Lake Nautajärvi (Finland) clastic–organic varves. *Palaeogeography, Palaeoclimatology, Palaeoecology*, *219*(3–4), 285–302. https://doi.org/10.1016/j.palaeo.2005.01.002

Ojala, A. E., Francus, P., Zolitschka, B., Besonen, M., & Lamoureux, S. F. (2012). Characteristics of sedimentary varve chronologies–a review. *Quaternary Science Reviews*, *43*, 45-60.

Ojala, A. E., Saarinen, T., & Salonen, V. P. (2000). Preconditions for the formation of annually laminated lake sediments in southern and central Finland. *Boreal Environment Research*, *5*(3), 243-255.

Okamoto, I., & Endoh, S. (1995). Water mass exchange between the main basin and Shiozu Bay. *Physical Processes in a Large Lake: Lake Biwa, Japan*, *48*, 31-42.

Oksanen, J., Guillaume Blanchet, F., Kindt, R., Legendre, P., Minchin, P.R., O'Hara, R.B., Simpson, G.L., Solymos, P., Henry, M., Stevens, H., Wagner, H. (2013). Vegan: Community Ecology Package. R Package Version 2.0-10. http://CRAN.Rproject. org/package¼vegan.

Oldfield, F. (2005). *Environmental change: key issues and alternative perspectives*. Cambridge University Press.

Oliva, M., Ruiz-Fernández, J., Barriendos, M., Benito, G., Cuadrat, J. M., Domínguez-Castro, F., García-Ruiz, J. M., Giralt, S., Gómez-Ortiz, A., Hernández, A., López-Costas, O., López-Moreno, J. I., López-Sáez, J. A., Martínez-Cortizas, A., Moreno, A., Prohom, M., Saz, M. A., Serrano, E., Tejedor, E., … Vicente-Serrano, S. M. (2018). The Little Ice Age in Iberian mountains. *Earth-Science Reviews*, *177*, 175–208. https://doi.org/10.1016/j.earscirev.2017.11.010

Olsen, J., Anderson, N. J., & Knudsen, M. F. (2012). Variability of the North Atlantic Oscillation over the past 5,200 years. *Nature Geoscience*, *5*(11), 808–812. https://doi.org/10.1038/ngeo1589

Olsen, J., Anderson, N. J., & Leng, M. J. (2013). Limnological controls on stable isotope records of late-Holocene palaeoenvironment change in SW Greenland: a paired lake study. *Quaternary Science Reviews*, *66*, 85-95.

Olsen, P. E. (1990). Tectonic, Climatic, and Biotic Modulation of Lacustrine Ecosystems--Examples from Newark Supergroup of Eastern North America: Chapter 13.

Ortega, P., Lehner, F., Swingedouw, D., Masson-Delmotte, V., Raible, C. C., Casado, M., & Yiou, P. (2015). A model-tested North Atlantic Oscillation reconstruction for the past millennium. *Nature*, *523*(7558), 71–74. https://doi.org/10.1038/nature14518

Osman, M. B., Coats, S., Das, S. B., McConnell, J. R., & Chellman, N. (2021). North Atlantic jet stream projections in the context of the past 1,250 years. *Proceedings of the National Academy of Sciences*, *118*(38), e2104105118.

Pacheco, J. M., Ferreira, T., Queiroz, G., Wallenstein, N., Coutinho, R., Cruz, J. V., ... & Goulart, C. (2013). Notas sobre a geologia do arquipélago dos Açores. *Geologia de Portugal*, *2*, 595-690.

PAGES Hydro2k Consortium. (2017). Comparing proxy and model estimates of hydroclimate variability and change over the Common Era. *Climate of the Past*, *13*(12), 1851–1900. https://doi.org/10.5194/cp-13-1851-2017

Paine, A. D. M. (1985). 'Ergodic' reasoning in geomorphology: Time for a review of the term? *Progress in Physical Geography: Earth and Environment*, *9*(1), 1–15. https://doi.org/10.1177/030913338500900101

Paredes, P., Fontes, J. C., Azevedo, E. B., & Pereira, L. S. (2017). Daily reference crop evapotranspiration in the humid environments of Azores islands using reduced data sets: Accuracy of FAO-PM temperature and Hargreaves-Samani methods. *Theoretical and Applied Climatology*, *134*(1–2), 595–611. https://doi.org/10.1007/s00704-017-2295-2

Parker, D., Folland, C., Scaife, A., Knight, J., Colman, A., Baines, P., & Dong, B. (2007). Decadal to multidecadal variability and the climate change background. *Journal of Geophysical Research: Atmospheres*, *112*(D18), 2007JD008411. https://doi.org/10.1029/2007JD008411

Parker, D.E., Legg, T.P. and Folland, C.K. (1992). 'A new daily Central England Temperature Series, 1772–1991' Int.J.Climatol. 12 , 317–342.

Parnell, J., Spinks, S., Andrews, S., Thayalan, W., & Bowden, S. (2015). High Molybdenum availability for evolution in a Mesoproterozoic lacustrine environment. *Nature Communications*, *6*(1), 6996.

Pawson, R. R. (2008). *Assessing the role of particulates in the fluvial organic carbon flux from eroding peatland systems*. The University of Manchester (United Kingdom).

Pedrazzi, D., Cappello, A., Zanon, V., & Del Negro, C. (2015). Impact of effusive eruptions from the Eguas–Carvão fissure system, São Miguel Island, Azores Archipelago (Portugal). *Journal of Volcanology and Geothermal Research*, *291*, 1–13. https://doi.org/10.1016/j.jvolgeores.2014.12.012

Pelletier, J. D. (2009). Controls on the height and spacing of eolian ripples and transverse dunes: A numerical modeling investigation. *Geomorphology*, *105*(3-4), 322-333.

Pérez-Peña, J. V., Azor, A., Azañón, J. M., & Keller, E. A. (2010). Active tectonics in the Sierra Nevada (Betic Cordillera, SE Spain): Insights from geomorphic indexes and drainage pattern analysis. *Geomorphology*, *119*(1-2), 74-87.

Perri, F. (2020). Chemical weathering of crystalline rocks in contrasting climatic conditions using geochemical proxies: An overview. *Palaeogeography, Palaeoclimatology, Palaeoecology*, *556*, 109873. https://doi.org/10.1016/j.palaeo.2020.109873

Perron, J. T., & Royden, L. (2013). An integral approach to bedrock river profile analysis. *Earth surface processes and landforms*, *38*(6), 570-576.

Peterson, B. J., & Fry, B. (1987). Stable isotopes in ecosystem studies. *Annual review of ecology and systematics*, *18*(1), 293-320.

Pham, S. V., Leavitt, P. R., McGowan, S., & Peres-Neto, P. (2008). Spatial variability of climate and land-use effects on lakes of the northern Great Plains. *Limnology and Oceanography*, *53*(2), 728–742. https://doi.org/10.4319/lo.2008.53.2.0728

Phillips, J. D., & Gomez, B. (2007). Controls on sediment export from the Waipaoa River basin, New Zealand. *Basin Research*, *19*(2), 241-252.

Pickrill, R. A., & Irwin, J. (1982). Predominant headwater inflow and its control of lake-river interactions in Lake Wakatipu. *New Zealand journal of marine and freshwater research*, *16*(2), 201-213.

Pickrill, R. A., & Irwin, J. (1983). Sedimentation in a deep glacier-fed lake—Lake Tekapo, New Zealand. *Sedimentology*, *30*(1), 63-75.

Pienitz, R., & Vincent, W. F. (2000). Effect of climate change relative to ozone depletion on UV exposure in subarctic lakes. *Nature*, *404*(6777), 484-487.

Pike, R. J., Evans, I. S., & Hengl, T. (2009). Geomorphometry: a brief guide. *Developments in soil science*, *33*, 3-30.

Pilskaln, C. H., & Johnson, T. C. (1991). Seasonal signals in Lake Malawi sediments. *Limnology and Oceanography*, *36*(3), 544-557.

Pinto, J. G., & Raible, C. C. (2012). Past and recent changes in the North Atlantic oscillation. *Wiley Interdisciplinary Reviews: Climate Change*, *3*(1), 79-90.

Piovano, E. L., Córdoba, F. E., & Stutz, S. (2014). *LIMNOGEOLOGY IN SOUTHERN SOUTH AMERICA: AN OVERVIEW*. *21*.

Pla, S., & Catalan, J. (2005). Chrysophyte cysts from lake sediments reveal the submillennial winter/spring climate variability in the northwestern Mediterranean region throughout the Holocene. *Climate Dynamics*, *24*(2–3), 263–278. https://doi.org/10.1007/s00382-004-0482-1

Plafker, G., & Ericksen, G. E. (1978). Nevados Huascarán Avalanches, Peru. In *Developments in Geotechnical Engineering* (Vol. 14, pp. 277–314). Elsevier. https://doi.org/10.1016/B978-0-444-41507-3.50016-7

Plisnier, P. D., Chitamwebwa, D., Mwape, L., Tshibangu, K., Langenberg, V., & Coenen, E. (1999). Limnological annual cycle inferred from physical-chemical fluctuations at three stations of Lake Tanganyika. *From limnology to fisheries: Lake Tanganyika and other large lakes*, 45-58.

Polissar, P. J. (2005). *Lake records of Holocene climate change, Cordillera de Mérida, Venezuela*. University of Massachusetts Amherst.

Porteiro, J. (2000). Lagoas dos Açores: elementos de suporte ao planeamento integrado. *Universidade dos Açores*.

Powers, L., Werne, J. P., Vanderwoude, A. J., Damsté, J. S. S., Hopmans, E. C., & Schouten, S. (2010). Applicability and calibration of the TEX86 paleothermometer in lakes. *Organic Geochemistry*, *41*(4), 404-413.

Prohom, M., Barriendos, M., & Sanchez-Lorenzo, A. (2016). Reconstruction and homogenization of the longest instrumental precipitation series in the Iberian Peninsula (Barcelona, 1786–2014). *International Journal of Climatology*, *36*(8), 3072–3087. https://doi.org/10.1002/joc.4537

Prothero, D. R., & Schwab, F. (2004). *Sedimentary geology*. Macmillan.

Quartau, R., Ramalho, R. S., Madeira, J., Santos, R., Rodrigues, A., Roque, C., ... & Da Silveira, A. B. (2018). Gravitational, erosional and depositional processes on volcanic ocean islands: Insights from the submarine morphology of Madeira Archipelago. *Earth and Planetary Science Letters*, *482*, 288-299.

Ragotzkie, R. A. (1978). Heat budgets of lakes. In *Lakes: chemistry, geology, physics* (pp. 1-19). New York, NY: Springer New York.

Raible, C.C., Lehner, F., González-Rouco, J.F., Fernández-Donado, L., 2014. Changing correlation structures of the Northern Hemisphere atmospheric circulation from 1000 to 2100 AD. Clim. Past 10, 537–550. https://doi.org/10.5194/cp-10-537-2014.

Ramalho, R. S., Quartau, R., Trenhaile, A. S., Mitchell, N. C., Woodroffe, C. D., & Ávila, S. P. (2013). Coastal evolution on volcanic oceanic islands: A complex interplay between volcanism, erosion, sedimentation, sea-level change and biogenic production. *Earth-Science Reviews*, *127*, 140-170.

Raposeiro, P. M., Hernández, A., Pla-Rabes, S., Gonçalves, V., Bao, R., Sáez, A., Shanahan, T., Benavente, M., de Boer, E. J., Richter, N., Gordon, V., Marques, H., Sousa, P. M., Souto, M., Matias, M. G., Aguiar, N., Pereira, C., Ritter, C., Rubio, M. J., … Giralt, S. (2021). Climate change facilitated the early colonization of the Azores Archipelago during medieval times. *Proceedings of the National Academy of Sciences*, *118*(41), e2108236118. https://doi.org/10.1073/pnas.2108236118

Raposeiro, P. M., Ritter, C., Abbott, M., Hernandez, A., Pimentel, A., Lasher, E., Płóciennik, M., Berlajolli, V., Kotrys, B., Pombal, X. P., Souto, M., Giralt, S., & Gonçalves, V. (2024). Late Holocene climate dynamics in the Azores archipelago. *Quaternary Science Reviews*, *331*, 108617. https://doi.org/10.1016/j.quascirev.2024.108617

Raposeiro, P. M., Rubio, M. J., González, A., Hernández, A., Sánchez-López, G., Vázquez-Loureiro, D., Rull, V., Bao, R., Costa, A. C., Gonçalves, V., Sáez, A., & Giralt, S. (2017). Impact of the historical introduction of exotic fishes on the chironomid community of Lake Azul (Azores Islands). *Palaeogeography, Palaeoclimatology, Palaeoecology*, *466*, 77–88. https://doi.org/10.1016/j.palaeo.2016.11.015

Raposeiro, P. M., Saez, A., Giralt, S., Costa, A. C., & Gonçalves, V. (2018). Causes of spatial distribution of subfossil diatom and chironomid assemblages in surface sediments of a remote deep island lake. *Hydrobiologia*, *815*(1), 141–163. https://doi.org/10.1007/s10750-018-3557-4

Räsänen, M. E., Auri, J. M., Huitti, J. V., Klap, A. K., & Virtasalo, J. J. (2009). A shift from lithostratigraphic to allostratigraphic classification of Quaternary glacial deposits. *GSA Today*, *19*(2), 4-11.

Rasmussen, J. B., Godbout, L., & Schallenberg, M. (1989). The humic content of lake water and its relationship to watershed and lake morphometry. *Limnology and Oceanography*, *34*(7), 1336-1343.

Ravelo, A. C., & Hillaire-Marcel, C. (2007). Chapter Eighteen The Use of Oxygen and Carbon Isotopes of Foraminifera in Paleoceanography. In *Developments in Marine Geology* (Vol. 1, pp. 735–764). Elsevier. https://doi.org/10.1016/S1572-5480(07)01023-8

Rawson, P. F., Allen, P. M., Brenchley, P. J., Cope, J. C. W., Gale, A. S., Evans, J. A., Gibbard, P. L., Gregory, F. J., Hailwood, E. A., Hesselbo, S. P., Knox, R. W. O'. B., Marshall, J. E. A., Oates, M., Riley, N. J., Smith, A. G., Trewin, N., Zalasiewicz, J.A. (2002. Stratigraphical Procedure. The Geological Society, London. 57 pp.

Rea, D. K., Owen, R. M., & Meyers, P. A. (1981). Sedimentary processes in the Great Lakes. *Reviews of Geophysics*, *19*(4), 635-648.

Reheis, M. C., & Redwine, J. L. (2008). Lake Manix shorelines and Afton Canyon terraces: Implications for incision of Afton Canyon. In *Special Paper 439: Late Cenozoic Drainage History of the Southwestern Great Basin and Lower Colorado River Region: Geologic and Biotic Perspectives* (Vol. 439, pp. 227–259). Geological Society of America. https://doi.org/10.1130/2008.2439(10)

Reid, I., & Frostick, L. E. (1986). Dynamics of bedload transport in Turkey Brook, a coarse-grained alluvial channel. *Earth Surface Processes and Landforms*, *11*(2), 143-155.

Reimer, P. J., Austin, W. E. N., Bard, E., Bayliss, A., Blackwell, P. G., Ramsey, C. B., Butzin, M., Cheng, H., Edwards, R. L., Friedrich, M., Grootes, P. M., Guilderson, T. P., Hajdas, I., Heaton, T. J., Hogg, A. G., Hughen, K. A., Kromer, B., Manning, S. W., Muscheler, R., … Talamo, S. (2020). The IntCal20 Northern Hemisphere Radiocarbon Age Calibration Curve (0–55 cal kBP). *Radiocarbon*, *62*(4), 725–757. https://doi.org/10.1017/RDC.2020.41

Reinfelds, I., & Nanson, G. (1993). Formation of braided river floodplains, Waimakariri River, New Zealand. *Sedimentology*, *40*(6), 1113–1127. https://doi.org/10.1111/j.1365-3091.1993.tb01382.x

Reynolds, C. S. (1973). The seasonal periodicity of planktonic diatoms in a shallow eutrophic lake. *Freshwater biology*, *3*(1), 89-110.

Reynolds, C. S. (1984). Phytoplankton periodicity: the interactions of form, function and environmental variability. *Freshwater biology*, *14*(2), 111-142.

Ricchi, A., Quartau, R., Ramalho, R. S., Romagnoli, C., Casalbore, D., & Zhao, Z. (2020). Imprints of volcanic, erosional, depositional, tectonic and mass-wasting processes in the morphology of Santa Maria insular shelf (Azores). *Marine Geology*, *424*, 106163.

Ricchi, A., Quartau, R., Ramalho, R. S., Romagnoli, C., Casalbore, D., da Cruz, J. V., ... & Vinhas, A. (2018). Marine terrace development on reefless volcanic islands: New insights from high-resolution marine geophysical data offshore Santa Maria Island (Azores Archipelago). *Marine Geology*, *406*, 42-56.

Richardson, T. L., Gibson, C. E., & Heaney, S. I. (2000). Temperature, growth and seasonal succession of phytoplankton in Lake Baikal, Siberia. *Freshwater biology*, *44*(3).

Richter, N., Russell, J. M., Amaral-Zettler, L., DeGroff, W., Raposeiro, P. M., Gonçalves, V., De Boer, E. J., Pla-Rabes, S., Hernández, A., Benavente, M., Ritter, C., Sáez, A., Bao, R., Trigo, R. M., Prego, R., & Giralt, S. (2022). Long-term hydroclimate variability in the sub-tropical North Atlantic and anthropogenic impacts on lake ecosystems: A case study from Flores Island, the Azores. *Quaternary Science Reviews*, *285*, 107525. https://doi.org/10.1016/j.quascirev.2022.107525

Ritter, C., Gonçalves, V., Pla-Rabes, S., de Boer, E. J., Bao, R., Sáez, A., Hernández, A., Sixto, M., Richter, N., Benavente, M., Prego, R., Giralt, S., & Raposeiro, P. M. (2022). The vanishing and the establishment of a new ecosystem on an oceanic island – Anthropogenic impacts with no return ticket. *Science of The Total Environment*, *830*, 154828. https://doi.org/10.1016/j.scitotenv.2022.154828

Robbins, J. A., Edgington, D. N., & Kemp, A. L. W. (1978). Comparative 210Pb, 137Cs, and Pollen Geochronologies of Sediments from Lakes Ontario and Erie. *Quaternary Research*, *10*(2), 256–278. https://doi.org/10.1016/0033-5894(78)90105-9

Rodrigues, T., Grimalt, J. O., Abrantes, F. G., Flores, J. A., & Lebreiro, S. M. (2009). Holocene interdependences of changes in sea surface temperature, productivity, and fluvial inputs in the Iberian continental shelf (Tagus mud patch): HOLOCENE CHANGES IN THE IBERIAN CONTINENTAL SHELF. *Geochemistry, Geophysics, Geosystems*, *10*(7), n/a-n/a. https://doi.org/10.1029/2008GC002367

Rodríguez-Puebla, C., & Nieto, S. (2010). Trends of precipitation over the Iberian Peninsula and the North Atlantic Oscillation under climate change conditions. *International Journal of Climatology*, *30*(12), 1807-1815.

Rogers, J. C. (1984). The association between the North Atlantic Oscillation and the Southern Oscillation in the northern hemisphere. *Monthly Weather Review*, *112*(10), 1999-2015.

Rosenmeier, M. F., Hodell, D. A., Brenner, M., Curtis, J. H., Martin, J. B., Anselmetti, F. S., ... & Guilderson, T. P. (2002). Influence of vegetation change on watershed hydrology: implications for paleoclimatic interpretation of lacustrine δ 18 O records. Journal of Paleolimnology, 27, 117-131.

Rosenzweig, C., Casassa, G., Karoly, D. J., Imeson, A., Liu, C., Menzel, A., Rawlins, S., Root, T. L., Seguin, B., & Tryjanowski, P. (2007). *Assessment of observed changes and responses in natural and managed systems*. https://doi.org/10.5167/UZH-33180

Rothwell, R. G. (1998). Sedimentary evidence relating to the tectonic evolution of the Lau Basin, SW Pacific, from ODP Sites 834–839 (ODP Leg 135). *Geological Society, London, Special Publications*, *131*(1), 211–229. https://doi.org/10.1144/GSL.SP.1998.131.01.14

Rothwell, R. G., Thomson, J., & Kähler, G. (1998). Low-sea-level emplacement of a very large Late Pleistocene ‘megaturbidite’ in the western Mediterranean Sea. *Nature*, *392*(6674), 377–380. https://doi.org/10.1038/32871

Round, F. E., & Crawford, R. M. (1981). The lines of evolution of the Bacillariophyta. I. Origin. *Proceedings of the Royal Society of London. Series B. Biological Sciences*, *211*(1183), 237-260.

Round, F. E., & Crawford, R. M. (1984). The lines of evolution of the Bacillariophyta-II. The centric series. *Proceedings of the Royal society of London. Series B. Biological sciences*, *221*(1223), 169-188.

Roundy, J. K., Ferguson, C. R., & Wood, E. F. (2014). Impact of land-atmospheric coupling in CFSv2 on drought prediction. *Climate Dynamics*, *43*(1–2), 421–434. https://doi.org/10.1007/s00382-013-1982-7

Royden, L., & Taylor Perron, J. (2013). Solutions of the stream power equation and application to the evolution of river longitudinal profiles. *Journal of Geophysical Research: Earth Surface*, *118*(2), 497-518.

Rubensdotter, L., & Rosqvist, G. (2003). The effect of geomorphological setting on Holocene lake sediment variability, northern Swedish Lapland. *Journal of Quaternary Science*, *18*(8), 757–767. https://doi.org/10.1002/jqs.800

Rubio de Inglés, M. J. (2016). Late Holocene Climate Variability in the North Atlantic based on biomarker reconstruction: The lake Azul (São Miguel, Azores archipielago) case. Universitat de Barcelona. 244 pp.

Ruiz-Fernández, A. C., Hillaire-Marcel, C., Páez-Osuna, F., Ghaleb, B., & Caballero, M. (2007). 210Pb chronology and trace metal geochemistry at Los Tuxtlas, Mexico, as evidenced by a sedimentary record from the Lago Verde crater lake. *Quaternary Research*, *67*(2), 181-192.

Ruiz-Fernández, A. C., Sanchez-Cabeza, J. A., Blaauw, M., Pérez-Bernal, L. H., Cardoso-Mohedano, J. G., Aquino-López, M. A., ... & Giralt, S. (2022). Historical reconstruction of sediment accumulation rates as an indicator of global change impacts in a tropical crater lake. *Journal of Paleolimnology*, *68*(4), 395-413.

Rull, V., González-Sampériz, P., Corella, J. P., Morellón, M., & Giralt, S. (2011). Vegetation changes in the southern Pyrenean flank during the last millennium in relation to climate and human activities: the Montcortès lacustrine record. *Journal of Paleolimnology*, *46*, 387-404

Rull, V., Lara, A., Rubio-Inglés, M. J., Giralt, S., Gonçalves, V., Raposeiro, P., Hernández, A., Sánchez-López, G., Vázquez-Loureiro, D., Bao, R., Masqué, P., & Sáez, A. (2017). Vegetation and landscape dynamics under natural and anthropogenic forcing on the Azores Islands: A 700-year pollen record from the São Miguel Island. *Quaternary Science Reviews*, *159*, 155–168. https://doi.org/10.1016/j.quascirev.2017.01.021

Rullkötter, J. (2001). Geochemistry, organic. *Encyclopedia of Physical Science and Technology, 3rd edition: Academic Press, San Diego*, *6*, 549-574.

Sabatier, P., Moernaut, J., Bertrand, S., Van Daele, M., Kremer, K., Chaumillon, E., & Arnaud, F. (2022). A Review of Event Deposits in Lake Sediments. *Quaternary*, *5*(3), 34. https://doi.org/10.3390/quat5030034

Sachse, D., Billault, I., Bowen, G.J., Chikaraishi, Y., Dawson, T.E., Feakins, S.J., Freeman, K.H., Magill, C.R., McInerney, F.A., Van Der Meer, M.T., Polissar, P., 2012. Molecular paleohydrology: interpreting the hydrogen-isotopic composition of lipid biomarkers from photosynthesizing organisms. Annu. Rev. Earth Planet Sci. 40, 221e249. https://doi.org/10.1146/annurev-earth-042711-105535.

Salvador, A. (Ed.). (1994). *International stratigraphic guide: a guide to stratigraphic classification, terminology, and procedure* (No. 30). Geological Society of America.

Salvany, J. M., & Ortí, F. (1994). Miocene glauberite deposits of Alcanadre, Ebro Basin, Spain: Sedimentary and diagenetic processes.

Sánchez-Cabeza, J., Masqué, P., & Ani-Ragolta, I. (1998). 210Pb and210Po analysis in sediments and soils by microwave acid digestion. *Journal of Radioanalytical and Nuclear Chemistry*, *227*(1–2), 19–22. https://doi.org/10.1007/bf02386425

Sánchez-López, G. (2016). North Atlantic Oscillation imprints in the Central Iberian Peninsula for the last two millennia: from ordination analyses to the Bayesian approach. Universitat de Barcelona. 283 pp.

Sánchez-López, G., Hernández, A., Pla-Rabes, S., Toro, M., Granados, I., Sigró, J., Trigo, R. M., Rubio-Inglés, M. J., Camarero, L., Valero-Garcés, B., & Giralt, S. (2015). The effects of the NAO on the ice phenology of Spanish alpine lakes. *Climatic Change*, *130*(2), 101–113. https://doi.org/10.1007/s10584-015-1353-y

Sánchez-López, G., Hernández, A., Pla-Rabes, S., Trigo, R. M., Toro, M., Granados, I., Sáez, A., Masqué, P., Pueyo, J. J., Rubio-Inglés, M. J., & Giralt, S. (2016). Climate reconstruction for the last two millennia in central Iberia: The role of East Atlantic (EA), North Atlantic Oscillation (NAO) and their interplay over the Iberian Peninsula. *Quaternary Science Reviews*, *149*, 135–150. https://doi.org/10.1016/j.quascirev.2016.07.021

Sancho, C., Peña, J. L., Muñoz, A., Benito, G., McDonald, E., Rhodes, E. J., & Longares, L. A. (2008). Holocene alluvial morphopedosedimentary record and environmental changes in the Bardenas Reales Natural Park (NE Spain). *Catena*, *73*(3), 225-238.

Schaefer, J. M., Codilean, A. T., Willenbring, J. K., Lu, Z. T., Keisling, B., Fülöp, R. H., & Val, P. (2022). Cosmogenic nuclide techniques. Nature Reviews Methods Primers, 2(1), 18.

Schaetzl, R. J. Anderson. S. (2005). Soils: Genesis and geomorphology. 817 pp.

Scheidegger, A. E. (1961). General theory of dispersion in porous media. *Journal of Geophysical Research*, *66*(10), 3273-3278.

Scherrer, S. C., Croci-Maspoli, M., Schwierz, C., & Appenzeller, C. (2006). Two-dimensional indices of atmospheric blocking and their statistical relationship with winter climate patterns in the Euro-Atlantic region. *International Journal of Climatology: A Journal of the Royal Meteorological Society*, *26*(2), 233-249.

Schettler, G., & Romer, R. L. (1998). Anthropogenic influences on Pb/Al and lead isotope signature in annually layered Holocene Maar lake sediments. *Applied Geochemistry*, *13*(6), 787-797.

Schindler, D. W. (1974). Eutrophication and recovery in experimental lakes: implications for lake management. *Science*, *184*(4139), 897-899.

Schindler, D. W. (1977). Evolution of phosphorus limitation in lakes: natural mechanisms compensate for deficiencies of nitrogen and carbon in eutrophied lakes. *Science*, *195*(4275), 260-262.

Schindler, D. W. (1997). Widespread effects of climatic warming on freshwater ecosystems in North America. *Hydrological processes*, *11*(8), 1043-1067.

Schindler, D. W., Bayley, S. E., Parker, B. R., Beaty, K. G., Cruikshank, D. R., Fee, E. J., Schindler, E. U., & Stainton, M. P. (1996a). The effects of climatic warming on the properties of boreal lakes and streams at the Experimental Lakes Area, northwestern Ontario. *Limnology and Oceanography*, *41*(5), 1004–1017. https://doi.org/10.4319/lo.1996.41.5.1004

Schindler, D. W., Bayley, S. E., Parker, B. R., Beaty, K. G., Cruikshank, D. R., Fee, E. J., Schindler, E. U., & Stainton, M. P. (1996b). The effects of climatic warming on the properties of boreal lakes and streams at the Experimental Lakes Area, northwestern Ontario. *Limnology and Oceanography*, *41*(5), 1004–1017. https://doi.org/10.4319/lo.1996.41.5.1004

Schnurrenberger, D., Russell, J., & Kelts, K. (2003). Classification of lacustrine sediments based on sedimentary components. *Journal of Paleolimnology*, *29*(2), 141–154. https://doi.org/10.1023/A:1023270324800

Scholz, C. A., Klitgord, K. D., Hutchinson, D. R., Ten Brink, U. S., Zonenshain, L. P., Golmshtok, A. Y., & Moore, T. C. (1993). Results of 1992 seismic reflection experiment in Lake Baikal. *Eos, Transactions American Geophysical Union*, *74*(41), 465-470.

Schrott, L., Hufschmidt, G., Hankammer, M., Hoffmann, T., & Dikau, R. (2003). Spatial distribution of sediment storage types and quantification of valley fill deposits in an alpine basin, Reintal, Bavarian Alps, Germany. *Geomorphology*, *55*(1–4), 45–63. https://doi.org/10.1016/S0169-555X(03)00131-4

Schwalb, A. (2003). Lacustrine ostracodes as stable isotope recorders of late-glacial and Holocene environmental dynamics and climate. *Journal of Paleolimnology*, *29*, 265-351.

Schweingruber, F. H., Kučerová, A., Adamec, L., & Doležal, J. (2020). *Anatomic atlas of aquatic and wetland plant stems*. Springer Nature.

Scotese, C. R., Song, H., Mills, B. J. W., & Van Der Meer, D. G. (2021). Phanerozoic paleotemperatures: The earth's changing climate during the last 540 million years. *Earth-Science Reviews*, *215*, 103503. https://doi.org/10.1016/j.earscirev.2021.103503

Scott, D. T., Baisden, W. T., Davies-Colley, R., Gomez, B., Hicks, D. M., Page, M. J., Preston, N. J., Trustrum, N. A., Tate, K. R., & Woods, R. A. (2006). Localized erosion affects national carbon budget. *Geophysical Research Letters*, *33*(1), 2005GL024644. https://doi.org/10.1029/2005GL024644

Searle, R. (1980). Tectonic pattern of the Azores spreading centre and triple junction. *Earth and Planetary Science Letters*, *51*(2), 415–434. https://doi.org/10.1016/0012-821X(80)90221-6

Seddon, A. W., Macias-Fauria, M., & Willis, K. J. (2015). Climate and abrupt vegetation change in Northern Europe since the last deglaciation. *The Holocene*, *25*(1), 25-36.

Seitzinger, S. P. (1988). Denitrification in freshwater and coastal marine ecosystems: ecological and geochemical significance. *Limnology and oceanography*, *33*(4part2), 702-724.

Semeniuk, C. A., & Semeniuk, V. (1995). A geomorphic approach to global classification for inland wetlands. *Classification and Inventory of the World's Wetlands*, 103-124.

Shanahan, T. M., Overpeck, J. T., Hubeny, J. B., King, J., Hu, F. S., Hughen, K., ... & Black, J. (2008). Scanning micro-X-ray fluorescence elemental mapping: A new tool for the study of laminated sediment records. *Geochemistry, Geophysics, Geosystems*, *9*(2).

Shanan, L. (1987). The impact of irrigation. *Land Transformation in Agriculture*, 115-131.

Shanmugam, G. (2013). Modern internal waves and internal tides along oceanic pycnoclines: Challenges and implications for ancient deep-marine baroclinic sands. AAPG bulletin, 97(5), 799-843.

Shen, J. (2013). Spatiotemporal variations of Chinese lakes and their driving mechanisms since the Last Glacial Maximum: A review and synthesis of lacustrine sediment archives. *Chinese Science Bulletin*, *58*, 17-31.

Shimada, T., Kashiwaya, K., Masuzawa, T., Hyodo, M. (2002). Hydro-environmental fluctuation in a lake–catchment system during the late Holocene inferred from Lake Yogo sediments. Trans

Shuman, B., Bartlein, P. J., & Webb III, T. (2005). The magnitudes of millennial-and orbital-scale climatic change in eastern North America during the Late Quaternary. *Quaternary Science Reviews*, *24*(20-21), 2194-2206.

Shunk, A. J., Driese, S. G., & Dunbar, J. A. (2009). Late Tertiary paleoclimatic interpretation from lacustrine rhythmites in the Gray Fossil Site, northeastern Tennessee, USA. *Journal of Paleolimnology*, *42*, 11-24.

Sidorchuk, A. (2005). Stochastic components in the gully erosion modelling. *Catena*, *63*(2-3), 299-317.

Siedler, G., Griffies, S. M., Gould, J., & Church, J. A. (2013). *Ocean circulation and climate: a 21st century perspective*. Academic Press.

Sime-Ngando, T., Boivin, P., Chapron, E., Jezequel, D., & Meybeck, M. (Eds.). (2016). Lake Pavin: History, geology, biogeochemistry, and sedimentology of a deep meromictic maar lake. Springer.

Singh, A. K., Dubey, C. A., Singh, D. S., Kumar, D., & Sharma, R. (2023). Sedimentary Parameters and Evolution of the Outwash Plain Deposits during Late Holocene in the Gangotri Glacier Region, Garhwal Himalaya, India. Journal of the Geological Society of India, 99(9), 1309-1316.

Skov, T., Buchaca, T., Amsinck, S. L., Landkildehus, F., Odgaard, B. V., Azevedo, J., ... & Jeppesen, E. (2010). Using invertebrate remains and pigments in the sediment to infer changes in trophic structure after fish introduction in Lake Fogo: a crater lake in the Azores. *Hydrobiologia*, *654*, 13-25.

Smith, E. T., Lee, C. C., Barnes, B. B., Adams, R. E., Pirhalla, D. E., Ransibrahmanakul, V., ... & Sheridan, S. C. (2020). A synoptic climatological analysis of the atmospheric drivers of water clarity variability in the Great Lakes. *Journal of Applied Meteorology and Climatology*, *59*(5), 915-935.

Smith, G. C., Covich, A. P., & Brasher, A. M. (2003). An ecological perspective on the biodiversity of tropical island streams. *BioScience*, *53*(11), 1048-1051.

Smith, N. D., & Ashley, G. (1985). Proglacial Lacustrine Environment. In G. M. Ashley, J. Shaw, & N. D. Smith (Eds.), *Glacial Sedimentary Environments* (Vol. 16, p. 0). SEPM Society for Sedimentary Geology. https://doi.org/10.2110/scn.85.02.0135

Smol, J. P. (2009). Pollution of lakes and rivers: a paleoenvironmental perspective. John Wiley & Sons.

Smol, J. P., Birks, H. J., & Last, W. M. (2001). *Tracking environmental change using lake sediments: Volume 4: Zoological indicators* (pp. xxi+-217). Springer Netherlands.

Sommerfield, C. K., & Wheatcroft, R. A. (2007). Late Holocene sediment accumulation on the northern California shelf: Oceanic, fluvial, and anthropogenic influences. *Geological Society of America Bulletin*, *119*(9–10), 1120–1134. https://doi.org/10.1130/B26019.1

Soreghan, M. J., & Cohen, A. S. (1996). Textural and compositional variability across littoral segments of Lake Tanganyika: the effect of asymmetric basin structure on sedimentation in large rift lakes. *AAPG bulletin*, *80*(3), 382-408.

Steinbauer, M. J., Grytnes, J. A., Jurasinski, G., Kulonen, A., Lenoir, J., Pauli, H., ... & Wipf, S. (2018). Accelerated increase in plant species richness on mountain summits is linked to warming. *Nature*, *556*(7700), 231-234.

Steinhilber, F., Beer, J., & Fröhlich, C. (2009). Total solar irradiance during the Holocene. *Geophysical Research Letters*, *36*(19), L19704. https://doi.org/10.1029/2009GL040142

Stephenson, D. B., Hannachi, A., & O'Neill, A. (2004). On the existence of multiple climate regimes. *Quarterly Journal of the Royal Meteorological Society*, *130*(597), 583–605. https://doi.org/10.1256/qj.02.146

Street-Perrott, F. A., & Roberts, N. (1983). Fluctuations in Closed-Basin Lakes as An Indicator of Past Atmospheric Circulation Patterns. In *Variations in the Global Water Budget* (pp. 331–345). Springer Netherlands. https://doi.org/10.1007/978-94-009-6954-4_26

Street-Perrott, F. A., Huang, Y., Perrott, R. A., Eglinton, G., Barker, P., Khelifa, L. B., ... & Olago, D. O. (1997). Impact of lower atmospheric carbon dioxide on tropical mountain ecosystems. *Science*, *278*(5342), 1422-1426.

Street-Perrott, F. A., & Barker, P. A. (2008). Biogenic silica: a neglected component of the coupled global continental biogeochemical cycles of carbon and silicon. *Earth Surface Processes and Landforms: The Journal of the British Geomorphological Research Group*, *33*(9), 1436-1457.

Stuiver, M., & Reimer, P. J. (1993). Extended 14C Data Base and Revised CALIB 3.0 14C Age Calibration Program. *Radiocarbon*, *35*(1), 215–230. https://doi.org/10.1017/S0033822200013904

Sturges, W. T., & Harrison, R. M. (1986). Bromine in marine aerosols and the origin, nature and quantity of natural atmospheric bromine. Atmospheric Environment (1967), 20(7), 1485-1496.

Sun, G., Noormets, A., Chen, J., & McNulty, S. G. (2008). Evapotranspiration estimates from eddy covariance towers and hydrologic modeling in managed forests in Northern Wisconsin, USA. agricultural and forest meteorology, 148(2), 257-267.

Suzuki, Y., & Takahashi, M. (1995). Growth responses of several diatom species isolated from various environments to temperature. *Journal of Phycology*, *31*(6), 880-888.

Takahashi, K., Yoshioka, T., Wada, E., & Sakamoto, M. (1990). Temporal variations in carbon isotope ratio of phytoplankton in a eutrophic lake. *Journal of Plankton Research*, *12*(4), 799-808.

Talbot, M. R. (2001). Nitrogen isotopes in palaeolimnology. *Tracking environmental change using lake sediments: physical and geochemical methods*, 401-439.

Talbot, M. R. & P. A. Allen. (1996). Lakes. In Reading, H. G. (ed.) Sedimentary Environments: Processes, Facies and Stratigraphy (3rd edition). Blackwell Science, London: 83–124.

Talbot, M. R., & Brendeland, K. I. (2001, December). Strontium isotopes as palaeohydrological tracers in the White Nile headwater lakes, East Africa. In *AGU Fall Meeting Abstracts* (Vol. 2001, pp. PP21C-05).

Talbot, M. R., & Johannessen, T. (1992). A high resolution palaeoclimatic record for the last 27,500 years in tropical West Africa from the carbon and nitrogen isotopic composition of lacustrine organic matter. *Earth and Planetary Science Letters*, *110*(1-4), 23-37.

Talbot, M. R., & Lærdal, T. (2000). The Late Pleistocene-Holocene palaeolimnology of Lake Victoria, East Africa, based upon elemental and isotopic analyses of sedimentary organic matter. *Journal of Paleolimnology*, *23*, 141-164.

Talbot, M.R. and Kelts, K. (1989). Introduction. In Talbot, M.R. and Kelts, K. (eds.), Phanerozoic Record of Lacustrine Basins and their Environmental Signals. Palaeogeogr., Palaeoclim., Palaeoecol. 70:1–5.

Taylor, G., & Eggleton, R. A. (2001). Regolith geology and geomorphology. John Wiley & Sons.

Tenzer, G. E., Myers, P. A., & Knoop, P. (1997). Sources and distribution of organic and carbonate carbon in surface sediments of Pyramid Lake, Nevada. *Journal of Sedimentary Research*, *67*(5), 884-890.

Thompson, S., & Eglinton, G. (1978). The fractionation of a recent sediment for organic geochemical analysis. *Geochimica et Cosmochimica Acta*, *42*(2), 199-207.

Thouret, J. C. (1999). Volcanic geomorphology—an overview. *Earth-science reviews*, *47*(1-2), 95-131.

Tiercelin, J. J., Cohen, A. S., Soreghan, M. J., & Lezzar, K. E. (1994). Pleistocene-modern deposits of the Lake Tanganyika Rift Basin, East Africa: A modern analog for lacustrine source rocks and reservoirs.

Tierney, J. E., Malevich, S. B., Gray, W., Vetter, L., & Thirumalai, K. (2019). Bayesian Calibration of the Mg/Ca Paleothermometer in Planktic Foraminifera. *Paleoceanography and Paleoclimatology*, *34*(12), 2005–2030. https://doi.org/10.1029/2019PA003744

Tierney, J. E., Poulsen, C. J., Montañez, I. P., Bhattacharya, T., Feng, R., Ford, H. L., Hönisch, B., Inglis, G. N., Petersen, S. V., Sagoo, N., Tabor, C. R., Thirumalai, K., Zhu, J., Burls, N. J., Foster, G. L., Goddéris, Y., Huber, B. T., Ivany, L. C., Kirtland Turner, S., … Zhang, Y. G. (2020). Past climates inform our future. *Science*, *370*(6517), eaay3701. https://doi.org/10.1126/science.aay3701

Tilman, D., Kilham, S. S., & Kilham, P. (1982). Phytoplankton community ecology: the role of limiting nutrients. *Annual review of Ecology and Systematics*, *13*(1), 349-372.

Treut, H. L., Somerville, R., Cubasch, U., Ding, Y., Mauritzen, C., Mokssit, A., Peterson, T., Prather, M., Allen, M., Auer, I., Biercamp, J., Covey, C., Fleming, J. R., García-Herrera, R., Gleckler, P., Haigh, J., Hegerl, G. C., Isaksen, K., Jones, J., … Prather, M. (2007). *Historical Overview of Climate Change Science*.

Trigo, R. M., Osborn, T. J., & Corte-Real, J. M. (2002). The North Atlantic Oscillation influence on Europe: climate impacts and associated physical mechanisms. *Climate research*, *20*(1), 9-17.

Trigo, R. M., Pozo-Vázquez, D., Osborn, T. J., Castro-Díez, Y., Gámiz-Fortis, S., & Esteban-Parra, M. J. (2004). North Atlantic Oscillation influence on precipitation, river flow and water resources in the Iberian Peninsula. *International Journal of Climatology: A Journal of the Royal Meteorological Society*, *24*(8), 925-944.

Trimble, S. W. (1999). Decreased rates of alluvial sediment storage in the Coon Creek Basin, Wisconsin, 1975-93. *Science*, *285*(5431), 1244-1246.

Trimble, S. W., & Crosson, P. (2000). US soil erosion rates--myth and reality. *Science*, *289*(5477), 248-250.

Trimble, S. W., & Lund, S. W. (1982). Soil conservation and the reduction of erosion and sedimentation in the Coon Creek Basin, Wisconsin (Vol. 1234). US Government Printing Office.

Troiani, F., Galve, J. P., Piacentini, D., Della Seta, M., & Guerrero, J. (2014). Spatial analysis of stream length-gradient (SL) index for detecting hillslope processes: a case of the Gállego River headwaters (Central Pyrenees, Spain). *Geomorphology*, *214*, 183-197.

Troiani, F., Piacentini, D., Della Seta, M., & Galve, J. P. (2017). Stream Length-gradient Hotspot and Cluster Analysis (SL-HCA) to fine-tune the detection and interpretation of knickzones on longitudinal profiles. *Catena*, *156*, 30-41.

Tye, R. S., & Coleman, J. M. (1989). Depositional processes and stratigraphy of fluvially dominated lacustrine deltas; Mississippi delta plain. Journal of Sedimentary Research, 59(6), 973-996.

Tylmann, W., Szpakowska, K., Ohlendorf, C., Woszczyk, M., & Zolitschka, B. (2012). Conditions for deposition of annually laminated sediments in small meromictic lakes: a case study of Lake Suminko (northern Poland). *Journal of Paleolimnology*, *47*, 55-70.

Tylmann, W., Zolitschka, B., Enters, D., & Ohlendorf, C. (2013). Laminated lake sediments in northeast Poland: distribution, preconditions for formation and potential for paleoenvironmental investigation. *Journal of Paleolimnology*, *50*, 487-503.

Ulfers, A., Zeeden, C., Wagner, B., Krastel, S., Buness, H., & Wonik, T. (2022). Borehole logging and seismic data from Lake Ohrid (North Macedonia/Albania) as a basis for age-depth modelling over the last one million years. *Quaternary Science Reviews*, *276*, 107295. https://doi.org/10.1016/j.quascirev.2021.107295

Unkel, I., Fernandez, M., Björck, S., Ljung, K., & Wohlfarth, B. (2010). Records of environmental changes during the Holocene from Isla de los Estados (54.4 S), southeastern Tierra del Fuego. Global and Planetary Change, 74(3-4), 99-113.

Unkel, S., Trendafilov, N. T., Hannachi, A., & Jolliffe, I. T. (2010). Independent exploratory factor analysis with application to atmospheric science data. Journal of Applied Statistics, 37(11), 1847-1862.

Urey, H. C. (1947). The thermodynamic properties of isotopic substances. *Journal of the Chemical Society (Resumed)*, 562-581.

Urrego, D. H., Bush, M. B., Silman, M. R., Correa-Metrio, A. Y., Ledru, M. P., Mayle, F. E., ... & Valencia, B. G. (2009). Millennial-scale ecological changes in tropical South America since the last glacial maximum. *Past climate variability in South America and surrounding regions: from the Last Glacial Maximum to the Holocene*, 283-300.

Valentin, C., Poesen, J., & Li, Y. (2005). Gully erosion: Impacts, factors and control. *Catena*, *63*(2-3), 132-153.

Valenzano, E., Scardino, G., Cipriano, G., Fago, P., Capolongo, D., De Giosa, F., ... & Mastronuzzi, G. (2018). Holocene morpho-sedimentary evolution of the Mar Piccolo basin (Taranto, Southern Italy). *Geogr. Fis. Din. Quat*, *41*, 119-135.

Valero-Garcés, B. L., & Kelts, K. R. (1995). A sedimentary facies model for perennial and meromictic saline lakes: Holocene Medicine Lake Basin, South Dakota, USA. *Journal of Paleolimnology*, *14*, 123-149.

Valero-Garcés, B. L., Laird, K. R., Fritz, S. C., Kelts, K., Ito, E., & Grimm, E. C. (1997). Holocene climate in the Northern Great Plains inferred from sediment stratigraphy, stable isotopes, carbonate geochemistry, diatoms, and pollen at Moon Lake, North Dakota. *Quaternary Research*, *48*(3), 359-369.

Van Daele, M., Moernaut, J., Silversmit, G., Schmidt, S., Fontijn, K., Heirman, K., ... & De Batist, M. (2014). The 600 yr eruptive history of Villarrica Volcano (Chile) revealed by annually laminated lake sediments. *Bulletin*, *126*(3-4), 481-498.

Vázquez-Loureiro, D., Gonçalves, V., Sáez, A., Hernández, A., Raposeiro, P. M., Giralt, S., Rubio-Inglés, M. J., Rull, V., & Bao, R. (2019). Diatom-inferred ecological responses of an oceanic lake system to volcanism and anthropogenic perturbations since 1290 CE. *Palaeogeography, Palaeoclimatology, Palaeoecology*, *534*, 109285. https://doi.org/10.1016/j.palaeo.2019.109285

Vázquez-Loureiro, D., Sáez, A., Gonçalves, V., Buchaca, T., Hernández, A., Raposeiro, P. M., De Boer, E. J., Masqué, P., Giralt, S., & Bao, R. (2023). Recent global warming induces the coupling of dissimilar long-term sedimentary signatures in two adjacent volcanic lakes (Azores Archipelago, Portugal). *Quaternary Science Reviews*, *303*, 107968. https://doi.org/10.1016/j.quascirev.2023.107968

Veizer, J., & Mackenzie, F. T. (2003). *Evolution of sedimentary rocks* (Vol. 7, p. 407).

Verburg, P., Hecky, R. E., & Kling, H. (2003). Ecological Consequences of a Century of Warming in Lake Tanganyika. *Science*, *301*(5632), 505–507. https://doi.org/10.1126/science.1084846

Verpoorter, C., Kutser, T., Seekell, D. A., & Tranvik, L. J. (2014). A global inventory of lakes based on high-resolution satellite imagery. *Geophysical Research Letters*, *41*(18), 6396–6402. https://doi.org/10.1002/2014GL060641

Vicente, P. P. J., Guillermo, B. R., Pedro, G. A. J., Miguel, A. J., Patricia, R. R., Cristina, R. C., ... & Alberto, A. S. L. (2024). *Landspy, a Python library and QGIS interface to landscape analysis and knickpoint evaluation* (No. EGU24-19443). Copernicus Meetings.

Vinther, B.M., Johnsen, S.J., Andersen, K.K., Clausen, H.B., Hansen, H.W., 2003a. NAO signal recorded in the stable isotopes of Greenland ice cores. Geophysical Research Letters 30, 1387.

Visbeck, M. (2009). A Station-Based Southern Annular Mode Index from 1884 to 2005. *Journal of Climate*, *22*(4), 940–950. https://doi.org/10.1175/2008JCLI2260.1

Vogel, H., Zanchetta, G., Sulpizio, R., Wagner, B., & Nowaczyk, N. (2010). A tephrostratigraphic record for the last glacial–interglacial cycle from Lake Ohrid, Albania and Macedonia. Journal of Quaternary Science: Published for the Quaternary Research Association, 25(3), 320-338.

Vogt, P. R., & Jung, W. Y. (2004). The Terceira Rift as hyper-slow, hotspot-dominated oblique spreading axis: A comparison with other slow-spreading plate boundaries. *Earth and Planetary Science Letters*, *218*(1–2), 77–90. https://doi.org/10.1016/S0012-821X(03)00627-7

Vogt, P. R., & Jung, W.-Y. (2018). The “Azores Geosyndrome” and Plate Tectonics: Research History, Synthesis, and Unsolved Puzzles. In U. Kueppers & C. Beier (Eds.), *Volcanoes of the Azores* (pp. 27–56). Springer Berlin Heidelberg. https://doi.org/10.1007/978-3-642-32226-6_3

Vollenweider, R. A. (1976). Rotsee, a source, not a sink for phosphorus? A comment to and a plea for nutrient balance studies. *Schweizerische Zeitschrift für Hydrologie*, *38*, 29-34.

Wagner, B., Sulpizio, R., Zanchetta, G., Wulf, S., Wessels, M., Daut, G., & Nowaczyk, N. (2008). The last 40 ka tephrostratigraphic record of Lake Ohrid, Albania and Macedonia: A very

distal archive for ash dispersal from Italian volcanoes. *Journal of Volcanology and Geothermal Research*, *177*(1), 71–80. https://doi.org/10.1016/j.jvolgeores.2007.08.018

Wakatsuki, T., Tanaka, Y., & Matsukura, Y. (2005). Soil slips on weathering-limited slopes underlain by coarse-grained granite or fine-grained gneiss near Seoul, Republic of Korea. *CATENA*, *60*(2), 181–203. https://doi.org/10.1016/j.catena.2004.11.003

Walker, B. H., Ludwig, D., Holling, C. S., & Peterman, R. M. (1981). Stability of semi-arid savanna grazing systems. The Journal of Ecology, 473-498.

Walker, I. R. (2001). Midges: Chironomidae and related diptera. *Tracking Environmental Change Using Lake Sediments: Volume 4: Zoological Indicators*, 43-66.

Walling, D. E. (1983). The sediment delivery problem. *Journal of hydrology*, *65*(1-3), 209-237.

Walling, D. E., & Kleo, A. H. A. (1979). Sediment yields of rivers in areas of low precipitation: a global view. *Proceedings... The Hydrology of areas of low precipitation*, *1979*.

Walsh, L. S., Martin, A. J., Ojha, T. P., & Fedenczuk, T. (2012). Correlations of fluvial knickzones with landslide dams, lithologic contacts, and faults in the southwestern Annapurna Range, central Nepalese Himalaya. *Journal of Geophysical Research: Earth Surface*, *117*(F1).

Wang, J., Yang, B., Ljungqvist, F.C., Luterbacher, J., Osborn, T.J., Briffa, K.R., Zorita, E. Internal and external forcing of multidecadal Atlantic climate variability over the past 1,200 years. (2017) Nature Geoscience, 10 (7), 512-517.

Wanner, H., Brönnimann, S., Casty, C., Gyalistras, D., Luterbacher, J., Schmutz, C., ... & Xoplaki, E. (2001). North Atlantic Oscillation–concepts and studies. *Surveys in geophysics*, *22*, 321-381.

Warburton, J. (1992). Observations of Bed Load Transport and Channel Bed Changes in a Proglacial Mountain Stream. *Arctic and Alpine Research*, *24*(3), 195. https://doi.org/10.2307/1551657

Wasson, R. J. (2003). A sediment budget for the Ganga–Brahmaputra catchment. Current science, 1041-1047.

Weckström, J., Korhola, A., & Blom, T. (1997). The relationship between diatoms and water temperature in thirty subarctic Fennoscandian lakes. *Arctic and Alpine Research*, *29*(1), 75-92.

Weerts, H. J. T., Westerhoff, W. E. (2007). Lithostratigraphy. In: Elias, S. (Ed.), Section 3: Quaternary Stratigraphy. Encyclopedia of Quaternary Sciences. Elsevier, Amsterdam, pp. 2826–2840.

Wehrli, B., Lotter, A. F., Schaller, T., & Sturm, M. (1997). High-resolution varve studies in Baldeggersee (Switzerland): project overview and limnological background data. *Aquatic Sciences*, *59*, 285-294.

Weirich, F. H. (1984). Turbidity currents: monitoring their occurrence and movement with a three-dimensional sensor network. *Science*, *224*(4647), 384-387.

Weirich, F. H. (1986). A study of the nature and incidence of density currents in a shallow glacial lake. *Annals of the Association of American Geographers*, *76*(3), 396-413.

Wells, S. G., & Harvey, A. M. (1987). *Sedimentologie and geomorphic variations in storm-generated alluvial fans, Howgill Fells, northwest England*.

Wentworth, C.K., 1922, A scale of grade and class terms for clastic sediments. The Journal of Geology, v. 30, p. 377–392. R Core Team (2021). R: A language and environment for statistical computing.

Wetzel, R. G. (2001). *Limnology: lake and river ecosystems*. gulf professional publishing.

Wetzel, R. G., Likens, G. E., Wetzel, R. G., & Likens, G. E. (2000). The heat budget of lakes. *Limnological analyses*, 45-56.

Whipple, K. X. (2004). BEDROCK RIVERS AND THE GEOMORPHOLOGY OF ACTIVE OROGENS. *Annual Review of Earth and Planetary Sciences*, *32*(1), 151–185. https://doi.org/10.1146/annurev.earth.32.101802.120356

White, I. D., Mottershead, D. N., & Harrison, S. J. (1998). *Environmental systems: an introductory text*. Psychology Press.

Whiting, P. J., Stamm, J. F., Moog, D. B., & Orndorff, R. L. (1999). Sediment-transporting flows in headwater streams. *Geological Society of America Bulletin*.

Wilby, R. L. (2007). A Review of Climate Change Impacts on the Built Environment. *CLIMATE CHANGE AND CITIES*, *33*(1).

Wilcock, P. R., & McArdell, B. W. (1993). Surface-based fractional transport rates: Mobilization thresholds and partial transport of a sand-gravel sediment. *Water Resources Research*, *29*(4), 1297–1312. https://doi.org/10.1029/92WR02748

Williamson, C. E., Dodds, W., Kratz, T. K., & Palmer, M. A. (2008). Lakes and streams as sentinels of environmental change in terrestrial and atmospheric processes. *Frontiers in Ecology and the Environment*, *6*(5), 247–254. https://doi.org/10.1890/070140

Williamson, C. E., Saros, J. E., Vincent, W. F., & Smol, J. P. (2009). Lakes and reservoirs as sentinels, integrators, and regulators of climate change. *Limnology and Oceanography*, *54*(6part2), 2273–2282. https://doi.org/10.4319/lo.2009.54.6_part_2.2273

Wilmshurst, J. M., Moar, N. T., Wood, J. R., Bellingham, P. J., Findlater, A. M., Robinson, J. J., & Stone, C. (2014). Use of pollen and ancient DNA as conservation baselines for offshore islands in New Zealand. *Conservation Biology*, *28*(1), 202-212.

Woollings, T., & Blackburn, M. (2012). The North Atlantic jet stream under climate change and its relation to the NAO and EA patterns. *Journal of Climate*, *25*(3), 886-902.

Woollings, T., Hannachi, A., & Hoskins, B. (2010). Variability of the North Atlantic eddy-driven jet stream. *Quarterly Journal of the Royal Meteorological Society*, *136*(649), 856-868.

Woolway, R. I., Jennings, E., Shatwell, T., Golub, M., Pierson, D. C., & Maberly, S. C. (2021). Lake heatwaves under climate change. *Nature*, *589*(7842), 402-407.

Woolway, R. I., Sharma, S., Weyhenmeyer, G. A., Debolskiy, A., Golub, M., Mercado-Bettín, D., ... & Jennings, E. (2021). Phenological shifts in lake stratification under climate change. *Nature communications*, *12*(1), 2318.

Worrall, F., Burt, T., & Adamson, J. (2003). Controls on the chemistry of runoff from an upland peat catchment. *Hydrological processes*, *17*(10), 2063-2083.

Wünnemann, B., Mischke, S., & Chen, F. (2006). A Holocene sedimentary record from Bosten Lake, China. *Palaeogeography, Palaeoclimatology, Palaeoecology*, *234*(2–4), 223–238. https://doi.org/10.1016/j.palaeo.2005.10.016

Wünnemann, B., Yan, D., & Ci, R. (2015). Morphodynamics and lake level variations at Paiku Co, southern Tibetan Plateau, China. *Geomorphology*, *246*, 489–501. https://doi.org/10.1016/j.geomorph.2015.07.007

Yatsu E (1986) Chikeigaku no ronri (Logic in geomorphology). In: Geographical Research Group of Chuo University (ed) Perspective of geography. Sozosha, Tokyo, 208p, pp 30–35 (in Japanese)

Yemane, K., Kahr, G., & Kelts, K. (1996). Imprints of post-glacial climates and palaeogeography in the detrital clay mineral assemblages of an Upper Permian fluviolacustrine Gondwana deposit from northern Malawi. *Palaeogeography, Palaeoclimatology, Palaeoecology*, *125*(1-4), 27-49.

Yokoyama, T. (1984). Stratigraphy of the quaternary system around Lake Biwa and geohistory of the ancient Lake Biwa. In: Horie S (ed) Lake Biwa. Dr. W. Junk, The Hague, 654p, pp 43–128.

Yuretich, R., Melles, M., Sarata, B., & Grobe, H. (1999). Clay minerals in the sediments of Lake Baikal; a useful climate proxy. *Journal of Sedimentary Research*, *69*(3), 588-596.

Zachos, J., Pagani, M., Sloan, L., Thomas, E., & Billups, K. (2001). Trends, Rhythms, and Aberrations in Global Climate 65 Ma to Present. *Science*, *292*(5517), 686–693. https://doi.org/10.1126/science.1059412

Zahrer, J., Dreibrodt, S., & Brauer, A. (2013). Evidence of the North Atlantic Oscillation in varve composition and diatom assemblages from recent, annually laminated sediments of Lake Belau, northern Germany. *Journal of Paleolimnology*, *50*, 231-244.

Zbyszeuwsky, G., A. Medeiros, O.V. Ferreira & C.T. Assunção. (1967). Carta Geológica de Portugal na escala 1:25000; notícia explicativa da folha da ilha do Corvo (Açores), 16 pp., Serv. Geol. Portugal., Lisboa.

Zecchin, M., & Catuneanu, O. (2013). High-resolution sequence stratigraphy of clastic shelves I: units and bounding surfaces. *Marine and Petroleum Geology*, *39*(1), 1-25.

Zhang, K., Kimball, J. S., Nemani, R. R., Running, S. W., Hong, Y., Gourley, J. J., & Yu, Z. (2015). Vegetation greening and climate change promote multidecadal rises of global land evapotranspiration. Scientific reports, 5(1), 15956.

Zhang, W., Wei, X., Jinhai, Z., Yuliang, Z., & Zhang, Y. (2012). Estimating suspended sediment loads in the Pearl River Delta region using sediment rating curves. *Continental Shelf Research*, *38*, 35–46. https://doi.org/10.1016/j.csr.2012.02.017

Zhang, X., Ward, B. B., & Sigman, D. M. (2020). Global nitrogen cycle: critical enzymes, organisms, and processes for nitrogen budgets and dynamics. *Chemical reviews*, *120*(12), 5308-5351.

ZillÉn, L., Snowball, I., Sandgren, P., & Stanton, T. (2003). Occurrence of varved lake sediment sequences in Varmland, west central Sweden: lake characteristics, varve chronology and AMS radiocarbon dating. *Boreas*, *32*(4), 612-626.

Zohary, T., Pollingher, U., Hadas, O., & Hambright, D. (1998). Bloom dynamics and sedimentation of Peridinium gatunense in Lake Kinneret. *Limnology and Oceanography*, *43*(2), 175-186.

Zolitschka, B., Francus, P., Ojala, A. E., & Schimmelmann, A. (2015). Varves in lake sediments–a review. Quaternary Science Reviews, 117, 1-41.

Zorita, E., & González-Rouco, F. (2002). Are temperature-sensitive proxies adequate for North Atlantic Oscillation reconstructions? *Geophysical Research Letters*, *29*(14). https://doi.org/10.1029/2002GL015404

Zubiate, L., McDermott, F., Sweeney, C., & O'Malley, M. (2017). Spatial variability in winter NAO–wind speed relationships in western Europe linked to concomitant states of the East Atlantic and Scandinavian patterns. *Quarterly Journal of the Royal Meteorological Society*, *143*(702), 552–562. https://doi.org/10.1002/qj.2943